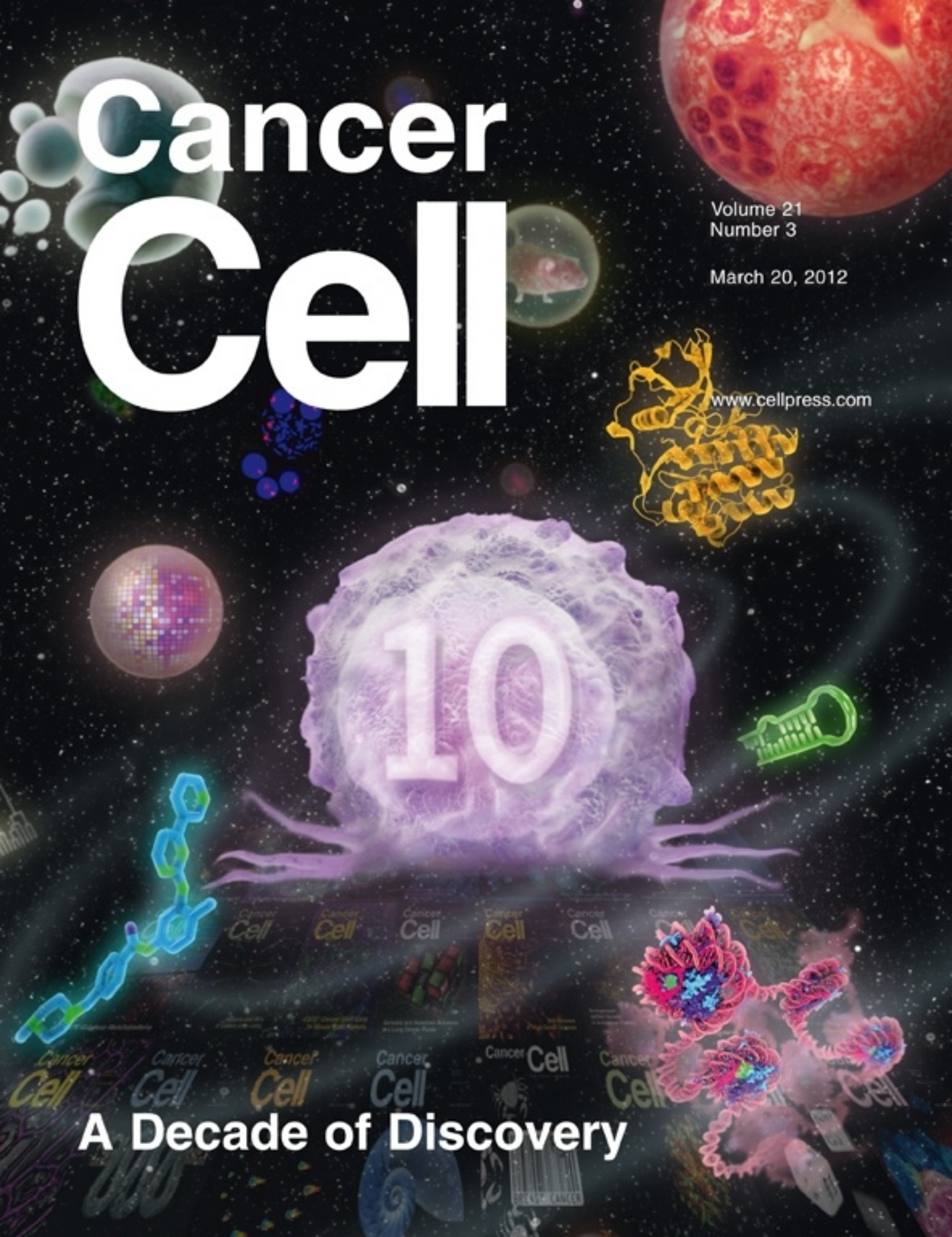
Cancer
Cell
Volume 21
Number 3
March 20, 2012
www.cellpress.com
10
A Decade of Discovery

Cancer Cell
Special Collection
10 YEARS OF EXCITING CANCER RESEARCH SINCE 2002

Cancer Stem Cells: Impact, Heterogeneity, and Uncertainty

Jeffrey A. Magee,[1] Elena Piskounova,[1] and Sean J. Morrison[1,*]
[1]Howard Hughes Medical Institute, Children's Research Institute, and Department of Pediatrics, University of Texas Southwestern Medical Center, Dallas, TX, 75390, USA
*Correspondence: sean.morrison@utsouthwestern.edu
DOI 10.1016/j.ccr.2012.03.003

The differentiation of tumorigenic cancer stem cells into nontumorigenic cancer cells confers heterogeneity to some cancers beyond that explained by clonal evolution or environmental differences. In such cancers, functional differences between tumorigenic and nontumorigenic cells influence response to therapy and prognosis. However, it remains uncertain whether the model applies to many, or few, cancers due to questions about the robustness of cancer stem cell markers and the extent to which existing assays underestimate the frequency of tumorigenic cells. In cancers with rapid genetic change, reversible changes in cell states, or biological variability among patients, the stem cell model may not be readily testable.

Sources of Heterogeneity within Cancer

Many tumors contain phenotypically and functionally heterogeneous cancer cells (Fidler and Hart, 1982; Fidler and Kripke, 1977; Heppner, 1984; Nowell, 1986). This heterogeneity among cancer cells in the same patient can arise in multiple ways. The most well-established mechanism involves intrinsic differences among cancer cells caused by stochastic genetic (Nowell, 1976) or epigenetic (Baylin and Jones, 2011) changes (clonal evolution; Figure 1A). Differences can also arise among cancer cells through extrinsic mechanisms in which different microenvironments within a tumor confer phenotypic and functional differences upon cancer cells in different locations (Figure 1B) (Polyak et al., 2009; Bissell and Hines, 2011). Finally, some cancers follow a stem cell model in which tumorigenic cancer stem cells "differentiate" into nontumorigenic cancer cells, creating a hierarchical organization (Figure 1C; Table 1) (Dick, 2008; Reya et al., 2001; Shackleton et al., 2009). The differentiation of cancer stem cells provides a mechanism for generating phenotypic and functional heterogeneity beyond the heterogeneity that can be attributed to clonal evolution or environmental differences (Figure 1D). However, the fact that heterogeneity can arise through multiple mechanisms means that heterogeneity alone does not imply the existence of a cancer stem cell hierarchy.

The Cancer Stem Cell Model

The cancer stem cell model is not a new idea (Hamburger and Salmon, 1977). It has been clear for decades that some cancers, including some germ lineage cancers (Kleinsmith and Pierce, 1964), some neuroblastomas (Shimada et al., 1984), and some myeloid leukemias (Fearon et al., 1986; Ogawa et al., 1970), can differentiate into progeny that have limited proliferative potential despite retaining the oncogenic mutations of their malignant progenitors.

Some germ lineage cancers contain rapidly dividing cells that differentiate into postmitotic derivatives (mature teratoma elements) in a process that resembles aberrant embryogenesis (Chaganti and Houldsworth, 2000). The presence of only mature differentiated cells in residual tumor masses after chemotherapy is a favorable prognostic factor, while the presence of residual undifferentiated cells predicts disease recurrence (Stenning et al., 1998). These and other data suggest that undifferentiated cells are primarily responsible for tumor growth and disease progression, consistent with the cancer stem cell model.

Neuroblastomas also exhibit variable degrees of differentiation (Ambros et al., 2002; Shimada et al., 1999a, 1999b, 1984). Neuroblastomas with widespread differentiation have a better prognosis than those with limited differentiation (Shimada et al., 1999b). Highly differentiated neuroblastic tumors are typically focal and can often be cured with surgery (Nitschke et al., 1988). Conversely, poorly differentiated neuroblastomas are often widely disseminated and are usually fatal despite aggressive treatment (Matthay et al., 2009, 1999; Shimada et al., 1999b). Therapies that promote differentiation significantly improve survival (Matthay et al., 2009, 1999). In some infants, disseminated tumors undergo spontaneous differentiation, leading to a favorable outcome even without therapy (Baker et al., 2010). While staging of neuroblastoma is complex and involves a number of variables other than differentiation status, these clinical observations are consistent with the cancer stem cell model in suggesting that undifferentiated neuroblastoma cells sometimes drive disease progression.

While the overt differentiation in some germ lineage cancers and some neuroblastomas provided clinical evidence consistent with the cancer stem cell model, these rare and unusual malignancies are of uncertain relevance to more prevalent adult cancers. Thus, the cancer stem cell model gained increased attention when evidence emerged supporting the model in leukemia and breast cancer. The advent of flow cytometry made it possible to separate phenotypically distinct subpopulations of live cancer cells to compare their tumorigenic potential. Using this approach, some human acute myeloid leukemias (AMLs) (Bonnet and Dick, 1997; Lapidot et al., 1994) and breast cancers (Al-Hajj et al., 2003) were found to follow the cancer stem cell model, suggesting that a broad spectrum of cancers might be hierarchically organized into tumorigenic and nontumorigenic components. In each of these studies, cells capable of forming leukemias/tumors were rare when transplanted into immunocompromised mice but could be enriched by selecting

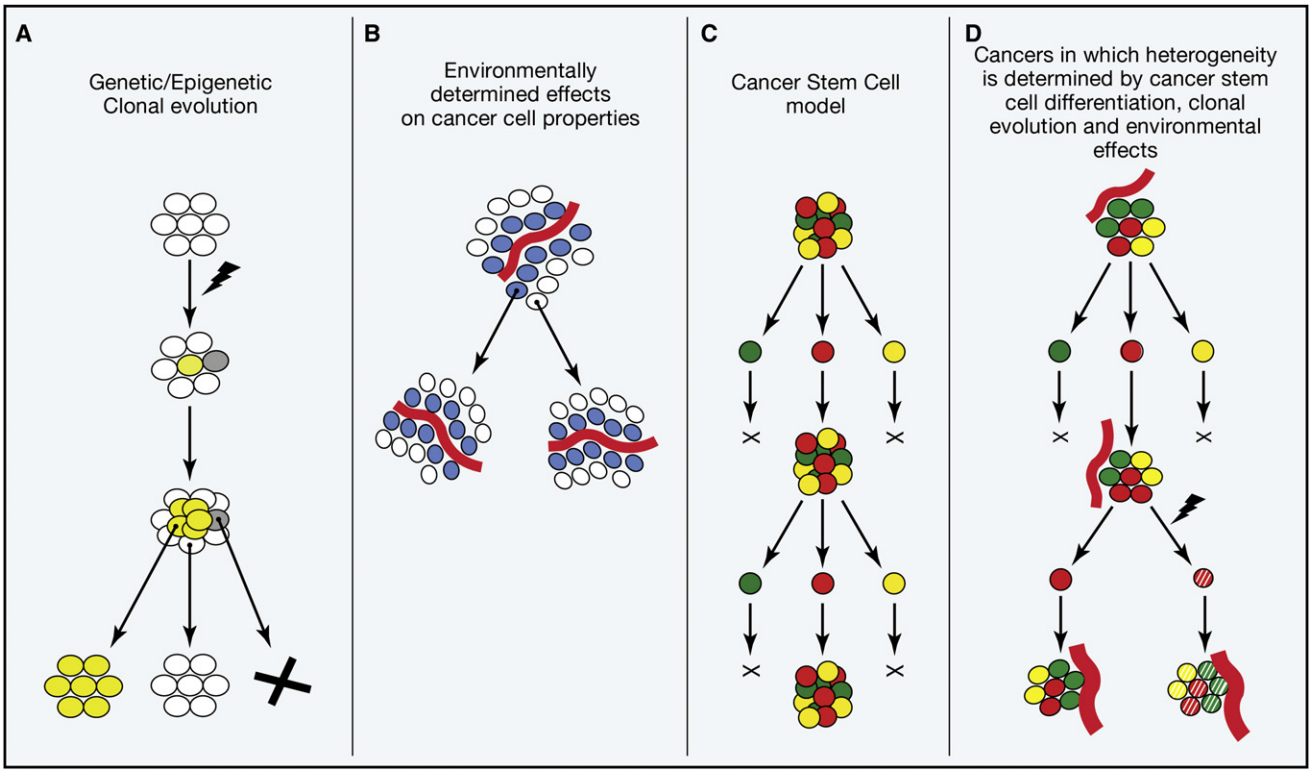

Figure 1. Sources of Heterogeneity within Cancer

(A) Heterogeneity can arise within tumors through stochastic genetic (Nowell, 1976) and epigenetic (Baylin and Jones, 2011) changes that confer heritable phenotypic and functional differences upon cancer cells. This process is known as clonal evolution because the genetic/epigenetic changes are subject to selection within tumors. This process tends to lead to more aggressive cancers over time; however, some cancer cells (gray) would be predicted to lose their tumorigenic capacity as a consequence of disadvantageous genetic changes.

(B) Heterogeneity can arise in response to extrinsic environmental differences within tumors: cancer cells (blue) adjacent to blood vessels (red) are different from cancer cells further from blood vessels (white) (Charles et al., 2010). The differences are shown as being reversible, though environmental differences could also cause irreversible changes in cancer cell properties.

(C) Cancers that follow the stem cell model contain intrinsically different subpopulations of tumorigenic (red) and nontumorigenic cells (yellow and green) organized in a hierarchy in which a minority population of tumorigenic cells gives rise to phenotypically diverse nontumorigenic cells. Nontumorigenic cells are thought to compose the bulk of tumors but have little capacity to contribute to cancer progression (Dick, 2008; Reya et al., 2001; Shackleton et al., 2009). Tumorigenic cells can be serially transplanted, re-establishing phenotypic heterogeneity with each passage.

(D) Cancers that follow the stem cell model are also subject to clonal evolution as well as heterogeneity from environmental differences within tumors. Thus, these sources of heterogeneity are not mutually exclusive and may each apply to variable extents depending on the cancer.

cells that expressed specific combinations of surface markers: leukemia-initiating cells were $CD34^{+}CD38^{-}$ (Bonnet and Dick, 1997; Lapidot et al., 1994) while breast cancer-initiating cells were $CD44^{+}CD24^{-/low}$ (Al-Hajj et al., 2003). This suggested that in some cancers only a small minority of cells can proliferate extensively and that some therapies that shrink tumors might not be curative because they fail to eliminate cancer stem cells.

Since these studies were published, other studies have taken similar approaches to provide evidence that other human cancers also follow the cancer stem cell model, including colon cancer (Dalerba et al., 2007; O'Brien et al., 2007; Ricci-Vitiani et al., 2007), pancreatic cancer (Li et al., 2007), brain tumors (Bao et al., 2006; Piccirillo et al., 2006; Singh et al., 2004) and ovarian cancer (Alvero et al., 2009; Curley et al., 2009; Stewart et al., 2011; Zhang et al., 2008b). In each case, the capacity to propagate the malignancy appeared to be restricted to a small, phenotypically distinct subpopulation of cancer cells. In tumorigenesis assays, many unfractionated cells had to be transplanted in order to transfer disease, suggesting that tumorigenic cells were rare. These studies suggested that many cancers follow the stem cell model and might be more effectively treated by targeting cancer stem cells.

Sources of Heterogeneity among Cancers

Despite these studies, the generalizability of the model remained uncertain. Does the model apply to all cancers, or only some? Do all AMLs and breast cancers follow the cancer stem cell model, or only in certain patients? Differences among cancers in driver mutations and in the cell-of-origin create great diversity in cancer biology. Sometimes these differences are reflected in the histopathology of the cancer, but in other cases they may influence the underlying biology without recognized effects on histopathology. Nonetheless, these sources of heterogeneity complicate the testing of the cancer stem cell model and mean that observations in a cancer from one patient may be true of cancers in certain other patients, but not all patients.

Some cancers, including hierarchically organized cancers that follow the stem cell model, can arise from normal stem cells

Table 1. Testing the Cancer Stem Cell Model

Properties of Cancers That Follow the Stem Cell Model	
	Experimental Evidence
Phenotypic and functional heterogeneity	Flow cytometry distinguishes phenotypically distinct subpopulations of cancer cells that are transplanted to test whether some are tumorigenic while others are nontumorigenic.
Hierarchical organization	Cancer stem cells are tumorigenic cells that give rise to a hierarchy of tumorigenic and nontumorigenic progeny. Upon transplantation, tumorigenic cells should give rise to more tumorigenic cells as well as phenotypically distinct nontumorigenic cells.
Properties Sometimes Ascribed to Cancer Stem Cells but Not Required by the Model	
	Experimental Evidence
Therapy resistance	Are tumorigenic cells more likely to survive therapy than nontumorigenic cells? Are tumorigenic cells enriched by therapy?
Rarity	Tumorigenic cells have been rare in many studies that supported the cancer stem cell model but, in principle, such cells do not have to be rare in a hierarchically organized cancer.
Quiescence	While cancer stem cells are sometimes claimed to be quiescent, little data support this assertion and the cell cycle distribution of most cancer stem cells is unknown.
Asymmetric division	Cancer stem cells are sometimes claimed to divide asymmetrically, but this has never been demonstrated in vivo and cannot be an obligate property because it would prevent the numerical expansion of cancer stem cells.
Derive from normal stem cells	Experimentally, cancer stem cells can arise from either normal stem cells or from restricted progenitors/differentiated cells. In practice, the cell-of-origin of most cancers is unknown.

through mutations that overactivate self-renewal mechanisms (Barker et al., 2009; Merlos-Suárez et al., 2011; Yang et al., 2008). Other cancers, including hierarchically organized cancers, can arise from restricted progenitors or differentiated cells as a result of mutations that ectopically activate self-renewal mechanisms in these cells (Figure 2A) (Cozzio et al., 2003; Huntly et al., 2004; Krivtsov et al., 2006; Schüller et al., 2008; Yang et al., 2008; Zhao et al., 2010). Thus, hierarchical organization in a cancer does not imply that it originated from normal stem cells, and the cancer stem cell model does not address the cell-of-origin (Wang and Dick, 2005). However, the cell-of-origin can influence the hierarchical organization of cancers as it influences the mutations that are competent to transform (Wang et al., 2010). The interaction of driver mutations with cellular context influences the frequency of leukemogenic cells and perhaps the degree of hierarchical organization (Heuser et al., 2009; Somervaille et al., 2009). Nonetheless, these inferences are all based upon experimentally induced cancers. The cell-of-origin for most cancers that spontaneously arise in patients has not been identified, at least not with precision, making it difficult to assess which biological differences among human cancers reflect differences in cell-of-origin.

Spatial differences in the cell-of-origin can also influence cancer properties. In some tissues, regional differences in cellular properties influence the driver mutations that are competent to transform. Medulloblastomas can arise either from Sonic Hedgehog pathway activation in granule neuron precursors of the cerebellum or from Wnt pathway activation in dorsal brainstem progenitors (Gibson et al., 2010; Schüller et al., 2008; Yang et al., 2008) (Figure 2B). Medulloblastomas are hierarchically organized, consistent with the cancer stem cell model (Read et al., 2009; Singh et al., 2004; Ward et al., 2009), so it is likely that the regional identity of the cell-of-origin influences cancer stem cell properties, though this has not yet been tested. Ependymomas that arise from different regions of the central nervous system have different mutations, different patterns of gene expression, and different prognoses (Johnson et al., 2010; Taylor et al., 2005). Because ependymomas appear to arise from radial glia and are hierarchically organized into tumorigenic and nontumorigenic components (Taylor et al., 2005), these results suggest that regional differences in radial glia lead to regional differences in driver mutations and cancer stem cell properties.

Temporal differences in the cell-of-origin also affect the properties of leukemogenic cells. Stem cell properties and self-renewal mechanisms change with age (He et al., 2009; Levi and Morrison, 2008). This likely alters the types of mutations that are competent to initiate cancers. Consistent with this, the mutation spectrum changes with age in human leukemias. Some driver mutations are found primarily in older patients (e.g., in FLT3, Nucleophosmin1, and Dnmt3a), whereas other mutations occur throughout life (e.g., in Ras) or more commonly in young patients (e.g., translocations involving AML1, MLL, and NUP98) (Figure 2C) (Armstrong and Look, 2005; Berman et al., 2011; Brown et al., 2007; Downing and Shannon, 2002; Falini et al., 2005; Ho et al., 2011; Kiyoi et al., 1999; Kottaridis et al., 2001; Ley et al., 2010; Meshinchi et al., 2001; Stirewalt et al., 2001; Thiede et al., 2006; Vogelstein et al., 1990; Zwaan et al., 2003). Because many AMLs are hierarchically organized (Lapidot et al., 1994; Yilmaz et al., 2006) and driver mutations influence the frequency of leukemogenic cells (Heuser et al., 2009; Somervaille et al., 2009), temporal changes in the cell-of-origin likely influence cancer stem cell properties.

Heterogeneity among Patients in Cancer Stem Cell Phenotype

Differences in driver mutations and cell-of-origin among patients raise the question of whether similar hierarchies of tumorigenic and nontumorigenic cells, with similar markers, are conserved among patients with similar cancers. Initial studies suggested that AMLs in many patients adopted a similar hierarchical organization in which rare leukemogenic cells were distinguished

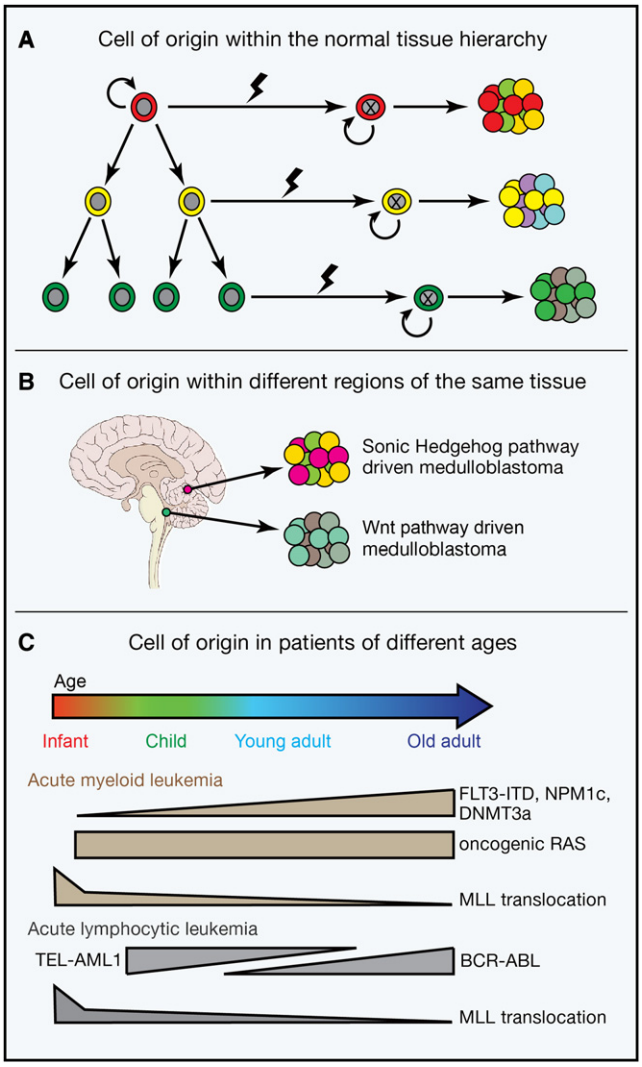

Figure 2. Sources of Heterogeneity among Cancers

Differences in the cell-of-origin can directly and indirectly influence the phenotype of tumorigenic cells and, perhaps, whether or not the cancer is hierarchically organized.

(A) Different cell types in a stem/progenitor cell hierarchy within a normal tissue may be transformed into cancer cells. The properties of the cell-of-origin influence the types of mutations that are competent to transform and the properties of the resulting cancer (Huntly et al., 2004; Wang et al., 2010).

(B) Spatial differences in the identity of the cell-of-origin within tissues influence the types of mutations that are competent to transform and the properties of the resulting cancer (Gibson et al., 2010; Johnson et al., 2010).

(C) Temporal differences in the cell-of-origin also influence the types of mutations that are competent to transform and the properties of the resulting cancer (J.A.M. and S.J.M., unpublished data), consistent with the observation that the driver mutation spectrum changes with age in patients (Downing and Shannon, 2002) (see text for references regarding age-related changes in the incidence of specific mutations).

from nonleukemogenic progeny by having a $CD34^+CD38^-$ surface marker phenotype, largely irrespective of AML subtype or blast cell maturation state (Bonnet and Dick, 1997; Lapidot et al., 1994). Many studies from other laboratories went on to characterize "leukemic stem cell" properties, such as gene expression signatures, by isolating $CD34^+CD38^-$ cells without verifying that these markers distinguished leukemogenic from nonleukemogenic cells in the patients they studied.

It was subsequently determined that there are leukemia-initiating cells among $CD34^-$ and $CD38^+$ cells in some AMLs (Sarry et al., 2011; Taussig et al., 2008, 2010). Dick and colleagues systematically addressed this issue by comparing the leukemogenic capacity of $CD34^+CD38^-$, $CD34^+CD38^+$, $CD34^-CD38^+$, and $CD34^-CD38^-$ AML cells from 16 patients (Eppert et al., 2011). In the 13 AMLs that engrafted, there was leukemogenic activity in the $CD34^+CD38^-$ fraction; however, leukemogenic cells were also detected in at least one other fraction in most patients. Most leukemogenic cells were contained in the $CD34^+CD38^-$ fraction in half of the patients and in the $CD34^+CD38^+$ fraction in the other half of patients. In one case, there were similar frequencies of leukemogenic cells in all fractions, and a second case had leukemogenic cells in 3 of 4 fractions. Leukemogenic activity is therefore not usually restricted to the $CD34^+CD38^-$ fraction and there is heterogeneity among patients in leukemogenic cell phenotype (Figure 3). Some AMLs might not follow the cancer stem cell model at all.

The frequency and phenotype of leukemogenic cells is also highly variable in mouse AMLs. Deletion of *Pten* from adult mouse hematopoietic cells leads to the development of AML upon transplantation into wild-type mice (Yilmaz et al., 2006). In these AMLs, leukemogenic activity is most highly enriched among rare cells with a surface marker phenotype similar to normal HSCs, but cells that express mature myeloid markers possess lower levels of leukemogenic activity. Mouse AMLs induced by MLL-AF9 expression appear to have much higher frequencies of leukemogenic cells than observed after *Pten* deletion (Krivtsov et al., 2006; Somervaille and Cleary, 2006; Somervaille et al., 2009). In these leukemias, cells bearing GMP-like surface markers have the highest frequency of leukemogenic cells (Krivtsov et al., 2006); however, leukemogenic activity is also found in other cell fractions (Somervaille and Cleary, 2006; Somervaille et al., 2009). Differences in oncogenic mutations can thus have profound effects on the frequency and phenotype of leukemia-initiating cells.

The same is true in solid cancers. Tumorigenic cells are enriched within the $CD44^+CD24^{-/low}$ population of some breast cancers (Al-Hajj et al., 2003). However, other breast cancers studied by Al-Hajj et al. had more phenotypically diverse breast cancer-initiating cells, demonstrating that the $CD44^+CD24^{-/low}$ surface marker phenotype does not universally distinguish tumorigenic from nontumorigenic breast cancer cells (Al-Hajj et al., 2003). In mouse models of mammary cancer, different driver mutations give rise to cancers that differ in the extent to which they follow the stem cell model (Cho et al., 2008; Vaillant et al., 2008; Zhang et al., 2008a); for example, CD61 enriched for cancer stem cell activity in mice with Wnt1 driven breast cancers but not in mice with Neu/ErbB2 driver breast cancers (Vaillant et al., 2008). Mouse models of lung cancer with different transforming mutations have tumorigenic cells with different surface marker phenotypes (Curtis et al., 2010). Thus, different oncogenic mutations give rise to cancers that differ in the extent to which they follow the cancer stem cell model and in tumorigenic cell phenotype.

These results demonstrate the importance of testing cancer stem cell markers in significant numbers of patients to

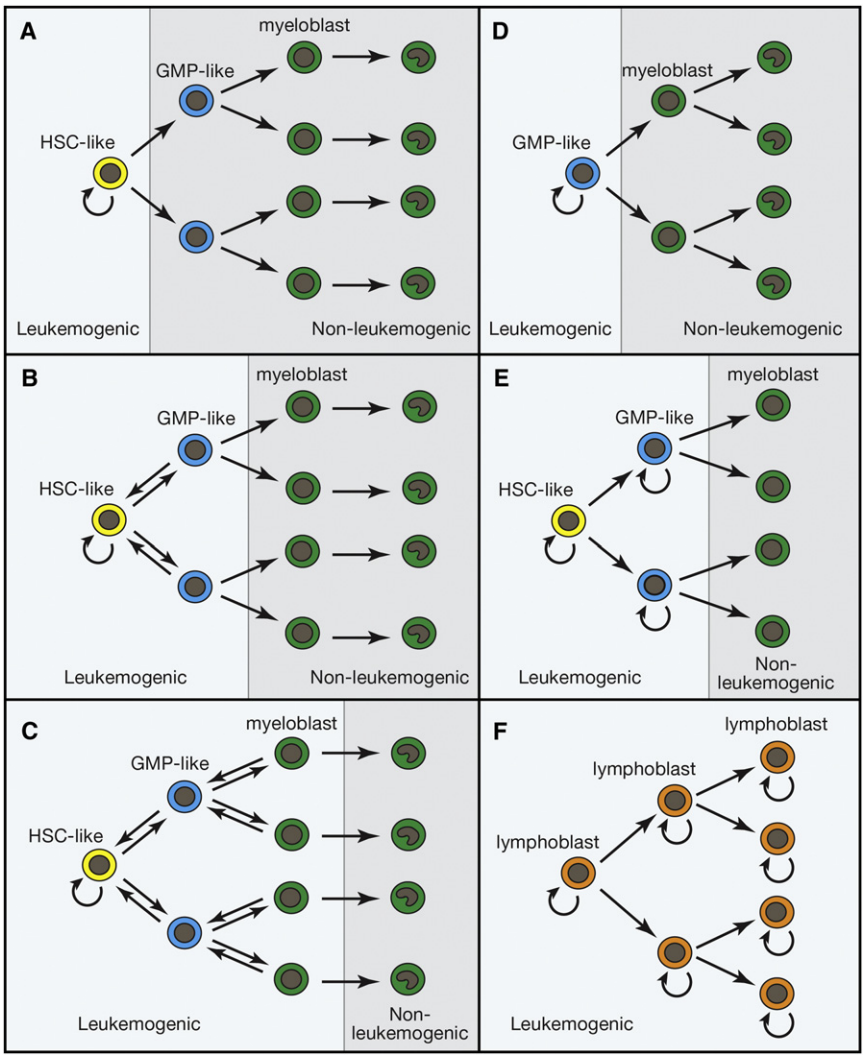

Figure 3. Variation among Leukemias in the Degree and Nature of Hierarchical Organization

Although most AMLs follow a cancer stem cell model, the surface marker phenotypes of the leukemogenic cells vary from patient to patient. (A–C) Different oncogenic mutations can transform cells at different levels within the hematopoiesis hierarchy (Wang et al., 2010), potentially influencing the frequency, spectrum, and phenotype of cells with leukemogenic potential. Interconversion between leukemogenic cell populations would allow any population to recapitulate the heterogeneity of the leukemogenic cell pool (Eppert et al., 2011; Sarry et al., 2011). (D) Some mutations, such as MLL-AF9 translocations, can confer leukemogenic activity upon restricted progenitors (Cozzio et al., 2003; Huntly et al., 2004; Krivtsov et al., 2006; Zhao et al., 2010). (E) If multiple populations have leukemogenic capacity but do not interconvert, then only the most immature cells can recapitulate the full heterogeneity of the parent leukemia, but multiple levels of the hierarchy may be able to drive disease progression (Goardon et al., 2011). (F) In some ALLs, many cells have leukemogenic activity despite heterogeneity in marker expression (le Viseur et al., 2008; Williams et al., 2007).

appreciate the heterogeneity among patients. Yet studies of cancer stem cell characteristics often assume that markers identified in one study can be applied without validation to other patients, to cell lines, or to cells transformed in culture. The conclusions in such studies may be undermined by heterogeneity among patients or by context- or oncogene-dependent effects on tumorigenic cell phenotype.

The Implications of the Cancer Stem Cell Model for Therapy

In cancers that follow the stem cell model, the functional differences between tumorigenic and nontumorigenic cells can have important implications for therapy. For example, the BCR-ABL inhibitor imatinib has been incredibly effective at restoring the health and prolonging the lives of patients with chronic myeloid leukemia (CML) (Druker et al., 2006); however, these patients must remain on imatinib indefinitely because many patients fail to completely eliminate BCR-ABL-expressing cells from their bone marrow (Bhatia et al., 2003; Chu et al., 2011) and even patients that achieve a complete molecular remission often relapse upon withdrawal of therapy (Rousselot et al., 2007).

These clinical observations appear to be explained by the persistence of rare imatinib-resistant CML stem cells (Chu et al., 2011; Graham et al., 2002; Holtz et al., 2002). A mouse model of CML-like disease driven by HIP1-PDGFR and AML1-ETO fusion proteins had leukemogenic and nonleukemogenic subpopulations of cancer cells distinguished by differences in surface marker expression (Oravecz-Wilson et al., 2009). The leukemogenic cells were rare and much more resistant to imatinib than their nonleukemogenic progeny. Imatinib treatment dramatically enriched leukemogenic cells despite reducing overall leukemia burden. Evidence has also been presented for radiation resistance in brain tumor-initiating cells (Bao et al., 2006) and breast cancer-initiating cells (Diehn et al., 2009).

While it has become fashionable to consider therapy resistance a defining feature of cancer stem cells, the sensitivity of tumorigenic and nontumorigenic cells to therapy depends upon the cancer and the therapy. Some therapies actually exploit the capacity of tumorigenic cells to differentiate into nontumorigenic cells by inducing differentiation. Acute promyelocytic leukemia is treated with arsenic trioxide and trans-retinoic acid, which induce rapid terminal differentiation, growth arrest, and apoptosis of the cancer cells (de Thé and Chen, 2010). Differentiation therapy has also been exploited experimentally in glioblastoma by treating with bone morphogenetic protein 4 (BMP4) to induce glial differentiation, reducing proliferation, tumor growth, and tumorigenic cell frequency (Piccirillo et al., 2006). BMP4 also promotes glial differentiation by normal CNS stem cells (Gross et al., 1996) suggesting tumorigenic cancer cells sometimes inherit differentiation pathways from normal

stem cells in the same tissue. Cis-retinoic acid also induces glial differentiation and improves survival in high-risk neuroblastoma patients (Matthay et al., 1999; Thiele et al., 1985). Thus, tumorigenic cells are specifically targeted by some therapies.

Therapy resistance can also arise through genetic mechanisms that are not necessarily related to cancer stem cells. While the intrinsic resistance of CML-initiating cells to imatinib allows these cells to persist in treated patients who are in remission, the ongoing administration of imatinib generally prevents relapse until the CML-initiating cells acquire an amplification of BCR-ABL or point mutations that confer imatinib resistance (Gorre et al., 2001; Roumiantsev et al., 2002). Melanomas carrying V600E BRAF mutations become resistant to the BRAF inhibitor vemurafenib through a variety of genetic mechanisms (Johannessen et al., 2010; Nazarian et al., 2010; Poulikakos et al., 2011; Poulikakos and Rosen, 2011; Villanueva et al., 2010), and we are unable to find any evidence that melanoma follows a cancer stem cell model (Quintana et al., 2010; Quintana et al., 2008). Therefore, cancer progression and therapy resistance may be influenced by the properties of cancers stem cells in cancers that follow the model, but therapy resistance and disease progression can also arise through genetic changes unrelated to the question of whether a cancer follows the stem cell model.

Tumorigenesis Assays

The xenotransplantation of human cancer cells into mice differs in a number of important respects from the growth of human cancer cells in patients. Mouse tissues differ from human tissues in terms of architecture and stromal cells (Kuperwasser et al., 2004). Mouse growth factors and adhesion molecules sometimes do not bind human receptors (Manz, 2007). Autologous immune cells are an important element of the tumor microenvironment as they can either promote or impair tumor growth (de Visser et al., 2006). Yet there are profound differences in immune regulation between the autologous and xenogeneic settings. Human cells transplanted into mice are subject to powerful xenogeneic immune responses that kill most human cells before they have an opportunity to proliferate (Auchincloss and Sachs, 1989). That is why human cancer cells must be transplanted into highly immunocompromised mice to assay tumorigenic capacity. Even NOD/SCID mice retain an attenuated xenogeneic barrier. Transplantation into more highly immunocompromised mice (such as NOD/SCID IL2Rγ^{null}) can significantly increase the frequency of tumorigenic cells that is detected in some, but not all, human cancers (Ishizawa et al., 2010; Kennedy et al., 2007; Quintana et al., 2008).

Some have speculated that less immunocompromised mice may represent ''better models'' for studying human cancers because the preservation of some immune activity makes these mice more similar to patients. However, the mechanisms by which mouse immune cells respond to transplanted human cells bear little resemblance to the mechanisms by which human immune cells sometimes respond to autologous cancer cells (Auchincloss and Sachs, 1989). No xenotransplantation assay can model the immune responses that sometimes occur in patients against their own tumors. Normal human hematopoietic stem cells (HSCs) and cancer-initiating cells are therefore more likely to be detected in more highly immunocompromised mice: NOD/SCID mice treated with anti-CD122 antibody to deplete NK cells or NOD/SCID IL2Rγ^{null} mice (Eppert et al., 2011; McDermott et al., 2010; Quintana et al., 2008).

It is also critical to recognize that transplantation assays, particularly xenotransplantation assays, test the potential of cells to form tumors, not their actual fate in the tumor in which they are born (Figure 4). There are many environmental variables in the tumor environment, such as hypoxia and immune responses, which can prevent cells that have the potential to form a tumor from actually doing so in their normal environment. Consequently, nobody knows whether many, or few, cells with tumorigenic potential actually contribute to disease progression in patients. The question of which cells are actually fated to contribute to disease progression is highly context dependent and is probably not testable in patients because of the experimental manipulations that would be required; however, this is testable by fate mapping of cells in mouse tumors. It will be interesting to compare the results of side-by-side fate-mapping experiments and transplantation assays to assess whether the cells that have the potential to form tumors upon transplantation are the same cells that drive disease progression in situ.

Tumorigenic Cells Are Abundant in Some Cancers

Not all hematopoietic malignancies contain rare cancer-initiating cells. Tumorgenic/leukemogenic cells are common in certain mouse models of B cell lymphoma, T cell lymphoma, and AML in which it is possible to transfer disease to wild-type recipients by transplanting only ten cells (Kelly et al., 2007). In a mouse model of B cell acute lymphoblastic leukemia (ALL), at least 50% of cancer cells are capable of transferring disease into wild-type recipient mice (Williams et al., 2007). In these malignancies, the abundance of tumorgenic/leukemogenic cells suggests that if there is any hierarchy it must be much more shallow than observed in many human AMLs, which so far have consistently appeared to have rare leukemogenic cells (Bonnet and Dick, 1997; Lapidot et al., 1994).

Tumorigenic cells are also common in some human cancers. When human melanomas were first transplanted into NOD/SCID mice, it was estimated that only one in a million melanoma cells were capable of forming tumors, and melanoma was proposed to follow a cancer stem cell model (Schatton et al., 2008). However, simple changes in tumorigenesis assay conditions (including the use of NOD/SCID IL2Rγ^{null} mice) increased the detected frequency of tumorigenic cells to one in four (Quintana et al., 2008). We now routinely transplant single cells directly from patients into NOD/SCID IL2Rγ^{null} mice and on average 30% of single cells form tumors (Quintana et al., 2010). We have quantified the frequency of tumorigenic cells from more than 30 patients with diverse stages and sites of disease, and in every case, the frequency of tumorigenic cells has been high, even in primary cutaneous melanomas obtained directly from patients (Quintana et al., 2010). Similar results have been published with mouse models of melanoma (Held et al., 2010). Thus, xenotransplantation assays sometimes dramatically underestimate the frequency of human cancer cells with tumorigenic potential.

Is melanoma unique among solid cancers in having common tumorigenic cells? We addressed this question in mouse models of malignant peripheral nerve sheath tumors (MPNSTs)

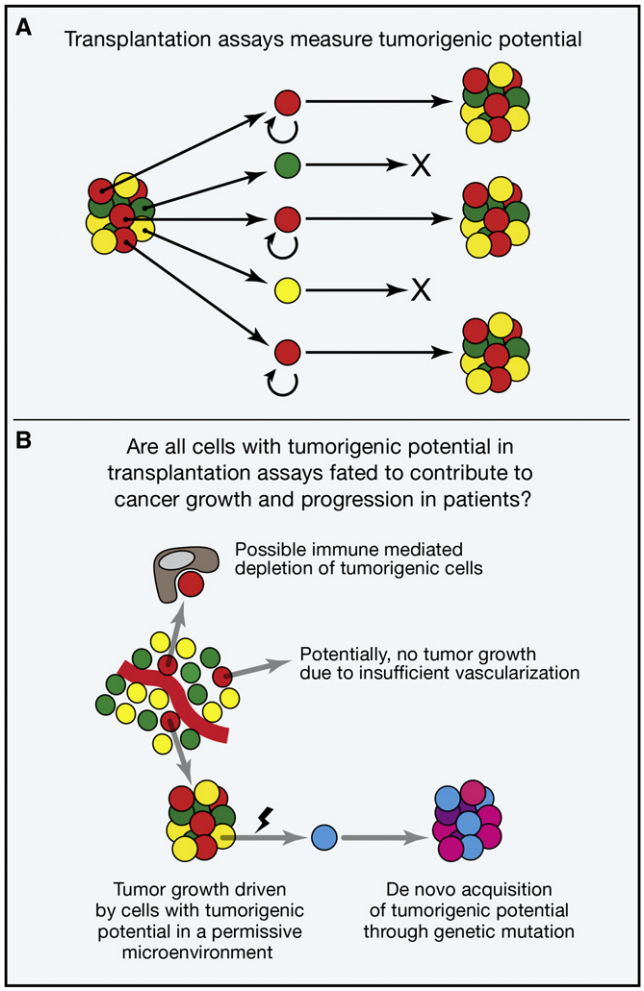

Figure 4. Fate versus Potential in Cancer

(A) Potential describes what cells can do in a permissive environment. The cancer stem cell model, and the transplantation assays (black arrows) on which it is largely based, address the potential of cancer cells to form tumors. (B) Fate reflects what cells actually do in a specific environment. In the context of cancer, the question is which cells are fated to contribute to tumor growth and disease progression in their actual environment in the patient. Many of the cells that have the potential to form tumors upon transplantation may not be fated to contribute to disease progression in a particular patient because they are not in a permissive environment. For example, some cancer cells undergo cell death due to hypoxia or immune effector activity. Some of these cells might have the potential to form a tumor if transplanted into another environment, but are fated to undergo cell death in the tumor environment in which they actually reside in the patient. There may also be cells that lack the ability to form a tumor upon transplantation but that are nonetheless fated to contribute to disease progression in the patient, such as if they acquire a new mutation that increases their proliferation. Transplantation assays only assess potential, not fate, in a patient and therefore should attempt to detect the full range of cells with the potential to form tumors. No transplantation assay mimics the environment within patient tissues and such assays are neither designed nor capable of assessing cell fate in patients. Consequently, very little is known about the spectrum of cells fated to contribute to tumor growth and disease progression in patients or the extent to which it overlaps with the spectrum of cells that can form a tumor upon transplantation.

(Buchstaller et al., 2012). We found that approximately 20% of mouse MPNST cells have the potential to form tumors, even when transplanted into fully immunocompetent mice. This suggests that tumorigenic cells may be common in a number of solid cancers, though it is important to note that we have not tested whether MPNSTs are hierarchically organized, and therefore, it is unknown whether this cancer has a shallow hierarchical organization.

An important question is whether we have systematically underestimated the frequency of tumorigenic cells by using transplantation assays that have not been optimized to detect the full range of cells with the potential to form tumors. Work on human HSCs and AML has identified numerous assay improvements that increased estimates of stem cell frequency by orders of magnitude (Eppert et al., 2011; Kennedy et al., 2007; McDermott et al., 2010; McKenzie et al., 2005; Notta et al., 2010), but assays for tumorigenic cells from solid cancers generally have not been studied to the same extent. Enzymatic dissociation conditions, sorting conditions, transplantation site, the extracellular matrix environment, and the recipient mouse (sex and strain) all affect the ability to detect tumorigenic cells. Other undiscovered assay parameters may also be important. Estimates of tumorigenic cell frequencies may continue to increase in many cancers as assays improve, though tumorigenic cells will likely remain rare in some cancers despite such improvements (Eppert et al., 2011; Ishizawa et al., 2010).

Do Tumorigenesis Assays Test the Ability to Recapitulate Tumor Heterogeneity?

A fundamental element of the stem cell model is that cancer stem cells give rise to phenotypically diverse progeny that recapitulate the heterogeneity of the tumor from which they derive (Figure 1C). This is presumed to occur through epigenetic mechanisms akin to the differentiation of normal stem cells; however, nobody has experimentally confirmed that epigenetic differences distinguish tumorigenic from nontumorigenic cells. The differentiation of cancer stem cells into nontumorigenic progeny is commonly assumed to be the major driver of heterogeneity in cancers that follow the stem cell model; however, the degree of genetic heterogeneity in such cancers is unknown. Therefore, some of the phenotypic and functional differences among cancer cells that have been attributed to the differentiation of cancer stem cells might derive from genetic differences that arise through clonal evolution (Figure 5A).

Since genetic changes are irreversible and stochastic, no tumorigenic cell can recapitulate the genetic heterogeneity of the tumor from which it derives. If the degree of genetic heterogeneity within a tumor is low, then cancer stem cells may be able to largely recapitulate the heterogeneity of the tumors from which they derive by differentiating into nontumorigenic cells (Figure 5B). However, if there is extensive genetic heterogeneity, then every tumorigenic cell may form a genetically distinct tumor and no tumorigenic cell will recapitulate the heterogeneity of the primary tumor (Figure 5C). Increasing evidence suggests that there is more genetic heterogeneity within tumors than previously thought (Navin et al., 2011; Yachida et al., 2010). However, driver mutations are rare among the genetic changes observed in cancer, so the degree of genetic heterogeneity that influences cancer cell function may be more modest. Nonetheless, if there is widespread genetic heterogeneity, functional and phenotypic differences among cancer cells cannot be assumed to be driven by epigenetic hierarchies rather than genetic differences (Campbell et al., 2010; Ding et al., 2010).

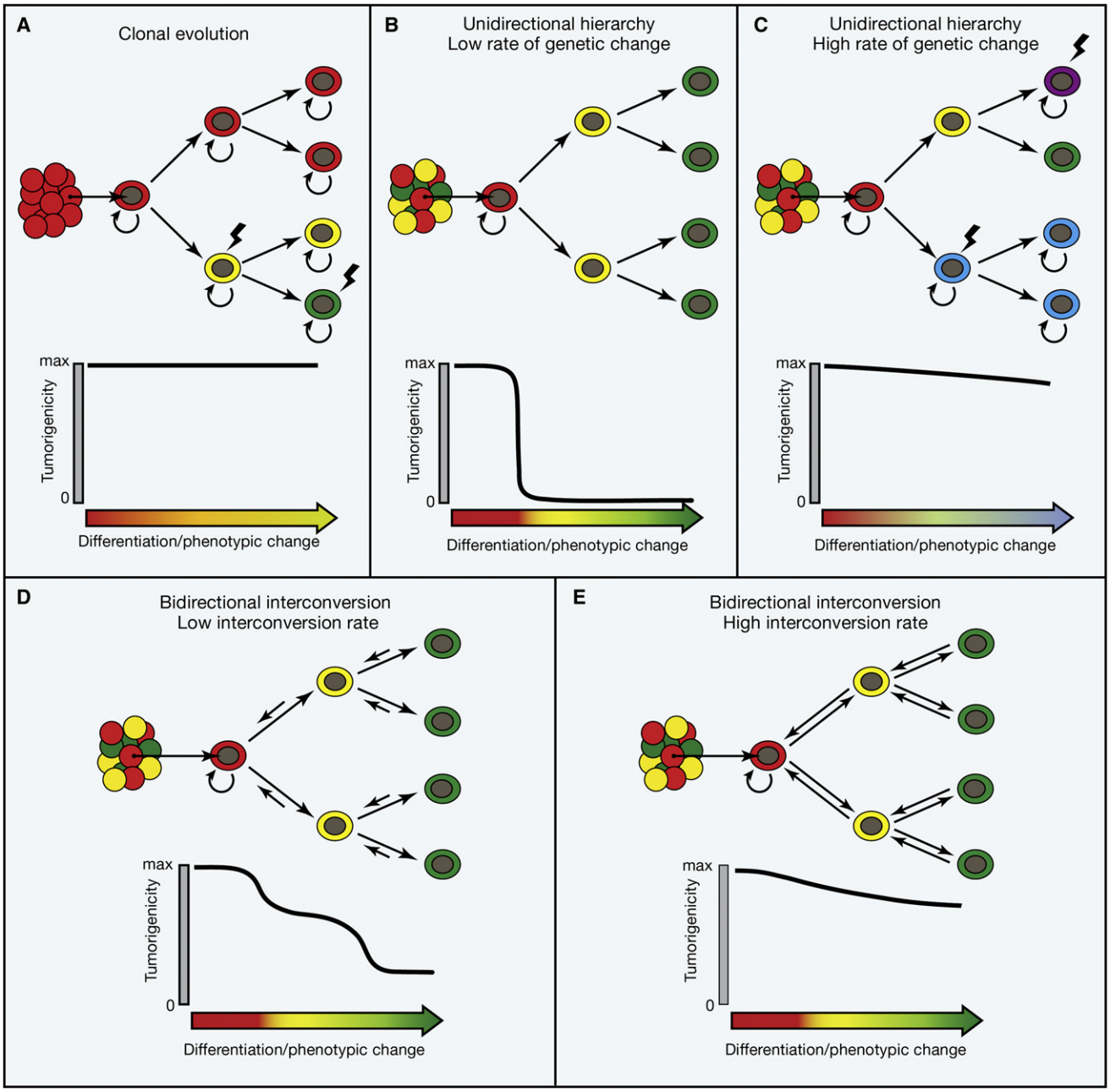

Figure 5. The Influences of Genetic Change and Reversible Transitions in Cell States on Hierarchical Organization in Cancer

(A) According to the clonal evolution model, many cancer cells have tumorigenic potential (circular self-renewal arrows) and heterogeneity arises through stochastic genetic/epigenetic changes (lightning bolt). Changes in cell phenotype are not necessarily associated with changes in tumorigenic potential.

(B) For cancers that follow a stem cell model in which only the cells at the top of the hierarchy retain tumorigenic capacity, the differentiation of these cells into nontumorigenic progeny creates tumor heterogeneity. Differentiation is associated with a loss of tumorigenic potential.

(C) For cancers with a high rate of genetic change, clones of cells within the hierarchy depicted in (B) may acquire tumorigenic potential as a consequence of new mutations. Phenotypic changes are sometimes associated with changes in tumorigenic potential and sometimes not. Note that it would be difficult to experimentally distinguish this model from the model in (A).

(D) A cancer that is hierarchically organized according to the cancer stem cell model but in which nontumorigenic cells can inefficiently revert to higher levels of the hierarchy. In this case, tumorigenic cells could be enriched or depleted using markers but "nontumorigenic" cells from the bottom of the hierarchy would always retain some tumorigenic capacity due to their ability to revert to tumorigenic states.

(E) A hierarchically organized cancer in which cells readily and reversibly interconvert between tumorigenic (red) and nontumorigenic (yellow and green) states. Note that it would be difficult to experimentally distinguish case (E) from case (C). In cancers that are genetically unstable or subject to efficient reversible cell transitions, the cancer stem cell model may be untestable, because it may be difficult to experimentally distinguish from cancers in which there is no hierarchy but where heterogeneity arises through clonal evolution.

In cancers that follow the stem cell model, cancer stem cells would be expected to undergo genetic change over time. Consistent with this, leukemia-initiating cells in B-ALLs undergo clonal evolution (Anderson et al., 2011; Notta et al., 2011), though these studies did not test whether the B-ALLs were hierarchically organized according to the cancer stem cell model. In cancers that do not follow the cancer stem cell model, genetic change would also occur over time and would be predicted to introduce phenotypic and functional heterogeneity. Thus, the cancer stem cell and clonal evolution models can be interacting, or independent, sources of heterogeneity depending on the cancer.

Another issue concerns the extent to which existing assays reliably test phenotypic heterogeneity. Some have suggested that melanomas have intrinsically different populations of tumorigenic and nontumorigenic cells that can be distinguished based on ABCB5 (Schatton et al., 2008) or CD271 (Civenni et al., 2011; Boiko et al., 2010) expression. However, neither of these markers correlate with the frequency of tumorigenic cells, and in our hands, small numbers of cells that are positive or negative for ABCB5 or CD271 have a similar capacity to form tumors and to recapitulate the phenotypic heterogeneity of the tumors from which they derive (Quintana et al., 2010). We also identified 20 other markers that are heterogeneously expressed by human melanoma cells and transplanted just 10 cells that were either positive or negative for each of these markers into NOD/SCID IL2Rγ^{null} mice (Quintana et al., 2010). All subpopulations exhibited a similar capacity to form phenotypically heterogeneous tumors. Thus, we have subdivided melanomas from many patients into almost 50 subpopulations of cells based on differences in marker expression and have not found any subpopulation that lacks the ability to form a phenotypically heterogeneous tumor.

The simplest interpretation of our data (Quintana et al., 2010) and other data (Pinner et al., 2009; Roesch et al., 2010) is that melanoma cells are phenotypically plastic, reversibly turning on and off markers. In contrast, Civenni et al. reported that both CD271$^+$ and CD271$^-$ melanoma cells formed tumors in NOD/SCID IL2Rγ^{null} mice but that the tumors formed by CD271$^-$ cells were not heterogeneous for CD271 expression and that only CD271$^+$ cells formed tumors in NOD/SCID mice (Civenni et al., 2011). They speculated that the difference relative to our results reflected different dissociation conditions. In our hands, both dissociation methods yield similar results with CD271$^+$ and CD271$^-$ melanoma cells each forming heterogeneous tumors that can be serially passaged, irrespective of whether they are transplanted in to NOD/SCID or NOD/SCID IL2Rγ^{null} mice (E. Quintana, U. Eskiocak, and S.J.M., unpublished data); however, if differences in enzymatic dissociation methods in solid cancers can sometimes generate reproducible differences in the phenotype of tumorigenic cells, this would illustrate the complexity of reproducing ''cancer stem cell'' markers.

If there are certain cells that reproducibly form tumors in NOD/SCID IL2Rγ^{null} mice and reproducibly fail to form tumors in NOD/SCID mice, what would this mean? Are some human cells more able to evade rejection by mouse immune cells? If so, does this have any physiological relevance for these cells in humans? If some tumorigenic cells are more able to generate phenotypically heterogeneous progeny than others, what does this mean? Could this reflect genetic differences among the cells (Campbell et al., 2010; Ding et al., 2010) rather than hierarchical epigenetic differences? Ultimately, a cell that has the potential to form a tumor in any assay has the potential to contribute to disease progression in a patient and cannot be ignored during therapy.

Uncertainty in Cancer Stem Cell Markers

In some cases, it has proven difficult to confirm markers that originally appeared to robustly distinguish tumorigenic from nontumorigenic cells; for example, CD133 was reported as a marker of tumorigenic brain cancer cells, and even large numbers of CD133-negative brain tumor cells were reported to lack the ability to form tumors (Bao et al., 2006; Singh et al., 2004). On this basis, gliomas and medulloblastomas were concluded to follow a cancer stem cell model. Yet subsequent studies found tumorigenic activity among both CD133$^+$ and CD133$^-$ brain tumor cells (Beier et al., 2007; Chen et al., 2010; Joo et al., 2008; Wang et al., 2008). These discrepancies could reflect differences among patients, methodological differences among laboratories, or ascertainment/tumor selection bias that led early studies to overestimate the robustness of markers. Work with other markers continues to support the conclusion that gliomas and medulloblastomas follow a cancer stem cell model (Read et al., 2009; Son et al., 2009; Ward et al., 2009); however, to confirm the existence and identity of cancer stem cells, it is necessary to identify markers that reproducibly distinguish tumorigenic and nontumorigenic cells, at least in specific subsets of patients.

Tumorigenic ovarian cancer cells have been reported to be enriched in the CD44$^+$ (Alvero et al., 2009), CD44$^+$CD117$^+$ (Zhang et al., 2008b), and CD133$^+$ (Curley et al., 2009) subpopulations of ovarian cancer cells. However, when Stewart et al. evaluated a large cohort of ovarian cancers, they were unable to find CD44$^+$CD117$^+$ cells in most ovarian cancers and the CD44$^+$CD117$^+$ cells they did find were depleted for tumorigenic activity (Stewart et al., 2011). CD133 enriched tumorigenic ovarian cancer cells in some cases and not in other cases. CD133 expression changed on some tumorigenic cells during passaging (Stewart et al., 2011). This suggests that CD133 only marks ovarian cancer stem cells under defined conditions in some patients and that the hierarchical organization of some ovarian cancers is not stable. It remains uncertain what fraction of ovarian cancers follow the stem cell model.

Cancer stem cell markers have proven difficult to broadly confirm in a number of solid cancers, raising questions about whether we have overestimated the number of cancers that follow this model and making it difficult to study the biology of these cells. Alternatively, it is possible that many cancers are hierarchically organized but that there is considerable diversity among patients in terms of the markers that distinguish tumorigenic from nontumorigenic cells. This is a key issue that must be resolved and which may require approaches other than the traditional dependence upon cell surface markers. For example, the separation of live cancer cells based on functional measures, such as signaling pathway activation (Vermeulen et al., 2010), might reduce phenotypic variability among tumorigenic cells. Unfortunately, the genetic approaches currently required to do this are only possible in mice where the use of inbred genetic

backgrounds and targeted mutations already reduce variability in cancer models relative to what is observed in patients.

Do Nontumorigenic Cells Sometimes Form Tumorigenic Cells?

Recent studies have suggested that the differentiation of cancer stem cells into nontumorigenic cells may be reversible (Chaffer et al., 2011; Gupta et al., 2011). In culture, immortalized human mammary epithelial cells (HMECs) undergo an epithelial-to-mesenchymal transition (EMT) following sustained expression of the transcription factors Snail or Twist, silencing of E-cadherin, or exposure to TGF-β (Mani et al., 2008; Morel et al., 2008; Scheel et al., 2011). This EMT was interpreted as conferring stem cell properties upon normal or transformed epithelial cells in culture, partly because the cells acquired a $CD44^+CD24^-$ phenotype, similar to breast cancer stem cells. The idea that cancer cells might reversibly transition between epigenetically defined tumorigenic and nontumorigenic states is appealing, partly because mechanisms that generate reversible heterogeneity can confer therapy resistance (Roesch et al., 2010; Sharma et al., 2010). However, it is not clear whether CD44 and CD24 consistently distinguish tumorigenic from nontumorigenic cells in cultured cell lines or whether nontumorigenic cells acquire tumorigenic potential by EMT in breast cancers in vivo.

The idea that nontumorigenic cancer cells could sometimes revert to having tumorigenic capacity is plausible given that restricted progenitors dedifferentiate into stem cells in certain normal tissues. In the *Drosophila* testis and ovary, spermatogonia and cytocytes dedifferentiate into germline stem cells under certain circumstances (Brawley and Matunis, 2004; Kai and Spradling, 2004). In mouse testis, spermatogonial progenitors can also dedifferentiate into spermatogonial stem cells (Barroca et al., 2009). So far this dedifferentiation has only been observed in normal tissues at low frequencies or under restricted circumstances. Nonetheless, if nontumorigenic cancer cells revert to a tumorigenic state at an appreciable rate in certain cancers, then this would undermine the ability to distinguish tumorigenic from nontumorigenic cells as even the ''nontumorigenic'' cells would be expected to form tumors at some level.

It is not clear whether the cancer stem cell model would effectively describe cancers in which there are tumorigenic and nontumorigenic states that can reversibly interconvert. If cells in the nontumorigenic state only convert to the tumorigenic state under restricted circumstances or with low efficiency, then it may still be possible to identify markers that distinguish populations that are enriched or depleted for tumorigenic capacity (Figure 5D). However, if cells in the nontumorigenic state convert to the tumorigenic state with high efficiency, it should not be possible to distinguish tumorigenic from nontumorigenic cells, potentially rendering the cancer stem cell model untestable in such cancers (Figure 5E). New models may be required to describe the heterogeneity in such cancers.

Cancer Stem Cells and Metastasis

Metastasis requires cells from a primary tumor to detach, invade the vascular or lymphatic system, migrate to distant sites, extravasate, then proliferate extensively and recruit new vasculature (Nguyen et al., 2009). There is much discussion regarding the metastasis of cancer stem cells, though nobody has actually tested whether the cells that are enriched for tumorigenic activity in transplantation assays are also enriched for the capacity to metastasize under physiological conditions. A fundamental question is whether metastatic potential is confined to a single population of tumorigenic cells or whether it arises stochastically through genetic or epigenetic changes that occur in many cancer cells without regard to their competence to form tumors prior to the stochastic change.

Some studies have suggested that subpopulations of tumorigenic pancreatic cancer (Hermann et al., 2007) and colon cancer (Pang et al., 2010) cells are enriched for the capacity to metastasize. However, the relationship between tumorigenic cells and metastasis has not yet been addressed systematically by examining all of the cancer cells that can be found in circulation and their tumorigenic capacity. Therefore, it remains uncertain whether nontumorigenic cancer cells have a similar capacity to disseminate as tumorigenic cells, or whether nontumorigenic cells from a primary tumor can sometimes acquire tumorigenic capacity after migrating to a new environment.

It has been proposed that cancer cells acquire metastatic potential by undergoing an EMT (Kalluri and Weinberg, 2009). As cancer cells lose their epithelial characteristics, they lose intracellular adhesions and polarity while acquiring more mesenchymal features such as the ability to migrate, invade, and resist apoptosis (Thiery et al., 2009). EMT has been proposed as a requisite step for breast cancer metastasis (Yang et al., 2004) and induction of an EMT also confers upon cultured cells a surface marker phenotype ($CD44^+CD24^-$) similar to tumorigenic breast cancer cells (Mani et al., 2008; Scheel et al., 2011). If cancer cells that have no tumorigenic capacity in transplantation assays can acquire this potential by undergoing an EMT, then any cancer cell could acquire metastatic potential.

Although the cancer stem cell model and work on EMTs focus on epigenetic differences between tumorigenic and nontumorigenic cells, there is good evidence that irreversible genetic mutations also confer metastatic potential (Vogelstein et al., 1988). In pancreatic cancer and medulloblastoma, genetically distinct subclones initiate metastatic disease (Campbell et al., 2010; Wu et al., 2012; Yachida et al., 2010). This raises the question of whether only cancer stem cells are competent to acquire genetic changes that confer metastatic potential or whether nontumorigenic cells can acquire genetic changes that confer both tumorigenic and metastatic potential. These fundamental questions remain to be studied in primary tumors in vivo, so the implications of the cancer stem cell model for metastasis are unresolved.

Conclusions and Future Directions

- Some cancers are hierarchically organized into undifferentiated cells that can drive disease progression and differentiated cells with less capacity to drive disease progression, consistent with the cancer stem cell model.
- Cancers that exhibit this kind of hierarchical organization have functional differences among undifferentiated and differentiated cancer cells that affect response to therapy and prognosis.

- There remain a number of uncertainties that make it difficult to assess whether many, or few, cancers follow the stem cell model. Some "cancer stem cell" markers have proven difficult to confirm, and tumorigenic cell frequencies can sometimes increase dramatically as a result of changes in assay conditions.
- Many studies have assumed that markers discovered in earlier studies were universally able to distinguish tumorigenic from nontumorigenic cells, even in independent patient cohorts or in cultured cell lines. Given the heterogeneity that is evident among patients and the context dependence of some markers, "cancer stem cell" markers should be confirmed in functional assays in each patient or under each experimental circumstance in which they are used.
- It remains unclear to what extent we have systematically underestimated tumorigenic cell frequencies by using assays that are not optimized for the engraftment of transplanted cells. In some cases, the underestimates may be modest and may not affect conclusions. In other cases, cancers thought to have only rare tumorigenic cells may actually have common tumorigenic cells.
- It will be necessary to systematically assess the degree to which changes in assay conditions affect the spectrum of cancer cells that can form tumors. If a cancer cell has the potential to proliferate extensively in any assay, then it has the potential to contribute to disease progression, and it is perilous to ignore that cell during therapy.
- It will be important to fate map cells within tumors thought to follow the cancer stem cell model to test whether only small populations of phenotypically distinct cells actually promote tumor growth and disease progression.
- Few studies have assessed the degree of genetic heterogeneity among cancer cells within the same tumor or the extent to which this causes phenotypic and functional differences. In some cancers, genetic heterogeneity may confound the assumption that heterogeneity arises from hierarchical epigenetic differences, rendering the cancer stem cell model difficult to test.
- It will be important to test whether primary tumors in vivo contain cells that reversibly transition between tumorigenic and nontumorigenic states. The cancer stem cell model may not effectively describe cancers in which the efficiency of interconversion is high.
- It will be necessary to distinguish cancers that follow the stem cell model from those that do not to avoid testing agents that target specific subpopulations of cancer cells in patients who have no chance of benefitting from them.

ACKNOWLEDGMENTS

This work was supported by the Howard Hughes Medical Institute and the Cancer Prevention and Research Institute of Texas. J.A.M. is supported by a grant from the National Institute of Child Health and Human Development to the University of Texas Southwestern Medical Center (K12 HD 068369-02).

REFERENCES

Al-Hajj, M., Wicha, M.S., Benito-Hernandez, A., Morrison, S.J., and Clarke, M.F. (2003). Proc. Natl. Acad. Sci. USA *100*, 3983–3988.

Alvero, A.B., Chen, R., Fu, H.H., Montagna, M., Schwartz, P.E., Rutherford, T., Silasi, D.A., Steffensen, K.D., Waldstrom, M., Visintin, I., et al. (2009). Cell Cycle *8*, 158–166.

Ambros, I.M., Hata, J., Joshi, V.V., Roald, B., Dehner, L.P., Tuchler, H., Potschger, U., and Shimada, H. (2002). Cancer *94*, 1574–1583.

Anderson, K., Lutz, C., van Delft, F.W., Bateman, C.M., Guo, Y., Colman, S.M., Kempski, H., Moorman, A.V., Titley, I., Swansbury, J., et al. (2011). Nature *469*, 356–361.

Armstrong, S.A., and Look, A.T. (2005). J. Clin. Oncol. *23*, 6306–6315.

Auchincloss, H., and Sachs, D.H. (1989). Transplantation and Graft Rejection. In Fundamental Immunology, W.E. Paul, ed. (New York: Raven Press), pp. 889–922.

Baker, D.L., Schmidt, M.L., Cohn, S.L., Maris, J.M., London, W.B., Buxton, A., Stram, D., Castleberry, R.P., Shimada, H., Sandler, A., et al. (2010). N. Engl. J. Med. *363*, 1313–1323.

Bao, S., Wu, Q., McLendon, R.E., Hao, Y., Shi, Q., Hjelmeland, A.B., Dewhirst, M.W., Bigner, D.D., and Rich, J.N. (2006). Nature *444*, 756–760.

Barker, N., Ridgway, R.A., van Es, J.H., van de Wetering, M., Begthel, H., van den Born, M., Danenberg, E., Clarke, A.R., Sansom, O.J., and Clevers, H. (2009). Nature *457*, 608–611.

Barroca, V., Lassalle, B., Coureuil, M., Louis, J.P., Le Page, F., Testart, J., Allemand, I., Riou, L., and Fouchet, P. (2009). Nat. Cell Biol. *11*, 190–196.

Baylin, S.B., and Jones, P.A. (2011). Nat. Rev. Cancer *11*, 726–734.

Beier, D., Hau, P., Proescholdt, M., Lohmeier, A., Wischhusen, J., Oefner, P.J., Aigner, L., Brawanski, A., Bogdahn, U., and Beier, C.P. (2007). Cancer Res. *67*, 4010–4015.

Berman, J.N., Gerbing, R.B., Alonzo, T.A., Ho, P.A., Miller, K., Hurwitz, C., Heerema, N.A., Hirsch, B., Raimondi, S.C., Lange, B., et al. (2011). Leukemia *25*, 1039–1042.

Bhatia, R., Holtz, M., Niu, N., Gray, R., Snyder, D.S., Sawyers, C.L., Arber, D.A., Slovak, M.L., and Forman, S.J. (2003). Blood *101*, 4701–4707.

Bissell, M.J., and Hines, W.C. (2011). Nat. Med. *17*, 320–329.

Boiko, A.D., Razorenova, O.V., van de Rijn, M., Swetter, S.M., Johnson, D.L., Ly, D.P., Butler, P.D., Yang, G.P., Joshua, B., Kaplan, M.J., et al. (2010). Nature *466*, 133–137.

Bonnet, D., and Dick, J.E. (1997). Nat. Med. *3*, 730–737.

Brawley, C., and Matunis, E. (2004). Science *304*, 1331–1334.

Brown, P., McIntyre, E., Rau, R., Meshinchi, S., Lacayo, N., Dahl, G., Alonzo, T.A., Chang, M., Arceci, R.J., and Small, D. (2007). Blood *110*, 979–985.

Buchstaller, J., McKeever, P.E., and Morrison, S.J. (2012). Cancer Cell *21*, 240–252.

Campbell, P.J., Yachida, S., Mudie, L.J., Stephens, P.J., Pleasance, E.D., Stebbings, L.A., Morsberger, L.A., Latimer, C., McLaren, S., Lin, M.L., et al. (2010). Nature *467*, 1109–1113.

Chaffer, C.L., Brueckmann, I., Scheel, C., Kaestli, A.J., Wiggins, P.A., Rodrigues, L.O., Brooks, M., Reinhardt, F., Su, Y., Polyak, K., et al. (2011). Proc. Natl. Acad. Sci. USA *108*, 7950–7955.

Chaganti, R.S., and Houldsworth, J. (2000). Cancer Res. *60*, 1475–1482.

Charles, N., Ozawa, T., Squatrito, M., Bleau, A.M., Brennan, C.W., Hambardzumyan, D., and Holland, E.C. (2010). Cell Stem Cell *6*, 141–152.

Chen, R., Nishimura, M.C., Bumbaca, S.M., Kharbanda, S., Forrest, W.F., Kasman, I.M., Greve, J.M., Soriano, R.H., Gilmour, L.L., Rivers, C.S., et al. (2010). Cancer Cell *17*, 362–375.

Cho, R.W., Wang, X., Diehn, M., Shedden, K., Chen, G.Y., Sherlock, G., Gurney, A., Lewicki, J., and Clarke, M.F. (2008). Stem Cells *26*, 364–371.

Chu, S., McDonald, T., Lin, A., Chakraborty, S., Huang, Q., Snyder, D.S., and Bhatia, R. (2011). Blood *118*, 5565–5572.

Civenni, G., Walter, A., Kobert, N., Mihic-Probst, D., Zipser, M., Belloni, B., Seifert, B., Moch, H., Dummer, R., van den Broek, M., et al. (2011). Cancer Res. *71*, 3098–3109.

Cozzio, A., Passegue, E., Ayton, P.M., Karsunky, H., Cleary, M.L., and Weissman, I.L. (2003). Genes Dev. *17*, 3029–3035.

Curley, M.D., Therrien, V.A., Cummings, C.L., Sergent, P.A., Koulouris, C.R., Friel, A.M., Roberts, D.J., Seiden, M.V., Scadden, D.T., Rueda, B.R., et al. (2009). Stem Cells *27*, 2875–2883.

Curtis, S.J., Sinkevicius, K.W., Li, D., Lau, A.N., Roach, R.R., Zamponi, R., Woolfenden, A.E., Kirsch, D.G., Wong, K.K., and Kim, C.F. (2010). Cell Stem Cell *7*, 127–133.

Dalerba, P., Dylla, S.J., Park, I.K., Liu, R., Wang, X., Cho, R.W., Hoey, T., Gurney, A., Huang, E.H., Simeone, D.M., et al. (2007). Proc. Natl. Acad. Sci. USA *104*, 10158–10163.

de Thé, H., and Chen, Z. (2010). Nat. Rev. Cancer *10*, 775–783.

de Visser, K.E., Eichten, A., and Coussens, L.M. (2006). Nat. Rev. Cancer *6*, 24–37.

Dick, J.E. (2008). Blood *112*, 4793–4807.

Diehn, M., Cho, R.W., Lobo, N.A., Kalisky, T., Dorie, M.J., Kulp, A.N., Qian, D., Lam, J.S., Ailles, L.E., Wong, M., et al. (2009). Nature *458*, 780–783.

Ding, L., Ellis, M.J., Li, S., Larson, D.E., Chen, K., Wallis, J.W., Harris, C.C., McLellan, M.D., Fulton, R.S., Fulton, L.L., et al. (2010). Nature *464*, 999–1005.

Downing, J.R., and Shannon, K.M. (2002). Cancer Cell *2*, 437–445.

Druker, B.J., Guilhot, F., O'Brien, S.G., Gathmann, I., Kantarjian, H., Gattermann, N., Deininger, M.W., Silver, R.T., Goldman, J.M., Stone, R.M., et al. (2006). N. Engl. J. Med. *355*, 2408–2417.

Eppert, K., Takenaka, K., Lechman, E.R., Waldron, L., Nilsson, B., van Galen, P., Metzeler, K.H., Poeppl, A., Ling, V., Beyene, J., et al. (2011). Nat. Med. *17*, 1086–1093.

Falini, B., Mecucci, C., Tiacci, E., Alcalay, M., Rosati, R., Pasqualucci, L., La Starza, R., Diverio, D., Colombo, E., Santucci, A., et al. (2005). N. Engl. J. Med. *352*, 254–266.

Fearon, E.R., Burke, P.J., Schiffer, C.A., Zehnbauer, B.A., and Vogelstein, B. (1986). N. Engl. J. Med. *315*, 15–24.

Fidler, I.J., and Kripke, M.L. (1977). Science *197*, 893–895.

Fidler, I.J., and Hart, I.R. (1982). Science *217*, 998–1003.

Gibson, P., Tong, Y., Robinson, G., Thompson, M.C., Currle, D.S., Eden, C., Kranenburg, T.A., Hogg, T., Poppleton, H., Martin, J., et al. (2010). Nature *468*, 1095–1099.

Goardon, N., Marchi, E., Atzberger, A., Quek, L., Schuh, A., Soneji, S., Woll, P., Mead, A., Alford, K.A., Rout, R., et al. (2011). Cancer Cell *19*, 138–152.

Gorre, M.E., Mohammed, M., Ellwood, K., Hsu, N., Paquette, R., Rao, P.N., and Sawyers, C.L. (2001). Science *293*, 876–880.

Graham, S.M., Jorgensen, H.G., Allan, E., Pearson, C., Alcorn, M.J., Richmond, L., and Holyoake, T.L. (2002). Blood *99*, 319–325.

Gross, R.E., Mehler, M.F., Mabie, P.C., Zang, Z., Santschi, L., and Kessler, J.A. (1996). Neuron *17*, 595–606.

Gupta, P.B., Fillmore, C.M., Jiang, G., Shapira, S.D., Tao, K., Kuperwasser, C., and Lander, E.S. (2011). Cell *146*, 633–644.

Hamburger, A.W., and Salmon, S.E. (1977). Science *197*, 461–463.

He, S., Nakada, D., and Morrison, S.J. (2009). Annu. Rev. Cell Dev. Biol. *25*, 377–406.

Held, M.A., Curley, D.P., Dankort, D., McMahon, M., Muthusamy, V., and Bosenberg, M.W. (2010). Cancer Res. *70*, 388–397.

Heppner, G.H. (1984). Cancer Res. *44*, 2259–2265.

Hermann, P.C., Huber, S.L., Herrler, T., Aicher, A., Ellwart, J.W., Guba, M., Bruns, C.J., and Heeschen, C. (2007). Cell Stem Cell *1*, 313–323.

Heuser, M., Sly, L.M., Argiropoulos, B., Kuchenbauer, F., Lai, C., Weng, A., Leung, M., Lin, G., Brookes, C., Fung, S., et al. (2009). Blood *114*, 3983–3993.

Ho, P.A., Kutny, M.A., Alonzo, T.A., Gerbing, R.B., Joaquin, J., Raimondi, S.C., Gamis, A.S., and Meshinchi, S. (2011). Pediatr. Blood Cancer *57*, 204–209.

Holtz, M.S., Slovak, M.L., Zhang, F., Sawyers, C.L., Forman, S.J., and Bhatia, R. (2002). Blood *99*, 3792–3800.

Huntly, B.J., Shigematsu, H., Deguchi, K., Lee, B.H., Mizuno, S., Duclos, N., Rowan, R., Amaral, S., Curley, D., Williams, I.R., et al. (2004). Cancer Cell *6*, 587–596.

Ishizawa, K., Rasheed, Z.A., Karisch, R., Wang, Q., Kowalski, J., Susky, E., Pereira, K., Karamboulas, C., Moghal, N., Rajeshkumar, N.V., et al. (2010). Cell Stem Cell *7*, 279–282.

Johannessen, C.M., Boehm, J.S., Kim, S.Y., Thomas, S.R., Wardwell, L., Johnson, L.A., Emery, C.M., Stransky, N., Cogdill, A.P., Barretina, J., et al. (2010). Nature *468*, 968–972.

Johnson, R.A., Wright, K.D., Poppleton, H., Mohankumar, K.M., Finkelstein, D., Pounds, S.B., Rand, V., Leary, S.E., White, E., Eden, C., et al. (2010). Nature *466*, 632–636.

Joo, K.M., Kim, S.Y., Jin, X., Song, S.Y., Kong, D.S., Lee, J.I., Jeon, J.W., Kim, M.H., Kang, B.G., Jung, Y., et al. (2008). Lab. Invest. *88*, 808–815.

Kai, T., and Spradling, A. (2004). Nature *428*, 564–569.

Kalluri, R., and Weinberg, R.A. (2009). J. Clin. Invest. *119*, 1420–1428.

Kelly, P.N., Dakic, A., Adams, J.M., Nutt, S.L., and Strasser, A. (2007). Science *317*, 337.

Kennedy, J.A., Barabe, F., Poeppl, A.G., Wang, J.C., and Dick, J.E. (2007). Science *318*, 1722.

Kiyoi, H., Naoe, T., Nakano, Y., Yokota, S., Minami, S., Miyawaki, S., Asou, N., Kuriyama, K., Jinnai, I., Shimazaki, C., et al. (1999). Blood *93*, 3074–3080.

Kleinsmith, L.J., and Pierce, G.B. (1964). Cancer Res. *24*, 1544–1551.

Kottaridis, P.D., Gale, R.E., Frew, M.E., Harrison, G., Langabeer, S.E., Belton, A.A., Walker, H., Wheatley, K., Bowen, D.T., Burnett, A.K., et al. (2001). Blood *98*, 1752–1759.

Krivtsov, A.V., Twomey, D., Feng, Z., Stubbs, M.C., Wang, Y., Faber, J., Levine, J.E., Wang, J., Hahn, W.C., Gilliland, D.G., et al. (2006). Nature *442*, 818–822.

Kuperwasser, C., Chavarria, T., Wu, M., Magrane, G., Gray, J.W., Carey, L., Richardson, A., and Weinberg, R.A. (2004). Proc. Natl. Acad. Sci. USA *101*, 4966–4971.

Lapidot, T., Sirard, C., Vormoor, J., Murdoch, B., Hoang, T., Caceres-Cortes, J., Minden, M., Paterson, B., Caligiuri, M.A., and Dick, J.E. (1994). Nature *17*, 645–648.

le Viseur, C., Hotfilder, M., Bomken, S., Wilson, K., Rottgers, S., Schrauder, A., Rosemann, A., Irving, J., Stam, R.W., Shultz, L.D., et al. (2008). Cancer Cell *14*, 47–58.

Levi, B.P., and Morrison, S.J. (2008). Cold Spring Harb. Symp. Quant. Biol. *73*, 539–553.

Ley, T.J., Ding, L., Walter, M.J., McLellan, M.D., Lamprecht, T., Larson, D.E., Kandoth, C., Payton, J.E., Baty, J., Welch, J., et al. (2010). N. Engl. J. Med. *363*, 2424–2433.

Li, C., Heidt, D.G., Dalerba, P., Burant, C.F., Zhang, L., Adsay, V., Wicha, M., Clarke, M.F., and Simeone, D.M. (2007). Cancer Res. *67*, 1030–1037.

Mani, S.A., Guo, W., Liao, M.J., Eaton, E.N., Ayyanan, A., Zhou, A.Y., Brooks, M., Reinhard, F., Zhang, C.C., Shipitsin, M., et al. (2008). Cell *133*, 704–715.

Manz, M.G. (2007). Immunity *26*, 537–541.

Matthay, K.K., Villablanca, J.G., Seeger, R.C., Stram, D.O., Harris, R.E., Ramsay, N.K., Swift, P., Shimada, H., Black, C.T., Brodeur, G.M., et al. (1999). N. Engl. J. Med. *341*, 1165–1173.

Matthay, K.K., Reynolds, C.P., Seeger, R.C., Shimada, H., Adkins, E.S., Haas-Kogan, D., Gerbing, R.B., London, W.B., and Villablanca, J.G. (2009). J. Clin. Oncol. *27*, 1007–1013.

McDermott, S.P., Eppert, K., Lechman, E.R., Doedens, M., and Dick, J.E. (2010). Blood *116*, 193–200.

McKenzie, J.L., Gan, O.I., Doedens, M., and Dick, J.E. (2005). Blood *106*, 1259–1261.

Merlos-Suárez, A., Barriga, F.M., Jung, P., Iglesias, M., Cespedes, M.V., Rossell, D., Sevillano, M., Hernando-Momblona, X., da Silva-Diz, V., Munoz, P., et al. (2011). Cell Stem Cell *8*, 511–524.

Meshinchi, S., Woods, W.G., Stirewalt, D.L., Sweetser, D.A., Buckley, J.D., Tjoa, T.K., Bernstein, I.D., and Radich, J.P. (2001). Blood *97*, 89–94.

Morel, A.P., Lievre, M., Thomas, C., Hinkal, G., Ansieau, S., and Puisieux, A. (2008). PLoS ONE *3*, e2888.

Navin, N., Kendall, J., Troge, J., Andrews, P., Rodgers, L., McIndoo, J., Cook, K., Stepansky, A., Levy, D., Esposito, D., et al. (2011). Nature *472*, 90–94.

Nazarian, R., Shi, H., Wang, Q., Kong, X., Koya, R.C., Lee, H., Chen, Z., Lee, M.K., Attar, N., Sazegar, H., et al. (2010). Nature *468*, 973–977.

Nguyen, D.X., Bos, P.D., and Massague, J. (2009). Nat. Rev. Cancer *9*, 274–284.

Nitschke, R., Smith, E.I., Shochat, S., Altshuler, G., Travers, H., Shuster, J.J., Hayes, F.A., Patterson, R., and McWilliams, N. (1988). J. Clin. Oncol. *6*, 1271–1279.

Notta, F., Doulatov, S., and Dick, J.E. (2010). Blood *115*, 3704–3707.

Notta, F., Mullighan, C.G., Wang, J.C., Poeppl, A., Doulatov, S., Phillips, L.A., Ma, J., Minden, M.D., Downing, J.R., and Dick, J.E. (2011). Nature *469*, 362–367.

Nowell, P.C. (1976). Science *194*, 23–28.

Nowell, P.C. (1986). Cancer Res. *46*, 2203–2207.

O'Brien, C.A., Pollett, A., Gallinger, S., and Dick, J.E. (2007). Nature *445*, 106–110.

Ogawa, M., Fried, J., Sakai, Y., Strife, A., and Clarkson, B.D. (1970). Cancer *25*, 1031–1049.

Oravecz-Wilson, K.I., Philips, S.T., Yilmaz, O.H., Ames, H.M., Li, L., Crawford, B.D., Gauvin, A.M., Lucas, P.C., Sitwala, K., Downing, J.R., et al. (2009). Cancer Cell *16*, 137–148.

Pang, R., Law, W.L., Chu, A.C., Poon, J.T., Lam, C.S., Chow, A.K., Ng, L., Cheung, L.W., Lan, X.R., Lan, H.Y., et al. (2010). Cell Stem Cell *6*, 603–615.

Piccirillo, S.G., Reynolds, B.A., Zanetti, N., Lamorte, G., Binda, E., Broggi, G., Brem, H., Olivi, A., Dimeco, F., and Vescovi, A.L. (2006). Nature *444*, 761–765.

Pinner, S., Jordan, P., Sharrock, K., Bazley, L., Collinson, L., Marais, R., Bonvin, E., Goding, C., and Sahai, E. (2009). Cancer Res. *69*, 7969–7977.

Polyak, K., Haviv, I., and Campbell, I.G. (2009). Trends Genet. *25*, 30–38.

Poulikakos, P.I., and Rosen, N. (2011). Cancer Cell *19*, 11–15.

Poulikakos, P.I., Persaud, Y., Janakiraman, M., Kong, X., Ng, C., Moriceau, G., Shi, H., Atefi, M., Titz, B., Gabay, M.T., et al. (2011). Nature *480*, 387–390.

Quintana, E., Shackleton, M., Sabel, M.S., Fullen, D.R., Johnson, T.M., and Morrison, S.J. (2008). Nature *456*, 593–598.

Quintana, E., Shackleton, M., Foster, H.R., Fullen, D.R., Sabel, M.S., Johnson, T.M., and Morrison, S.J. (2010). Cancer Cell *18*, 510–523.

Read, T.A., Fogarty, M.P., Markant, S.L., McLendon, R.E., Wei, Z., Ellison, D.W., Febbo, P.G., and Wechsler-Reya, R.J. (2009). Cancer Cell *15*, 135–147.

Reya, T., Morrison, S.J., Clarke, M.F., and Weissman, I.L. (2001). Nature *414*, 105–111.

Ricci-Vitiani, L., Lombardi, D.G., Pilozzi, E., Biffoni, M., Todaro, M., Peschle, C., and De Maria, R. (2007). Nature *445*, 111–115.

Roesch, A., Fukunaga-Kalabis, M., Schmidt, E.C., Zabierowski, S.E., Brafford, P.A., Vultur, A., Basu, D., Gimotty, P., Vogt, T., and Herlyn, M. (2010). Cell *141*, 583–594.

Roumiantsev, S., Shah, N.P., Gorre, M.E., Nicoll, J., Brasher, B.B., Sawyers, C.L., and Van Etten, R.A. (2002). Proc. Natl. Acad. Sci. USA *99*, 10700–10705.

Rousselot, P., Huguet, F., Rea, D., Legros, L., Cayuela, J.M., Maarek, O., Blanchet, O., Marit, G., Gluckman, E., Reiffers, J., et al. (2007). Blood *109*, 58–60.

Sarry, J.E., Murphy, K., Perry, R., Sanchez, P.V., Secreto, A., Keefer, C., Swider, C.R., Strzelecki, A.C., Cavelier, C., Recher, C., et al. (2011). J. Clin. Invest. *121*, 384–395.

Schatton, T., Murphy, G.F., Frank, N.Y., Yamaura, K., Waaga-Gasser, A.M., Gasser, M., Zhan, Q., Jordan, S., Duncan, L.M., Weishaupt, C., et al. (2008). Nature *451*, 345–349.

Scheel, C., Eaton, E.N., Li, S.H., Chaffer, C.L., Reinhardt, F., Kah, K.J., Bell, G., Guo, W., Rubin, J., Richardson, A.L., et al. (2011). Cell *145*, 926–940.

Schüller, U., Heine, V.M., Mao, J., Kho, A.T., Dillon, A.K., Han, Y.G., Huillard, E., Sun, T., Ligon, A.H., Qian, Y., et al. (2008). Cancer Cell *14*, 123–134.

Shackleton, M., Quintana, E., Fearon, E.R., and Morrison, S.J. (2009). Cell *138*, 822–829.

Sharma, S.V., Lee, D.Y., Li, B., Quinlan, M.P., Takahashi, F., Maheswaran, S., McDermott, U., Azizian, N., Zou, L., Fischbach, M.A., et al. (2010). Cell *141*, 69–80.

Shimada, H., Chatten, J., Newton, W.A., Jr., Sachs, N., Hamoudi, A.B., Chiba, T., Marsden, H.B., and Misugi, K. (1984). J. Natl. Cancer Inst. *73*, 405–416.

Shimada, H., Ambros, I.M., Dehner, L.P., Hata, J., Joshi, V.V., and Roald, B. (1999a). Cancer *86*, 349–363.

Shimada, H., Ambros, I.M., Dehner, L.P., Hata, J., Joshi, V.V., Roald, B., Stram, D.O., Gerbing, R.B., Lukens, J.N., Matthay, K.K., et al. (1999b). Cancer *86*, 364–372.

Singh, S.K., Hawkins, C., Clarke, I.D., Squire, J.A., Bayani, J., Hide, T., Henkelman, R.M., Cusimano, M.D., and Dirks, P.B. (2004). Nature *432*, 396–401.

Somervaille, T.C., and Cleary, M.L. (2006). Cancer Cell *10*, 257–268.

Somervaille, T.C., Matheny, C.J., Spencer, G.J., Iwasaki, M., Rinn, J.L., Witten, D.M., Chang, H.Y., Shurtleff, S.A., Downing, J.R., and Cleary, M.L. (2009). Cell Stem Cell *4*, 129–140.

Son, M.J., Woolard, K., Nam, D.H., Lee, J., and Fine, H.A. (2009). Cell Stem Cell *4*, 440–452.

Stenning, S.P., Parkinson, M.C., Fisher, C., Mead, G.M., Cook, P.A., Fossa, S.D., Horwich, A., Jones, W.G., Newlands, E.S., Oliver, R.T., et al. (1998). Cancer *83*, 1409–1419.

Stewart, J.M., Shaw, P.A., Gedye, C., Bernardini, M.Q., Neel, B.G., and Ailles, L.E. (2011). Proc. Natl. Acad. Sci. USA *108*, 6468–6473.

Stirewalt, D.L., Kopecky, K.J., Meshinchi, S., Appelbaum, F.R., Slovak, M.L., Willman, C.L., and Radich, J.P. (2001). Blood *97*, 3589–3595.

Taussig, D.C., Miraki-Moud, F., Anjos-Afonso, F., Pearce, D.J., Allen, K., Ridler, C., Lillington, D., Oakervee, H., Cavenagh, J., Agrawal, S.G., et al. (2008). Blood *112*, 568–575.

Taussig, D.C., Vargaftig, J., Miraki-Moud, F., Griessinger, E., Sharrock, K., Luke, T., Lillington, D., Oakervee, H., Cavenagh, J., Agrawal, S.G., et al. (2010). Blood *115*, 1976–1984.

Taylor, M.D., Poppleton, H., Fuller, C., Su, X., Liu, Y., Jensen, P., Magdaleno, S., Dalton, J., Calabrese, C., Board, J., et al. (2005). Cancer Cell *8*, 323–335.

Thiede, C., Koch, S., Creutzig, E., Steudel, C., Illmer, T., Schaich, M., and Ehninger, G. (2006). Blood *107*, 4011–4020.

Thiele, C.J., Reynolds, C.P., and Israel, M.A. (1985). Nature *313*, 404–406.

Thiery, J.P., Acloque, H., Huang, R.Y., and Nieto, M.A. (2009). Cell *139*, 871–890.

Vaillant, F., Asselin-Labat, M.L., Shackleton, M., Forrest, N.C., Lindeman, G.J., and Visvader, J.E. (2008). Cancer Res. *68*, 7711–7717.

Vermeulen, L., De Sousa, E.M.F., van der Heijden, M., Cameron, K., de Jong, J.H., Borovski, T., Tuynman, J.B., Todaro, M., Merz, C., Rodermond, H., et al. (2010). Nat. Cell Biol. *12*, 468–476.

Villanueva, J., Vultur, A., Lee, J.T., Somasundaram, R., Fukunaga-Kalabis, M., Cipolla, A.K., Wubbenhorst, B., Xu, X., Gimotty, P.A., Kee, D., et al. (2010). Cancer Cell *18*, 683–695.

Vogelstein, B., Fearon, E.R., Hamilton, S.R., Kern, S.E., Preisinger, A.C., Leppert, M., Nakamura, Y., White, R., Smits, A.M., and Bos, J.L. (1988). N. Engl. J. Med. *319*, 525–532.

Vogelstein, B., Civin, C.I., Preisinger, A.C., Krischer, J.P., Steuber, P., Ravindranath, Y., Weinstein, H., Elfferich, P., and Bos, J. (1990). Genes Chromosomes Cancer *2*, 159–162.

Wang, J.C., and Dick, J.E. (2005). Trends Cell Biol. *15*, 494–501.

Wang, J., Sakariassen, P.O., Tsinkalovsky, O., Immervoll, H., Boe, S.O., Svendsen, A., Prestegarden, L., Rosland, G., Thorsen, F., Stuhr, L., et al. (2008). Int. J. Cancer *122*, 761–768.

Wang, Y., Krivtsov, A.V., Sinha, A.U., North, T.E., Goessling, W., Feng, Z., Zon, L.I., and Armstrong, S.A. (2010). Science *327*, 1650–1653.

Ward, R.J., Lee, L., Graham, K., Satkunendran, T., Yoshikawa, K., Ling, E., Harper, L., Austin, R., Nieuwenhuis, E., Clarke, I.D., et al. (2009). Cancer Res. *69*, 4682–4690.

Williams, R.T., den Besten, W., and Sherr, C.J. (2007). Genes Dev. *21*, 2283–2287.

Wu, X., Northcott, P.A., Dubuc, A., Dupuy, A.J., Shih, D.J., Witt, H., Croul, S., Bouffet, E., Fults, D.W., Eberhart, C.G., et al. (2012). Nature *482*, 529–533.

Yachida, S., Jones, S., Bozic, I., Antal, T., Leary, R., Fu, B., Kamiyama, M., Hruban, R.H., Eshleman, J.R., Nowak, M.A., et al. (2010). Nature *467*, 1114–1117.

Yang, J., Mani, S.A., Donaher, J.L., Ramaswamy, S., Itzykson, R.A., Come, C., Savagner, P., Gitelman, I., Richardson, A., and Weinberg, R.A. (2004). Cell *117*, 927–939.

Yang, Z.J., Ellis, T., Markant, S.L., Read, T.A., Kessler, J.D., Bourboulas, M., Schuller, U., Machold, R., Fishell, G., Rowitch, D.H., et al. (2008). Cancer Cell *14*, 135–145.

Yilmaz, O.H., Valdez, R., Theisen, B.K., Guo, W., Ferguson, D.O., Wu, H., and Morrison, S.J. (2006). Nature *441*, 475–482.

Zhang, M., Behbod, F., Atkinson, R.L., Landis, M.D., Kittrell, F., Edwards, D., Medina, D., Tsimelzon, A., Hilsenbeck, S., Green, J.E., et al. (2008a). Cancer Res. *68*, 4674–4682.

Zhang, S., Balch, C., Chan, M.W., Lai, H.C., Matei, D., Schilder, J.M., Yan, P.S., Huang, T.H., and Nephew, K.P. (2008b). Cancer Res. *68*, 4311–4320.

Zhao, Z., Zuber, J., Diaz-Flores, E., Lintault, L., Kogan, S.C., Shannon, K., and Lowe, S.W. (2010). Genes Dev. *24*, 1389–1402.

Zwaan, C.M., Meshinchi, S., Radich, J.P., Veerman, A.J., Huismans, D.R., Munske, L., Podleschny, M., Hahlen, K., Pieters, R., Zimmermann, M., et al. (2003). Blood *102*, 2387–2394.

Cancer Cell
Special Collection
10 YEARS OF EXCITING CANCER RESEARCH SINCE 2002

Metabolic Reprogramming: A Cancer Hallmark Even Warburg Did Not Anticipate

Patrick S. Ward[1,2] and Craig B. Thompson[1,*]
[1]Cancer Biology and Genetics Program, Memorial Sloan-Kettering Cancer Center, New York, NY 10065, USA
[2]Cell and Molecular Biology Graduate Group, Perelman School of Medicine at the University of Pennsylvania, Philadelphia, PA 19104, USA
*Correspondence: craig@mskcc.org
DOI 10.1016/j.ccr.2012.02.014

Cancer metabolism has long been equated with aerobic glycolysis, seen by early biochemists as primitive and inefficient. Despite these early beliefs, the metabolic signatures of cancer cells are not passive responses to damaged mitochondria but result from oncogene-directed metabolic reprogramming required to support anabolic growth. Recent evidence suggests that metabolites themselves can be oncogenic by altering cell signaling and blocking cellular differentiation. No longer can cancer-associated alterations in metabolism be viewed as an indirect response to cell proliferation and survival signals. We contend that altered metabolism has attained the status of a core hallmark of cancer.

The propensity for proliferating cells to secrete a significant fraction of glucose carbon through fermentation was first elucidated in yeast. Otto Warburg extended these observations to mammalian cells, finding that proliferating ascites tumor cells converted the majority of their glucose carbon to lactate, even in oxygen-rich conditions. Warburg hypothesized that this altered metabolism was specific to cancer cells, and that it arose from mitochondrial defects that inhibited their ability to effectively oxidize glucose carbon to CO_2. An extension of this hypothesis was that dysfunctional mitochondria caused cancer (Koppenol et al., 2011). Warburg's seminal finding has been observed in a wide variety of cancers. These observations have been exploited clinically using ^{18}F-deoxyglucose positron emission tomography (FDG-PET). However, in contrast to Warburg's original hypothesis, damaged mitochondria are not at the root of the aerobic glycolysis exhibited by most tumor cells. Most tumor mitochondria are not defective in their ability to carry out oxidative phosphorylation. Instead, in proliferating cells, mitochondrial metabolism is reprogrammed to meet the challenges of macromolecular synthesis. This possibility was never considered by Warburg and his contemporaries.

Advances in cancer metabolism research over the last decade have enhanced our understanding of how aerobic glycolysis and other metabolic alterations observed in cancer cells support the anabolic requirements associated with cell growth and proliferation. It has become clear that anabolic metabolism is under complex regulatory control directed by growth-factor signal transduction in nontransformed cells. Yet despite these advances, the repeated refrain from traditional biochemists is that altered metabolism is merely an indirect phenomenon in cancer, a secondary effect that pales in importance to the activation of primary proliferation and survival signals (Hanahan and Weinberg, 2011). Most proto-oncogenes and tumor suppressor genes encode components of signal transduction pathways. Their roles in carcinogenesis have traditionally been attributed to their ability to regulate the cell cycle and sustain proliferative signaling while also helping cells evade growth suppression and/or cell death (Hanahan and Weinberg, 2011). But evidence for an alternative concept, that the primary functions of activated oncogenes and inactivated tumor suppressors are to reprogram cellular metabolism, has continued to build over the past several years. Evidence is also developing for the proposal that proto-oncogenes and tumor suppressors primarily evolved to regulate metabolism.

We begin this review by discussing how proliferative cell metabolism differs from quiescent cell metabolism on the basis of active metabolic reprogramming by proto-oncogenes and tumor suppressors. Much of this reprogramming depends on utilizing mitochondria as functional biosynthetic organelles. We then further develop the idea that altered metabolism is a primary feature selected for during tumorigenesis. Recent advances have demonstrated that altered metabolism in cancer extends beyond adaptations to meet the increased anabolic requirements of a growing and dividing cell. Changes in cancer cell metabolism can also influence cellular differentiation status, and in some cases these changes arise from oncogenic alterations in metabolic enzymes themselves.

Quiescent versus Proliferating Cells: Both Use Mitochondria, but to Different Ends

Most nonproliferating, differentiated cells depend on the efficiency of ATP production through oxidative phosphorylation to maintain their integrity. As a result, such cells metabolize glucose to pyruvate through glycolysis, and then completely oxidize most of this pyruvate to CO_2 through the tricarboxylic acid (TCA) cycle of the mitochondria, where oxygen is the final acceptor in an electron transport chain that generates an electrochemical gradient facilitating ATP production. The elucidation of the TCA cycle and how cells maximize ATP production to maintain themselves was one of the great discoveries of the last century.

In vivo, metazoan cells are surrounded by an abundance of nutrients. However, unlike prokaryotes or single-cell eukaryotes, animal cells are not cell autonomous for nutrient uptake. Instead, just to survive, metazoan cells compete for limiting levels of growth factors that direct nutrient uptake (Rathmell et al., 2000). To survive under such conditions, differentiated cells adopt a catabolic metabolism focused on maximizing the efficiency of ATP production from limited nutrients (Deberardinis

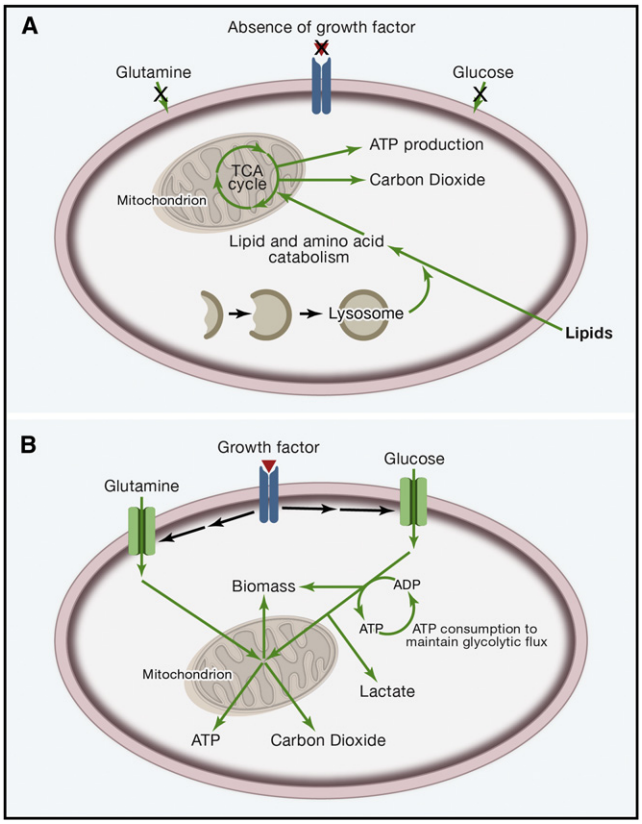

Figure 1. Metabolism in Quiescent versus Proliferating Cells: Both Use Mitochondria

(A) In the absence of instructional growth factor signaling, cells in multicellular organisms lack the ability to take up sufficient nutrients to maintain themselves. Neglected cells will undergo autophagy and catabolize amino acids and lipids through the TCA cycle, assuming sufficient oxygen is available. This oxidative metabolism maximizes ATP production.

(B) Cells that receive instructional growth factor signaling are directed to increase their uptake of nutrients, most notably glucose and glutamine. The increased nutrient uptake can then support the anabolic requirements of cell growth: mainly lipid, protein, and nucleotide synthesis (biomass). Excess carbon is secreted as lactate. Proliferating cells may also use strategies to decrease their ATP production while increasing their ATP consumption. These strategies maintain the ADP:ATP ratio necessary to sustain glycolytic flux. Green arrows represent metabolic pathways, while black arrows represent signaling.

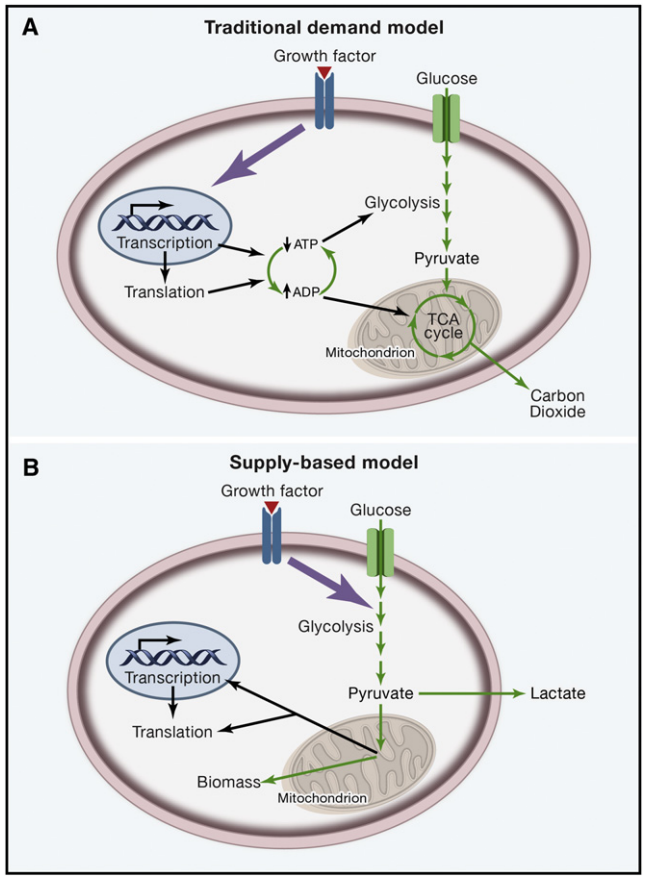

Figure 2. Metabolism Is a Direct, Not Indirect, Response to Growth Factor Signaling

(A) The traditional demand-based model of how metabolism is altered in proliferating cells. In response to growth factor signaling, increased transcription and translation consume free energy and decrease the ATP:ADP ratio. This leads to enhanced flux of glucose carbon through glycolysis and the TCA cycle for the purpose of producing more ATP.

(B) Supply-based model of how metabolism changes in proliferating cells. Growth factor signaling directly reprograms nutrient uptake and metabolism. Increased nutrient flux through glycolysis and the mitochondria in response to growth factor signaling is used for biomass production. Metabolism also impacts transcription and translation through mechanisms independent of ATP availability.

et al., 2006; Lum et al., 2005; Vander Heiden et al., 2009) (Figure 1A). In contrast, when growth factors are abundant, cells increase their nutrient uptake and adopt an anabolic metabolism (Bauer et al., 2004) (Figure 1B). As a consequence of intracellular abundance of nutrients, growth-factor-stimulated cells adapt to their largesse by initiating cell division in a manner analogous to that of single-cell eukaryotes exposed to nutrient-rich medium (Boer et al., 2010; Conlon and Raff, 2003; Fantes and Nurse, 1977). In cancer cells, the instructional signaling pathways downstream of growth factor receptors can be constitutively activated in the absence of extracellular growth factors.

Altered Metabolism Is a Direct Response to Growth-Factor Signaling

The traditional cancer model posits that the altered metabolism associated with cell proliferation occurs as a secondary response to cell cycle and proliferative signaling. In this model, the demand for free energy to sustain transcription and translation drives a decrease in the ATP:ADP ratio, leading to subsequent allosteric effects on rate-limiting metabolic enzymes (Figure 2A). While traditional allosteric regulation certainly occurs in proliferating cells, strong evidence now exists to support an alternative model. In this supply-based model, changes in metabolic fluxes occur in primary response to growth-factor signaling, independent of changes in ATP and other mechanisms worked out by early biochemists (Figure 2B). The reprogramming of cellular metabolism toward macromolecular synthesis is critical to supplying enough nucleotides, proteins, and lipids for a cell to double its total biomass and then divide to produce two daughter cells. In contrast to the catabolic metabolism of differentiated cells, this anabolic metabolism fundamental to cell growth and proliferation is not focused on maximizing ATP

yield. Rather than ATP, proliferating cells are in much greater need of reduced carbon and reduced nitrogen, as well as cytosolic NADPH for reductive biosynthetic reactions.

The recognition that proliferating cells do not maximize ATP production through mitochondrial oxidative phosphorylation has contributed to the continuing misconception that proliferating cells, particularly cancer cells, do not utilize mitochondria. In fact, most cancer cells and proliferating normal cells still derive a significant fraction of their ATP through oxidative phosphorylation. However, in proliferating cells, in contrast to quiescent cells, this oxidative phosphorylation-dependent production of ATP appears secondary to the use of mitochondrial enzymes in the synthesis of anabolic precursors.

PI3K/Akt/mTORC1 Activation: Driving Anabolic Metabolism and Tumorigenesis by Reprogramming Mitochondria

Activation of the PI3K/Akt pathway is perhaps the most common lesion in spontaneous human cancers. Activated PI3K/Akt leads to enhanced glucose uptake and glycolysis (Buzzai et al., 2005; Elstrom et al., 2004). Pivotal to this induction is increased glucose transporter expression on the cell surface, activation of hexokinase to capture glucose intracellularly through phosphorylation, and Akt-induced, phosphofructokinase-2-dependent allosteric activation of phosphofructokinase-1 to commit glucose to glycolytic metabolism (Deprez et al., 1997; Gottlob et al., 2001; Kohn et al., 1996; Rathmell et al., 2003). However, the PI3K/Akt pathway also promotes glucose carbon flux into biosynthetic pathways that rely upon functional mitochondrial metabolism (Figure 3). For example, fatty acid, cholesterol, and isoprenoid synthesis all require acetyl-CoA (Wakil et al., 1957). The pyruvate dehydrogenase (PDH) complex that converts glucose-derived pyruvate into acetyl-CoA is solely mitochondrial (Linn et al., 1969). Mitochondrial acetyl-CoA then cannot be directly exported to the cytoplasm but instead must first condense with oxaloacetate to form citrate through the activity of another exclusively mitochondrial enzyme, citrate synthase (Stern et al., 1952). Citrate can then be exported to the cytosol, where it can be converted back to acetyl-CoA by ATP-citrate lyase (ACL) (Srere, 1959). Akt facilitates this diversion of mitochondrial citrate from the TCA cycle to acetyl-CoA production by phosphorylating and activating ACL (Bauer et al., 2005; Berwick et al., 2002; Hatzivassiliou et al., 2005). RNAi knockdown or pharmacologic inhibition of ACL is particularly effective at decreasing the in vitro proliferation of cells with increased glucose uptake. ACL knockdown can also diminish Akt-driven tumorigenesis in vivo (Bauer et al., 2005; Hatzivassiliou et al., 2005). ACL's breakdown of citrate is also pivotal to preventing a cytosolic accumulation of citrate. Citrate is a major negative allosteric regulator of glycolysis (Stryer, 1995). Taken together, these findings demonstrate that the reprogramming of mitochondrial citrate metabolism is a central aspect of PI3K/Akt oncogenic activity.

Downstream of PI3K/Akt, the well-characterized cell growth regulator mTORC1 also has many effects intertwined with mitochondrial metabolism. mTORC1 is best known for enhancing protein synthesis. Several amino acid precursors are derived from the transamination of mitochondrial intermediates. Oxaloacetate can be transaminated to produce aspartate which can serve as a precursor for asparagine, and α-ketoglutarate can be transaminated to produce glutamate, which in turn can be converted to proline, arginine, and glutamine. Most cancers depend on these syntheses rather than exogenous supplies. This is consistent with how most tumors other than childhood leukemia are resistant to the effects of depleting the blood of asparagine through the intravenous use of L-asparaginase (Clarkson et al., 1970; Tallal et al., 1970). mTORC1 has also been shown to have direct effects on promoting mitochondrial biogenesis, in part via a transcriptional complex that promotes the function of PGC-1α (Bentzinger et al., 2008; Cunningham et al., 2007; Ramanathan and Schreiber, 2009; Schieke et al., 2006). Finally, a study isolating the cell-intrinsic consequences of mTORC1 activation demonstrated that SREBP-mediated de novo lipogenesis is a critical component of mTORC1-driven proliferation (Düvel et al., 2010). As discussed above, de novo lipogenesis in mammalian cells depends on mitochondrial citrate production.

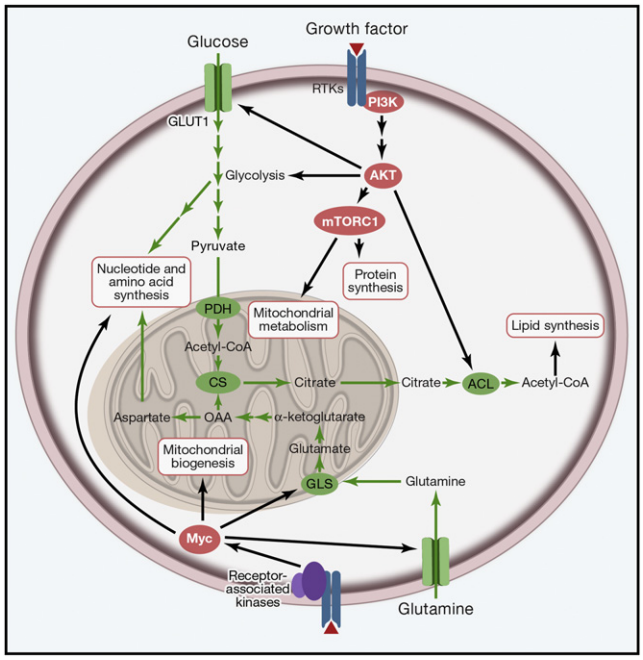

Figure 3. Alterations in Classic Oncogenes Directly Reprogram Cell Metabolism to Increase Nutrient Uptake and Biosynthesis

PI3K/Akt signaling downstream of receptor tyrosine kinase (RTK) activation increases glucose uptake through the transporter GLUT1, and increases flux through glycolysis. Branches of glycolytic metabolism contribute to nucleotide and amino acid synthesis. Akt also activates ATP-citrate lyase (ACL), promoting the conversion of mitochondria-derived citrate to acetyl-CoA for lipid synthesis. Mitochondrial citrate can be synthesized when glucose-derived acetyl-CoA, generated by pyruvate dehydrogenase (PDH), condenses with glutamine-derived oxaloacetate (OAA) via the activity of citrate synthase (CS). mTORC1 promotes protein synthesis and mitochondrial metabolism. Myc increases glutamine uptake and the conversion of glutamine into a mitochondrial carbon source by promoting the expression of the enzyme glutaminase (GLS). Myc also promotes mitochondrial biogenesis. In addition, Myc promotes nucleotide and amino acid synthesis, both through direct transcriptional regulation and through increasing the synthesis of mitochondrial metabolite precursors.

HIF-1-Mediated Inhibition of Carbon Flux into Mitochondria Can Be Antiproliferative

Notably, Düvel et al. (2010) found that the other major target of mTORC1 activation, hypoxia-inducible factor 1 (HIF-1), is not

critical for mTORC1-driven proliferation. This may seem surprising in light of HIF-1's often-cited ability to promote the enhanced glycolysis characteristic of cancer cells. However, HIF-1 activation has the additional effect of inhibiting mitochondrial metabolism of glucose carbon, in part by promoting the expression of pyruvate dehydrogenase kinase 1 (PDK1) to inhibit PDH activity (Kim et al., 2006; Papandreou et al., 2006). By diverting pyruvate into lactate, HIF-1 blocks glucose carbon incorporation into mitochondrial citrate which is critical for lipid synthesis (Lum et al., 2007). This block correlates with the antiproliferative effect of HIF-1 observed in hematopoietic and renal cells (Lum et al., 2007) and fits with recent genetic evidence of HIF-1 acting as a tumor suppressor in some cancers (Shen et al., 2011).

There are cancers that do exhibit decreased flux of glucose-derived pyruvate into the mitochondria relative to normal tissues. However, as will be discussed later in this review, these cancers still rely on mitochondrial metabolic flux. In place of oxidative metabolism of both glucose and glutamine, these cancers preferentially perform reductive and carboxylating biosynthetic reactions from glutamine carbon (Le et al., 2012; Metallo et al., 2012; Mullen et al., 2012; Wise et al., 2011).

Myc Activation Also Impacts Mitochondrial Metabolism

Like PI3K, Akt, and mTORC1, the Myc transcription factor has important metabolic roles beyond enhancing glycolysis. Myc promotes mitochondrial gene expression and mitochondrial biogenesis (Li et al., 2005). Oncogenic Myc has also been shown to promote the mitochondrial utilization of glutamine by enhancing the expression of glutaminase (GLS), which deamidates glutamine to glutamate. Cells expressing oncogenic Myc are glutamine-addicted and undergo apoptosis when glutamine is withdrawn from the culture medium. While the role of glutamine as a nitrogen donor is important for the proliferation of these cells, their viability depends on glutamine as a carbon source for mitochondrial metabolism (DeBerardinis et al., 2007; Fan et al., 2010; Gao et al., 2009; Wise et al., 2008; Yuneva et al., 2007). Recently, it was observed that the growth of tumor xenografts from Myc-expressing B cells can be impaired by pharmacological inhibition of GLS (Le et al., 2012). These data provide further evidence that reprogrammed glutamine metabolism is critical to the growth and survival of Myc-driven malignancies. Upstream of Myc, RhoGTPases have also been linked to the activation of GLS and glutamine dependence. Either siRNA knockdown or pharmacological inhibition of GLS can inhibit Rho-GTPase-induced transformation and proliferation (Wang et al., 2010).

Did Proto-Oncogenes and Tumor Suppressors Arise in Evolution as Components of Metabolic Regulation?

The weight of the evidence to date supports the concept that reprogramming of cellular metabolism is a primary and fundamental aspect of transformation resulting from mutations in proto-oncogenes and tumor suppressors. Proliferative metabolism is heavily dependent on the reprogramming of mitochondria to serve a synthetic rather than a degradative role. Metabolic changes associated with proliferating cells do not simply occur passively in response to damaged mitochondria or changes in ATP levels.

A related concept concerns the possibility that proto-oncogenes and tumor suppressors arose in evolution as components of metabolic regulation. Consistent with this hypothesis, activation of the tumor suppressor p53 has been shown to be critical for cell survival following glucose depletion (Jones et al., 2005). Subsequent reports have linked this metabolic stress response of p53 to increased fatty acid oxidation (Assaily et al., 2011; Zaugg et al., 2011). In tumors, the loss of p53 can enhance glycolysis and anabolic synthesis from glycolytic intermediates (Bensaad et al., 2006; Kondoh et al., 2005; Matoba et al., 2006). However, mitochondrial metabolism continues to be critical in cells with metabolic reprogramming arising from p53 loss. Treatment with the antidiabetic drug metformin, an inhibitor of complex 1 of the mitochondrial electron transport chain (El-Mir et al., 2000; Owen et al., 2000), is especially toxic to p53-deficient tumor cells (Buzzai et al., 2007).

Oncogenic mutations in proto-oncogenes can be selected for in tumor populations subjected to metabolic stress. Yun et al. (2009) showed that depriving colon carcinoma cells of glucose increased the rate at which activating mutations in Ras grew out. Surviving clones were better able to cope with limited glucose due to their upregulation of the transporter GLUT1. Some clones demonstrated *KRAS* mutations, and mutant KRAS was shown to upregulate GLUT1 expression and confer sensitivity to glycolytic inhibition. Importantly, increased glycolytic metabolism from activated Ras does not stem from defective mitochondrial pathways. Even for Ras-mediated tumorigenesis, the importance of intact mitochondrial oxidative metabolism has been confirmed in vivo (Guo et al., 2011; Weinberg et al., 2010).

Metabolic Enzymes Can Be Alternatively Spliced to Isoforms that Support Anabolic Growth

In addition to activating oncogenes like Ras, preferentially expressing specific isoforms of metabolic enzymes can provide cancer cells with a mechanism to select for metabolic alterations during tumorigenesis. For example, proliferating cells almost universally express the M2 isoform of pyruvate kinase M (PKM2). Pyruvate kinase is a glycolytic enzyme that converts phosphoenolpyruvate (PEP) to pyruvate, with concomitant generation of ATP. In contrast to the M1 isoform of pyruvate kinase (PKM1) that is the predominant isoform in most adult differentiated tissues, the PKM2 splice variant is the major isoform in embryonic tissues and in all cancer cells examined to date (Mazurek, 2011). Other significant genes for proliferative cell metabolism are also alternatively spliced. The phosphofructokinase/fructose-2,6-bisphosphatase B3 gene (*PFKFB3*) is highly expressed in human tumors and has six splice variants. Two splice variants predominate in high-grade astrocytoma and colon carcinoma and enhance glycolytic flux, while other splice variants are limited to low-grade tumors and normal tissues (Bando et al., 2005; Zscharnack et al., 2009). An alternatively spliced isoform of *GLS* may also be important for the mitochondrial glutamine metabolism of tumor cells (Cassago et al., 2012).

The most extensively characterized of these alternatively spliced metabolic enzymes remains pyruvate kinase. The preferential expression of PKM2 in proliferating cells suggested a protumorigenic role for this splice variant, and xenograft models

subsequently demonstrated that PKM2-expressing cells have a growth advantage in vivo compared with PKM1-expressing cells (Christofk et al., 2008a). However, in what might seem paradoxical for an isoform associated with proliferating and highly glycolytic cells, PKM2 has intrinsically lower enzymatic activity than PKM1. PKM2 is also uniquely sensitive to inhibition by tyrosine kinase signaling downstream of growth factor receptors, in contrast to PKM1 which is constitutively active (Christofk et al., 2008b; Hitosugi et al., 2009). Current evidence suggests that the decreased activity of PKM2 is selected to facilitate anabolic metabolism (Figure 4). With less rapid conversion of PEP to pyruvate, the accumulation of upstream glycolytic intermediates and subsequent shunting of these intermediates into anabolic pathways branching off glycolysis can result. These pathways include pyrimidine biosynthesis (Mazurek et al., 2001). They may also include the glycerol synthesis and serine/glycine synthesis pathways.

The Primary Role of PKM2 Expression in Proliferating Cells Is to Facilitate Anabolic Metabolism

Accompanying the resurgence of interest in the metabolic effects of PKM2 have been recent reports on "non-metabolic" functions of PKM2 (Luo et al., 2011; Yang et al., 2011). These studies are the latest variations on a theme from work spanning over a decade that have identified at least 11 proteins that bind to PKM2 (Garcia-Gonzalo et al., 2003; Le Mellay et al., 2002; Mazurek et al., 2001, 2007; Shimada et al., 2008; Siwko and Mochly-Rosen, 2007; Spoden et al., 2009; Williams et al., 1998; Wu et al., 2008; Zwerschke et al., 1999). Several of these are nuclear proteins, suggesting that PKM2 may, under certain conditions, translocate to the nucleus to fulfill nonmetabolic, putatively transcriptional functions (Hoshino et al., 2007; Ignacak and Stachurska, 2003; Lee et al., 2008; Spoden et al., 2008; Steták et al., 2007). However, other studies have added further strength to the concept that reduced pyruvate kinase enzymatic activity in the cytoplasm, leading to enhanced anabolic metabolism from glycolytic intermediates, is the primary role for PKM2 expression in proliferating cells. A recent study showed that in cancer cells, elevation of reactive oxygen species (ROS) can inactivate the active, tetrameric form of the cytosolic PKM2 enzyme (Anastasiou et al., 2011). Another report showed that PKM2 has a unique lysine residue which is acetylated in tumor cells, targeting it for degradation by chaperone-mediated autophagy (Lv et al., 2011). Both of these findings are consistent with PKM2 primarily acting as a glycolytic switch that can be rapidly inactivated in tumor cells by multiple mechanisms, all of which facilitate the shunting of glucose carbon/glycolytic intermediates into branching anabolic pathways.

A major paradox remaining with PKM2 is that cells expressing PKM2 produce more glucose-derived pyruvate than PKM1-expressing cells, despite having a form of the pyruvate kinase enzyme that is less active and more sensitive to inhibition. One way to get around the PKM2 bottleneck and maintain/enhance pyruvate production may be through a proposed alternative glycolytic pathway involving an enzymatic activity not yet purified that dephosphorylates PEP to pyruvate without the generation of ATP (Vander Heiden et al., 2010). Another answer to this paradox may emanate from the serine synthetic pathway. The decreased enzymatic activity of PKM2 can promote the accumulation of the 3-phosphoglycerate glycolytic intermediate that serves as the entry point for the serine synthetic pathway branch off glycolysis. The little-studied enzyme serine dehydratase can then directly convert serine to pyruvate. A third explanation may lie in the oscillatory activity of PKM2 from the inactive dimer to the active tetramer form. Regulatory inputs into PKM2 like tyrosine phosphorylation and ROS destabilize the tetrameric form of PKM2 (Anastasiou et al., 2011; Christofk et al., 2008b; Hitosugi et al., 2009), but other inputs present in glycolytic cancer cells like fructose-1,6-bisphosphate and serine can continually allosterically activate and/or promote reformation of the PKM2 tetramer (Ashizawa et al., 1991; Eigenbrodt et al., 1983). Thus, PKM2 may be continually switching from inactive to active forms in cells, resulting in an apparent upregulation of flux through anabolic glycolytic branching pathways while also maintaining reasonable net flux of glucose carbon through PEP to pyruvate. With such an oscillatory system, small changes in the levels of any of the above-mentioned PKM2 regulatory inputs can cause exquisite, rapid adjustments to glycolytic flux. This would be predicted to be advantageous for proliferating cells in the setting of variable extracellular nutrient availability. The capability for oscillatory regulation of PKM2 could also provide an explanation for why tumor cells do not select for altered glycolytic metabolism

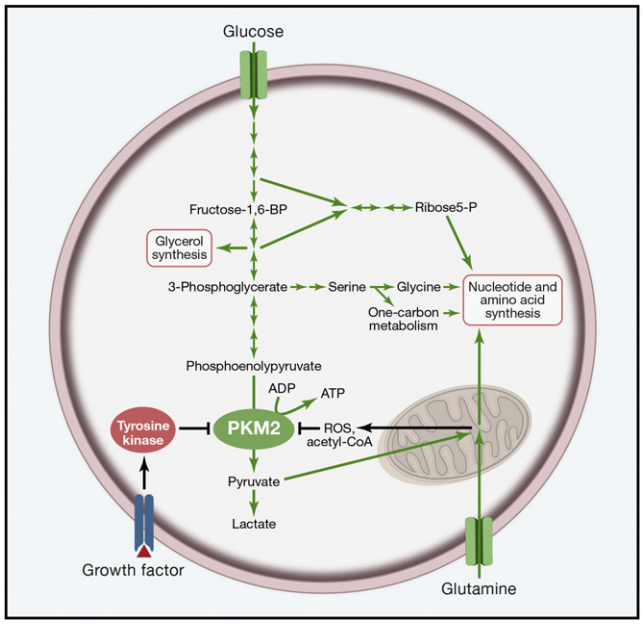

Figure 4. Pyruvate Kinase M2 Expression in Proliferating Cells Is Regulated by Signaling and Mitochondrial Metabolism to Facilitate Macromolecular Synthesis

Pyruvate kinase M2 (PKM2) is a less active isoform of the terminal glycolytic enzyme pyruvate kinase. It is also uniquely inhibited downstream of tyrosine kinase signaling. The decreased enzymatic activity of PKM2 in the cytoplasm promotes the accumulation of upstream glycolytic intermediates and their shunting into anabolic pathways. These pathways include the serine synthetic pathway that contributes to nucleotide and amino acid production. When mitochondrial metabolism is excessive, reactive oxygen species (ROS) from the mitochondria can feed back to inhibit PKM2 activity. Acetylation of PKM2, dependent on acetyl-CoA availability, may also promote PKM2 degradation and further contribute to increased flux through anabolic synthesis pathways branching off glycolysis.

upstream of PKM2 through deletions and/or loss-of-function mutations of other glycolytic enzymes.

Amplification of Metabolic Enzymes in Cancer

In addition to regulation by alternative splicing, the expression of metabolic enzymes may also be regulated by increases in gene copy number in cancer cells. The gene encoding hexokinase II, which catalyzes the first reaction of glycolysis converting glucose to glucose-6-phosphate, is amplified in hepatoma cells (Rempel et al., 1996), and fatty acid synthase has been reported to exhibit copy-number gain in prostate cancer (Shah et al., 2006). More recently, two independent groups have identified amplification of the gene encoding phosphoglycerate dehydrogenase in breast cancer and melanoma, resulting in increased flux through the serine/glycine synthesis pathway (Locasale et al., 2011; Possemato et al., 2011). As described above, the expression of PKM2 may provide an independent mechanism to enhance flux through the serine/glycine synthesis pathway. This enhanced flux may provide multiple metabolic advantages in addition to serine and glycine production. One proposed function is facilitating α-ketoglutarate production for mitochondrial metabolism (Possemato et al., 2011). Additional proposed functions include the generation of precursors for pyrimidine synthesis and the production of sarcosine, a glycine-derived metabolite linked to prostate cancer progression (Sreekumar et al., 2009; Zhang et al., 2012). Other important functions for flux through the serine synthesis pathway are likely.

Oncogenic Mutations in Metabolic Enzymes: The Discovery of IDH1 Mutations and the Oncometabolite 2-Hydroxyglutarate

While the preference for all tumor cells to express PKM2 versus PKM1 is striking and likely selected for to facilitate anabolic metabolism, PKM2 is present in most proliferating cells and is not specific to cancer (Mazurek, 2011). The strongest evidence to date that altered metabolism is selected for by cancer cells during tumorigenesis has come with the recent elucidation of somatic mutations in metabolic enzymes. Mutations in the cytosolic $NADP^+$-dependent isocitrate dehydrogenase 1 gene (*IDH1*) were first found to be recurrent in glioma and acute myeloid leukemia (AML) through whole-genome sequencing (Mardis et al., 2009; Parsons et al., 2008). The initially described mutations were remarkably selective for a specific arginine residue in the enzyme active site, R132. All mutations were missense, and all mutations were heterozygous with retention of the remaining wild-type *IDH1* allele. These characteristics suggested that the mutants acquired an altered function. Yet this contrasted with initial data demonstrating that the tumor-specific mutations in IDH1 and IDH2 resulted in loss of their normal enzymatic activity to interconvert isocitrate and α-ketoglutarate (Yan et al., 2009). The heterozygous nature of the mutations was then explained away with the report that IDH1 mutants can dominantly inhibit the wild-type IDH1 in cells (Zhao et al., 2009).

An alternative explanation came with the report that IDH1 mutations at R132 are not simply loss-of-function mutations for isocitrate and α-ketoglutarate interconversion, but also acquire a novel reductive activity to convert α-ketoglutarate to 2-hydroxyglutarate (2HG), a rare metabolite found only in trace amounts in mammalian cells under normal conditions (Dang et al., 2009). However, it still remained unclear whether 2HG was truly a pathogenic "oncometabolite" resulting from IDH1 mutation or was just the byproduct of a loss-of-function mutation. Whether 2HG production or the loss of IDH1 normal function played a more important role in tumorigenesis remained uncertain.

2HG Is a Biomarker and Common Feature of Both IDH1 and IDH2 Mutations

A potential answer to whether 2HG production was relevant to tumorigenesis arrived with the study of mutations in IDH2, the mitochondrial homolog of IDH1. Up to this point a small fraction of gliomas lacking IDH1 mutations were known to harbor mutations at IDH2 R172, the analogous residue to IDH1 R132 (Yan et al., 2009). However, given the rarity of these IDH2 mutations, they had not been characterized for 2HG production. The discovery of IDH2 R172 mutations in AML as well as glioma samples prompted the study of whether these mutations also conferred the reductive enzymatic activity to produce 2HG. Enzymatic assays and measurement of 2HG levels in primary AML samples confirmed that these IDH2 R172 mutations result in 2HG elevation (Gross et al., 2010; Ward et al., 2010).

It was then investigated whether the measurement of 2HG levels in primary tumor samples with unknown *IDH* mutation status could serve as a metabolite screening test for both cytosolic IDH1 and mitochondrial IDH2 mutations. AML samples with low to undetectable 2HG were subsequently sequenced and determined to be IDH1 and IDH2 wild-types, and several samples with elevated 2HG were found to have neomorphic mutations at either IDH1 R132 or IDH2 R172 (Gross et al., 2010). However, some 2HG-elevated AML samples lacked IDH1 R132 or IDH2 R172 mutations. When more comprehensive sequencing of *IDH1* and *IDH2* was performed, it was found that the common feature of this remaining subset of 2HG-elevated AMLs was another mutation in IDH2, occurring at R140 (Ward et al., 2010). This discovery provided additional evidence that 2HG production was the primary feature being selected for in tumors.

In addition to intensifying efforts to find the cellular targets of 2HG, the discovery of the 2HG-producing IDH1 and IDH2 mutations suggested that 2HG measurement might have clinical utility in diagnosis and disease monitoring. While much work is still needed in this area, serum 2HG levels have successfully correlated with IDH1 R132 mutations in AML, and recent data have suggested that ^{1}H magnetic resonance spectroscopy can be applied for 2HG detection in vivo for glioma (Andronesi et al., 2012; Choi et al., 2012; Gross et al., 2010; Pope et al., 2012). These methods may have advantages over relying on invasive-solid-tumor biopsies or isolating leukemic blast cells to obtain material for sequencing of *IDH1* and *IDH2*. Screening tumors and body fluids by 2HG status also has potentially increased applicability given the recent report that additional IDH mutations can produce 2HG (Ward et al., 2011). These additional alleles may account for the recently described subset of 2HG-elevated chondrosarcoma samples that lacked the most common *IDH1* or *IDH2* mutations but were not examined for other IDH alterations (Amary et al., 2011). Metabolite screening approaches can also distinguish neomorphic IDH mutations from SNPs and sequencing artifacts with no effect on IDH

enzyme activity, as well as from an apparently rare subset of loss-of-function, non-2HG-producing IDH mutations that may play a secondary tumorigenic role in altering cellular redox (Ward et al., 2011).

Metabolites as Oncogenes: Dysregulating Epigenetics and Cellular Differentiation

Consideration of the tumor subtypes where IDH mutations were most prevalent, the finding that IDH mutations occurred early in disease progression (Watanabe et al., 2009), and the lack of evidence that 2HG was acting as a mutagen (Mardis et al., 2009) led to investigation of whether 2HG accumulation might lead to impairment in cellular differentiation. Evidence in support of this hypothesis was first provided in 32D myeloid cells and in mouse primary bone marrow cells cultured ex vivo. In both cell types, the overexpression of IDH mutants blocked acquisition of mature myeloid markers while increasing the expression of stem-cell markers (Figueroa et al., 2010).

How could a small organic acid, 2HG, mediate such an effect? Numerous reports have now highlighted the ability of 2HG to inhibit several α-ketoglutarate-dependent dioxygenase enzymes (Figure 5). Contradictory claims exist regarding the ability of 2HG to inhibit the prolyl hydroxylase that targets HIF-1 for degradation (PHD2) to modulate HIF levels in cells. Several independent groups have failed to observe a direct link between 2HG and PHD2 inhibition. The weight of the evidence now suggests that regulation of HIF-1 stability through decreased PHD2 activity is not the primary effect of IDH mutations (Chowdhury et al., 2011; Dang et al., 2009; Jin et al., 2011; Mardis et al., 2009; Metellus et al., 2011; Williams et al., 2011). In contrast, multiple groups have found that IDH mutant expression and 2HG elevation can inhibit the TET family of enzymes that hydroxylate 5′-methylcytosine (Figueroa et al., 2010; Turcan et al., 2012; Xu et al., 2011). α-ketoglutarate-dependent TET activity produces 5′-hydroxymethylcytosine. This product can be an intermediate in either passive or active DNA demethylation through pathways that are still under active investigation. The biological relevance of TET inhibition by 2HG has strong genetic evidence: neomorphic mutations of *IDH1* or *IDH2* and *TET2* loss-of-function mutations were found to be mutually exclusive in a large AML cohort. Moreover, *TET2* mutant AML samples displayed an overlapping DNA hypermethylation signature with samples having *IDH1* or *IDH2* mutations, and shRNA knockdown of TET2 recapitulated the effect of IDH mutant overexpression on blocking hematopoietic cell differentiation (Figueroa et al., 2010).

The Oncometabolite 2HG Does More than Inhibit TET Activity and DNA Demethylation

Similar to hematologic malignancies, in gliomas and chondrosarcomas *IDH1* or *IDH2* mutations have been linked with altered DNA methylation profiles (Noushmehr et al., 2010; Pansuriya et al., 2011; Turcan et al., 2012). However, in gliomas and chondrosarcomas, there is no evidence of mutations in TET enzymes. This could potentially be due to the fact that redundant TET enzymes are expressed in glial and chondrosarcoma precursor cells, making it difficult to inactivate TET family function by mutation in such cells. Alternatively, other chromatin-modifying α-ketoglutarate-dependent dioxygenase enzymes may be inhibited by 2HG in these cells. Although one initial report implicated a broad array of enzymes that were affected by 2HG (Xu et al., 2011), a later report suggested greater specificity of 2HG for some specific Jumonji C domain histone demethylases (Chowdhury et al., 2011). Most recently, it has been reported that the mark most altered with stable, as opposed to transient, expression of IDH mutation is methylation at histone H3 lysine 9 (H3K9) (Lu et al., 2012). By studying the differentiation of 3T3-L1 fibroblasts into mature adipocytes, this study found that inhibition of H3K9 demethylation by 2HG, or siRNA knockdown of an H3K9 demethylase, was sufficient to block cell differentiation in the absence of changes in DNA methylation. This study also examined the effect of IDH mutation in immortalized astrocytes and found that a progressive accumulation of H3K9 methylation preceded the increase in DNA methylation. The

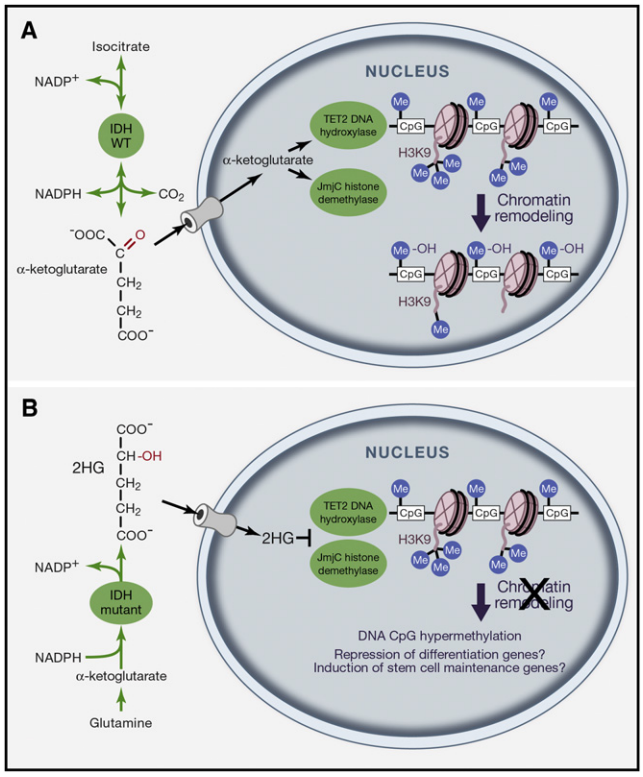

Figure 5. IDH1 and IDH2 Mutants Convert Glutamine Carbon to the Oncometabolite 2-Hydroxyglutarate to Dysregulate Epigenetics and Cell Differentiation

(A) α-ketoglutarate, produced in part by wild-type isocitrate dehydrogenase (IDH), can enter the nucleus and be used as a substrate for dioxygenase enzymes that modify epigenetic marks. These enzymes include the TET2 DNA hydroxylase enzyme, which converts 5-methylcytosine to 5-hydroxymethylcytosine, typically at CpG dinucleotides. 5-hydroxymethylcytosine may be an intermediate in either active or passive DNA demethylation. α-ketoglutarate is also a substrate for JmjC domain histone demethylase enzymes that demethylate lysine residues on histone tails.

(B) The common feature of cancer-associated mutations in cytosolic IDH1 and mitochondrial IDH2 is the acquisition of a neomorphic enzymatic activity. This activity converts glutamine-derived α-ketoglutarate to the oncometabolite 2HG. 2HG can competitively inhibit α-ketoglutarate-dependent enzymes like TET2 and the JmjC histone demethylases, thereby impairing normal epigenetic regulation. This results in altered histone methylation marks, in some cases DNA hypermethylation at CpG islands, and dysregulated cellular differentiation.

2HG-induced alterations in histone and DNA methylation are likely synergistic, and the precise relationship between these marks is the focus of continued investigation. For now, these findings provide further evidence that IDH mutation can impair differentiation in nontransformed cells from multiple cells of origin, and that this impairment is linked to 2HG-mediated epigenetic dysregulation.

Non-cell-autonomous effects of 2HG may also be important in some tumors. 2HG can inhibit the prolyl hydroxylase that regulates collagen synthesis (Xu et al., 2011). This inhibition could impact the tumor microenvironment and partly account for the diffuse nature of lower-grade gliomas. However, determination of whether this and other effects of 2HG are ultimately important for tumorigenesis will require careful future studies.

2HG Is Not the Only Oncometabolite

Will we find other novel oncometabolites like 2HG? We should consider basing the search for new oncometabolites on those metabolites already known to cause disease in pediatric inborn errors of metabolism (IEMs). 2HG exemplifies how advances in research on IEMs can inform research on cancer metabolism, and vice versa. Methods developed by those studying 2HG aciduria were used to demonstrate that *R*(−)-2HG (also known as D-2HG) is the exclusive 2HG stereoisomer produced by IDH1 and IDH2 mutants (Dang et al., 2009; Ward et al., 2010). Likewise, following the discovery of 2HG-producing *IDH2 R140* mutations in leukemia, researchers looked for and successfully found germline *IDH2 R140* mutations in D-2HG aciduria. *IDH2 R140* mutations now account for nearly half of all cases of this devastating disease (Kranendijk et al., 2010). While interest has surrounded 2HG due to its apparent novelty as a metabolite not found in normal nondiseased cells, there are situations where 2HG appears in the absence of metabolic enzyme mutations. For example, in human cells proliferating in hypoxia, α-ketoglutarate can accumulate and be metabolized through an enhanced reductive activity of wild-type IDH2 in the mitochondria, leading to 2HG accumulation in the absence of IDH mutation (Wise et al., 2011). The ability of 2HG to alter epigenetics may reflect its evolutionary ancient status as a signal for elevated glutamine/glutamate metabolism and/or oxygen deficiency.

With this broadened view of what constitutes an oncometabolite, one could argue that the discoveries of two other oncometabolites, succinate and fumarate, preceded that of 2HG. Loss-of-function mutations in the TCA cycle enzymes succinate dehydrogenase (SDH) and fumarate hydratase (FH) have been known for several years to occur in pheochromocytoma, paraganglioma, leiomyoma, and renal carcinoma. It was initially hypothesized that these mutations contribute to cancer through mitochondrial damage producing elevated ROS (Eng et al., 2003). However, potential tumorigenic effects were soon linked to the elevated levels of succinate and fumarate arising from loss of SDH function and FH function, respectively. Succinate was initially found to impair PHD2, the α-ketoglutarate-dependent enzyme regulating HIF stability, through product inhibition (Selak et al., 2005). Subsequent work confirmed that fumarate could inhibit PHD2 (Isaacs et al., 2005) and that succinate could also inhibit the related enzyme PHD3 (Lee et al., 2005). These observations linked the elevated HIF levels observed in SDH- and FH-deficient tumors to the activity of the succinate and fumarate metabolites. Recent work has suggested that fumarate may have other important roles that predominate in FH deficiency. For example, fumarate can modify cysteine residues to inhibit a negative regulator of the Nrf2 transcription factor. This posttranslational modification leads to the upregulation of antioxidant response genes (Adam et al., 2011; Ooi et al., 2011).

There are still many unanswered questions regarding the biology of SDH- and FH-deficient tumors. In light of the emerging epigenetic effects of 2HG, it is intriguing that succinate has been shown to alter histone demethylase activity in yeast (Smith et al., 2007). Perhaps elevated succinate and fumarate resulting from SDH and FH mutations can promote tumorigenesis in part through epigenetic modulation.

Textbook Biochemical Pathways Often Do Not Apply to Proliferating Cells

What has received little appreciation since the work of Krebs and his colleagues is that for many proliferating cells, the major problem is not how to maximize ATP yield, but rather how to maximize the flux of carbon into macromolecular synthetic pathways. In fact, it was first demonstrated in 1973 that glycolysis in proliferating cells is limited by the rate of ATP consumption and not ATP production, as glycolytic enzymes can be inhibited when ATP levels are high (Scholnick et al., 1973). Recent work has revisited how proliferating cells maintain glycolytic flux by either minimizing ATP production or enhancing ATP consumption. The proposed alternative glycolytic pathway to get around the PKM2 bottleneck may be one way to accomplish this (Vander Heiden et al., 2010). In this alternative pathway, the high-energy phosphate of PEP is transferred not to ADP but instead to a histidine residue on an upstream glycolytic enzyme. This alternative transfer therefore decouples the PEP→pyruvate conversion from ATP production. Another study found that cells with activated PI3K/Akt upregulate the activity of ENTPD5, an endoplasmic reticulum enzyme involved in glycosylation reactions and linked to ATP hydrolysis (Fang et al., 2010).

One pathway that supports cell proliferation and is not found in most textbooks is the ability of TCA-cycle enzymes to facilitate reductive carboxylation rather than oxidative metabolism. While this may seem heretical, IDH-dependent reductive carboxylation of α-ketoglutarate to isocitrate was described in early metabolic literature (Ochoa, 1948) and has been investigated since then as a way to produce citrate and fatty acids from α-ketoglutarate derived from glutamine (Holleran et al., 1995; Ward et al., 2010; Yoo et al., 2008). Recently, three independent reports implicated IDH-dependent reductive carboxylation as playing a particularly important role in proliferating cells that exhibit decreased flux of glucose-derived pyruvate into the mitochondria. This occurs in hypoxic cells or in cells harboring defects in mitochondrial oxidative phosphorylation (Metallo et al., 2012; Mullen et al., 2012; Wise et al., 2011). There are conflicting conclusions over whether the reductive flux of glutamine-derived carbon is primarily dependent upon cytosolic IDH1 or mitochondrial IDH2. These findings could all be correct if a mitochondrial-cytosolic NADPH shuttle exists using these enzymes (Figure 6). Although NADPH mitochondrial-cytosolic shuttles have not been previously described, it would allow high-energy electrons from NADPH in one compartment to be donated to α-ketoglutarate through reductive carboxylation and then transported to the other compartment

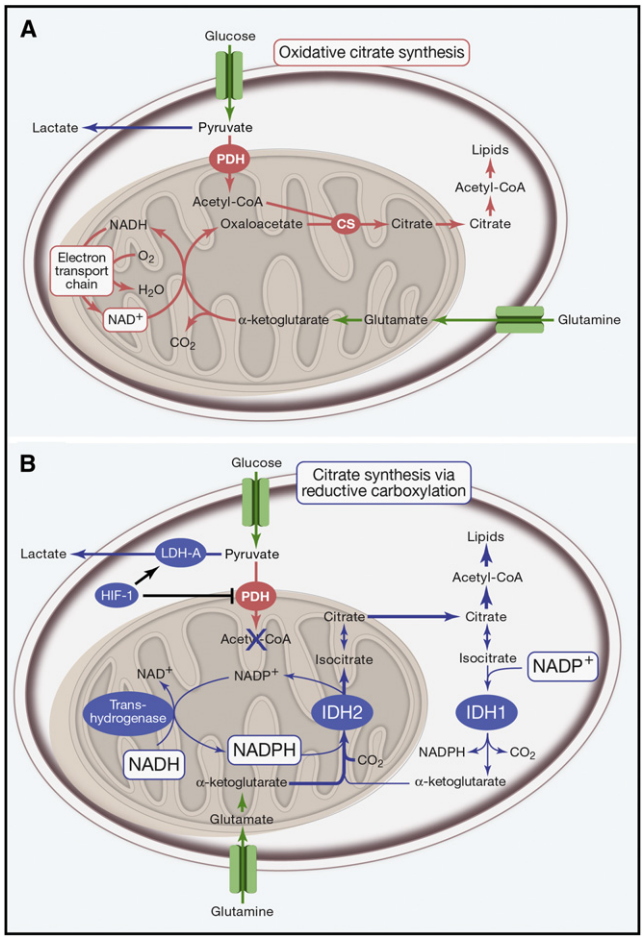

Figure 6. Hypoxia and HIF-1 Activation Promote an Alternative Pathway for Citrate Synthesis through Reductive Metabolism of Glutamine

(A) In proliferating cells under normoxic conditions, citrate is synthesized from both glucose and glutamine. Glucose carbon provides acetyl-CoA through the activity of PDH. Glutamine carbon provides oxaloacetate through oxidative mitochondrial metabolism dependent on NAD^+. Glucose-derived acetyl-CoA and glutamine-derived oxaloacetate condense to form citrate via the activity of citrate synthase (CS). Citrate can be exported to the cytosol for lipid synthesis. (B) In cells proliferating in hypoxia and/or with HIF-1 activation, glucose is diverted away from mitochondrial acetyl-CoA and citrate production. Citrate can be maintained through an alternative pathway of reductive carboxylation, which we propose to rely on reverse flux of glutamine-derived α-ketoglutarate through IDH2. This reverse flux in the mitochondria would promote electron export from the mitochondria when the activity of the electron transport chain is inhibited because of the lack of oxygen as an electron acceptor. Mitochondrial reverse flux can be accomplished by NADH conversion to NADPH by mitochondrial transhydrogenase and the resulting NADPH use in α-ketoglutarate carboxylation. When citrate/isocitrate is exported to the cytosol, some may be metabolized in the oxidative direction by IDH1 and contribute to a shuttle that produces cytosolic NADPH.

in the form of isocitrate/citrate for oxidation and regeneration of α-ketoglutarate and NADPH. Further work is needed to test this concept, but knowledge regarding cellular redox suggests the reductive flux is likely to occur in the mitochondria. Mitochondria have a high NADH:NAD^+ ratio, particularly in hypoxia (Chance and Thorell, 1959; Frezza et al., 2011), and NADH can be converted to NADPH within the mitochondria via a transhydrogenase that is absent from the cytosol (Rydström, 2006).

Unlike ATP, cytosolic NADPH might be limiting for cell proliferation. It is critical for providing reducing equivalents for fatty acid and cholesterol biosynthesis, as well as for modulating oxidative stress. Historically, the oxidative pentose phosphate pathway, branching off glycolysis at glucose-6-phosphate dehydrogenase (G6PD), has been considered the major NADPH-producing pathway. However, we offer that the repeated human experiment should be considered: millions of men are affected by the X-linked disorder of G6PD deficiency, yet cohort studies have not detected a decrease in cancer incidence in G6PD-deficient men (Cocco et al., 1998; Ferraris et al., 1988), and smaller case control studies have also failed to demonstrate a relationship (Forteleoni et al., 1988; Pisano et al., 1991). These studies focused on men with the Mediterranean variant of *G6PD*, an allele demonstrating severe enzyme deficiency with less than 10% of normal activity. The relationship between other disease-associated G6PD variants and cancer has not been rigorously tested. Notably, Ferraris et al. also examined females with mosaicism for the Mediterranean variant of *G6PD* (due to random X inactivation) who developed clonal hematological disorders. Neoplastic clones did not demonstrate preferential expression of the wild-type G6PD allele. Collectively, these data raise the possibility that significant flux through G6PD to generate NADPH is not necessarily critical for cell proliferation or tumorigenesis. While this hypothesis deserves further study, it would account for the observed propensity of tumor cells to synthesize pentose phosphates through a G6PD-independent pathway (Boros et al., 2000; Zhao et al., 2010). It would also fit with the importance of glucose carbon being metabolized through other branches of glycolytic metabolism, including serine synthesis (as discussed above) and the hexosamine pathway (Wellen et al., 2010). However, exactly which alternative NADPH-generating pathways are most important remain unclear. Further work in this area would benefit from improved methods for measuring NADPH.

Challenges Ahead for Studying the Metabolic Hallmarks of Cancer

Despite rapid technological advances in studying cell metabolism, we remain unable to reliably distinguish cytosolic metabolites from those in the mitochondria and other compartments. Current fractionation methods often lead to metabolite leakage. Even within one subcellular compartment, there may be distinct pools of metabolites resulting from channeling between metabolic enzymes. A related challenge lies in the quantitative measurement of metabolic flux, i.e., measuring the movement of carbon, nitrogen, and other atoms through metabolic pathways rather than simply measuring the steady-state levels of individual metabolites. While critical fluxes have been quantified in cultured cancer cells, and methods for these analyses continue to improve (DeBerardinis et al., 2007; Mancuso et al., 2004; Yuan et al., 2008), many obstacles remain, such as cellular compartmentalization and the reliance of most cell culture on complex, incompletely defined media.

Non-cell-autonomous effects of tumor metabolism represent another emerging challenge. For example, lactate produced by tumor cells can acidify the surrounding microenvironment and potentially promote tumor invasion, and some tumors may exhibit a symbiosis between lactate-producing cells and

lactate-consuming cells (Sonveaux et al., 2008). In addition, fatty acid exchange between omental adipocytes and ovarian carcinoma cells has been documented (Nieman et al., 2011). These areas appear ripe for further study.

Over the past decade, the study of metabolism has returned to its rightful place at the forefront of cancer research. Although Warburg was wrong about mitochondria, he was prescient in his focus on metabolism. Data now support the concepts that altered metabolism results from active reprogramming by altered oncogenes and tumor suppressors, and that metabolic adaptations can be clonally selected during tumorigenesis. Altered metabolism should now be considered a core hallmark of cancer. There is much work to be done.

ACKNOWLEDGMENTS

We thank members of the Thompson Laboratory, particularly Chao Lu and Lydia Finley, and Anthony Mancuso for helpful discussions. The Thompson Laboratory is supported in part by grants from the NCI and NIH. P.S.W. is also supported in part by the University of Pennsylvania Medical Scientist Training Program. C.B.T. has multiple patent applications relevant to the issues discussed in this review. These patent applications are assigned to the University of Pennsylvania. C.B.T. is a co-founder of Agios Pharmaceuticals and a member of the board of directors of Merck.

REFERENCES

Adam, J., Hatipoglu, E., O'Flaherty, L., Ternette, N., Sahgal, N., Lockstone, H., Baban, D., Nye, E., Stamp, G.W., Wolhuter, K., et al. (2011). Cancer Cell *20*, 524–537.

Amary, M.F., Damato, S., Halai, D., Eskandarpour, M., Berisha, F., Bonar, F., McCarthy, S., Fantin, V.R., Straley, K.S., Lobo, S., et al. (2011). Nat. Genet. *43*, 1262–1265.

Anastasiou, D., Poulogiannis, G., Asara, J.M., Boxer, M.B., Jiang, J.K., Shen, M., Bellinger, G., Sasaki, A.T., Locasale, J.W., Auld, D.S., et al. (2011). Science *334*, 1278–1283.

Andronesi, O.C., Kim, G.S., Gerstner, E., Batchelor, T., Tzika, A.A., Fantin, V.R., Vander Heiden, M.G., and Sorensen, A.G. (2012). Sci. Transl. Med. *4*, 116ra4.

Ashizawa, K., Willingham, M.C., Liang, C.M., and Cheng, S.Y. (1991). J. Biol. Chem. *266*, 16842–16846.

Assaily, W., Rubinger, D.A., Wheaton, K., Lin, Y., Ma, W., Xuan, W., Brown-Endres, L., Tsuchihara, K., Mak, T.W., and Benchimol, S. (2011). Mol. Cell *44*, 491–501.

Bando, H., Atsumi, T., Nishio, T., Niwa, H., Mishima, S., Shimizu, C., Yoshioka, N., Bucala, R., and Koike, T. (2005). Clin. Cancer Res. *11*, 5784–5792.

Bauer, D.E., Harris, M.H., Plas, D.R., Lum, J.J., Hammerman, P.S., Rathmell, J.C., Riley, J.L., and Thompson, C.B. (2004). FASEB J. *18*, 1303–1305.

Bauer, D.E., Hatzivassiliou, G., Zhao, F., Andreadis, C., and Thompson, C.B. (2005). Oncogene *24*, 6314–6322.

Bensaad, K., Tsuruta, A., Selak, M.A., Vidal, M.N., Nakano, K., Bartrons, R., Gottlieb, E., and Vousden, K.H. (2006). Cell *126*, 107–120.

Bentzinger, C.F., Romanino, K., Cloëtta, D., Lin, S., Mascarenhas, J.B., Oliveri, F., Xia, J., Casanova, E., Costa, C.F., Brink, M., et al. (2008). Cell Metab. *8*, 411–424.

Berwick, D.C., Hers, I., Heesom, K.J., Moule, S.K., and Tavare, J.M. (2002). J. Biol. Chem. *277*, 33895–33900.

Boer, V.M., Crutchfield, C.A., Bradley, P.H., Botstein, D., and Rabinowitz, J.D. (2010). Mol. Biol. Cell *21*, 198–211.

Boros, L.G., Torday, J.S., Lim, S., Bassilian, S., Cascante, M., and Lee, W.N. (2000). Cancer Res. *60*, 1183–1185.

Buzzai, M., Bauer, D.E., Jones, R.G., Deberardinis, R.J., Hatzivassiliou, G., Elstrom, R.L., and Thompson, C.B. (2005). Oncogene *24*, 4165–4173.

Buzzai, M., Jones, R.G., Amaravadi, R.K., Lum, J.J., DeBerardinis, R.J., Zhao, F., Viollet, B., and Thompson, C.B. (2007). Cancer Res. *67*, 6745–6752.

Cassago, A., Ferreira, A.P., Ferreira, I.M., Fornezari, C., Gomes, E.R., Greene, K.S., Pereira, H.M., Garratt, R.C., Dias, S.M., and Ambrosio, A.L. (2012). Proc. Natl. Acad. Sci. USA *109*, 1092–1097.

Chance, B., and Thorell, B. (1959). J. Biol. Chem. *234*, 3044–3050.

Choi, C., Ganji, S.K., Deberardinis, R.J., Hatanpaa, K.J., Rakheja, D., Kovacs, Z., Yang, X.L., Mashimo, T., Raisanen, J.M., Marin-Valencia, I., et al. (2012). Nat Med. Published online January 26, 2012. 10.1038/nm.2682.

Chowdhury, R., Yeoh, K.K., Tian, Y.M., Hillringhaus, L., Bagg, E.A., Rose, N.R., Leung, I.K., Li, X.S., Woon, E.C., Yang, M., et al. (2011). EMBO Rep. *12*, 463–469.

Christofk, H.R., Vander Heiden, M.G., Harris, M.H., Ramanathan, A., Gerszten, R.E., Wei, R., Fleming, M.D., Schreiber, S.L., and Cantley, L.C. (2008a). Nature *452*, 230–233.

Christofk, H.R., Vander Heiden, M.G., Wu, N., Asara, J.M., and Cantley, L.C. (2008b). Nature *452*, 181–186.

Clarkson, B., Krakoff, I., Burchenal, J., Karnofsky, D., Golbey, R., Dowling, M., Oettgen, H., and Lipton, A. (1970). Cancer *25*, 279–305.

Cocco, P., Todde, P., Fornera, S., Manca, M.B., Manca, P., and Sias, A.R. (1998). Blood *91*, 706–709.

Conlon, I., and Raff, M. (2003). J. Biol. *2*, 7.

Cunningham, J.T., Rodgers, J.T., Arlow, D.H., Vazquez, F., Mootha, V.K., and Puigserver, P. (2007). Nature *450*, 736–740.

Dang, L., White, D.W., Gross, S., Bennett, B.D., Bittinger, M.A., Driggers, E.M., Fantin, V.R., Jang, H.G., Jin, S., Keenan, M.C., et al. (2009). Nature *462*, 739–744.

Deberardinis, R.J., Lum, J.J., and Thompson, C.B. (2006). J. Biol. Chem. *281*, 37372–37380.

DeBerardinis, R.J., Mancuso, A., Daikhin, E., Nissim, I., Yudkoff, M., Wehrli, S., and Thompson, C.B. (2007). Proc. Natl. Acad. Sci. USA *104*, 19345–19350.

Deprez, J., Vertommen, D., Alessi, D.R., Hue, L., and Rider, M.H. (1997). J. Biol. Chem. *272*, 17269–17275.

Düvel, K., Yecies, J.L., Menon, S., Raman, P., Lipovsky, A.I., Souza, A.L., Triantafellow, E., Ma, Q., Gorski, R., Cleaver, S., et al. (2010). Mol. Cell *39*, 171–183.

Eigenbrodt, E., Leib, S., Krämer, W., Friis, R.R., and Schoner, W. (1983). Biomed. Biochim. Acta *42*, S278–S282.

El-Mir, M.Y., Nogueira, V., Fontaine, E., Avéret, N., Rigoulet, M., and Leverve, X. (2000). J. Biol. Chem. *275*, 223–228.

Elstrom, R.L., Bauer, D.E., Buzzai, M., Karnauskas, R., Harris, M.H., Plas, D.R., Zhuang, H., Cinalli, R.M., Alavi, A., Rudin, C.M., and Thompson, C.B. (2004). Cancer Res. *64*, 3892–3899.

Eng, C., Kiuru, M., Fernandez, M.J., and Aaltonen, L.A. (2003). Nat. Rev. Cancer *3*, 193–202.

Fan, Y., Dickman, K.G., and Zong, W.X. (2010). J. Biol. Chem. *285*, 7324–7333.

Fang, M., Shen, Z., Huang, S., Zhao, L., Chen, S., Mak, T.W., and Wang, X. (2010). Cell *143*, 711–724.

Fantes, P., and Nurse, P. (1977). Exp. Cell Res. *107*, 377–386.

Ferraris, A.M., Broccia, G., Meloni, T., Forteleoni, G., and Gaetani, G.F. (1988). Am. J. Hum. Genet. *42*, 516–520.

Figueroa, M.E., Abdel-Wahab, O., Lu, C., Ward, P.S., Patel, J., Shih, A., Li, Y., Bhagwat, N., Vasanthakumar, A., Fernandez, H.F., et al. (2010). Cancer Cell *18*, 553–567.

Forteleoni, G., Argiolas, L., Farris, A., Ferraris, A.M., Gaetani, G.F., and Meloni, T. (1988). Tumori *74*, 665–667.

Frezza, C., Zheng, L., Tennant, D.A., Papkovsky, D.B., Hedley, B.A., Kalna, G., Watson, D.G., and Gottlieb, E. (2011). PLoS ONE *6*, e24411.

Gao, P., Tchernyshyov, I., Chang, T.C., Lee, Y.S., Kita, K., Ochi, T., Zeller, K.I., De Marzo, A.M., Van Eyk, J.E., Mendell, J.T., and Dang, C.V. (2009). Nature *458*, 762–765.

Garcia-Gonzalo, F.R., Cruz, C., Muñoz, P., Mazurek, S., Eigenbrodt, E., Ventura, F., Bartrons, R., and Rosa, J.L. (2003). FEBS Lett. *539*, 78–84.

Gottlob, K., Majewski, N., Kennedy, S., Kandel, E., Robey, R.B., and Hay, N. (2001). Genes Dev. *15*, 1406–1418.

Gross, S., Cairns, R.A., Minden, M.D., Driggers, E.M., Bittinger, M.A., Jang, H.G., Sasaki, M., Jin, S., Schenkein, D.P., Su, S.M., et al. (2010). J. Exp. Med. *207*, 339–344.

Guo, J.Y., Chen, H.Y., Mathew, R., Fan, J., Strohecker, A.M., Karsli-Uzunbas, G., Kamphorst, J.J., Chen, G., Lemons, J.M., Karantza, V., et al. (2011). Genes Dev. *25*, 460–470.

Hanahan, D., and Weinberg, R.A. (2011). Cell *144*, 646–674.

Hatzivassiliou, G., Zhao, F., Bauer, D.E., Andreadis, C., Shaw, A.N., Dhanak, D., Hingorani, S.R., Tuveson, D.A., and Thompson, C.B. (2005). Cancer Cell *8*, 311–321.

Hitosugi, T., Kang, S., Vander Heiden, M.G., Chung, T.W., Elf, S., Lythgoe, K., Dong, S., Lonial, S., Wang, X., Chen, G.Z., et al. (2009). Sci. Signal. *2*, ra73.

Holleran, A.L., Briscoe, D.A., Fiskum, G., and Kelleher, J.K. (1995). Mol. Cell. Biochem. *152*, 95–101.

Hoshino, A., Hirst, J.A., and Fujii, H. (2007). J. Biol. Chem. *282*, 17706–17711.

Ignacak, J., and Stachurska, M.B. (2003). Comp. Biochem. Physiol. B Biochem. Mol. Biol. *134*, 425–433.

Isaacs, J.S., Jung, Y.J., Mole, D.R., Lee, S., Torres-Cabala, C., Chung, Y.L., Merino, M., Trepel, J., Zbar, B., Toro, J., et al. (2005). Cancer Cell *8*, 143–153.

Jin, G., Reitman, Z.J., Spasojevic, I., Batinic-Haberle, I., Yang, J., Schmidt-Kittler, O., Bigner, D.D., and Yan, H. (2011). PLoS ONE *6*, e16812.

Jones, R.G., Plas, D.R., Kubek, S., Buzzai, M., Mu, J., Xu, Y., Birnbaum, M.J., and Thompson, C.B. (2005). Mol. Cell *18*, 283–293.

Kim, J.W., Tchernyshyov, I., Semenza, G.L., and Dang, C.V. (2006). Cell Metab. *3*, 177–185.

Kohn, A.D., Summers, S.A., Birnbaum, M.J., and Roth, R.A. (1996). J. Biol. Chem. *271*, 31372–31378.

Kondoh, H., Lleonart, M.E., Gil, J., Wang, J., Degan, P., Peters, G., Martinez, D., Carnero, A., and Beach, D. (2005). Cancer Res. *65*, 177–185.

Koppenol, W.H., Bounds, P.L., and Dang, C.V. (2011). Nat. Rev. Cancer *11*, 325–337.

Kranendijk, M., Struys, E.A., van Schaftingen, E., Gibson, K.M., Kanhai, W.A., van der Knaap, M.S., Amiel, J., Buist, N.R., Das, A.M., de Klerk, J.B., et al. (2010). Science *330*, 336.

Le, A., Lane, A.N., Hamaker, M., Bose, S., Gouw, A., Barbi, J., Tsukamoto, T., Rojas, C.J., Slusher, B.S., Zhang, H., et al. (2012). Cell Metab. *15*, 110–121.

Le Mellay, V., Houben, R., Troppmair, J., Hagemann, C., Mazurek, S., Frey, U., Beigel, J., Weber, C., Benz, R., Eigenbrodt, E., and Rapp, U.R. (2002). Adv. Enzyme Regul. *42*, 317–332.

Lee, J., Kim, H.K., Han, Y.M., and Kim, J. (2008). Int. J. Biochem. Cell Biol. *40*, 1043–1054.

Lee, S., Nakamura, E., Yang, H., Wei, W., Linggi, M.S., Sajan, M.P., Farese, R.V., Freeman, R.S., Carter, B.D., Kaelin, W.G., Jr., and Schlisio, S. (2005). Cancer Cell *8*, 155–167.

Li, F., Wang, Y., Zeller, K.I., Potter, J.J., Wonsey, D.R., O'Donnell, K.A., Kim, J.W., Yustein, J.T., Lee, L.A., and Dang, C.V. (2005). Mol. Cell. Biol. *25*, 6225–6234.

Linn, T.C., Pettit, F.H., and Reed, L.J. (1969). Proc. Natl. Acad. Sci. USA *62*, 234–241.

Locasale, J.W., Grassian, A.R., Melman, T., Lyssiotis, C.A., Mattaini, K.R., Bass, A.J., Heffron, G., Metallo, C.M., Muranen, T., Sharfi, H., et al. (2011). Nat. Genet. *43*, 869–874.

Lu, C., Ward, P.S., Kapoor, G.S., Rohle, D., Turcan, S., Abdel-Wahab, O., Edwards, C., Khanin, R., Figueroa, M.E., Melnick, A., et al. (2012). Nature. Published online February 15, 2012. 10.1038/nature10860.

Lum, J.J., Bauer, D.E., Kong, M., Harris, M.H., Li, C., Lindsten, T., and Thompson, C.B. (2005). Cell *120*, 237–248.

Lum, J.J., Bui, T., Gruber, M., Gordan, J.D., DeBerardinis, R.J., Covello, K.L., Simon, M.C., and Thompson, C.B. (2007). Genes Dev. *21*, 1037–1049.

Luo, W., Hu, H., Chang, R., Zhong, J., Knabel, M., O'Meally, R., Cole, R.N., Pandey, A., and Semenza, G.L. (2011). Cell *145*, 732–744.

Lv, L., Li, D., Zhao, D., Lin, R., Chu, Y., Zhang, H., Zha, Z., Liu, Y., Li, Z., Xu, Y., et al. (2011). Mol. Cell *42*, 719–730.

Mancuso, A., Beardsley, N.J., Wehrli, S., Pickup, S., Matschinsky, F.M., and Glickson, J.D. (2004). Biotechnol. Bioeng. *87*, 835–848.

Mardis, E.R., Ding, L., Dooling, D.J., Larson, D.E., McLellan, M.D., Chen, K., Koboldt, D.C., Fulton, R.S., Delehaunty, K.D., McGrath, S.D., et al. (2009). N. Engl. J. Med. *361*, 1058–1066.

Matoba, S., Kang, J.G., Patino, W.D., Wragg, A., Boehm, M., Gavrilova, O., Hurley, P.J., Bunz, F., and Hwang, P.M. (2006). Science *312*, 1650–1653.

Mazurek, S. (2011). Int. J. Biochem. Cell Biol. *43*, 969–980.

Mazurek, S., Zwerschke, W., Jansen-Dürr, P., and Eigenbrodt, E. (2001). Biochem. J. *356*, 247–256.

Mazurek, S., Drexler, H.C., Troppmair, J., Eigenbrodt, E., and Rapp, U.R. (2007). Anticancer Res. *27* (6B), 3963–3971.

Metallo, C.M., Gameiro, P.A., Bell, E.L., Mattaini, K.R., Yang, J., Hiller, K., Jewell, C.M., Johnson, Z.R., Irvine, D.J., Guarente, L., et al. (2012). Nature *481*, 380–384.

Metellus, P., Colin, C., Taieb, D., Guedj, E., Nanni-Metellus, I., de Paula, A.M., Colavolpe, C., Fuentes, S., Dufour, H., Barrie, M., et al. (2011). J. Neurooncol. *105*, 591–600.

Mullen, A.R., Wheaton, W.W., Jin, E.S., Chen, P.H., Sullivan, L.B., Cheng, T., Yang, Y., Linehan, W.M., Chandel, N.S., and DeBerardinis, R.J. (2012). Nature *481*, 385–388.

Nieman, K.M., Kenny, H.A., Penicka, C.V., Ladanyi, A., Buell-Gutbrod, R., Zillhardt, M.R., Romero, I.L., Carey, M.S., Mills, G.B., Hotamisligil, G.S., et al. (2011). Nat. Med. *17*, 1498–1503.

Noushmehr, H., Weisenberger, D.J., Diefes, K., Phillips, H.S., Pujara, K., Berman, B.P., Pan, F., Pelloski, C.E., Sulman, E.P., Bhat, K.P., et al; Cancer Genome Atlas Research Network. (2010). Cancer Cell *17*, 510–522.

Ochoa, S. (1948). J. Biol. Chem. *174*, 133–157.

Ooi, A., Wong, J.C., Petillo, D., Roossien, D., Perrier-Trudova, V., Whitten, D., Min, B.W., Tan, M.H., Zhang, Z., Yang, X.J., et al. (2011). Cancer Cell *20*, 511–523.

Owen, M.R., Doran, E., and Halestrap, A.P. (2000). Biochem. J. *348*, 607–614.

Pansuriya, T.C., van Eijk, R., d'Adamo, P., van Ruler, M.A., Kuijjer, M.L., Oosting, J., Cleton-Jansen, A.M., van Oosterwijk, J.G., Verbeke, S.L., Meijer, D., et al. (2011). Nat. Genet. *43*, 1256–1261.

Papandreou, I., Cairns, R.A., Fontana, L., Lim, A.L., and Denko, N.C. (2006). Cell Metab. *3*, 187–197.

Parsons, D.W., Jones, S., Zhang, X., Lin, J.C., Leary, R.J., Angenendt, P., Mankoo, P., Carter, H., Siu, I.M., Gallia, G.L., et al. (2008). Science *321*, 1807–1812.

Pisano, M., Cocco, P., Cherchi, R., Onnis, R., and Cherchi, P. (1991). Tumori *77*, 12–15.

Pope, W.B., Prins, R.M., Albert Thomas, M., Nagarajan, R., Yen, K.E., Bittinger, M.A., Salamon, N., Chou, A.P., Yong, W.H., Soto, H., et al. (2012). J. Neurooncol. *107*, 197–205.

Possemato, R., Marks, K.M., Shaul, Y.D., Pacold, M.E., Kim, D., Birsoy, K., Sethumadhavan, S., Woo, H.K., Jang, H.G., Jha, A.K., et al. (2011). Nature *476*, 346–350.

Ramanathan, A., and Schreiber, S.L. (2009). Proc. Natl. Acad. Sci. USA *106*, 22229–22232.

Rathmell, J.C., Vander Heiden, M.G., Harris, M.H., Frauwirth, K.A., and Thompson, C.B. (2000). Mol. Cell *6*, 683–692.

Rathmell, J.C., Fox, C.J., Plas, D.R., Hammerman, P.S., Cinalli, R.M., and Thompson, C.B. (2003). Mol. Cell. Biol. *23*, 7315–7328.

Rempel, A., Mathupala, S.P., Griffin, C.A., Hawkins, A.L., and Pedersen, P.L. (1996). Cancer Res. *56*, 2468–2471.

Rydström, J. (2006). Biochim. Biophys. Acta *1757*, 721–726.

Schieke, S.M., Phillips, D., McCoy, J.P., Jr., Aponte, A.M., Shen, R.F., Balaban, R.S., and Finkel, T. (2006). J. Biol. Chem. *281*, 27643–27652.

Scholnick, P., Lang, D., and Racker, E. (1973). J. Biol. Chem. *248*, 5175.

Selak, M.A., Armour, S.M., MacKenzie, E.D., Boulahbel, H., Watson, D.G., Mansfield, K.D., Pan, Y., Simon, M.C., Thompson, C.B., and Gottlieb, E. (2005). Cancer Cell *7*, 77–85.

Shah, U.S., Dhir, R., Gollin, S.M., Chandran, U.R., Lewis, D., Acquafondata, M., and Pflug, B.R. (2006). Hum. Pathol. *37*, 401–409.

Shen, C., Beroukhim, R., Schumacher, S.E., Zhou, J., Chang, M., Signoretti, S., and Kaelin, W.G., Jr. (2011). Cancer Discov *1*, 222–235.

Shimada, N., Shinagawa, T., and Ishii, S. (2008). Genes Cells *13*, 245–254.

Siwko, S., and Mochly-Rosen, D. (2007). Int. J. Biochem. Cell Biol. *39*, 978–987.

Smith, E.H., Janknecht, R., and Maher, L.J., 3rd. (2007). Hum. Mol. Genet. *16*, 3136–3148.

Sonveaux, P., Végran, F., Schroeder, T., Wergin, M.C., Verrax, J., Rabbani, Z.N., De Saedeleer, C.J., Kennedy, K.M., Diepart, C., Jordan, B.F., et al. (2008). J. Clin. Invest. *118*, 3930–3942.

Spoden, G.A., Mazurek, S., Morandell, D., Bacher, N., Ausserlechner, M.J., Jansen-Dürr, P., Eigenbrodt, E., and Zwerschke, W. (2008). Int. J. Cancer *123*, 312–321.

Spoden, G.A., Morandell, D., Ehehalt, D., Fiedler, M., Jansen-Dürr, P., Hermann, M., and Zwerschke, W. (2009). J. Cell. Biochem. *107*, 293–302.

Sreekumar, A., Poisson, L.M., Rajendiran, T.M., Khan, A.P., Cao, Q., Yu, J., Laxman, B., Mehra, R., Lonigro, R.J., Li, Y., et al. (2009). Nature *457*, 910–914.

Srere, P.A. (1959). J. Biol. Chem. *234*, 2544–2547.

Stern, J.R., Ochoa, S., and Lynen, F. (1952). J. Biol. Chem. *198*, 313–321.

Steták, A., Veress, R., Ovádi, J., Csermely, P., Kéri, G., and Ullrich, A. (2007). Cancer Res. *67*, 1602–1608.

Stryer, L. (1995). Biochemistry, Fourth Edition (New York: W.H. Feeman and Company).

Tallal, L., Tan, C., Oettgen, H., Wollner, N., McCarthy, M., Helson, L., Burchenal, J., Karnofsky, D., and Murphy, M.L. (1970). Cancer *25*, 306–320.

Turcan, S., Rohle, D., Goenka, A., Walsh, L.A., Fang, F., Yilmaz, E., Campos, C., Fabius, A.W., Lu, C., Ward, P.S., et al. (2012). Nature. Published online February 15, 2012. 10.1038/nature10866.

Vander Heiden, M.G., Cantley, L.C., and Thompson, C.B. (2009). Science *324*, 1029–1033.

Vander Heiden, M.G., Locasale, J.W., Swanson, K.D., Sharfi, H., Heffron, G.J., Amador-Noguez, D., Christofk, H.R., Wagner, G., Rabinowitz, J.D., Asara, J.M., and Cantley, L.C. (2010). Science *329*, 1492–1499.

Wakil, S.J., Porter, J.W., and Gibson, D.M. (1957). Biochim. Biophys. Acta *24*, 453–461.

Wang, J.B., Erickson, J.W., Fuji, R., Ramachandran, S., Gao, P., Dinavahi, R., Wilson, K.F., Ambrosio, A.L., Dias, S.M., Dang, C.V., and Cerione, R.A. (2010). Cancer Cell *18*, 207–219.

Ward, P.S., Patel, J., Wise, D.R., Abdel-Wahab, O., Bennett, B.D., Coller, H.A., Cross, J.R., Fantin, V.R., Hedvat, C.V., Perl, A.E., et al. (2010). Cancer Cell *17*, 225–234.

Ward, P.S., Cross, J.R., Lu, C., Weigert, O., Abel-Wahab, O., Levine, R.L., Weinstock, D.M., Sharp, K.A., and Thompson, C.B. (2011). Oncogene. Published online September 26, 2011. 10.1038/onc.2011.416.

Watanabe, T., Nobusawa, S., Kleihues, P., and Ohgaki, H. (2009). Am. J. Pathol. *174*, 1149–1153.

Weinberg, F., Hamanaka, R., Wheaton, W.W., Weinberg, S., Joseph, J., Lopez, M., Kalyanaraman, B., Mutlu, G.M., Budinger, G.R., and Chandel, N.S. (2010). Proc. Natl. Acad. Sci. USA *107*, 8788–8793.

Wellen, K.E., Lu, C., Mancuso, A., Lemons, J.M., Ryczko, M., Dennis, J.W., Rabinowitz, J.D., Coller, H.A., and Thompson, C.B. (2010). Genes Dev. *24*, 2784–2799.

Williams, J.M., Chen, G.C., Zhu, L., and Rest, R.F. (1998). Mol. Microbiol. *27*, 171–186.

Williams, S.C., Karajannis, M.A., Chiriboga, L., Golfinos, J.G., von Deimling, A., and Zagzag, D. (2011). Acta Neuropathol. *121*, 279–281.

Wise, D.R., DeBerardinis, R.J., Mancuso, A., Sayed, N., Zhang, X.Y., Pfeiffer, H.K., Nissim, I., Daikhin, E., Yudkoff, M., McMahon, S.B., and Thompson, C.B. (2008). Proc. Natl. Acad. Sci. USA *105*, 18782–18787.

Wise, D.R., Ward, P.S., Shay, J.E., Cross, J.R., Gruber, J.J., Sachdeva, U.M., Platt, J.M., DeMatteo, R.G., Simon, M.C., and Thompson, C.B. (2011). Proc. Natl. Acad. Sci. USA *108*, 19611–19616.

Wu, X., Zhou, Y., Zhang, K., Liu, Q., and Guo, D. (2008). FEBS Lett. *582*, 2155–2160.

Xu, W., Yang, H., Liu, Y., Yang, Y., Wang, P., Kim, S.H., Ito, S., Yang, C., Wang, P., Xiao, M.T., et al. (2011). Cancer Cell *19*, 17–30.

Yan, H., Parsons, D.W., Jin, G., McLendon, R., Rasheed, B.A., Yuan, W., Kos, I., Batinic-Haberle, I., Jones, S., Riggins, G.J., et al. (2009). N. Engl. J. Med. *360*, 765–773.

Yang, W., Xia, Y., Ji, H., Zheng, Y., Liang, J., Huang, W., Gao, X., Aldape, K., and Lu, Z. (2011). Nature *480*, 118–122.

Yoo, H., Antoniewicz, M.R., Stephanopoulos, G., and Kelleher, J.K. (2008). J. Biol. Chem. *283*, 20621–20627.

Yuan, J., Bennett, B.D., and Rabinowitz, J.D. (2008). Nat. Protoc. *3*, 1328–1340.

Yun, J., Rago, C., Cheong, I., Pagliarini, R., Angenendt, P., Rajagopalan, H., Schmidt, K., Willson, J.K., Markowitz, S., Zhou, S., et al. (2009). Science *325*, 1555–1559.

Yuneva, M., Zamboni, N., Oefner, P., Sachidanandam, R., and Lazebnik, Y. (2007). J. Cell Biol. *178*, 93–105.

Zaugg, K., Yao, Y., Reilly, P.T., Kannan, K., Kiarash, R., Mason, J., Huang, P., Sawyer, S.K., Fuerth, B., Faubert, B., et al. (2011). Genes Dev. *25*, 1041–1051.

Zhang, W.C., Shyh-Chang, N., Yang, H., Rai, A., Umashankar, S., Ma, S., Soh, B.S., Sun, L.L., Tai, B.C., Nga, M.E., et al. (2012). Cell *148*, 259–272.

Zhao, F., Mancuso, A., Bui, T.V., Tong, X., Gruber, J.J., Swider, C.R., Sanchez, P.V., Lum, J.J., Sayed, N., Melo, J.V., et al. (2010). Oncogene *29*, 2962–2972.

Zhao, S., Lin, Y., Xu, W., Jiang, W., Zha, Z., Wang, P., Yu, W., Li, Z., Gong, L., Peng, Y., et al. (2009). Science *324*, 261–265.

Zscharnack, K., Kessler, R., Bleichert, F., Warnke, J.P., and Eschrich, K. (2009). Neuropathol. Appl. Neurobiol. *35*, 566–578.

Zwerschke, W., Mazurek, S., Massimi, P., Banks, L., Eigenbrodt, E., and Jansen-Dürr, P. (1999). Proc. Natl. Acad. Sci. USA *96*, 1291–1296.

Cancer Cell Special Collection 10 YEARS OF EXCITING CANCER RESEARCH SINCE 2002

Accessories to the Crime: Functions of Cells Recruited to the Tumor Microenvironment

Douglas Hanahan[1,*] and Lisa M. Coussens[2,*]
[1]The Swiss Institute for Experimental Cancer Research (ISREC), School of Life Sciences, Swiss Federal Institute of Technology Lausanne (EPFL), CH-1015 Lausanne, Switzerland
[2]Department of Cell and Developmental Biology and Knight Cancer Institute, Oregon Health and Science University, 3181 SW Sam Jackson Park Road, Portland, OR 97239-3098, USA
*Correspondence: douglas.hanahan@epfl.ch (D.H.), coussenl@ohsu.edu (L.M.C.)
DOI 10.1016/j.ccr.2012.02.022

Mutationally corrupted cancer (stem) cells are the driving force of tumor development and progression. Yet, these transformed cells cannot do it alone. Assemblages of ostensibly normal tissue and bone marrow-derived (stromal) cells are recruited to constitute tumorigenic microenvironments. Most of the hallmarks of cancer are enabled and sustained to varying degrees through contributions from repertoires of stromal cell types and distinctive subcell types. Their contributory functions to hallmark capabilities are increasingly well understood, as are the reciprocal communications with neoplastic cancer cells that mediate their recruitment, activation, programming, and persistence. This enhanced understanding presents interesting new targets for anticancer therapy.

The overarching focus of cancer research for the past four decades has been on the malignant cancer cell, seeking to understand the dominant oncogenes and tumor suppressor genes whose respective activation/upregulation or loss of function serve to impart aberrant properties on normal cells, thus contributing to their transformation into the cancerous cells that form the basis for malignancy. New tools and new data have continued to enrich our knowledge and insights into properties of malignant cells and the genetic aberrations that endow the proliferative foundation of cancer as a chronic disease. Whole-genome resequencing and genome-wide epigenetic and transcriptional profiling are presenting an avalanche of new data, with great expectations and concomitant challenges to distill it into a clarity of mechanism that can, in turn, be translated into more effective therapies. With rare exception, today's therapies for most forms of human cancer remain incompletely effective and transitory, despite knowledge of driving oncogenes and crucial oncogenic signaling pathways amenable to pharmacological intervention with targeted therapies. The challenge of distillation is, in fact, even more daunting if one incorporates the diversity of human cancers arising from distinctive cells of origin in different tissues and organs, with variable parameters of tumor development and progression, oncogenic mutation, prognosis, and response to therapy.

The hallmarks of cancer (Hanahan and Weinberg, 2000) were conceived to suggest a conceptual rationale—an underlying commonality—for this diversity and disparity in cancer cell genotypes and phenotypes, positing that the spectrum of cancers reflects different solutions to the same challenge to a prospective outlaw cell, being able to circumvent the intrinsic barriers and protective functions that have evolved in higher organisms to prevent unauthorized, chronic cell proliferation. A second premise was the now-increasingly accepted importance of the tumor microenvironment (TME), embodied in the concept that cancer cells do not manifest the disease alone, but rather conscript and corrupt resident and recruited normal cell types to serve as contributing members to the outlaw society of cells. Collaborative interactions between neoplastic cancer cells and their supporting stroma coalesce into the ectopic, chronically proliferative (and often disseminating) organ-like structures that typify most human cancers, in the form of tumors and local invasions, metastases, or vascular niches nurturing hematopoietic malignancies. Thus, in the past decade, the TME and its constituent "stromal" cells have collectively risen in prominence, now embracing a broad field of investigation. While some aspects of stroma have been long appreciated, in particular, the contributions of tumor angiogenesis and remodeled extracellular matrix (ECM) (Bissell et al., 1982; Dvorak, 1986; Folkman, 1974), the larger impact of the TME on tumor growth and progression, and on the resilience of most cancers in the face of therapy, is increasingly evident, but perhaps still not fully appreciated. This perspective, therefore, seeks to document the diverse functional contributions that stromal cell constituents of tumors can make toward cancer phenotypes, by illustrating how different stromal cell types demonstrably contribute to the core and emergent hallmarks of cancer, namely, sustaining proliferative signaling, evading growth suppressors, resisting cell death, enabling replicative immortality, inducing angiogenesis, activating invasion and metastasis, reprogramming energy metabolism, and evading immune destruction. As will be seen below, stromal cells types are significantly influencing most of the hallmark capabilities, highlighting the realization that malignant cancer cells, despite all their mutational entitlement, do not act alone in elaborating the disease.

Contributions of Stromal Cell Types to Hallmark Capabilities

While the contributions of certain stromal cell types to particular hallmarks is self-evident, in particular, that of endothelial cells to tumor angiogenesis, there are much broader contributions of stromal cells to the hallmarks of cancer (and hence to the nature of the disease). We present below illustrative but not

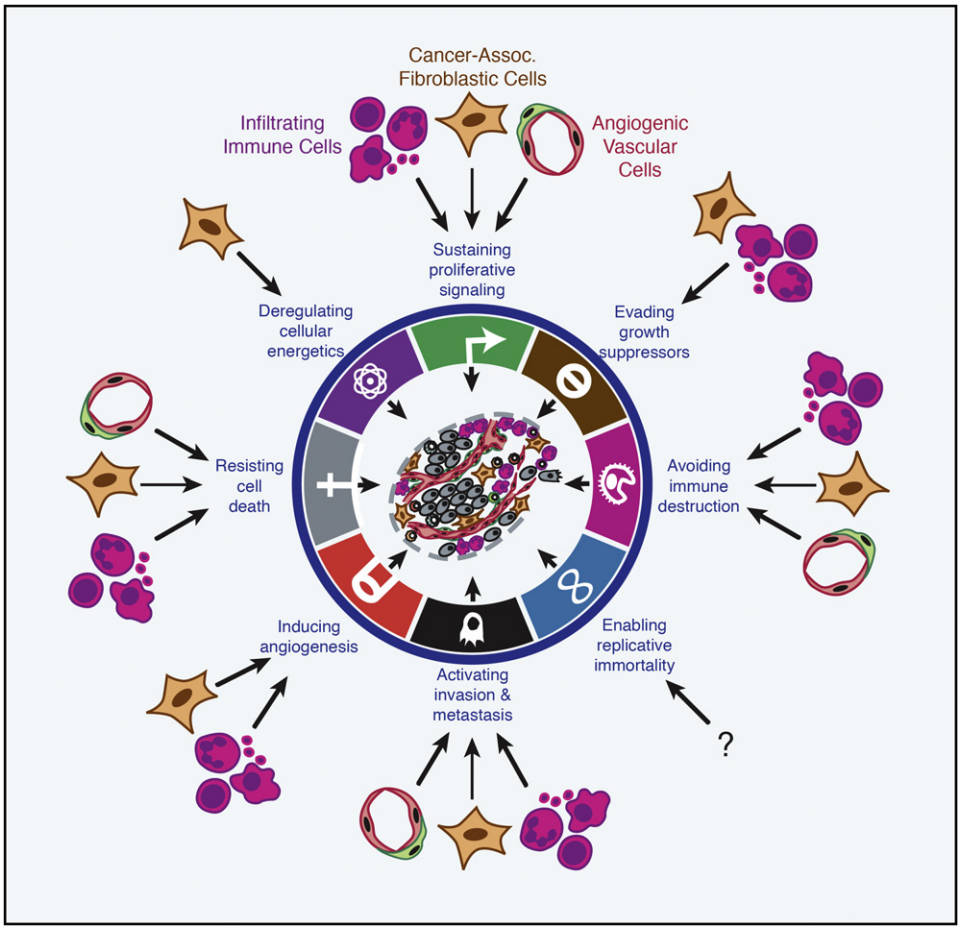

Figure 1. Multifactoral Contributions of Activated/Recruited Stromal Calls to the Hallmarks of Cancer
Of the eight acquired hallmark capabilities—six core and two emerging (Hanahan and Weinberg, 2011)—seven demonstrably involve contributions by stromal cells of the tumor microenvironment. The stromal cells can be divided into three general classes, depicted here by their involvement in particular hallmarks, illustrating the diversity of their functional contributions. Notably, the importance of each of these stromal cell classes varies with tumor type and organ, governed by parameters of the distinctive tumor microenvironments and underlying oncogenetic alterations in cancer cells and cancer stem cells that arise in primary tumors, and their invasive and metastatic colonizations. Moreover, distinctive cell types and subcell types within these classes can exert variable roles in enabling these capabilities, and in some cases by opposing them, as elaborated in the text and in Figure 2.

comprehensive examples of the functional roles that stromal cells play in enabling the various hallmark capabilities. Moreover, while we recognize that within each stromal subtype a spectrum of subpopulations exist, most notably in the case of cells in the innate immune system (myeloid-lineage cells), for simplicity, and to appeal to a general audience, we refer to these various subgroups within the general population as opposed to discussing activities of each, since comprehensive reviews describing these intricacies are available (Chow et al., 2011; Gabrilovich and Nagaraj, 2009; Mantovani et al., 2011; Porta et al., 2011). The breadth of stromal cell contributions to hallmark capabilities is illustrated in Figure 1, in which we have grouped the generic constituents of the stromal component of the TME into three general classes: angiogenic vascular cells (AVCs), infiltrating immune cells (IICs), and cancer-associated fibroblastic cells (CAFs).

Sustaining Proliferative Signaling

Although driving oncogenic mutations conveying chronic proliferative stimuli in neoplastic cells are definitive for, and considered essential to, many forms of human cancer, virtually every stromal cell type has demonstrable ability to support hyperproliferation of cancer cells in one context or another. As such, paracrine and juxtacrine mitogenic signals supplied by stromal cell types may potentially be involved in different tumor types at virtually any stage of tumorigenesis and progression, ranging from the initiation of aberrant proliferation to the development of adaptive resistance to therapies targeting such driving oncogenic signals.

Angiogenic Vascular Cells. Certainly the most well-established extrinsic modulator of cancer cell (and thus tumor) growth is lesional neovascularization (Folkman, 1974), involving the tube-forming endothelial cells and their supporting pericytes that comprise the angiogenic vasculature (Armulik et al., 2005). It has long been evident in mouse models that the induction of angiogenesis, the "angiogenic switch" (Folkman et al., 1989), increases the rates of cancer cell proliferation in neoplasias and tumors (Bergers et al., 1999; Hanahan and Folkman, 1996), and that inhibition of angiogenesis can impair such

hyperproliferation (Bergers et al., 1999; Brem et al., 1993; Carmeliet and Jain, 2011; Ferrara and Alitalo, 1999; Parangi et al., 1996; Shaheen et al., 1999), presumably reflecting reduced bioavailability of blood-borne mitogenic growth factors, with or without concomitant antiapoptotic survival factors (see below). Notably, the (mitogenic) effects on cancer cells of angiogenic switching and its inhibition in human tumors remains only inferential, in large part due to a paucity of analyses involving serial biopsies of lesions during malignant progression, and throughout the course of therapeutic response and relapse/resistance to angiogenesis inhibitors.

Recently, AVCs have been implicated in local supply of growth-promoting trophic factors that are expressed and secreted—independent from blood-borne factors—by the endothelial cells, potentially acting to stimulate in a paracrine fashion multiple hallmark capabilities (Butler et al., 2010); the generality and importance of such "nonvascular" local support of cancer cell proliferation and other capabilities by tumor endothelial cells (and pericytes) is yet to be established.

Infiltrating Immune Cells. Although "inflammation and cancer" has become a rubric for the intersection of tumors with the immune system, many tumors show subtle infiltrations of immune cells that do not meet the classical definition of an inflammatory immune response, and yet are functionally instrumental in the tumor phenotypes discussed below; thus, we adopt the terminology of IICs to encompass both classic inflammation and more subtle involvement of immune cells in the TME. That said, virtually all adult solid tumors (carcinomas most notably) contain infiltrates of diverse leukocyte subsets including both myeloid- and lymphoid-lineage cells (Tlsty and Coussens, 2006), whose complexity and activation status vary depending on the tissue/organ locale, and stage of malignancy (Mantovani et al., 2008; Ruffell et al., 2011). IICs supply direct and indirect mitogenic growth mediators that stimulate proliferation of neoplastic cells, as well as other stromal cell types in their vicinity (Balkwill et al., 2005). Notable examples include epidermal growth factor (EGF), transforming growth factor-β (TGF-β), tumor necrosis factor-α (TNF-α), fibroblast growth factors (FGFs), various interleukins (ILs), chemokines, histamine, and heparins (Balkwill et al., 2005). In addition, IICs express diverse classes of proteolytic enzymes (metallo, serine, and cysteine proteases) that can selectively cleave and thereby modify the structure and function of extracellular matrix (ECM), for example, uncaging bioactive mitogenic agents (Lu et al., 2011a). While such effects are reflective of typical leukocyte activities ascribed to repair of tissue damage (Dvorak et al., 2011; Tlsty and Coussens, 2006), the chronic presence of paracrine and juxtacrine mitogenic signaling molecules provided by IICs can supply evolving neoplastic cells with signals that help sustain their unchecked proliferation.

A recent study (Guerra et al., 2011) adds another intriguing contribution of IICs to the proliferative hallmark, demonstrating that inflammation of a pancreas harboring ductal epithelial cells with an activating mutation in the *K-ras* oncogene can obviate triggering of oncogene-induced cell senescence that otherwise limits hyperproliferation and malignant progression of nascent (initiated) pancreatic cancer cells; treatment of such cancer-predisposed mice with anti-inflammatory drugs restores oncogene-induced senescence, and impairs development of pancreatic cancer. The identity of the immune cell (sub)-type and of the paracrine signal(s) it supplies to inhibit oncogene-induced senescence remain to be elucidated, as does the potential involvement in other tumor types of this microenvironmental mechanism for circumventing senescence barriers to oncogene-driven hyperproliferation.

Cancer-Associated Fibroblastic Cells. Likely also reflecting corrupted wound healing and tissue repair mechanisms, a variety of fibroblastic cells can be recruited and/or activated to contribute to this and other hallmark capabilities (for recent reviews, see Cirri and Chiarugi, 2011; Franco et al., 2010; Pietras and Ostman, 2010; Räsänen and Vaheri, 2010). Thus, connective tissue fibroblasts proximal to neoplastic growths can be activated, and mesenchymal progenitors—in particular, mesenchymal stem cells (MSCs), both local and bone marrow derived—can be recruited and induced to differentiate into myofibroblasts defined in part by expression of alpha smooth muscle actin (αSMA) (Paunescu et al., 2011), or into adipocytes defined by expression of fatty acid binding protein-4 (FABP4) (Rosen and MacDougald, 2006). We group these similarly fibroblastic and yet distinctive cell types into a stromal cell class collectively referred to as CAFs (Hanahan and Weinberg, 2011, and references therein). Each of these CAF subtypes can contribute to a variety of tumor-promoting functions, with the potential to impact on multiple hallmark capabilities; their diversity in characteristics and in functional contributions in different organ-specific TMEs are increasingly well delineated, and appreciated. Thus, for example, CAFs can express and secrete signaling proteins that include mitogenic epithelial growth factors—hepatocyte growth factor (HGF), EGF family members, insulin-like growth factor-1 (IGF-1), stromal cell-derived factor-1 (SDF-1/CXCL12), and a variety of FGFs—with the capability to stimulate cancer cell proliferation (Cirri and Chiarugi, 2011; Erez et al., 2010; Franco et al., 2010; Kalluri and Zeisberg, 2006; Orimo et al., 2005; Räsänen and Vaheri, 2010; Rosen and MacDougald, 2006; Spaeth et al., 2009). CAFs can also orchestrate functional attributes associated with epithelial-to-mesenchymal transition (EMT) via secretion of TGF-β (Chaffer and Weinberg, 2011), which can also affect other hallmark traits noted below. In addition, both activated adipocytes and activated fibroblasts can express spectrums of "proinflammatory" mediators (Celis et al., 2005; Dirat et al., 2011; Erez et al., 2010), thereby recruiting and activating IICs that, in turn, provide mitogenic signals to cancer cells, as well as other cell types in the TME. The signals that activate, recruit, and "fine-tune" or "educate" CAFs are complex and variable between different tumor types, as are the particular roles they are implicated to play, in particular, TMEs, mirroring the complexity of IICs and of the oncogenic transformation events and mutational ontogeny of the cancer cells.

Evading Growth Suppressors

Although suppression of unscheduled/chronic proliferation of incipient cancer cells is largely thought to involve cell intrinsic mechanisms, principally involving the p53 and pRb tumor suppressor pathways, there are intriguing examples of stromal cells in the TME helping cancer cells evade various forms of growth suppression, as illustrated by the following examples.

Cancer-Associated, and Normal, Fibroblastic Cells. The roster of induced gains of function that enable CAFs to support multiple

hallmark tumor phenotypes does not currently include paracrine factors that demonstrably short-circuit cancer cell-intrinsic growth suppressor pathways. There is, however, compelling evidence for causal loss of function elicited during the conversion of normal fibroblasts into CAFs. Experiments performed in coculture systems have clearly demonstrated that normal connective tissue fibroblasts (but not CAFs) from various organs can inhibit growth of cancer cells, in a process that requires contact of the "normal" fibroblasts with cancer cells, suggestive of roles (along with epithelial contact inhibition) in governing epithelial homeostasis and proliferative quiescence (Bissell and Hines, 2011; Flaberg et al., 2011). Thus, "normal" fibroblasts may serve as extrinsic epithelial growth suppressors, such that CAFs contribute to this particular hallmark capability by what they have lost from their cell of origin during the course of being reprogrammed ("educated") as CAFs. An additional possibility, currently speculative, is that tissue fibroblasts activated into CAF-like states by other aberrant conditions (e.g., fibrosis, edema, or infection) might also produce proteases or other paracrine factors that disrupt normal epithelial architecture, thereby relieving the intrinsic growth suppression mediated by epithelial cell-cell adhesion, allowing initiation of neoplastic development.

Infiltrating Immune Cells. Epithelial cells are subject to an extrinsic form of growth suppression involving cell-cell and cell-ECM adhesion molecules that via their adhesive interactions transmit antigrowth signals to the cell cycle machinery; such antigrowth signals can, for example, overrule the proliferation-inducing signals of driving oncogenes such as c-Myc (Hezel and Bardeesy, 2008; Partanen et al., 2009). IICs express and secrete a variety of proteolytic enzymes (metallo, serine, and cysteine proteinases and heparanase) that, in addition to liberating mitogenic growth factors, can selectively cleave cell-cell and cell-ECM adhesion molecules, and/or ECM molecules (ligands for the latter), thereby disabling growth suppressing adhesion complexes maintaining homeostasis (Lu et al., 2011a; Mohamed and Sloane, 2006; Pontiggia et al., 2011; Xu et al., 2009).

Resisting Cell Death

Tissues are endowed with embedded regulatory programs for controlling aberrant proliferation of resident cells, as well as for inhibiting "invasion" of foreign cell types, which act by inducing one form or another of cell death, of which apoptosis is the most prominent. Thus, in order to sustain their proliferative capacity and thrive ectopically, neoplastic cells must either develop intrinsic resistance to local cell death programs or instead coordinate development of cell extrinsic programs that safeguard their survival. Recent investigations have revealed the stromal/extrinsic capabilities for evading the tissue-protective mission of cell death programs that not only foster ectopic proliferation and survival of neoplastic cells, but also help to blunt effectiveness of cytotoxic and targeted therapy.

Angiogenic Vascular Cells. It is well established that vascularization of incipient neoplasias and tumors serves to attenuate cell death that would otherwise result from hypoxia and lack of serum-derived nutrients and survival factors. Indeed, the aforementioned studies from the 1990s report reduced apoptosis scaling hand-in-hand with increased proliferation of cancer cells following activation of the angiogenic switch, and conversely increased apoptosis resulting from pharmacological or genetic impairment of angiogenesis. Induction of both apoptosis and necrosis are almost invariable results of appreciable destruction of tumor vasculature, as contrasted to the alternative "normalization" of the tumor vasculature that results from weaker inhibitors of tumor angiogenesis and neovascularization (De Bock et al., 2011; Goel et al., 2011). The role of angiogenesis in limiting apoptosis is aptly illustrated by the effects of vascular disrupting agents that destroy the tumor vasculature, causing acute hypoxia and rampant cell death inside treated tumors, leaving behind hollow acellular cores enveloped by a rim of viable cells that survive by co-opting adjacent tissue vasculature (Daenen et al., 2009). Such studies establish vascularization, be it "abnormal" or "normalized," as essential to the hallmark capability for limiting cancer cell death.

Infiltrating Immune Cells. Heterotypic and homotypic cell adhesion molecules provide various cell types—in their proper tissue microenvironments (e.g., organized epithelia) —with survival signals that help to maintain tissue integrity and homeostasis, such that cell detachment and loss of adhesion triggers apoptosis. One mechanism used by cancer cells to become independent of such dependence on homotypic survival signals involves IICs, which by binding to cancer cells take the place of their disconnected epithelial brethren, conveying on them the ability to survive in ectopic microenvironments by suppressing the triggering of cell death pathways. Thus, for example, α4-integrin-expressing tumor-associated macrophages (TAMs) act in a juxtacrine manner to promote survival of metastatic breast cancer cells in lung by binding *vascular cell adhesion molecule-1 (VCAM-1*) expressed on breast cancer cells. The α4-integrin/VCAM-1 interaction specifically activates Ezrin—a mediator of receptor tyrosine signaling—in breast carcinoma cells, which, in turn, induces PI3K/AKT signaling and suppression of apoptosis (Chen et al., 2011). A similar mechanism fosters expansion of macrometastatic breast cancer in bone (Lu et al., 2011c). In addition, TAMs also protect breast cancer cells from chemotherapy (taxol, etoposide, and doxorubicin)-induced cell death by a cathepsin protease-dependent mechanism (Shree et al., 2011). Collectively, these studies reveal the capability of macrophages (and monocytes) to provide survival signals to cancer cells that limits the impact on neoplastic progression of cancer cell death programs triggered by a variety of tissue-protective and therapy-induced mechanisms.

Cancer-Associated Fibroblastic Cells. A number of studies have implicated CAFs in the capability to limit the impact on tumor growth and progression of cancer cell apoptosis (Kalluri and Zeisberg, 2006; Loeffler et al., 2006; Pietras and Ostman, 2010). One modality involves the secretion of diffusible paracrine survival factors such as IGF-1 and IGF-2. A second relates to synthesis of ECM molecules and ECM-remodeling proteases that contribute to formation of a neoplastic ECM, distinctive from normal tissue stroma, that provides nondiffusible survival signals (e.g., ligands for antiapoptotic integrins); functional studies have implicated CAF-derived ECM in modulating cancer cell survival, among other traits (Lu et al., 2011a). Moreover, cancer-associated adipocytes, analogous to IICs, blunt the cytotoxic effects of radiation therapy and confer a radioresistant phenotype to breast cancer cells dependent on adipocyte-derived IL-6 (Bochet et al., 2011). While the generality (and relevance to human tumors) of these prosurvival effects has yet to be

established, it can be envisioned that such contributions by CAFs will prove to be operative in many forms of human cancer, and may also have differential clinical implications for individual patients with the same tumor type, such as obese patients whose cancers have been associated with more aggressive characteristics (Khandekar et al., 2011).

Enabling Replicative Immortality?

Stabilizing telomere length and functionality to enable limitless replication of cancer cells is the essence of this hallmark, one that is seemingly independent of the TME, in that there is currently no substantive evidence for stromal contributions to telomere stabilization in cancer cells. While it could be argued that abrogation of senescence-inducing signals from normal stromal fibroblasts or antagonistic IICs is involved in enabling this hallmark, we consider that triggering such senescence is more likely involved in a first line of tissue defense focused on opposing (along with cell death and cell cycle arrest) inappropriate proliferation, long before replicative immortality becomes a factor, and thus stromal involvement in senescence and its circumvention is most logically associated with the proliferation and growth suppression hallmarks.

Inducing Angiogenesis

In adult tissues, most blood vessels are quiescent, and angiogenesis (growth of new blood vessels from pre-existing ones) occurs only during the female reproductive cycle and under certain pathophysiological conditions, such as tissue remodeling associated with wound healing (Carmeliet and Jain, 2011). Whereas the cellular and molecular programs are common to both physiological and tumor angiogenesis, constitutively activated proangiogenic signaling in tumors make tumor-associated vessels distinctly irregular, chaotic, and inherently unstable (De Bock et al., 2011; McDonald and Choyke, 2003; Morikawa et al., 2002). Interestingly, tumors with reduced levels of such hyperactive angiogenic stimulation—resultant to limited abundance of vascular endothelial growth factor (VEGF) and other angiogenic regulatory factors in their TME, or to pharmacological suppression of VEGF—evidence so-called "vascular normalization," in which vessels are less torturous, with better pericyte coverage, and improved and less erratic blood flow (De Bock et al., 2011; Goel et al., 2011; Jain, 2005). Historically, tumor angiogenesis was envisioned to be principally regulated by cancer cells expressing proangiogenic factors, which is indeed one mechanism; there is, however, now abundant evidence that stromal cells in the TME are instrumental in switching on and sustaining chronic angiogenesis in many tumor types, as illustrated in the following examples.

Infiltrating Immune Cells. There is a tight interplay between IICs and vascular cells. Endothelial cells mediate leukocyte recruitment by expressing a repertoire of leukocyte adhesion molecules, while IICs produce a diverse assortment of soluble factors that influence endothelial cell behavior. Myeloid cells implicated in these interactions include subsets of granulocytes (neutrophils, basophils, and eosinophils), dendritic cells, TAMs, Tie2-expressing monocytes, immature myeloid cells (iMCs)/myeloid-derived suppressor cells (MDSCs), and mast cells. The soluble mediators produced by IICs implicated in regulating aspects of the angiogenic process include cytokines (VEGF, bFGF, TNF-α, TGF-β, platelet-derived growth factor [PDGF], placental growth factor [PIGF]), Neuropilin-1, chemokines (CXCL12, IL-8/CXCL8), matrix metalloproteinases (MMPs, including MMP-2, -7, -9, -12, and -14), serine proteases (urokinase-type plasminogen activator), cysteine cathepsin proteases, DNA-damaging molecules (reactive oxygen species), histamine, and other bioactive mediators (nitric oxide). All of these effectors have demonstrated capabilities to regulate vascular cell survival, proliferation, and motility, along with tissue remodeling, culminating in new vessel formation (De Palma and Coussens, 2008).

TAMs regulate tumor angiogenesis largely through their production of VEGF-A; this connection is illustrated by restoration, via ectopic VEGF overexpression, of tumor angiogenesis otherwise impaired by macrophage depletion (Lin et al., 2007). Conversely, genetic deletion of the *VEGF-A* gene in macrophages attenuates tumor angiogenesis and results in a morphologically more normal vasculature, much as is seen with pharmacological inhibitors of VEGF signaling (Stockmann et al., 2008). In some mouse models of cancer, production of MMP-9 by TAMs increases bioavailability of otherwise limited (ECM sequestered) VEGF-A, thus providing an alternative, but still VEGF-dependent route for promoting angiogenesis (Bergers et al., 2000; Du et al., 2008; Giraudo et al., 2004). Similarly, TAM production of the VEGF family member PIGF stimulates angiogenesis in some tumors (Rolny et al., 2011) and thus TAMs may present a mechanism for acquiring resistance to anti-VEGF-A/VEGFR therapies (Fischer et al., 2007; Motzer et al., 2006; Willett et al., 2005).

The significance of TAMs as anticancer therapeutic targets has recently been emphasized by several studies reporting that reprogramming of tumor-promoting TAMs toward a phenotype embodied in conventional "antigen-presenting" macrophages can blunt tumor growth via processes that include impaired angiogenesis and vascular normalization. For example, histidine-rich glycoprotein HRG, a host-produced protein deposited in tumor stroma, can induce such a reprogramming of TAMs, resulting in vascular normalization and improved responses to chemotherapy (Rolny et al., 2011). Similar findings were reported by blockade of colony stimulating factor-1 (CSF-1) signaling, which resulted in macrophage depletion in mammary tumors, concomitant with reduced vascular density and improved responses to chemotherapy (Denardo et al., 2011). Common to both studies was enhanced anti-tumor immune responses by cytotoxic T lymphocytes (CTLs), thus indicating the complexity of dialogs by diverse stromal cell types in tumors, and the power of targeting one subtype to thereby subvert or alter bioactivities of other counterpart stromal cells.

While not as well studied, mast cells have long been recognized for their ability to foster tumor angiogenesis (Kessler et al., 1976). Recruitment of mast cells to human papilloma virus-induced squamous carcinomas (Coussens et al., 1999) or *Myc*-induced pancreatic β cell tumors (Soucek et al., 2007) is required for macroscopic tumor expansion; treatment with mast cell inhibitors results in impaired induction and persistence of angiogenesis, thereby elevating hypoxia and cell death of both cancer cells and endothelial cells (Soucek et al., 2007). Mast cells are reservoirs of potent vascular mediators including VEGF, Angiopoietin-1, IL-8/CXCL8, histamine, and heparin; mast cells can also release proteases (e.g., MMP-9) that liberate ECM-sequestered proangiogenic growth factors (Bergers et al., 2000; Coussens et al., 1999), or indirectly regulate AVCs—in the

case of tryptase—via cleavage of protease-activated receptor-2 (PAR2) on CAFs, which activates proangiogenic signaling programs (Khazaie et al., 2011).

Other IICs associated with tumor angiogenesis include neutrophils and their myeloid progenitors, which produce MMP-9 and are demonstrably involved in angiogenic switching in some tumors (Nozawa et al., 2006; Pahler et al., 2008; Shojaei et al., 2007), and platelets, the enucleated minicells spun off from megakeryocytes whose principle role involves induction of blood clotting in response to bleeding. Platelets release distinctive granules containing either pro- or antiangiogenic regulatory molecules, and have been implicated in angiogenesis for decades (Sabrkhany et al., 2011); the precise roles and importance of platelets and the mechanisms of their regulated degranulation has been elusive. Recent studies however have reported that candidate effectors in platelets can be genetically manipulated (Labelle et al., 2011), thus enabling an avenue to clarify their roles in tumor angiogenesis.

Cancer-Associated Fibroblastic Cells. There is abundant evidence that CAFs are involved in orchestrating tumor angiogenesis in a variety of tumor types. First, CAFs in different TMEs can produce a number of proangiogenic signaling proteins, including VEGF, FGF2 plus other FGFs, and IL-8/CXCL8 and PDGF-C; of note, PDGF-C may rescue angiogenesis in some anti-VEGF resistant tumors (Crawford et al., 2009). In addition, CAFs as well as normal connective tissue fibroblasts are major biosynthetic sources of ECM proteins, in which angiogenic growth factors are sequestered. In contrast to typical normal fibroblasts, CAFs can also produce a variety of ECM-degrading enzymes that release such latent angiogenic factors (bFGF, VEGF, TGF-β), rendering them bioavailable to their receptors on endothelial cells (Kalluri and Zeisberg, 2006; Pietras and Ostman, 2010; Räsänen and Vaheri, 2010). Finally, CAFs can produce chemoattractants for proangiogenic macrophages, neutrophils, and other myeloid cells, thereby indirectly orchestrating tumor angiogenesis (Räsänen and Vaheri, 2010; Vong and Kalluri, 2011), as well as directly stimulating recruitment of endothelial precursor cells via secretion of CXCL12 (Orimo and Weinberg, 2007).

Activating Invasion and Metastasis

All three classes of stromal cell are implicated as contributors in one context or another to the capability for invasion and metastasis, as the following examples illustrate.

Angiogenic Vascular Cells. The characteristics of chronically angiogenic (and morphologically abnormal) tumor vasculature have the added effect of contributing to cancer cell dissemination in the course of metastasis. Many tumors express high levels of the proangiogenic factor VEGF, also known and first identified as vascular permeability factor (Senger et al., 1983). VEGF signaling through VEGFR2 loosens tight junctions interconnecting endothelial tube cells, rendering vasculature permeable to leakage of blood into the interstitial TME, and concomitantly lowering barriers for intravasation of cancer cells into the circulation, particularly in tumors with high interstitial fluid pressure, which therefore counteracts pressure inside the vasculature. Tumor vasculature hyperstimulated by VEGF often has reduced pericyte coverage and looser association of such pericytes with endothelium, the significance of which has been revealed in studies where genetic or pharmacologic perturbation of pericyte coverage facilitates metastatic dissemination of cancer cells (Cooke et al., 2012; Xian et al., 2006). Hypoxia in and around tumor vessels also contributes to metastatic dissemination of cancer cells through the actions of genes regulated by hypoxia inducible (HIF) transcription factors, including VEGF and inducible nitric oxide synthase (iNOS), among many mediators. Notably, differential expression of HIFs by endothelial cells (and IICs) is particularly significant for metastasis (Branco-Price et al., 2012; Takeda et al., 2010), as they variably alter vascular tension and function, largely dependent on nitric oxide, which, in turn, loosens pericyte coverage (Kashiwagi et al., 2005), contributing thereby to metastatic success. Such studies establish the concept, still to be generalized, that impaired vascular integrity disables a significant barrier to blood-borne metastasis, and thus facilitates dissemination of cancer cells from primary human tumors.

The vasculature plays a similar role in metastatic seeding at distant sites, where an intact normal endothelium with intimate pericyte coverage can be envisaged to block cancer cell extravasation from the blood into normal parenchyma. Indeed, it is increasingly evident that metastatic primary tumors can precondition the vasculature in metastatic sites with factors such as VEGF, supplied systemically or produced locally by the disseminated cancer cells they spawn; the actions of VEGF on the endothelium at incipient metastatic sites facilitates both loosening of vessel walls for extravasation, and subsequent induction of angiogenesis to support metastatic tumor growth. Still to be clarified is the identification and possible roles of factors produced by endothelial cells and pericytes that contribute to metastatic processes.

Infiltrating Immune Cells. Functional studies spanning the last decade have unambiguously established and elaborated the roles of IICs in fostering metastasis. Mast cells and macrophages in primary tumor TMEs provide a wide range of proteases, including serine, cysteine, and metalloproteases (Kessenbrock et al., 2010; van Kempen et al., 2006) that foster ectopic tissue invasion by remodeling structural components of ECM (fibrillar collagens, elastins, or fibrin), which in turn provide conduits for malignant cell egress, as well as generating ECM fragments with proinvasive signaling activities. For example, the proteolytic activities of MMP-2 expressed by macrophages and other leukocytes effects the release of cryptic ECM fragments by cleaving laminin-5 γ2 chains that, in turn, mimic EGF receptor (EGFR) ligands and thus induce cell motility and invasion (Giannelli et al., 1997; Pirilä et al., 2003). Leukocyte-derived MMP-7 processes proheparin-bound-EGF (HB-EGF) into its bioactive form in pancreatic carcinoma cells (Cheng et al., 2007), resulting in repressed E-cadherin-mediated cell adhesion and potentiation of invasive growth (Wang et al., 2007a). Leukocyte-derived MMP-7 and cathepsin B further facilitate tumor cell motility and invasion by directly cleaving extracellular domains of E-cadherin (Gocheva et al., 2006; Vasiljeva et al., 2006). IIC-derived TNF-α enhances invasive/migratory phenotypes of breast, skin, and ovarian cancer cells through activation of downstream signaling cascades, including the Jun N-terminal kinase (JNK) and nuclear factor κB (NFκB) transcription factors, resulting in induced gene expression of proinvasive factors, e.g., EMMPRIN (extracellular matrix metalloprotease inducer) and MIF (migration inhibitory factor), whose expression enhances

MMP-2 and MMP-9 secretion and activity (Balkwill, 2009). Macrophage-derived TNF-α also potentiates Wnt/beta-catenin signaling during gastric carcinogenesis by activating Akt signaling and GSK3beta phosphorylation in initiated gastric epithelial cells independent of the NFκB pathway (Oguma et al., 2008).

IIC mediators also inhibit expression of known metastasis suppressor genes. T cells and macrophages infiltrating prostate cancers produce the TNF-α-related cytokine RANKL (Receptor Activator for NFκB Ligand). RANKL, through interaction with its receptor RANK, activates Inhibitor of NFκB Kinase α (IKKα), leading to transcriptional repression of the metastatic tumor suppressor gene *maspin* (Abraham et al., 2003; Sager et al., 1997); maspin inhibits metastasis by impairing cancer cell invasion, in part by altering expression of integrin adhesion molecules that anchor and thereby restrict cell mobility (Chen and Yates, 2006). Abrogation of IKKα activity restores *maspin* gene expression and significantly reduces lymphatic and pulmonary metastasis of prostatic tumor cells, further strengthening the causality link (Luo et al., 2007). Notably, in prostate cancer metastasis to bone, RANKL bioavailability, and hence suppression of mapsin in cancer cells, is regulated by osteoclast-supplied MMP-7, illustrating another means by which stromal cells in metastatic microenvironments can provide paracrine support for metastatic colonization (Gorden et al., 2007; Lynch et al., 2005).

Concentration gradients of growth factors established by leukocytes also coordinate tumor cell movement toward, and intravasation into, tumor-associated vasculature. For example, macrophages are the primary source of EGF in the developing mammary gland and in mouse models of breast cancer (Leek et al., 2000; Lewis and Pollard, 2006). EGF promotes invasion/chemotaxis and intravasation of breast carcinoma cells through a paracrine loop operative between tumor cells and macrophages that are required for mammary cancer cell migration (Wyckoff et al., 2004) via cofilin-dependent actin polymerization (Wang et al., 2007b). Transcriptome profiling has revealed that the TAMs participating in this paracrine interplay represent a unique subpopulation that associates intimately with tumor vessels (Ojalvo et al., 2010).

Long suspected but largely below the radar are platelets. A recent report solidified these suspicions (Labelle et al., 2011), revealing that platelets induce a transitory EMT by physically associating with blood-borne cancer cells, facilitating extravasation and seeding of metastases. Functional genetic studies demonstrated that the invasion- and metastasis-promoting activity of platelets involves platelet-derived TGF-ß ligand as well as an inducer of NFκB signaling that requires physical contact of platelets with cancer cells (suggestive perhaps of the membrane-bound Notch ligands). Thus, platelets can be added to the roster of tumor-promoting hematopoietic cells that facilitate invasion and metastasis. It is intriguing to consider the possibility that platelets might intravasate into premalignant tissues or primary tumors via leaky tumor vasculature, contributing therein to induction of EMT and locally invasive growth.

Cancer-Associated Fibroblastic Cells. There are increasing examples wherein CAFs modulate the capability of cancer cells to invade locally or establish secondary tumors at distant metastatic sites. One prominent CAF-derived effector of this capability is the c-Met ligand HGF, which stimulates via heightened c-Met signaling both invasiveness and proliferation. A second, CAF-derived effector, TGF-β, is demonstrably involved in activating EMT programs in certain cancer cells, thereby enabling their capability for invasion and metastasis (Chaffer and Weinberg, 2011); likely additional CAF mediators will prove to be involved in different contexts; thus, for example, CAF/MSC secretion of CCL5 stimulates breast cancer metastasis (Karnoub et al., 2007). Moreover, CAFs produce a distinctive (from normal fibroblasts) repertoire of ECM proteins as well as a variety of ECM remodeling enzymes that further modify the TME, rendering it more supportive of cancer cell invasion, both proximal to the CAFs as well in adjacent normal tissue (Chaffer and Weinberg, 2011; Cirri and Chiarugi, 2011; Kalluri and Zeisberg, 2006; Pietras and Ostman, 2010). CAFs are detected at the invasive fronts in some tumors, consistent with an active collaboration with cancer cells in invasion; such CAFs may reflect comigrating cells as well as normal tissue fibroblasts that have been reprogrammed by signals (e.g., PDGF and sonic hedgehog) released by cancer cells (or IICs). Such reprogramming is also evident in metastasis, where emigrating cancer cells induce expression of the ECM molecule periostin, necessary for efficient colonization in a mouse model of metastatic breast cancer (Malanchi et al., 2012). In another model system, cancer cells disseminate through the circulation in conjunction with primary tumor-derived CAFs (Duda et al., 2010), bringing the foundations of a TME to the metastatic site, a variation on the theme discussed above whereby cancer cells disseminate in association with macrophages or other myeloid cells.

Given the observations that fibrotic breast disease and increased breast density predispose to breast cancer, and that environmentally induced fibrotic disorders increase incidence of lung, skin, and pancreatic cancer, it is evident that the intensity of fibroblastic proliferation, accumulation and assembly may play other influential roles in tumor development and progression. Breast carcinogenesis is accompanied by lysyl oxidase-mediated crosslinking of collagen fibrils (largely produced by CAFs) that imparts a proinvasive phenotype on mammary cancer cells, which is dependent on enhanced PI3 kinase (PI3K) signaling, and associated with integrin clustering and increased presence of focal adhesions (Levental et al., 2009). Notably, genetic or pharmacological blockade of lysyl oxidase-mediated collagen crosslinking impedes late-stage cancer progression in mouse models of mammary carcinogenesis (Levental et al., 2009). Moreover, ablation of CAFs with an inhibitor of hedgehog signaling improves therapeutic delivery of cytotoxic drugs in a mouse model of pancreatic ductal adenocarcinoma, revealing that the desmoplastic stroma erected by CAFs represents a barrier to effective biodistribution of chemotherapy (Olive et al., 2009). The structural effects of CAFs on TMEs have been further revealed by studies perturbing other CAF-derived mediators. Notably, inhibiting either TGF-β, its type I receptor (Kano et al., 2007; Sounni et al., 2010), or the PDGF receptors (Pietras et al., 2001) similarly reduces interstitial fluid pressure in certain tumors, resulting in improved tumor hemodynamics and more favorable biodistribution of drugs, so too does reducing the abundance of the ECM component hyaluronic acid in the TME (Provenzano et al., 2012). Thus, in addition to producing soluble factors that modulate hallmark

phenotypes, CAFs can profoundly alter the physical parameters of the TME in some tumor types, consequently impacting delivery of therapeutics.

Evading Immune Destruction

Angiogenic Vascular Cells. Although the aberrant morphology of the angiogenic tumor vasculature—loosened interconnections between endothelial cells and less intimate association and coverage by pericytes—evidently facilitates transit of cells across the vascular wall in both directions, there is abundant evidence that such routes of transit are in many cases insufficient for the massive influx of natural killer (NK) cells, CTLs, and NK T cells needed to achieve effective killing of cancer cells in tumors. As such, the tumor vasculature contributes to the hallmark capability of evading immune destruction by its inability to support intensive T cell inflammation. Numerous studies have documented this barrier to T cell influx, seen by the absence in tumors of high endothelial venules (HEVs) (Onrust et al., 1996), vascular structures serving as portals for mass transit of lymphocytes into and out of activated lymph nodes and heavily inflamed tissues. More recently, regulatory signals that render tumor vasculature nonpermissive for HEVs and such mass transit of CTLs have been identified, and their modulation was found to break down inflammatory barriers (Fisher et al., 2011; Manzur et al., 2008). Thus, an added benefit of ''anti-angiogenic'' strategies involving inhibition of VEGF signaling and of its consequent vascular abnormalities may be in enabling tumor immunity via HEV induction in the normalized vasculature (Goel et al., 2011; Manzur et al., 2008).

Infiltrating Immune Cells. IIC phenotypes in some tumors are similar to the resolution phase of wound healing, wherein the TME contains significant leukocytic infiltrations that convey immunosuppressive activity (ability to block antitumor CTL or NK/T cell-mediated killing of aberrant cells). These assemblages include regulatory T cells (T_{reg}), iMCs/MDSCs, TAMs programmed by Th2-type cytokines, and neutrophil and mast cell subtypes that collectively endow cancer cells with a mechanism to escape killing by T cells (Ruffell et al., 2010).

Macrophage progenitors exposed to a variety of immune-regulatory cytokines (IL-4, IL-13, etc.) and other factors (thymic stromal lymphopoietin, immune complexes, etc.) can differentiate to become alternatively activated TAMs with various tumor-promoting properties, as elaborated above. Among their distinctive phenotypes is absence of cytotoxic activity typified by conventional tissue macrophages (Qian and Pollard, 2010), instead manifesting an ability to block $CD8^+$ T cell proliferation or infiltration though release of factors with immunosuppressive potential (Denardo et al., 2011; Doedens et al., 2010; Kryczek et al., 2006; Movahedi et al., 2010). TAMs also indirectly foster immune suppression through recruitment of T_{reg} cells via the chemokine CCL22 (Curiel et al., 2004). In murine tumor models, suppression of $CD8^+$ T cell proliferation by TAMs is at least partly dependent on metabolism of L-arginine via arginase-1 or iNOS (Doedens et al., 2010; Movahedi et al., 2010) resulting in production of oxygen radicals or nitrogen species (Lu et al., 2011b; Molon et al., 2011). In human TAMs, suppression of $CD8^+$ T cells can occur independent of L-arginine metabolism (Kryczek et al., 2006) and may instead rely on macrophage expression of ligands for T cell costimulatory receptors that mediate T cell inhibition (Topalian et al., 2012), as has been described for hepatocellular (Kuang et al., 2009) and ovarian (Kryczek et al., 2006) cancer. Data from human tumors indicate that the presence of TAMs expressing immune-suppressive markers correlates with reduced survival of patients with several types of solid tumors, and notably inversely correlates with $CD8^+$ T cell density in human breast cancer (Denardo et al., 2011).

iMCs encompass a diverse population of myeloid cells characterized in part by coexpression of surface markers CD11b and Gr1, and include monocytes variably referred to as MDSCs, inflammatory monocytes, and neutrophils (Ostrand-Rosenberg, 2008). MDSCs and iMCs are functionally characterized by their suppression of T cell proliferation via arginase I, inducible nitric oxide synthase expression, and perioxynitrite, and, at the same time, by their ability to promote generation of T_{reg} cells (Ostrand-Rosenberg, 2008).

While the immunosuppressive activity of mast cells is not well described, it is clear that in addition to their prominent mitogenic and proangiogenic activities as discussed above, they also indirectly regulate immunosuppression (Wasiuk et al., 2009), by releasing cytokines that recruit CTL-suppressing MDSCs and T_{regs}. T_{regs} are also recruited into neoplastic tissues by other cytokines, most notably CCL2 and TGF-β; their abundance (and hence their indictment as tumor promoting) correlates with poor outcome for several cancer types (van der Vliet et al., 2007). T_{regs} typically play an important physiological role in suppressing responses to self-antigens, thereby preventing autoimmunity, and as such can be corrupted to dampen anti-tumor immunity. A related immunosuppressive strategy involves expression of the lymphatic chemokine CCL21 in tumors; CCL21 instructs lymphoid neogenesis and immune tolerization involving MDSCs and T_{regs} so as to prevent autoimmunity; thus, when CCL-21 is ectopically expressed in tumors, it can contribute to suppression of antitumor immunity by altering the differentiation and function of IICs, biasing toward tumor-promoting subtypes (Shields et al., 2010).

Cancer-Associated Fibroblastic Cells. In addition to producing chemokines and other signals that recruit IICs, CAFs can demonstrably inhibit cytotoxic T cells and NK/T cells, in part by producing TGF-ß, thereby blunting destructive inflammatory responses that might otherwise disrupt tumor growth and progression (Stover et al., 2007).

Reprogramming Energy Metabolism

There is now broad appreciation that cancer cells have altered metabolism to support chronic proliferation, in particular, flexible utilization of fuel sources and modes of consuming them to generate energy and biomaterials; most notable is the activation of aerobic glycolysis that complements the output of (sometimes reduced) oxidative phosphorylation for such purposes. While much of metabolic reprogramming is considered to be cell intrinsic to the cancer cells, there are both evident and emergent extrinsic modulators in the TME.

Angiogenic Vascular Cells. Variations in the density and functionality of the angiogenic tumor vasculature are well-established modulators of energy metabolism for the cancer cell; in particular, inadequate vascular function can result in hypoxia, activating the HIF response system, which among its myriad of effects can stimulate aerobic glycolysis, enabling cancer cells to survive and proliferate more effectively in conditions of vascular insufficiency, thereby concomitantly enhancing the

capability for invasive growth. It is of course arguable whether this effect on metabolism truly represents a functional contribution of tumor vasculature to the cancer cell and hence to malignant phenotypes, as opposed to a reaction to its impaired functionality, but the net result remains the same, that the nature of the aberrant vasculature of the TME impacts cancer cell metabolism.

Infiltrating Immune Cells. A specific role for IICs as regulators of altered energy metabolism in cancer cells is beginning to emerge (Trinchieri, 2011). While definitive genetic studies unambiguously linking IICs to tumor cell metabolism are still on the horizon, it has been reported that alternatively activated macrophages are implicated in the altered metabolism of tumors, as well as in the development of metabolic pathologies (Biswas and Mantovani, 2012).

Cancer-Associated Fibroblastic Cells. There is an intriguing line of evidence linking CAFs to an unconventional form of aerobic glycolysis, in which CAFs are induced by reactive oxygen species released by cancer cells to switch on aerobic glycolysis, secreting lactate and pyruvate that, in turn, can serve as fuel for cancer cell proliferation (Rattigan et al., 2012; Sotgia et al., 2012). A particular subclass of CAF, in which the intracellular scaffold protein Caveolin-1 is downregulated (by reactive oxygen species), displays this metabolic support phenotype, resulting in an activated TME that drives early tumor recurrence, metastasis, and poor clinical outcome in breast and prostate cancers (Sotgia et al., 2011). While yet to be generalized, the results (and the association of reduced Caveolin-1 in CAFs with poor prognosis) suggest that heterotypic supply of energy sources to cancer cells may prove to be yet another profound contribution made by CAFs to the TME, above and beyond the aforementioned roles in orchestrating cell proliferation (and survival), angiogenesis, invasion, and metastasis.

Recent data have also revealed that adipocytes similarly engage in ''metabolic coupling'' with cancer cells and thereby promote tumor progression (Martinez-Outschoorn et al., 2012) (Nieman et al., 2011). Metastatic ovarian carcinoma typically seeds into adipose tissue in peritoneum, resulting in reprogramming of proximal adipocytes toward a more catabolic state. In this state, ''activated'' adipocytes generate free fatty acids that are utilized by metastatic ovarian cancer cells to generate ATP via mitochondrial β-oxidation. Mitochondrial metabolism in metastatic ovarian cancer cells is fostered, thereby protecting them from apoptotic cell death, as well as improving chemoresistance, and enhancing their colonization into macrometastatic lesions (Nieman et al., 2011). Looking ahead, it will be interesting to determine if re-educated adipocytes are involved in tumor metabolism in other cancer types, perhaps in partnership with conventional fibroblast-derived CAFs, which as noted above are implicated in metabolic fueling of breast cancer cells (Sotgia et al., 2012).

Thus, a remarkable symbiotic relationship in energy metabolism is emerging between CAFs and cancer cells, in which CAFs in different TMEs can exchange energy sources with cancer cells to optimize metabolic efficiency and tumor growth, involving the alternative use of glucose and lactate, and other energy-rich molecules. The nature of the symbiosis can evidently vary depending on the TME: in some cases, the CAFs switch on aerobic glycolysis, utilizing glucose and secreting lactate that is taken up by cancer cells and used as fuel (Balliet et al., 2011; Ertel et al., 2012; Martinez-Outschoorn et al., 2012; Sotgia et al., 2012). In other cases, the symbiosis is opposite: cancer cells switch on aerobic glycolysis, utilizing glucose and exporting lactate, which the CAFs then take up and use as fuel to drive their tumor-promoting functional activities (Rattigan et al., 2012). No doubt further variations of the energy-sharing theme, and intricacies of mechanism, will be revealed as other TMEs are assessed for their metabolic phenotypes.

Beyond The Hallmarks: Supporting Cancer Stem Cells

It has become evident in the past decade that most if not all malignancies contain a heterogeneous subpopulation of cancer cells with stem-like properties—cancer stem cells (CSCs)—that are instrumental in the pathologic manifestation of cancer, variably affecting initiation, persistence in the face of intrinsic barriers to expansive proliferation, metastatic progression, and the ability to rebound from ostensibly efficacious cancer therapies. Once again, this crucial dimension of the cancer cell is not strictly autonomous; rather, stromal cells demonstrably support CSCs. All three stromal cell classes have been implicated in functional support of CSCs in different neoplastic contexts, including, for example, (1) endothelial cells, pericytes, and perivascular IICs organized into specialized vascular niches in primary tumors (Calabrese et al., 2007) as well as metastatic sites (Kaplan et al., 2005; Lyden et al., 2001; Psaila and Lyden, 2009), and (2) the myofibroblastic/MSC subtype of CAFs, likely also present in metastatic vascular stem cell niches (Kidd et al., 2009; Korkaya et al., 2011; Liu et al., 2011; Spaeth et al., 2008, 2009); similar niche-forming cells may also nurture CSCs inside primary tumors.

In sum, there is compelling evidence for the insidious roles that normal cells play in cancer, having been recruited and/or activated to serve as members of corrupt TMEs, contributing to the functional capabilities embodied in most of the hallmarks of cancer (Figure 1). Their contributions are diverse and variable from one organ and oncogenic foundation in cancer (stem) cells to another. The three general classes of stromal cell contain multiple cell types and subcell types, of which major subtypes and their ascribed functions (in various neoplastic contexts) are summarized in Figure 2.

Challenges in Charting Human Tumor Microenvironments

Much of the functional and correlative evidence presented above implicating stromal mechanisms has come from experiments performed in model systems, principally tumors growing and progressing in genetically engineered mouse models of cancer (GEMM) and human xenotransplant mice (increasingly now primary patient-derived xenotransplants [PDX]), as well as in cell and organ coculture assays. Moreover, the challenges in performing precise genetic manipulations of stromal cells in experimental tumors is considerable, and as such, some of the predicted contributions have not been definitively established in terms of their functional significance in relation to the driving forces embodied in the mutationally transformed cancer cells. And even then, a bigger question remains: do human cancers and their foundation in cancer cells (and cancer stem cells) develop, progress, metastasize, and acquire drug resistance with similar support by accessory cells recruited and redirected

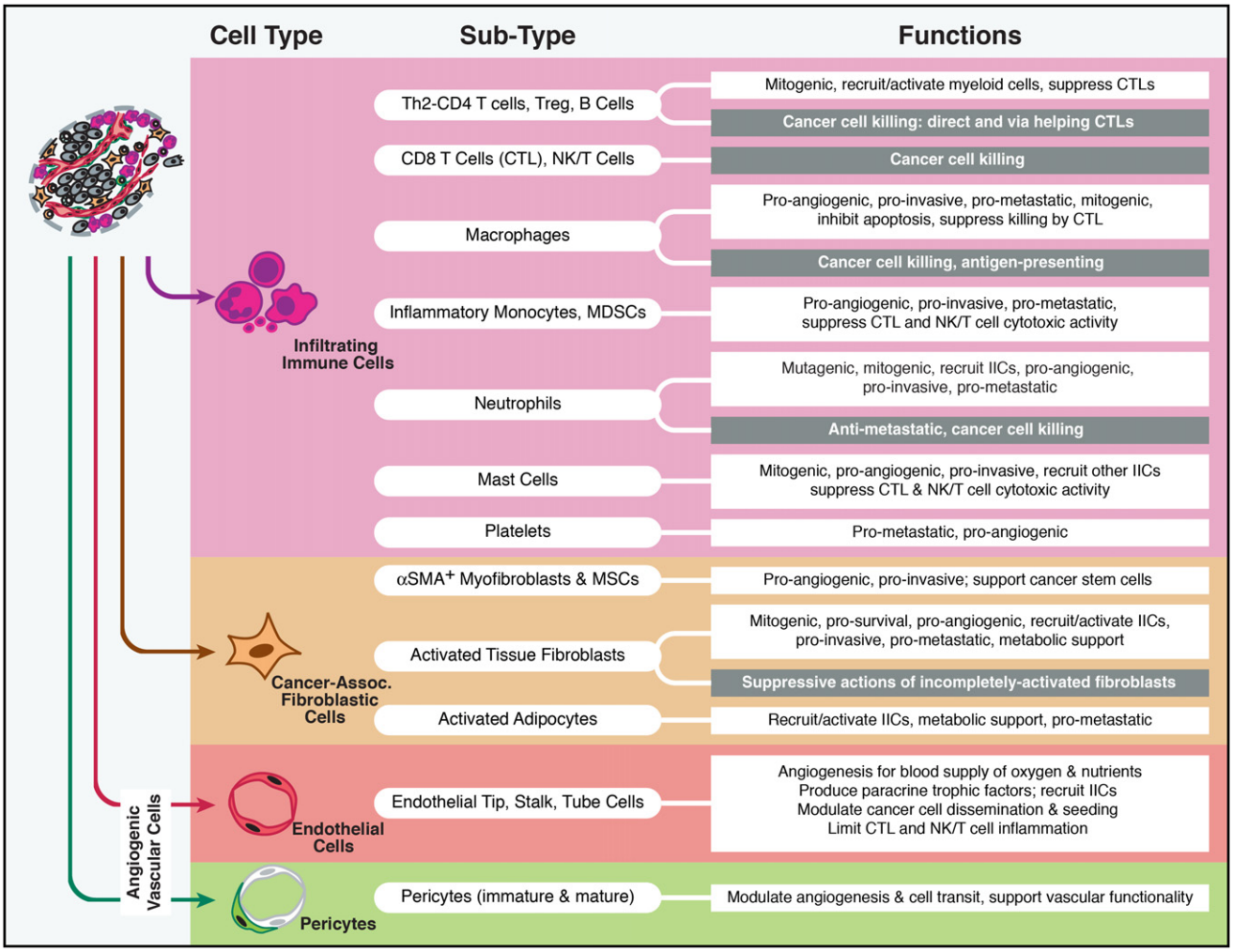

Figure 2. Multiple Stromal Cell Types and Subcell Types of the Tumor Microenvironment Can Variably Contribute to, or in Some Cases Oppose, Acquisition of the Seven Hallmark Functional Capabilities in Different Organ Sites, Tumor Types and Subtypes, and Stages of Progression

Major stromal cell subtypes are indicated, along with a synopsis of key functional contributions that such cell subtypes can make. The antagonistic functions of certain subcell types are highlighted in gray. The lists of subtypes and of their key functions are not comprehensive, but rather prominent examples. Not listed are molecular regulatory signals for, and effector agents of, the noted functions. Both lists will certainly be refined in coming years. Also not shown are the crucial cancer cells and cancer stem cells, with which these stromal cells dynamically interact to manifest cancer phenotypes (Hanahan and Weinberg, 2011). Th2, helper type 2; CD4 T cell, CD4-positive lymphocyte; Treg, regulatory T cell; CTL, cytotoxic T lymphocyte; NK/T, natural killer and natural killer T cell; MDSCs, myeloid-derived suppressor cells; αSMA, alpha smooth muscle actin; MSCs, mesenchymal stem cells.

to constitute an essential TME? And, how can their roles and functional importance be clarified across the broad spectrum of human malignancies, factoring in differences to the histologically distinct stages of tumor development and progression, the molecular genetic subtypes being recognized for many human cancers, and the individual patient to patient variations that are increasingly appreciated? Certainly, there is epidemiological evidence associating abundance of particular stromal cell types—density of neovascularization and abundance of tumor-promoting versus tumor antagonizing IICs—with prognosis in various human cancers (Balkwill and Mantovani, 2011). Beyond epidemiology, the path toward clarification is challenging. One possible approach may involve integration of representative mouse models of particular cancers (GEMM and PDX) with morphology-retaining biopsies and surgical resections from cancer patients: hypotheses and knowledge developed via functional studies in mouse models could be validated by analyzing the primary human samples for predicted determinants indicative of functional correlation. Among the analytic techniques that can be envisioned are (1) advanced histochemical methodology (multicolor immunostaining and in situ RNA hybridization); (2) precise laser capture microdissection of stromal cell types and subtypes populating lesions, facilitated by selective antibody capture, followed by bimolecular analysis, including deep sequencing of mRNA and miRNA; and (3) purification by flow cytometry—also using antibody and other cell surface identifiers—of viable stromal subcell types, followed by cell bioassays and molecular genetic analyses, again leveraging tools and knowledge from the model system(s) to ask if the human lesion manifests similar stromal cells and

functional effectors. Crosstalk and coordinated signaling pathways between neoplastic cells and stromal cell types identified in mouse models seem likely to prove indicative of similar (if not identical) interactions operating in cognate human tumors, but the challenge will be to establish the correlation. Initial glimpses into the power of evaluating human tumor stroma for risk prediction has provided tantalizing information indicating that aspects of the TME significantly correlate with overall survival, as well as response to therapy (Beck et al., 2011; Denardo et al., 2011; Finak et al., 2008). Advancements in noninvasive imaging and analysis of blood-borne tumor-derived material may also prove of value for profiling the constituents of the tumor stroma (Daldrup-Link et al., 2011; Weissleder, 2006). The future challenge is considerable, but the imperative to pursue it is clear, as there is little doubt that the TME and its conscripted stromal cells will prove to be instrumental factors in many human malignancies.

Prospects and Obstacles for Therapeutic Targeting of Function-Enabling Stromal Cell Types

The demonstrable roles that stromal cells can in principle play in enabling or enhancing multiple hallmark capabilities (Figures 1 and 2) in different TMEs clearly motivates therapeutic targeting strategies aimed to abrogate their contributions. The task, however, will not be easy. A case in point involves antiangiogenic therapy, anticipated for decades as a paradigm-shifting approach to treating human cancer, by abrogating an essential hallmark capability. Potent angiogenic inhibitors have been developed, principally aimed at the VEGF and other proangiogenic signaling pathways. Several such drugs have successfully surpassed the efficacy bar in phase 3 clinical trials, and are consequently approved for use in particular cancer indications, representing a proof of principle that a hallmark-enabling stromal cell type is a valid therapeutic target. The reality check, however, is that clinical responses are typically transitory, and survival benefit limited in duration, indicative of the development of adaptive resistance; the explanation is likely multifactorial, based on preclinical studies in mouse models, which have revealed in some cases evasion of the signaling blockage (Casanovas et al., 2005), in others recruitment of additional or different subtypes of proangiogenic IICs or CAFs (Priceman et al., 2010; Shojaei et al., 2007), and in others shifting to heightened dependence on invasion and metastasis to co-opt normal tissue vasculature instead of producing a neovasculature (Ebos and Kerbel, 2011; Pàez-Ribes et al., 2009; Sennino et al., 2012). While sobering, such results nevertheless suggest solutions: if mechanisms of adaptive-evasive resistance to antiangiogenic therapy that are operative in particular cancer types can be identified and cotargeted, perhaps antiangiogenic therapy in such cancers can be rendered more enduring. There is similar promise, and likely pitfalls, in targeting CAFs and specific IIC subtypes, in regard to the goal of short-circuiting the multiple functional contributions they make to hallmark capabilities. One can anticipate both beneficial effects, and adaptive resistance. In regard to targeting tumor-promoting IICs, there are both encouraging examples (Denardo et al., 2011; Giraudo et al., 2004; Mazzieri et al., 2011; Pietras et al., 2008; Shree et al., 2011), and sobering cases of adaptive resistance, including substitution of a targeted subtype by another with redundant capabilities (Casanovas, 2011; Pahler et al., 2008). Here again, identification of resistance mechanisms may enable combinatorial strategies that counteract adaptive resistance when targeting CAFs and IICs and their functional contributions to hallmark capabilities, improving therapeutic efficacy. Such promise, however, may be qualified by yet another confounding complexity that will likely need to be addressed: individual patient heterogeneity. Thus, it may prove instrumental to factor into the equation individual variations in tumors from different patients. While ostensibly of the same type and histological and/or molecular genetic subtype, individual tumors may nevertheless have profound (and subtle) differences —in cancer cells and likely in the character or abundance of stromal cell (sub)-types that impact critical attributes of the TME, thereby consequently determining the extent of beneficial responses to mechanism-guided therapeutic (co)-targeting; this emerging realization is spawning the frontier of personalized cancer therapy (Haber et al., 2011; Martini et al., 2011). As alluded above, technology development and more routine protocols for informative tumor biopsy may allow the precise constitution of function-enhancing/enabling stromal cell types in a patient's (primary and/or metastatic) TME to be revealed, allowing fine tuning of therapeutic strategies with greater potential for beneficial impact on the disease.

Conclusions

Cancer medicine is increasingly moving toward a new era of personalized diagnostics and therapeutics that aggressively embraces integrative approaches (De Palma and Hanahan, 2012). Looking forward, combinatorial strategies will target not only cancer cell-intrinsic pathways, but also cancer cell-extrinsic cells, pathways, and mediators at play in the TME. As the strategic goal of deciphering the roles of the TME in primary and metastatic tumor locales progresses, new discoveries can be envisioned to produce innovative multitargeting strategies that will be able to more thoroughly extinguish primary and metastatic disease, while circumventing elucidated adaptive resistance mechanisms to such therapies, profoundly altering the prognosis for many forms of human cancer (De Palma and Hanahan, 2012).

ACKNOWLEDGMENTS

We than Terry Schoop of OFC Graphics, Kensington, CA, for refinement and preparation of the figures, and Dr. Michele De Palma for critical reading of the manuscript.

REFERENCES

Abraham, S., Zhang, W., Greenberg, N., and Zhang, M. (2003). J. Urol. *169*, 1157–1161.

Armulik, A., Abramsson, A., and Betsholtz, C. (2005). Circ. Res. *97*, 512–523.

Balkwill, F. (2009). Nat. Rev. Cancer *9*, 361–371.

Balkwill, F., Charles, K.A., and Mantovani, A. (2005). Cancer Cell *7*, 211–217.

Balkwill, F.R., and Mantovani, A. (2011). Semin. Cancer Biol.

Balliet, R.M., Capparelli, C., Guido, C., Pestell, T.G., Martinez-Outschoorn, U.E., Lin, Z., Whitaker-Menezes, D., Chiavarina, B., Pestell, R.G., Howell, A., et al. (2011). Cell Cycle *10*, 4065–4073.

Beck, A.H., Sangoi, A.R., Leung, S.M., Marinelli, R.J., Nielsen, T.O., van de Vijver, M.J., West, R.B., van de Rijn, M., and Koller, D. (2011). Sci. Trans. Med. *3*, 108ra113.

Bergers, G., Javaherian, K., Lo, K.M., Folkman, J., and Hanahan, D. (1999). Science *284*, 808–812.

Bergers, G., Brekken, R., McMahon, G., Vu, T.H., Itoh, T., Tamaki, K., Tanzawa, K., Thorpe, P., Itohara, S., Werb, Z., and Hanahan, D. (2000). Nat. Cell Biol. *2*, 737–744.

Bissell, M.J., and Hines, W.C. (2011). Nat. Med. *17*, 320–329.

Bissell, M.J., Hall, H.G., and Parry, G. (1982). J. Theor. Biol. *99*, 31–68.

Biswas, S.K., and Mantovani, A. (2012). Cell Metab., in press.

Bochet, L., Meulle, A., Imbert, S., Salles, B., Valet, P., and Muller, C. (2011). Biochem. Biophys. Res. Commun. *411*, 102–106.

Branco-Price, C., Zhang, N., Schnelle, M., Evans, C., Katschinski, D.M., Liao, D., Ellies, L., and Johnson, R.S. (2012). Cancer Cell *21*, 52–65.

Brem, H., Gresser, I., Grosfeld, J., and Folkman, J. (1993). J. Pediatr. Surg. *28*, 1253–1257.

Butler, J.M., Kobayashi, H., and Rafii, S. (2010). Nat. Rev. Cancer *10*, 138–146.

Calabrese, C., Poppleton, H., Kocak, M., Hogg, T.L., Fuller, C., Hamner, B., Oh, E.Y., Gaber, M.W., Finklestein, D., Allen, M., et al. (2007). Cancer Cell *11*, 69–82.

Carmeliet, P., and Jain, R.K. (2011). Nature *473*, 298–307.

Casanovas, O. (2011). J. Clin. Invest. *121*, 1244–1247.

Casanovas, O., Hicklin, D.J., Bergers, G., and Hanahan, D. (2005). Cancer Cell *8*, 299–309.

Celis, J.E., Moreira, J.M., Cabezón, T., Gromov, P., Friis, E., Rank, F., and Gromova, I. (2005). Mol. Cell. Proteomics *4*, 492–522.

Chaffer, C.L., and Weinberg, R.A. (2011). Science *331*, 1559–1564.

Chen, E.I., and Yates, J.R. (2006). IUBMB Life *58*, 25–29.

Chen, Q., Zhang, X.H., and Massagué, J. (2011). Cancer Cell *20*, 538–549.

Cheng, K., Xie, G., and Raufman, J.P. (2007). Biochem. Pharmacol. *73*, 1001–1012.

Chow, A., Brown, B.D., and Merad, M. (2011). Nat. Rev. Immunol. *11*, 788–798.

Cirri, P., and Chiarugi, P. (2011). Cancer Metastasis Rev. Published online November 11, 2011.

Cooke, V.G., LeBleu, V.S., Keskin, D., Khan, Z., O'Connell, J.T., Teng, Y., Duncan, M.B., Xie, L., Maeda, G., Vong, S., et al. (2012). Cancer Cell *21*, 66–81.

Coussens, L.M., Raymond, W.W., Bergers, G., Laig-Webster, M., Behrendtsen, O., Werb, Z., Caughey, G.H., and Hanahan, D. (1999). Genes Dev. *13*, 1382–1397.

Crawford, Y., Kasman, I., Yu, L., Zhong, C., Wu, X., Modrusan, Z., Kaminker, J., and Ferrara, N. (2009). Cancer Cell *15*, 21–34.

Curiel, T.J., Coukos, G., Zou, L., Alvarez, X., Cheng, P., Mottram, P., Evdemon-Hogan, M., Conejo-Garcia, J.R., Zhang, L., Burow, M., et al. (2004). Nat. Med. *10*, 942–949.

Daenen, L.G., Shaked, Y., Man, S., Xu, P., Voest, E.E., Hoffman, R.M., Chaplin, D.J., and Kerbel, R.S. (2009). Mol. Cancer Ther. *8*, 2872–2881.

Daldrup-Link, H.E., Golovko, D., Ruffell, B., Denardo, D.G., Castaneda, R., Ansari, C., Rao, J., Tikhomirov, G.A., Wendland, M.F., Corot, C., and Coussens, L.M. (2011). Clin. Cancer Res. *17*, 5695–5704.

De Bock, K., Cauwenberghs, S., and Carmeliet, P. (2011). Curr. Opin. Genet. Dev. *21*, 73–79.

De Palma, M., and Coussens, L.M. (2008). Immune cells and inflammatory mediators as regulators of tumor angiogenesis. In Angiogenesis: An Integrative Approach from Science to Medicine, W.D. Figg and J. Folkman, eds. (New York: Springer), pp. 225–238.

De Palma, M., and Hanahan, D. (2012). Mol. Oncol.. 10.1016/j.molonc.2012.01.011.

Denardo, D.G., Brennan, D.J., Rexhepaj, E., Ruffell, B., Shiao, S.L., Madden, S.F., Gallagher, W.M., Wadhwani, N., Keil, S.D., Junaid, S.A., et al. (2011). Cancer Discov *1*, 54–67.

Dirat, B., Bochet, L., Dabek, M., Daviaud, D., Dauvillier, S., Majed, B., Wang, Y.Y., Meulle, A., Salles, B., Le Gonidec, S., et al. (2011). Cancer Res. *71*, 2455–2465.

Doedens, A.L., Stockmann, C., Rubinstein, M.P., Liao, D., Zhang, N., DeNardo, D.G., Coussens, L.M., Karin, M., Goldrath, A.W., and Johnson, R.S. (2010). Cancer Res. *70*, 7465–7475.

Du, R., Lu, K.V., Petritsch, C., Liu, P., Ganss, R., Passegué, E., Song, H., Vandenberg, S., Johnson, R.S., Werb, Z., and Bergers, G. (2008). Cancer Cell *13*, 206–220.

Duda, D.G., Duyverman, A.M., Kohno, M., Snuderl, M., Steller, E.J., Fukumura, D., and Jain, R.K. (2010). Proc. Natl. Acad. Sci. USA *107*, 21677–21682.

Dvorak, H.F. (1986). N. Engl. J. Med. *315*, 1650–1659.

Dvorak, H.F., Weaver, V.M., Tlsty, T.D., and Bergers, G. (2011). J. Surg. Oncol. *103*, 468–474.

Ebos, J.M., and Kerbel, R.S. (2011). Nat Rev Clin Oncol *8*, 210–221.

Erez, N., Truitt, M., Olson, P., Arron, S.T., and Hanahan, D. (2010). Cancer Cell *17*, 135–147.

Ertel, A., Tsirigos, A., Whitaker-Menezes, D., Birbe, R.C., Pavlides, S., Martinez-Outschoorn, U.E., Pestell, R.G., Howell, A., Sotgia, F., and Lisanti, M.P. (2012). Cell Cycle *11*, 253–263.

Ferrara, N., and Alitalo, K. (1999). Nat. Med. *5*, 1359–1364.

Finak, G., Bertos, N., Pepin, F., Sadekova, S., Souleimanova, M., Zhao, H., Chen, H., Omeroglu, G., Meterissian, S., Omeroglu, A., et al. (2008). Nat. Med. *14*, 518–527.

Fischer, C., Jonckx, B., Mazzone, M., Zacchigna, S., Loges, S., Pattarini, L., Chorianopoulos, E., Liesenborghs, L., Koch, M., De Mol, M., et al. (2007). Cell *131*, 463–475.

Fisher, D.T., Chen, Q., Skitzki, J.J., Muhitch, J.B., Zhou, L., Appenheimer, M.M., Vardam, T.D., Weis, E.L., Passanese, J., Wang, W.C., et al. (2011). J. Clin. Invest. *121*, 3846–3859.

Flaberg, E., Markasz, L., Petranyi, G., Stuber, G., Dicso, F., Alchihabi, N., Oláh, E., Csízy, I., Józsa, T., Andrén, O., et al. (2011). Int. J. Cancer *128*, 2793–2802.

Folkman, J. (1974). Adv. Cancer Res. *19*, 331–358.

Folkman, J., Watson, K., Ingber, D., and Hanahan, D. (1989). Nature *339*, 58–61.

Franco, O.E., Shaw, A.K., Strand, D.W., and Hayward, S.W. (2010). Semin. Cell Dev. Biol. *21*, 33–39.

Gabrilovich, D.I., and Nagaraj, S. (2009). Nat. Rev. Immunol. *9*, 162–174.

Giannelli, G., Falk-Marzillier, J., Schiraldi, O., Stetler-Stevenson, W.G., and Quaranta, V. (1997). Science *277*, 225–228.

Giraudo, E., Inoue, M., and Hanahan, D. (2004). J. Clin. Invest. *114*, 623–633.

Gocheva, V., Zeng, W., Ke, D., Klimstra, D., Reinheckel, T., Peters, C., Hanahan, D., and Joyce, J.A. (2006). Genes Dev. *20*, 543–556.

Goel, S., Duda, D.G., Xu, L., Munn, L.L., Boucher, Y., Fukumura, D., and Jain, R.K. (2011). Physiol. Rev. *91*, 1071–1121.

Gorden, D.L., Fingleton, B., Crawford, H.C., Jansen, D.E., Lepage, M., and Matrisian, L.M. (2007). Int. J. Cancer *121*, 495–500.

Guerra, C., Collado, M., Navas, C., Schuhmacher, A.J., Hernández-Porras, I., Cañamero, M., Rodriguez-Justo, M., Serrano, M., and Barbacid, M. (2011). Cancer Cell *19*, 728–739.

Haber, D.A., Gray, N.S., and Baselga, J. (2011). Cell *145*, 19–24.

Hanahan, D., and Folkman, J. (1996). Cell *86*, 353–364.

Hanahan, D., and Weinberg, R.A. (2000). Cell *100*, 57–70.

Hanahan, D., and Weinberg, R.A. (2011). Cell *144*, 646–674.

Hezel, A.F., and Bardeesy, N. (2008). Oncogene *27*, 6908–6919.

Jain, R.K. (2005). Science *307*, 58–62.

Kalluri, R., and Zeisberg, M. (2006). Nat. Rev. Cancer *6*, 392–401.

Kano, M.R., Bae, Y., Iwata, C., Morishita, Y., Yashiro, M., Oka, M., Fujii, T., Komuro, A., Kiyono, K., Kaminishi, M., et al. (2007). Proc. Natl. Acad. Sci. USA *104*, 3460–3465.

Kaplan, R.N., Riba, R.D., Zacharoulis, S., Bramley, A.H., Vincent, L., Costa, C., MacDonald, D.D., Jin, D.K., Shido, K., Kerns, S.A., et al. (2005). Nature *438*, 820–827.

Karnoub, A.E., Dash, A.B., Vo, A.P., Sullivan, A., Brooks, M.W., Bell, G.W., Richardson, A.L., Polyak, K., Tubo, R., and Weinberg, R.A. (2007). Nature *449*, 557–563.

Kashiwagi, S., Izumi, Y., Gohongi, T., Demou, Z.N., Xu, L., Huang, P.L., Buerk, D.G., Munn, L.L., Jain, R.K., and Fukumura, D. (2005). J. Clin. Invest. *115*, 1816–1827.

Kessenbrock, K., Plaks, V., and Werb, Z. (2010). Cell *141*, 52–67.

Kessler, D.A., Langer, R.S., Pless, N.A., and Folkman, J. (1976). Int. J. Cancer *18*, 703–709.

Khandekar, M.J., Cohen, P., and Spiegelman, B.M. (2011). Nat. Rev. Cancer *11*, 886–895.

Khazaie, K., Blatner, N.R., Khan, M.W., Gounari, F., Gounaris, E., Dennis, K., Bonertz, A., Tsai, F.N., Strouch, M.J., Cheon, E., et al. (2011). Cancer Metastasis Rev. *30*, 45–60.

Kidd, S., Spaeth, E., Dembinski, J.L., Dietrich, M., Watson, K., Klopp, A., Battula, V.L., Weil, M., Andreeff, M., and Marini, F.C. (2009). Stem Cells *27*, 2614–2623.

Korkaya, H., Liu, S., and Wicha, M.S. (2011). J. Clin. Invest. *121*, 3804–3809.

Kryczek, I., Zou, L., Rodriguez, P., Zhu, G., Wei, S., Mottram, P., Brumlik, M., Cheng, P., Curiel, T., Myers, L., et al. (2006). J. Exp. Med. *203*, 871–881.

Kuang, D.M., Zhao, Q., Peng, C., Xu, J., Zhang, J.P., Wu, C., and Zheng, L. (2009). J. Exp. Med. *206*, 1327–1337.

Labelle, M., Begum, S., and Hynes, R.O. (2011). Cancer Cell *20*, 576–590.

Leek, R.D., Hunt, N.C., Landers, R.J., Lewis, C.E., Royds, J.A., and Harris, A.L. (2000). J. Pathol. *190*, 430–436.

Levental, K.R., Yu, H., Kass, L., Lakins, J.N., Egeblad, M., Erler, J.T., Fong, S.F., Csiszar, K., Giaccia, A., Weninger, W., et al. (2009). Cell *139*, 891–906.

Lewis, C.E., and Pollard, J.W. (2006). Cancer Res. *66*, 605–612.

Lin, E.Y., Li, J.F., Bricard, G., Wang, W., Deng, Y., Sellers, R., Porcelli, S.A., and Pollard, J.W. (2007). Mol. Oncol. *1*, 288–302.

Liu, S., Ginestier, C., Ou, S.J., Clouthier, S.G., Patel, S.H., Monville, F., Korkaya, H., Heath, A., Dutcher, J., Kleer, C.G., et al. (2011). Cancer Res. *71*, 614–624.

Loeffler, M., Krüger, J.A., Niethammer, A.G., and Reisfeld, R.A. (2006). J. Clin. Invest. *116*, 1955–1962.

Lu, P., Takai, K., Weaver, V.M., and Werb, Z. (2011a). Cold Spring Harb. Perspect. Biol. *3*. 10.1101/cshperspect.a005058.

Lu, T., Ramakrishnan, R., Altiok, S., Youn, J.I., Cheng, P., Celis, E., Pisarev, V., Sherman, S., Sporn, M.B., and Gabrilovich, D. (2011b). J. Clin. Invest. *121*, 4015–4029.

Lu, X., Mu, E., Wei, Y., Riethdorf, S., Yang, Q., Yuan, M., Yan, J., Hua, Y., Tiede, B.J., Lu, X., et al. (2011c). Cancer Cell *20*, 701–714.

Luo, J.L., Tan, W., Ricono, J.M., Korchynskyi, O., Zhang, M., Gonias, S.L., Cheresh, D.A., and Karin, M. (2007). Nature *446*, 690–694.

Lyden, D., Hattori, K., Dias, S., Costa, C., Blaikie, P., Butros, L., Chadburn, A., Heissig, B., Marks, W., Witte, L., et al. (2001). Nat. Med. *7*, 1194–1201.

Lynch, C.C., Hikosaka, A., Acuff, H.B., Martin, M.D., Kawai, N., Singh, R.K., Vargo-Gogola, T.C., Begtrup, J.L., Peterson, T.E., Fingleton, B., et al. (2005). Cancer Cell *7*, 485–496.

Malanchi, I., Santamaria-Martínez, A., Susanto, E., Peng, H., Lehr, H.A., Delaloye, J.F., and Huelsken, J. (2012). Nature *481*, 85–89.

Mantovani, A., Allavena, P., Sica, A., and Balkwill, F. (2008). Nature *454*, 436–444.

Mantovani, A., Cassatella, M.A., Costantini, C., and Jaillon, S. (2011). Nat. Rev. Immunol. *11*, 519–531.

Manzur, M., Hamzah, J., and Ganss, R. (2008). Cell Cycle *7*, 2452–2455.

Martinez-Outschoorn, U.E., Sotgia, F., and Lisanti, M.P. (2012). Cell Metab. *15*, 4–5.

Martini, M., Vecchione, L., Siena, S., Tejpar, S., and Bardelli, A. (2011). Nat. Rev. Clin. Oncol. *9*, 87–97.

Mazzieri, R., Pucci, F., Moi, D., Zonari, E., Ranghetti, A., Berti, A., Politi, L.S., Gentner, B., Brown, J.L., Naldini, L., and De Palma, M. (2011). Cancer Cell *19*, 512–526.

McDonald, D.M., and Choyke, P.L. (2003). Nat. Med. *9*, 713–725.

Mohamed, M.M., and Sloane, B.F. (2006). Nat. Rev. Cancer *6*, 764–775.

Molon, B., Ugel, S., Del Pozzo, F., Soldani, C., Zilio, S., Avella, D., De Palma, A., Mauri, P., Monegal, A., Rescigno, M., et al. (2011). J. Exp. Med. *208*, 1949–1962.

Morikawa, S., Baluk, P., Kaidoh, T., Haskell, A., Jain, R.K., and McDonald, D.M. (2002). Am. J. Pathol. *160*, 985–1000.

Motzer, R.J., Michaelson, M.D., Redman, B.G., Hudes, G.R., Wilding, G., Figlin, R.A., Ginsberg, M.S., Kim, S.T., Baum, C.M., DePrimo, S.E., et al. (2006). J. Clin. Oncol. *24*, 16–24.

Movahedi, K., Laoui, D., Gysemans, C., Baeten, M., Stangé, G., Van den Bossche, J., Mack, M., Pipeleers, D., In't Veld, P., De Baetselier, P., and Van Ginderachter, J.A. (2010). Cancer Res. *70*, 5728–5739.

Nieman, K.M., Kenny, H.A., Penicka, C.V., Ladanyi, A., Buell-Gutbrod, R., Zillhardt, M.R., Romero, I.L., Carey, M.S., Mills, G.B., Hotamisligil, G.S., et al. (2011). Nat. Med. *17*, 1498–1503.

Nozawa, H., Chiu, C., and Hanahan, D. (2006). Proc. Natl. Acad. Sci. USA *103*, 12493–12498.

Oguma, K., Oshima, H., Aoki, M., Uchio, R., Naka, K., Nakamura, S., Hirao, A., Saya, H., Taketo, M.M., and Oshima, M. (2008). EMBO J. *27*, 1671–1681.

Ojalvo, L.S., Whittaker, C.A., Condeelis, J.S., and Pollard, J.W. (2010). J. Immunol. *184*, 702–712.

Olive, K.P., Jacobetz, M.A., Davidson, C.J., Gopinathan, A., McIntyre, D., Honess, D., Madhu, B., Goldgraben, M.A., Caldwell, M.E., Allard, D., et al. (2009). Science *324*, 1457–1461.

Onrust, S.V., Hartl, P.M., Rosen, S.D., and Hanahan, D. (1996). J. Clin. Invest. *97*, 54–64.

Orimo, A., and Weinberg, R.A. (2007). Cancer Biol. Ther. *6*, 618–619.

Orimo, A., Gupta, P.B., Sgroi, D.C., Arenzana-Seisdedos, F., Delaunay, T., Naeem, R., Carey, V.J., Richardson, A.L., and Weinberg, R.A. (2005). Cell *121*, 335–348.

Ostrand-Rosenberg, S. (2008). Curr. Opin. Genet. Dev. *18*, 11–18.

Pàez-Ribes, M., Allen, E., Hudock, J., Takeda, T., Okuyama, H., Viñals, F., Inoue, M., Bergers, G., Hanahan, D., and Casanovas, O. (2009). Cancer Cell *15*, 220–231.

Pahler, J.C., Tazzyman, S., Erez, N., Chen, Y.Y., Murdoch, C., Nozawa, H., Lewis, C.E., and Hanahan, D. (2008). Neoplasia *10*, 329–340.

Parangi, S., O'Reilly, M., Christofori, G., Holmgren, L., Grosfeld, J., Folkman, J., and Hanahan, D. (1996). Proc. Natl. Acad. Sci. USA *93*, 2002–2007.

Partanen, J.I., Nieminen, A.I., and Klefstrom, J. (2009). Cell Cycle *8*, 716–724.

Paunescu, V., Bojin, F.M., Tatu, C.A., Gavriliuc, O.I., Rosca, A., Gruia, A.T., Tanasie, G., Bunu, C., Crisnic, D., Gherghiceanu, M., et al. (2011). J. Cell. Mol. Med. *15*, 635–646.

Pietras, K., and Ostman, A. (2010). Exp. Cell Res. *316*, 1324–1331.

Pietras, K., Ostman, A., Sjöquist, M., Buchdunger, E., Reed, R.K., Heldin, C.H., and Rubin, K. (2001). Cancer Res. *61*, 2929–2934.

Pietras, K., Pahler, J., Bergers, G., and Hanahan, D. (2008). PLoS Med. *5*, e19.

Pirilä, E., Ramamurthy, N.S., Sorsa, T., Salo, T., Hietanen, J., and Maisi, P. (2003). Dig. Dis. Sci. *48*, 93–98.

Pontiggia, O., Sampayo, R., Raffo, D., Motter, A., Xu, R., Bissell, M.J., de Kier Joffé, E.B., and Simian, M. (2011). Breast Cancer Res. Treat. Published online September 21, 2011.

Porta, C., Riboldi, E., Totaro, M.G., Strauss, L., Sica, A., and Mantovani, A. (2011). Immunotherapy *3*, 1185–1202.

Priceman, S.J., Sung, J.L., Shaposhnik, Z., Burton, J.B., Torres-Collado, A.X., Moughon, D.L., Johnson, M., Lusis, A.J., Cohen, D.A., Iruela-Arispe, M.L., and Wu, L. (2010). Blood *115*, 1461–1471.

Provenzano, P.P., Cuevas, C., Chang, A.E., Goel, V.K., Von Hoff, D.D., and Hingorani, S.R. (2012). Cancer Cell, in press.

Psaila, B., and Lyden, D. (2009). Nat. Rev. Cancer *9*, 285–293.

Qian, B.Z., and Pollard, J.W. (2010). Cell *141*, 39–51.

Räsänen, K., and Vaheri, A. (2010). Exp. Cell Res. *316*, 2713–2722.

Rattigan, Y.I., Patel, B.B., Ackerstaff, E., Sukenick, G., Koutcher, J.A., Glod, J.W., and Banerjee, D. (2012). Exp. Cell Res. *318*, 326–335.

Rolny, C., Mazzone, M., Tugues, S., Laoui, D., Johansson, I., Coulon, C., Squadrito, M.L., Segura, I., Li, X., Knevels, E., et al. (2011). Cancer Cell *19*, 31–44.

Rosen, E.D., and MacDougald, O.A. (2006). Nat. Rev. Mol. Cell Biol. *7*, 885–896.

Ruffell, B., DeNardo, D.G., Affara, N.I., and Coussens, L.M. (2010). Cytokine Growth Factor Rev. *21*, 3–10.

Ruffell, B., Au, A., Rugo, H.S., Esserman, L.J., Hwang, E.S., and Coussens, L.M. (2011). Proc. Natl. Acad. Sci. USA. *109*, 2796–2801.

Sabrkhany, S., Griffioen, A.W., and Oude Egbrink, M.G. (2011). Biochim. Biophys. Acta *1815*, 189–196.

Sager, R., Sheng, S., Pemberton, P., and Hendrix, M.J. (1997). Adv. Exp. Med. Biol. *425*, 77–88.

Senger, D.R., Galli, S.J., Dvorak, A.M., Perruzzi, C.A., Harvey, V.S., and Dvorak, H.F. (1983). Science *219*, 983–985.

Sennino, B., Ishiguro-Oonuma, T., Wei, Y., Naylor, R.N., Williamson, C.W., Bhagwandin, V., Tabruyn, S.P., You, W.-K., Chapman, H.A., Christensen, J.G., et al. (2012). Cancer Discovery. Published online February 24, 2012. 10.1158/2159-8290.

Shaheen, R.M., Davis, D.W., Liu, W., Zebrowski, B.K., Wilson, M.R., Bucana, C.D., McConkey, D.J., McMahon, G., and Ellis, L.M. (1999). Cancer Res. *59*, 5412–5416.

Shields, J.D., Kourtis, I.C., Tomei, A.A., Roberts, J.M., and Swartz, M.A. (2010). Science *328*, 749–752.

Shojaei, F., Wu, X., Malik, A.K., Zhong, C., Baldwin, M.E., Schanz, S., Fuh, G., Gerber, H.P., and Ferrara, N. (2007). Nat. Biotechnol. *25*, 911–920.

Shree, T., Olson, O.C., Elie, B.T., Kester, J.C., Garfall, A.L., Simpson, K., Bell-McGuinn, K.M., Zabor, E.C., Brogi, E., and Joyce, J.A. (2011). Genes Dev. *25*, 2465–2479.

Sotgia, F., Martinez-Outschoorn, U.E., Pavlides, S., Howell, A., Pestell, R.G., and Lisanti, M.P. (2011). Breast Cancer Res. *13*, 213.

Sotgia, F., Martinez-Outschoorn, U.E., Howell, A., Pestell, R.G., Pavlides, S., and Lisanti, M.P. (2012). Annu. Rev. Pathol. *7*, 423–467.

Soucek, L., Lawlor, E.R., Soto, D., Shchors, K., Swigart, L.B., and Evan, G.I. (2007). Nat. Med. *13*, 1211–1218.

Sounni, N.E., Dehne, K., van Kempan, L.C.L., Egeblad, M., Affara, N.I., Cuevas, I., Wiesen, J., Junankar, S., Korets, L.V., Lee, J., et al. (2010). Dis. Model Mech. *3*, 317–332.

Spaeth, E., Klopp, A., Dembinski, J., Andreeff, M., and Marini, F. (2008). Gene Ther. *15*, 730–738.

Spaeth, E.L., Dembinski, J.L., Sasser, A.K., Watson, K., Klopp, A., Hall, B., Andreeff, M., and Marini, F. (2009). PLoS ONE *4*, e4992.

Stockmann, C., Doedens, A., Weidemann, A., Zhang, N., Takeda, N., Greenberg, J.I., Cheresh, D.A., and Johnson, R.S. (2008). Nature *456*, 814–818.

Stover, D.G., Bierie, B., and Moses, H.L. (2007). J. Cell. Biochem. *101*, 851–861.

Takeda, N., O'Dea, E.L., Doedens, A., Kim, J.W., Weidemann, A., Stockmann, C., Asagiri, M., Simon, M.C., Hoffmann, A., and Johnson, R.S. (2010). Genes Dev. *24*, 491–501.

Tlsty, T.D., and Coussens, L.M. (2006). Annu. Rev. Pathol. *1*, 119–150.

Topalian, S.L., Drake, C.G., and Pardoll, D.M. (2012). Curr. Opin. Immunol. Published online January 12, 2012.

Trinchieri, G. (2011). Annu. Rev. Immunol. Published online March 24, 2011.

van der Vliet, H.J., Koon, H.B., Atkins, M.B., Balk, S.P., and Exley, M.A. (2007). J. Immunother. *30*, 591–595.

van Kempen, L.C., de Visser, K.E., and Coussens, L.M. (2006). Eur. J. Cancer *42*, 728–734.

Vasiljeva, O., Papazoglou, A., Krüger, A., Brodoefel, H., Korovin, M., Deussing, J., Augustin, N., Nielsen, B.S., Almholt, K., Bogyo, M., et al. (2006). Cancer Res. *66*, 5242–5250.

Vong, S., and Kalluri, R. (2011). The role of stromal myofibroblast and extracellular matrix in tumor angiogenesis. Genes Cancer. Published online October 5, 2011.

Wang, F., Sloss, C., Zhang, X., Lee, S.W., and Cusack, J.C. (2007a). Cancer Res. *67*, 8486–8493.

Wang, W., Wyckoff, J.B., Goswami, S., Wang, Y., Sidani, M., Segall, J.E., and Condeelis, J.S. (2007b). Cancer Res. *67*, 3505–3511.

Wasiuk, A., de Vries, V.C., Hartmann, K., Roers, A., and Noelle, R.J. (2009). Clin. Exp. Immunol. *155*, 140–146.

Weissleder, R. (2006). Science *312*, 1168–1171.

Willett, C.G., Boucher, Y., Duda, D.G., di Tomaso, E., Munn, L.L., Tong, R.T., Kozin, S.V., Petit, L., Jain, R.K., Chung, D.C., et al. (2005). J. Clin. Oncol. *23*, 8136–8139.

Wyckoff, J., Wang, W., Lin, E.Y., Wang, Y., Pixley, F., Stanley, E.R., Graf, T., Pollard, J.W., Segall, J., and Condeelis, J. (2004). Cancer Res. *64*, 7022–7029.

Xian, X., Håkansson, J., Ståhlberg, A., Lindblom, P., Betsholtz, C., Gerhardt, H., and Semb, H. (2006). J. Clin. Invest. *116*, 642–651.

Xu, R., Boudreau, A., and Bissell, M.J. (2009). Cancer Metastasis Rev. *28*, 167–176.

Targeting Epigenetic Misregulation in Synovial Sarcoma

Joshua J. Waterfall[1] and Paul S. Meltzer[1,*]
[1]Genetics Branch, Center for Cancer Research, National Cancer Institute, Bethesda, MD 20892, USA
*Correspondence: pmeltzer@mail.nih.gov
DOI 10.1016/j.ccr.2012.02.023

Like many sarcomas, synovial sarcoma is driven by a characteristic oncogenic transcription factor fusion, SS18-SSX. In this issue of *Cancer Cell*, Su et al. elucidate the protein partners necessary for target gene misregulation and demonstrate a direct effect of histone deacetylase inhibitors on the SS18-SSX complex composition, expression misregulation, and apoptosis.

It has been more than 25 years since the recurrent translocation between chromosomes 18 and X in synovial sarcoma (SS) was first reported (Limon et al., 1986) and 18 years since the cloning of the productive fusion between *SYT/SS18* on chromosome 18 and *SSX* on chromosome X generated by this translocation (Clark et al., 1994). Although there have been great advancements in understanding the basic biology of this rare cancer, therapeutic strategies and clinical outcomes have remained largely unchanged since the 1980s, and large tumors, metastatic disease, and relapse are frequently impossible to control. In a new study, Su et al. (2012 [in this issue of *Cancer Cell*]) not only provide deep insight into the molecular mechanisms at work in SS but also suggest an unexpected explanation for the sensitivity of SS to histone deacetylase (HDAC) inhibition in preclinical models. Beyond helping to guide current clinical trials of HDAC inhibitors in SS, this study has implications for other transcription factor-fusion driven malignancies.

Sarcomas are a heterogeneous group of tumors of mesenchymal origin. Although representing less than 1% of adult neoplasms, they account for ~15% of all pediatric malignancies. As in leukemia and lymphoma, chromosome translocations that create oncogenic fusion proteins are common in sarcomas and are often pathognomonic for the particular sarcoma type (Davis and Meltzer, 2007). Interestingly, a large number of these fusion proteins involve transcription factors, and the misregulation of target gene expression is a clear driving mechanism of malignancy. SS contains fusions of the transcriptional coactivator SYT/SS18 with the SSX family of transcriptional corepressors (most frequently SSX1 or SSX2). The fusion protein typically contains nearly the entirety of SS18 and the C-terminal domains of SSX, which contain the strongest repressive activities (de Bruijn et al., 2007). Although the typical location near the synovial joints of the limbs gave rise to its name, SS occurs in many other sites, and in fact most likely originates in a myogenic progenitor compartment rather than synovial tissue (Haldar et al., 2007). SS are classified histologically as monophasic SS, in which all tumor cells exhibit a spindle cell morphology; biphasic SS, which contains a mixture of spindle cells and cells showing epithelial differentiation; and more rarely, poorly differentiated SS.

Su et al. (2012) began by identifying interactors of the endogenous SS18-SSX fusion protein in an SS cell line and immediately made two very important discoveries. The first reveals how SS18-SSX is recruited to specific genomic locations, an important unresolved question in the field because the fusion protein lacks direct DNA binding domains. Of interest, one interactor identified was the sequence specific transcriptional activator activating transcription factor 2 (ATF2). In follow-up experiments, the authors established that, at least for a set of important target genes, SS18-SSX is recruited directly to promoters by ATF2. The second important discovery was the interaction of SS18-SSX with the transcriptional corepressor transducin-like enhancer of split 1 (TLE1). High levels of TLE family members, especially TLE1, have been identified as potential biomarkers for SS (Terry et al., 2007), but their functional role in the disease has been unclear. The authors demonstrate that TLE1 serves as a bridge for tethering transcriptional repressors such as HDAC1 and PRC2 to SS18-SSX. Furthermore, the authors demonstrate for several genes normally activated by ATF2 that SS18-SSX recruits dominant repressive activities mediated by TLE1/HDAC1 and PRC2. Thus, an elegant model is developed to explain the effects of the SS18-SSX: targeting to DNA through the interaction of the SS18 moiety with the transcriptional activator ATF2 and recruitment of the repressive HDAC and PRC2 to ATF2 targets through the SSX portion of the fusion protein. At least for certain target genes, the repressive activities dominate, and aberrant gene repression contributes to the tumor phenotype. Consistent with this model, disruption of the complex by RNAi depletion of its components leads to target gene derepression and increased apoptosis. Perhaps most intriguing and of immediate therapeutic relevance is the discovery that HDAC inhibitor treatment disrupts the interaction between TLE1 and the fusion protein, thus releasing the HDAC and PRC2 complexes from ATF2 target promoters and derepressing target gene expression. While the mechanism could certainly be indirect, one possibility would be that either TLE1 or SS18-SSX is itself acetylated, thereby destabilizing the interaction. HDAC inhibitors are of significant clinical interest, with vorinostat and romidepsin now FDA-approved for treatment of cutaneous T cell lymphoma. Since they appear to target a core mechanism of SS, it is certainly plausible that this class of drugs will provide significant benefits to patients.

Although the new study firmly establishes these molecular mechanisms of the oncogenic fusion protein and the target genes investigated are certainly interesting ones, there is as yet no cohesive explanation of how normal progenitor cells are transformed by SS18-SSX. Which pathways are affected? Is it purely aberrant repression of pathways such as differentiation, cell death, and/or senescence that drive the disease? The glandular structures apparent in the biphasic subtype of SS suggest that the tumor is not characterized by a simple block of normal mesenchymal differentiation but raises the possibility that the cells are being driven into an aberrant state. A deeper dissection of the transcriptional networks misregulated by SSX18-SSX will be necessary to more fully understand the functional consequences of SSX18-SSX activity.

It is worth noting the relevance of these discoveries to other malignancies. Oncogenic fusions involving transcription factors is a common theme in malignancies of mesenechymal and hematopoetic lineages as well as in certain epithelial tumors such as prostate cancer. ATF, TLE, Polycomb, and HDAC family members have all been implicated in a wide array of cancer types through altered expression levels as well as somatic mutations. Perhaps most relevant to the SS results, endometrial stromal sarcoma (ESS) is often driven by fusions of the zinc finger transcription factor JAZF1 with Polycomb proteins SUZ12 or PHF1, or fusion of PHF1 and EPC1 (Chiang et al., 2011). Presumably, this leads to mislocalization of Polycomb complexes on the chromatin and misregulation of target genes. ESS has also been shown to be sensitive to HDAC inhibitors (Hrzenjak et al., 2008). While acute promyeloctic leukemia (APL) and SS are quite different diseases, the PML-retinoic acid receptor alpha (RARα) fusion which defines APL also functions largely through pathological recruitment of HDACs and PRC2 (Villa et al., 2007). In normal physiology the RARα switches between repressing target gene expression when retinoic acid (RA) levels are low and the receptor is unliganded and activating target gene expression when RA levels are high and bind the receptor. The oncogenic mechanism of the PML-RARα fusion is persistent association with corepressors regardless of physiological RA concentrations. The standard and typically successful treatment for APL is all-trans retinoic acid, which leads to release of corepressors from PML-RARα, derepression of target genes, terminal differentiation, and apoptosis.

The study of Su et al. (2012) is a significant addition to our understanding of the basic biological mechanisms of SS and highlights the commonly underappreciated role of transcriptional repression by oncogenic transcription factor-fusions. The phase I and II clinical trials for HDAC inhibitors in sarcoma currently underway, the outcomes of which are much anticipated, now have a stronger biological rationale and context for interpretation of their results. Most intriguingly, the effects of HDAC inhibitors on multiprotein complex composition and possibly on non-histone targets are likely to be of more general importance in numerous systems.

REFERENCES

Chiang, S., Ali, R., Melnyk, N., McAlpine, J.N., Huntsman, D.G., Gilks, C.B., Lee, C.H., and Oliva, E. (2011). Am. J. Surg. Pathol. *35*, 1364–1372.

Clark, J., Rocques, P.J., Crew, A.J., Gill, S., Shipley, J., Chan, A.M., Gusterson, B.A., and Cooper, C.S. (1994). Nat. Genet. *7*, 502–508.

Davis, S.R., and Meltzer, P.S. (2007). Cancer Cell *11*, 305–307.

de Bruijn, D.R., Nap, J.P., and van Kessel, A.G. (2007). Genes Chromosomes Cancer *46*, 107–117.

Haldar, M., Hancock, J.D., Coffin, C.M., Lessnick, S.L., and Capecchi, M.R. (2007). Cancer Cell *11*, 375–388.

Hrzenjak, A., Kremser, M.L., Strohmeier, B., Moinfar, F., Zatloukal, K., and Denk, H. (2008). J. Pathol. *216*, 495–504.

Limon, J., Dal Cin, P., and Sandberg, A.A. (1986). Cancer Genet. Cytogenet. *23*, 87–91.

Su, L., Sampaio, A.V., Jones, K.B., Pacheco, M., Goytain, A., Lin, S., Poulin, N., Yi, L., Rossi, F.M., Kast, J., et al. (2012). Cancer Cell *21*, this issue, 333–347.

Terry, J., Saito, T., Subramanian, S., Ruttan, C., Antonescu, C.R., Goldblum, J.R., Downs-Kelly, E., Corless, C.L., Rubin, B.P., van de Rijn, M., et al. (2007). Am. J. Surg. Pathol. *31*, 240–246.

Villa, R., Pasini, D., Gutierrez, A., Morey, L., Occhionorelli, M., Viré, E., Nomdedeu, J.F., Jenuwein, T., Pelicci, P.G., et al. (2007). Cancer Cell *11*, 513–525.

ALK and MYCN: When Two Oncogenes Are Better than One

Zhihui Liu[1] and Carol J. Thiele[1,*]
[1]Pediatric Oncology Branch, Center for Cancer Research, National Cancer Institute, 9000 Rockville Pike, Bethesda, MD 20892, USA
*Correspondence: ct47a@nih.gov
DOI 10.1016/j.ccr.2012.03.004

Mutations of *ALK* are frequently observed in *MYCN*-amplified neuroblastomas and correlate with poor clinical outcome, but how these oncogenes cooperate in neuroblastoma development remains unclear. In this issue of *Cancer Cell,* Zhu et al. describe a mechanism by which ALK and MYCN synergistically induce neuroblastoma in the zebrafish model system.

Neuroblastoma (NB) is the most common childhood malignant solid tumor of the sympathetic nervous system (Maris, 2010). Numerous chromosomal abnormalities, including deletions of chromosome arms 1p, 11q, gain of 17q, and amplification of *MYCN* on chromosome 2p, are associated with NB. The overall prevalence of *MYCN* amplification is about 20% and is a genetic marker of poor prognosis that has been used for treatment stratification of NB patients since the late 1980s (Maris, 2010). During the past 40 years, the outcome of children with high-risk NB has shown marked improvements. However, the 5 year event-free survival is only 50% for these patients, and there are significant toxicities associated with current treatments. Until recently, no recurrent mutations in druggable targets had been identified. The discovery of activating mutations in the *ALK* oncogene in both hereditary (80%) and sporadic (7%–8%) NB provides an opportunity for targeted therapy (reviewed in Azarova et al., 2011).

The *ALK* oncogene was identified initially as a gene that fused with *NPM* through 2;5 chromosome translocation in cases of anaplastic large-cell lymphoma (Morris et al., 1994). Although the wild-type (WT) ALK is preferentially expressed in the central and peripheral nervous systems, its physiologic role, ligands, and signaling pathways remain largely obscure (Azarova et al., 2011). In a series of elegant studies, activating mutations in ALK were identified in primary NB tumors, and their oncogenic potential was demonstrated. WT ALK was also thought to possess oncogenic activity in NB cells when its expression level surpasses a threshold (Azarova et al., 2011).

A question in the field has been whether *ALK* mutations alone are sufficient to cause neuroblastoma. The finding that *ALK* mutations occur in equal frequencies across all genomic NB subtypes and in both low- and high-risk tumors seemed to be inconsistent with *ALK* being the sole "driver" oncogene in NB. One clue came with the finding that a common mutation *ALK F1174L* is observed at a higher frequency in *MYCN*-amplified tumors (Azarova et al., 2011). Moreover, overexpression of WT or mutant ALK stimulated *MYCN* transcription in neuroblastoma cell lines, and coexpressing activated ALK and MYCN increased NIH 3T3 cell transformation in vitro (Schönherr et al., 2012). Amplification of *ALK* also occurs in about 2%–3% of NB, but almost exclusively in those with *MYCN*-amplification (Azarova et al., 2011). Taken together, these studies raised the possibility of a positive cooperative effect between the dysregulation of both ALK and MYCN.

In this issue of *Cancer Cell*, Zhu et al. (2012) explore these questions by generating a series of transgenic zebrafish models to assess the tumorigenicity of ALK, ALK F1174L, and MYCN alone or together. Using the dopamine-β-hydroxylase promoter to drive EGFP-MYCN expression, Zhu et al. (2012) first investigated whether MYCN transgenic zebrafish can develop NB as had been shown in mice (Weiss et al., 1997). They showed that MYCN-induced zebrafish NB at a low frequency (17.3%), with these tumors sharing histologic, immunocytochemical, and ultrastructural features with human NB. Zebrafish NB arise from neuroblasts that migrate into the interrenal gland (equivalent to the human adrenal gland) late in development (~21 days post fertilization), and the sympathoadrenal precursors coexpress neuronal-specific Hu proteins and the catecholaminergic enzymes TH and DβH.

Zebrafish expressing ALK or ALK F1174L transgene alone did not develop NB. To address whether ALK and MYCN genetically interact, Zhu et al. (2012) generated transgenic zebrafishes that expressed the human ALK, or ALK F1174L, together with MYCN. Tumor onset was accelerated in fish expressing both MYCN and ALK F1174L compared to those expressing MCYN alone, and the penetrance in the MYCN/ALK F1174L fish was 3-fold higher than MYCN fish. Like the tumors in the MYCN fishes, tumors in MYCN/ALK F1174L fish arise in the interrenal gland and resemble human NB. This suggests that ALK mutations may be "initiating" events and need a "second hit", such as dysregulated MYCN, to fully transform cells. This provides a context which might explain the findings of *ALK* mutations in the tumors of low risk, good prognosis NB patients.

So how does ALK accelerate tumor onset and increase penetrance in MYCN transgenic fish? Zhu et al. (2012) found that the number of Hu^+ neuroblasts was significantly increased in MYCN transgenic fish compared with controls at 3–5 weeks post fertilization (wpf) (Figure 1). These MYCN-overexpressing neuroblasts fail to differentiate, resulting in reduced numbers of chromaffin cells. Moreover, at 5–7 wpf, the number of Hu^+ neuroblasts in the interrenal gland decreased significantly due to apoptotic cell death. These findings indicate that overexpression of MYCN causes expansion of sympathoadrenal neuroblasts

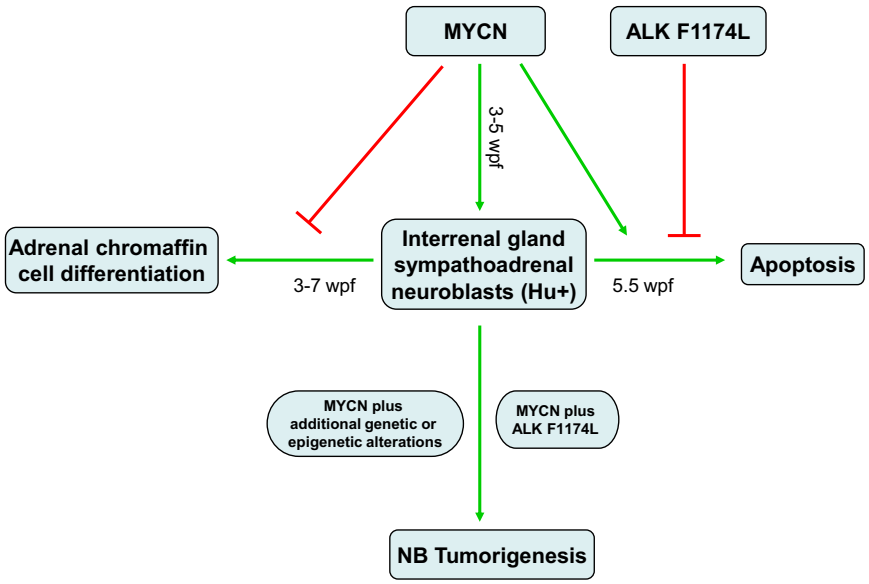

Figure 1. MYCN and ALK F1174L Synergistically Impact Neuroblastoma Tumorigenesis
In zebrafish, the MYCN overexpression causes expansion of the sympathoadrenal neuroblasts from 3 to 5 wpf, and the MYCN overexpressing neuroblasts fail to differentiate into chromaffin cells. Only a small group of zebrafish (17%) with MYCN overexpression developed neuroblastoma; others won't because MYCN overexpression also triggers an apoptotic response at 5.5 wpf. The activated ALK F1174L provides a cell survival signal that blocks the apoptotic response of MYCN-overexpressing neuroblasts at this juncture in development, so the tumor penetrance in the MYCN/ALK F1174L coexpressing transgenic fish is 3-fold higher (56%).

and prevents their differentiation, yet it also induces a developmentally-timed apoptotic response (Figure 1). However, in the presence of activated ALK, these cells survive but fail to differentiate resulting in the continued accumulation of Hu^+ neuroblasts and the development of highly penetrant, fully transformed NB (Figure 1). For the MYCN-only transgenic fish that develop tumors, it is possible that additional genetic alterations cooperate with MYCN to contribute to NB formation. Zhu et al. (2012) ruled out mutations in the tyrosine kinase domain of the zebrafish *alk* gene and loss of capsase-8 expression that is known to occur in *MYCN*-amplified human NB. Thus, other genetic mutations or epigenetic events that activate prosurvival pathways may occur with MYCN overexpression in these tumors. In fact, recent studies showed that the Myc family (including MYCN) directly upregulates the transcription of all core components of the Polycomb Repressive Complex 2 (PRC2) to maintain embryonic stem cell pluripotency (Neri et al., 2012). Dysregulation of EZH2 (a subunit of PRC2) has been shown to silence differentiation-associated genes with tumor suppressor activity in undifferentiated human NB (Wang et al., 2012). In this zebrafish model system, WT or activated ALK expression alone is not sufficient for the development of NB but requires overexpression of MYCN. It remains to be clarified if increased expression of ALK via the use of a stronger promoter or protein stabilization will result in tumorigenesis on its own.

The results from Zhu et al. (2012) demonstrate that ALK and MYCN collaboratively contribute to NB development, with ALK F1174L attenuating MYCN-induced apoptosis perhaps by activating pro-survival pathways. A clinical Phase I/II trial targeting ALK is underway in children with solid tumors, including those with NB using Crizotinib, the FDA-approved ALK/MET inhibitor. Given the clinical experience with targeted agents and the development of drug resistance, it is unlikely that targeting ALK alone will lead to durable responses. Multi-modality therapeutic approaches will be needed. The general view has been that transcription factors such as MYCN are less amenable to targeted therapeutic approaches. However, the recent identification of inhibitors of BET (bromodomain and extraterminal subfamily of human bromodomain proteins), which decrease MYCN mRNA levels in *MYCN*-amplified NB cell lines (Mertz et al., 2011) and strategies to destabilize MYCN protein (Hogarty and Maris, 2012), indicate it may be feasible to target MYCN. The zebrafish MYCN-ALK F1174L NB tumor model serves not only to understand developmental alterations leading to tumor formation but it can also serve as a platform for evaluating unbiased drug screens as well as the next generation of targeted approaches.

REFERENCES

Azarova, A.M., Gautam, G., and George, R.E. (2011). Semin. Cancer Biol. *21*, 267–275.

Hogarty, M.D., and Maris, J.M. (2012). Cancer Cell *21*, 145–147.

Maris, J.M. (2010). N. Engl. J. Med. *362*, 2202–2211.

Mertz, J.A., Conery, A.R., Bryant, B.M., Sandy, P., Balasubramanian, S., Mele, D.A., Bergeron, L., and Sims, R.J., 3rd. (2011). Proc. Natl. Acad. Sci. USA *108*, 16669–16674.

Morris, S.W., Kirstein, M.N., Valentine, M.B., Dittmer, K.G., Shapiro, D.N., Saltman, D.L., and Look, A.T. (1994). Science *263*, 1281–1284.

Neri, F., Zippo, A., Krepelova, A., Cherubini, A., Rocchigiani, M., and Oliviero, S. (2012). Mol. Cell. Biol. *32*, 840–851.

Schönherr, C., Ruuth, K., Kamaraj, S., Wang, C.L., Yang, H.L., Combaret, V., Djos, A., Martinsson, T., Christensen, J.G., Palmer, R.H., and Hallberg, B. (2012). Oncogene. Published online January 30, 2012. 10.1038/onc.2012.12.

Wang, C., Liu, Z., Woo, C.W., Li, Z., Wang, L., Wei, J.S., Marquez, V.E., Bates, S.E., Jin, Q., Khan, J., et al. (2012). Cancer Res. *72*, 315–324.

Weiss, W.A., Aldape, K., Mohapatra, G., Feuerstein, B.G., and Bishop, J.M. (1997). EMBO J. *16*, 2985–2995.

Zhu, S., Lee, J.S., Guo, F., Shin, J., Perez-Atayde, A.R., Kutok, J.L., Rodig, S.J., Neuberg, D.S., Helman, D., Feng, H., et al. (2012). Cancer Cell *21*, this issue, 362–373.

Targeting Tumor Architecture to Favor Drug Penetration: A New Weapon to Combat Chemoresistance in Pancreatic Cancer?

Man Yu[1] and Ian F. Tannock[1,2,*]
[1]Ontario Cancer Institute/Princess Margaret Hospital, University Health Network and University of Toronto, Toronto, ON M5G 2M9, Canada
[2]Division of Medical Oncology and Hematology, Princess Margaret Hospital, University Health Network and University of Toronto, Toronto, ON M5G 2M9, Canada
*Correspondence: ian.tannock@uhn.ca
DOI 10.1016/j.ccr.2012.03.002

Pancreatic ductal adenocarcinoma (PDA) responds poorly to chemotherapy. In this issue of *Cancer Cell*, Provenzano et al. identify hyaluronan as a pivotal determinant of elevated interstitial fluid pressures (IFP) and vascular collapse in PDA. PEGPH20 treatment ablates stromal hyaluronan, normalizes IFP, and increases accessibility of tumor cells to anticancer drugs.

Pancreatic ductal adenocarcinoma (PDA) is among the most lethal human malignancies due to its insidious onset and resistance to therapy. Most anticancer drugs, including standard-of-care gemcitabine and novel molecular targeted therapies that have displayed impressive activity against PDA cells in culture and in some preclinical animal models, yield little success in the clinic (Li et al., 2010). Sensitivity of neoplastic cells in such models is a poor predictor of clinical effectiveness.

In addition to epigenetic and genetic alterations in cancer cells that influence drug sensitivity, the tumor microenvironment mediates responses of solid tumors to chemotherapy (Trédan et al., 2007). The vasculature of solid tumors is disorganized compared to that in normal tissues, with variable blood flow and large distances between functional capillaries. This leads to gradients from tumor blood vessels of nutrients, with regions of hypoxia and extracellular acidity and gradients in tumor cell proliferation (Figure 1). Anticancer drugs are delivered through blood vessels, and gradients in their concentration are established within tumors; cells distal from blood vessels are likely to be resistant to systemic therapy because of low drug concentration and because most drugs, including many targeted agents, are more active against rapidly-proliferating cells. A dense extracellular matrix (ECM) and stromal components of tumors increase interstitial fluid pressure (IFP), which limits ability of larger molecules, including therapeutic antibodies, to penetrate tumor tissue by convection; if IFP exceeds capillary pressure, vascular collapse will occur, limiting delivery of all drugs (and nutrients) to the tumor. The above factors are particularly relevant to PDA, which usually has a dense desmoplastic stroma with fibrotic connective tissue that surrounds the tumor and may account for >80% of tumor volume (Erkan et al., 2010). This leads to a microenvironment with low blood perfusion and hypoxia, serving as a "wall-like" barrier to diminish the delivery of anticancer drugs and stimulating aggressive tumor cell behavior (Neesse et al., 2011). The amount of reactive stroma is an independent predictor for poor prognosis of patients with PDA (Erkan et al., 2008). Hence, targeting non-neoplastic components within the microenvironment provides an opportunity for developing more effective therapies.

In this issue of *Cancer Cell*, Provenzano et al. (2012) characterize histologically various stromal components in preinvasive, invasive, and metastatic pancreatic tissues in mice and humans. They and others have shown that autochthonous PDA in $Kras^{LSL\text{-}G12D/+}$;*Cre* and $Kras^{LSL\text{-}G12D/+}$;$Trp^{53LSL\text{-}R172H/+}$;*Cre* conditional knockout mice provide excellent models for human PDA (see also Olive et al., 2009). Provenzano and colleagues demonstrate that the content of collagen and glycosaminoglycans increases progressively with histopathological grade from early precusor lesions to invasive and metastatic PDA tumors. The expression and abundance of hyaluroic acid (HA), a large linear glycosaminoglycan associated with inflammation, wound repair, and tissue remodelling (Toole, 2004), are elevated during carcinogenesis. These findings, along with similar observations in other solid tumors (Toole, 2004), suggest that accumulation of HA contributes to neoplastic transformation, tumor progression, and drug resistance in PDA. Using three-dimensional matrices, the investigators demonstrate that the presence of HA can directly elevate IFP. The authors measure IFP in murine PDA and find a range of 75–130 mm Hg, much larger than values in the normal pancreas or than capillary blood pressure (range: 8–13 mm Hg). These extremely high levels of IFP induce vascular collapse and limit availability of drugs to the tumor.

In this issue of *Cancer Cell*, Provenzano et al. (2012) then evaluate intravenous administration of PEGPH20, a HA-targeting enzymatic agent, in mice bearing autochtonous PDA. PEGPH20 depletes HA in the tumor matrix, resulting in a marked reduction in IFP, increased diameter of $CD31^{+}$ blood vessels, increased patent vessels, and improved penetration of doxorubicin in PDA. They compare treatment with gemcitabine with or without PEGPH20 in cohorts of mice bearing autochtonous PDA. Gemcitabine alone has negligible effects, but the combination leads to reduced tumor size and increased apoptosis of tumor cells with all tumors responding after three cycles. Combined treatment decreases metastatic tumor burden and increases overall

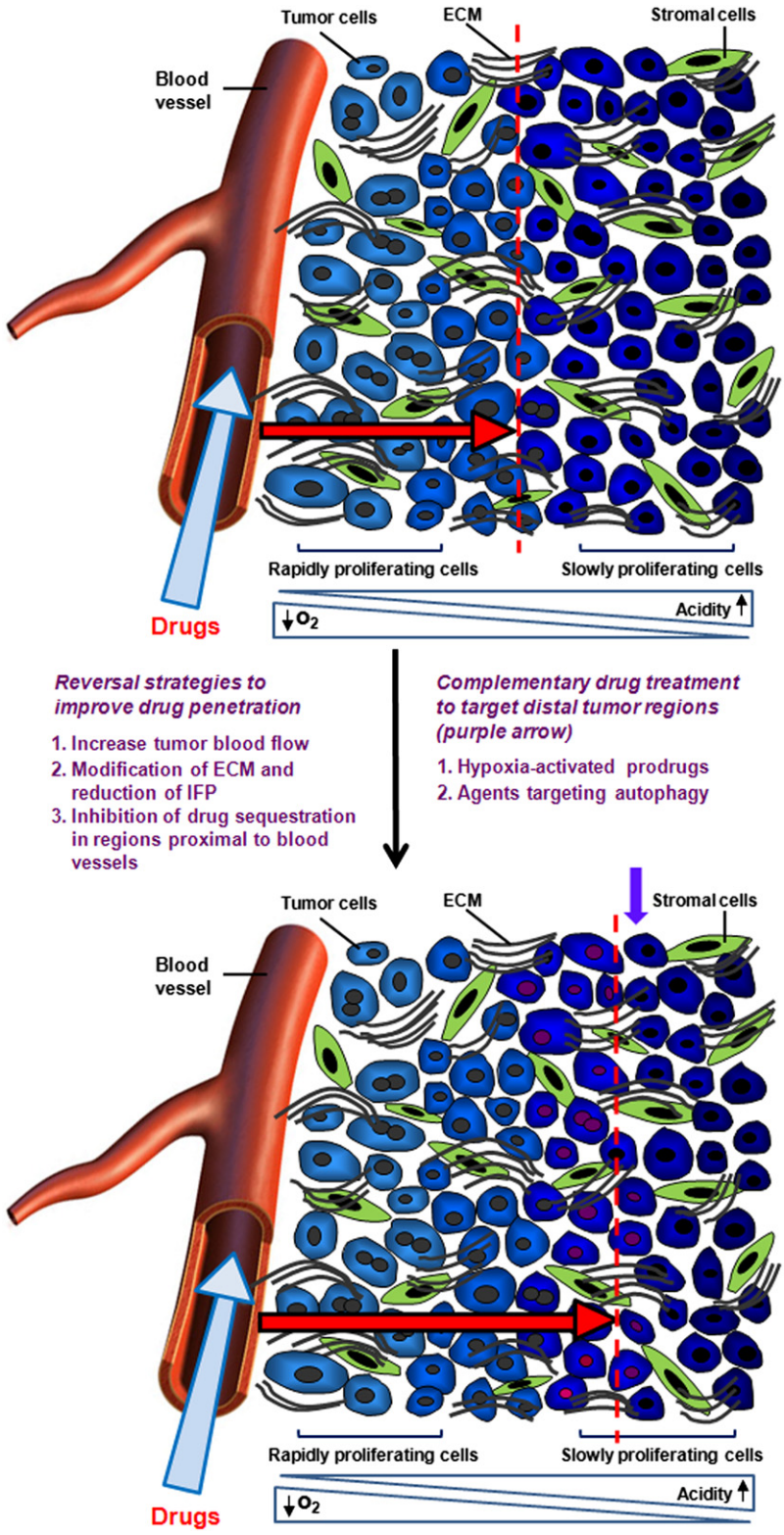

Figure 1. Strategies to Overcome the Effects of Limited Drug Distribution in Solid Tumors
Drug distribution in solid tumors is determined by various factors including molecular size and charge, consumption of drugs by cells proximal to blood vessels, and the volume and organization of the extracellular matrix (ECM). As shown by Provenzano et al. (2012), modification of the ECM can lead to a decrease of high interstitial fluid pressure (IFP) and an increase of tumor blood flow, allowing greater access of cytotoxic agents to tumor cells. Other strategies to improve drug distribution (indicated schematically by red arrows and dashed lines) include augmentation of tumor blood flow and inhibition of drug sequestration in cells close to blood vessels. Combined treatment with conventional therapeutics and drugs that both diffuse to and target cells distant from blood vessels (e.g., hypoxia-activated prodrugs and agents that target autophagy) may also improve therapeutic effectiveness.

survival of animals when compared to either agent used alone. These therapeutic effects are accompanied by extensive remodeling of tumor stroma and maintainance of a functional vasculature. In light of these promising results and encouraging data from phase I clinical trials, a phase II trial has been intitiated to investigate the effects of gemcitabine + PEGPH20 in the treatment of patients with advanced, previously-untreated PDA (http://www.clinicaltrials.gov).

Other investigators have used strategies to improve vascular perfusion and drug delivery in PDA. Olive et al. (2009) reported that depletion of tumor-associated stromal fibroblasts by disrupting Hedgehog signaling increased intratumoral vascular density transiently via neoangiogenesis and resulted in improved delivery and greater antitumor activity of gemcitabine using the same mouse model of PDA. Two drugs that inhibit the Hedgehog pathway (GDC-0449 and LDE225) are being evaluated with chemotherapy in phase II clinical trials for PDA (http://www.clinicaltrials.gov).

Will these strategies translate into improved outcome for people with advanced PDA? Targeting the tumor microenvironment is an innovative approach worthy of study in cinical trials, especially for a disease where other strategies have yielded only minor improvements in outcome. However, all mice in the preclinical trials conducted by Provenzano et al. (2012) eventually die of their tumors. Even if enzymatic treatment can lead to vascular remodeling and increased perfusion in human PDA, there remain gradients in drug concentration in relation to tumor blood vesseels and resistance of poorly-nourished slowly-proliferating cells to anticancer drugs, a problem common to solid tumors (Trédan et al., 2007). As shown by Huxham et al. (2004), tumor repopulation is intiated from cells distant from blood vessels when transplanted

human colorectal xenografts are treated with gemcitabine.

The major contributions of Olive et al. (2009) and Provenzano et al. (2012) are in demonstrating the importance of the microenvironment of PDA, and of solid tumors in general, in determining resistance to drug therapy. The majority of research on drug resistance has concentrated on molecular properties of individual cancer cells. Although intrinsic sensitivity is important, it is only part of the story—stated simply, if a drug does not get to some of the tumor cells, they will not be killed no matter how sensitive they might be to the drug in cell culture. More research should focus on strategies that recognize the importance of the tumor microenvironment and drug delivery in limiting therapeutic efficacy. There are several approaches to this problem, some of which are outlined in Figure 1. They include strategies to target the ECM with enzymes such as PEGPH20 or inhibition of Hedgehog signaling, strategies to decrease drug sequestration in cells proximal to blood vessels thereby allowing better distribution of drugs to distal cells, and combination treatment using "conventional" therapeutics together with drugs that both diffuse to and target specifically cells distant from blood vessels. Promising drugs for the latter include hypoxia-activated prodrugs and agents that attack the process of autophagy, a survival mechanism for stressed tumor cells (Trédan et al., 2007; Yang et al., 2011).

In summary, the efficiency of systemic chemotherapy for PDA in particular and for solid tumors in general is hindered by poor delivery of drugs to some tumor regions and by effects of the tumor microenvironment on drug activity. As Provenzano and coworkers show convincingly, agents that improve drug delivery by modifying factors relating to the tumor microenvironment represent an important future direction for cancer therapy.

REFERENCES

Erkan, M., Michalski, C.W., Rieder, S., Reiser-Erkan, C., Abiatari, I., Kolb, A., Giese, N.A., Esposito, I., Friess, H., and Kleeff, J. (2008). Clin. Gastroenterol. Hepatol. *6*, 1155–1161.

Erkan, M., Reiser-Erkan, C., Michalski, C.W., and Kleeff, J. (2010). Exp. Oncol. *32*, 128–131.

Huxham, L.A., Kyle, A.H., Baker, J.H., Nykilchuk, L.K., and Minchinton, A.I. (2004). Cancer Res. *64*, 6537–6541.

Li, J., Wientjes, M.G., and Au, J.L. (2010). AAPS J. *12*, 223–232.

Neesse, A., Michl, P., Frese, K.K., Feig, C., Cook, N., Jacobetz, M.A., Lolkema, M.P., Buchholz, M., Olive, K.P., Gress, T.M., and Tuveson, D.A. (2011). Gut *60*, 861–868.

Olive, K.P., Jacobetz, M.A., Davidson, C.J., Gopinathan, A., McIntyre, D., Honess, D., Madhu, B., Goldgraben, M.A., Caldwell, M.E., Allard, D., et al. (2009). Science *324*, 1457–1461.

Provenzano, P.P., Cuevas, C., Chang, A.E., Goel, V.K., Von Hoff, D.D., and Hingorani, S. (2012). Cancer Cell *21*, this issue, 418–429.

Toole, B.P. (2004). Nat. Rev. Cancer *4*, 528–539.

Trédan, O., Galmarini, C.M., Patel, K., and Tannock, I.F. (2007). J. Natl. Cancer Inst. *99*, 1441–1454.

Yang, Z.J., Chee, C.E., Huang, S., and Sinicrope, F.A. (2011). Mol. Cancer Ther. *10*, 1533–1541.

A Tell-Tail Sign of Chromatin: Histone Mutations Drive Pediatric Glioblastoma

Esther Rheinbay,[1,2,3,4] David N. Louis,[2] Bradley E. Bernstein,[1,2,3,*] and Mario L. Suvà[1,2,3]
[1]Howard Hughes Medical Institute, Chevy Chase, MD 20815, USA
[2]Department of Pathology, Center for Cancer Research, Massachusetts General Hospital and Harvard Medical School, Boston, MA 02114, USA
[3]Broad Institute of Harvard and MIT, Cambridge, MA 02142, USA
[4]Bioinformatics Program, Boston University, Boston, MA 02215, USA
*Correspondence: bernstein.bradley@mgh.harvard.edu
DOI 10.1016/j.ccr.2012.03.001

Recent genomic analyses of pediatric glioblastoma, a poorly understood tumor with dismal outcome, have identified mutations in histone H3 variants that affect critical amino acids in the tail. The findings extend discoveries of chromatin regulator inactivation and gain-of-function mutations by documenting alteration of a modifiable histone residue in human cancer.

Brain tumors are the most common solid neoplasms of childhood and the primary cause of cancer-related deaths in children. Although their pathological classification is complex, most high-grade brain tumors in children are categorized as either embryonal (such as medulloblastoma) or glial (such as the diffusely infiltrative glioblastoma [GBM]). An anatomical variant of high-grade glioma, diffuse intrinsic pontine glioma (DIPG), is a particularly vexing clinical challenge given its location in the neurologically critical brain stem. Over the past few decades, major progress has been made in the understanding and treatment of children with medulloblastomas, but little real progress has been made in the treatment of children with malignant diffuse gliomas. Consistent prognostic estimates have been difficult to establish, since the clinical behavior of childhood diffuse gliomas is not as stereotypical as that of their more common adult counterpart.

human colorectal xenografts are treated with gemcitabine.

The major contributions of Olive et al. (2009) and Provenzano et al. (2012) are in demonstrating the importance of the microenvironment of PDA, and of solid tumors in general, in determining resistance to drug therapy. The majority of research on drug resistance has concentrated on molecular properties of individual cancer cells. Although intrinsic sensitivity is important, it is only part of the story—stated simply, if a drug does not get to some of the tumor cells, they will not be killed no matter how sensitive they might be to the drug in cell culture. More research should focus on strategies that recognize the importance of the tumor microenvironment and drug delivery in limiting therapeutic efficacy. There are several approaches to this problem, some of which are outlined in Figure 1. They include strategies to target the ECM with enzymes such as PEGPH20 or inhibition of Hedgehog signaling, strategies to decrease drug sequestration in cells proximal to blood vessels thereby allowing better distribution of drugs to distal cells, and combination treatment using "conventional" therapeutics together with drugs that both diffuse to and target specifically cells distant from blood vessels. Promising drugs for the latter include hypoxia-activated prodrugs and agents that attack the process of autophagy, a survival mechanism for stressed tumor cells (Trédan et al., 2007; Yang et al., 2011).

In summary, the efficiency of systemic chemotherapy for PDA in particular and for solid tumors in general is hindered by poor delivery of drugs to some tumor regions and by effects of the tumor microenvironment on drug activity. As Provenzano and coworkers show convincingly, agents that improve drug delivery by modifying factors relating to the tumor microenvironment represent an important future direction for cancer therapy.

REFERENCES

Erkan, M., Michalski, C.W., Rieder, S., Reiser-Erkan, C., Abiatari, I., Kolb, A., Giese, N.A., Esposito, I., Friess, H., and Kleeff, J. (2008). Clin. Gastroenterol. Hepatol. *6*, 1155–1161.

Erkan, M., Reiser-Erkan, C., Michalski, C.W., and Kleeff, J. (2010). Exp. Oncol. *32*, 128–131.

Huxham, L.A., Kyle, A.H., Baker, J.H., Nykilchuk, L.K., and Minchinton, A.I. (2004). Cancer Res. *64*, 6537–6541.

Li, J., Wientjes, M.G., and Au, J.L. (2010). AAPS J. *12*, 223–232.

Neesse, A., Michl, P., Frese, K.K., Feig, C., Cook, N., Jacobetz, M.A., Lolkema, M.P., Buchholz, M., Olive, K.P., Gress, T.M., and Tuveson, D.A. (2011). Gut *60*, 861–868.

Olive, K.P., Jacobetz, M.A., Davidson, C.J., Gopinathan, A., McIntyre, D., Honess, D., Madhu, B., Goldgraben, M.A., Caldwell, M.E., Allard, D., et al. (2009). Science *324*, 1457–1461.

Provenzano, P.P., Cuevas, C., Chang, A.E., Goel, V.K., Von Hoff, D.D., and Hingorani, S. (2012). Cancer Cell *21*, this issue, 418–429.

Toole, B.P. (2004). Nat. Rev. Cancer *4*, 528–539.

Trédan, O., Galmarini, C.M., Patel, K., and Tannock, I.F. (2007). J. Natl. Cancer Inst. *99*, 1441–1454.

Yang, Z.J., Chee, C.E., Huang, S., and Sinicrope, F.A. (2011). Mol. Cancer Ther. *10*, 1533–1541.

A Tell-Tail Sign of Chromatin: Histone Mutations Drive Pediatric Glioblastoma

Esther Rheinbay,[1,2,3,4] David N. Louis,[2] Bradley E. Bernstein,[1,2,3,*] and Mario L. Suvà[1,2,3]
[1]Howard Hughes Medical Institute, Chevy Chase, MD 20815, USA
[2]Department of Pathology, Center for Cancer Research, Massachusetts General Hospital and Harvard Medical School, Boston, MA 02114, USA
[3]Broad Institute of Harvard and MIT, Cambridge, MA 02142, USA
[4]Bioinformatics Program, Boston University, Boston, MA 02215, USA
*Correspondence: bernstein.bradley@mgh.harvard.edu
DOI 10.1016/j.ccr.2012.03.001

Recent genomic analyses of pediatric glioblastoma, a poorly understood tumor with dismal outcome, have identified mutations in histone H3 variants that affect critical amino acids in the tail. The findings extend discoveries of chromatin regulator inactivation and gain-of-function mutations by documenting alteration of a modifiable histone residue in human cancer.

Brain tumors are the most common solid neoplasms of childhood and the primary cause of cancer-related deaths in children. Although their pathological classification is complex, most high-grade brain tumors in children are categorized as either embryonal (such as medulloblastoma) or glial (such as the diffusely infiltrative glioblastoma [GBM]). An anatomical variant of high-grade glioma, diffuse intrinsic pontine glioma (DIPG), is a particularly vexing clinical challenge given its location in the neurologically critical brain stem. Over the past few decades, major progress has been made in the understanding and treatment of children with medulloblastomas, but little real progress has been made in the treatment of children with malignant diffuse gliomas. Consistent prognostic estimates have been difficult to establish, since the clinical behavior of childhood diffuse gliomas is not as stereotypical as that of their more common adult counterpart.

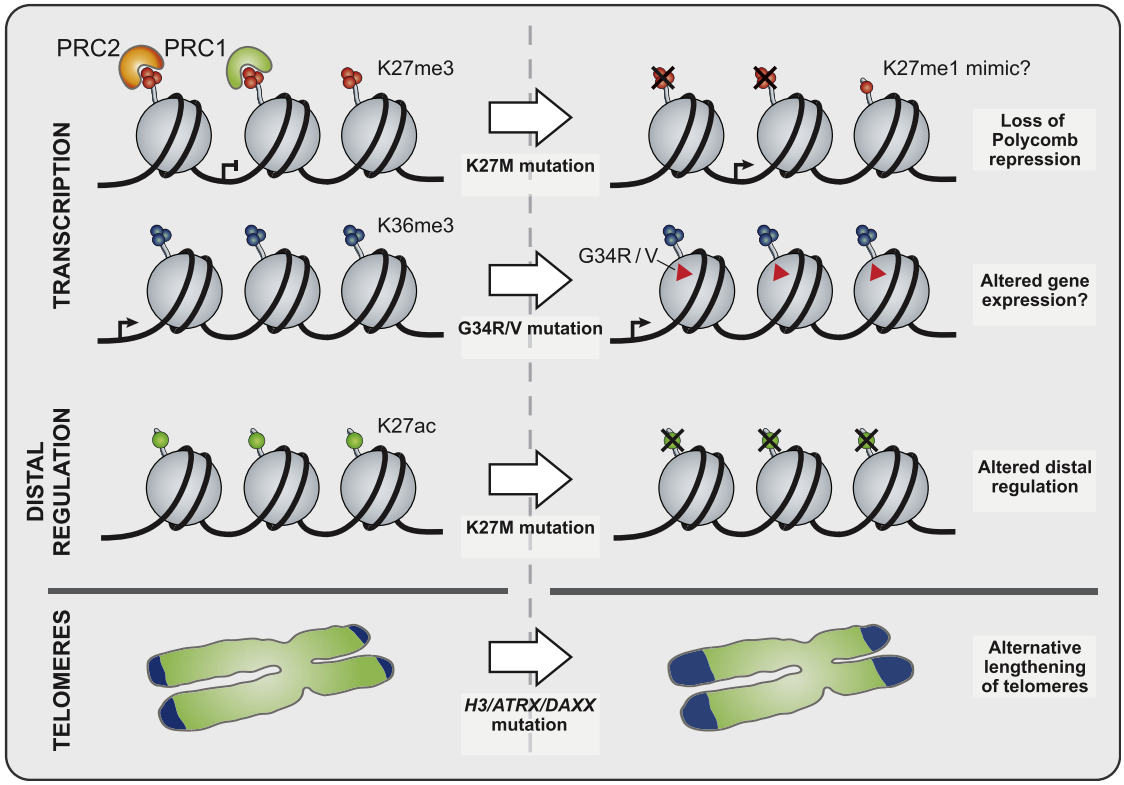

Figure 1. Model Depicts Possible Consequences of Histone and *ATRX/DAXX* Mutations
(Top) Histone H3 mutations may influence transcriptional regulation through loss of H3K27me3, which may impede repression by Polycomb-repressive complexes PRC1 and PRC2. K27M may also mimic H3K27me1. Structural changes through G34R/V mutation may indirectly affect H3K36 methylation. The K27M change may also affect distal elements, which are frequently marked by H3K27 acetylation.
(Bottom) Alternatively or in addition, *H3F3A* and *ATRX/DAXX* mutants may lead to alternative telomere lengthening.

Moreover, in recent years, it has become clear that although pediatric diffuse gliomas appear histologically identical to adult glioma, they have different underlying genetic compositions (Paugh et al., 2010). For example, whereas *IDH1* or *IDH2* mutations are found in the majority of grade II and III diffuse gliomas in adults and are thought to constitute early genetic events, they are rare in pre-adolescent children (Paugh et al., 2010). *TP53* mutations, a cardinal feature of diffuse astrocytic gliomas in adults, are far less common in diffuse gliomas in the first few years of life (Pollack et al., 2001), and combined loss of chromosome arms 1p and 19q, the classic genetic finding in diffuse oligodendrogliomas in adults, is exceedingly rare in pediatric oligodendrogliomas (Kreiger et al., 2005). Although it has been clear that pediatric diffuse gliomas are clinically and genetically different from their adult counterparts, no distinct genetic marker and key pathogenic mechanism has yet been discovered.

Two independent studies used whole-genome or whole-exome sequencing to interrogate the cancer genome of pediatric diffuse glioma (Schwartzentruber et al., 2012; Wu et al., 2012). In an extensive survey, Schwartzentruber et al. (2012) performed initial whole-exome sequencing of 48 pediatric GBMs, and 6 matched normal samples and discovered recurrent mutations in the *H3F3A* gene, encoding histone H3.3, in 31% of cases. These mutations were highly specific and comprised either K27M (9 of 48 cases), G34R (5 of 48 cases) or G34V (1 case). Interestingly, in an additional cohort of 784 adult and pediatric gliomas, *H3F3A* mutations were found in only 3% of adult GBMs but in 32% of pediatric GBMs and 18% of pediatric anaplastic astrocytomas. Wu et al. (2012) found *H3F3A* K27M mutations through whole-genome sequencing of 7 DIPGs and targeted sequencing of 43 additional DIPGs and 36 pediatric GBMs. Notably, K27M mutations were also found in the canonical histone H3.1 (*HIST1H3B*) in 18% of DIPGs. All histone alterations identified in the two studies are heterozygous, suggesting that these are gain-of-function mutations.

Histone H3.3 is deposited at active gene loci in the genome as well as at pericentromeres and telomeres. Unlike its canonical counterpart H3.1, H3.3 is incorporated into chromatin independently of the cell replication cycle (Talbert and Henikoff, 2010). The two mutations found in the two studies are located in the histone tail that is subject to extensive post-translational modification. In particular, the K27M mutation will block two widely studied modifications: K27 methylation, associated with Polycomb-mediated gene repression (Simon and Kingston, 2009), and K27 acetylation, present at active promoters and enhancers (Zhou et al., 2011). Although H3G34 is not itself subject to post-translational modification, it resides in close proximity to a lysine at position 36 (H3K36), whose methylation status is associated with transcriptional elongation (Zhou et al., 2011). In support of an indirect effect on

H3K36, Schwartzentruber et al. (2012) show that H3K36 methylation levels are increased in a tumor with G34R mutation. In addition, expression profiling of K27M and G34R/V mutant GBMs demonstrated differences in expression patterns of neural development genes, likely reflecting different effects of the two mutations on gene regulation.

Although H3.3 mutations conceivably affect gene regulatory functions, the selective advantage in pediatric GBM may actually relate to telomere maintenance and/or heterochromatin stability. Deposition of H3.3 within these genomic contexts is mediated by the ATRX-DAXX complex (Goldberg et al., 2010). Schwartzentruber et al. (2012) identified recurrent mutations in *ATRX* (14/48 cases) and its binding partner *DAXX* (2/48 cases). Overall, 21 of 48 (44%) pediatric GBMs had mutations in *H3F3A, ATRX*, or *DAXX*. Mutation of the ATRX-DAXX complex and either H3.3 tail mutation correlated with loss of ATRX expression in a pediatric GBM tissue array and an alternative lengthening of telomeres phenotype in GBM. Interestingly, although *IDH1* mutations were identified in 4 of 48 pediatric GBM, they were mutually exclusive with *H3F3A/ATRX/DAXX* mutations in this cohort.

Links between chromatin and cancer were initially drawn by oncogenic fusions containing chromatin proteins and by the anti-proliferative properties of chemical inhibitors of histone deacetylases (Baylin and Jones, 2011). These have been strengthened recently as an increasing number of whole-genome and exome cancer sequencing studies have identified prevalent mutations in histone modifying enzymes, nucleosome remodelers, and other regulatory proteins in chromatin. Although such findings are suggestive of direct roles for histone modifications, they fall short of definitive proof given that modifying enzymes also have nonhistone targets and frequently reside within large complexes with multi-faceted functions. Thus, the studies now presented by Schwartzentruber et al. (2012) and Wu et al. (2012) extend our understanding of how defects in chromatin contribute to cancer fitness by providing the first evidence of somatic mutations directly affecting a modifiable residue in histone proteins (Figure 1). Further study is essential to understand the mechanisms by which these and other alterations to the chromatin machinery contribute to malignant transformation and how they may be exploited for improved diagnosis and therapy.

ACKNOWLEDGMENTS

The authors thank Leslie Gaffney from the Broad Institute for assistance with the figure.

REFERENCES

Baylin, S.B., and Jones, P.A. (2011). Nat. Rev. Cancer *11*, 726–734.

Goldberg, A.D., Banaszynski, L.A., Noh, K.M., Lewis, P.W., Elsaesser, S.J., Stadler, S., Dewell, S., Law, M., Guo, X., Li, X., et al. (2010). Cell *140*, 678–691.

Kreiger, P.A., Okada, Y., Simon, S., Rorke, L.B., Louis, D.N., and Golden, J.A. (2005). Acta Neuropathol. *109*, 387–392.

Paugh, B.S., Qu, C., Jones, C., Liu, Z., Adamowicz-Brice, M., Zhang, J., Bax, D.A., Coyle, B., Barrow, J., Hargrave, D., et al. (2010). J. Clin. Oncol. *28*, 3061–3068.

Pollack, I.F., Finkelstein, S.D., Burnham, J., Holmes, E.J., Hamilton, R.L., Yates, A.J., Finlay, J.L., and Sposto, R.; Children's Cancer Group. (2001). Cancer Res. *61*, 7404–7407.

Schwartzentruber, J., Korshunov, A., Liu, X.Y., Jones, D.T., Pfaff, E., Jacob, K., Sturm, D., Fontebasso, A.M., Quang, D.A., Tönjes, M., et al. (2012). Nature *482*, 226–231.

Simon, J.A., and Kingston, R.E. (2009). Nat. Rev. Mol. Cell Biol. *10*, 697–708.

Talbert, P.B., and Henikoff, S. (2010). Nat. Rev. Mol. Cell Biol. *11*, 264–275.

Wu, G., Broniscer, A., McEachron, T.A., Lu, C., Paugh, B.S., Becksfort, J., Qu, C., Ding, L., Huether, R., Parker, M., et al; St. Jude Children's Research Hospital–Washington University Pediatric Cancer Genome Project. (2012). Nat. Genet. *44*, 251–253.

Zhou, V.W., Goren, A., and Bernstein, B.E. (2011). Nat. Rev. Genet. *12*, 7–18.

Cancer Cell
Article

Deconstruction of the SS18-SSX Fusion Oncoprotein Complex: Insights into Disease Etiology and Therapeutics

Le Su,[1] Arthur V. Sampaio,[1] Kevin B. Jones,[3,4] Marina Pacheco,[2] Angela Goytain,[2] Shujun Lin,[1] Neal Poulin,[2] Lin Yi,[1] Fabio M. Rossi,[1] Juergen Kast,[1] Mario R. Capecchi,[4] T. Michael Underhill,[1,*] and Torsten O. Nielsen[2]
[1]Biomedical Research Centre, University of British Columbia, Vancouver, British Columbia V6T 1Z3, Canada
[2]Genetic Pathology Evaluation Centre, 509-2660 Oak Street, Vancouver V6H 3Z6, Canada
[3]Department of Orthopaedics and Center for Children's Cancer Research, Huntsman Cancer Institute
[4]Department of Human Genetics and Howard Hughes Medical Institute
University of Utah, Salt Lake City, UT 84112, USA
*Correspondence: tunderhi@brc.ubc.ca
DOI 10.1016/j.ccr.2012.01.010

SUMMARY

Synovial sarcoma is a translocation-associated sarcoma where the underlying chromosomal event generates *SS18-SSX* fusion transcripts. In vitro and in vivo studies have shown that the SS18-SSX fusion oncoprotein is both necessary and sufficient to support tumorigenesis; however, its mechanism of action remains poorly defined. We have purified a core SS18-SSX complex and discovered that SS18-SSX serves as a bridge between activating transcription factor 2 (ATF2) and transducin-like enhancer of split 1 (TLE1), resulting in repression of ATF2 target genes. Disruption of these components by siRNA knockdown or treatment with HDAC inhibitors rescues target gene expression, leading to growth suppression and apoptosis. Together, these studies define a fundamental role for aberrant ATF2 transcriptional dysregulation in the etiology of synovial sarcoma.

INTRODUCTION

Synovial sarcoma is an aggressive soft tissue tumor of adolescents and young adults (Haldar et al., 2008). Histologically, these tumors can display monophasic (spindle-shaped mesenchymal cells), biphasic (similar but with focal epithelial differentiation), or poorly differentiated (small blue round cells generic with some other translocation-associated sarcomas) morphology. Treatment consists of wide local tumor excision and radiation, which cures local disease. Metastatic disease is usually fatal despite treatment with conventional chemotherapy agents such as doxorubicin and ifosfamide, which confer at best a temporary response.

Almost all synovial sarcomas carry a demonstrable, pathognomonic t(X;18) reciprocal translocation fusing *SS18* to an *SSX* gene. Clinical diagnosis can be molecularly confirmed by the identification of this event by karyotyping, RT-PCR, or FISH techniques, although recently, transducin-like enhancer of split 1 (TLE1) has emerged as a useful immunohistochemical marker that may obviate the need to resort to molecular testing (Jagdis et al., 2009). A variety of studies have shown that the resulting SS18-SSX fusion functions as an oncoprotein; heterologous expression induces transformation of rat fibroblasts, and continued expression is needed for tumor cell survival (Nagai et al., 2001). Most convincingly, in transgenic mice conditional overexpression of SS18-SSX2 in the myogenic progenitor compartment, but not other compartments, leads to the appearance of both monophasic and biphasic synovial sarcoma tumors with full penetrance (Haldar et al., 2007). Together, these studies indicate that the SS18-SSX fusion protein exhibits oncogenic activity and is both necessary and sufficient for tumorigenesis.

Significance

Synovial sarcoma is a cancer of adolescents and young adults for which conventional chemotherapy has limited benefit, and metastatic disease is usually fatal. Preclinical studies have shown sensitivity to HDAC inhibitors, which are being evaluated in clinical trials. However, the mechanistic basis of SS18-SSX-mediated tumorigenesis and HDAC inhibitor action in synovial sarcoma has not been defined. Herein, we identify ATF2 as the DNA-binding partner of SS18-SSX and show that HDAC inhibitors reverse the epigenetic repressor activity of the SS18-SSX oncoprotein complex by preventing TLE1 recruitment. These findings thus uncover a role for HDAC inhibitors in fusion oncoprotein complex assembly, and may inform concurrent investigations on other types of translocation-associated cancer.

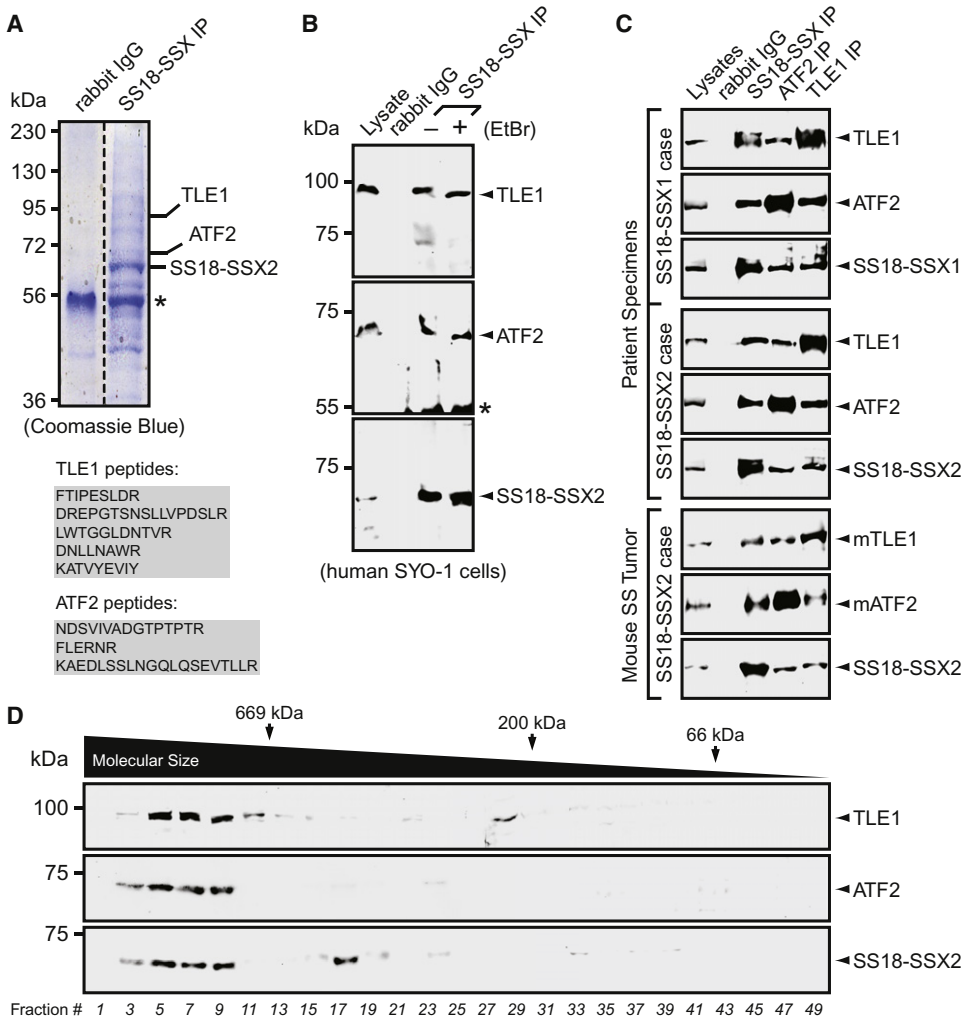

Figure 1. SS18-SSX Associates with ATF2 and TLE1 in Synovial Sarcoma

(A) Coomassie-stained gel of the SS18-SSX complex in SYO-1 cells. ATF2 and TLE1 were identified by mass spectrometry. Asterisk indicates IgG bands.

(B) Western blot analysis of the SS18-SSX precipitates (in the presence or absence of EtBr) in SYO-1 cells. Rabbit IgG was used as a negative control.

(C) Reciprocal IP of SS18-SSX, ATF2, and TLE1 showing their interactions in human and mouse synovial sarcoma (SS) tumors.

(D) Glycerol-gradient fractionation profile of SS18-SSX2, ATF2, and TLE1 in SYO-1 cells.

See also Figure S1.

The SS18-SSX fusion protein retains a C-terminal repressor domain from either of two highly similar cancer-testis antigens, SSX1 or SSX2 (SSX4 has also been reported in rare cases), which is fused to the N terminus of SS18, a transcriptional coactivator (Ladanyi, 2001). The resulting fusion proteins SS18-SSX1 and SS18-SSX2 have no apparent DNA-binding motif, yet appear to function predominantly in transcriptional regulation (Lim et al., 1998). The control of gene expression by SS18-SSX is believed to involve chromatin remodeling, due to its colocalization with both Trithorax (TrxG) and Polycomb group (PcG) complexes, maintaining chromatin in a poised bivalent state (de Bruijn et al., 2006; Lubieniecka et al., 2008; Soulez et al., 1999). Similar to other sarcoma-associated fusion oncoproteins, expression of SS18-SSX contributes to aberrant transcriptional activity and dysregulated gene expression. Because SS18-SSX itself lacks direct DNA-binding domains or activity, it has been challenging to identify target genes or to decipher its mechanism of action. In this article we explore the mechanism of SS18-SSX-mediated repression and its connection with the antitumor action of HDAC inhibitors by identifying the key constituents of SS18-SSX transcriptional complexes in synovial sarcoma.

RESULTS

Identification of ATF2 and TLE1 within an SS18-SSX Complex

To study transcriptional regulation governed by SS18-SSX, we used a validated antibody (RA2009; see Figure S1A available online) to isolate endogenous SS18-SSX2 and its interactants from human synovial sarcoma SYO-1 cells (Figure 1A). Mass spectroscopy further confirmed the presence of SS18-SSX2

(Figure S1B) and identified several known cofactors, including histone deacetylases (Figure S1C). This approach also allowed us to capture multiple peptides corresponding to two previously uncharacterized components, activating transcription factor 2 (ATF2) and TLE1 (Figure S1C). Both of these are master transcriptional regulators that are highly conserved across different species. ATF2 is a DNA-binding protein that recognizes the cAMP-responsive element (CRE) via its leucine zipper domain and recruits histone acetyltransferases (HATs) to increase transcription (Kawasaki et al., 2000). However, the other component TLE1 is a *Groucho* corepressor that usually interacts with transcriptional activators and functions as a competitive inhibitor to repress transcription (Ali et al., 2010). TLE1 is known to be highly expressed in synovial sarcoma (Terry et al., 2007) and has recently been demonstrated to be a robust diagnostic marker for synovial sarcoma, although its biological function in this disease has been unclear (Foo et al., 2011; Jagdis et al., 2009; Knösel et al., 2010).

To validate the proteomic data, immunoprecipitation (IP) was performed in two human synovial sarcoma cell lines (SYO-1 and FUJI), and this shows that both ATF2 and TLE1 are specifically precipitated with anti-SS18-SSX, but not with rabbit IgG (Figures 1B and S1D). Interaction of SS18-SSX2 with both ATF2 and TLE1 was preserved in the presence of ethidium bromide (EtBr, Figure 1B), which suggests that this fusion oncoprotein complex forms independently of DNA. ATF2 and TLE1 association with both SS18-SSX1 and SS18-SSX2 fusion proteins was verified by reciprocal IP using RA2009, ATF2, and TLE1 antibodies (Figure 1C) using patient primary tumors confirmed to express *SS18-SSX1* and *SS18-SSX2* (Figure S1E). Importantly, we find that the mouse homologs of ATF2 (mATF2) and TLE1 (mTLE1/Grg1) are also bound to the human fusion protein in cell cultures derived from tumors from *SS18-SSX2* conditional overexpression mice (Figure 1C) (Haldar et al., 2007). The specificity of ATF2-TLE1 association was confirmed by reciprocal IP using a clear cell sarcoma cell line (DTC-1) where, in the absence of the SS18-SSX fusion oncoprotein, ATF2 and TLE1 no longer coimmunoprecipitated (Figure S1F). This raised the possibility that SS18-SSX serves as a scaffold to link ATF2 and TLE1. Indeed, glycerol-gradient fractionation on human synovial sarcoma SYO-1 cells revealed a coelution profile of ATF2 and TLE1 with SS18-SSX2 (Figures 1D and S1G), indicating that ATF2 and TLE1 occur in the same SS18-SSX complex. We also observed several fundamental chromatin-remodeling factors (SMARCA2, HDAC1, and EZH2) in a major overlapping peak with SS18-SSX2 (Figure S1G).

To obtain further evidence of the observed disease-specific abnormal association of ATF2 with TLE1, a small interfering RNA (siRNA)-based method was used to deplete endogenous SS18-SSX2 and its complex components ATF2 and TLE1 in human SYO-1 and mouse synovial sarcoma cells (Figures S2A and S2B), and the consequences of cell survival were assessed. Similar to SS18-SSX2 knockdown, both ATF2/mATF2 silencing and TLE1/mTLE1 silencing reduce synovial sarcoma cell growth (Figures 2A and S2C) and impair the ability of human and mouse tumor cells to form colonies (Figures 2B and S2D). These knockdown cells appear to undergo apoptosis because depletion of either ATF2 or TLE1 induces an enrichment in the Annexin-V$^+$ fraction (Figure 2C) and also stimulates Caspase-3 activation (Figure S2E). Together, these data demonstrate that ATF2 and TLE1 functionally associate with SS18-SSX to form an endogenous complex in synovial sarcoma important for tumor cell survival.

Copurification of ATF2 and TLE1 Requires SS18-SSX

To gain molecular insights into SS18-SSX complex assembly, reciprocal IP was performed on human SYO-1 cells transfected with nonspecific, SS18-SSX2, ATF2, or TLE1 siRNA. Western blot analysis shows that ATF2 and TLE1 coimmunoprecipitation is dependent upon SS18-SSX2 (Figure 3A). By contrast, recruitment of ATF2 and TLE1 to SS18-SSX2 seems to be independent of each other because depletion of ATF2 (or TLE1) has no significant impact on SS18-SSX2 association with TLE1 (or ATF2) (Figure 3B). To further confirm binding specificity, HEK293 cell lines stably expressing Myc-tagged *SS18*, *SS18-SSX2*, or empty vector were generated (Figure S3A). Analysis of the anti-Myc-tag precipitates reveals the coexistence of ATF2 and TLE1 with recombinant SS18-SSX2 (Figure 3C). The lack of TLE1, but not ATF2, in the Myc-SS18 precipitates (Figure 3C) indicates that ATF2 and TLE1 recruitment involves different protein domains of SS18-SSX2. Reciprocal IP of ATF2 and TLE1 also supports this concept by showing that their connection depends on the presence of SS18-SSX2 and does not occur with SS18 alone (Figures S3B and S3C). Consistent with these data, we find that compared to control cells, ATF2 and TLE1 migrate as individual glycerol-gradient peaks in *SS18-SSX2*-knockdown cells (Figure 3D), implying that they are not found in a shared complex in the absence of SS18-SSX. The shared change in ATF2 and TLE1 distribution in glycerol-gradient sedimentation was also observed in HEK293 stable cell lines with and without the fusion oncoprotein (Figure S3D). To address which domains of SS18-SSX are responsible for ATF2 and TLE1 binding, we next generated *SS18-SSX2* deletion mutants (Figures 3E and S3E) (Nagai et al., 2001) and performed reciprocal IP using the antibodies specific to Myc-tag, ATF2, and TLE1 in HEK293 cells. The results suggest that the N-terminal SNH (SYT N-terminal homolog) domain is responsible for the interaction of SS18-SSX2 with ATF2, whereas TLE1 specifically interacts with the repressor domain (SSXRD) of SS18-SSX2 (Figure 3F). In aggregate these data further reinforce that S18-SSX fusion oncoprotein serves as a scaffold protein to bridge the *Groucho* corepressor TLE1 to transcription factor ATF2 in synovial sarcoma (Figure 3G).

SS18-SSX/TLE1 Functions to Repress ATF2 Target Gene Expression

Recent studies have identified the tumor suppressor *Early Growth Response 1* (*EGR1*) as a direct target of SS18-SSX (Lubieniecka et al., 2008). This gene was used to study the mechanisms underlying SS18-SSX occupancy of its targets. Chromatin immunoprecipitation (ChIP) with antibodies to ATF2, TLE1, and SS18-SSX identifies a common occupied DNA region around 100 bp upstream of the transcription start site of the human *EGR1* locus (Figure 4A). Sequence analysis of this promoter area reveals a consensus CRE site (5′-TCACGTCA-3′), which has been well defined in previous studies as a putative ATF2-binding element, and is phylogenetically conserved across diverse species (Faour et al., 2005; Hayakawa et al.,

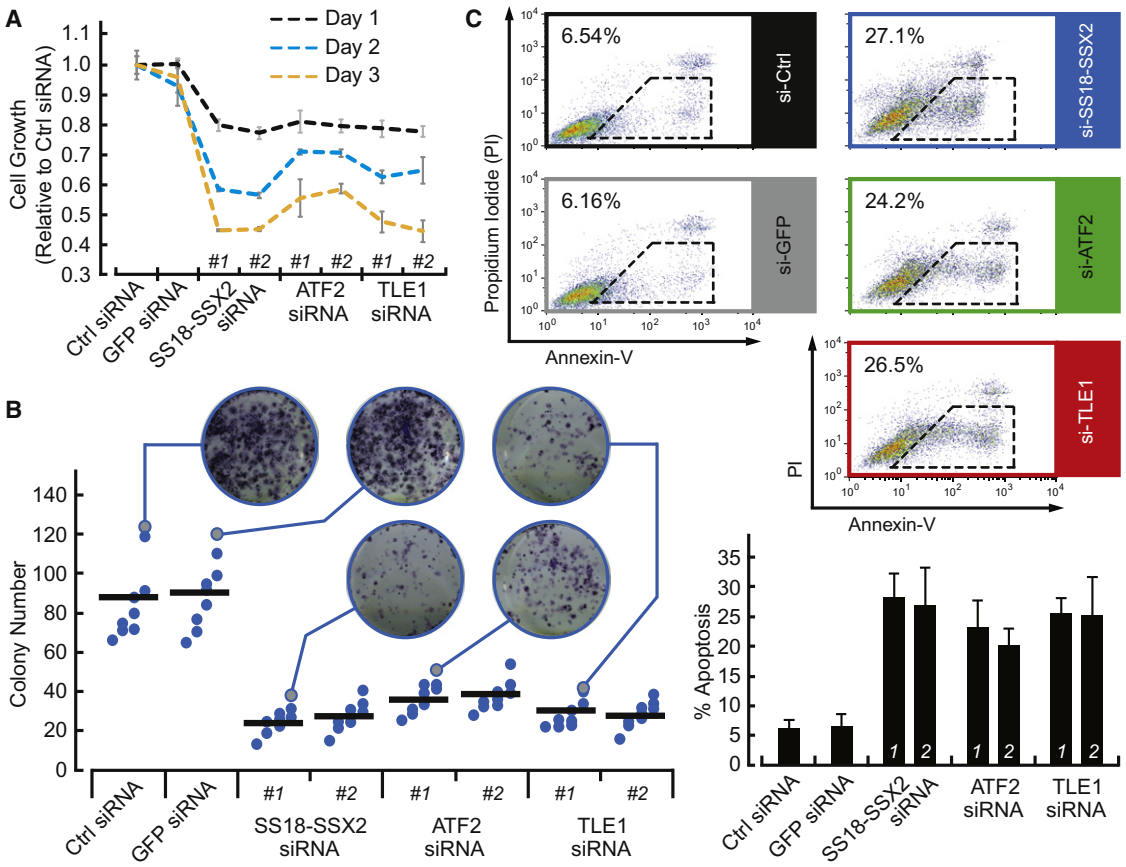

Figure 2. Disruption of the SS18-SSX Complex Reduces Synovial Sarcoma Cell Growth

(A) The effect of SS18-SSX2, ATF2, and TLE1 knockdown on SYO-1 cell growth. Data represent mean ± SD of three experiments.

(B) Colony formation assays on SYO-1 cells at 8 days after indicated siRNA transfections. Representative images for crystal violet stain, and quantitation of number of colonies by ImageJ software. The black bars represent the mean.

(C) Flow cytometric analysis of apoptotic SYO-1 cells transfected with indicated siRNA following 72 hr. Percentages of Annexin-V$^+$ cells are shown (n = 3). Bar charts are mean ± SD.

See also Figure S2.

2004). This indicates that the transcription factor ATF2 may have a critical role in the recruitment of the SS18-SSX complex to target promoters. To test this possibility, we first examined the ATF2 cellular location because ATF2 has been shown to dynamically shuttle between the nucleus and cytoplasm in a context-dependent manner (Bhoumik et al., 2008; Liu et al., 2006; Maekawa et al., 2007). Immunohistochemical and immunofluorescent analysis of ATF2 in patient synovial sarcoma specimens and SYO-1 cells, respectively, shows that ATF2 is predominantly located in the nucleus (Figures 4B and 4C).

To examine the transcriptional activity of ATF2, published and in-house microarray expression profiles of patient specimens were interrogated (Baird et al., 2005; Nakayama et al., 2010; Nielsen et al., 2002) for the expression of known ATF2 target genes. In addition to two known SS18-SSX targets *EGR1* and *Nuclear Protein 1* (*NUPR1*, or *Candidate of Metastasis 1*, *COM1*) (Ishida et al., 2007), a set of seven more genes (Figure 5A) was chosen for further investigation because their promoters contain validated CRE sites for ATF2 binding (Figure S4A) (Hayakawa et al., 2004). These CRE sites are also conserved between humans and mice, and their protein products are involved in controlling cell cycle, apoptosis, and other cellular signaling pathways (Lopez-Bergami et al., 2010). To validate these candidate genes, ChIP was performed on *SS18-SSX1*- and *SS18-SSX2*-positive clinical tumor frozen tissue specimens. Site-specific quantitative PCR (qPCR) shows that both SS18-SSX1 and -SSX2 fusion proteins, together with ATF2 and TLE1, bind to the CRE-containing regions (Figures 5B, 5C, S4B, and S4C). However, we were unable to detect any nonspecific recruitment of these factors (Figures 5B, 5C, S4B, and S4C), implying a possible predominant role for the ATF2-binding element in directing SS18-SSX promoter occupancy. To further evaluate SS18-SSX DNA-binding activity, nuclear proteins were extracted from HEK293 stable cell lines with and without the fusion oncoprotein and incubated with infrared dye-labeled CRE oligonucleotides. An electrophoretic mobility shift assay (EMSA) identifies a specific protein-DNA complex, which is supershifted by the antibody against Myc-tag in Myc-SS18-SSX2-expressing cells, but not in control cells (Figure 5D). Consistently, a similar protein-DNA complex is also observed in human SYO-1 cells where it is supershifted by the antibodies to SS18-SSX, ATF2, and TLE1 (Figure 5E).

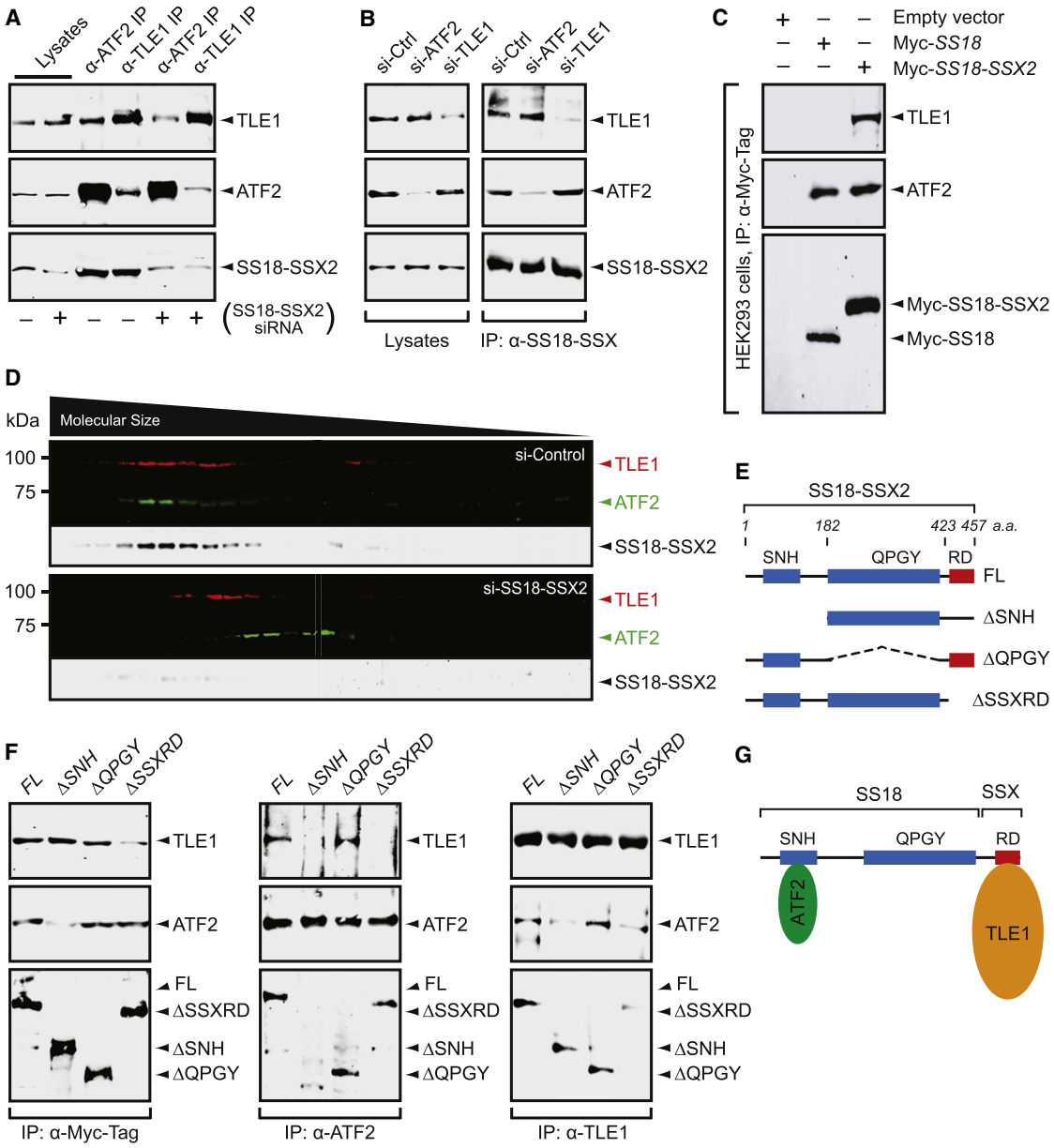

Figure 3. Molecular Association of SS18-SSX with ATF2 and TLE1

(A) Reciprocal IP of ATF2 and TLE1 in control and SS18-SSX2 knockdown SYO-1 cells. Western blot analysis of whole-cell lysates following SS18-SSX2 knockdown are shown on the left.

(B) Western blot analysis of the extracts of control, ATF2, and TLE1 knockdown SYO-1 cells immunoprecipitated by the anti-SS18-SSX antibody.

(C) Myc IP analysis of HEK293 cells stably expressing empty vector, Myc-tagged WT *SS18* or *SS18-SSX2*.

(D) Sedimentation profile of control and SS18-SSX2 knockdown SYO-1 cell extracts by 10%–40% glycerol gradients.

(E) Schematic representing C-terminal Myc-tagged *SS18-SSX2* truncation and deletion constructs. FL, full-length fusion oncoprotein; SNH, SYT N-terminal homolog; QPGY, glycine-/proline-/glutamine-/tyrosine-domain; SSXRD, SSX repressor domain.

(F) Mapping the interface in SS18-SSX2 for its association with ATF2 and TLE1 by reciprocal IP experiments with the Myc, ATF2, and TLE1 antibodies in HEK293 cells expressing the SS18-SSX2 constructs as described in (E).

(G) Schematic model illustrating the scaffolding role of SS18-SSX in ATF2 and TLE1 association.

See also Figure S3.

To further establish a direct link between ATF2 and recruitment of SS18-SSX, we used a specific siRNA to reduce the expression of ATF2 in human SYO-1 cells (Figure S5A). ChIP analyses reveal that loss of ATF2 significantly compromises the association of SS18-SSX2 and TLE1 with target gene promoters (Figure 6A). Furthermore, RT-qPCR analysis shows that transcript abundance of multiple ATF2 targets is increased after depleting ATF2 or SS18-SSX2 (Figure 6B). Consistent with this, in the

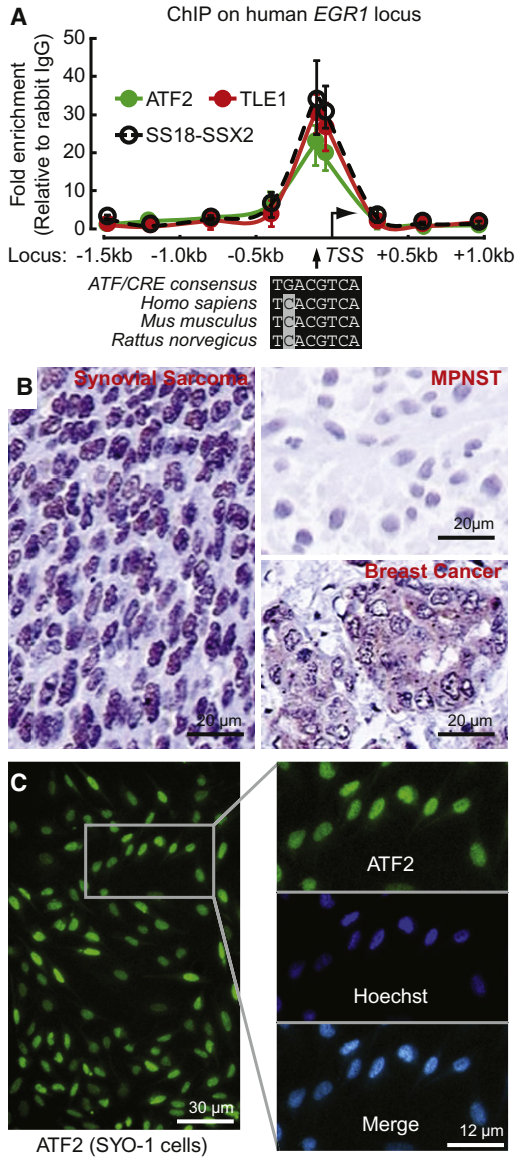

Figure 4. ATF2 Is Recruited to the *EGR1* Promoter along with TLE1 and SS18-SSX and Is Localized to the Nucleus in Synovial Sarcoma

(A) Binding of SS18-SSX, ATF2, and TLE1 across the human *EGR1* locus was assessed by ChIP and site-specific qPCR. Data shown are the mean ± SD of three experiments where values are expressed relative to rabbit IgG.

(B) Endogenous ATF2 protein is localized to the nucleus in primary synovial sarcoma tissues by immunohistochemistry. Malignant peripheral nerve sheath tumor (MPNST) was used as an ATF2-negative control, and cytoplasmic ATF2 staining is shown in a breast cancer case for comparison.

(C) Immunofluorescence analysis of ATF2 nuclear localization in SYO-1 cells. Hoechst staining defines the nuclei. The box defines the area that was expanded and shown in the right panel.

mouse model of synovial sarcoma, SS18-SSX2 and TLE1 binding to target gene promoters is abrogated after ATF2 depletion (Figures 6C and S5B). Notably, an increased transcript level of either *Egr1* or *Atf3* was also observed in mATF2- and SS18-SSX2-knockdown mouse synovial sarcoma cells (Figure 6D). To confirm the specificity of this effect, wild-type (WT) or dn ATF2 was transfected into HEK293 cells in the presence or absence of the fusion protein SS18-SSX2. As shown in Figure S5C, compared with the dn form, overexpression of WT ATF2 in control cells significantly increases *EGR1* and *ATF3* transcript levels. However, this effect is no longer observed in *SS18-SSX2*-expressing cells, indicating that in the presence of SS18-SSX2, ATF2 transactivational activity is reduced. In agreement with the RT-qPCR data, transfection of an *ATF3* reporter gene in human SYO-1 cells shows that the promoter activity for this ATF2 target gene is increased ~4-fold after *SS18-SSX2* depletion, whereas this stimulation is not seen in a construct with two point mutations in the CRE site of the *ATF3* promoter (Figure 6E). Thus, these experiments demonstrate that the SS18-SSX complex occupies ATF2 target genes, and this is dependent upon its interaction with ATF2.

TLE1 also appears to be a functionally important component of the SS18-SSX complex (Figures 2A–2C). To assess whether TLE1 influences SS18-SSX transcriptional activity, TLE1 was knocked down in synovial sarcoma cells. Unlike ATF2 knockdown, depletion of TLE1 affects neither SS18-SSX2 nor ATF2 recruitment to target promoters *EGR1* and *ATF3* (Figure 7A). However, an appreciable increase in transcript levels for both tested target genes is detected by RT-qPCR in TLE1 knockdown cells, compared to control cells (Figure 7B). The specificity of this effect was further confirmed by showing that TLE1 depletion only induces *EGR1* and *ATF3* transcription in HEK293 cells in the presence of Myc-SS18-SSX2 (Figures S6A and S6B). These results indicate that SS18-SSX negatively regulates the transcription of its target genes via collaborating with TLE1. To gain molecular insights into the role of TLE1 in SS18-SSX-mediated repression, histone modifications were analyzed because previous work linked SS18-SSX recruitment to histone H3 lysine 27 trimethylation (H3K27me3), a key mark of gene repression (Lopez-Bergami et al., 2010). *TLE1* knockdown in SYO-1 cells results in a pronounced reduction in H3K27me3 levels at the same *EGR1* and *ATF3* promoter regions occupied by SS18-SSX, whereas the levels of trimethylated histone H3 at lysine 4 (H3K4me3), used as controls, are unchanged (Figure 7C). Given that H3K27me3 is a hallmark of PcG-dependent gene silencing (Cao et al., 2002; Müller et al., 2002), we asked whether TLE1 serves to link the PcG complex to SS18-SSX, thereby promoting repression of target genes. TLE1 has previously been shown to have a close relationship with the catalytic subunits of the PcG complex (Chen et al., 1999; Dasen et al., 2001; Higa et al., 2006). To test this directly in synovial sarcoma, human SYO-1 and primary SS18-SSX2 mouse model tumor cells were used for reciprocal IP analysis. In both cases, coprecipitation of TLE1 leads to enrichment of the PcG component, enhancer of zeste 2 (EZH2), and its functional cofactor, histone deacetylase 1 (HDAC1) (Figure S6C). Similar interactions were obtained with other core PcG subunits, such as the embryonic ectoderm development (EED) protein and suppressor of zeste 12 homolog (SUZ12) (Figures S6D and S6E). These same components of the HDAC/PcG complex had also been identified in mass spectrometric analysis of SS18-SSX2-enriched proteins (Figure S1C), and not surprisingly, EZH2 interactions are maintained in the absence of ATF2 but require TLE1 (Figure 7D). Consistent with these findings, ChIP analysis demonstrates that depletion of TLE1 is associated with a concomitant

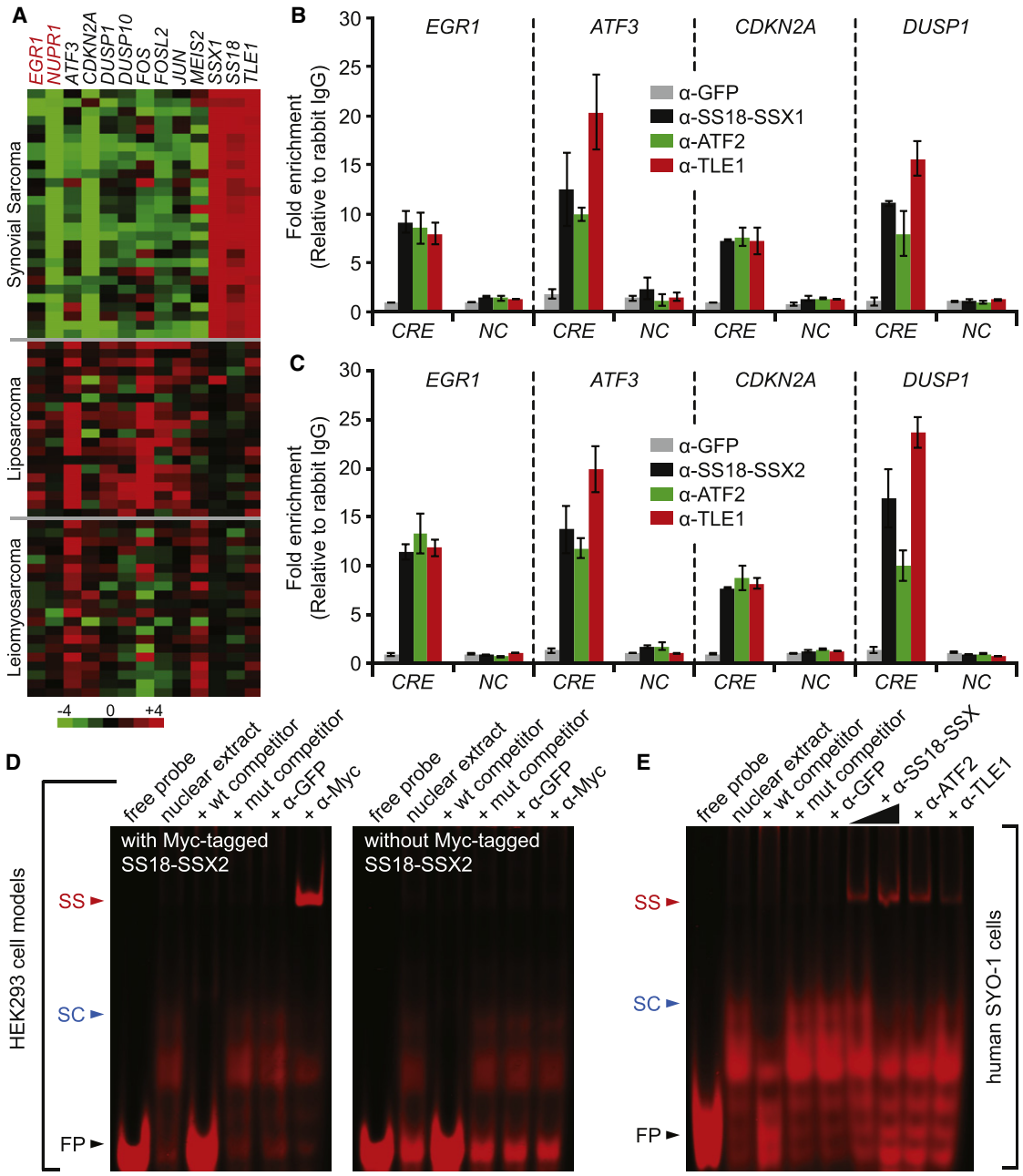

Figure 5. SS18-SSX Is Recruited to Genes with an ATF/CRE

(A) Heat map from meta-analysis of Affymetrix HG-U133_Plus_2 arrays, from Gene Expression Omnibus accession numbers GSE21050 (PMID 20581836) and GSE20196 (PMID: 20975339). Quantile normalized GCRMA expression values are given in log base 2 and calculated relative to the median expression for each gene.

(B and C) ChIP results of primary synovial sarcoma specimens showing SS18-SSX, ATF2, and TLE1 recruitment to the promoter regions of indicated genes. (B) and (C) represent synovial sarcomas containing either SS18-SSX1 or SS18-SSX2 fusion oncoproteins, respectively. The ChIP enrichment was normalized to Rabbit IgG, anti-GFP ChIP was used as the negative control, and ChIP assays were also carried out using non-CRE (NC) containing portions of the respective gene promoters. Bar charts are mean ± SD.

(D and E) EMSA competition and supershift assays showing SS18-SSX2 DNA-binding activity in HEK293 cell models (D) and SYO-1 cells (E). SS, supershift; SC, SS18-SSX:CRE complex; FP, free probe.

See also Figure S4.

decrease in HDAC1 and EZH2 occupancy on both *EGR1* and *ATF3* target promoter regions (Figure 7E), suggesting that TLE1 functionally regulates HDAC/PcG recruitment to SS18-SSX target promoters. Reciprocal IP of TLE1, HDAC1, and EZH2 in normal human and mouse fibroblast cells (CCL153 and NIH/3T3) shows association of these three proteins

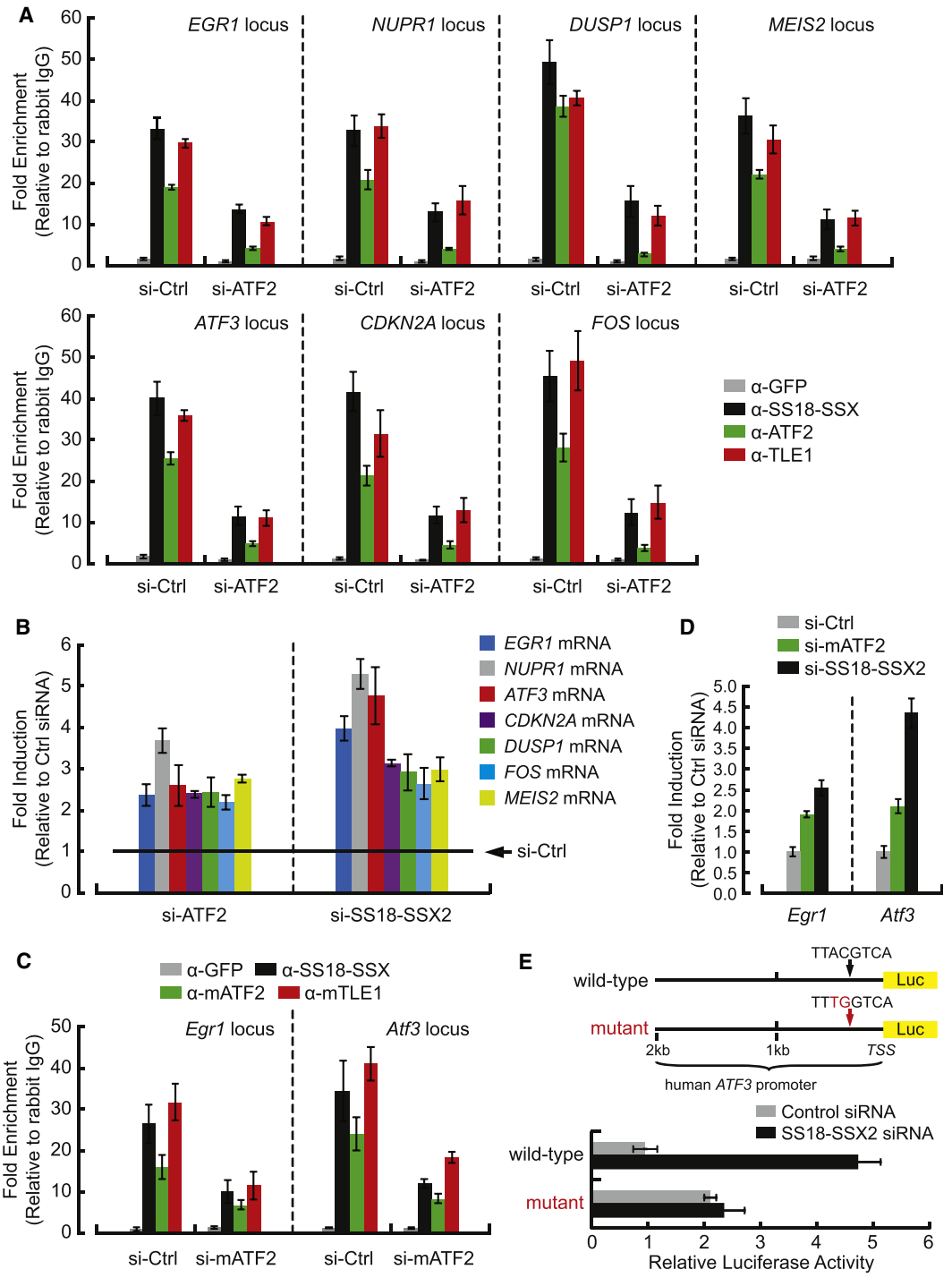

Figure 6. ATF2 Is Critical for DNA Binding of the SS18-SSX Complex

(A and C) Binding of SS18-SSX, ATF2, and TLE1 to representative target promoters was determined by ChIP-qPCR in human SYO-1 (A) and mouse SS tumor cells (C) transfected with control or ATF2/mATF2 siRNA.

(B and D) RT-qPCR analysis of indicated ATF2 target gene expression in human SYO-1 cells (B) and mouse SS tumor cells (D) transfected with control, ATF2/mATF2, or SS18-SSX2 siRNA. Transcript levels were normalized to 18S rRNA, and depicted as a fold change between control and knockdown cells.

(E) Luciferase reporter assays showing the human *ATF3* promoter activity in control and SS18-SSX2 knockdown SYO-1 cells. The reporter constructs were made with the WT *ATF3* promoter regions with or without indicated base substitutions in the ATF/CRE site.

Bar charts are mean ± SD.

See also Figure S5.

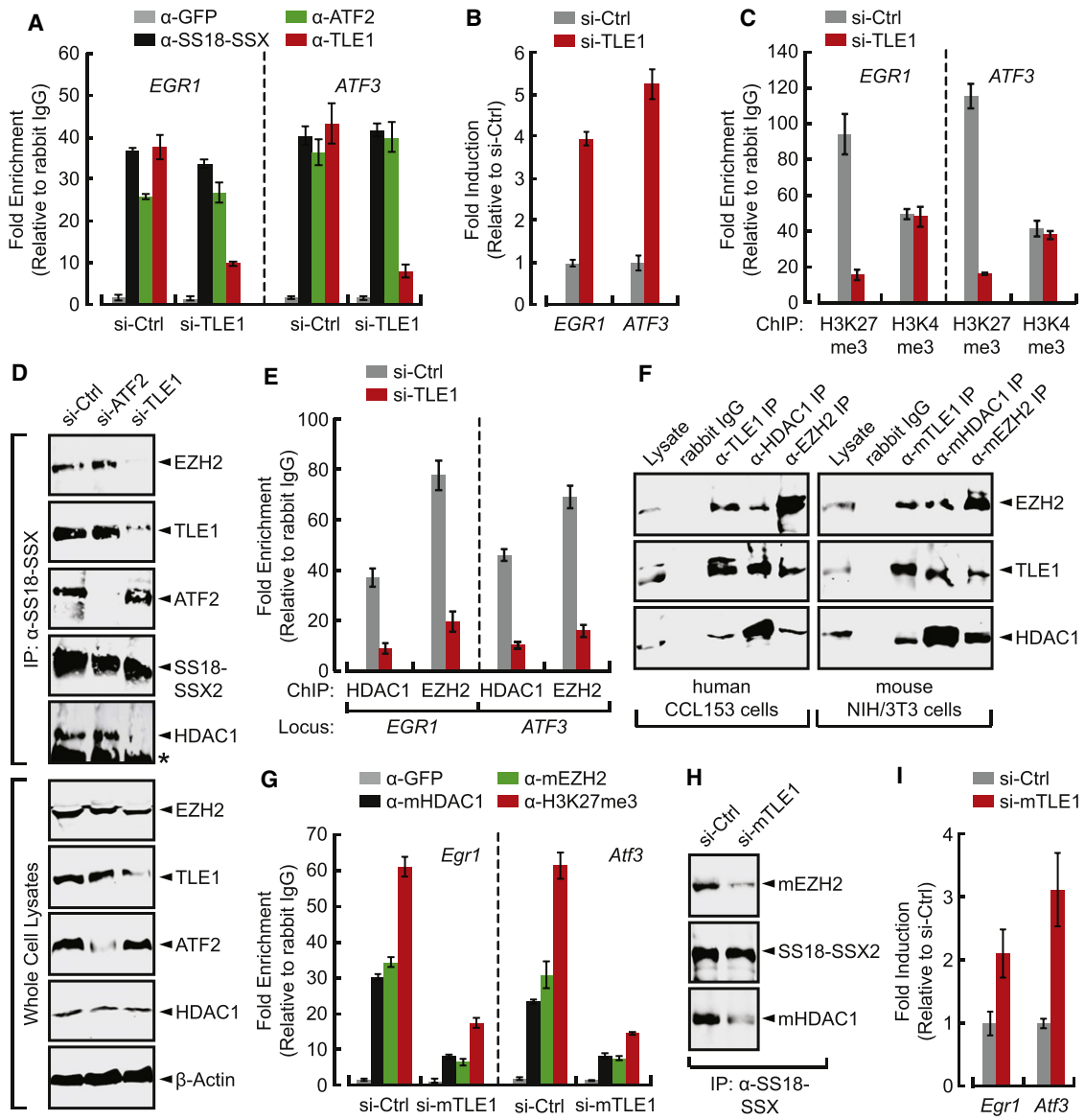

Figure 7. TLE1 Contributes to SS18-SSX-Mediated Repression

(A, C, and E) ChIP-qPCR analysis of the human *EGR1* and *ATF3* promoters in control and TLE1 knockdown SYO-1 cells. The GFP antibody was used as a negative control for ChIP assays. Columns represent mean ± SD (n = 3).

(B) RT-qPCR analysis for human *EGR1* and *ATF3* gene transcripts in SYO-1 cells before and after TLE1 depletion. Transcript levels were normalized to 18S rRNA, and depicted as a fold change between control and TLE1 knockdown SYO-1 cells.

(D) SS18-SSX IP assay showing its association with HDAC1 and EZH2 in control, ATF2, and TLE1 knockdown SYO-1 cells. Asterisk indicates IgG bands.

(F) Reciprocal IP with the TLE1, HDAC1, and EZH2 antibodies showing their interaction in normal human (left) and mouse (right) fibroblast cells.

(G) ChIP-qPCR analysis of control and mTLE1 knockdown mouse synovial sarcoma cells using the indicated antibodies.

(H) Association of SS18-SSX2 with HDAC1 and EZH2 was determined by IP in mouse SS tumor cells transfected with control or mTLE1 siRNA.

(I) RT-qPCR analysis of *Egr1* and *Atf3* gene transcripts in mouse tumor cells transfected with control or mTLE1 siRNA for 48 hr. Changes in expression were normalized to control cells.

Columns represent mean ± SD (n = 3). Bar charts are mean ± SD.

See also Figure S6.

(Figure 7F), and also raises the possibility that TLE1-containing complexes are shared between cancerous and normal cells. In accordance with observations in human tumor cells, TLE1 also has a critical role in assembling HDAC1 and EZH2 into the SS18-SSX complex and maintaining H3K27me3 levels and transcriptional repression on the SS18-SSX-bound promoter regions in the mouse synovial sarcoma model (Figures 7G–7I and S6F). Taken together, these results indicate that TLE1 is responsible for SS18-SSX-mediated gene silencing by an HDAC/PcG-directed epigenetic mechanism.

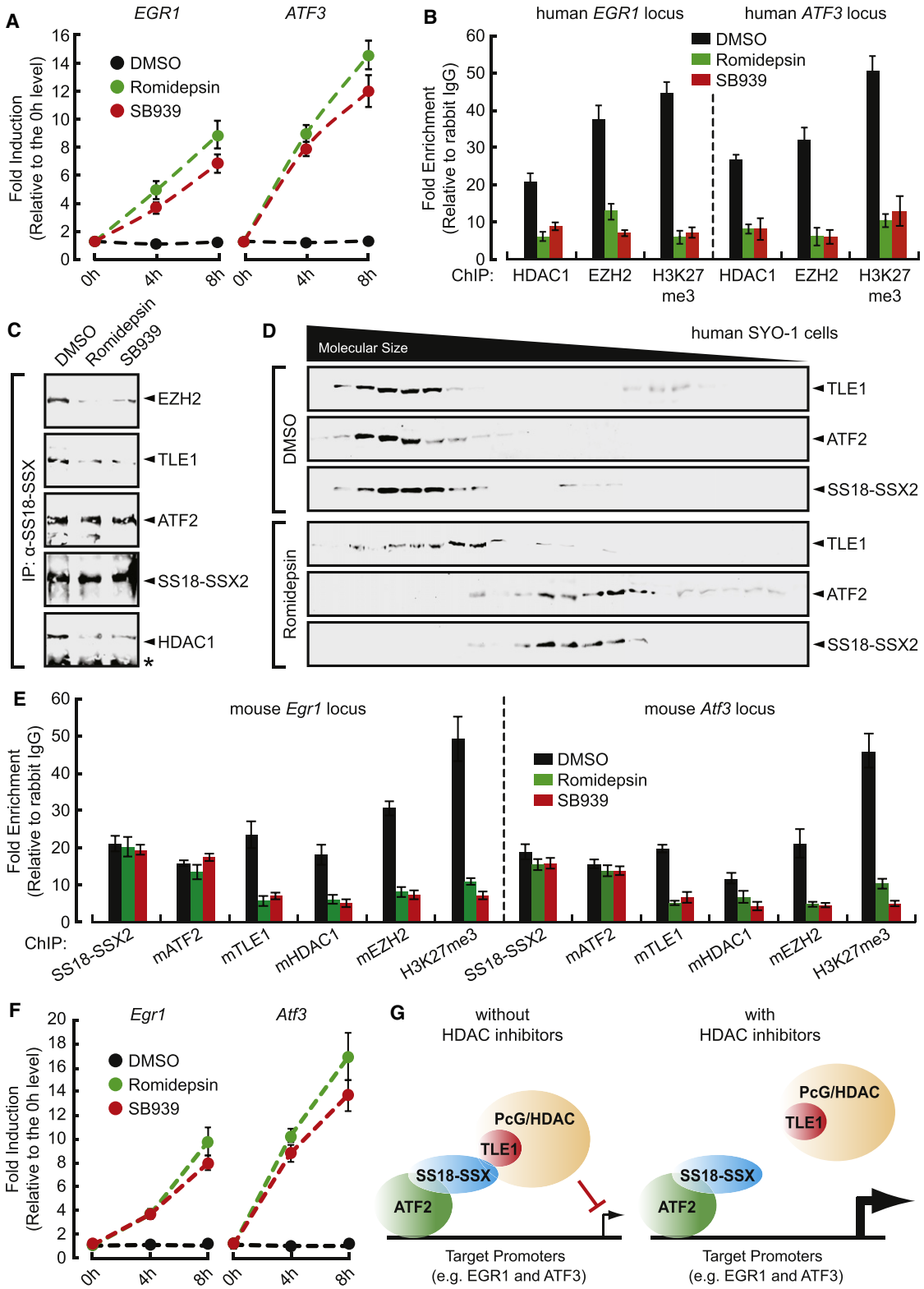

Figure 8. Effect of HDAC Inhibitors on TLE1 Recruitment and SS18-SSX-Mediated Gene Silencing

(A) RT-qPCR analysis of human *EGR1* and *ATF3* gene transcripts in SYO-1 cells treated with DMSO, romidepsin, or SB939 for 8 hr. Changes in expression were normalized to the 0 hr time point.

(B and E) ChIP-qPCR analysis of the *EGR1* and *ATF3* promoters in SYO-1 and mouse synovial sarcoma cells treated with DMSO, romidepsin, or SB939 for 8 hr. The antibodies used in ChIP assays are shown at the bottom of each panel.

HDAC Inhibitors Impact SS18-SSX Target Gene Expression through Modulation of TLE1 Complex Recruitment

The involvement of HDAC/PcG components in the repressor activity of the SS18-SSX complex suggests that HDAC or PcG proteins could be therapeutic targets for the treatment of synovial sarcoma. Indeed, it has been shown that repression of HDAC activity by small molecule inhibitors can effectively suppress synovial sarcoma by reversing SS18-SSX-mediated epigenetic silencing (Lubieniecka et al., 2008; Su et al., 2010). To further examine the importance of HDAC proteins in regulating SS18-SSX activity, HDAC1 (identified as a core SS18-SSX complex subunit, Figure S1C) was knocked down. Similar to the published effects of HDAC inhibitors, depletion of HDAC1 from SYO-1 cells results in *EGR1* reactivation (Figure S7A), and is also associated with decreased cell growth and increased cell death (Figures S7B and S7C). Transcript levels for the SS18-SSX target genes *EGR1* and *ATF3*, as well as other identified targets, increase following addition of romidepsin or SB939 (clinical-grade HDAC inhibitors) (Figures 8A and S7D). H3K27me3 repressive marks are decreased on the *EGR1* and *ATF3* promoters during HDAC inhibitor treatment (Figure 8B). Further analysis under the same conditions reveals a concomitant reduction in localization of HDAC1 and EZH2 to these ATF2 target promoters, even though their protein levels are unaffected (Figures 8B and S7E). Consistent with this observation, HDAC inhibitor treatment of SYO-1 cells reduces HDAC1 and EZH2 appearance in the SS18-SSX complex (Figure 8C). Interestingly, HDAC1 and EZH2 remain bound to TLE1 before and after exposure to romidepsin (Figure S7F). As noted above, HDAC/PcG components are recruited to SS18-SSX through TLE1 (Figures 7D and 7E), and we thus hypothesized that HDAC inhibitors block HDAC/PcG activity by altering the behavior of TLE1. In support of this possibility, glycerol-gradient sedimentation was performed using vehicle (DMSO)- or romidepsin-treated SYO-1 cell extracts. Western blot analysis shows that SS18-SSX2 and TLE1 are located in two separate elution peaks after HDAC inhibitor treatment, whereas the coelution of ATF2 with the fusion protein appears to be stable under both conditions (Figure 8D). To directly test the effect of HDAC inhibitors on TLE1 recruitment, the interaction of TLE1 with SS18-SSX was assessed in the presence of romidepsin or SB939 (Figure 8C). Under these conditions, both HDAC inhibitors block the association of TLE1 with SS18-SSX and its DNA-binding partner ATF2. ChIP analysis in HDAC inhibitor-treated SYO-1 cells demonstrates the removal of TLE1 from target promoters, whereas SS18-SSX2 and ATF2 remain resident (Figure S7G). A similar abrogation of TLE1, HDAC1, and EZH2 occupancy on the *Egr1* and *Atf3* promoters is observed in mouse synovial sarcoma cells following HDAC inhibitor treatment (Figure 8E). Congruent with this, romidepsin and SB939 induce a time-dependent increase in the expression of both *Egr1* and *Atf3* (Figure 8F), in accordance with a significant decrease in H3K27me3 levels on their promoter regions (Figure 8E). Taken together, these findings suggest that HDAC inhibitors derepress SS18-SSX target genes, at least in part through disrupting the recruitment of TLE1 and its associated HDAC/PcG proteins to the SS18-SSX complex, thus leading to loss of the repressive H3K27me3 mark and restored gene expression.

DISCUSSION

The nature through which SS18-SSX dysregulates transcription is a long-standing question in the synovial sarcoma field. Previous studies have shown that SS18-SSX can interact with components of the TrxG transcriptional activator complexes (Nagai et al., 2001; Thaete et al., 1999), as well it has been found to colocalize with PcG repressor factors (Soulez et al., 1999). Although these observations suggest a potential role for chromatin remodeling in SS18-SSX-mediated gene silencing, it remained unclear how SS18-SSX controls the TrxG-PcG balance and, more importantly, how this fusion oncoprotein regulates gene expression in the absence of any known DNA-binding domain. In this study we identify a core SS18-SSX transcriptional complex that is required for epigenetic silencing of tumor suppressor genes in synovial sarcoma. For assembly of this complex, the SS18-SSX fusion oncoprotein serves as a scaffolding protein to connect together two important transcriptional regulators: ATF2 and TLE1. SS18-SSX alone cannot bind to DNA, and its recruitment to target promoters is dependent on the sequence-specific transcriptional activator ATF2. In this manner, SS18-SSX recruitment of a TLE1-containing repressor complex functions to silence ATF2 target genes.

Modulation of ATF2 has also been identified in other cancers, and interestingly, both activation and inhibition of ATF2 have been linked to tumorigenesis indicating that ATF2 function in cancer is context dependent (Lopez-Bergami et al., 2010). For instance in melanoma, activation of ATF2, which is associated with predominantly nuclear localization, appears to be important for tumorigenesis and metastasis. Conversely, in other cancers, loss or decreased expression of ATF2 is associated with an increased incidence of tumorigenesis and metastasis (Maekawa et al., 2007, 2008). Putative *ATF2*-inactivating mutations in lung cancer have been identified, and in melanoma increased ATF2 cytoplasmic localization is associated with reduced tumorigenic potential and a better prognosis (Berger et al., 2003; Woo et al., 2002). *Atf2* heterozygous mice exhibit an increased incidence of breast cancer after a long latency period (>60 weeks), suggesting that an additional hit(s) is required for tumor progression in this background (Maekawa

(C) SS18-SSX IP assay in DMSO-, romidepsin-, and SB939-treated SYO-1 cells. ATF2 and TLE1 protein levels were determined by western blot analysis of whole-cell lysates (Figure S7E). Asterisk indicates IgG bands.
(D) Glycerol-gradient sedimentation analysis of DMSO- and romidepsin-treated SYO-1 cell extracts 8 hr following treatment.
(F) Transcript levels for *Egr1* and *Atf3* were measured by RT-qPCR in mouse SS tumor cells treated with DMSO, romidepsin, or SB939 for 8 hr, and depicted as a fold change relative to the 0 hr time point.
(G) Model of how the SS18-SSX complex regulates transcription before and after HDAC inhibitor treatment.
Bar charts are mean ± SD.
See also Figure S7.

et al., 2007). However, this second hit may in part involve loss of ATF2 because in all tumors examined ATF2 was undetectable. In a skin cancer model in mice, deletion of *Atf2* was sufficient to increase the appearance of precancerous lesions (Bhoumik et al., 2008). However, in this model loss of ATF2 appears to promote tumorigenesis and is unlikely involved in initiation. Together, these studies support a fundamental role for ATF2 in tumorigenesis, and highlight the varied mechanisms employed to inactivate its function.

In synovial sarcoma, ATF2 function is disrupted through a mechanism in which the fusion oncoprotein couples ATF2 to a TLE1-containing complex. Interestingly, whereas ATF2 shows predominantly nuclear localization, the presence of the fusion oncoprotein in turn leads to repression of ATF2 target genes. Repression of ATF2 targets is observed in both synovial sarcoma-derived cell lines and in primary tumors. Furthermore, restoration of ATF2 transcriptional activity and/or the expression of some ATF2 target genes leads to growth suppression and apoptosis in synovial sarcoma cells, indicating that loss of ATF2 function is important for the maintenance of the tumor cell phenotype. Importantly, loss of TLE1 phenocopies loss of ATF2, and leads to upregulation of several ATF2 target genes. In this regard, TLE1 appears to function in a dn manner on ATF2-mediated transactivation, by mediating HDAC/PcG-directed gene silencing of ATF2 targets. It should be noted that TLE1 expression is an important clinical feature for distinguishing synovial sarcoma from other soft tissue tumors (Jagdis et al., 2009; Knösel et al., 2010; Terry et al., 2007). However, the relevance of TLE1 as a specific biomarker for this disease remains controversial (Foo et al., 2011; Kosemehmetoglu et al., 2009), in part due to an absence of supportive functional data. Herein, we define a fundamental role for TLE1 in the etiology of synovial sarcoma and provide a biological rationale for its use as a diagnostic biomarker and potential therapeutic target in synovial sarcoma.

Synovial sarcomas have been shown to be highly sensitive to HDAC inhibitors in preclinical models (Ito et al., 2005; Liu et al., 2008), and herein, we find that the interaction between SS18-SSX and TLE1 is critical in regulating the epigenetic reprogramming that occurs following HDAC inhibitor treatment. Based on these findings, we propose a model (Figure 8G) wherein HDAC inhibitors relieve SS18-SSX-mediated repression at ATF2 target genes most likely through removal of TLE1 and its associated HDAC/PcG factors from SS18-SSX. Consequently, as was also observed with TLE1 knockdown, HDAC/PcG complexes are no longer recruited to ATF2 target promoters. In support of this concept, TLE1 depletion similarly results in diminished H3K27me3 signals and elevated transcript levels for ATF2/SS18-SSX target genes. The mechanisms underlying HDAC inhibitor-induced disruption of SS18-SSX-TLE1 interaction are currently unknown but are being investigated. In summary our findings provide fundamental insights into the nature of the SS18-SSX transcriptional complex, including a DNA-binding partner protein (ATF2) and abnormal recruitment of enzymatic epigenetic corepressors via TLE1. This information provides a biological rationale for including synovial sarcoma in clinical trials of HDAC inhibitors (NCT01112384, NCT00918489, NCT00878800) and a framework for identifying therapeutic strategies to treat this deadly disease.

EXPERIMENTAL PROCEDURES

Cells, Tissues, and Chemicals

Human synovial sarcoma cell lines SYO-1 and FUJI were kindly provided by Dr. Akira Kawai (National Cancer Centre Hospital, Tokyo) and Dr. Kazuo Nagashima (Hokkaido University School of Medicine, Sapporo, Japan) and maintained in RPMI-640 medium with 10% fetal bovine serum (FBS) (Invitrogen). HEK293 cells stably expressing Myc-tagged SS18 or SS18-SSX2 were grown in DMEM with 10% FBS and 400 μg/ml Zeocin (Invitrogen). Primary mouse synovial sarcoma cells were isolated from tumors of female *Myf5-Cre/SSM2* mice as described previously (Haldar et al., 2007), and cultured in DMEM with 10% FBS. All cells were maintained at 37°C, 95% humidity, and 5% CO_2.

Human subjects in this study provided informed consent for use of tissues for research purposes following procedures approved by the Clinical Research Ethics Board of the University of British Columbia (projects H08-0717 "Sarcoma tissue bank" and H06-00013 "Molecular targets for therapy of sarcoma").

HDAC inhibitors romidepsin (FK228, Depsipeptide, or NSC-630176) and SB939 were obtained from the Developmental Therapeutic Branch of the National Cancer Institute (Bethesda, MD, USA) and S*BIO (Singapore, Singapore), respectively. DMSO was purchased from Sigma-Aldrich.

Plasmid DNA Constructs

To define the domains within SS18-SSX2 that interact with ATF2 and TLE1, variants missing the SNH or QPGY domain of SS18 and the SSXRD domain of SSX2 were generated via gene synthesis (Integrated DNA Technologies [IDT]) and subcloned as EcoR1-Not1 fragments into the mammalian expression vector pcDNA4/myc-HisA (Life Technologies). All genes were engineered to remove the stop, allowing readthrough to generate a C-terminal Myc-6XHis tag.

IP and Western Blots

For IP, cells were washed twice with ice-cold PBS, and incubated with RIPA buffer (Santa Cruz Biotechnology) for 35 min on ice. Whole-cell lysates were centrifuged at 4°C, at full speed in a microcentrifuge for 15 min, and the supernatants were mixed with 15 μl of protein A/G agarose beads (Santa Cruz Biotechnology) for 45 min at 4°C for preclearing. For IP, 500 μg of precleared proteins was incubated with 1.5 μg of indicated antibody at 4°C overnight, followed by the addition of 25 μl of protein A/G agarose beads. After a 3 hr incubation at 4°C, the beads were precipitated, washed once with RIPA buffer and twice with ice-cold PBS, and boiled in 2× loading dye for 5 min. Samples were separated by 10%–12% SDS-PAGE and transferred to nitrocellulose membranes (Bio-Rad Laboratories). Blots were incubated with indicated antibodies (see below for details). Signals were visualized using the Odyssey Infrared System (LI-COR Biosciences).

Mass Spectrometry

Coomassie blue-stained bands were excised from the gel and reduced with dithiothreitol (DTT), followed by alkylation with iodoacetamide (IAA). Gel bands were digested with Trypsin at 37°C overnight as described (Shevchenko et al., 1996). Proteolytically digested peptides were then extracted from the gel pieces, reconstituted in formic acid (FA), and analyzed on a QStar XL LC-MS/MS (Applied Biosystems). The MS/MS peaks were submitted to Mascot and gpmDB for peptide sequence database search (Wong et al., 2009). Both of these databases were employed to confirm peptide/protein identification in this study.

Immunofluorescence and Immunohistochemistry

SYO-1 cells were cultured on glass coverslips, fixed with 3:1 acetone-methanol at −20°C for 7 min, and blocked with 5% BSA for 30 min. Cells were then incubated with a polyclonal ATF2 rabbit antibody (Santa Cruz Biotechnology) at 4°C overnight, followed by three washes with ice-cold PBS. After incubation with Alexa Fluor-Conjugated anti-Rabbit secondary antibody (New England Biolabs), the coverslips were mounted in 50% glycerol and 2% DABCO (Sigma-Aldrich). The cellular localization of ATF2 was analyzed under a fluorescence microscope (Zeiss).

Primary synovial sarcoma, malignant peripheral nerve sheath, and breast cancer samples were embedded in paraffin, and stained with the same ATF2 antibody used in immunofluorescence. All immunostainings were performed with avidin-biotin-peroxidase complex technique (VECTASTAIN) in combination with diaminobenzidine (DAB), and counterstained with hematoxylin and eosin (H&E) on surgical pathology specimens as described previously (Pacheco et al., 2010; Terry et al., 2007). Negative controls were carried out with rabbit IgG.

Glycerol-Gradient Sedimentation

Nuclear extracts were prepared from SYO-1 and HEK293 stable cell lines using the Pierce NE-PER Nuclear Extraction kit. Samples were then subjected to a 10%–40% glycerol gradient in 4.8 ml buffer (150 mM NaCl, 10 mM HEPES [pH 7.5], 2 mM DTT, 1 mM EDTA, and 0.1% Triton X-100), and centrifuged at 40,000 rpm for 16 hr at 4°C in a SW50.1 rotor (Beckman). Fractions (160 μl) were collected starting from the top of the gradient, followed by SDS-PAGE and western blot analysis. To determine molecular weight (mol wt) of fractions, marker proteins thyroglobulin (mol wt 669 kDa), β-amylase (mol wt 200 kDa), and BSA (mol wt 66 kDa) were spiked into the gradients and detected using their respective antibodies.

RNA Interference

The siRNAs specific for ATF2/mATF2, TLE1/mTLE1, and HDAC1 were purchased from Dharmacon and Santa Cruz Biotechnology, respectively. Two different SS18-SSX2 siRNAs were synthesized by IDT as described in previous studies (Garcia et al., 2011; Lubieniecka et al., 2008). At 60% confluence, cells were transfected with the indicated siRNA using Lipofectamine RNAiMAX transfection reagent (Invitrogen) according to the manufacturer's instructions. Except where indicated, lysates or RNA was harvested 48 hr post-transfection, and used for IP, glycerol gradients, reporter gene assays, RT-qPCR, and western blots. Knockdown efficiency was determined by RT-qPCR.

Cell Growth and Colony Formation Assay

To measure cell growth rate, human and mouse synovial sarcoma cells were cultured at 60% confluence on 48-well plates, and transfected with the indicated siRNA using Lipofectamine RNAiMAX transfection reagent. At various times after transfection, cell growth was monitored by MTT assay (Life Technologies) and normalized to control cells to give relative growth rate of cells. For colony formation assay, control and knockdown cells were replated on 6-well plates at a density of 1×10^3 cells per well. After 8 days of incubation, cells were fixed with 10% formalin and stained with 0.1% crystal violet, and the colonies counted by using ImageJ software as described (Junttila et al., 2007).

Cell Death and Apoptosis Assay

Cells were cultured with propidium iodide (PI) at a concentration of 500 ng/ml, followed by transfection with the indicated siRNA. Cell death was indicated by PI-positive cells, and visualized under a fluorescence microscope (Zeiss). For analysis of apoptosis, cells were harvested 72 hr after siRNA transfection, and suspended in Annexin-V-FITC-PI dye (Invitrogen). After adding Annexin-V binding buffer, the samples were run through a FACS scan flow cytometer (Becton Dickinson) as described (Kawase et al., 2009). Summit for MoFlo Acquisition and Sort Control Software was used to quantify apoptosis (Annexin-V positive cells).

ChIP

ChIP experiments were performed following the Active Motif protocol as described (Su et al., 2010). Briefly, 5×10^7 cells or 150 mg synovial sarcoma tissues were crosslinked with 1% formaldehyde prior to lysis and homogenization. Crosslinked DNA was sheared using a Bioruptor-UCD300 sonicator (Diagenode) for 15 × 25 s pulses (60 s pause between pulses) at 4°C. After centrifugation, the supernatants were precleared with Protein G beads for 30 min at 4°C, and incubated with the indicated antibody at 4°C overnight. After 4 hr incubation with Protein G beads, the precipitates were washed four times with different washing buffers (Active Motif), eluted with 1% SDS, and incubated at 65°C overnight to reverse crosslinking. ChIP-enriched DNA was purified using the QIAGEN PCR Purification kit, and subjected to SYBR Green qPCR analysis (Roche) using various primer sets (Supplemental Experimental Procedures).

EMSA

The *ATF/CRE* probe was purchased from LI-COR, and labeled on the 5′ end of each strand with Infrared Dye-700 nm. The WT and mutant *ATF/CRE* competitor probes were obtained from Santa Cruz Biotechnology. Binding reactions were performed in the dark at room temperature for 30 min in 25 μl of EMSA buffer (250 mM NaCl, 20 mM HEPES [pH 7.9], 2 mM DTT, 20% glycerol, 0.5% Tween 20) as described before (Boyle et al., 2009). Samples were separated on 4% polyacrylamide gels (29.2:0.8 acrylamide-bisacrylamide in 100 mM Tris, 100 mM borate, and 10 mM EDTA). The extent of gel shift was then visualized on the Odyssey Infrared scanner (LI-COR).

Luciferase Reporter Assay

For luciferase reporter assays, transient transfections were performed using FuGENE 6 transfection reagent (Roche). SYO-1 cells were subcultured in 24-well plates, and transfected with the WT or mutant human *ATF3* promoter-firefly luciferase reporter plasmid together with renilla luciferase expression vector. After 24 hr incubation, the control or SS18-SSX2-specific siRNA was introduced using Lipofectamine RNAiMAX transfection reagent. Cells were harvested at 48 hr after siRNA transfection and analyzed using the Dual-Luciferase Reporter Assay system (Promega). Firefly luciferase was normalized to renilla luciferase activity to control for differences in transfection efficiency and to generate relative luciferase activity.

Real-Time qPCR

Total RNA was isolated and then reverse transcribed to cDNA using the QIAGEN RNeasy Mini kit and the high-capacity cDNA reverse transcription kit (Applied Biosystems), respectively, as described previously (Su et al., 2010). TaqMan gene expression assays were performed by using the ABI-7500 Fast Real-Time PCR System with specific primer/probe sets (Applied Biosystems). All transcript levels were normalized to 18S ribosomal RNA (rRNA) expression.

Antibodies

The rabbit polyclonal antibody (RA2009) against SS18-SSX was kindly provided by Dr. Diederik R.H. de Bruijn (Radboud University Nijmegen Medical Centre, Nijmegen, The Netherlands). The antibodies for SS18 (H-80), SSX (C-9), ATF2 (C-19), TLE1 (M-101 and N-18), HDAC1 (10E2), β-Actin (N-21), Caspase-3 (H-277), and EGR1 (588) were purchased from Santa Cruz Biotechnology. The H3K4me3 (Upstate; 05-745) and H3k27me3 (Upstate; 07-449) antibodies were used for ChIP. For IP and western blots, we also used the following antibodies: Myc (Cell Signaling; #2278); HDAC1 (Abcam; ab1767); EZH2 (Active Motif; #39639); EED (Abcam; ab4469); SUZ12 (Abcam; ab12073); Caspase-3 (Cell Signaling; #9668); and GFP (Cell Signaling; #2555).

SUPPLEMENTAL INFORMATION

Supplemental Information includes seven figures and Supplemental Experimental Procedures and can be found with this article online at doi:10.1016/j.ccr.2012.01.010.

ACKNOWLEDGMENTS

We thank Dr. Diederik R.H. de Bruijn (Radboud University Nijmegen Medical Centre, Nijmegen, The Netherlands) for rabbit polyclonal antibody against SS18-SSX and enlightened discussion of SS18-SSX ChIP data, and Drs. Junya Kawauchi and Shigetaka Kitajima (Tokyo Medical and Dental University, Tokyo) for human *ATF3* promoter-luciferase reporter plasmids. Romidepsin was generously provided by Celgene (Gloucester Pharmaceuticals) and the National Cancer Institute, and SB939 was provided by S*BIO (Singapore). This work was supported by grants from the Canadian Cancer Society Research Institute (Grant #018355) and the Terry Fox Foundation and CIHR Institute of Cancer (TFF 105265). K.B.J. receives career development support from the National Cancer Institute (NIH) K08CA138764 and additional support from the Paul Nabil Bustany Fund for Synovial Sarcoma

Research. T.M.U. was supported by an Arthritis Society Investigator award. T.O.N. is a Michael Smith Foundation of Health Research senior scholar.

Received: July 26, 2011
Revised: November 23, 2011
Accepted: January 24, 2012
Published: March 19, 2012

REFERENCES

Ali, S.A., Zaidi, S.K., Dobson, J.R., Shakoori, A.R., Lian, J.B., Stein, J.L., van Wijnen, A.J., and Stein, G.S. (2010). Transcriptional corepressor TLE1 functions with Runx2 in epigenetic repression of ribosomal RNA genes. Proc. Natl. Acad. Sci. USA *107*, 4165–4169.

Baird, K., Davis, S., Antonescu, C.R., Harper, U.L., Walker, R.L., Chen, Y., Glatfelter, A.A., Duray, P.H., and Meltzer, P.S. (2005). Gene expression profiling of human sarcomas: insights into sarcoma biology. Cancer Res. *65*, 9226–9235.

Berger, A.J., Kluger, H.M., Li, N., Kielhorn, E., Halaban, R., Ronai, Z., and Rimm, D.L. (2003). Subcellular localization of activating transcription factor 2 in melanoma specimens predicts patient survival. Cancer Res. *63*, 8103–8107.

Bhoumik, A., Fichtman, B., Derossi, C., Breitwieser, W., Kluger, H.M., Davis, S., Subtil, A., Meltzer, P., Krajewski, S., Jones, N., and Ronai, Z. (2008). Suppressor role of activating transcription factor 2 (ATF2) in skin cancer. Proc. Natl. Acad. Sci. USA *105*, 1674–1679.

Boyle, P., Le Su, E., Rochon, A., Shearer, H.L., Murmu, J., Chu, J.Y., Fobert, P.R., and Després, C. (2009). The BTB/POZ domain of the *Arabidopsis* disease resistance protein NPR1 interacts with the repression domain of TGA2 to negate its function. Plant Cell *21*, 3700–3713.

Cao, R., Wang, L., Wang, H., Xia, L., Erdjument-Bromage, H., Tempst, P., Jones, R.S., and Zhang, Y. (2002). Role of histone H3 lysine 27 methylation in Polycomb-group silencing. Science *298*, 1039–1043.

Chen, G., Fernandez, J., Mische, S., and Courey, A.J. (1999). A functional interaction between the histone deacetylase Rpd3 and the corepressor groucho in *Drosophila* development. Genes Dev. *13*, 2218–2230.

Dasen, J.S., Barbera, J.P., Herman, T.S., Connell, S.O., Olson, L., Ju, B., Tollkuhn, J., Baek, S.H., Rose, D.W., and Rosenfeld, M.G. (2001). Temporal regulation of a paired-like homeodomain repressor/TLE corepressor complex and a related activator is required for pituitary organogenesis. Genes Dev. *15*, 3193–3207.

de Bruijn, D.R., Allander, S.V., van Dijk, A.H., Willemse, M.P., Thijssen, J., van Groningen, J.J., Meltzer, P.S., and van Kessel, A.G. (2006). The synovial-sarcoma-associated SS18-SSX2 fusion protein induces epigenetic gene (de) regulation. Cancer Res. *66*, 9474–9482.

Faour, W.H., Alaaeddine, N., Mancini, A., He, Q.W., Jovanovic, D., and Di Battista, J.A. (2005). Early growth response factor-1 mediates prostaglandin E2-dependent transcriptional suppression of cytokine-induced tumor necrosis factor-alpha gene expression in human macrophages and rheumatoid arthritis-affected synovial fibroblasts. J. Biol. Chem. *280*, 9536–9546.

Foo, W.C., Cruise, M.W., Wick, M.R., and Hornick, J.L. (2011). Immunohistochemical staining for TLE1 distinguishes synovial sarcoma from histologic mimics. Am. J. Clin. Pathol. *135*, 839–844.

Garcia, C.B., Shaffer, C.M., Alfaro, M.P., Smith, A.L., Sun, J., Zhao, Z., Young, P.P., Vansaun, M.N., and Eid, J.E. (2011). Reprogramming of mesenchymal stem cells by the synovial sarcoma-associated oncogene SYT-SSX2. Oncogene, in press. Published online September 26, 2011. 10.1038/onc.2011.418.

Haldar, M., Hancock, J.D., Coffin, C.M., Lessnick, S.L., and Capecchi, M.R. (2007). A conditional mouse model of synovial sarcoma: insights into a myogenic origin. Cancer Cell *11*, 375–388.

Haldar, M., Randall, R.L., and Capecchi, M.R. (2008). Synovial sarcoma: from genetics to genetic-based animal modeling. Clin. Orthop. Relat. Res. *466*, 2156–2167.

Hayakawa, J., Mittal, S., Wang, Y., Korkmaz, K.S., Adamson, E., English, C., Ohmichi, M., McClelland, M., and Mercola, D. (2004). Identification of promoters bound by c-Jun/ATF2 during rapid large-scale gene activation following genotoxic stress. Mol. Cell *16*, 521–535.

Higa, L.A., Wu, M., Ye, T., Kobayashi, R., Sun, H., and Zhang, H. (2006). CUL4-DDB1 ubiquitin ligase interacts with multiple WD40-repeat proteins and regulates histone methylation. Nat. Cell Biol. *8*, 1277–1283.

Ishida, M., Miyamoto, M., Naitoh, S., Tatsuda, D., Hasegawa, T., Nemoto, T., Yokozeki, H., Nishioka, K., Matsukage, A., Ohki, M., and Ohta, T. (2007). The SYT-SSX fusion protein down-regulates the cell proliferation regulator COM1 in t(x;18) synovial sarcoma. Mol. Cell. Biol. *27*, 1348–1355.

Ito, T., Ouchida, M., Morimoto, Y., Yoshida, A., Jitsumori, Y., Ozaki, T., Sonobe, H., Inoue, H., and Shimizu, K. (2005). Significant growth suppression of synovial sarcomas by the histone deacetylase inhibitor FK228 in vitro and in vivo. Cancer Lett. *224*, 311–319.

Jagdis, A., Rubin, B.P., Tubbs, R.R., Pacheco, M., and Nielsen, T.O. (2009). Prospective evaluation of TLE1 as a diagnostic immunohistochemical marker in synovial sarcoma. Am. J. Surg. Pathol. *33*, 1743–1751.

Junttila, M.R., Puustinen, P., Niemelä, M., Ahola, R., Arnold, H., Böttzauw, T., Ala-aho, R., Nielsen, C., Ivaska, J., Taya, Y., et al. (2007). CIP2A inhibits PP2A in human malignancies. Cell *130*, 51–62.

Kawasaki, H., Schiltz, L., Chiu, R., Itakura, K., Taira, K., Nakatani, Y., and Yokoyama, K.K. (2000). ATF-2 has intrinsic histone acetyltransferase activity which is modulated by phosphorylation. Nature *405*, 195–200.

Kawase, T., Ohki, R., Shibata, T., Tsutsumi, S., Kamimura, N., Inazawa, J., Ohta, T., Ichikawa, H., Aburatani, H., Tashiro, F., and Taya, Y. (2009). PH domain-only protein PHLDA3 is a p53-regulated repressor of Akt. Cell *136*, 535–550.

Knösel, T., Heretsch, S., Altendorf-Hofmann, A., Richter, P., Katenkamp, K., Katenkamp, D., Berndt, A., and Petersen, I. (2010). TLE1 is a robust diagnostic biomarker for synovial sarcomas and correlates with t(X;18): analysis of 319 cases. Eur. J. Cancer *46*, 1170–1176.

Kosemehmetoglu, K., Vrana, J.A., and Folpe, A.L. (2009). TLE1 expression is not specific for synovial sarcoma: a whole section study of 163 soft tissue and bone neoplasms. Mod. Pathol. *22*, 872–878.

Ladanyi, M. (2001). Fusions of the SYT and SSX genes in synovial sarcoma. Oncogene *20*, 5755–5762.

Lim, F.L., Soulez, M., Koczan, D., Thiesen, H.J., and Knight, J.C. (1998). A KRAB-related domain and a novel transcription repression domain in proteins encoded by SSX genes that are disrupted in human sarcomas. Oncogene *17*, 2013–2018.

Liu, H., Deng, X., Shyu, Y.J., Li, J.J., Taparowsky, E.J., and Hu, C.D. (2006). Mutual regulation of c-Jun and ATF2 by transcriptional activation and subcellular localization. EMBO J. *25*, 1058–1069.

Liu, S., Cheng, H., Kwan, W., Lubieniecka, J.M., and Nielsen, T.O. (2008). Histone deacetylase inhibitors induce growth arrest, apoptosis, and differentiation in clear cell sarcoma models. Mol. Cancer Ther. *7*, 1751–1761.

Lopez-Bergami, P., Lau, E., and Ronai, Z. (2010). Emerging roles of ATF2 and the dynamic AP1 network in cancer. Nat. Rev. Cancer *10*, 65–76.

Lubieniecka, J.M., de Bruijn, D.R., Su, L., van Dijk, A.H., Subramanian, S., van de Rijn, M., Poulin, N., van Kessel, A.G., and Nielsen, T.O. (2008). Histone deacetylase inhibitors reverse SS18-SSX-mediated polycomb silencing of the tumor suppressor early growth response 1 in synovial sarcoma. Cancer Res. *68*, 4303–4310.

Maekawa, T., Shinagawa, T., Sano, Y., Sakuma, T., Nomura, S., Nagasaki, K., Miki, Y., Saito-Ohara, F., Inazawa, J., Kohno, T., et al. (2007). Reduced levels of ATF-2 predispose mice to mammary tumors. Mol. Cell. Biol. *27*, 1730–1744.

Maekawa, T., Sano, Y., Shinagawa, T., Rahman, Z., Sakuma, T., Nomura, S., Licht, J.D., and Ishii, S. (2008). ATF-2 controls transcription of Maspin and GADD45 alpha genes independently from p53 to suppress mammary tumors. Oncogene *27*, 1045–1054.

Müller, J., Hart, C.M., Francis, N.J., Vargas, M.L., Sengupta, A., Wild, B., Miller, E.L., O'Connor, M.B., Kingston, R.E., and Simon, J.A. (2002). Histone methyltransferase activity of a *Drosophila* Polycomb group repressor complex. Cell *111*, 197–208.

Nagai, M., Tanaka, S., Tsuda, M., Endo, S., Kato, H., Sonobe, H., Minami, A., Hiraga, H., Nishihara, H., Sawa, H., and Nagashima, K. (2001). Analysis of transforming activity of human synovial sarcoma-associated chimeric protein SYT-SSX1 bound to chromatin remodeling factor hBRM/hSNF2 alpha. Proc. Natl. Acad. Sci. USA *98*, 3843–3848.

Nakayama, R., Mitani, S., Nakagawa, T., Hasegawa, T., Kawai, A., Morioka, H., Yabe, H., Toyama, Y., Ogose, A., Toguchida, J., et al. (2010). Gene expression profiling of synovial sarcoma: distinct signature of poorly differentiated type. Am. J. Surg. Pathol. *34*, 1599–1607.

Nielsen, T.O., West, R.B., Linn, S.C., Alter, O., Knowling, M.A., O'Connell, J.X., Zhu, S., Fero, M., Sherlock, G., Pollack, J.R., et al. (2002). Molecular characterisation of soft tissue tumours: a gene expression study. Lancet *359*, 1301–1307.

Pacheco, M., Horsman, D.E., Hayes, M.M., Clarkson, P.W., Huwait, H., and Nielsen, T.O. (2010). Small blue round cell tumor of the interosseous membrane bearing a t(2;22)(q34;q12)/EWS-CREB1 translocation: a case report. Mol. Cytogenet. *3*, 12.

Shevchenko, A., Jensen, O.N., Podtelejnikov, A.V., Sagliocco, F., Wilm, M., Vorm, O., Mortensen, P., Shevchenko, A., Boucherie, H., and Mann, M. (1996). Linking genome and proteome by mass spectrometry: large-scale identification of yeast proteins from two dimensional gels. Proc. Natl. Acad. Sci. USA *93*, 14440–14445.

Soulez, M., Saurin, A.J., Freemont, P.S., and Knight, J.C. (1999). SSX and the synovial-sarcoma-specific chimaeric protein SYT-SSX co-localize with the human Polycomb group complex. Oncogene *18*, 2739–2746.

Su, L., Cheng, H., Sampaio, A.V., Nielsen, T.O., and Underhill, T.M. (2010). EGR1 reactivation by histone deacetylase inhibitors promotes synovial sarcoma cell death through the PTEN tumor suppressor. Oncogene *29*, 4352–4361.

Terry, J., Saito, T., Subramanian, S., Ruttan, C., Antonescu, C.R., Goldblum, J.R., Downs-Kelly, E., Corless, C.L., Rubin, B.P., van de Rijn, M., et al. (2007). TLE1 as a diagnostic immunohistochemical marker for synovial sarcoma emerging from gene expression profiling studies. Am. J. Surg. Pathol. *31*, 240–246.

Thaete, C., Brett, D., Monaghan, P., Whitehouse, S., Rennie, G., Rayner, E., Cooper, C.S., and Goodwin, G. (1999). Functional domains of the SYT and SYT-SSX synovial sarcoma translocation proteins and co-localization with the SNF protein BRM in the nucleus. Hum. Mol. Genet. *8*, 585–591.

Wong, J.P., Reboul, E., Molday, R.S., and Kast, J. (2009). A carboxy-terminal affinity tag for the purification and mass spectrometric characterization of integral membrane proteins. J. Proteome Res. *8*, 2388–2396.

Woo, I.S., Kohno, T., Inoue, K., Ishii, S., and Yokota, J. (2002). Infrequent mutations of the activating transcription factor-2 gene in human lung cancer, neuroblastoma and breast cancer. Int. J. Oncol. *20*, 527–531.

Cancer Cell
Article

NKX2-1/TITF1/TTF-1-Induced ROR1 Is Required to Sustain EGFR Survival Signaling in Lung Adenocarcinoma

Tomoya Yamaguchi,[1] Kiyoshi Yanagisawa,[1,2] Ryoji Sugiyama,[1] Yasuyuki Hosono,[1] Yukako Shimada,[1] Chinatsu Arima,[1] Seiichi Kato,[3] Shuta Tomida,[1] Motoshi Suzuki,[1] Hirotaka Osada,[4] and Takashi Takahashi[1,*]
[1]Division of Molecular Carcinogenesis, Center for Neurological Diseases and Cancer, Nagoya University Graduate School of Medicine, Showa-ku, Nagoya 466-8550, Japan
[2]Institute for Advanced Research, Nagoya University, Chikusa-ku, Nagoya 464-8601, Japan
[3]Department of Pathology and Laboratory Medicine, Nagoya University Hospital, Showa-ku, Nagoya 466-8550, Japan
[4]Division of Molecular Oncology, Aichi Cancer Center Research Institute, Chikusa-ku, Nagoya 464-8681, Japan
*Correspondence: tak@med.nagoya-u.ac.jp
DOI 10.1016/j.ccr.2012.02.008

SUMMARY

We and others previously identified *NKX2-1*, also known as *TITF1* and *TTF-1*, as a lineage-survival oncogene in lung adenocarcinomas. Here we show that NKX2-1 induces the expression of the receptor tyrosine kinase-like orphan receptor 1 (*ROR1*), which in turn sustains a favorable balance between prosurvival PI3K-AKT and pro-apoptotic p38 signaling, in part through ROR1 kinase-dependent c-Src activation, as well as kinase activity-independent sustainment of the EGFR-ERBB3 association, ERBB3 phosphorylation, and consequential PI3K activation. Notably, ROR1 knockdown effectively inhibited lung adenocarcinoma cell lines, irrespective of their EGFR status, including those with resistance to the EGFR tyrosine kinase inhibitor gefitinib. Our findings thus identify ROR1 as an "Achilles' heel" in lung adenocarcinoma, warranting future development of therapeutic strategies for this devastating cancer.

INTRODUCTION

It is well understood that oncogene addiction is present in certain cancers, with lung adenocarcinomas carrying epidermal growth factor receptor (EGFR) mutations among the best examples (Weinstein, 2002). Emerging evidence, though currently sparse, suggests that "lineage-specific transcription factors" with developmental roles in normal progenitor cells of particular lineages may also confer dependency for survival to certain types of cancer cells (Garraway and Sellers, 2006). The basic helix-loop-helix (bHLH) transcription factor MITF in melanoma has been proposed as an archetypal prototype. Along this line, our previous studies demonstrated that achaete-scute homolog 1 (ASH1)/achaete-scute complex-like 1, a bHLH protein indispensable for pulmonary neuroendocrine cell development, is also required for survival of lung cancers with neuroendocrine features, such as small cell lung cancers (Nishikawa et al., 2011; Osada et al., 2005, 2008).

Lung cancer is the leading cause of cancer death, whereas adenocarcinomas arising from peripheral lung are the most frequent histological type and exhibit the highest degree of heterogeneity. NKX2-1, a homeodomain transcription factor also known as TITF1 and TTF-1, plays an essential role in peripheral lung development, and NKX2-1 deficiency in mice results in lung aplasia (Kimura et al., 1996). We previously reported that NKX2-1 is a reliable lineage marker for terminal respiratory unit (TRU) cells, as well as for "TRU-type" adenocarcinomas with distinct gene expression profiles, which show abundant

Significance

NKX2-1-induced ROR1 is required to sustain a favorable balance between prosurvival PI3K-AKT signaling and the pro-apoptotic p38 pathway; the collapse of which elicits "oncogenic shock." ROR1 was also identified as a receptor tyrosine kinase with a "sustainer role" for the EGFR-ERBB3-mediated signaling. Mechanisms, such as a secondary EGFR mutation, MET amplification, and HGF overexpression, may arise in lung adenocarcinomas of patients undergoing EGFR-TKI treatment and lead to tumor resistance of the treatment. Such diverse mechanisms make it difficult to predict which should be targeted to prevent expansion of resistant clones. From a clinical point of view, it is thus of particular interest that ROR1 inhibition appears to be effective in treatment of gefitinib-resistant lung adenocarcinomas with various resistance mechanisms.

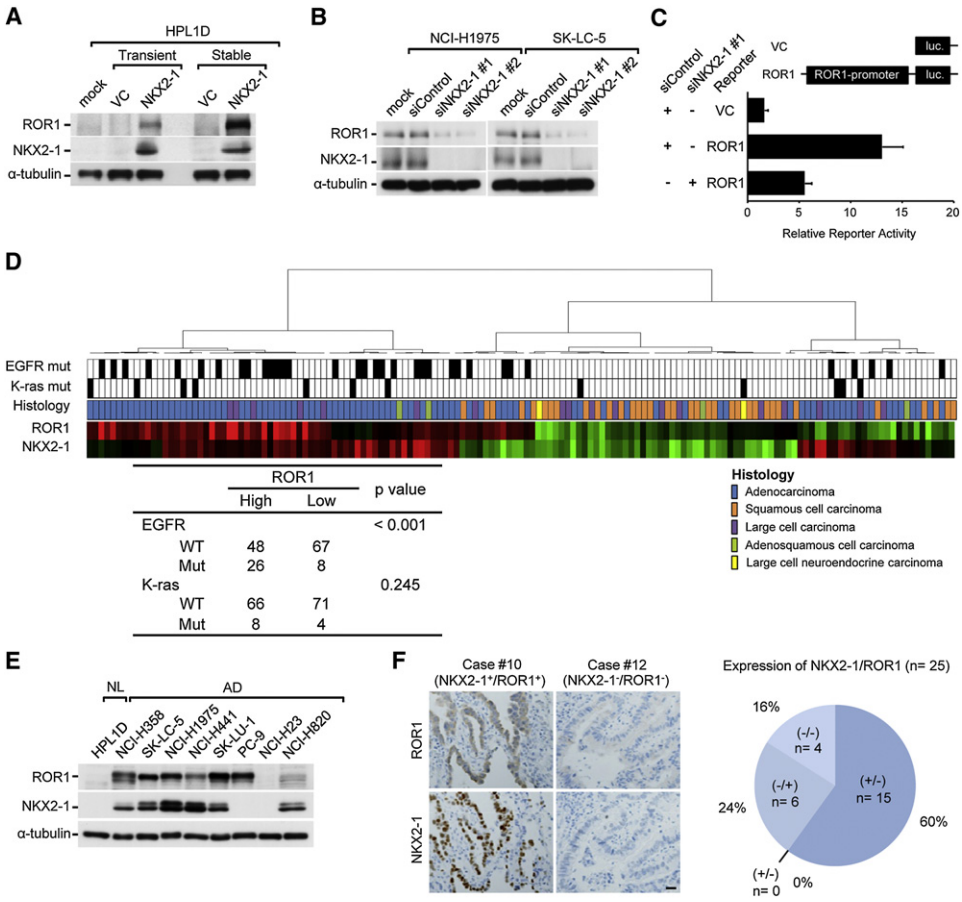

Figure 1. *ROR1* Is Transactivated by NKX2-1

(A) WB analysis of NKX2-1-transfected HPL1D.

(B) WB analysis of siNKX2-1-introduced NKX2-1$^+$/ROR1$^+$ lung adenocarcinoma cell lines. siControl, negative control siRNA; siNKX2-1 #1 and #2, siRNAs against NKX2-1.

(C) Luciferase reporter assay of ROR1 promoter showing reduced activity in response to NKX2-1 silencing in a stable NKX2-1 transfectant of HPL1D. Data are shown as the mean ± SD (n = 3).

(D) Hierarchical clustering analysis of non-small-cell lung cancers using a microarray dataset along with information regarding the relationship of *ROR1* expression with *EGFR* and *K-ras* mutations.

(E) Western blot analysis of ROR1 and NKX2-1 in lung adenocarcinoma and normal lung epithelial cell lines. NL, normal lung; AD, lung adenocarcinoma.

(F) Representative ROR1 staining in lung adenocarcinoma specimens and a summary of immunohistochemical analysis (n = 25). Scale bar, 100 μm. See also Figure S1 and Table S1.

NKX2-1 expression, as well as characteristic clinicopathologic and genetic features, including a significant association with *EGFR* mutations (Takeuchi et al., 2006; Yatabe et al., 2002, 2005). We further identified NKX2-1 as a lineage-survival oncogene in lung adenocarcinoma (Tanaka et al., 2007); other investigators reached similar conclusions through genome-wide searches for focal genomic aberrations (Kendall et al., 2007; Kwei et al., 2008; Weir et al., 2007).

Previous findings, including ours, thus clearly indicate the requirement of sustained NKX2-1 expression for lung adenocarcinoma survival, though how NKX2-1 mediates survival signals remains elusive. It should be noted that NKX2-1 itself is well known to play indispensable roles in the maintenance of normal lung physiology, such as transcriptional activation of surfactant protein genes (Boggaram, 2009). In the present study, we therefore aimed to elucidate downstream signaling by NKX2-1, since such understanding appears to be a crucial step in the development of a therapeutic strategy for targeting NKX2-1-mediated survival signaling.

RESULTS

Identification of ROR1 as a Direct Transcriptional Target for NKX2-1

To better understand how NKX2-1 mediates survival signals in lung adenocarcinomas, we performed microarray analysis using HPL1D, an immortalized human peripheral lung epithelial cell line (Masuda et al., 1997), which was stably introduced with NKX2-1. Consequently, *ROR1* was identified among the most highly upregulated genes (Figure S1A available online). NKX2-1-mediated ROR1 induction was validated by western blot analysis using NKX2-1 transfectants (Figure 1A), as well as

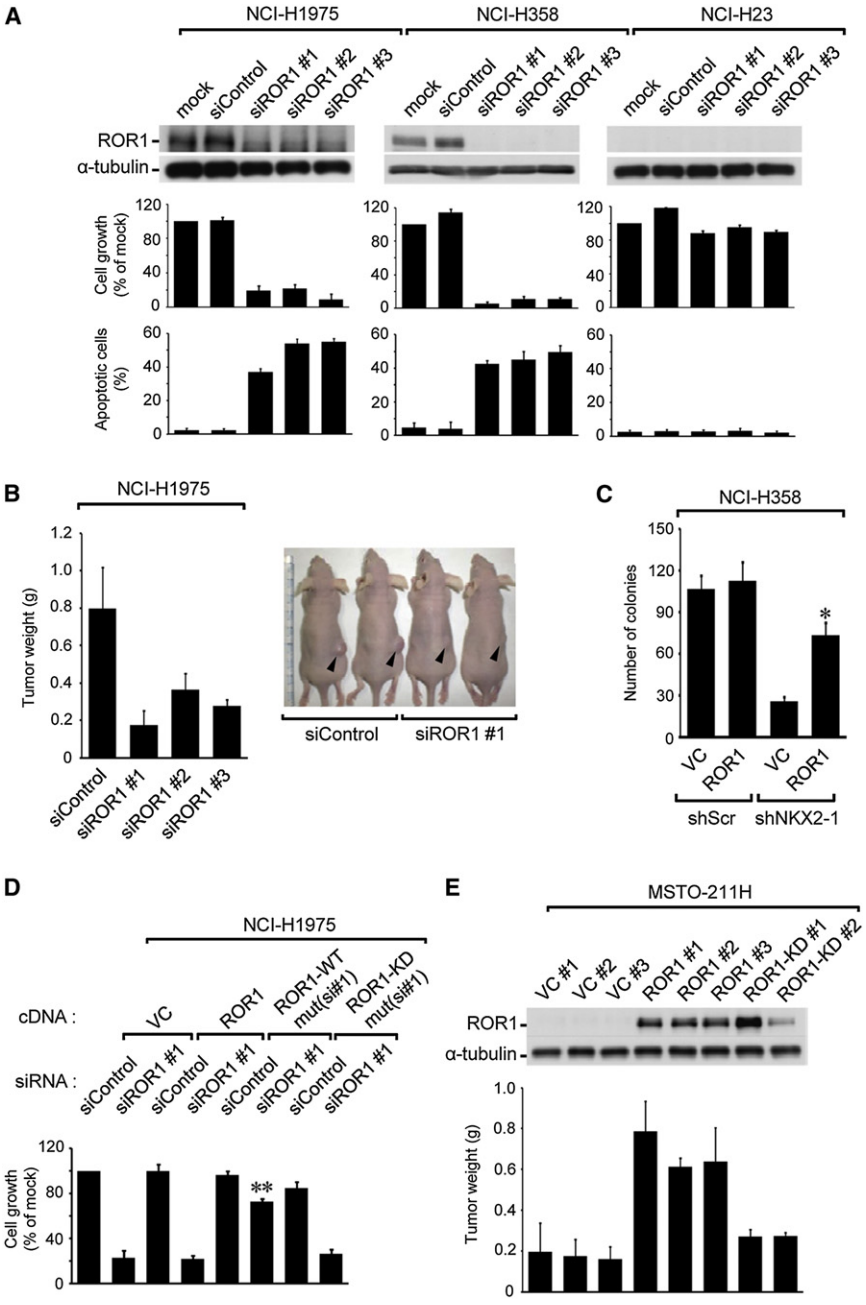

Figure 2. ROR1 Sustains Lung Adenocarcinoma Survival

(A) Assays for measuring the effects of ROR1 knockdown in growth inhibition and apoptosis induction in lung adenocarcinoma cell lines. siControl, negative control siRNA; siROR1 #1 to #3, siRNA against ROR1. Data are shown as the mean ± SD (n = 3).

(B) In vivo treatment of xenografts with ROR1 siRNA. Two weeks after intratumoral siRNA injection, photographs were obtained and tumor weights measured. Data are shown as the mean ± SD (n = 7).

(C) Alleviation of siNKX2-1-mediated growth inhibition by ROR1 introduction. Colonies were counted two weeks after cotransfection of the expression vectors of ROR1 and short hairpin RNA against NKX2-1 in NKX2-1^{+}/ROR1^{+} NCI-H358. Data are shown as the mean ± SD (n = 3). *$p < 0.05$ versus VC+shNKX2-1, as determined by Student's t test.

(D) Colorimetric assays of cells treated with siROR1, along with wild-type ROR1 [ROR1-mut(si#1)] or kinase-dead ROR1 [ROR1-KD mut(si#1)], each with silent mutations at the siRNA binding site. Data are shown as the mean ± SD (n = 3). **$p < 0.001$ versus siROR1#1+ROR1, as determined by Student's t test.

(E) In vivo tumor growth assay in stable wild-type or kinase-dead ROR1 transfectants of MSTO-211H. Three weeks after subcutaneous inoculation, tumor weights were measured. Data are shown as the mean ± SD (n = 5). See also Figure S2.

lung adenocarcinoma cell lines treated with siRNA against NKX2-1 (siNKX2-1; Figure 1B). A luciferase reporter assay with the 1.0 kb human ROR1 promoter region showed its NKX2-1-dependent activation (Figure 1C), and a chromatin immunoprecipitation (ChIP) assay revealed direct binding of NKX2-1 to the ROR1 promoter (Figure S1B), demonstrating that *ROR1* is a direct transcriptional target for NKX2-1. Co-expression of *NKX2-1* and *ROR1* was preferentially observed in adenocarcinomas in analysis of our previous microarray dataset of 149 non-small lung cancer patients (Figure 1D; Takeuchi et al., 2006; GEO accession number: GSE11969), whereas the presence of *EGFR* mutations was found to be associated with a high expression of *ROR1*. A similar association between NKX2-1 and ROR1 expression was also confirmed at the protein level in panels of lung adenocarcinoma cell lines and tumor specimens (Figures 1E and 1F and Table S1). However, we also noted some instances of NKX2-1^{-}/ROR1^{+}, suggesting that the expression of ROR1 may be also regulated by other transcription factors.

Involvement of ROR1 in NKX2-1-Mediated Survival Signaling in Lung Adenocarcinomas

Next, we examined whether ROR1 knockdown affects survival in lung adenocarcinoma cells. siROR1 treatment was shown to induce significant growth inhibition of ROR1-positive lung adenocarcinoma cell lines in association with apoptosis induction, whereas ROR1-negative lung adenocarcinoma cell lines, as well as primary normal lung epithelial cells, did not show any growth inhibition (Figures 2A and S2A–S2C). In addition, intratumoral injection of ROR1 siRNAs with atelocollagen significantly reduced in vivo growth of NCI-H1975 xenografts (Figure 2B). We also investigated whether exogenously introduced ROR1 could mitigate NKX2-1-knockdown-induced growth inhibition. Forced ROR1 expression resulted in significant, though not complete, alleviation of growth inhibition imposed by the expression of short hairpin RNA against NKX2-1 in NKX2-1^{+}/ROR1^{+} NCI-H358 cells,

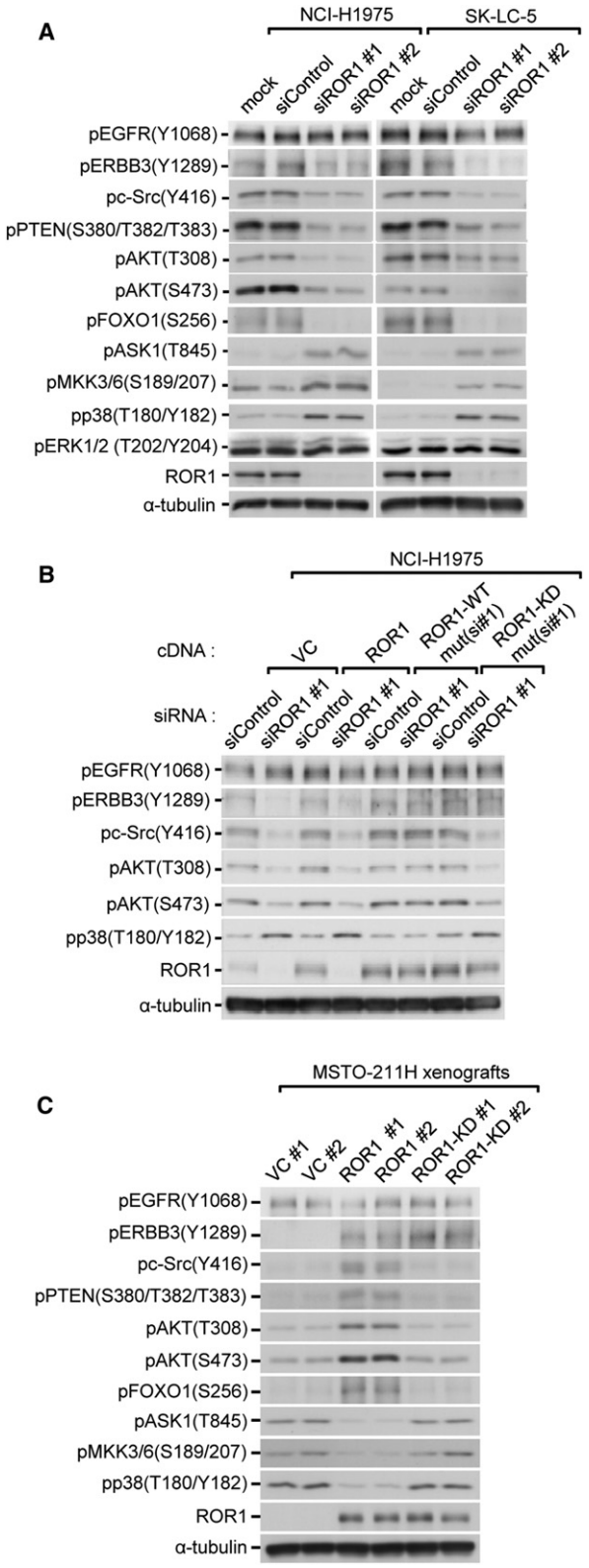

Figure 3. ROR1 Affects Both PI3K-AKT Prosurvival and Pro-Apoptotic p38 Signaling

(A) WB analysis of the prosurvival and pro-apoptotic signaling molecules in siROR1-treated adenocarcinoma cells.

(B) WB analysis of lung adenocarcinoma cells concurrently treated with siROR1 and RNAi-resistant wild-type ROR1 [ROR1-mut(si#1)] or kinase-dead ROR1 [ROR1-KD mut(si#1)].

(C) WB analysis of signaling molecules in ROR1 stable transfectants. ROR1-KD, kinase-dead ROR1. See also Figure S3.

supporting the notion that NKX2-1-induced survival signaling is conferred, at least in part, through induction of ROR1 (Figure 2C). Interestingly, we found that the wild-type but not kinase-dead ROR1 with silent mutations at the siRNA binding site was able to counteract siROR1-induced growth inhibition (Figure 2D). Concordantly, forced expression of wild-type ROR1 but not kinase-dead ROR1 in ROR1-negative MSTO-211H cells at a level comparable to that in NCI-H1975 cells enhanced in vivo growth of the xenografts (Figures 2E, S2D, and S2E), suggesting that ROR1 kinase activity is required to fully confer a growth advantage.

Identification of ROR1-EGFR Interaction Sustaining EGFR-ERBB3-PI3K Signaling

We also examined how ROR1 mediates survival signals in lung adenocarcinomas. ROR1 knockdown decreased phosphorylations of ERBB3, c-Src, and AKT in NKX2-1^{+}/ROR1^{+} NCI-H1975, SK-LC-5, and NCI-H358 cells (Figures 3A, S3A, and S3B). siROR1 treatment also reduced phosphorylation of FOXO1, downstream of AKT, whereas p38 phosphorylation was induced in siROR1-treated cells, in association with increased phosphorylations of its upstream kinases ASK1 and MKK3/6. In contrast, phosphorylations of EGFR and ERK1/2 were not affected by ROR1 knockdown. Introduction of exogenous wild-type ROR1 with silent mutations at the siRNA binding site cancelled effects on downstream signaling, demonstrating the specificity of siRNA-mediated ROR1 knockdown (Figure 3B). We noted that forced expression of kinase-dead ROR1 with the silent mutations restored ERBB3 phosphorylation, whereas it failed to mitigate siROR1-induced effects on c-Src, p38, and AKT phosphorylations (Figure 3B). Conversely, opposite effects on the phosphorylations of potential downstream molecules were observed in wild-type, but not kinase-dead, ROR1-introduced MSTO-211H xenografts, whereas increased ERBB3 phosphorylation was detected in both wild-type and kinase-dead ROR1-introduced xenografts (Figure 3C).

EGFR by itself is an efficient initiator of ERK through homodimer formation, though it is a poor activator of PI3K signaling (Sharma and Settleman, 2009). In addition, EGF-induced EGFR activation is linked to PI3K through phosphorylation of intrinsically kinase-deficient ERBB3 but not EGFR in lung adenocarcinoma cells (Engelman et al., 2005; Rothenberg et al., 2008). We found that ROR1 knockdown selectively diminished EGF treatment-induced ERBB3 phosphorylation without appreciably affecting the phosphorylation of EGFR itself in NCI-H1975 and SK-LC-5 cells (Figure 4A), which appeared to be consistent with the lack of effects seen with ROR1 knockdown on ERK phosphorylation. ROR1 knockdown also abrogated EGF-induced phosphorylation of AKT and FOXO1, whereas decreased c-Src phosphorylation and induction of p38 phosphorylation were elicited by siROR1 treatment regardless of the presence or absence of EGF. Marked nuclear retention, hence activation of apoptosis-inducing FOXO1, a target of the

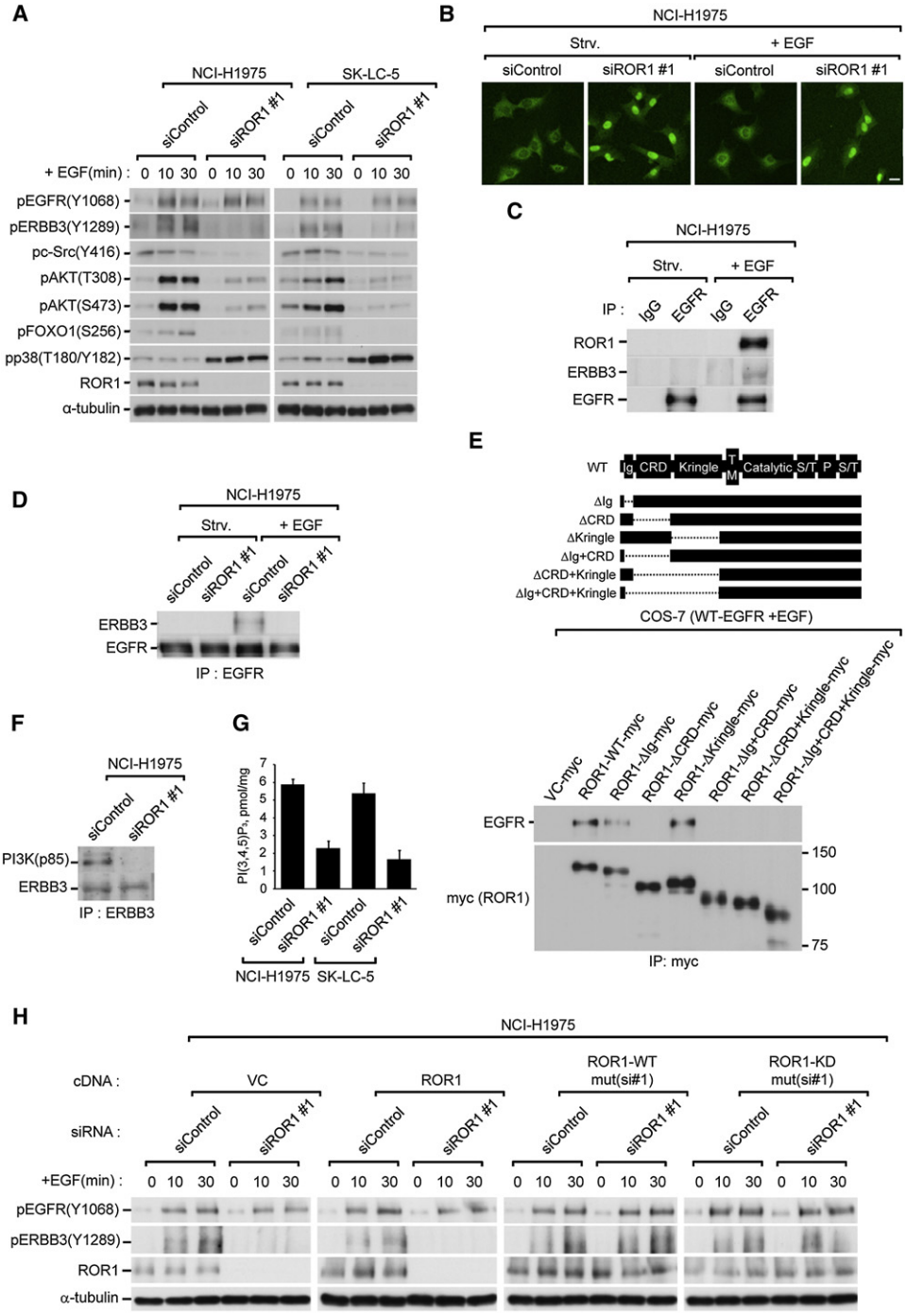

Figure 4. ROR1 Sustains EGF-Induced Signaling through ERBB3

(A) WB analysis of downstream molecules in EGF-treated and ROR1-silenced NCI-H1975 and SK-LC-5.

(B) Immunofluorescence staining of FOXO1 in ROR1-silenced NCI-H1975 in the presence or absence of EGF. Scale bar, 30 μm. Strv, serum starved.

(C) IP-WB analysis of EGF-stimulated association of EGFR with ROR1 or ERBB3 in NCI-H1975. Strv, serum starved.

(D) IP-WB analysis of EGFR-ERBB3 association in response to EGF, with and without siROR1 treatment, in NCI-H1975. Strv, serum starved.

(E) IP-WB analysis of ROR1-EGFR association in COS-7 cotransfected with EGFR and various ROR1 deletion mutants.

(F) IP-WB analysis of the interaction between ERBB3 and p85 (PI3K), with and without siROR1 treatment, in NCI-H1975.

(G) In vitro PI3K assay with immunoprecipitated PI3K from siROR1-treated NCI-H1975 or SK-LC-5 cell lysates. Data are shown as the mean ± SD (n = 3).

(H) WB analysis of EGF-induced EGFR and ERBB3 phosphorylation in the presence or absence of siROR1 treatment in siRNA-resistant wild-type [ROR1-mut(si#1)] or kinase-dead [ROR1-mut(si#1)] ROR1-introduced NCI-H1975 cells. See also Figure S4.

PI3K-AKT axis (Calnan and Brunet, 2008), was also observed in response to siROR1 treatment (Figure 4B). Interestingly, EGF treatment induced an association of ROR1 with EGFR in NCI-H1975 cells, as well as in COS-7 cells cotransfected with both ROR1 and EGFR (Figures 4C and S4A, respectively). Immunoprecipitation (IP)-western blot (WB) analysis also revealed that ROR1 knockdown significantly reduced co-immunoprecipitation of EGFR with ERBB3 in EGF-stimulated NCI-H1975 cells (Figure 4D). It was further shown that a cysteine-rich domain of the extracellular domain of ROR1 is required for association with EGFR (Figures 4E and S4B). In line with enhancement of EGF-induced ERBB3 phosphorylation by ROR1, its knockdown led to significantly reduced binding of the p85 subunit of PI3K to ERBB3 (Figure 4F). In addition, an in vitro PI3K assay using PI3K immunoprecipitated from siROR1-treated NCI-H1975 and SK-LC-5 cell lysates showed reduced conversion of PIP_3 (Figure 4G), demonstrating that ROR1 knockdown negatively affects PI3K activity. Interestingly, both wild-type and kinase-dead ROR1 with silent mutations at the siRNA binding site were able to restore EGF-induced ERBB3 phosphorylation in NCI-H1975 cells, indicating that ROR1 kinase activity is not indispensable in this regard (Figure 4H). Taken together, these findings indicated that ROR1 kinase activity is not indispensable for sustaining ROR1-EGFR interaction, EGFR-ERBB3 interaction, and ERBB3 phosphorylation, whereas ROR1 kinase activity is required to fully sustain downstream signaling and survival, suggesting the involvement of additional downstream signaling.

Identification of c-Src as a Downstream Molecule in ROR1-Mediated Survival Signaling

We accordingly sought an additional, underlying mechanism by which ROR1 fully sustains survival signaling in lung adenocarcinomas. Contrasting changes in c-Src Y416 phosphorylation in response to altered ROR1 expression caught our attention, since it suggested a possible, functional relationship. We found that introduction of constitutively active c-Src noticeably alleviated ROR1-silencing-induced effects, including growth inhibition, and reduced phosphorylations of PTEN and AKT, both of which are known to be downstream of c-Src (Figure 5A; Hennessy et al., 2005; Martin, 2001). ROR1 knockdown-induced p38 phosphorylation was also clearly counteracted by the introduction of constitutively active c-Src. Of note, c-Src inactivation by either siRNAs or a c-Src inhibitor (SKI-1) had effects very similar to ROR1 knockdown in terms of both growth inhibition and signaling in ROR1-positive NCI-H1975 and SK-LC-5 cells (Figures 5B), whereas ROR1-negative NCI-H23 cells had virtually no response to c-Src inhibition (Figure S5A). IP-WB analysis revealed the interactions of exogenously introduced ROR1 with exogenous c-Src in COS-7 cells (Figure 5C) and endogenous c-Src in 293T cells (Figure S5B), whereas IP-WB analysis also revealed the interaction between endogenous ROR1 and c-Src proteins in NCI-H1975 cells (Figure 5D). In addition, an in vitro pull-down assay using GST-tagged ROR1 showed an interaction with endogenous c-Src in NCI-H1975 cell lysates (Figure S5C), as well as with a purified c-Src protein (Figure S5D). An in vitro ROR1 kinase assay using endogenous c-Src as a substrate in ROR1-negative NCI-H23 and 293T cells (Figures S5E and S5F), as well as exogenous kinase-dead c-Src the same as that in NIH/3T3 cells (Figure 5E), revealed robust c-Src phosphorylation. Furthermore, an association of ROR1 with the SH3 domain of c-Src was demonstrated by IP-WB analysis (Figure 5F), as well as by a GST pull-down assay (Figure S5G). In accordance with a previous report—in which it was reported that protein-protein interactions of c-Src are mediated by binding of its SH3 domain with proline-rich stretches of the binding partners (Yeatman, 2004)—the interaction between c-Src and ROR1 required the presence of the proline-rich domain but not kinase activity of ROR1 (Figure 5G). Whereas PTEN has been shown to be tyrosine-phosphorylated and negatively regulated by c-Src (Lu et al., 2003; Nagata et al., 2004), we observed a decrease tyrosine phosphorylation and S380/T382/T383 phosphorylation of PTEN in NCI-H1975 and SK-LC-5 cells with ROR1 knockdown (Figure S5H). ROR1 knockdown-induced growth inhibition was alleviated to a considerable extent by silencing of PTEN or p38 in NCI-H1975 cells (Figure 5H). Increase in c-Src phosphorylation in siPTEN-treated NCI-H1975 cells may reflect incomplete repression of PTEN activity, considering that PTEN dephosphorylates c-Src (Zhang et al., 2011). Although Wnt5a was recently suggested to mediate NF-κB signaling as an ROR1 ligand (Fukuda et al., 2008), our preliminary data suggest that this may not be the case in lung adenocarcinomas (Figures S5I and S5J).

Dispensable c-Src Binding of ROR1 for ROR1-EGFR Association and Sustainment of EGFR-ERBB3 Interaction

We next examined whether c-Src binding of ROR1 is required to sustain ROR1-EGFR and EGFR-ERBB3 interactions. IP-WB analysis of COS-7 cells transiently cotransfected with various forms of ROR1 and EGFR revealed that the interaction between ROR1 and EGFR does not require either ROR1 kinase activity or the c-Src-interacting proline-rich domain of ROR1 (Figure 6A). Similarly, whereas an EGF-induced interaction between EGFR and ERBB3 was markedly enhanced by the presence of ROR1, both kinase activity and a proline-rich domain of ROR1 were shown to be dispensable for these interactions (Figure 6B). In addition, c-Src knockdown did not cause any appreciable changes in the interaction between ROR1 and EGFR or between EGFR and ERBB3 (Figure 6C). Thus, the present findings suggest that ROR1 mediates survival signals, at least in part, by two distinct mechanisms: ROR1 kinase-dependent c-Src-mediated signaling and ROR1-kinase independent sustainment of EGFR-ERBB3-PI3K signaling. In this regard, it is interesting that rescue from siROR1-mediated effects by introduction of exogenous wild-type ROR1 with silent mutations at the siRNA binding site was significantly counteracted by concurrent treatment with sic-Src in both NCI-H1975 and NCI-H358, whereas such rescue was significantly counteracted by concurrent treatment with siERBB3 in only NCI-H1975 but not NCI-H358 cells (Figure 7A), suggesting possible cellular context-dependent differences in contributions of ROR1-sustained downstream signaling. This finding also appeared to be consistent with differential sensitivity to sic-Src and siERBB3 treatment between NCI-H1975 and NCI-H358 cells (Figure S6A). The relative insensitivity to siERBB3 of NCI-H358 cells with a K-ras mutation may be consistent with a previous report of the ineffectiveness of treatment with a PI3K inhibitor alone in lung adenocarcinomas occurring in *K-ras* transgenic mice (Engelman et al., 2008). It was

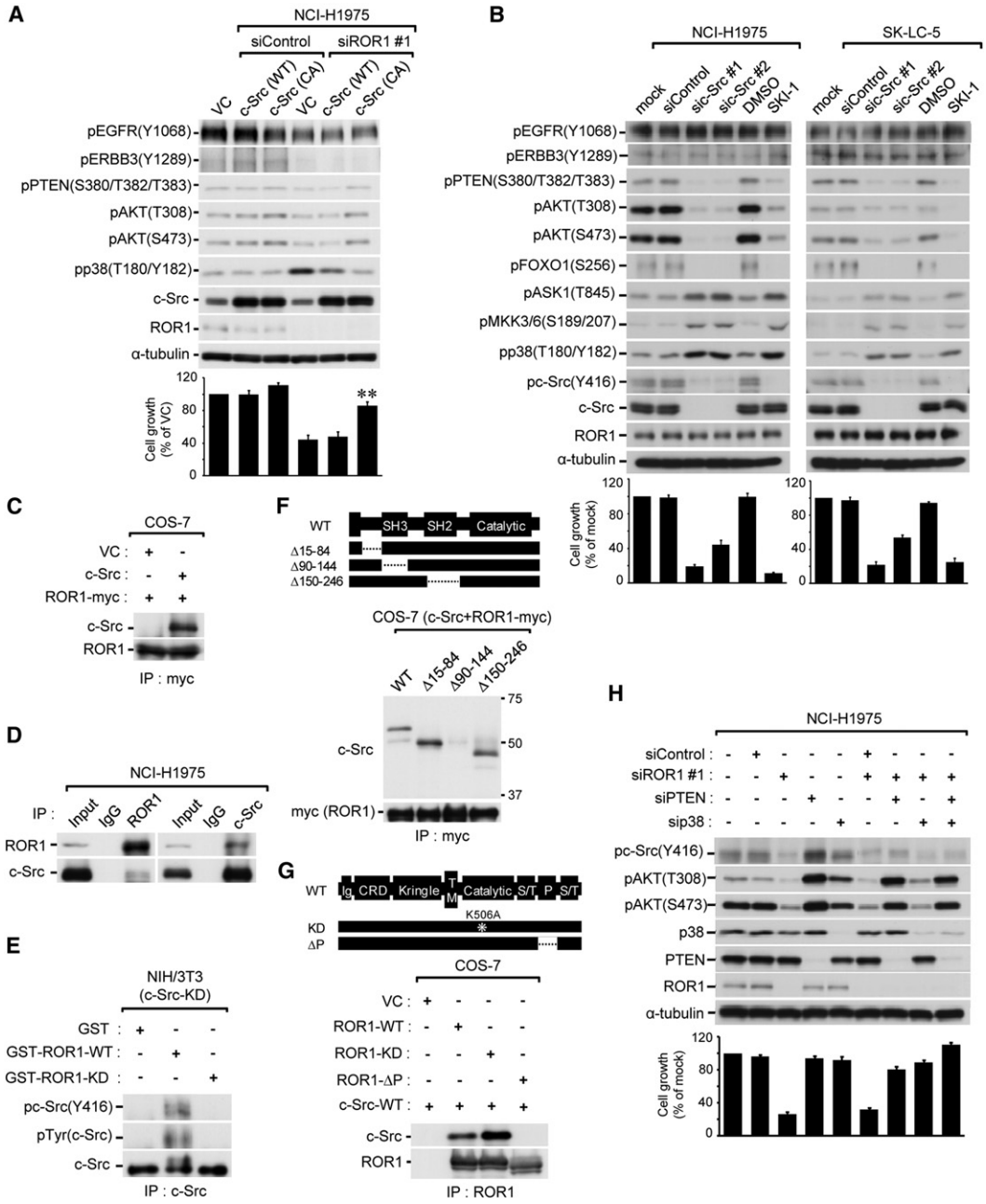

Figure 5. ROR1 Binds to and Phosphorylates c-Src

(A) WB (top panel) and colorimetric (bottom panel) analyses of NCI-H1975 cells introduced with siROR1 and c-Src. VC, empty vector control; WT, wild-type c-Src; CA, constitutive active c-Src. Data are shown as the mean ± SD (n = 3). **p < 0.001 versus VC+siROR1#1, as determined by Student's t test.

(B) Western blot (top panel) and colorimetric (bottom panel) analyses showing effects of c-Src inactivation by either siRNAs or a c-Src inhibitor (SKI-1). Data are shown as the mean ± SD (n = 3).

(C) IP-WB analysis of the interaction between exogenous ROR1 and c-Src in COS-7.

(D) IP-WB analysis of endogenous ROR1 and c-Src using cell lysates of NCI-H1975. IgG, negative control.

(E) In vitro ROR1 kinase assay using immunoprecipitated as a substrate in kinase-dead c-Src-transfected NIH/3T3.

(F) IP-WB analysis of the ROR1-c-Src interaction using COS-7 cotransfected with myc-tagged ROR1 and various deletion mutants of c-Src.

(G) IP-WB analyses of the ROR1-c-Src interaction using mutant ROR1 constructs. WT, wild-type; KD, kinase-dead; ΔP, ROR1 lacking proline-rich region.

(H) WB (top panel) and colorimetric (bottom panel) analyses of NCI-H1975 cosilenced for ROR1, PTEN, and/or p38. Data are shown as the mean ± SD (n = 3). See also Figure S5.

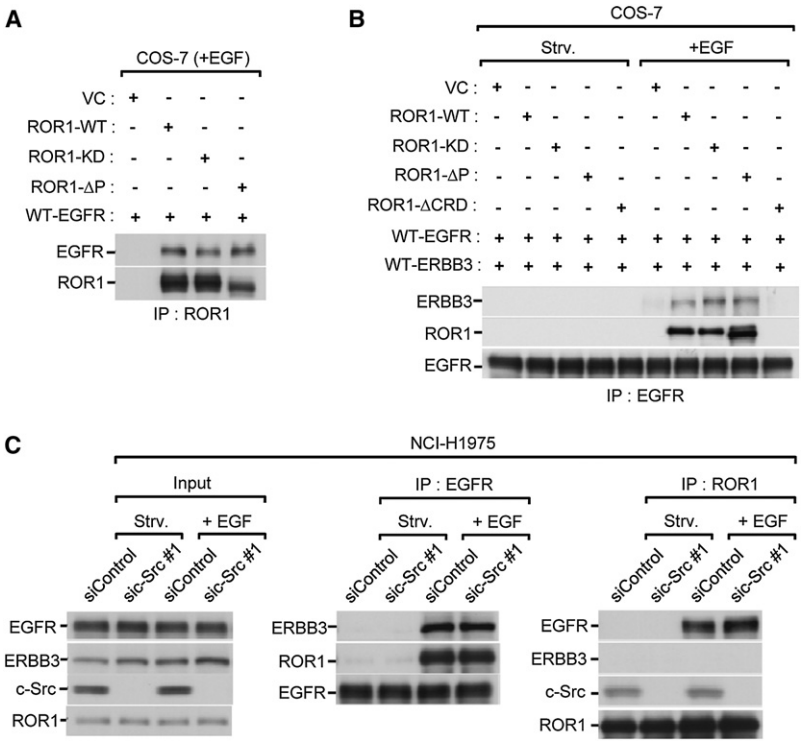

Figure 6. ROR1 Sustains EGFR-ERBB3 Interaction Independent of c-Src Binding

(A) IP-WB analysis of COS-7 cells co-introduced with EGFR and various forms of ROR1. WT, wild-type; KD, kinase-dead; ΔP, ROR1 lacking proline-rich region.

(B) IP-WB analysis of COS-7 cells co-introduced with various forms of ROR1, together with EGFR and ERBB3. Strv, serum starved.

(C) IP-WB analysis of the interactions among ROR1, EGFR, and ERBB3 in NCI-H1975 cells treated, with and without sic-Src. Strv, serum starved.

observed that sic-Src treatment in vivo similarly inhibited both growth and signaling in xenografts of two independent MSTO-211H clones overexpressing ROR1, supporting the notion that c-Src plays a crucial role as a downstream effector in this setting (Figures 7B and S6B).

ROR1 Inhibition as a Therapeutic Option Irrespective of EGFR Status

It is of particular interest that ROR1 knockdown inhibited the growth of NCI-H1975 cells, because this line carries double EGFR mutations L858R and T790M, the latter of which is a well-recognized mutation that confers resistance to EGFR TKI (Kobayashi et al., 2005; Pao et al., 2005). We similarly observed growth inhibition by ROR1 knockdown in another EGFR TKI-resistant lung adenocarcinoma cell line, NCI-H820, which carries delE746-T751 and T790M EGFR mutations, together with MET amplification (Figures 8A and S7A; Bean et al., 2007; Engelman et al., 2007; Turke et al., 2010). HGF overexpression has been postulated as an additional mechanism for resistance to EGFR TKI by switching dependency from EGFR to MET (Yano et al., 2008). However, treatment with siROR1 overcame HGF-mediated resistance to gefitinib in the PC-9 lung adenocarcinoma cell line with an activating EGFR mutation, which was accompanied with reduction in HGF-elicited MET-transduced increase in AKT phosphorylation, as well as decreased c-Src and increased p38 phosphorylations (Figure 8B). It was also noted that siROR1 treatment enhanced growth inhibition in PC-9 cells when applied along with gefitinib in the absence of HGF (Figure S7B). Whereas gefitinib diminished ERBB3 phosphorylation to a nearly negligible level in the NCI-H358 lung adenocarcinoma cell line, which is known to be relatively sensitive to gefitinib despite wild-type EGFR status (Engelman et al., 2005), concurrent siROR1 treatment with gefitinib further enhanced inhibition of cell growth in association with a clear reduction in remaining AKT phosphorylation (Figure 8C). Together, these findings suggest that ROR1 inhibition may be a therapeutic option for ROR1-positive lung adenocarcinomas irrespective of their EGFR status.

DISCUSSION

Accumulated evidence indicates that NKX2-1, a lineage-specific transcription factor with essential roles in peripheral lung development (Maeda et al., 2007), is expressed in a major fraction of lung adenocarcinomas (Yatabe et al., 2002). Although previous studies, including ours, demonstrated the requirement of sustained NKX2-1 expression for lung adenocarcinoma survival (Kendall et al., 2007; Kwei et al., 2008; Tanaka et al., 2007; Weir et al., 2007), the mechanism by which NKX2-1 mediates, survival signals remains elusive. The present study clearly showed that ROR1 is a direct transcriptional target of NKX2-1 and is crucially involved in sustainment of a favorable balance between prosurvival PI3K-AKT signaling and the pro-apoptotic p38 pathway (Figures 8D), collapse of which elicits "oncogenic shock" (Sharma et al., 2006). Our previous studies revealed a significant association of *NKX2-1* expression with *EGFR* mutations in lung adenocarcinomas (Takeuchi et al., 2006; Yatabe et al., 2005), suggesting their potential functional linkage. In this regard, the present findings suggest that NKX2-1 and EGFR may be functionally interrelated with each other through NKX2-1-mediated ROR1 induction in lung adenocarcinoma cells, which conceivably contributes to the development of lung adenocarcinomas with characteristic features. In addition, when considering the significant, yet incomplete, rescue from siNKX2-1-induced growth inhibition by ROR1 overexpression, an additional downstream target(s) may be involved in NKX2-1-mediated survival signaling.

The present results also demonstrate that ROR1 employs distinct kinase-dependent and -independent mechanisms to sustain a favorable balance between PI3K-AKT-mediated prosurvival signaling and the pro-apoptotic p38 pathway (Figure 8D). EGFR exists in a conformation that is unable to interact with ERBB3 and requires a ligand-engagement-elicited conformational change of the extracellular domain for dimerization-competence acquisition (Linggi and Carpenter, 2006). We found

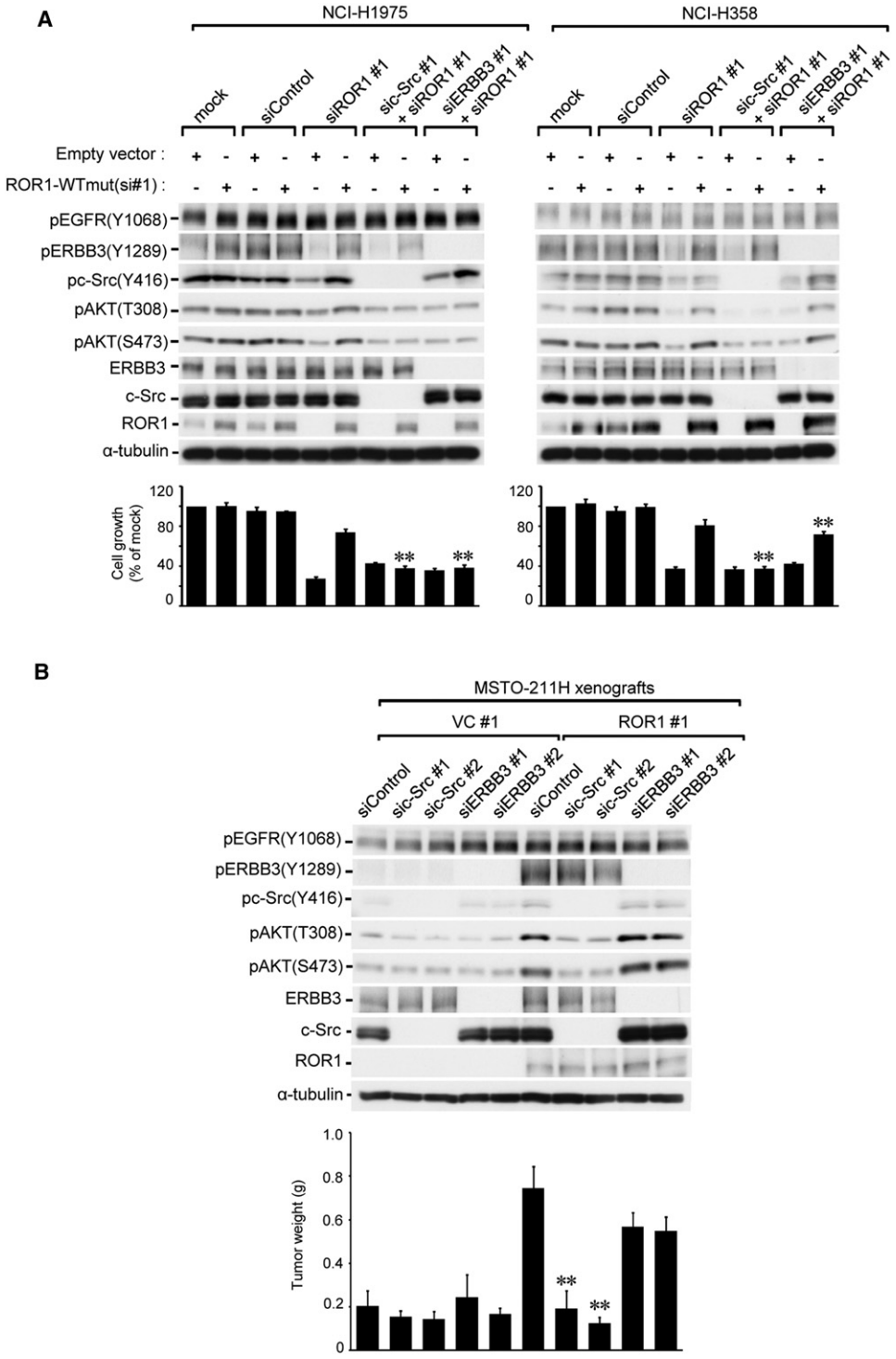

Figure 7. ROR1 Sustains Downstream Signaling via c-Src and ERBB3 in a Cellular Context-Dependent Manner

(A) Colorimetric assay (bottom panel) and WB analysis (top panel) of NCI-H1975 and NCI-H358 cells introduced with RNAi-resistant wild-type ROR1 [ROR1-mut(si#1)] and treated with siROR1, along with either sic-Src or siERBB3. Data are shown as the mean ± SD (n = 3). **$p < 0.001$ versus siROR1#1+ROR1-WTmut(si#1), as determined by Student's t test.

(B) In vivo tumor growth assay (bottom panel) and WB analysis (top panel) of xenografts of MSTO-211H, stably expressing exogenous ROR1, which were treated in vivo with sic-Src or siERBB3. Data are shown as the mean ± SD (n = 6). **$p < 0.001$ versus siControl +ROR1, as determined by Student's t test. See also Figure S6.

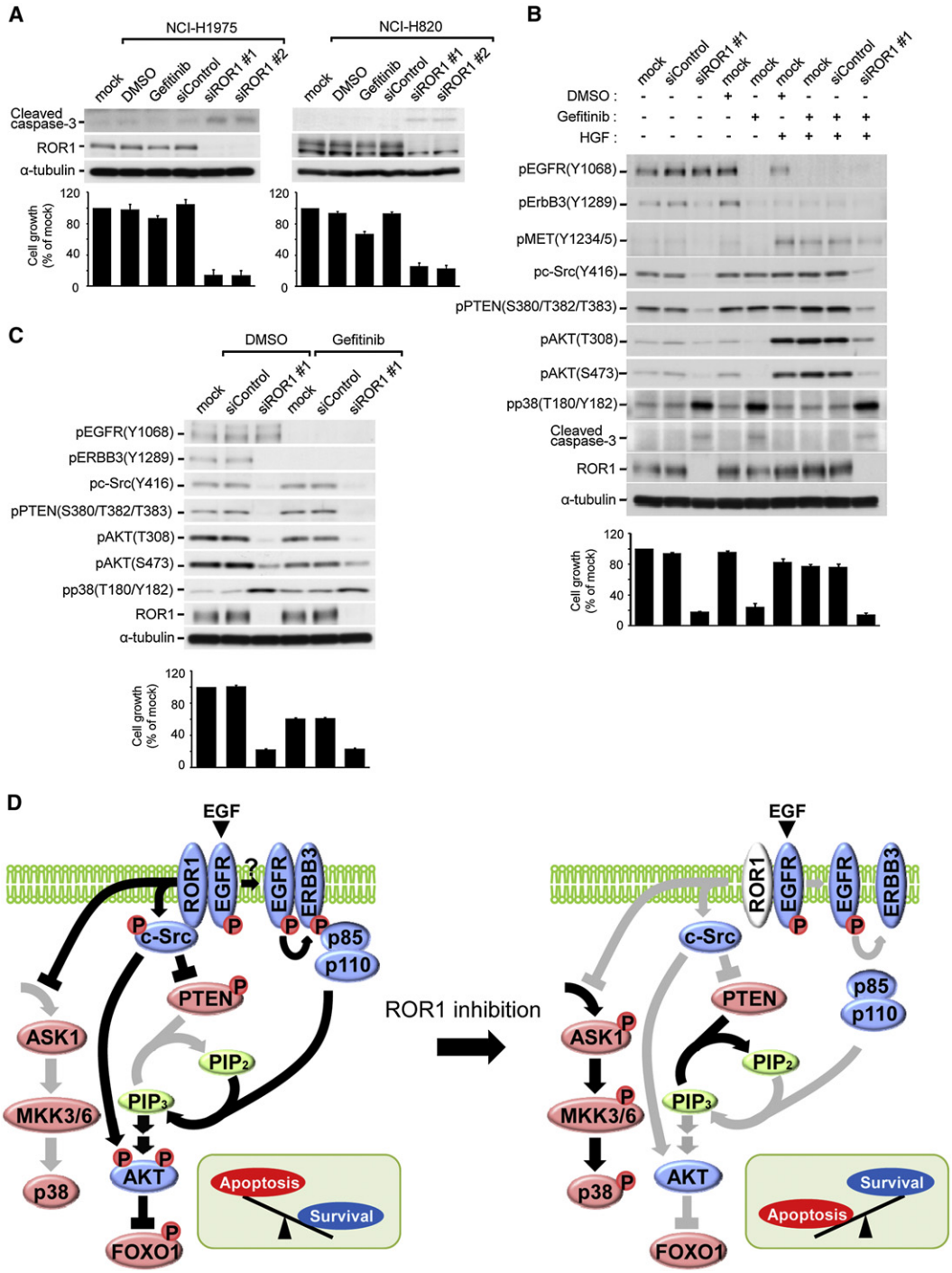

Figure 8. ROR1 Repression Inhibits Lung Adenocarcinomas, Irrespective of the EGFR Status

(A) WB analysis of cleaved caspase-3 (top panel) and a colorimetric assay (bottom panel) of NCI-H1975 and NCI-H820 knocked down for ROR1. Data are shown as the mean ± SD (n = 3).

(B) WB analysis of downstream molecules and a colorimetric assay of gefitinib and/or HGF treatment of siROR1-teated PC-9 cells. Data are shown as the mean ± SD (n = 3).

(C) Effects of siROR1 treatment in the relatively gefitinib-sensitive lung adenocarcinoma cell line NCI-H358. Data are shown as the mean ± SD (n = 3).

(D) Proposed model of how ROR1 plays a key role in sustaining a favorable balance between prosurvival and pro-apoptotic signaling. Two distinct mechanisms appear to coexist in sustaining prosurvival signaling: (1) ROR1 kinase-dependent c-Src activation and (2) kinase-independent sustainment of EGFR-ERBB3 association and consequential ERBB3 phosphorylation. See also Figure S7.

that ROR1 plays a role independent of its kinase activity in sustainment of EGF-induced signaling of the EGFR-ERBB3-PI3K axis, which is well known to play a crucial role in lung adenocarcinomas. Interestingly, we also observed that EGF treatment elicited robust phosphorylations of both EGFR at Y1068 and ERK, even in cells knocked down for ROR1. These findings indicate that ROR1 interaction with EGFR is selectively required for sustainment of signaling along the EGFR-ERBB3-PI3K axis through EGFR-ERBB3 heterodimerization and resultant ERBB3 phosphorylation but not for signaling toward the ERK pathway through autophosphorylation and homodimerization of EGFR. It is anticipated that future studies detailing the high-resolution structures of these receptors would provide insight into how ROR1 participates in this process with such specificity.

We previously showed that ROR1 physically interacts with and phosphorylates c-Src, which is a critical component of multiple signaling pathways important for cancer development (Yeatman, 2004). In addition, we noted that PTEN negative regulation of PI3K-AKT signaling appears to be, at least in part, under the influence of ROR1 expression, a finding consistent with previous reports on PTEN as a c-Src substrate (Lu et al., 2003; Nagata et al., 2004). It is also interesting to note that c-Src-mediated tyrosine phosphorylation has been proposed to trigger T308 and S473 phosphorylations by PDK1 and mTORC2, respectively, leading to AKT activation (Bellacosa et al., 1998; Chen et al., 2001; Jiang and Qiu, 2003) and lending support for the notion that ROR1-mediated c-Src activation may be also involved in this prerequisite process for robust AKT activation in lung adenocarcinoma cells. Thus, ROR1 appears to play a role independent of kinase activity in sustainment of EGF-induced signaling through the EGFR-ERBB3-PI3K axis, which is further upheld by ROR1 downstream through its kinase-dependent c-Src activation. It is also possible that there may be additional substrates of ROR1, as is generally the case in receptor tyrosine kinase signaling.

Taken together, the present findings identify ROR1 as an "Achilles' heel" in lung adenocarcinomas. Mechanisms, such as secondary EGFR mutation, MET amplification, and HGF overexpression, may arise in lung adenocarcinomas in patients undergoing EGFR-TKI treatment, leading to resistance to treatment by the tumors. The existence of such diverse mechanisms make it difficult to predict which should be targeted to prevent expansion of resistant clones (Bean et al., 2007; Engelman et al., 2007; Turke et al., 2010; Yano et al., 2008). From a clinical point of view, it is of particular interest that ROR1 inhibition appears to be effective for treatment of gefitinib-resistant lung adenocarcinomas with various resistance mechanisms. To date, very little is known about the functions of ROR1 and its role in human cancers, in accordance with its name, that is, tyrosine kinase-like orphan receptor 1 (Forrester, 2002; Green et al., 2008; Minami et al., 2010). Interestingly, upregulation of ROR1 was recently reported in chronic lymphocytic leukemia (Baskar et al., 2008; Daneshmanesh et al., 2008; Fukuda et al., 2008). In addition, it is notable that NKX2-1 is expressed in small cell lung cancers at a high frequency (Kitamura et al., 2009). Future development of therapeutic means including ROR1-specific antibodies and small molecules that inhibit both or either of the two distinct prosurvival signal-sustaining functions is greatly anticipated for attempts to reduce the intolerable death toll from currently "hard-to-cure" lung adenocarcinomas, as well as possibly other ROR1-positive cancers.

EXPERIMENTAL PROCEDURES

Cell Lines and Tissues

NCI-H1975, NCI-H820, NCI-H441, NCI-H358, NCI-H23, and PC-9 cells were purchased from the American Type Culture Collection. The derivations and culture conditions of other human cancer cell lines, as well as the immortalized human lung epithelial cell line HPL1D, have been reported (Tanaka et al., 2007). Their characteristics are summarized in Table S1. Human cancer and normal tissues as well as primary normal lung epithelial cells were obtained under approval from the institutional review board of Nagoya University with written informed consent from each patient.

Constructs

The methods used for the construction of the expression constructs of full-length human NKX2-1 cDNA in pCMV-puro (pCMVpuro-NKX2-1), as well as of short hairpin RNA (shRNA) against NKX2-1 in pH1RNAneo (pH1RNAneo-shNKX2-1), have been described (Tanaka et al., 2007). Full-length human ROR1 cDNA (OriGene Technologies, Rockville, MDs) was inserted into a pCMV-puro vector, and the entire open reading frame of the resulting construct (pCMVpuro-ROR1) was thoroughly sequenced. pCMVpuro-ROR1-KD (an inactivating K506A mutation at the ATP binding site), pCMVpuro-ROR1-ΔP, and pCMVpuro-ROR1-ΔCRD were constructed by in vitro mutagenesis using KOD-plus-DNA polymerase (Toyobo, Osaka, Japan). In addition, a myc-tagged derivative of pIRESpuro2-ROR1 (pIRESpuro2-ROR1-myc) and its derivatives (pIRESpuro2-ROR1-ΔN-myc and pIRESpuro2-ROR1-ΔC-myc) were constructed. pIRESpuro2-ROR1-ΔIg-myc, pIRESpuro2-ROR1-ΔCRD-myc, pIRESpuro2-ROR1-ΔKringle-myc, pIRESpuro2-ROR1-ΔIg+CRD-myc, pIRESpuro2-ROR1-ΔCRD+Kringle-myc, and pIRESpuro2-ROR1-ΔIg+CRD+Kringle-myc were also constructed by in vitro mutagenesis using a KOD-plus-DNA polymerase.

Full-length human EGFR cDNA was purchased from Riken and inserted into a pCMV-puro vector (pCMVpuro-EGFR). Full-length human ERBB3 cDNA (pcDNA5/FRT-ERBB3) was kindly provided by N. Taniguchi (Osaka University, Osaka, Japan). pNeo-MSV-c-Src wild-type (WT), constitutive active (CA), and kinase dead (KD) were kindly provided by T. Hunter (Salk Institute, La Jolla, CA; Broome and Hunter, 1996), and the inserts were transferred into pCMVpuro, resulting in the following: pCMVpuro-WT-c-Src, pCMVpuro-CA-c-Src, and pCMVpuro-KD-c-Src. pRC-CMV-c-Src wild-type (WT), Δ15-84 (Δ15), Δ90-144 (Δ90), and Δ150-246 (Δ150) were kindly provided by S.J. Shattil (University of California San Diego, San Diego, CA, USA; Arias-Salgado et al., 2003).

Microarray Analysis

HPL1D cells stably expressing NKX2-1 (HPL1D-NKX2-1) were generated by transfecting pCMVpuro-NKX2-1 using FuGENE6, followed by puromycin selection. RNA was extracted from HPL1D-NKX2-1 and its empty control vector HPL1D-VC and then analyzed in dye-swapped duplicate using a low RNA fluorescent linear amplification kit and 44K whole human genome microarrays (Agilent Technologies, Santa Clara, CA), in accordance with the manufacturer's instructions. HPL1D cells were also transiently transfected with NKX2-1, selected with puromycin for three days, and harvested for validation of ROR1 induction by western blot analysis.

Western Blot and Immunoprecipitation-Western Blot Analyses

Western blot and immunoprecipitation-western blot analyses were performed using standard procedures with Immobilon-P filters (Millipore, Billerica, MA) and an enhanced chemiluminescence system (GE Healthcare, Buckinghamshire, UK). For analysis of physical interactions between ROR1 and c-Src, pIRESpuro2-ROR1-myc was transfected with various c-Src expression constructs, including wild-type (WT), Δ15-84 c-Src (Δ15), Δ90-144 c-Src (Δ90), or Δ150-246 c-Src (Δ150). Similarly, wild-type c-Src was transfected with pCMVpuro-ROR1 (ROR1), pCMVpuro-ROR1-K506A (ROR1-KD), or pCMVpuro-ROR1–ΔP (ROR1-ΔP). Cells were harvested 24 hr after transfection with the lysis buffer containing 20 mM Tris-HCl (pH 7.5), 150 mM NaCl,

1 mM EDTA, 1 mM EGTA, 1% Triton X-100, 2.5 mM sodium pyrophosphate, 1 mM β-glycerophosphate, 1 mM Na_3VO_4, 1 μg/ml leupeptin, 1 mM PMSF, and Complete (EDTA-free protease inhibitor mixture; Roche, Mannheim, Germany). For analysis of physical interactions among ROR1, EGFR, and ERBB3, pCMVpuro-EGFR and/or pcDNA5/FRT-ERBB3 were transfected with various ROR1 expression constructs, including wild-type (WT), ΔN, ΔC, ΔIg, ΔCRD, ΔKringle, ΔIg+CRD, ΔCRD+Kringle, and ΔIg+CRD+Kringle. Cells were serum-starved for 24 hr, treated with 20 ng/ml of EGF 48 hr after transfection for up to 30 min, and then harvested to analyze their interactions through immunoprecipitation-western blot analysis. A NP-40 lysis buffer containing 20 mM Tris-HCl (pH 8.0), 137 mM NaCl, 2 mM EDTA, 1% NP-40, 10% Glycerol, and 1 mM Na_3VO_4 was used to investigate the physical interactions among ROR1, EGFR, and ERBB3.

Clarification of ROR1-RNAi Effects

pCMVpuro-ROR1-WT-mut(si#1) and pCMVpuro-ROR1-KD-mut(si#1), which carry multiple silent mutations at the binding site of siROR1#1, were constructed by in vitro mutagenesis using KOD-plus-DNA Polymerase (Toyobo) and the oligonucleotide primer 5′-CAACAGTGGACAGAGTTCCAG-3′ (mutated residues are underlined). NCI-H1975 and NCI-H358 at 2.0×10^6 were transfected with an empty pCMVpuro vector (VC), pCMVpuro-ROR1 (ROR1), pCMVpuro-ROR1-WT-mut(si#1) [ROR1-WT-mut(si#1)], or pCMVpuro-ROR1-KD-mut(si#1) [ROR1-KD-mut(si#1)], followed by puromycin selection (1.5 μg/ml) for three days. The resulting bulk transfectants were then re-seeded into 6-well plates and further introduced with siROR1 alone or along with either sic-Src or siERBB3 on the next day. Cells were harvested for western blot analysis at three days or a colorimetric assay at five days after siRNA transfection. For rescue experiments of ERBB3 phosphorylation, NCI-H1975 cells expressing ROR1-WT-mut(si#1) or ROR1-KD-mut(si#1) were transfected with siROR1 or siControl and then serum-starved for 24 hr. After treatment with 20 ng/ml of EGF for various time periods, western blot analyses were performed.

Analyses of Functional Relationships of ROR1 with NKX2-1 and c-Src

In order to analyze the effects of exogenous ROR1 expression in shNKX2-1-treated lung adenocarcinoma cells, pH1RNAneo-shNKX2-1 and pCMVpuro-ROR1 were cotransfected into NCI-H358 at a ratio of 1:4, followed by neomycin selection for two weeks before counting the number of colonies. The functional relationship between ROR1 and c-Src was analyzed in NCI-H1975 cells by transfection of pCMVpuro-WT-c-Src or pCMVpuro-CA-c-Src; then, transfected cells were selected with puromycin for three days. The resulting bulk transfectants were then re-seed into 6-well plates and further introduced with siROR1 or siControl. Cells were harvested for western blot analysis at 72 hr after siRNA transfection. A colorimetric assay was performed five days after siRNA transfection. NCI-H1975, SK-LC-5, and NCI-H23 cells were also treated with the Src kinase inhibitor SKI-1 at 5 μM for 6 hr and harvested for western blot analysis. For a colorimetric assay, cells were treated with 5 μM SKI-1 for five days.

In Vivo Tumorigenicity Assays

NCI-H1975 cells at 1.0×10^7 were subcutaneously inoculated into the lower flanks of 8-week-old athymic nude mice (Japan SLC, Shizuoka, Japan). One week after inoculation, a mixture of 1 nmol of siRNAs (siROR1 #1, #2, and #3) and 200 μl of atelocollagen (Koken, Tokyo, Japan) was injected into the tumors, which had an average volume of 50 mm^3. Tumor weights were measured two weeks after siRNA injection. In vivo tumorigenicity assays were also performed by subcutaneous inoculation of 1.0×10^7 MSTO-211H cells stably expressing wild-type ROR1 (ROR1#1 and #2), kinase-dead ROR1 (ROR1-KD#1 and #2), or those introduced with an empty vector (VC#1 and #2) into the lower flanks of 8-week-old athymic nude mice (Japan SLC). In this experiment, tumor weights were determined three weeks after inoculation. In addition, tumors were analyzed by western blot analysis for detection of various protein expressions. For analysis of the effects of c-Src or ERBB3 knockdown in the ROR1 transfectants, a mixture of 1 nmol siRNAs (siControl, sic-Src #1, sic-Src #2, siERBB3 #1, or siERBB3 #2) and 200 μl atelocollagen was injected into the tumors at one week after inoculation. Tumor weights were measured two weeks after siRNA injection and various protein expressions were analyzed by western blot analysis. All animal experiments were performed in compliance with the regulations for animal experiments of Nagoya University.

EGF, HGF, and/or Gefitinib Treatment in Cells Knocked Down for ROR1

NCI-H1975 and SK-LC-5 cells (1.0×10^5) were transfected with 20 nM siROR1 or siControl and then serum-starved for 24 hr. After treatment with 20 ng/ml of EGF for various time periods, western blot and immunofluorescent staining analyses were performed. NCI-H1975, NCI-H820, and NCI-H358 cells (1.0×10^5) were transfected with 20 nM siROR1 or siControl, then cultured for three days before treatment with 1 μM gefitinib for 6 hr, and harvested for western blot analysis. For a colorimetric assay, cells (5.0×10^4) were transfected with the siRNAs and then continuously exposed to 1 μM gefitinib for four days. Similarly, three days after siRNA transfection, PC-9 cells were treated with 1 μM gefitinib and/or 50 ng/ml of HGF for 6 hr and then harvested for western blot analysis. Effects on cell proliferation were also examined by a colorimetric assay after a four-day exposure to 1 μM gefitinib and/or 50 ng/ml of HGF, which was initiated the day after siRNA transfection.

ACCESSION NUMBERS

The raw microarray data have been deposited in the Gene Expression Omnibus databases under accession number GSE25830.

SUPPLEMENTAL INFORMATION

Supplemental Information includes seven figures, one table, and Supplemental Experimental Procedures and can be found with this article online at doi:10.1016/j.ccr.2012.02.008.

ACKNOWLEDGMENTS

We thank T. Hunter and S.J. Shattil for providing the c-Src constructs and N. Taniguchi for the ERBB3 construct. This work was supported in part by grants-in-aid for Scientific Research on Priority Areas and Scientific Research on Innovative Areas from the Ministry of Education, Culture, Sports, Science, and Technology (MEXT) of Japan, as well as grants-in-aid for Scientific Research (A) and Young Scientists (B) from the Japan Society for the Promotion of Science (JSPS).

Received: July 15, 2011
Revised: December 7, 2011
Accepted: February 2, 2012
Published: March 19, 2012

REFERENCES

Arias-Salgado, E.G., Lizano, S., Sarkar, S., Brugge, J.S., Ginsberg, M.H., and Shattil, S.J. (2003). Src kinase activation by direct interaction with the integrin beta cytoplasmic domain. Proc. Natl. Acad. Sci. USA *100*, 13298–13302.

Baskar, S., Kwong, K.Y., Hofer, T., Levy, J.M., Kennedy, M.G., Lee, E., Staudt, L.M., Wilson, W.H., Wiestner, A., and Rader, C. (2008). Unique cell surface expression of receptor tyrosine kinase ROR1 in human B-cell chronic lymphocytic leukemia. Clin. Cancer Res. *14*, 396–404.

Bean, J., Brennan, C., Shih, J.Y., Riely, G., Viale, A., Wang, L., Chitale, D., Motoi, N., Szoke, J., Broderick, S., et al. (2007). MET amplification occurs with or without T790M mutations in EGFR mutant lung tumors with acquired resistance to gefitinib or erlotinib. Proc. Natl. Acad. Sci. USA *104*, 20932–20937.

Bellacosa, A., Chan, T.O., Ahmed, N.N., Datta, K., Malstrom, S., Stokoe, D., McCormick, F., Feng, J., and Tsichlis, P. (1998). Akt activation by growth factors is a multiple-step process: the role of the PH domain. Oncogene *17*, 313–325.

Boggaram, V. (2009). Thyroid transcription factor-1 (TTF-1/Nkx2.1/TITF1) gene regulation in the lung. Clin. Sci. *116*, 27–35.

Broome, M.A., and Hunter, T. (1996). Requirement for c-Src catalytic activity and the SH3 domain in platelet-derived growth factor BB and epidermal growth factor mitogenic signaling. J. Biol. Chem. *271*, 16798–16806.

Calnan, D.R., and Brunet, A. (2008). The FoxO code. Oncogene *27*, 2276–2288.

Chen, R., Kim, O., Yang, J., Sato, K., Eisenmann, K.M., McCarthy, J., Chen, H., and Qiu, Y. (2001). Regulation of Akt/PKB activation by tyrosine phosphorylation. J. Biol. Chem. *276*, 31858–31862.

Daneshmanesh, A.H., Mikaelsson, E., Jeddi-Tehrani, M., Bayat, A.A., Ghods, R., Ostadkarampour, M., Akhondi, M., Lagercrantz, S., Larsson, C., Osterborg, A., et al. (2008). Ror1, a cell surface receptor tyrosine kinase is expressed in chronic lymphocytic leukemia and may serve as a putative target for therapy. Int. J. Cancer *123*, 1190–1195.

Engelman, J.A., Jänne, P.A., Mermel, C., Pearlberg, J., Mukohara, T., Fleet, C., Cichowski, K., Johnson, B.E., and Cantley, L.C. (2005). ErbB-3 mediates phosphoinositide 3-kinase activity in gefitinib-sensitive non-small cell lung cancer cell lines. Proc. Natl. Acad. Sci. USA *102*, 3788–3793.

Engelman, J.A., Zejnullahu, K., Mitsudomi, T., Song, Y., Hyland, C., Park, J.O., Lindeman, N., Gale, C.M., Zhao, X., Christensen, J., et al. (2007). MET amplification leads to gefitinib resistance in lung cancer by activating ERBB3 signaling. Science *316*, 1039–1043.

Engelman, J.A., Chen, L., Tan, X., Crosby, K., Guimaraes, A.R., Upadhyay, R., Maira, M., McNamara, K., Perera, S.A., Song, Y., et al. (2008). Effective use of PI3K and MEK inhibitors to treat mutant Kras G12D and PIK3CA H1047R murine lung cancers. Nat. Med. *14*, 1351–1356.

Forrester, W.C. (2002). The Ror receptor tyrosine kinase family. Cell. Mol. Life Sci. *59*, 83–96.

Fukuda, T., Chen, L., Endo, T., Tang, L., Lu, D., Castro, J.E., Widhopf, G.F., 2nd, Rassenti, L.Z., Cantwell, M.J., Prussak, C.E., et al. (2008). Antisera induced by infusions of autologous Ad-CD154-leukemia B cells identify ROR1 as an oncofetal antigen and receptor for Wnt5a. Proc. Natl. Acad. Sci. USA *105*, 3047–3052.

Garraway, L.A., and Sellers, W.R. (2006). Lineage dependency and lineage-survival oncogenes in human cancer. Nat. Rev. Cancer *6*, 593–602.

Green, J.L., Kuntz, S.G., and Sternberg, P.W. (2008). Ror receptor tyrosine kinases: orphans no more. Trends Cell Biol. *18*, 536–544.

Hennessy, B.T., Smith, D.L., Ram, P.T., Lu, Y., and Mills, G.B. (2005). Exploiting the PI3K/AKT pathway for cancer drug discovery. Nat. Rev. Drug Discov. *4*, 988–1004.

Jiang, T., and Qiu, Y. (2003). Interaction between Src and a C-terminal proline-rich motif of Akt is required for Akt activation. J. Biol. Chem. *278*, 15789–15793.

Kendall, J., Liu, Q., Bakleh, A., Krasnitz, A., Nguyen, K.C., Lakshmi, B., Gerald, W.L., Powers, S., and Mu, D. (2007). Oncogenic cooperation and coamplification of developmental transcription factor genes in lung cancer. Proc. Natl. Acad. Sci. USA *104*, 16663–16668.

Kimura, S., Hara, Y., Pineau, T., Fernandez-Salguero, P., Fox, C.H., Ward, J.M., and Gonzalez, F.J. (1996). The T/ebp null mouse: thyroid-specific enhancer-binding protein is essential for the organogenesis of the thyroid, lung, ventral forebrain, and pituitary. Genes Dev. *10*, 60–69.

Kitamura, H., Yazawa, T., Sato, H., Okudela, K., and Shimoyamada, H. (2009). Small cell lung cancer: significance of RB alterations and TTF-1 expression in its carcinogenesis, phenotype, and biology. Endocr. Pathol. *20*, 101–107.

Kobayashi, S., Boggon, T.J., Dayaram, T., Jänne, P.A., Kocher, O., Meyerson, M., Johnson, B.E., Eck, M.J., Tenen, D.G., and Halmos, B. (2005). EGFR mutation and resistance of non-small-cell lung cancer to gefitinib. N. Engl. J. Med. *352*, 786–792.

Kwei, K.A., Kim, Y.H., Girard, L., Kao, J., Pacyna-Gengelbach, M., Salari, K., Lee, J., Choi, Y.L., Sato, M., Wang, P., et al. (2008). Genomic profiling identifies TITF1 as a lineage-specific oncogene amplified in lung cancer. Oncogene *27*, 3635–3640.

Linggi, B., and Carpenter, G. (2006). ErbB receptors: new insights on mechanisms and biology. Trends Cell Biol. *16*, 649–656.

Lu, Y., Yu, Q., Liu, J.H., Zhang, J., Wang, H., Koul, D., McMurray, J.S., Fang, X., Yung, W.K., Siminovitch, K.A., and Mills, G.B. (2003). Src family protein-tyrosine kinases alter the function of PTEN to regulate phosphatidylinositol 3-kinase/AKT cascades. J. Biol. Chem. *278*, 40057–40066.

Maeda, Y., Davé, V., and Whitsett, J.A. (2007). Transcriptional control of lung morphogenesis. Physiol. Rev. *87*, 219–244.

Martin, G.S. (2001). The hunting of the Src. Nat. Rev. Mol. Cell Biol. *2*, 467–475.

Masuda, A., Kondo, M., Saito, T., Yatabe, Y., Kobayashi, T., Okamoto, M., Suyama, M., Takahashi, T., and Takahashi, T. (1997). Establishment of human peripheral lung epithelial cell lines (HPL1) retaining differentiated characteristics and responsiveness to epidermal growth factor, hepatocyte growth factor, and transforming growth factor beta1. Cancer Res. *57*, 4898–4904.

Minami, Y., Oishi, I., Endo, M., and Nishita, M. (2010). Ror-family receptor tyrosine kinases in noncanonical Wnt signaling: their implications in developmental morphogenesis and human diseases. Dev. Dyn. *239*, 1–15.

Nagata, Y., Lan, K.H., Zhou, X., Tan, M., Esteva, F.J., Sahin, A.A., Klos, K.S., Li, P., Monia, B.P., Nguyen, N.T., et al. (2004). PTEN activation contributes to tumor inhibition by trastuzumab, and loss of PTEN predicts trastuzumab resistance in patients. Cancer Cell *6*, 117–127.

Nishikawa, E., Osada, H., Okazaki, Y., Arima, C., Tomida, S., Tatematsu, Y., Taguchi, A., Shimada, Y., Yanagisawa, K., Yatabe, Y., et al. (2011). miR-375 is activated by ASH1 and inhibits YAP1 in a lineage-dependent manner in lung cancer. Cancer Res. *71*, 6165–6173.

Osada, H., Tatematsu, Y., Yatabe, Y., Horio, Y., and Takahashi, T. (2005). ASH1 gene is a specific therapeutic target for lung cancers with neuroendocrine features. Cancer Res. *65*, 10680–10685.

Osada, H., Tomida, S., Yatabe, Y., Tatematsu, Y., Takeuchi, T., Murakami, H., Kondo, Y., Sekido, Y., and Takahashi, T. (2008). Roles of achaete-scute homologue 1 in DKK1 and E-cadherin repression and neuroendocrine differentiation in lung cancer. Cancer Res. *68*, 1647–1655.

Pao, W., Miller, V.A., Politi, K.A., Riely, G.J., Somwar, R., Zakowski, M.F., Kris, M.G., and Varmus, H. (2005). Acquired resistance of lung adenocarcinomas to gefitinib or erlotinib is associated with a second mutation in the EGFR kinase domain. PLoS Med. *2*, e73.

Rothenberg, S.M., Engelman, J.A., Le, S., Riese, D.J., 2nd, Haber, D.A., and Settleman, J. (2008). Modeling oncogene addiction using RNA interference. Proc. Natl. Acad. Sci. USA *105*, 12480–12484.

Sharma, S.V., Gajowniczek, P., Way, I.P., Lee, D.Y., Jiang, J., Yuza, Y., Classon, M., Haber, D.A., and Settleman, J. (2006). A common signaling cascade may underlie "addiction" to the Src, BCR-ABL, and EGF receptor oncogenes. Cancer Cell *10*, 425–435.

Sharma, S.V., and Settleman, J. (2009). ErbBs in lung cancer. Exp. Cell Res. *315*, 557–571.

Takeuchi, T., Tomida, S., Yatabe, Y., Kosaka, T., Osada, H., Yanagisawa, K., Mitsudomi, T., and Takahashi, T. (2006). Expression profile-defined classification of lung adenocarcinoma shows close relationship with underlying major genetic changes and clinicopathologic behaviors. J. Clin. Oncol. *24*, 1679–1688.

Tanaka, H., Yanagisawa, K., Shinjo, K., Taguchi, A., Maeno, K., Tomida, S., Shimada, Y., Osada, H., Kosaka, T., Matsubara, H., et al. (2007). Lineage-specific dependency of lung adenocarcinomas on the lung development regulator TTF-1. Cancer Res. *67*, 6007–6011.

Turke, A.B., Zejnullahu, K., Wu, Y.L., Song, Y., Dias-Santagata, D., Lifshits, E., Toschi, L., Rogers, A., Mok, T., Sequist, L., et al. (2010). Preexistence and clonal selection of MET amplification in EGFR mutant NSCLC. Cancer Cell *17*, 77–88.

Weinstein, I.B. (2002). Cancer. Addiction to oncogenes—the Achilles heal of cancer. Science *297*, 63–64.

Weir, B.A., Woo, M.S., Getz, G., Perner, S., Ding, L., Beroukhim, R., Lin, W.M., Province, M.A., Kraja, A., Johnson, L.A., et al. (2007). Characterizing the cancer genome in lung adenocarcinoma. Nature *450*, 893–898.

Yano, S., Wang, W., Li, Q., Matsumoto, K., Sakurama, H., Nakamura, T., Ogino, H., Kakiuchi, S., Hanibuchi, M., Nishioka, Y., et al. (2008). Hepatocyte growth factor induces gefitinib resistance of lung adenocarcinoma with epidermal growth factor receptor-activating mutations. Cancer Res. *68*, 9479–9487.

Yatabe, Y., Mitsudomi, T., and Takahashi, T. (2002). TTF-1 expression in pulmonary adenocarcinomas. Am. J. Surg. Pathol. *26*, 767–773.

Yatabe, Y., Kosaka, T., Takahashi, T., and Mitsudomi, T. (2005). EGFR mutation is specific for terminal respiratory unit type adenocarcinoma. Am. J. Surg. Pathol. *29*, 633–639.

Yeatman, T.J. (2004). A renaissance for SRC. Nat. Rev. Cancer *4*, 470–480.

Zhang, S., Huang, W.C., Li, P., Guo, H., Poh, S.B., Brady, S.W., Xiong, Y., Tseng, L.M., Li, S.H., Ding, Z., et al. (2011). Combating trastuzumab resistance by targeting SRC, a common node downstream of multiple resistance pathways. Nat. Med. *17*, 461–469.

Cancer Cell
Article

Activated ALK Collaborates with MYCN in Neuroblastoma Pathogenesis

Shizhen Zhu,[1,6] Jeong-Soo Lee,[1,6,8] Feng Guo,[1] Jimann Shin,[1,9] Antonio R. Perez-Atayde,[2] Jeffery L. Kutok,[3,10] Scott J. Rodig,[3] Donna S. Neuberg,[4] Daniel Helman,[1] Hui Feng,[1] Rodney A. Stewart,[1,7] Wenchao Wang,[1] Rani E. George,[1,5] John P. Kanki,[1] and A. Thomas Look[1,5,*]

[1]Department of Pediatric Oncology, Dana-Farber Cancer Institute
[2]Department of Pathology, Children's Hospital Boston
[3]Department of Pathology, Brigham and Women's Hospital
[4]Department of Biostatistics and Computational Biology, Dana-Farber Cancer Institute
[5]Division of Hematology/Oncology, Children's Hospital Boston
Harvard Medical School, Boston, MA 02115, USA
[6]These authors contributed equally to this work
[7]Present address: Huntsman Cancer Institute, Department of Oncological Sciences, University of Utah, Salt Lake City, UT 84112, USA
[8]Present address: Korea Research Institute of Bioscience and Biotechnology, Aging Research Center, Daejeon 305-806, Korea
[9]Present address: Department of Developmental Biology, Washington University School of Medicine, Saint Louis, MO 63110, USA
[10]Present address: Molecular Pathology, Infinity Pharmaceuticals, Cambridge, MA 02139, USA
*Correspondence: thomas_look@dfci.harvard.edu
DOI 10.1016/j.ccr.2012.02.010

SUMMARY

Amplification of the *MYCN* oncogene in childhood neuroblastoma is often accompanied by mutational activation of *ALK* (anaplastic lymphoma kinase), suggesting their pathogenic cooperation. We generated a transgenic zebrafish model of neuroblastoma in which MYCN-induced tumors arise from a subpopulation of neuroblasts that migrate into the adrenal medulla analog following organogenesis. Coexpression of activated *ALK* with *MYCN* in this model triples the disease penetrance and markedly accelerates tumor onset. *MYCN* overexpression induces adrenal sympathetic neuroblast hyperplasia, blocks chromaffin cell differentiation, and ultimately triggers a developmentally-timed apoptotic response in the hyperplastic sympathoadrenal cells. Coexpression of activated *ALK* with *MYCN* provides prosurvival signals that block this apoptotic response and allow continued expansion and oncogenic transformation of hyperplastic neuroblasts, thus promoting progression to neuroblastoma.

INTRODUCTION

Neuroblastoma is a childhood solid tumor that arises in the peripheral sympathetic nervous system (PSNS), typically in the adrenal medulla or paraspinal ganglia, during embryogenesis (Brodeur, 2003; Maris, 2010). When disseminated at diagnosis in older children, the disease carries a very poor prognosis despite the use of intensive therapies. Amplification of the *MYCN* oncogene is found in tumor cells from ~20% of neuroblastoma patients and is the most reliable marker of a poor prognosis (Brodeur, 2003; Maris et al., 2007). Overexpression of *MYCN* in the PSNS of transgenic mice, using the rat tyrosine hydroxylase (*TH*) promoter, results in tumors that closely resemble human neuroblastoma arising in the sympathetic ganglia (Chesler and Weiss, 2011; Weiss et al., 1997), indicating that aberrant expression of *MYCN* promotes the development of this tumor in vivo.

The anaplastic lymphoma kinase (*ALK*) gene encodes a receptor tyrosine kinase that is normally expressed at high levels in the nervous system and was originally identified as a fusion

Significance

Neuroblastoma is an important developmental tumor arising in the peripheral sympathetic nervous system, which accounts for ~10% of cancer-related deaths in childhood. The ALK receptor tyrosine kinase is mutationally activated in a subset of primary neuroblastomas, but the mechanisms through which ALK signaling cooperates with MYCN overexpression in neuroblastoma pathogenesis remain unclear. By generating a transgenic zebrafish model that overexpresses human *MYCN* and activated *ALK* in the fish analog of the adrenal medulla, we now show that upregulated *MYCN* mediates sympathetic neuroblast hyperplasia, which is mitigated by a developmentally-timed apoptotic response. Activated ALK blocks neuroblast apoptosis at this critical time in development, establishing a mechanism for the synergistic relationship between these two oncoproteins in the pathogenesis of neuroblastoma.

protein with nucleophosmin in cases of anaplastic large cell lymphoma (Morris et al., 1994). Activation of ALK can regulate cellular proliferation, differentiation and apoptosis via a number of different signaling pathways, including PI3K/AKT, RAS/MAPK, and STAT3, but its precise physiologic role remains elusive (Chiarle et al., 2008; Palmer et al., 2009). Recently, we and others reported that amplification of the *ALK* gene occurs only in *MYCN*-amplified primary neuroblastomas and that within this group ~15% of cases have *ALK* amplification (George et al., 2008; Mossé et al., 2008). Activating *ALK* mutations were also identified in both familial and sporadic neuroblastoma cases, including but not limited to a subset with *MYCN* amplification, further implicating this kinase in neuroblastoma pathogenesis (Chen et al., 2008; George et al., 2008; Janoueix-Lerosey et al., 2008; Mossé et al., 2008). Mechanisms through which signaling by aberrantly activated ALK cooperates with MYCN overexpression to enhance neuroblastoma development remain undefined, posing a major obstacle to the development of effective targeted treatments for this devastating disease.

We have generated a transgenic zebrafish model in which overexpression of human *MYCN* in the PSNS induces tumors in the fish analog of the adrenal medulla that closely resemble human neuroblastoma. Using this model system, we undertook studies to explore mechanistically the interaction between mutationally activated ALK and MYCN overexpression during neuroblastoma pathogenesis in the PSNS.

RESULTS

Transgenic EGFP Expression in the PSNS

We first isolated a 5.2 kb promoter fragment upstream of the coding sequence of the zebrafish dopamine-β-hydroxylase gene (*dβh*), which encodes the rate-limiting enzyme for noradrenalin synthesis. This fragment was used to drive expression of enhanced green fluorescent protein (EGFP) in a stable zebrafish transgenic line, *Tg(dβh:EGFP)*, designated DβH in this article. In juvenile and adult transgenic zebrafish, EGFP was specifically expressed by sympathetic neurons of the superior cervical ganglia (Figures 1A–1C), the first sympathetic ganglion to develop in early embryogenesis, and by each sequential segmental ganglion of the sympathetic chain (Figures 1A, 1B, and 1D). EGFP was also expressed by sympathoadrenal cells of the interrenal gland (Figures 1A, 1B, and 1E), the zebrafish equivalent of the human adrenal gland (Hsu et al., 2003). In the interrenal gland, the EGFP-expressing cells can be visualized within a discrete region in the ventral aspect of the head kidney, intermixed with adrenal cortical cells that are TH- and EGFP-negative (Figure 1E). The specificity of EGFP expression for sympathoadrenal cells when driven by the *dβh* promoter fragment is demonstrated by coexpression of endogenous TH (Figures 1C–1E), another enzyme expressed by sympathetic neurons and chromaffin cells (An et al., 2002; O'Brien et al., 2004).

Zebrafish Expressing *MYCN* Develop Neuroblastoma

Using a coinjection strategy (Langenau et al., 2008), we generated a stable transgenic zebrafish line, *Tg(dβh:EGFP-MYCN)*, designated MYCN in this article, that overexpresses the human *MYCN* gene fused to EGFP under control of the *dβh* promoter. In MYCN transgenic fish the expansion of cells expressing EGFP as tumors developed was readily detectable in living fish by immunofluorescence microscopy (Figure 2A). $EGFP^+$ tumor masses were found in the anterior abdomen, corresponding to the interrenal gland, and were composed of small, undifferentiated, round-tumor cells with hyperchromatic nuclei, often forming nests (Figure 2B). Tumor cells were strongly immunoreactive for TH and the pan-neuronal markers Hu and Synaptophysin (Figure 2C), indicating their PSNS-related neuronal origin (Gould et al., 1986; Marusich et al., 1994; Teitelman et al., 1979). Normal interrenal chromaffin cells also expressed TH, but not Hu or Synaptophysin (Figure 2C), indicating that the neuroblastomas arose from sympathetic neuroblast precursors and not chromaffin cells, as is the case in human neuroblastoma (Figure 2E).

Neuroblastoma is frequently considered in the differential diagnosis of malignant small round-cell tumors of childhood, and electron microscopy is a helpful tool for distinguishing among these malignancies. A diagnosis of neuroblastoma can be established ultrastructurally by demonstrating the presence of neurosecretory granules within the cytoplasm or cytoplasmic processes of tumor cells (Figure 2E) (Mierau et al., 1998). These neurosecretory granules were evident in the tumors we identified in the zebrafish (Figure 2D), strengthening their association with childhood neuroblastoma. The histopathological, immunohistochemical and ultrastructural features of neuroblastoma are shown in Figure 2E, to illustrate their similarities with those of neuroblastomas induced by *MYCN* overexpression in zebrafish (Figures 2B–2D) (Hoshi et al., 2008; Mierau et al., 1998; Molenaar et al., 1990; Taxy, 1980; Tornóczky et al., 2007). These findings support our use of this model to investigate activated ALK as a contributor to MYCN-driven tumorigenesis.

ALK Accelerates MYCN-Induced Neuroblastoma

We and others have implicated activating mutations of *ALK* in the pathogenesis of neuroblastoma, including cases that also show *MYCN* amplification (De Brouwer et al., 2010; George et al., 2008; Mossé et al., 2008). To address whether *ALK* and *MYCN* genetically interact during neuroblastoma induction, we generated a second stable transgenic zebrafish line that expresses the human *ALK* gene harboring the *F1174L* mutation, one of the most prevalent somatic activating mutations found in neuroblastoma patients and human cell lines (Chen et al., 2008; George et al., 2008). The *dβh:EGFP* and *dβh:ALKF1174L* constructs were coinjected into zebrafish embryos at the one-cell stage to generate a transgenic line expressing both the EGFP and activated *ALK* transgenes, *Tg(dβh:EGFP;dβh:ALKF1174L)*, designated ALK in this article. EGFP was specifically expressed by sympathoadrenal cells in the interrenal gland of the ALK transgenic fish at 5 weeks postfertilization (wpf), and *ALK* was coexpressed with EGFP by the same cells (Figure S1A available online). This transgenic line was bred to the MYCN heterozygous transgenic line, and the offspring were monitored for evidence of tumors. All of the expected genotypes were represented in the offspring of this cross: (1) MYCN; (2) ALK; (3) MYCN;ALK; and (4) wild-type (WT) AB fish lacking either transgene. A tumor watch was performed on a total of 1,156 sorted offspring. The fish were isolated in individual tanks as soon as tumors appeared; and were sacrificed for molecular and pathologic analyses when there was evidence of tumor progression.

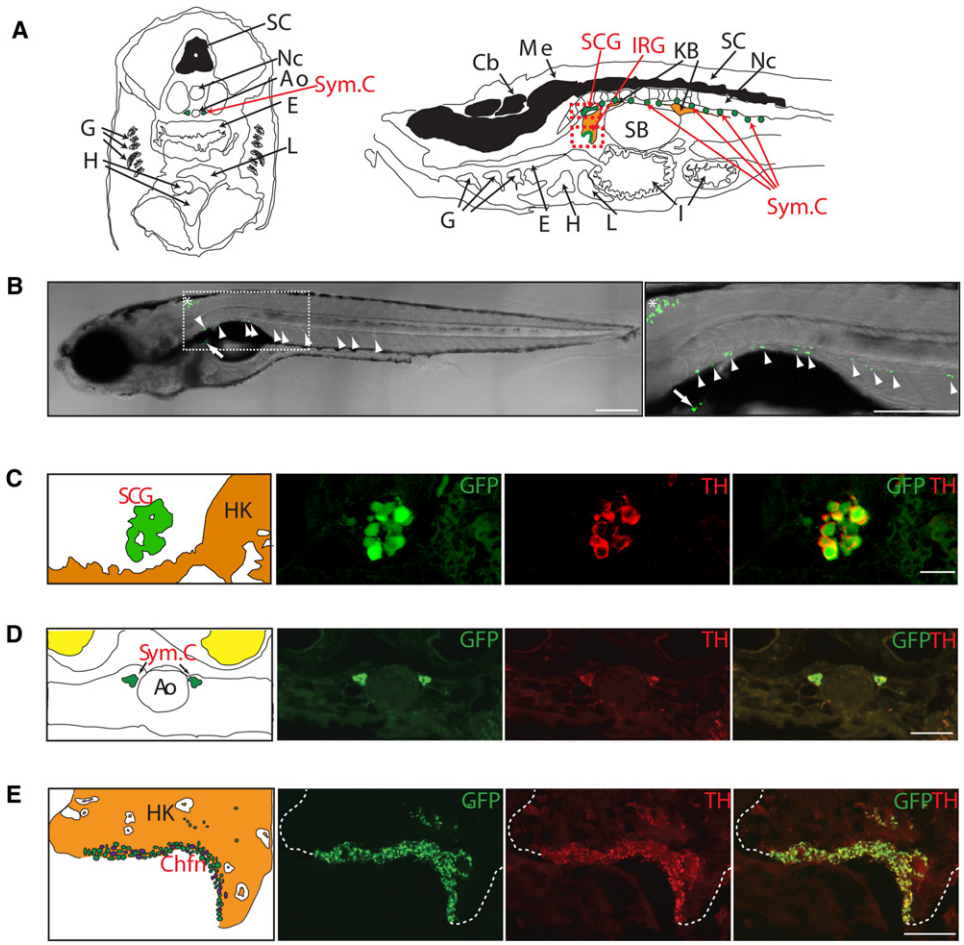

Figure 1. Transgenic Gene Expression in the Sympathetic Neurons and the Interrenal Gland

(A) Left: Schematic of a transverse section illustrating zebrafish anatomical structures, dorsal upward. Right: Schematic of a sagittal section illustrating zebrafish anatomical structures, anterior to left.

(B) EGFP expression (green) in the zebrafish chain of sympathetic ganglia (arrowheads), the IRG (arrow), and medulla oblongata (asterisk) at 3 wpf. Lateral view of confocal-brightfield image, anterior to left. The magnified view of the boxed region is shown on the right. Scale bar represents 500 μm.

(C) EGFP is coexpressed with TH in the SCG at 6 wpf (sagittal section); TH coexpression is indicated in red. Scale bar represents 20 μm.

(D) EGFP is coexpressed with TH in the chain of sympathetic ganglia at 6 wpf (transverse section). TH coexpression is indicated in red. Scale bar represents 20 μm.

(E) EGFP is coexpressed with TH in the IRG at 8 months postfertilization (mpf) (sagittal section). TH coexpression is indicated in red. Scale bar represents 100 μm. Ao, aorta; Cb, cerebellum; Chfn, chromaffin cells; E, esophagus; G, gill; H, heart; HK, head kidney; I, intestine; IRG, interregnal gland; KB, kidney body; L, liver; Me, medulla; Nc, notochord; SB, swim bladder; SC, spinal cord; SCG, superior cervical ganglion; Sym.C, sympathetic chain. See also Figure S1.

The first 23 tumors arose between 5–7 weeks of age, and all had the compound transgenic genotype, MYCN;ALK (Figure 3A). The expression of MYCN and ALK proteins and *ALK* RNA was confirmed in the tumors of these compound transgenic fish by immunohistochemical and RT-PCR analyses, respectively (Figures S1B and S1C). Tumors continued to arise after 9 weeks of age in both the MYCN-only and the MYCN;ALK compound transgenic lines, but their rate of induction was much higher in the latter group (Figure 3A). Tumor penetrance in the MYCN;ALK compound transgenic fish was also much higher: 55.6% versus 17.3% for the MYCN transgenic fish ($p < 0.0001$; Figure 3A). Although germline mutations of *ALK* cause hereditary neuroblastoma (Mossé et al., 2008), tumors did not develop in fish expressing this transgene alone over the 6-month monitoring period (Figure 3A). Tumors in the compound transgenic fish arose in the interrenal gland, as did those in the MYCN fish, and these tumors were comparable histologically, immunohistochemically, and ultrastructurally (Figure S2) to human neuroblastoma (Figure 2E).

To control for possible founder effects in our transgenic lines, and to examine whether overexpression of wild-type *ALK* (ALKWT) as well as mutationally activated *ALK* could collaborate with MYCN in neuroblastoma pathogenesis, we overexpressed either activated human *ALK* or human *ALKWT* in MYCN fish. For this experiment, we coinjected the following constructs into the one-cell stage of MYCN transgenic and control embryos: (1) *dβh-ALKF1174L* with *dβh-mCherry*; (2) *dβh-ALKWT* with *dβh-mCherry*; or (3) *dβh-mCherry* alone. We have shown that this

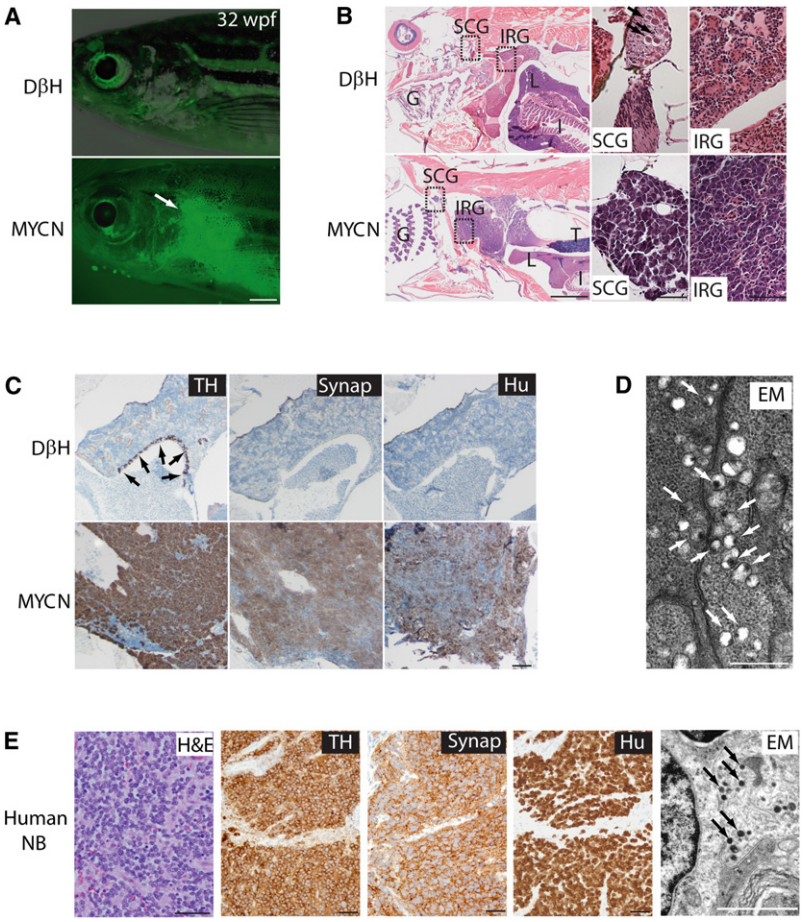

Figure 2. Neuroblastomas Arise in *MYCN*-Expressing Transgenic Zebrafish

(A) Top: DβH fish. Bottom: MYCN fish with EGFP-expressing tumor (arrow) at 32 weeks postfertilization (wpf). Scale bar represents 1 mm.

(B) Top: H&E-stained sagittal sections of DβH fish. Boxes indicate the SCG and the IRG, and are magnified in the right panels. Bottom: H&E-stained sagittal sections of MYCN fish with neuroblastic tumors. Boxes indicate the SCG and the IRG and are magnified in the right panels. Arrows indicate SCG neurons. The majority of tumors arise in the IRG of MYCN fish, although as seen in this example, tumor cells in the SCG were occasionally observed in individual fish that also had tumors in the IRG. G, gill; L, liver; I, intestine; IRG, interregnal gland; SCG, superior cervical ganglion; T, testis. Scale bars represent 50 μm.

(C) Top: Sagittal sections through the interregnal gland of DβH fish. Chromaffin cells of the interregnal gland express TH (arrows). Bottom: Sagittal sections through the interregnal gland of a MYCN fish with EGFP-expressing tumor. Cells throughout the tumor in the interregnal gland express TH, Synaptophysin (Synap), and Hu. Scale bar represents 100 μm.

(D) Electron microscopy (EM) reveals neurosecretory granules in the *MYCN*-expressing tumors (arrows). Scale bar represents 500 nm.

(E) Pathological, immunohistochemical, and ultrastructural analyses of a human neuroblastoma. Arrows point to neurosecretory granules. Scale bars represent 500 μm (left panel), 100 μm (middle panels), and 2 μm (right panel), respectively. See also Figure S2.

coinjection strategy results in cointegration into DNA and coexpression of the two coinjected transgenes as mosaics in a subset of cells in ~50% of the injected embryos (Langenau et al., 2008). Thus, the expression of mCherry served as a marker for the coexpression of *ALK* in tissues of the mosaic primary injected animals. When these animals were monitored for the tumor onset, neuroblastomas were not observed in any of the siblings that did not inherit the *MYCN* transgene and were injected with either the *ALKWT* or *ALKF1174L* transgenes, emphasizing that overexpression of *MYCN* is required for tumorigenesis in this model. Eight tumors arose by 9 wpf in the MYCN fish coinjected with *dβh-ALKF1174L* and *dβh-mCherry* (Figures 3B and S3A), whereas none were observed by 9 wpf in the MYCN line coinjected with *dβh-ALKWT* and *dβh-mCherry* ($p = 0.002$; Figures 3B and S3B) or with *dβh-mCherry* alone ($p = 0.007$; Figures 3B and S3C). In addition, four tumors in the MYCN line coinjected with *dβh-ALKWT* and *dβh-mCherry* and five tumors in the MYCN line injected with *dβh-mCherry* alone were identified after 11 wpf (Figure 3B), similar to the time of tumor onset in the uninjected MYCN line (Figure 3A). These findings show that activated ALK cooperates with *MYCN* overexpression to accelerate the onset of neuroblastoma, regardless of the integration site in individual mosaic animals, and that overexpression of *ALKWT* at the levels driven by the *dβh* promoter does not appear to collaborate with MYCN to induce neuroblastoma in this model system.

MYCN-Induced Loss of Sympathoadrenal Cells

To investigate the cellular basis for MYCN-induced neuroblastoma and its modification by constitutively activated ALK, we examined the development of sympathoadrenal cells in (1) DβH; (2) MYCN; (3) ALK; and (4) MYCN;ALK transgenic fish during the embryonic and larval stages. During normal development, PSNS cells arise from the neural crest and migrate ventrally to locations adjacent to the dorsal aorta (Huber, 2006). After forming the superior cervical ganglia, a subset of sympathoadrenal cells migrate further to invade the mesonephros and differentiate to form chromaffin cells in the interrenal gland (An et al., 2002; Huber, 2006; Stewart et al., 2004). We identified cells of the developing superior cervical ganglia at 80 hr postfertilization (hpf) in living DβH transgenic fish and in whole-mount in situ hybridization preparations with *dbh*- and *th*- riboprobes (Figure 4A), indicating that EGFP expression in the developing embryonic PSNS of this transgenic line recapitulates the normal endogenous expression patterns of *dβh* and *th* (Figure 4A). By 80 hpf, EGFP was apparent in the superior cervical ganglia, as well as in non-PSNS dopaminergic neurons, such as the medulla oblongata and cranial ganglia (Figure 4A). By contrast, most MYCN transgenic embryos (~80%) failed to express a detectable level of EGFP fused to human *MYCN* in the superior cervical ganglia at 80 hpf, even though the fusion protein was clearly expressed in non-PSNS tissues (Figure 4B),

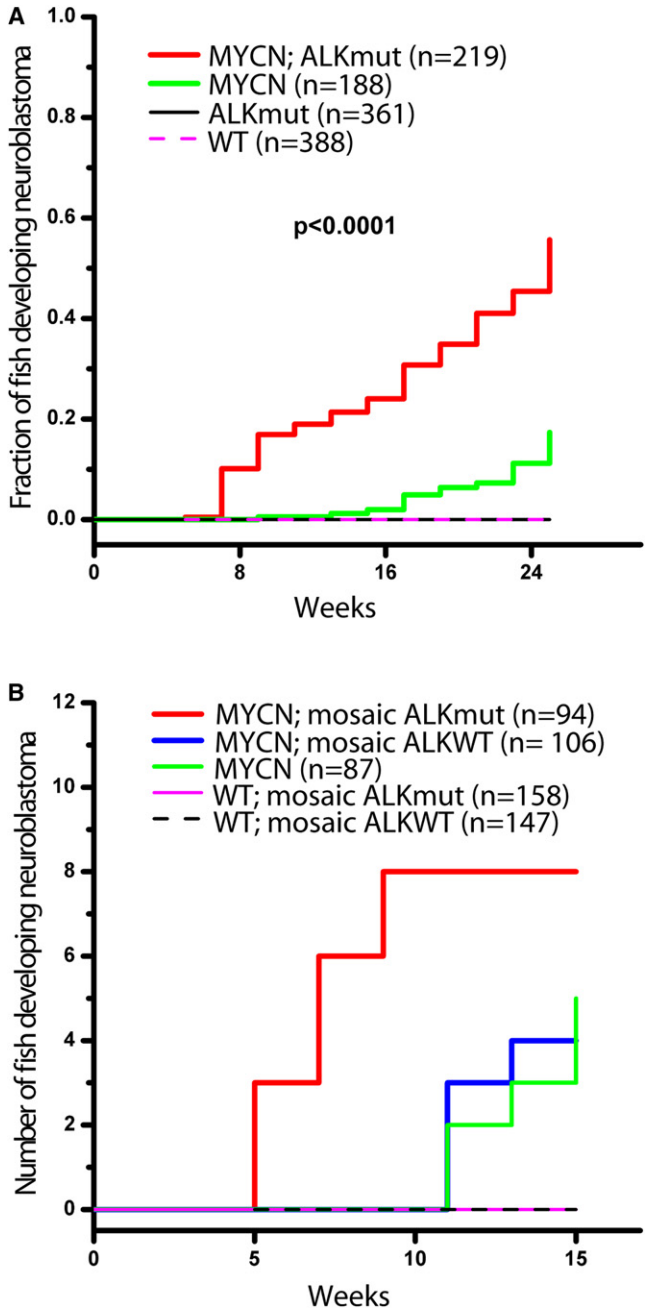

Figure 3. Activated ALK Accelerates Disease Onset and Increases the Penetrance of MYCN-Induced Neuroblastoma

(A) Cumulative frequency of neuroblastoma in stable transgenic zebrafish by Kaplan-Meier analysis. ALKmut represents stable transgenic fish expressing the *ALK (F1174L)* transgene. WT, wild-type.

(B) Onset of neuroblastoma in MYCN transgenic fish or wild-type (WT) fish as mosaics coinjected with the following DNA constructs: (1) *dβh-ALKF1174L* and *dβh-mCherry* (mosaic ALKmut); (2) *dβh-ALKWT* and *dβh-mCherry* (mosaic ALKWT); or (3) *dβh-mCherry* alone. The difference between tumor onset by 9 wpf in the MYCN fish coinjected with *dβh-ALKF1174L* and *dβh-mCherry* (MYCN; mosaic ALKmut) and that in the MYCN line coinjected with *dβh-ALKWT* and *dβh-mCherry* (MYCN; mosaic ALKWT) or *dβh-mCherry* alone (MYCN) is significant at p = 0.002 and p = 0.007, respectively, with two-tailed Fisher exact test. See also Figure S3.

and in most animals, the absence of detectable sympathoadrenal cells persisted through 10 dpf (Figure S4C). The lack of EGFP expression is consistent with the markedly reduced numbers of sympathoadrenal cells in MYCN embryos indicated by the loss of cells with endogenous *th* and *dβh* RNA expression by whole-mount in situ hybridization (Figures 4B versus 4A). Because *th* and *dβh* are markers for differentiated sympathoadrenal cells, the absence of cells expressing *EGFP-MYCN* under control of the *dβh* promoter could reflect either *MYCN*-induced apoptosis or an arrest in sympathoadrenal progenitor cell differentiation.

To distinguish between these possibilities, we first performed TUNEL and anti-activated Caspase-3 staining on sections of 36, 51, and 72 hpf MYCN versus DβH transgenic fish. We found no evidence of TUNEL- or anti-activated Caspase-3-positive cells in the superior cervical ganglia or regions where sympathoadrenal cells would be expected to form (Figure S5; data not shown), suggesting that the absence of detectable sympathoadrenal cells is not due to cell death, but rather to a failure to initiate the PSNS developmental program at this early time in development. To test this possibility, we performed whole-mount in situ hybridization at 54 hpf and 80 hpf for expression of the *phox2b*, *zash1a*, and *AP-2 alpha* (*tfap2a*) genes, which encode transcription factors required for sympathoadrenal cell specification and maintenance (Figure 5) (Guillemot et al., 1993; Lucas et al., 2006; Pattyn et al., 1999). Each of these sympathoadrenal cell progenitor markers was readily detectable in the superior cervical ganglia region of control embryos, but undetectable in MYCN transgenic embryos at these stages, indicating that specification of the earliest identifiable sympathoadrenal cell progenitors was blocked by expression of the *EGFP-MYCN* fusion gene. The suppression of sympathoadrenal cell development by *EGFP-MYCN* appears to be tissue-specific, because expression of the *EGFP-MYCN* by non-PSNS dopaminergic neuronal cells in these embryos was largely unaffected, including expression by cells of the locus coeruleus, medulla oblongata, and cranial ganglia (Figures 4B versus 4A and S4C).

To investigate the possibility that neuroblastoma might arise from residual EGFP-MYCN+ sympathoadrenal cells that can be identified at 3 dpf in ~20% of the transgenic embryos, we analyzed these embryos in more detail at 5 dpf. At this time, neurons of the superior cervical ganglia in control DβH transgenic fish express EGFP and are both TH^+ and Hu+ (arrows in Figure S4A), whereas chromaffin cells lose Hu expression as they differentiate into chromaffin cells, reflecting a loss of their neuronal phenotype (arrowheads in Figure S4A). Interestingly, the small populations of EGFP+ cells observed in the superior cervical ganglia of MYCN animals were heterogeneous in their immunoreactivity patterns, including cells that were TH^+/Hu− (arrowheads in Figure S4B), TH−/Hu− (double arrowheads in Figure S4B), or TH^+/Hu+ (data not shown). However, these residual cells did not appear to contribute to neuroblastoma development, as there was no difference in the time of disease onset in the 20% of fish that had small numbers of residual cells at 5 dpf compared to the majority of MYCN transgenic fish, which lacked detectable cells in the superior cervical ganglia (Table S1).

Expression of mutant *ALK F1174L* in ALK transgenic fish did not affect the development of sympathoadrenal cells, as shown

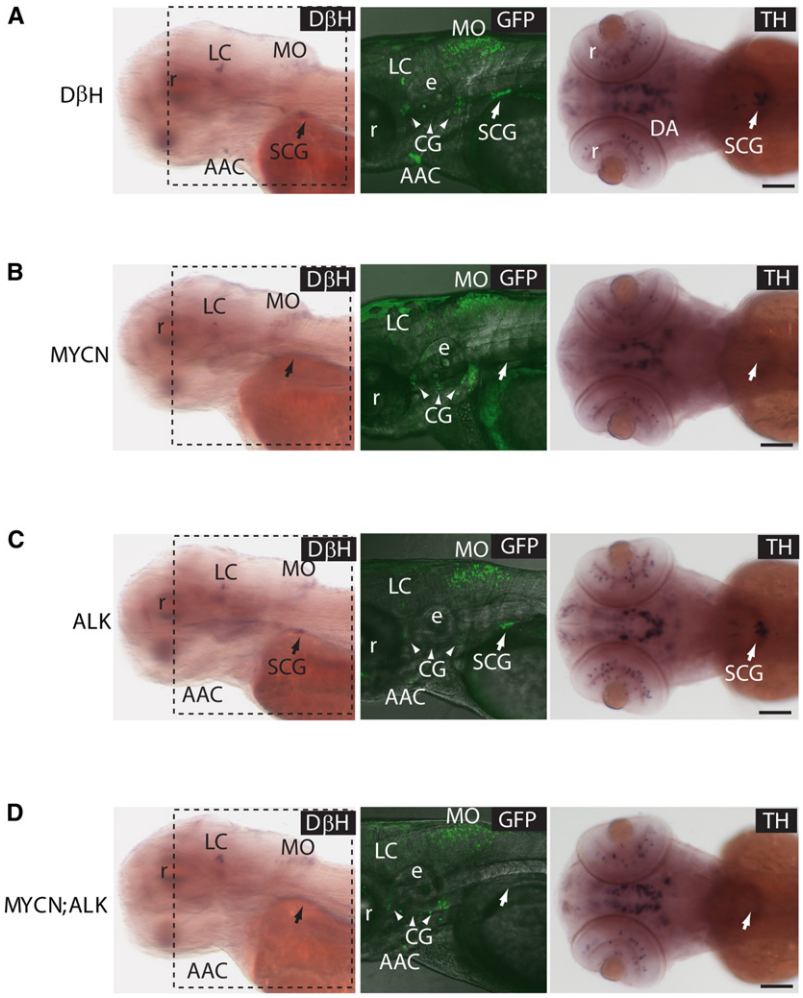

Figure 4. *MYCN* Expression Causes Sympathoadrenal Cell Loss

(A) DβH transgenic line. Oblique views of *dβh* RNA expression (left panels); lateral views of EGFP expression in merged confocal-brightfield images (middle panels); dorsal views of *th* RNA expression (right panels). Arrows point to the SCG, and arrowheads point to the CG. Scale bar represents 100 μm.

(B) MYCN transgenic line. *MYCN* expression causes loss of cells in the SCG (arrows). Scale bar represents 100 μm.

(C) ALK transgenic line. *ALK* expression does not interfere with the SCG development (arrows). Scale bar represents 100 μm.

(D) MYCN;ALK transgenic line. Loss of cells in the SCG is not rescued by activated *ALK* expression (arrows). Scale bar represents 100 μm. AAC, arch-associated catecholaminergic neurons; CG (arrowheads), cranial ganglia; DA, diencephalic dopaminergic neurons; e, ear; LC, locus coeruleus; MO, medulla oblongata; r, retina; SCG, superior cervical ganglion. See also Figure S4 and Table S1.

by EGFP fluorescence and expression of the *th* and *dβh* RNAs (Figures 4C and S4C). Furthermore, the expression of activated *ALK* in the presence of *MYCN* in MYCN;ALK transgenic embryos did not rescue the loss of sympathoadrenal cells observed in the MYCN transgenic embryos (Figures 4D and S4C). Thus, although activated ALK clearly cooperates with MYCN in tumorigenesis, this interplay does not depend on any ability of ALK to reverse the pronounced MYCN-induced suppression of sympathoadrenal cell development during early embryonic and larval stages.

Hyperplasic Hu+ Cells in the Interrenal Gland

Analysis of the PSNS during the first 10 days of life in MYCN transgenic zebrafish revealed the profound capacity of high level of MYCN to suppress the development of sympathoadrenal cells, but did not provide any insight into why these transgenic fish developed neuroblastoma. Because the first tumors arose in MYCN;ALK transgenic fish between 5–7 wpf, we examined the interrenal gland of MYCN transgenic zebrafish beginning at 3 wpf to identify the cells that give rise to neuroblastoma. In DβH control animals, we observed GFP+/Hu+/TH$^+$ neuroblast cells in both the mediolateral (Figure 6A) and lateral regions of the developing interrenal gland (Figure S6). The number of Hu+ neuroblasts quantified from sections through both interrenal gland regions remained low between 3–7 wpf (Figure 6B); Hu+ cell numbers in ALK transgenic fish were comparable to those in controls (Figure 6B). By contrast, the numbers of Hu+ neuroblasts were significantly increased in MYCN transgenic fish, as compared to those in controls at 3 wpf (Figure 6B, $p = 0.03$). In 9 of 16 MYCN transgenic fish examined, the numbers of Hu+ neuroblasts were markedly increased at 5 wpf (Figures 6A and 6B, $p = 0.004$). However, at 7 wpf, 11 of 16 MYCN fish lacked detectable Hu+ neuroblasts in the interrenal gland (Figure 6B), indicating that during this 2-week period these cells were either eliminated or had differentiated, thus losing their expression of the neuronal marker Hu. In MYCN;ALK compound transgenic fish the numbers of Hu+ cells also increased during the 3- to 5-week period, but in contrast to transgenic fish expressing *MYCN* alone, the Hu+ cell numbers continued to increase in 6 of 12 fish at 7 wpf (Figure 6B, $p = 0.03$). Thus, Hu+ cells continue to expand in only a small fraction of transgenic animals expressing *MYCN* alone after 5 wpf, whereas a much higher fraction of the double transgenic MYCN;ALK animals showed progressive expansion of Hu+ cells, mirroring the much higher fraction of these animals that develop fully transformed neuroblastoma (Figure 3A).

To assess the effects of *MYCN* and activated *ALK* expression on the differentiation of Hu+, TH$^+$ neuroblast into Hu−, TH$^+$ adrenal chromaffin cells, we quantified the numbers of Hu−, GFP+ cells within the interrenal gland of each of the zebrafish lines over time. We found increasing numbers of these cells between 3–7 wpf in both control DβH and ALK transgenic zebrafish, indicating the differentiation of the Hu+ neuroblast precursors into chromaffin cells (Figures 7A–7C). By contrast, the Hu−, GFP+ chromaffin cells did not increase normally and remained at very low levels between 3–7 wpf in *MYCN*-overexpressing fish relative to control animals, regardless of whether

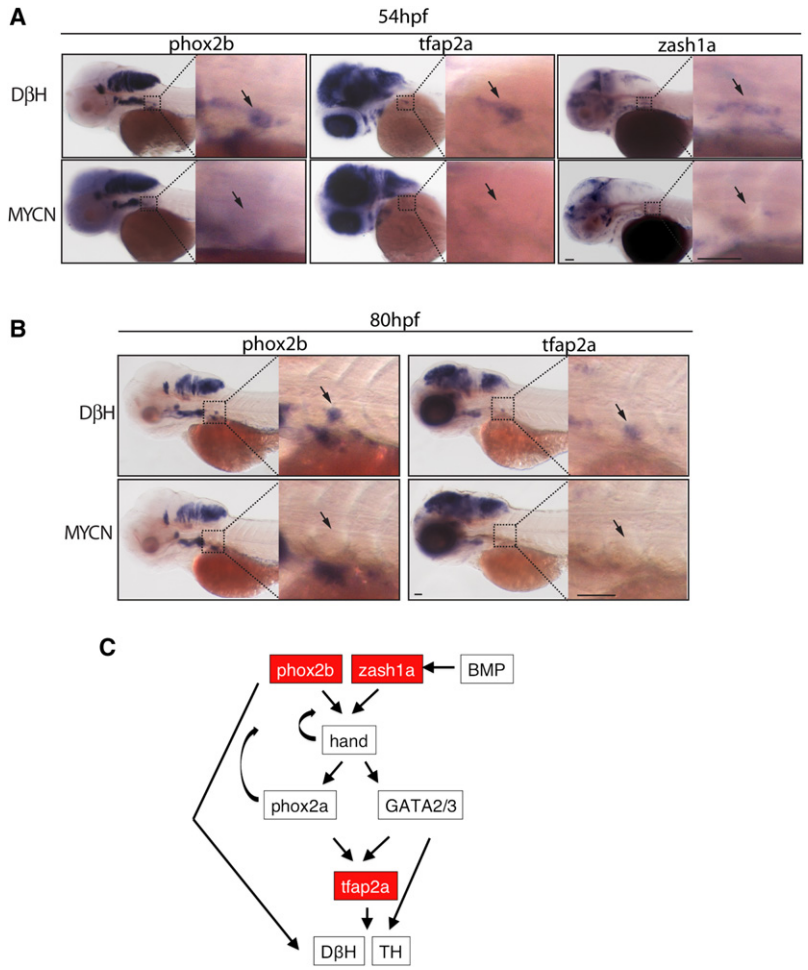

Figure 5. Expression of Early Sympathoadrenal Markers Is Absent in MYCN Transgenic Embryos during Early Development

(A and B) Top panels: DβH; lower panels: MYCN transgenic fish. Expression of sympathoadrenal cell markers at 54 hpf (A) and 80 hpf (B). The magnified view of the boxed region is shown on the right. Arrows point to the superior cervical ganglion. Scale bars represent 50 μm (left panels) and 100 μm (right panels, magnified view).

(C) Diagram of the genetic interactions of sympathoadrenal genes during early development. Arrows indicate the activation of target genes. Curved arrows indicate positive feedback regulation. See also Figure S5.

the fish also expressed the activated *ALK* transgene (Figures 7A–7C). At 7 wpf, we identified two MYCN transgenic fish and two MYCN;ALK fish with some expansion of Hu−/TH$^+$ chromaffin cells (Figure 7C). Thus, in a small subset of *MYCN*-overexpressing fish, the sympathoadrenal cells manage to differentiate, lose the Hu neuronal marker and expand at 7 weeks of age despite activated *ALK* overexpression. The chromaffin cell expansion seems to be self-limited, because all of the tumors that arise in these fish express the Hu pan-neuronal marker (Figures 2C and S2C).

To determine whether the loss of Hu+ cells in the transgenic fish expressing *MYCN* alone between 5–7 wpf was due to apoptotic cell death, we assessed the expression of activated Caspase-3 as an indicator of apoptotic cell death. An important difference was observed at 5.5 wpf: transgenic fish expressing *MYCN* alone showed significant numbers of apoptotic cells coexpressing Hu and activated Caspase-3 (Figures 8B, 8C and S7C), providing the basis for the profound loss of these cells by 7 wpf. By contrast, in *MYCN*;*ALK* transgenic fish, we rarely observed apoptotic cells expressing both Hu and activated Caspase-3 (Figures 8B, 8C and S7D), consistent with the continued increase in Hu+ cell numbers at 7 wpf in this group (Figure 6B). Neuroblastomas that develop in MYCN transgenic animals coexpress GFP, TH, and Hu, regardless of whether the animals also express the activated *ALK* transgene. Thus, the expanding neuroblast cell populations that we identified at 7 wpf in MYCN transgenic animals appear to give rise to fully transformed tumors a few weeks later, and a fraction of the fish with these hyperplastic precursors was markedly increased by coexpression of activated *ALK*, accounting for the increased penetrance of neuroblastoma in the compound transgenic line (Figure 3A). Taken together, these findings indicate that overexpression of *MYCN* prevents the differentiation of neuroblast precursors into adrenal chromaffin cells, and induces a developmentally-timed apoptotic response at 5.5 wpf in most MYCN transgenic fish. However, concomitant expression of activated *ALK* in these cells promotes cell survival without altering the MYCN-induced block in differentiation, resulting in the continued accumulation of Hu+ neuroblasts that culminates in the development of highly penetrant, fully transformed neuroblastoma.

DISCUSSION

Early in the embryogenesis of our transgenic zebrafish, *MYCN* overexpression results in a profound loss of neural crest-derived cells within the sympathoadrenal cell lineage. Nevertheless, these animals can develop neuroblastoma, and both the onset and penetrance of the disease are markedly enhanced by coexpression of a transgene encoding the activated *ALK* receptor tyrosine kinase. Thus, our zebrafish model clearly demonstrates a synergistic relationship between these two genes in neuroblastoma pathogenesis. Using multiparameter confocal microscopy and immunohistochemistry to examine embryos throughout early development, we show that MYCN-induced neuroblastoma does not arise from the earliest cells populating the superior cervical ganglia (3–6 dpf), but rather from neuroblasts that migrate into the interrenal gland later in development (~21 dpf), after the kidney has developed. The interrenal gland is the zebrafish equivalent of the human adrenal gland, and sympathoadrenal precursors in the interrenal gland coexpress neuronal-specific Hu proteins and the catecholaminergic enzymes TH and Dβh. The interrenal gland origin

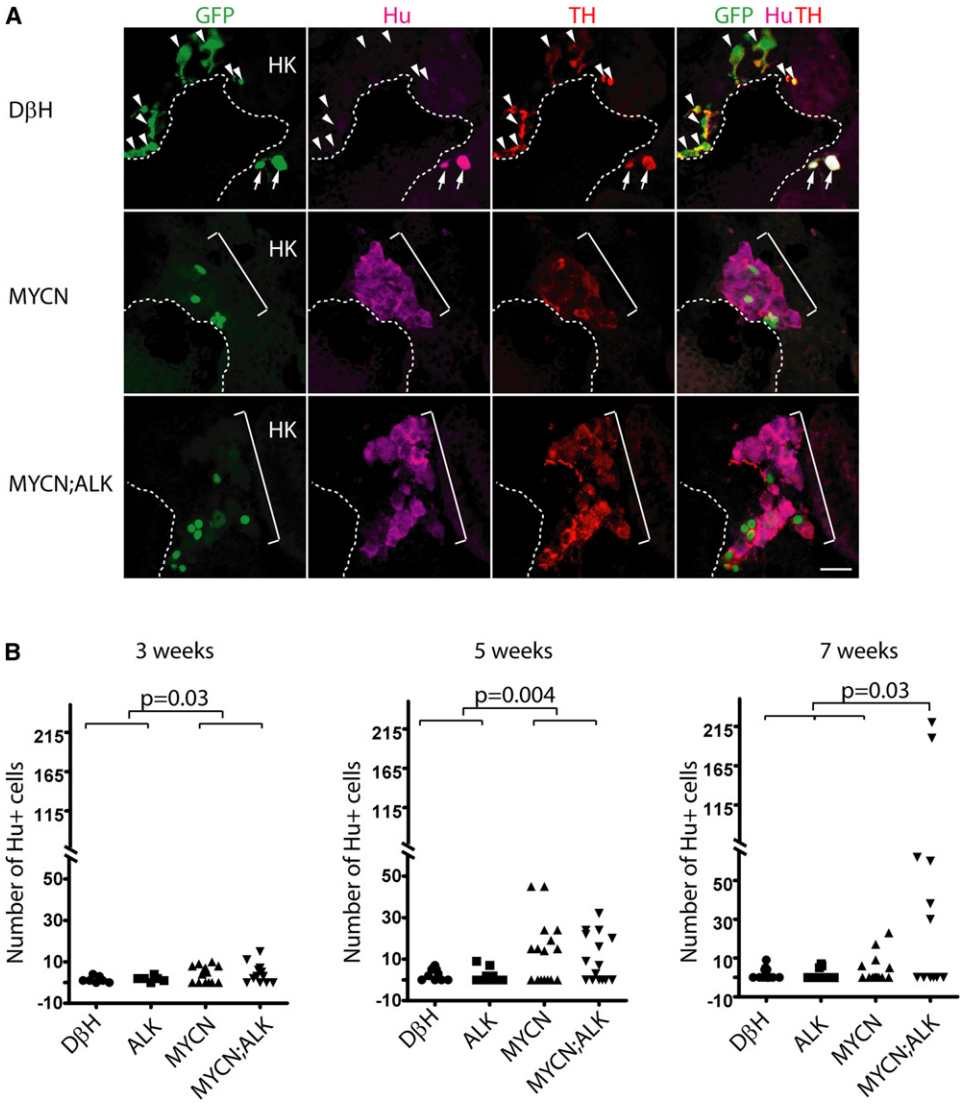

Figure 6. MYCN Causes Hu+ Cell Hyperplasia in the Interrenal Gland

(A) Sagittal sections through the interrenal gland in DβH (top panels), MYCN (middle panels), and MYCN;ALK (lower panels) transgenic fish at 5wpf (dorsal up, anterior left). EGFP, green; Hu, magenta; TH, red. Representative sections through the interrenal gland in DβH fish contain three to five GFP+/Hu+/TH$^+$ sympathetic neuroblasts (arrows) and many GFP+/Hu−/TH$^+$ chromaffin cells (arrowheads). Hu+ cell numbers increase in MYCN and MYCN;ALK fish (brackets), and can be GFP+ and TH$^+$. Dotted lines indicate the head kidney (HK) boundary. Scale bar represents 20 μm.

(B) Numbers of Hu+ interrenal gland cells in DβH, ALK, MYCN, and MYCN;ALK transgenic fish at 3, 5, and 7 weeks. Means of Hu+ cell numbers were compared by the two-tailed Wilcoxon signed-rank test. See also Figure S6.

of neuroblastoma in zebrafish recapitulates the adrenal medullary site of origin observed in ~50% of the children with this tumor (Janoueix-Lerosey et al., 2010), in contrast to the murine *MYCN* transgenic model, where tumors arise from hyperplastic neuroblasts predominately in the sympathetic cervical ganglia complex and the superior cervical ganglia (Alam et al., 2009; Hansford et al., 2004). In the study by Hansford et al. (2004), these hyperplastic neuroblasts regressed due to apoptotic cell death in normal and hemizygous transgenic animals, but frequently progressed to fully transformed neuroblastoma in homozygous transgenic animals. The similarities and differences between the murine and zebrafish transgenic models afford complementary opportunities to investigate mechanisms underlying sympathoadrenal cell transformation within the distinct anatomical locations that comprise the PSNS.

Using the zebrafish model, we now show that expression of aberrantly activated *ALK* potentiates the oncogenic effects of MYCN by blocking the apoptotic death of *MYCN*-overexpressing sympathoadrenal neuroblasts. The death of these cells occurs within a well-defined developmental window, 5.5 wpf, indicating that although overexpression of *MYCN* causes aberrant expansion of these cells from 3 to 5 wpf, it also triggers an apoptotic response at 5.5 wpf. By monitoring the appearance of more differentiated adrenal chromaffin cell numbers in animals

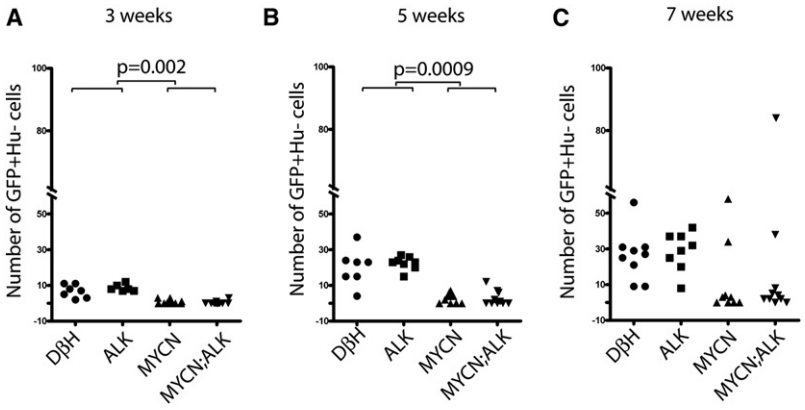

Figure 7. *MYCN* Expression Blocks Chromaffin Cell Differentiation in the Interrenal Gland

Numbers of GFP+/Hu− chromaffin cells in the interrenal gland in DβH, ALK, MYCN, and MYCN;ALK transgenic fish at 3 weeks (A), 5 weeks (B), and 7 weeks (C). Means of GFP+/Hu− cell numbers were compared by the two-tailed Wilcoxon signed-rank test.

of each genotype, we show that these *MYCN*-overexpressing neuroblasts fail to differentiate, resulting in reduced numbers of Hu−, TH^+, Dβh+ chromaffin cells. The MYCN-induced apoptotic response in these cells does not seem to result from the types of constitutive MYC- or MYCN-induced apoptotic signaling that has been described by others (Fanidi et al., 1992; Finch et al., 2006; Nilsson and Cleveland, 2003), because the *MYCN*-overexpressing immature neuroblasts in our transgenic fish do not undergo apoptosis during their expansion to 5 wpf. Rather, the apoptotic death of these cells appears to result from a conflict between aberrant proliferative signals emanating from overexpressed *MYCN* and other developmentally timed signals that specify chromaffin cell fate. Thus, activated ALK provides a cell survival signal that blunts the apoptotic response of *MYCN*-overexpressing neuroblasts at this juncture in development, but does not restore the ability of these cells to differentiate. For the 17% of MYCN-only transgenic fish that develop tumors, it is likely that additional genetic alterations cooperate with this oncogene to contribute to neuroblastoma transformation. Nevertheless, we did not detect somatic missense mutations within the tyrosine kinase domain of the zebrafish *alk*

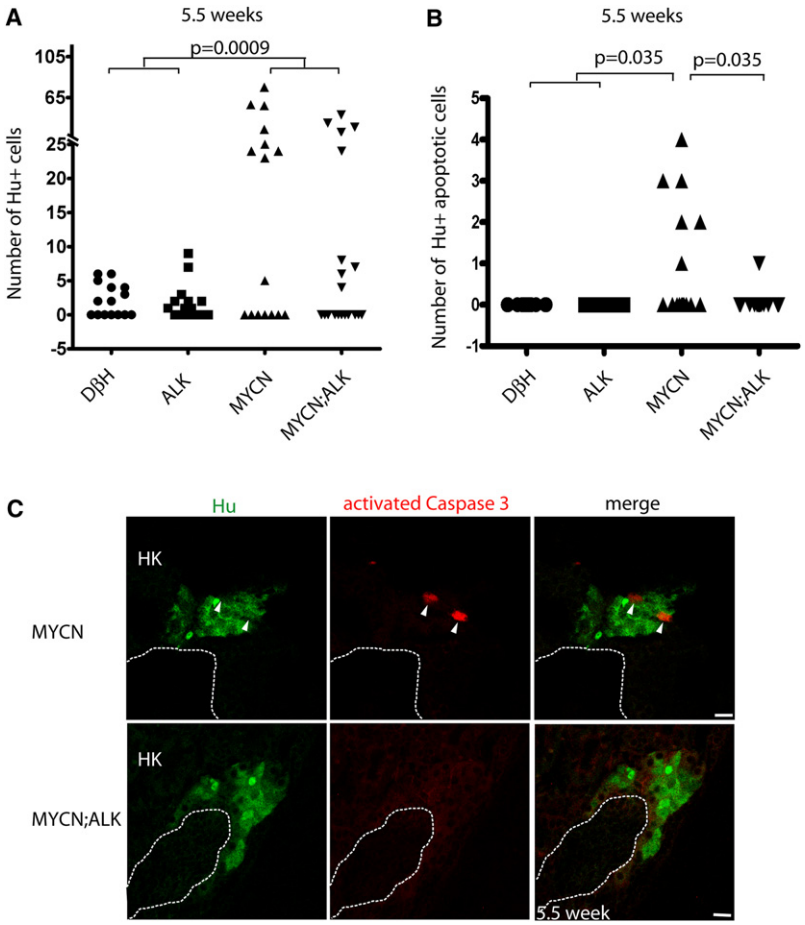

Figure 8. ALK Inhibits a Developmentally-Timed Apoptotic Response Triggered by *MYCN* Overexpression in the Interrenal Gland

(A) Numbers of Hu+ interrenal gland cells in the DβH, ALK, MYCN, and MYCN;ALK fish at 5.5 wpf. Means of Hu+ cell numbers were compared by the two-tailed Wilcoxon signed-rank test.

(B) Numbers of apoptotic Hu+ interrenal gland cells in the DβH, ALK, MYCN, and MYCN;ALK fish at 5.5 wpf. The numbers of transgenic fish at 5.5 wpf with apoptotic Hu+ cells in the interrenal gland were compared by two-tailed Fisher exact test.

(C) Sagittal sections through the interrenal gland in MYCN (top panels) and MYCN;ALK (bottom panels) transgenic fish at 5.5 wpf (dorsal up, anterior left). Hu, green; activated Caspase-3, red. Hu+, activated Caspase-3+ apoptotic cells were detected in the MYCN transgenic fish (arrowheads). Dotted lines indicate the head kidney (HK) boundary. Scale bars represent 10 μm. See also Figure S7.

gene in ten tumors from MYCN-only transgenic fish, or a loss of *capsase-8* expression, which has been implicated in the pathogenesis of human neuroblastoma with *MYCN* amplification. Thus, mutations or epigenetic events that activate prosurvival pathways other than those mediated by *alk* activation or *capsase-8* loss of function appear to interact with *MYCN* overexpression in these tumors.

The mutant *ALK (F1174L)* gene that we expressed in our zebrafish model has not been observed in the germline of human patients with familial neuroblastoma. This suggests that it may generate signals that are incompatible with normal human embryogenesis, making it more potent than the *R1275Q* mutation, the most common heritable mutation in familial neuroblastoma. In our transgenic zebrafish model, the *ALK (F1174L)* mutation is tolerated in the germline, presumably because it is driven in a tissue-specific manner in sympathoadrenal cells by the *dβh* promoter. In our model system, overexpression of *MYCN* is required for the development of neuroblastoma and activated *ALK* expression is not sufficient, even though germline mutations of *ALK* can function as an initiating event in human neuroblastoma, and these tumors may or may not have *MYCN* amplification (Mossé et al., 2008). Further study in the zebrafish model will be required to determine whether mutational events other than *MYCN* overexpression can cooperate with activated ALK to induce neuroblastoma.

The potent anti-apoptotic effect of activated *ALK* expression combined with *MYCN* overexpression might be expected to mediate greater resistance to drug-induced apoptosis and a poorer outcome for patients whose tumors have both amplified *MYCN* and an activating *ALK* mutation. This prediction gains support from a recent meta-analysis of *ALK* mutations in childhood neuroblastoma with *MYCN* amplification, which showed that the mutant *ALK (F1174L)* gene is expressed in a high proportion of childhood tumors with *MYCN* amplification, and that these children have an especially poor outcome (De Brouwer et al., 2010). A new ALK small molecule inhibitor, crizotinib (PF-02341066), has produced encouraging results in a recently completed phase II trial for patients with non-small-cell lung cancer that harbors activating *ALK* rearrangements, including *EML4-ALK or RANBP2-ALK* (Butrynski et al., 2010; Kwak et al., 2010; Sasaki et al., 2010), and has been approved by the FDA for use in patients with such tumors. A phase I trial of the same inhibitor was recently initiated in children with solid tumors, including those with neuroblastoma harboring either mutated or amplified *ALK*. Despite these advances, a recent report indicates that the *ALK (F1174L)* mutation confers resistance to crizotinib (Sasaki et al., 2010), which will likely interfere with the activity of this drug against neuroblastomas harboring this mutation. We suggest that the zebrafish model described in this article will provide a useful platform for testing alternative small molecule inhibitors of *F1174L*-activated *ALK*, or key targets within its downstream pathways, to improve the treatment of this aggressive form of childhood neuroblastoma.

EXPERIMENTAL PROCEDURES

Zebrafish

Zebrafish were the AB background strain. Embryos were staged according to Kimmel et al. (1995). All zebrafish studies and maintenance of the animals were in accord with Dana-Farber Cancer Institute IACUC-approved protocol #02-107.

DNA Constructs for Transgenesis

The 5.2-kb promoter region of the *dβh* gene was amplified by PCR from a zebrafish BAC clone and subcloned into vectors to drive the expression of several genes, including *Tg(dβh:EGFP)*, *Tg(dβh:EGFP-MYCN)*, and *Tg(dβh:EGFP;dβh:ALKF1174L)* in tissues normally expressing the *dβh* gene. Embryos were injected with these DNA constructs at the one-cell stage and grown to adulthood. Fin clips from the offspring were genotyped for the stable integration and germline transmission of the transgenes. The *Tg(dβh:EGFP)*, *Tg(dβh:EGFP-MYCN)*, and *Tg(dβh:EGFP;dβh:ALKF1174L)* zebrafish lines are designated the "DβH," "MYCN," and "ALK" transgenic line in this article, respectively.

Tumor Watch of Transgenic Fish

MYCN and ALK heterozygous transgenic fish were crossed, and offspring were screened every 2 weeks starting from 5 wpf for fluorescent EGFP-expressing cell masses indicative of tumors. In addition, for Figure 3B, either activated human *ALK* or wild-type human *ALK* (*ALKWT*) were overexpressed in MYCN fish as mosaics by coinjecting the following constructs into the one-cell stage of MYCN transgenic and control embryos: (1) *dβh-ALKF1174L* with *dβh-mCherry*; (2) *dβh-ALKWT* with *dβh-mCherry*; or (3) *dβh-mCherry* alone. The primary injected embryos were raised and monitored for the onset of tumorigenesis as described above. Fish with tumors were separated and analyzed further by H&E staining and immunohistochemical assays.

RNA In Situ Hybridization, Cryosectioning, Paraffin Sectioning, and Immunostaining

RNA in situ hybridization assays were performed according to Thisse and Thisse (Thisse and Thisse, 2008). Constructs for making RNA probes to detect *dβh*, *th*, *phox2b*, and *tfap2a* expression have been described (Stewart et al., 2006). Fish were fixed with 4% paraformaldehyde and embedded in agar/sucrose or paraffin blocks for cryosectioning or paraffin sectioning, respectively. Sections were immunostained by conventional protocols (Macdonald, 1999) using antibodies against GFP, TH, Hu, Synaptophysin, and ALK.

Electron Microscopy and Imaging

Transmission electron microscopy (TEM) of tumor cells was carried out at the Harvard Medical School EM Facility with a Tecnai G^2 Spirit BioTWIN scope equipped with an AMT 2k CCD camera. A Zeiss LSM 510 META confocal microscope and Leica SP5X Laser Scanning Confocal Microscope were used to capture fluorescent images at high magnification, and a Leica M420 stereoscopic microscope captured bright field and low-magnification fluorescent images. Images were processed with Leica LAS AF Lite, Improvision Openlab v5 and Adobe Photoshop software.

Additional methods are presented in Supplemental Experimental Procedures.

ACCESSION NUMBERS

The GenBank accession number for the *dβh* promoter sequence reported in this paper is JQ727685.

SUPPLEMENTAL INFORMATION

Supplemental Information includes seven figures, one table, and Supplemental Experimental Procedures and can be found with this article online at doi:10.1016/j.ccr.2012.02.010.

ACKNOWLEDGMENTS

This work was supported by a grant CA104605 from the National Cancer Institute, NIH (A.T.L.), a Young Investigator Award from Children's Tumor Foundation and Neuroblastoma Foundation (J.S.L.), a fellowship from the Friends for Life (S.Z., R.E.G.), a fellowship from the Hope Street Kids Foundation (J.S.L.), a fellowship from Durand Family Fund for Pediatric Neuroblastoma Research (J.S.L.), a fellowship from the David A. Abraham Fund and Pediatric Low Grade

Astrocytoma Foundation (J.S.), an award K99CA134743 from the National Cancer Institute, NIH (H.F.), an award R00 NS058608 from NIH/NINDS (R.A.S.), and a grant from the National Institutes of Health and the Children's Oncology Group (R.E.G.). We thank John Gilbert for editing the manuscript and critical comments, and Greg Molind, Lu Zhang, Derek Walsh, and John P. Lyons for excellent care of our zebrafish facility.

Received: May 26, 2011
Revised: November 23, 2011
Accepted: February 7, 2012
Published: March 19, 2012

REFERENCES

Alam, G., Cui, H., Shi, H., Yang, L., Ding, J., Mao, L., Maltese, W.A., and Ding, H.F. (2009). MYCN promotes the expansion of Phox2B-positive neuronal progenitors to drive neuroblastoma development. Am. J. Pathol. *175*, 856–866.

An, M., Luo, R., and Henion, P.D. (2002). Differentiation and maturation of zebrafish dorsal root and sympathetic ganglion neurons. J. Comp. Neurol. *446*, 267–275.

Brodeur, G.M. (2003). Neuroblastoma: biological insights into a clinical enigma. Nat. Rev. Cancer *3*, 203–216.

Butrynski, J.E., D'Adamo, D.R., Hornick, J.L., Dal Cin, P., Antonescu, C.R., Jhanwar, S.C., Ladanyi, M., Capelletti, M., Rodig, S.J., Ramaiya, N., et al. (2010). Crizotinib in ALK-rearranged inflammatory myofibroblastic tumor. N. Engl. J. Med. *363*, 1727–1733.

Chen, Y., Takita, J., Choi, Y.L., Kato, M., Ohira, M., Sanada, M., Wang, L., Soda, M., Kikuchi, A., Igarashi, T., et al. (2008). Oncogenic mutations of ALK kinase in neuroblastoma. Nature *455*, 971–974.

Chesler, L., and Weiss, W.A. (2011). Genetically engineered murine models—contribution to our understanding of the genetics, molecular pathology and therapeutic targeting of neuroblastoma. Semin. Cancer Biol. *21*, 245–255.

Chiarle, R., Voena, C., Ambrogio, C., Piva, R., and Inghirami, G. (2008). The anaplastic lymphoma kinase in the pathogenesis of cancer. Nat. Rev. Cancer *8*, 11–23.

De Brouwer, S., De Preter, K., Kumps, C., Zabrocki, P., Porcu, M., Westerhout, E.M., Lakeman, A., Vandesompele, J., Hoebeeck, J., Van Maerken, T., et al. (2010). Meta-analysis of neuroblastomas reveals a skewed ALK mutation spectrum in tumors with MYCN amplification. Clin. Cancer Res. *16*, 4353–4362.

Fanidi, A., Harrington, E.A., and Evan, G.I. (1992). Cooperative interaction between c-myc and bcl-2 proto-oncogenes. Nature *359*, 554–556.

Finch, A., Prescott, J., Shchors, K., Hunt, A., Soucek, L., Dansen, T.B., Swigart, L.B., and Evan, G.I. (2006). Bcl-xL gain of function and p19 ARF loss of function cooperate oncogenically with Myc in vivo by distinct mechanisms. Cancer Cell *10*, 113–120.

George, R.E., Sanda, T., Hanna, M., Fröhling, S., Luther, W., 2nd, Zhang, J., Ahn, Y., Zhou, W., London, W.B., McGrady, P., et al. (2008). Activating mutations in ALK provide a therapeutic target in neuroblastoma. Nature *455*, 975–978.

Gould, V.E., Lee, I., Wiedenmann, B., Moll, R., Chejfec, G., and Franke, W.W. (1986). Synaptophysin: a novel marker for neurons, certain neuroendocrine cells, and their neoplasms. Hum. Pathol. *17*, 979–983.

Guillemot, F., Lo, L.C., Johnson, J.E., Auerbach, A., Anderson, D.J., and Joyner, A.L. (1993). Mammalian achaete-scute homolog 1 is required for the early development of olfactory and autonomic neurons. Cell *75*, 463–476.

Hansford, L.M., Thomas, W.D., Keating, J.M., Burkhart, C.A., Peaston, A.E., Norris, M.D., Haber, M., Armati, P.J., Weiss, W.A., and Marshall, G.M. (2004). Mechanisms of embryonal tumor initiation: distinct roles for MycN expression and MYCN amplification. Proc. Natl. Acad. Sci. USA *101*, 12664–12669.

Hoshi, N., Hitomi, J., Kusakabe, T., Fukuda, T., Hirota, M., and Suzuki, T. (2008). Distinct morphological and immunohistochemical features and different growth rates among four human neuroblastomas heterotransplanted into nude mice. Med. Mol. Morphol. *41*, 151–159.

Hsu, H.J., Lin, G., and Chung, B.C. (2003). Parallel early development of zebrafish interrenal glands and pronephros: differential control by wt1 and ff1b. Development *130*, 2107–2116.

Huber, K. (2006). The sympathoadrenal cell lineage: specification, diversification, and new perspectives. Dev. Biol. *298*, 335–343.

Janoueix-Lerosey, I., Lequin, D., Brugières, L., Ribeiro, A., de Pontual, L., Combaret, V., Raynal, V., Puisieux, A., Schleiermacher, G., Pierron, G., et al. (2008). Somatic and germline activating mutations of the ALK kinase receptor in neuroblastoma. Nature *455*, 967–970.

Janoueix-Lerosey, I., Schleiermacher, G., and Delattre, O. (2010). Molecular pathogenesis of peripheral neuroblastic tumors. Oncogene *29*, 1566–1579.

Kimmel, C.B., Ballard, W.W., Kimmel, S.R., Ullmann, B., and Schilling, T.F. (1995). Stages of embryonic development of the zebrafish. Dev. Dyn. *203*, 253–310.

Kwak, E.L., Bang, Y.J., Camidge, D.R., Shaw, A.T., Solomon, B., Maki, R.G., Ou, S.H., Dezube, B.J., Jänne, P.A., Costa, D.B., et al. (2010). Anaplastic lymphoma kinase inhibition in non-small-cell lung cancer. N. Engl. J. Med. *363*, 1693–1703.

Langenau, D.M., Keefe, M.D., Storer, N.Y., Jette, C.A., Smith, A.C., Ceol, C.J., Bourque, C., Look, A.T., and Zon, L.I. (2008). Co-injection strategies to modify radiation sensitivity and tumor initiation in transgenic Zebrafish. Oncogene *27*, 4242–4248.

Lucas, M.E., Müller, F., Rüdiger, R., Henion, P.D., and Rohrer, H. (2006). The bHLH transcription factor hand2 is essential for noradrenergic differentiation of sympathetic neurons. Development *133*, 4015–4024.

Macdonald, R. (1999). Zebrafish immunohistochemistry. Methods Mol. Biol. *127*, 77–88.

Maris, J.M. (2010). Recent advances in neuroblastoma. N. Engl. J. Med. *362*, 2202–2211.

Maris, J.M., Hogarty, M.D., Bagatell, R., and Cohn, S.L. (2007). Neuroblastoma. Lancet *369*, 2106–2120.

Marusich, M.F., Furneaux, H.M., Henion, P.D., and Weston, J.A. (1994). Hu neuronal proteins are expressed in proliferating neurogenic cells. J. Neurobiol. *25*, 143–155.

Mierau, G.W., Weeks, D.A., and Hicks, M.J. (1998). Role of electron microscopy and other special techniques in the diagnosis of childhood round cell tumors. Hum. Pathol. *29*, 1347–1355.

Molenaar, W.M., Baker, D.L., Pleasure, D., Lee, V.M., and Trojanowski, J.Q. (1990). The neuroendocrine and neural profiles of neuroblastomas, ganglioneuroblastomas, and ganglioneuromas. Am. J. Pathol. *136*, 375–382.

Morris, S.W., Kirstein, M.N., Valentine, M.B., Dittmer, K.G., Shapiro, D.N., Saltman, D.L., and Look, A.T. (1994). Fusion of a kinase gene, ALK, to a nucleolar protein gene, NPM, in non-Hodgkin's lymphoma. Science *263*, 1281–1284.

Mossé, Y.P., Laudenslager, M., Longo, L., Cole, K.A., Wood, A., Attiyeh, E.F., Laquaglia, M.J., Sennett, R., Lynch, J.E., Perri, P., et al. (2008). Identification of ALK as a major familial neuroblastoma predisposition gene. Nature *455*, 930–935.

Nilsson, J.A., and Cleveland, J.L. (2003). Myc pathways provoking cell suicide and cancer. Oncogene *22*, 9007–9021.

O'Brien, E.K., d'Alençon, C., Bonde, G., Li, W., Schoenebeck, J., Allende, M.L., Gelb, B.D., Yelon, D., Eisen, J.S., and Cornell, R.A. (2004). Transcription factor Ap-2alpha is necessary for development of embryonic melanophores, autonomic neurons and pharyngeal skeleton in zebrafish. Dev. Biol. *265*, 246–261.

Palmer, R.H., Vernersson, E., Grabbe, C., and Hallberg, B. (2009). Anaplastic lymphoma kinase: signalling in development and disease. Biochem. J. *420*, 345–361.

Pattyn, A., Morin, X., Cremer, H., Goridis, C., and Brunet, J.F. (1999). The homeobox gene Phox2b is essential for the development of autonomic neural crest derivatives. Nature *399*, 366–370.

Sasaki, T., Okuda, K., Zheng, W., Butrynski, J., Capelletti, M., Wang, L., Gray, N.S., Wilner, K., Christensen, J.G., Demetri, G.I., et al. (2010). The neuroblastoma-associated F1174L ALK mutation causes resistance to an ALK kinase inhibitor in ALK-translocated cancers. Cancer Res. *70*, 10038–10043.

Stewart, R.A., Look, A.T., Kanki, J.P., and Henion, P.D. (2004). Development of the peripheral sympathetic nervous system in zebrafish. Methods Cell Biol. *76*, 237–260.

Stewart, R.A., Arduini, B.L., Berghmans, S., George, R.E., Kanki, J.P., Henion, P.D., and Look, A.T. (2006). Zebrafish foxd3 is selectively required for neural crest specification, migration and survival. Dev. Biol. *292*, 174–188.

Taxy, J.B. (1980). Electron microscopy in the diagnosis of neuroblastoma. Arch. Pathol. Lab. Med. *104*, 355–360.

Teitelman, G., Baker, H., Joh, T.H., and Reis, D.J. (1979). Appearance of catecholamine-synthesizing enzymes during development of rat sympathetic nervous system: possible role of tissue environment. Proc. Natl. Acad. Sci. USA *76*, 509–513.

Thisse, C., and Thisse, B. (2008). High-resolution in situ hybridization to whole-mount zebrafish embryos. Nat. Protoc. *3*, 59–69.

Tornóczky, T., Semjén, D., Shimada, H., and Ambros, I.M. (2007). Pathology of peripheral neuroblastic tumors: significance of prominent nucleoli in undifferentiated/poorly differentiated neuroblastoma. Pathol. Oncol. Res. *13*, 269–275.

Weiss, W.A., Aldape, K., Mohapatra, G., Feuerstein, B.G., and Bishop, J.M. (1997). Targeted expression of MYCN causes neuroblastoma in transgenic mice. EMBO J. *16*, 2985–2995.

Cancer Cell
Article

The Crosstalk of mTOR/S6K1 and Hedgehog Pathways

Yan Wang,[1] Qingqing Ding,[1] Chia-Jui Yen,[1] Weiya Xia,[1] Julie G. Izzo,[2,3] Jing-Yu Lang,[1] Chia-Wei Li,[1] Jennifer L. Hsu,[1,8,14] Stephanie A. Miller,[1] Xuemei Wang,[4] Dung-Fang Lee,[1,9] Jung-Mao Hsu,[1,9] Longfei Huo,[1] Adam M. LaBaff,[1,9] Dongping Liu,[1] Tzu-Hsuan Huang,[1] Chien-Chen Lai,[7,10] Fuu-Jen Tsai,[6] Wei-Chao Chang,[8,11] Chung-Hsuan Chen,[11] Tsung-Teh Wu,[12] Navtej S. Buttar,[13] Kenneth K. Wang,[13] Yun Wu,[5] Huamin Wang,[5] Jaffer Ajani,[3] and Mien-Chie Hung[1,8,9,14,*]

[1]Department of Molecular and Cellular Oncology
[2]Department of Experimental Therapeutics
[3]Department of Gastrointestinal Medical Oncology
[4]Department of Biostatistics
[5]Department of Pathology
University of Texas, MD Anderson Cancer Center, Houston, TX 77030, USA
[6]Department of Medical Research
[7]Graduate Institute of Chinese Medical Science
[8]Center for Molecular Medicine and Graduate Institute of Cancer Biology
China Medical University, 40402 Taichung, Taiwan
[9]Graduate School of Biomedical Sciences, University of Texas, Houston, TX 77030, USA
[10]Institute of Molecular Biology, National Chung Hsing University, Taichung 402, Taiwan
[11]Genomics Research Center, Academia Sinica, Taipei 115, Taiwan
[12]Department of Anatomic Pathology
[13]Division of Gastroenterology and Hepatology
Mayo Clinic, Rochester, MN 55905, USA
[14]Asia University, Taichung 41354, Taiwan
*Correspondence: mhung@mdanderson.org
DOI 10.1016/j.ccr.2011.12.028

SUMMARY

Esophageal adenocarcinoma (EAC) is the most prevalent esophageal cancer type in the United States. The TNF-α/mTOR pathway is known to mediate the development of EAC. Additionally, aberrant activation of Gli1, downstream effector of the Hedgehog (HH) pathway, has been observed in EAC. In this study, we found that an activated mTOR/S6K1 pathway promotes Gli1 transcriptional activity and oncogenic function through S6K1-mediated Gli1 phosphorylation at Ser84, which releases Gli1 from its endogenous inhibitor, SuFu. Moreover, elimination of S6K1 activation by an mTOR pathway inhibitor enhances the killing effects of the HH pathway inhibitor. Together, our results established a crosstalk between the mTOR/S6K1 and HH pathways, which provides a mechanism for SMO-independent Gli1 activation and also a rationale for combination therapy for EAC.

INTRODUCTION

Esophageal adenocarcinoma (EAC) is one of the most aggressive cancers in the world, characterized by high mortality and poor prognosis (Jemal et al., 2009). In the United States, EAC has increased at a frequency of 5%–10% per year since the 1980s, making it the fastest growing malignancy (Jemal et al., 2009). Despite multidisciplinary therapeutic approaches, EAC remains a virulent disease with an overall five-year survival rate <20% (Hongo et al., 2009). It is very urgent to identify therapeutic targets for prevention and establish biomarkers useful for early detection of high-risk populations. Esophageal chronic

Significance

The Hedgehog pathway plays a crucial role in many types of cancers, and several chemicals targeting SMO, the key mediator of canonical Hedgehog pathway, are being tested in clinical trials for cancer therapy. Although these chemicals have shown potential efficacy, the development of resistance has been also observed. Our data demonstrate that mTOR/S6K1 directly activates Gli1 independent of SMO, which results in the resistance of tumor cells to inhibitors targeting SMO. However, an mTOR inhibitor could enhance the inhibitory effects of SMO inhibitors on the tumor cells. Therefore, the combination of the inhibitors against the mTOR/S6K1 and Hedgehog pathways may be more effective in cancer target therapy.

inflammation induced by gastro-esophageal reflux disease is an important factor contributing to EAC (Lambert and Hainaut, 2007a, 2007b), and some inflammation-related cytokines have been found to play pivotal roles in the development of EAC, especially tumor necrosis factor (TNF)-α (Eksteen et al., 2001).

Our previous work has shown that TNF-α activates the mTOR pathway through IKKβ to stimulate the development and progression of EAC (Yen et al., 2008). The mechanistic target of rapamycin (mTOR) is a serine/threonine protein kinase, and its activation leads to the phosphorylation of S6K1 and 4E-BP1 (Guertin and Sabatini, 2007). S6K1 is also a serine/threonine kinase, and its phosphorylation by mTOR activates its function to promote the mRNA translation of target genes (Guertin and Sabatini, 2007). For 4E-BP1, however, phosphorylation by mTOR inactivates its function and de-represses its inhibition on cap-dependent translation (Guertin and Sabatini, 2007). The mTOR pathway has been established pivotally to be involved in many aspects of molecular and cellular biology, including mRNA translation, ribosome biogenesis, cell growth and survival, nutrient metabolism, immunosuppression, and aging, as well as cancers (Guertin and Sabatini, 2007). Moreover, the mTOR pathway is activated by TNF-α to promote angiogenesis (Lee et al., 2007a), which facilitates the chronic inflammation-induced cancers, including breast cancers (Lee et al., 2007a) and esophageal cancers (EC; Hildebrandt et al., 2009; Yen et al., 2008).

The Hedgehog (HH) signal pathway is also considered to be crucially involved in the development of esophageal cancers because it is overactivated and correlated with lymph node metastasis (Katoh and Katoh, 2009a; Lee et al., 2009). The HH pathway was identified first in *Drosophila* as an important regulator for proper embryonic patterning and is highly conserved from *Drosophila* to mammals (Ingham and McMahon, 2001). Three HH ligands have been identified in mammals: Sonic Hedgehog (SHH), Indian Hedgehog (IHH), and Desert Hedgehog (DHH; Ng and Curran, 2011), which are secreted and initiate signaling in receiving cells by binding and inactivating the HH receptor Patched 1 (PTCH1). Inhibition of PTCH1 releases the G-coupled receptor-like signal transducer Smoothened (SMO). SMO then activates glioma-associated oncogenes (Gli) through blocking their inhibitory partner, suppressor of fused (SuFu; Ng and Curran, 2011). Gli proteins, including Gli1, 2, and 3, are zinc finger transcription factors. Activated Gli proteins translocate into the nucleus and stimulate the transcription of HH pathway target genes, including Gli1, PTCH1, and many survival-promoting molecules (Jiang and Hui, 2008; Ng and Curran, 2011). Besides being activated by HH ligands-PTCH1-SMO axis, also known as the canonical HH pathway (Jenkins, 2009), Gli proteins, mainly Gli1, have been reported to be activated by AKT (Katoh and Katoh, 2009b; Stecca et al., 2007), MAPK/ERK (Seto et al., 2009), and KRAS (Nolan-Stevaux et al., 2009) in HH ligands-PTCH1-SMO axis-independent or SMO-independent manner (Ng and Curran, 2011). Although the canonical pathway has been well established, how Gli1 is regulated in a SMO-independent manner is still a puzzle.

Although both mTOR and HH pathways have been considered as drug targets in gastrointestinal (GI) cancer, including esophageal cancers (Wiedmann and Caca, 2005), the correlation between the two pathways has not been yet reported. Additionally, whether there is a relationship between TNF-α and HH pathway in EAC is also not clear. Therefore, in this work, we explored whether the TNF-α/mTOR pathway is involved in the activation of the HH pathway in EAC.

RESULTS

TNF-α Promotes Gli1 Activity through the mTOR Pathway

Because Gli protein activity is a useful readout for the HH pathway (Jiang and Hui, 2008), we employed a Gli-dependent luciferase reporter system (Sasaki et al., 1997) to evaluate the influence of TNF-α on the HH pathway in three EAC cell lines: BE3, SKGT-4, and OE33 (Boonstra et al., 2010). We observed that TNF-α increases the expression of the reporter (Figure 1A) and the mRNA levels of four Gli target genes (Figure 1B). Therefore, TNF-α can activate the HH pathway in the EAC cells. Then, we compared the activity of HH pathway in EAC cells stimulated by SHH or TNF-α. We found that there is constitutive activation of HH pathway in EAC cell lines, which can be inhibited by SMO inhibitors, cyclopamine and GDC-0449 (Scales and de Sauvage, 2009). Both SHH and TNF-α increased the activity of HH pathway in EAC cells with higher intensity from SHH (Figure S1A available online).

To investigate whether TNF-α induces Gli activity through SMO-dependent HH pathway, we pretreated the EAC cells with cyclopamine followed by TNF-α. Interestingly, cyclopamine did not affect the TNF-α-induced Gli activity (Figure 1C). Similarly, knock-down of SMO did not inhibit the TNF-α-induced Gli activity (Figure S1B). Therefore, TNF-α activates Gli function in a SMO-independent manner. To determine whether the mTOR pathway is involved in the regulation of Gli function by TNF-α, we used rapamycin and WYE-354 to block the mTOR pathway (Richard et al., 2010). Surprisingly, both compounds impaired TNF-α-stimulated Gli activation (Figures 1C and S1C). Therefore, TNF-α-stimulated Gli activation might require the activation of mTOR pathway. To further evaluate this possibility, we overexpressed wild-type mTOR or a rapamycin-resistant mTOR (mTORS2035T; Brown et al., 1995) in EAC cells followed by treatment of TNF-α alone or plus rapamycin. Western blot results confirmed that rapamycin blocked activation of mTOR pathway in mTOR-overexpressed cells but not in mTORS2035T-overexpressed cells (Figure S1D). Consistently, rapamycin suppressed the TNF-α-stimulated Gli reporter expression in mTOR-transfected EAC cells but barely had effect on mTORS2035T-transfected EAC cells (Figure 1F). Collectively, these results suggest that TNF-α activates Gli proteins through mTOR pathway.

Although Gli1, Gli2, and Gli3 all can regulate the expression of the Gli reporter (Jiang and Hui, 2008; Ng and Curran, 2011), only Gli1 knock-down impaired the TNF-α-stimulated expression of Gli reporter (Figure S1E), which suggests that TNF-α selectively activated Gli1. Consistently, TNF-α treatment rapidly induced Gli1 nuclear accumulation without obvious changes in the total protein level of Gli1 (Figure 1D, top panel). Rapamycin (Figure 1D, middle panel), but not cyclopamine (Figure 1D, bottom panel), blocked TNF-α-induced Gli1 nuclear accumulation, which was further supported by the immunofluorescence staining (Figures 1E, S1F, and S1G). Therefore, TNF-α promotes Gli1 nuclear localization and activation through the mTOR pathway.

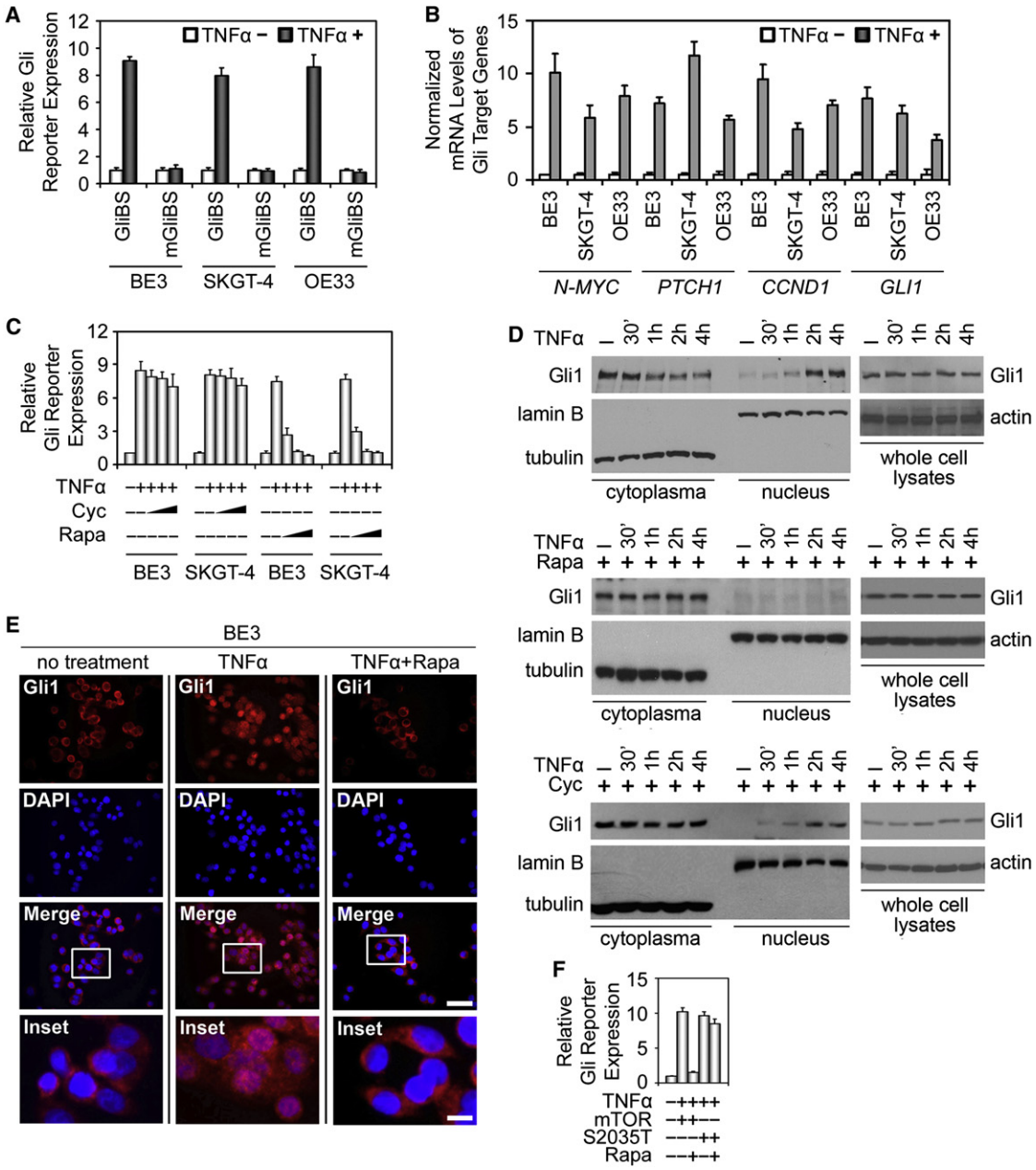

Figure 1. TNF-α Regulates Gli1 Transcriptional Activity

(A) Luciferase assay for Gli transcriptional activity in esophageal adenocarcinoma (EAC) cell lines with or without TNF-α (5 ng/ml) stimulation. The EAC cells were transfected using GliBS-Lucferase or mGliBS-Luciferase with CMV-Renilla at a 10:1 ratio, serum-starved overnight, and then treated with TNF-α for 24 hr. GliBS is Gli-responsive reporter, and mGliBS is Gli-unresponsive reporter. Error bars represent SD (n = 5).

(B) The mRNA levels of Gli1 target genes in the EAC cell lines with or without TNF-α (5 ng/ml) stimulation were examined by real-time PCR and normalized to the mRNA level of *ACTIN*. Error bars represent SD (n = 4).

(C) EAC cells were cotreated with TNF-α (5 ng/ml) and cyclopamine (Cyc; 0.5, 1, and 5 μM) or TNF-α (5 ng/ml) and rapamycin (Rapa; 10, 50, and 100 nM) for 24 hr and then subjected to luciferase assay. Error bars represent SD (n = 5 for cyclopamine treatment and n = 4 for rapamycin treatment).

(D) BE3 cells were treated with TNF-α (5 ng/ml) alone (top panel) or cotreated with TNF-α and rapamycin (50 nM, middle panel) or cyclopamine (1 μM, bottom panel) for indicated time course. Then, the cells were lysed for cell fractionation followed by western blotting. Lamin B and tubulin were used as markers for the nucleus and the cytoplasm, respectively.

(E) Immunofluorescent analysis of Gli1 in BE3 cells treated with TNF-α (5 ng/ml) alone or cotreated with TNF-α and rapamycin (50 nM). Scale bar = 100 μm for original picture and 25 μm for inset. Dapi was used to stain nuclei.

(F) Luciferase assay for Gli reporter using BE3 cells transfected with wild-type mTOR or rapamycin-resistant mTOR (mTORS2035T) followed by treatment of TNF-α alone or in combination with rapamycin (50 nM). Error bars represent SD (n = 4).

See also Figure S1.

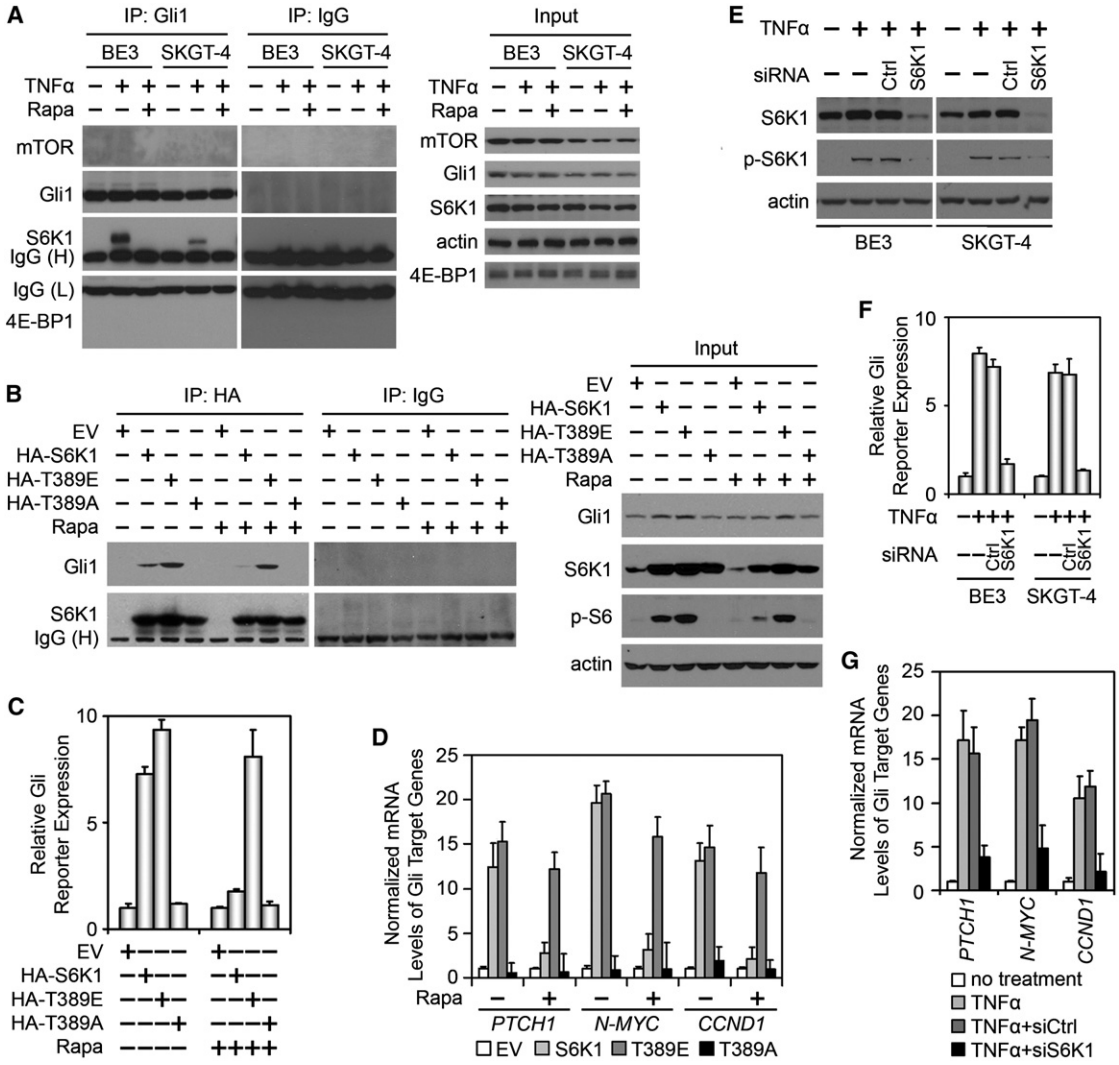

Figure 2. S6K1 Mediates the Regulation of Gli1 by TNF-α

(A) BE3 or SKGT4 cells were treated with TNF-α (5 ng/ml) alone or cotreated with TNF-α and rapamycin (50 nM) for 6 hr, and then the cells were lysed and subjected to IP-western blot assay to examine the interactions between mTOR pathway components with Gli1.

(B) BE3 cells were transiently transfected with HA-tagged wild-type S6K1 (HA-S6K1), constitutively activated S6K1T389E (HA-T389E), function-loss S6K1T389A (HA-T389A), or empty vector (EV). After 24 hr of the transfection, the cells were treated with or without rapamycin (100 nM) for additional 6 hr followed by lysis and IP-western assay to test the interaction between S6K1 variants and Gli1. Phosphorylated S6 (p-S6) was used as marker for S6K1 activation.

(C) BE3 cells were transiently transfected with Gli-firefly and CMV-renilla reporters in combination with HA-S6K1, HA-T389E, HA-T389A, or EV. After 24 hr of the transfection, the cells were treated with or without rapamycin (100 nM) for additional 24 hr followed by luciferase assay to measure the expression of Gli reporter. Error bars represent SD (n = 3).

(D) The mRNA levels of Gli1 target genes in the BE3 cells transiently transfected with HA-S6K1, HA-T389E, HA-T389A, or EV followed by treatment with or without rapamycin (100 nM) measured via real-time PCR. The mRNA levels of Gli1 target genes were normalized to the mRNA level of *ACTIN*. Error bars represent SD (n = 3).

(E) Western blot analysis using the EAC cells transfected with control siRNA (Ctrl) or siRNA targeting S6K1 followed by TNF-α treatment.

(F) EAC cells were transiently transfected with control siRNA (Ctrl) or siRNA targeting S6K1. After 48 hr of the transfection, the cells were further transfected with Gli-firefly and CMV-renilla reporters with or without TNF-α for additional 24 hr followed by luciferase assay. Error bars represent SD (n = 3).

(G) BE3 cells were transiently transfected with control siRNA (Ctrl) or siRNA targeting S6K1 followed by treatment with TNF-α or only treated with TNF-α. The mRNA levels of Gli1 target genes in these cells were measured respectively through real-time PCR and normalized to the mRNA level of *ACTIN*. Error bars represent SD (n = 3).

See also Figure S2.

S6K1 Mediates the Regulation of Gli1 by TNF-α

To investigate how the mTOR pathway activates Gli1 activity, we examined whether Gli1 interacts with the components of mTOR pathway. Without TNF-α, no interactions were found between Gli1 and mTOR pathway components; with TNF-α stimulation, however, a clear interaction was observed between Gli1 and S6K1 but not between Gli1 and mTOR or 4EB-P1 (Figures 2A and S2A). Since Gli1 function is inhibited by SuFu, we also

examined whether there are any interactions between the mTOR pathway components and SuFu. Unlike Gli1, SuFu did not interact with mTOR, S6K1, or 4EB-P1, regardless of TNF-α treatment (Figure S2B). Moreover, neither Gli2 nor Gli3 bound to mTOR, S6K1, or 4EB-P1 (Figures S2C and S2D). Taken together, the mTOR pathway might regulate Gli1 via S6K1.

Because S6K1 bound to Gli1 only under TNF-α stimulation, we hypothesized that S6K1 might need to be activated to interact with Gli1. To address this point, wild-type S6K1, constitutively activated S6K1 (S6K1T389E), or function-loss S6K1 (S6K1T389A; Holz et al., 2005) was transfected into the BE3 cells. S6K1 and S6K1T389E increased S6K1 activity, as indicated by increase of phosphorylation of S6, a substrate of S6K1 (Figure 2B). Rapamycin could inhibit the activity of S6K1, but not S6K1T389E (Figure 2B; Holz et al., 2005). Both S6K1 and S6K1T389E interacted with Gli1, and rapamycin effectively inhibited the interaction between S6K1 and Gli1, but not between S6K1T389E and Gli1 (Figure 2B). In addition, ectopic expression of S6K1T389A did not interact with Gli1 (Figure 2B). Furthermore, ectopic expression of S6K1 or S6K1T389E, but not S6K1T389A, increased the expression of Gli reporter and Gli1 target genes (Figures 2C and 2D). Rapamycin blocked the effects of S6K1 on Gli reporter expression but did not affect that of S6K1T389E (Figures 2C and 2D). Thus, only the activated S6K1 formed complex with Gli1 and enhanced its activity.

To investigate whether S6K1 mediates the regulation of Gli1 by TNF-α, we knocked down S6K1 (Figure 2E) and tested the regulation of Gli1 by TNF-α. The results indicated that the TNF-α-stimulated Gli1 activity and expression of Gli target genes were impeded by S6K1 knock-down (Figures 2F and 2G). Additionally, the inhibition of TNF-α-stimulated Gli1 activation by siRNA, which targeted 3′UTR region of S6K1 mRNA, was rescued by expression of an exogenous S6K1 lacking of 3′UTRs but not by expression of exogenous S6K1T389A or a kinase-dead S6K1 (S6K1 K100R; Holz et al., 2005; Figures S2E and S2F). Therefore, activated S6K1 is required for the regulation of Gli1 by the TNF-α/mTOR pathway.

Gli1 Is Phosphorylated by S6K1 and Required for TNF-α/mTOR/S6K1-Mediated Cell Proliferation

Since S6K1 is a serine/threonine kinase, we asked whether S6K1 regulates Gli1 through phosphorylation. Indeed, serine/threonine phosphorylation of Gli1 was observed with the ectopic expression of S6K1 or S6K1T389E (Figure 3A) but not of S6K1T389A or S6K1K100R (Figure 3A). Furthermore, an in vitro kinase assay showed that only the Gli1 fragment containing 1-500aa, Gli1F1, was phosphorylated by S6K1 but not by S6K1K100R (Figure 3B). The phosphorylation level of Gli1F1 fragment is comparable to that of S6, suggesting that Gli1 was a substrate of S6K1 in vitro. We identified 79-KKRALS-84 (Figure S3A), which is highly conserved from fruit fly to human (Figure 3C), as one potential S6K1-recognizing motif (K/RxRxxS/T) in Gli1F1. When Ser84 was mutated to alanine (Gli1S84A), phosphorylation of Gli1 by S6K1 disappeared (Figure 3D), suggesting that the Ser84 in Gli1 is the site phosphorylated by S6K1 in vitro.

To assess whether this phosphorylation occurs in vivo, we performed mass spectrometric analysis using BE3 cells treated with TNF-α alone or TNF-α and rapamycin. The results showed that the phosphorylation of Gli1 Ser84 was detected in cells treated with TNF-α but not in cells treated with rapamycin and TNF-α (Figure S3B). Thus, the activation of the mTOR/S6K1 pathway contributes to the phosphorylation of Gli1 Ser84. To further investigate endogenous Gli1 phosphorylation by TNF-α or S6K1, we developed a mouse polyclonal antibody that specifically recognizes phosphorylated Ser84 of Gli1 (p-Gli1S84). This antibody recognized TNF-α-stimulated flag-Gli1 but not without TNF-α or flag-Gli1S84A, regardless of TNF-α treatment (Figure S3C). Using this antibody, we found that TNF-α stimulation or S6K1 ectopic expression effectively induced Gli1 Ser84 phosphorylation (Figure 3E), which was diminished by the addition of rapamycin (Figure 3E). Notably, phosphorylated Gli1 was observed mainly in the nucleus (Figure 3F), which implied that the phosphorylated Gli1 might be functionally activated. The TNF-α-stimulated phosphorylation of Gli1 was largely inhibited when S6K1 was knocked down by siRNA targeting 3′UTR but could be effectively rescued by exogenous S6K1 (Figure 3G). Together, the results suggest that S6K1 mediates the regulation of Gli1 by the TNF-α/mTOR pathway through phosphorylating Gli1 at Ser84.

We also investigated if Gli1 activation is required for the effects of the TNF-α/mTOR/S6K1 pathway on cellular oncogenecity. We detected clear signals of p-Gli1S84 in BE3 and OE33 (Figure S3D), and knock-down of Gli1 impaired the TNF-α-stimulated, as well as S6K1 ectopic, expression-increased cell viability, proliferation, and invasion (Figures S3E and S3F). Thus, the activation of Gli1 by S6K1 is functionally involved in the TNF-α/mTOR pathway.

Besides TNF-α, we tested whether other mTOR pathway stimulators led to Gli1 phosphorylation. Amino acids also induced the phosphorylation of Gli1S84 in BE3 cells (Figure S3H). Furthermore, the phosphorylation of Gli1S84 in $TSC2^{-/-}$ MEFs, which has constitutive activation of the mTOR pathway and S6K1, is increased compared with $TSC^{+/+}$ MEFs (Figure S3G). Therefore, the activation of the mTOR pathway is an important stimulator for Gli1 phosphorylation in both cancer and noncancerous cells.

The mTOR pathway includes two complexes. The first is mTOR complex 1 (mTORC1), which requires raptor and activates S6K1, and the second is mTORC2, which requires rictor and activates AKT (Zoncu et al., 2011). Rapamycin and WYE-354 inhibit both mTORC1 and mTORC2 (Richard et al., 2010). Therefore, we asked whether mTORC2 also regulates Gli1 phosphorylation. Although knock-down of mTOR or raptor impaired the TNF-α-mediated Gli1 phosphorylation and activation, knock-down of rictor did not (Figures 3H and S3I), indicating that only mTORC1 plays a role in the regulation of Gli1.

Gli1 Phosphorylation by S6K1 Augments the Gli1 Function and Inhibits SuFu Binding

Since Gli1 is regulated by S6K1 in EAC cells, we wanted to know if Gli1 is required for EAC transformation. We established BE3 stable clones with Gli1 knock-down (Figure 4A), and as expected, transcription of Gli1 target genes decreased with Gli1 knock-down (Figure 4B). Moreover, Gli1 knock-down also decreased cell proliferation (Figures 4C and 4D), migration (Figure S4A), invasion (Figure S4B), and anchorage-independent growth ability (Figure S4C). Thus, Gli1 is functionally required for EAC cells. Then, to understand the effects of Ser84

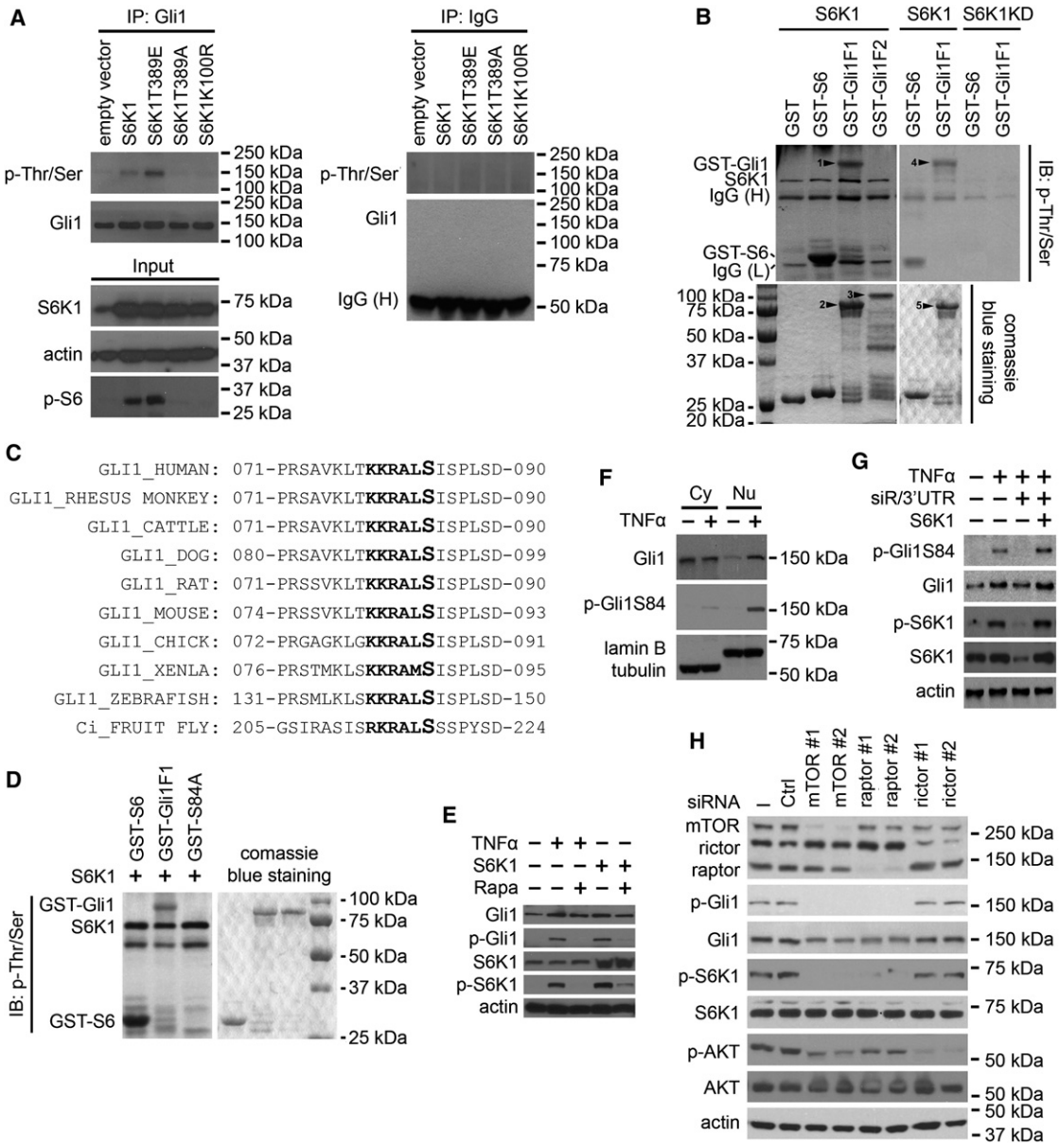

Figure 3. S6K1 Phosphorylates Gli1 at Ser84

(A) The empty vector, wild-type S6K1, S6K1T389E, S6K1T389A, or kinase-dead S6K1 (S6K1K100R) was introduced into the BE3 cells, and endogenous Gli1 was immunoprecipitated for western blot analysis. The phosphorylation was examined using anti-phospho-serine/threonine antibody.

(B) In vitro kinase assay using purified Gli1 fragment, containing 1–500 amino acids (Gli1F1), or Gli1F2, containing amino acid 501 to the end, plus purified wild-type S6K1 kinase or kinase-dead S6K1 (S6K1KD). Arrowheads 1 and 4 show phosphorylated Gli1F1 detected using anti-phospho-serine/threonine antibody; arrowheads 2 and 5 are purified Gli1F1 protein; and arrowhead 3 is purified Gli1F2 protein. The phosphorylation of S6 acts as a positive control.

(C) The S6K1 recognizing motif in Gli1 from fruit fly to human.

(D) In vitro kinase assay using purified Gli1F1 or Gli1F1 with the alanine substitution of serine 84 (S84A) plus purified S6K1.

(E) With the absence or presence of rapamycin (100 nM), BE3 cells were transiently transfected with S6K1 expression plasmid or treated with TNF-α (5 ng/ml). The phosphorylation of Gli1S84 was detected using phosphor-Gli1S84-specific antibody in western blot analysis.

(F) BE3 cells were treated with TNF-α (5 ng/ml) for 6 hr, and then the cells were lysed for cell fractionation and subsequent western blot analysis. The phosphorylation of Gli1S84 was detected using phosphor-Gli1S84-specific antibody. Lamin B and tubulin were used as markers for the nucleus and cytoplasm, respectively.

(G) BE3 cells were treated with TNF-α alone, or TNF-α plus siRNA targeting S6K1 mRNA 3′UTR with or without transfection of S6K1 expression plasmid, and then the cells were lysed for western blot analysis.

(H) Western blot analysis of BE3 cells transfected with control siRNA, or siRNA targeting mTOR, raptor, and rictor, respectively.

See also Figure S3.

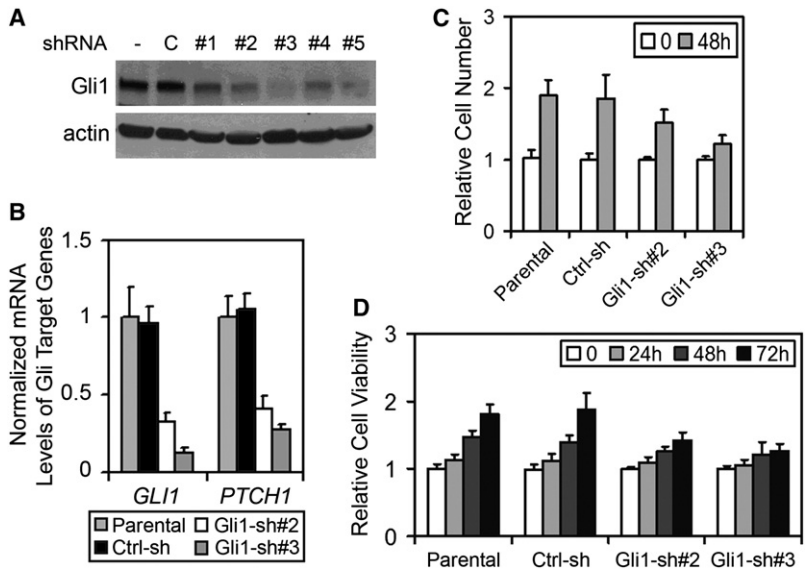

Figure 4. Knock-Down of Gli1 in EAC Cells Decreases Cell Proliferation, Migration, Invasion, and Colony Formation

(A) The BE3 stable clones with Gli1 knock-down. C, non-silencing control shRNA; #1–5, five different Gli1 shRNAs.

(B) The mRNA levels of Gli1 target genes in the BE3 stable clones with Gli1 knock-down measured via real-time PCR and normalized to the mRNA level of *ACTIN*. Error bars represent SD (n = 3).

(C) Cell counting analysis of the BE3 stable clones with Gli1 knock-down. All cells were counted, and then 1×10^5 cells were seeded in 10 cm dishes. Error bars represent SD (n = 3).

(D) MTT (3-(4,5-Dimethylthiazol-2-yl)-2,5-diphenyltetrazolium bromide) assay of the BE3 stable clones with Gli1 knock-down. All cells were counted, and then 3,000 cells were seeded in each well of a 96-well plate. Error bars represent SD (n = 3).

See also Figure S4.

phosphorylation on Gli1 function, we generated stable clones of BE3 cells expressing wild-type Gli1 (BE3/Gli1), Gli1S84A (BE3/S84A), Gli1S84E (BE3/S84E), or with the empty vector (BE3/EV). For Gli1S84E, Ser84 was mutated into glutamine to mimic constitutive phosphorylation of Gli1 at Ser84. We found that with similar Gli1 expression levels, BE3/S84E bore much higher Gli1 transcriptional activity and mRNA levels of Gli1 target genes among all the stable clones (Figures 5A and 5B). Consistently, the immunofluorescence staining showed that the level of nuclear Gli1 was much higher in BE3/S84E cells than BE3/Gli1 and BE3/S84A (Figure 5C). To further confirm that the functional difference was due to the mutations of Gli1, we treated these cells with TNF-α alone or together with rapamycin and found that TNF-α markedly induced the Gli1 transcriptional activity in BE3/Gli1, which was inhibited by cotreatment of rapamycin, but did not affect the Gli1 activity in BE3/S84E and BE3/S84A (Figure S5A). The results suggest that both S84E and S84A mutants were insensitive to TNF-α stimulation. The immunofluorescence staining further showed that TNF-α could enhance Gli1 nuclear localization in BE3/Gli1 cells but not in BE3/S84E or BE3/S84A cells (Figures 5C and S5B). Moreover, the p-Gli1S84 level also increased with TNF-α stimulation but gradually decreased with increased rapamycin dose (Figure S5C). Taken together, TNF-α-stimulated S84 phosphorylation increases Gli1 nuclear localization and transcriptional activity, and S84E and S84A mutants, mimicking phosphorylated and nonphosphorylated Gli1, respectively, are no longer sensitive to TNF-α.

Many reports have described Gli1 as an oncogene (Jiang and Hui, 2008; Ng and Curran, 2011); hence, we investigated the relationship between Gli1 phosphorylation and its tumorigenic functions. Gli1S84E and wild-type Gli1 but not Gli1S84A increased cell proliferation (Figure S5D). The Gli1S84E stable clones also exhibited the highest level of colony formation activity in soft-agar assay (Figure S5E). BE3/S84E exhibited much higher invasive ability than BE3/Gli1 and BE3/S84A (Figure S5F). These results support that the phosphorylation of Gli1 at Ser84 enhances Gli1 function. To further address why the wild-type Gli1 did not show strong biological activities in Figures S5E–S5F, we treated the BE3/Gli1 stable clone with TNF-α. Interestingly, we observed increased cell proliferation, anchorage-independent growth, and invasion (Figures S5G–S5I). Notably, TNF-α did not affect the BE3/S84E and BE3/S84A stable cells (Figures S5G–S5I). Therefore, the TNF-α/mTOR pathway promotes Gli1 function mostly via the Gli1 Ser84 phosphorylation. Furthermore, we tested the tumorigenicity of these cells by subcutaneously injecting them into the nude mice. Consistent with our in vitro data, BE3/S84E had the strongest tumorigenicity among all stable cells. Whereas BE3/Gli1 also led to tumor growth in nude mice, the tumors were smaller than those from BE3/S84E. BE3/EV and BE3/S84A induced only small tumor formation (Figures 5D and S5J). All these data indicated that Gli1 Ser84 is a key site for Gli1 activity, and its phosphorylation by S6K1 enhances Gli1 function as an oncogene.

It has been reported that without HH ligand stimulation, Gli1 function is inhibited by SuFu (Cheng and Yue, 2008). We therefore investigated whether Gli1 Ser84 phosphorylation affects its binding with SuFu. A co-immunoprecipitation experiment showed that the interaction between SuFu and Gli1 was markedly decreased in BE3/S84E compared with BE3/Gli1 and BE3/S84A (Figure 5E), which suggested that the Ser84 phosphorylation in Gli1 possibly reduced its binding to SuFu. Similarly, SuFu strongly interacted with exogenous Gli1WT and Gli1S84A but only weakly with Gli1S84E (Figure S5K). Furthermore, both TNF-α treatment and S6K1 ectopic expression decreased the binding between SuFu and Gli1, which was fully reversed by rapamycin administration (Figure 5F). Taken together, TNF-α/S6K1-induced phosphorylation of Gli1Ser84 attenuates SuFu-mediated Gli1 inhibition.

S6K1 and Gli1 Are Positively Correlated in Human Tumor Tissues

To investigate the significance of Gli1 regulation by S6K1 in human EAC tissues, we first validated suitability by immunohistochemistry (IHC) of the anti-Gli1 antibody that we would use,

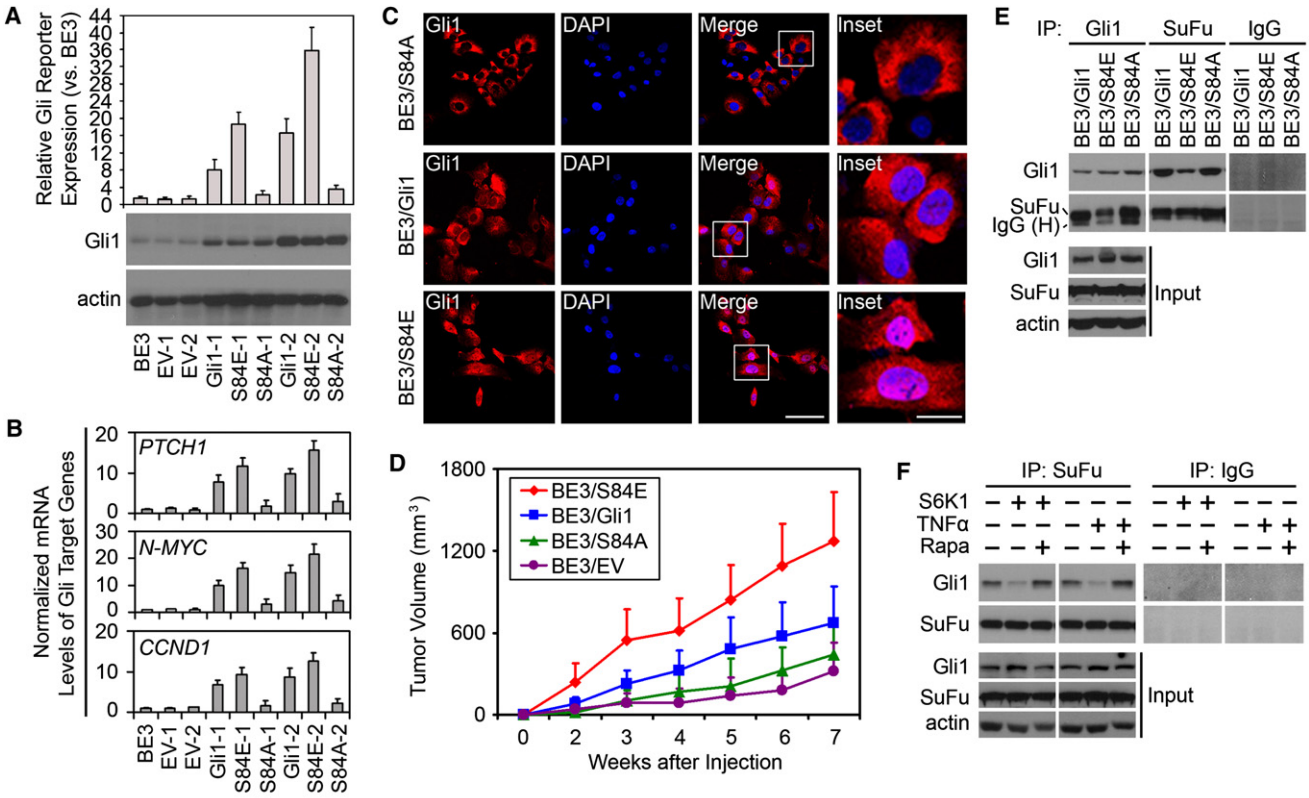

Figure 5. Functional Effects of S6K1-mediated Gli1 Phosphorylation

(A) Gli1 protein levels and Gli reporter activity in BE3 parental cells and the stable clones established from BE3 parental cells. EV, empty vector; S84A, alanine mutant of Gli1 Ser84; S84E, glutamine mutant of Gli1 Ser84. Error bars represent SD (n = 3).

(B) The mRNA levels of the Gli1 target genes in BE3 parental cells and stable clones were examined through real-time PCR and normalized to the level of *ACTIN*. Error bars represent SD (n = 3).

(C) Immunofluorescent analysis of Gli1 in the BE3 stable clones. Scale bar = 100 μm for original picture and 25 μm for inset. DAPI was used to stain nuclei.

(D) In vivo tumorigenesis assay of the stable clones in nude mice. BE3 stable cells (1×10^5) were subcutaneously injected into the right flank of nude mice, and tumor volume was measured and calculated using the formula $l \times w^2$, where l is the longest diameter and w is the shortest diameter. Error bars represent SD (n = 5).

(E) Interactions between Gli1 and SuFu in the stable clones through IP-western analysis.

(F) Endogenous interactions between Gli1 and SuFu in BE3 cells with the treatment of TNF-α (5 ng/ml) or ectopic expression of S6K1 with or without rapamycin (50 nM).

See also Figure S5.

even though it had been used for IHC before (Di Marcotullio et al., 2006; Fukaya et al., 2006). Consistent with a previous report (Kolterud et al., 2009), the staining in normal mouse colon tissues using this antibody showed that the Gli1 signal (brown color indicated by the arrows) is mainly localized in stromal cells (Figure S6A, left panel). Furthermore, western blot analysis of EAC cell lines using this antibody showed a single band at about 150 kDa (Figure S6B), which is consistent with the Gli1 molecular weight. When Gli1 was knocked down, the signal detected by the antibody concomitantly decreased compared with that from the parental or control siRNA-transfected cells (Figure S6C). This antibody was raised against amino acids 781–1080 of Gli1, and the Gli1 staining was completely blocked by a GST-Gli1 fragment containing amino acids 501–1160 but not by the fragment containing amino acids 1–500 (Figure S6D). Therefore, this anti-Gli1 antibody is applicable for IHC experiment.

We then evaluated the levels of Gli1 and p-S6K1 in 107 EAC tissue specimens by IHC (Figures 6A and 6B). Expression of both proteins was found in most cases. Eighty out of the 107 for p-S6K1 (74.8%) and 87 of the 107 (81.3%) for Gli1 were positive (Figure 6A), and there was a strong correlation between the levels of p-S6K1 and Gli1 (Figure 6C). We also collected 15 samples from rat Barrett's esophagus models (Yen et al., 2008) and found that there were no p-S6K1 or Gli1 signals in normal esophageal squamous cells but observed strong signals of both p-S6K1 and Gli1 in three of five BE and three of five EAC tissue samples (Figure S6E). Together, these data further support the notion that the activation of mTOR/S6K1 and Gli1 pathways is involved in the transformation of esophagus. To ensure the Gli1S84 phosphorylation also exists in human EAC tumor tissues, we first tested the applicability of the anti-p-Gli1S84 antibody for IHC. We found that the staining of p-Gli1 could be blocked by phosphorylated Gli1 peptide used for

A

protein	n	negative	positive			
		0%	>0-10%	>10-25%	>25-50%	>50%
p-S6K1 (T389)	107	27 (25%)	31 (29%)	15 (14%)	21 (20%)	13 (12%)
Gli1	107	20 (19%)	18 (17%)	9 (8%)	31 (29%)	29 (27%)

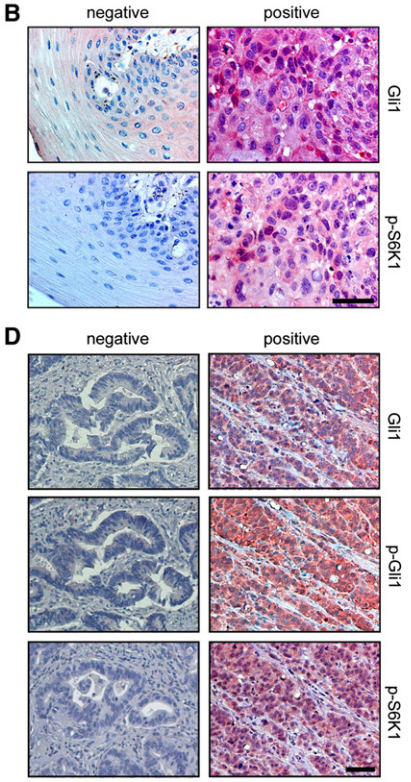

C

		Gli1		total
		negative	positive	
p-S6K1	negative	12	15	27
	positive	8	72	80
total		20	87	107
p = 0.0002				

E

		Gli1		total
		negative	positive	
p-S6K1	negative	15	15	30
	positive	8	32	40
total		23	47	70
p = 0.0108				

F

		p-Gli1		total
		negative	positive	
p-S6K1	negative	23	7	30
	positive	12	28	40
total		35	35	70
p = 0.0002				

G

$Gli1^+$ tissues		p-Gli1		total
		negative	positive	
p-S6K1	negative	8	7	15
	positive	4	28	32
total		12	35	47
p = 0.0093				

Figure 6. Correlations between p-S6K1T389 and Gli1 or p-Gli1S84 in EAC

(A) Statistic analysis of immunohistochemistry (IHC) staining of Gli1 and p-S6K1 from human EAC tissues.

(B) Representative IHC staining results for Gli1 and p-S6K1 in human EAC tissues. Scale bar = 50 μm.

(C) Statistic analysis for Gli1 and p-S6K1 correlation from the IHC staining results in human EAC tissues.

(D) Representative IHC staining results for p-Gli1 or p-S6K1 in human EAC tissue microarray. Scale bar = 50 μm.

(E) Statistic analysis for Gli1 and p-S6K1 correlation from the IHC staining results in human EAC tissue microarray.

(F) Statistic analysis for p-Gli1 and p-S6K1 correlation from the IHC staining results in human EAC tissue microarray.

(G) Statistic analysis for p-Gli1 and p-S6K1 correlation in the Gli1 positive subpopulation of human EAC tissue microarray.

See also Figure S6.

developing the antibody but not by the same nonphosphorylated peptide (Figure S6F). Moreover, using the same set of mouse colon tissues used above, we could not detect any signal of p-S6K1 and, as expected, the signal of p-Gli1 is also negative (Figure S6A, middle and right panels). Therefore, the p-Gli1 antibody is applicable for IHC. We then examined the Gli1, p-Gli1, and p-S6K1 in human EAC tissue microarray (n = 70), and the result again showed that there was a strongly positive correlation between p-S6K1 and Gli1 or p-Gli1 (Figures S6G and 6D–6F). All p-Gli1-positive tissues are also Gli1-positive, and among the Gli1-positive tissues, there is also a strong positive correlation between p-Gli1 and p-S6K1 (Figure 6G). Thus, the phosphorylation of Gli1 also exists in human EAC tumor tissues. Additionally, using human tissue microarray with multiple cancer types, we found a positive correlation between p-S6K1 and Gli1 (Figures S6H and S6I), suggesting that the regulation of Gli1 by S6K1 might be not limited to EAC and is worthwhile to be tested in multiple kinds of cancers in the future.

A Combination Therapy that Targets Both Canonical HH and mTOR/S6K1 Pathways in EAC Cells Provides Better Therapeutic Effects

Consistent with the previous reports (Berman et al., 2003; Sims-Mourtada et al., 2006), we detected the activated form of SHH protein, the amino terminal domain of SHH (SHH-N; Ng and Curran, 2011), in the EAC cell lines (Figure 7A). In addition, SHH treatment dramatically increased expression of Gli reporter (Figure S7A) and Gli1 target genes (Figure 7B). Hence, the EAC cell lines exhibit activated canonical HH pathway. Because our data have shown that in EAC cell lines mTOR/S6K1-mediated Gli1 activation is SMO-independent, we speculated that mTOR/S6K1/Gli1 should enhance the resistance of EAC cells to SMO inhibitors. As expected, the IC_{50} value of cyclopamine or GDC-0449 in BE3/S84E was much higher than that for BE3/EV, BE3/Gli1, and BE3/S84A (Figure 7C). Moreover, TNF-α treatment increased the resistance of BE3/Gli1, but not BE3/S84A, to cyclopamine or GDC-0449 (Figure 7D), suggesting that Gli1S84 phosphorylation enhances cell resistance to SMO inhibitors. Then, we examined whether a combination of inhibitors of HH and mTOR pathways would be more effective for these EAC cell lines. To avoid the killing effect of rapamycin, we first determined that 10 nM rapamycin was sufficient to inhibit the activation of S6K1 in BE3 cells but did not significantly inhibit cell viability (Figure S7B). Thus, we used 10 nM rapamycin for all subsequent experiments. We found that rapamycin treatment enhanced the efficacy of cyclopamine or GDC-0449 in the EAC cell lines (Figure 7E). Moreover, knock-down of SMO also inhibited cell viability, and rapamycin treatment further enhanced the inhibitory effect (Figure S7C). Interestingly, the effects of rapamycin on SMO inhibitors existed in BE3/Gli1 cells but not in BE3/S84E cells (Figure 7F). Therefore, the mTOR inhibitor could enhance SMO inhibitor effects in vitro through eliminating the phosphorylation of Gli1S84. For further examination of the crosstalk of mTOR and HH pathways in vivo, we performed an in vivo combination therapy using GDC-0449 and another mTOR inhibitor, RAD-001, which is widely used in combination with other antitumor drugs in clinical trials (Piguet et al., 2011; Price et al., 2010; Quek et al., 2011). We subcutaneously inoculated mice with BE3 cells and treated them with GDC-0449, RAD-001, or both and found that though

low dose RAD001 did not inhibit tumor growth, it enhanced the tumor-inhibitory effect of GDC-0449 (Figure 7G). Therefore, the combination of the inhibitors targeting the two pathways could produce better efficacy for targeted therapy.

SMO-Independent Activation of Gli1 by AKT and ERK Requires mTOR/S6K1

It has been reported that AKT and MAPK/ERK also activate HH pathway in a SMO-independent manner. Interestingly, AKT and ERK can activate the mTOR/S6K1 pathway by inhibiting the TSC1/2 complex (Lee et al., 2007a; Ma et al., 2005; Ozes et al., 2001). This prompted us to test if the mTOR/S6K1 pathway is required for the activation of Gli1 by the two kinases. Through ectopic expression of AKT or ERK, we found that Gli1 activity increased, which could be blocked by rapamycin (Figure S8). Moreover, the activation of AKT or ERK also stimulated the phosphorylation of S6K1T389 and Gli1Ser84, which was inhibited by rapamycin (Figure 8A). However, AKT and ERK lost the ability to induce Gli1 phosphorylation when S6K1 was knocked down (Figure 8B). Therefore, our results indicated that the mTOR/S6K1/Gli1 pathway might mediate the previously reported AKT and ERK-stimulated Gli1 activation (Figure 8C).

DISCUSSION

In this study, we demonstrate a SMO-independent activation of Gli1 by the mTOR/S6K1 pathway, in which activated S6K1 phosphorylates Gli1 at Ser84, resulting in its release from SuFu binding and translocation into the nucleus to activate its target genes (Figure 8C). We previously reported that the mTOR/S6K1 pathway facilitates progression from inflammation and tumorigenesis through upregulation of VEGF, as well as the subsequent angiogenesis (Lee et al., 2007a). In addition, TNF-α/mTOR can be activated by chronic inflammation in the esophagus (Yen et al., 2008). Our work herein further implies that the mTOR/S6K1 pathway might also promote EAC through the activation of Gli1. Since Gli1 is known as an oncogene (Ng and Curran, 2011), our results also provide further evidence to support the concept that chronic inflammation is an important stimulator for tumorigenesis of the esophagus (Lambert and Hainaut, 2007a, 2007b).

The canonical HH pathway is well known to have a tight negative feedback regulation, which blocks the HH ligands and inhibits SMO activation through Gli1-promoted transcription of PTCH and HH interacting protein (Katoh and Katoh, 2006). When SMO is inactivated, SuFu binds to and inhibits Gli1 function (Katoh and Katoh, 2006). Function-loss-mutation of SuFu has been shown to result in tumorigenesis due to the aberrant activation of the HH pathway (Cheng and Yue, 2008; Lee et al., 2007b). Therefore, SuFu is an important negative regulator for the HH pathway and acts as a tumor suppressor. In this study, we found that the phosphorylation of Gli1 by S6K1 blocked the interaction between SuFu and Gli1, allowing Gli1 to translocate into the nucleus to activate transcription of HH target genes. Thus, in contrast to the canonical HH pathway, SMO inhibitors do not seem to affect S6K1-mediated Gli1 activation, suggesting that the S6K1-mediated release of SuFu from Gli1 occurs independently of SMO. In fact, SMO inhibitors, such as cyclopamine and GDC-0449, had little effects on the mTOR/S6K1-mediated Gli1 activation. These findings suggest that the mTOR/S6K1 pathway can act as a positive modulator to amplify and fuel Gli1 activation to promote tumorigenesis and disease progression.

The HH pathway has been considered as a therapeutic target for GI cancers, including esophageal cancers (Lee et al., 2009; Wiedmann and Caca, 2005). Several SMO inhibitors, including GDC-0449, are currently being tested in clinical trials, which are either structurally derived from or functionally similar to cyclopamine (Scales and de Sauvage, 2009; Stanton and Peng, 2010). Our data showed that the administration of GDC-0449 indeed decreased the EAC tumor size, supporting that GDC-0449 also could be used for treating EAC (Figure 7G). In this study, however, we disclose a SMO-independent activation of Gli1 by the mTOR/S6K1 pathway, which cannot be inhibited by SMO inhibitors but is sensitive to inhibitors of the mTOR pathways. Cotreatment with mTOR/S6K1 and SMO inhibitors, RAD001 and GDC-0449, indeed showed better inhibitory effects on tumor growth in vivo than did single drug treatment. Therefore, our results strongly suggest that a combination of inhibitors targeting the two pathways may be a more effective strategy to treat EAC.

In addition, through the immunostaining analysis of human EAC tissues, we found that in about 40% (28/70) of patients, all of the p-Gli1, Gli1, and p-S6K1 were positive, suggesting that these patients may bear both canonical HH pathway and mTOR/S6K1-mediated SMO-independent Gli1 activation. Based on the current study, we would predict that this population of patients may not have full response to GDC-0449 treatment alone but could benefit from the proposed cotreatment of inhibitors targeting both the mTOR and HH pathways. Therefore, a preselection procedure might be required for the patients before receiving the SMO inhibitors to determine whether the cotreatment strategy should be applied. It is worthwhile to mention that many inhibitors targeting these two pathways are being tested in clinical trials, such as GDC-0449 and IPI-926, targeting the HH pathway (Stanton and Peng, 2010), and RAD001 and AP23573, targeting the mTOR pathway (Konings et al., 2009). Thus, exploring a vast array of possible therapeutic combinations will be useful to simultaneously target these pathways.

Although SMO inhibitors are known to inhibit several types of cancer and have shown hopeful tumor-inhibitory effects, the development of resistance due to the constitutive activation mutation of SMO or overactivation of PI3K/AKT pathway has been reported (Metcalfe and de Sauvage, 2011). Buonamici et al. further showed that the resistance of medulloblastoma to SMO inhibitors could be decreased through a combination of SMO and PI3K/AKT inhibitors (Buonamici et al., 2010). Interestingly, PI3K/AKT and RAS/MEK/ERK have been also found to activate Gli1 in a SMO-independent manner (Katoh and Katoh, 2009b; Seto et al., 2009; Stecca et al., 2007), though the mechanisms are not well understood. Because AKT and ERK can activate the mTOR/S6K1 pathway (Ma et al., 2005; Ozes et al., 2001) and activation of Gli1 by AKT or ERK requires S6K1 (Figure 8B), our finding that S6K1 phosphorylates Gli1 and enhances its function provides a molecular mechanism not only for mTOR/S6K1-mediated but also AKT or ERK-induced SMO-independent Gli1 activation (Figure 8C). Thus, our results also provide a potential explanation for the resistance of tumor cells to SMO inhibitors. Similarly, our study offers a rationale for combining

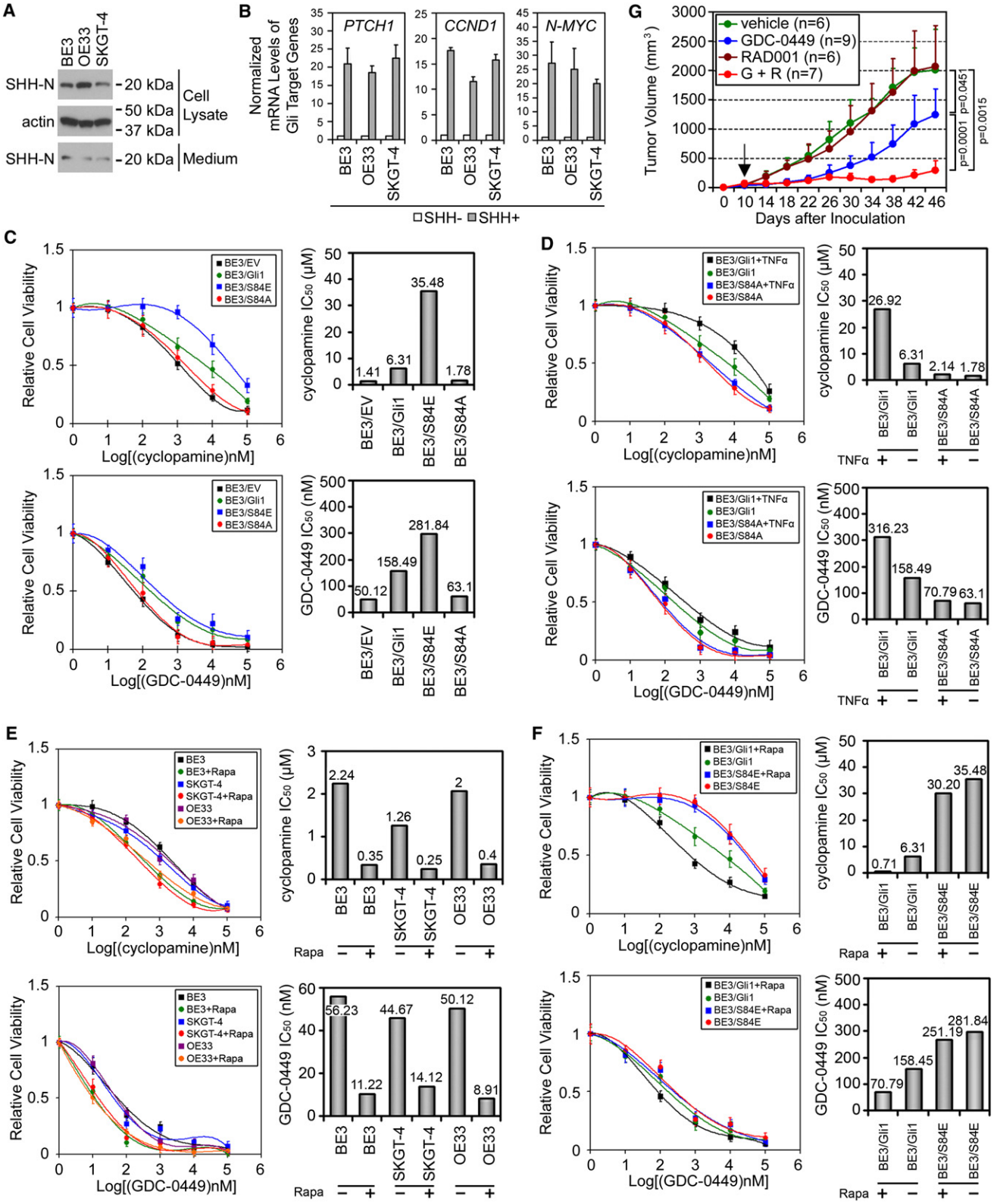

Figure 7. Effects of mTOR and/or HH Pathway Inhibitors on EAC Cells

(A) The expression of activated SHH (SHH-N) in EAC cell lines and the cell culture medium.

(B) The mRNA levels of Gli1 target genes in EAC cell lines with or without SHH treatment (1 μg/ml) induces the upregulation of. The mRNA levels of Gli1 target genes are normalized to *ACTIN*. Error bars represent SD (n = 3).

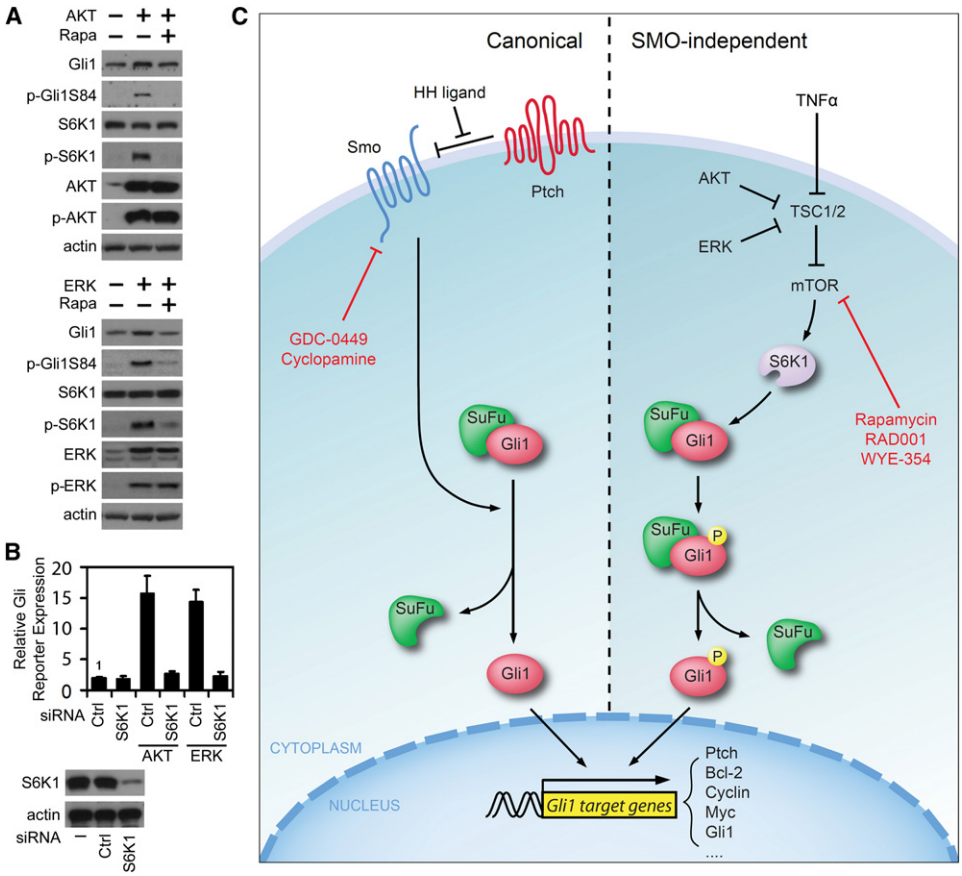

Figure 8. AKT and ERK Can Activate Gli1 through mTOR/S6K1 Pathway

(A) The regulation of S6K1 and Gli1 by ectopically expressed AKT or ERK in HeLa cells with or without rapamycin (50 nM).

(B) The influence of S6K1 knock-down on the AKT or ERK-stimulated HH pathway in HeLa cells. Error bars represent SD (n = 3).

(C) Schematic diagram for the canonical HH pathway stimulated by HH ligands and SMO-independent Gli1 activation stimulated by the mTOR/S6K1 pathway.

See also Figure S8.

SMO with mTOR/S6K1 inhibitors to increase the effectiveness for treating EAC.

Taken together, our current study identifies Gli1 as a substrate for S6K1 and establishes a crosstalk between the mTOR/S6K1 and HH pathways, providing a mechanism for SMO-independent Gli1 activation. Our data also suggest that the combination of the inhibitors to these two pathways has a more potent inhibitory effect on the EAC cells than single agent alone. Moreover, we also found the correlation between p-S6K1 and Gli1 of multiple cancer types using tissue microarray, indicating that the combined targeted therapy, targeting both the mTOR/S6K1 and HH pathways, may be effective for treatment of EAC, as well as other cancers.

EXPERIMENTAL PROCEDURES

Human Tissues

Human EAC specimens for immunohistochemistry were obtained retrospectively from patients undergoing complete esophageal surgical resection, as primary treatment, at MD Anderson Cancer Center (MDACC) between January 1986 and December 1997. The specimen collection was conducted in accordance with the protocols approved by the Institutional Review Board at MD Anderson Cancer Center, and written informed consent was obtained from

(C) IC_{50} of cyclopamine (top two panels) or GDC-0449 (bottom two panels) for the Gli1 stable clones. Error bars represent SD (n = 4).

(D) IC_{50} of cyclopamine (top two panels) or GDC-0449 (bottom two panels) for the Gli1 stable clones with existence of TNF-α (5 ng/ml). Error bars represent SD (n = 4).

(E) IC_{50} of cyclopamine (top two panels) or GDC-0449 (bottom two panels) for EAC cells pretreated with rapamycin (Rapa, 10 nM). Error bars represent SD (n = 4).

(F) IC_{50} of cyclopamine (top two panels) or GDC-0449 (bottom two panels) for the Gli1 stable clones with rapamycin (Rapa, 50 nM) treatment. Error bars represent SD (n = 4).

(G) In vivo combination therapy for subcutaneously inoculated tumors from BE3 cells using GDC-0449 (50 mg/kg) or RAD001 (10 mg/kg). BE3 cells 1×10^6 were subcutaneously injected into the right flank of nude mice, and the tumor cells were allowed to grow for 10 days (the arrow) before initiation of drug treatment. The vehicle, GDC-0449, RAD001, or combination of GDC-0449 and RAD001, was orally administrated, qd. The tumor volume measured and calculated using the formula $l \times w^2$, where l is the longest diameter and w is the shortest diameter. Error bars represent SD (n = 5).

See also Figure S7.

patients in all cases at time of enrollment. The multiple tissue microarrays were purchased from US Biomax, Inc. (BC00112 and MTU241; Rockville, MD, USA).

Immunoprecipitation, Immunoblotting, and In Vitro Kinase Assays

Immunoprecipitation and immunoblotting were performed as previously described (Lee et al., 2007a). For in vitro kinase assay, the BL21 competent cells were transformed with pGEX-6P-1, pGEX-6P-1-S6, pGEX-6P-1-Gli1F1, or pGEX-6P-1-Gli1F2 vectors. After overnight growth, the cells were lysed, and the target proteins were purified using the GST antibody crosslinked agarose beads (Thermo Scientific, Hudson, NH, USA) in accordance with the manufacturer's instruction. In addition, 90% confluent BE3 cells were transfected with HA-S6K1, HA-S6K1T389E, HA-S6K1T389A, or HA-S6K1K100R, and 24 hr after transfection, the cells were lysed and immunoprecipitated with anti-HA antibody. Purified GST protein or GST fusion proteins were incubated with purified HA-S6K1 or HA-S6K1 mutants in the presence of 50 mM ATP in a kinase buffer for 30 min at 30°C. Reaction products were subjected to SDS-PAGE (sodium dodecyl sulfate polyacrylamide gel electrophoresis (SDS-PAGE) and then blotted with phosphor-Thr/Ser antibody.

IC_{50} Evaluation for Cyclopamine and GDC-0449

Cells were seeded in 96-well plates at the density of 5,000 cells/well. After overnight growth, the cells were exposed to increasing concentrations, ranging from 1 nM to 100 μM for cyclopamine or GDC-0449, with or without 10 nM rapamycin, for 48 hr. The concentrations required to inhibit cell growth by 50% (IC_{50}) were calculated from survival curves.

Rat Model of BE and EAC

The rat model was established as previously described (Yen et al., 2008). The excised esophageal tissues from normal esophagus, BE, or EAC were fixed in 10% buffered formalin for 24 hr and then transferred to 80% ethanol. The tissue was longitudinally divided into slices for immunohistochemistry staining.

Tumorigenicity Assay and Combination Therapy In Vivo

All animal experiments were approved by the Institutional Animal Care and Use Committee (IACUC) at MD Anderson Cancer Center. Nude female mice were housed under standard conditions. For tumorigenicity assay, 1×10^5 BE3 stable cells were subcutaneously injected in right flank. The resulting tumors were measured with calipers weekly, and tumor volume was determined using the formula $l \times w^2$, where l is the longest diameter and w is the shortest diameter. For combination therapy, 1×10^6 BE3 cells were subcutaneously injected in right flanks of nude mice and allowed to grow for 10 days before drug treatment. GDC-0449 was formulated in MCT (0.5% methylcellulose and 0.5% Tween 80) and RAD001 in water. GDC-0449 (50 mg/kg) and RAD001 (10 mg/kg) were dosed qd (quaque die (qd) by oral gavage. The tumors were measured with calipers every 4 days. Data were presented as tumor volume (mean ± SD). Statistical analysis was done using the Student's t test by the program SPSS for Windows.

Statistical Analyses

Statistical analyses were performed with the Student's t test, Spearman rank correlation test, or Fisher's exact test as indicated. A p value of <0.05 was considered statistically significant. All data analyses were performed using the program SPSS for Windows.

All other experimental procedures are described in the Supplemental Experimental Procedures.

SUPPLEMENTAL INFORMATION

Supplemental Information includes eight figures and Supplemental Experimental Procedures and can be found with this article online at doi:10.1016/j.ccr.2011.12.028.

ACKNOWLEDGMENTS

We thank Dr. Anthony E. Oro for providing the Gli1-expressing plasmid; Rune Toftgård for SuFu-expressing plasmid; and Dr. Hiroshi Sasaki for Gli1-reporter plasmids. We thank Jer-Yen Yang for insightful discussion and Su Zhang, Jian-Guang Shi, Zhen-Bo Han, and Jin-Fong Lee for technical assistance. This work was supported by the National Institutes of Health (CA109311and CA099031 to M.-C.H and CCSG Core Grant CA16672); the Kadoorie Charitable Foundation; the Center for Biological Pathway at the University of Texas, MD Anderson Cancer Center; Susan G. Komen (SAC110016 to M.-C.H), the Sister Institution Fund of China Medical University and Hospital and the University of Texas, MD Anderson Cancer Center; Department of Health Cancer Research Center of Excellence (DOH101-TD-C-111-005, Taiwan; NSC100-2321-B-039-002, Taiwan; NSC99-2632-B-039-001-MY3, Taiwan); the Dallas, Park, Sultan, Smith, and Cantu Family funds (to J.A.); the Reivercreek and Schecter Private foundations (to J.A.); Kevin and Frazier funds (to J.A.); National Cancer Institute (CA142072, CA127672, and CA129906 to J.A.); and the University of Texas, MD Anderson Cancer Center Multidisciplinary Research Program Funding.

Received: July 8, 2011
Revised: October 13, 2011
Accepted: December 30, 2011
Published: March 19, 2012

REFERENCES

Berman, D.M., Karhadkar, S.S., Maitra, A., Montes De Oca, R., Gerstenblith, M.R., Briggs, K., Parker, A.R., Shimada, Y., Eshleman, J.R., Watkins, D.N., and Beachy, P.A. (2003). Widespread requirement for Hedgehog ligand stimulation in growth of digestive tract tumours. Nature *425*, 846–851.

Boonstra, J.J., van Marion, R., Beer, D.G., Lin, L., Chaves, P., Ribeiro, C., Pereira, A.D., Roque, L., Darnton, S.J., Altorki, N.K., et al. (2010). Verification and unmasking of widely used human esophageal adenocarcinoma cell lines. J. Natl. Cancer Inst. *102*, 271–274.

Brown, E.J., Beal, P.A., Keith, C.T., Chen, J., Shin, T.B., and Schreiber, S.L. (1995). Control of p70 s6 kinase by kinase activity of FRAP in vivo. Nature *377*, 441–446.

Buonamici, S., Williams, J., Morrissey, M., Wang, A., Guo, R., Vattay, A., Hsiao, K., Yuan, J., Green, J., Ospina, B., et al. (2010). Interfering with resistance to smoothened antagonists by inhibition of the PI3K pathway in medulloblastoma. Sci Transl Med *2*, 51ra70.

Cheng, S.Y., and Yue, S. (2008). Role and regulation of human tumor suppressor SUFU in Hedgehog signaling. Adv. Cancer Res. *101*, 29–43.

Di Marcotullio, L., Ferretti, E., Greco, A., De Smaele, E., Po, A., Sico, M.A., Alimandi, M., Giannini, G., Maroder, M., Screpanti, I., and Gulino, A. (2006). Numb is a suppressor of Hedgehog signalling and targets Gli1 for Itch-dependent ubiquitination. Nat. Cell Biol. *8*, 1415–1423.

Eksteen, J.A., Scott, P.A., Perry, I., and Jankowski, J.A. (2001). Inflammation promotes Barrett's metaplasia and cancer: a unique role for TNFalpha. Eur. J. Cancer Prev. *10*, 163–166.

Fukaya, M., Isohata, N., Ohta, H., Aoyagi, K., Ochiya, T., Saeki, N., Yanagihara, K., Nakanishi, Y., Taniguchi, H., Sakamoto, H., et al. (2006). Hedgehog signal activation in gastric pit cell and in diffuse-type gastric cancer. Gastroenterology *131*, 14–29.

Guertin, D.A., and Sabatini, D.M. (2007). Defining the role of mTOR in cancer. Cancer Cell *12*, 9–22.

Hildebrandt, M.A., Yang, H., Hung, M.C., Izzo, J.G., Huang, M., Lin, J., Ajani, J.A., and Wu, X. (2009). Genetic variations in the PI3K/PTEN/AKT/mTOR pathway are associated with clinical outcomes in esophageal cancer patients treated with chemoradiotherapy. J. Clin. Oncol. *27*, 857–871.

Holz, M.K., Ballif, B.A., Gygi, S.P., and Blenis, J. (2005). mTOR and S6K1 mediate assembly of the translation preinitiation complex through dynamic protein interchange and ordered phosphorylation events. Cell *123*, 569–580.

Hongo, M., Nagasaki, Y., and Shoji, T. (2009). Epidemiology of esophageal cancer: Orient to Occident. Effects of chronology, geography and ethnicity. J. Gastroenterol. Hepatol. *24*, 729–735.

Ingham, P.W., and McMahon, A.P. (2001). Hedgehog signaling in animal development: paradigms and principles. Genes Dev. *15*, 3059–3087.

Jemal, A., Siegel, R., Ward, E., Hao, Y., Xu, J., and Thun, M.J. (2009). Cancer statistics, 2009. CA Cancer J. Clin. *59*, 225–249.

Jenkins, D. (2009). Hedgehog signalling: emerging evidence for non-canonical pathways. Cell. Signal. *21*, 1023–1034.

Jiang, J., and Hui, C.C. (2008). Hedgehog signaling in development and cancer. Dev. Cell *15*, 801–812.

Katoh, Y., and Katoh, M. (2006). Hedgehog signaling pathway and gastrointestinal stem cell signaling network (review). Int. J. Mol. Med. *18*, 1019–1023.

Katoh, Y., and Katoh, M. (2009a). Hedgehog target genes: mechanisms of carcinogenesis induced by aberrant hedgehog signaling activation. Curr. Mol. Med. *9*, 873–886.

Katoh, Y., and Katoh, M. (2009b). Integrative genomic analyses on GLI1: positive regulation of GLI1 by Hedgehog-GLI, TGFbeta-Smads, and RTK-PI3K-AKT signals, and negative regulation of GLI1 by Notch-CSL-HES/HEY, and GPCR-Gs-PKA signals. Int. J. Oncol. *35*, 187–192.

Kolterud, A., Grosse, A.S., Zacharias, W.J., Walton, K.D., Kretovich, K.E., Madison, B.B., Waghray, M., Ferris, J.E., Hu, C., Merchant, J.L., et al. (2009). Paracrine Hedgehog signaling in stomach and intestine: new roles for hedgehog in gastrointestinal patterning. Gastroenterology *137*, 618–628.

Konings, I.R., Verweij, J., Wiemer, E.A., and Sleijfer, S. (2009). The applicability of mTOR inhibition in solid tumors. Curr. Cancer Drug Targets *9*, 439–450.

Lambert, R., and Hainaut, P. (2007a). Esophageal cancer: cases and causes (part I). Endoscopy *39*, 550–555.

Lambert, R., and Hainaut, P. (2007b). Esophageal cancer: the precursors (part II). Endoscopy *39*, 659–664.

Lee, D.F., Kuo, H.P., Chen, C.T., Hsu, J.M., Chou, C.K., Wei, Y., Sun, H.L., Li, L.Y., Ping, B., Huang, W.C., et al. (2007a). IKK beta suppression of TSC1 links inflammation and tumor angiogenesis via the mTOR pathway. Cell *130*, 440–455.

Lee, D.Y., Deng, Z., Wang, C.H., and Yang, B.B. (2007b). MicroRNA-378 promotes cell survival, tumor growth, and angiogenesis by targeting SuFu and Fus-1 expression. Proc. Natl. Acad. Sci. USA *104*, 20350–20355.

Lee, W., Patel, J.H., and Lockhart, A.C. (2009). Novel targets in esophageal and gastric cancer: beyond antiangiogenesis. Expert Opin. Investig. Drugs *18*, 1351–1364.

Ma, L., Chen, Z., Erdjument-Bromage, H., Tempst, P., and Pandolfi, P.P. (2005). Phosphorylation and functional inactivation of TSC2 by Erk implications for tuberous sclerosis and cancer pathogenesis. Cell *121*, 179–193.

Metcalfe, C., and de Sauvage, F.J. (2011). Hedgehog fights back: mechanisms of acquired resistance against Smoothened antagonists. Cancer Res. *71*, 5057–5061.

Ng, J.M., and Curran, T. (2011). The Hedgehog's tale: developing strategies for targeting cancer. Nat. Rev. Cancer *11*, 493–501.

Nolan-Stevaux, O., Lau, J., Truitt, M.L., Chu, G.C., Hebrok, M., Fernández-Zapico, M.E., and Hanahan, D. (2009). GLI1 is regulated through Smoothened-independent mechanisms in neoplastic pancreatic ducts and mediates PDAC cell survival and transformation. Genes Dev. *23*, 24–36.

Ozes, O.N., Akca, H., Mayo, L.D., Gustin, J.A., Maehama, T., Dixon, J.E., and Donner, D.B. (2001). A phosphatidylinositol 3-kinase/Akt/mTOR pathway mediates and PTEN antagonizes tumor necrosis factor inhibition of insulin signaling through insulin receptor substrate-1. Proc. Natl. Acad. Sci. USA *98*, 4640–4645.

Piguet, A.C., Saar, B., Hlushchuk, R., St-Pierre, M.V., McSheehy, P.M., Radojevic, V., Afthinos, M., Terracciano, L., Djonov, V., and Dufour, J.F. (2011). Everolimus augments the effects of sorafenib in a syngeneic orthotopic model of hepatocellular carcinoma. Mol. Cancer Ther. *10*, 1007–1017.

Price, K.A., Azzoli, C.G., Krug, L.M., Pietanza, M.C., Rizvi, N.A., Pao, W., Kris, M.G., Riely, G.J., Heelan, R.T., Arcila, M.E., and Miller, V.A. (2010). Phase II trial of gefitinib and everolimus in advanced non-small cell lung cancer. J. Thorac. Oncol. *5*, 1623–1629.

Quek, R., Wang, Q., Morgan, J.A., Shapiro, G.I., Butrynski, J.E., Ramaiya, N., Huftalen, T., Jederlinic, N., Manola, J., Wagner, A.J., et al. (2011). Combination mTOR and IGF-1R inhibition: phase I trial of everolimus and figitumumab in patients with advanced sarcomas and other solid tumors. Clin. Cancer Res. *17*, 871–879.

Richard, D.J., Verheijen, J.C., and Zask, A. (2010). Recent advances in the development of selective, ATP-competitive inhibitors of mTOR. Curr. Opin. Drug Discov. Devel. *13*, 428–440.

Sasaki, H., Hui, C., Nakafuku, M., and Kondoh, H. (1997). A binding site for Gli proteins is essential for HNF-3beta floor plate enhancer activity in transgenics and can respond to Shh in vitro. Development *124*, 1313–1322.

Scales, S.J., and de Sauvage, F.J. (2009). Mechanisms of Hedgehog pathway activation in cancer and implications for therapy. Trends Pharmacol. Sci. *30*, 303–312.

Seto, M., Ohta, M., Asaoka, Y., Ikenoue, T., Tada, M., Miyabayashi, K., Mohri, D., Tanaka, Y., Ijichi, H., Tateishi, K., et al. (2009). Regulation of the hedgehog signaling by the mitogen-activated protein kinase cascade in gastric cancer. Mol. Carcinog. *48*, 703–712.

Sims-Mourtada, J., Izzo, J.G., Apisarnthanarax, S., Wu, T.T., Malhotra, U., Luthra, R., Liao, Z., Komaki, R., van der Kogel, A., Ajani, J., and Chao, K.S. (2006). Hedgehog: an attribute to tumor regrowth after chemoradiotherapy and a target to improve radiation response. Clin. Cancer Res. *12*, 6565–6572.

Stanton, B.Z., and Peng, L.F. (2010). Small-molecule modulators of the Sonic Hedgehog signaling pathway. Mol. Biosyst. *6*, 44–54.

Stecca, B., Mas, C., Clement, V., Zbinden, M., Correa, R., Piguet, V., Beermann, F., and Ruiz I Altaba, A. (2007). Melanomas require HEDGEHOG-GLI signaling regulated by interactions between GLI1 and the RAS-MEK/AKT pathways. Proc. Natl. Acad. Sci. USA *104*, 5895–5900.

Wiedmann, M.W., and Caca, K. (2005). Molecularly targeted therapy for gastrointestinal cancer. Curr. Cancer Drug Targets *5*, 171–193.

Yen, C.J., Izzo, J.G., Lee, D.F., Guha, S., Wei, Y., Wu, T.T., Chen, C.T., Kuo, H.P., Hsu, J.M., Sun, H.L., et al. (2008). Bile acid exposure up-regulates tuberous sclerosis complex 1/mammalian target of rapamycin pathway in Barrett's-associated esophageal adenocarcinoma. Cancer Res. *68*, 2632–2640.

Zoncu, R., Efeyan, A., and Sabatini, D.M. (2011). mTOR: from growth signal integration to cancer, diabetes and ageing. Nat. Rev. Mol. Cell Biol. *12*, 21–35.

Cancer Cell
Article

Treatment-Emergent Mutations in NAEβ Confer Resistance to the NEDD8-Activating Enzyme Inhibitor MLN4924

Michael A. Milhollen,[1] Michael P. Thomas,[1] Usha Narayanan,[1] Tary Traore,[1] Jessica Riceberg,[1] Benjamin S. Amidon,[1] Neil F. Bence,[1] Joseph B. Bolen,[1] James Brownell,[1] Lawrence R. Dick,[1] Huay-Keng Loke,[1] Alice A. McDonald,[1] Jingya Ma,[1] Mark G. Manfredi,[1] Todd B. Sells,[1] Mike D. Sintchak,[1] Xiaofeng Yang,[1] Qing Xu,[1] Erik M. Koenig,[1] James M. Gavin,[1] and Peter G. Smith[1,*]
[1]Discovery, Millennium Pharmaceuticals, Inc., Cambridge, MA 02139, USA
*Correspondence: peter_smith@h3biomedicine.com
DOI 10.1016/j.ccr.2012.02.009

SUMMARY

MLN4924 is an investigational small-molecule inhibitor of NEDD8-activating enzyme (NAE) in clinical trials for the treatment of cancer. MLN4924 is a mechanism-based inhibitor, with enzyme inhibition occurring through the formation of a tight-binding NEDD8-MLN4924 adduct. In cell and xenograft models of cancer, we identified treatment-emergent heterozygous mutations in the adenosine triphosphate binding pocket and NEDD8-binding cleft of *NAEβ* as the primary mechanism of resistance to MLN4924. Biochemical analyses of *NAEβ* mutants revealed slower rates of adduct formation and reduced adduct affinity for the mutant enzymes. A compound with tighter binding properties was able to potently inhibit mutant enzymes in cells. These data provide rationales for patient selection and the development of next-generation NAE inhibitors designed to overcome treatment-emergent *NAEβ* mutations.

INTRODUCTION

Targeting ubiquitin and ubiquitin-like protein (UBL) pathways with small molecule inhibitors is an emerging therapeutic strategy for a variety of diseases (Schulman and Harper, 2009). Of the seventeen identified UBLs, many play critical roles in the modulation of cancer cell growth and survival pathways through their control of protein homeostasis (Nalepa et al., 2006). Our efforts to inhibit enzymes that control UBL conjugation led to the identification of MLN4924, an investigational small molecule inhibitor of the NEDD8-activating enzyme (NAE; Soucy et al., 2009a). The inhibition of NAE by MLN4924 results in the inactivation of a family of E3 ubiquitin ligases, which results in DNA re-replication and inhibition of nuclear factor (NF)-κB signaling, leading to cancer cell death (Milhollen et al., 2010, 2011). MLN4924 is currently in clinical trials and has shown clinical activity in some solid tumor and hematologic malignancies (Wang et al., 2011). Therefore, we sought to define mechanisms of resistance to MLN4924 in preclinical models of cancer.

The inhibition of NAE by MLN4924 occurs through the formation of a NEDD8-MLN4924 covalent adduct resembling NEDD8-AMP, a process that requires NAE catalytic activity (Brownell et al., 2010). Importantly, the NEDD8-MLN4924 adduct is a tight binding inhibitor of NAE, and it has been proposed that the tight binding nature of the inhibitor-protein adduct is crucial for MLN4924 potency (Brownell et al., 2010). The best characterized substrates of NEDD8 conjugation are the cullin scaffold proteins of the cullin-RING ligase (CRL) complexes, which control the ubiquitination and proteasomal destruction of numerous cancer-relevant proteins (Soucy et al., 2009b; Watson et al., 2011). Thus, inhibition of NAE and NEDD8 conjugation by MLN4924 leads to the inhibition of CRL activity and perturbation of cellular protein homeostasis (Soucy et al., 2009a). The evaluation of MLN4924 in cellular and tumor xenograft studies has revealed two distinct mechanisms of action. The first is the

Significance

There are numerous examples of target-based mutations leading to treatment-emergent resistance in oncology (e.g., with imatinib). This has enabled drug discovery efforts resulting in the identification of superior and/or second-generation inhibitors. As a result of this trend, predicting and responding to resistance is critical to the full exploitation of an oncology target and to promptly meeting the needs of patients. Compelled by clinical activity of MLN4924 in acute myelogenous leukemia, we sought to preemptively define the landscape of resistance mechanisms and identified treatment-induced mutations of *NAEβ*. If resistance occurs in the clinic, these findings will accelerate our assessment of the molecular cause and provide insights into the development of second-generation NAE inhibitors.

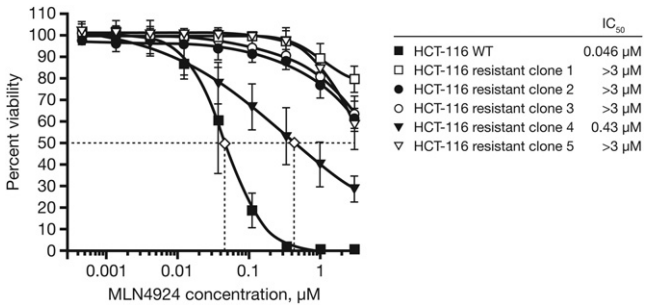

Figure 1. MLN4924-Resistant HCT-116 Clones Show Reduced Sensitivity to MLN4924

HCT-116 WT cells and resistant clones were treated with DMSO or various concentrations of MLN4924 for 96 hr, and cell viability was assessed with an ATPlite assay. Data shown are mean ± standard deviation (n = 3 experiments). See also Figure S1.

induction of DNA re-replication, DNA damage, and cell death through MLN4924-mediated dysregulation of the $CRL1^{SKP2}$ and $CRL4^{DDB1}$ substrate CDT1 (Milhollen et al., 2011). It has been shown that p53 status does not impact the induction of DNA re-replication but may make cells more prone to undergo apoptosis or senescence, depending on the appropriate genetic background (Milhollen et al., 2011; Lin et al., 2010a, 2010b). The second mechanism is the inhibition of NF-κB pathway activity in NF-κB-dependent diffuse large B cell lymphomas (DLBCL), primarily through dysregulation of $CRL1^{\beta TRCP}$-mediated turnover of phosphorylated IκBα (Milhollen et al., 2010). In addition, preclinical models of acute myelogenous leukemia (AML) are sensitive to MLN4924 inhibition in both cell lines and primary patient blasts through mechanisms related to CDT1 dysregulation, NF-κB inhibition, and induction of reactive oxygen species (Swords et al., 2010). These data highlight the therapeutic potential of MLN4924 in a diverse set of preclinical cancer models.

MLN4924 is currently undergoing phase I clinical testing in a variety of solid tumor and hematological malignancies (Wang et al., 2011). Clinical activity has been described in patients with AML with reports of 3 of 15 patients achieving a complete response on MLN4924 therapy (Wang et al., 2011). With initial signs of clinical activity with a pathway inhibitor, it is increasingly important to identify potential mediators of resistance in preclinical models that can be predictive of clinical observations (Sellers, 2011). Thus, we utilized cellular and tumor xenograft models of cancer as an approach to study acquired resistance to MLN4924.

In this report we describe the emergence of heterozygous mutations in the NAEβ (UBA3) subunit of NAE in cell lines and xenograft models of cancer following selection pressure with MLN4924. We evaluate how such mutations may reduce compound potency and present evidence in cells and xenografts regarding pathway inhibition, levels of NAEβ-bound NEDD8-MLN4924 adduct, and recovery of pathway activity following inhibition. Finally, we investigate a pan-E1 inhibitor with tighter binding properties and its ability to inhibit NEDD8 conjugation in MLN4924-resistant cells carrying a mutation in NAEβ.

Table 1. Heterozygous Mutations in *NAEβ* Detected in MLN4924-Resistant HCT-116, NCI-H460, and Calu-6 clones

Cell Line	NAEβ Status Sanger	Sequenom
HCT-116 parental	WT	WT
HCT-116.1	A171T	A171T
HCT-116.2	A171T	A171T
HCT-116.3	A171T	A171T
HCT-116.4	C324Y	C324Y
HCT-116.5	G201V	G201V
NCI-H460 parental	WT	WT
NCI-H460.1	E204K	E204K
NCI-H460.2	A171D	A171D
Calu-6 parental	WT	WT
Calu-6.1	N209K	N209K

See also Figure S2 and Tables S1, S2, and S4.

RESULTS

Clonal Selection of Tumor Cell Lines that Are Resistant to MLN4924 Show Reduced Pathway Inhibition In Vitro and Contain a Mutation in *NAEβ*

Three solid tumor cell lines (HCT-116 colorectal, NCI-H460 lung, and Calu-6 lung) that have been shown to undergo DNA re-replication in response to NAE inhibition (Soucy et al., 2009a) were chosen to study potential mechanisms of resistance to MLN4924. These cell lines have differential sensitivity to MLN4924-induced cytotoxicity, with EC_{50} values (cell viability assay) of 46, 80, and 1070 nM for HCT-116, Calu-6, and NCI-H460 cells, respectively. Cells were exposed to high concentrations of MLN4924 ($\geq EC_{90}$ concentrations) for four days, which resulted in almost-complete cell kill, and five resistant clones were obtained for HCT-116 cells. One HCT-116 clone was found to be 10-fold less sensitive to MLN4924, and four had EC_{50} values greater than 3 μM (Figure 1). Similarly, one Calu-6 clone and two NCI-H460 clones were isolated and found to have EC_{50} values of >10 μM (Figure S1 available online). The MLN4924-resistant HCT-116 cell clones remained sensitive to other chemotherapies (bortezomib, doxorubicin, and SN-38; Figure S1), suggesting that the resistance mechanism is not a shared mechanism with other agents.

To determine whether changes in the NEDD8 pathway may explain the resistance to MLN4924, cells were evaluated for changes in gene transcript levels or the presence of DNA mutations in *NAEβ*, *NAE1*, *NEDD8*, *COPS5*, or *UBC12*, the primary E2 for neddylation. No substantial changes were found in mRNA levels of neddylation pathway genes (Figure S2A). Changes were observed in mRNA levels of adenosine triphosphate (ATP)-binding cassette-transporter proteins; however, MLN4924 activity was unaffected by co-incubation with drug efflux inhibitors (Figure S2B). DNA sequencing revealed no treatment-emergent DNA mutations in *NAE1*, *UBC12*, *COPS5*, or *NEDD8*; however, heterozygous mutations in *NAEβ* were detected by Sanger sequencing in all resistant cell lines (Tables 1 and S1). These mutations were confirmed using additional mass spectrometry-based and next-generation sequencing

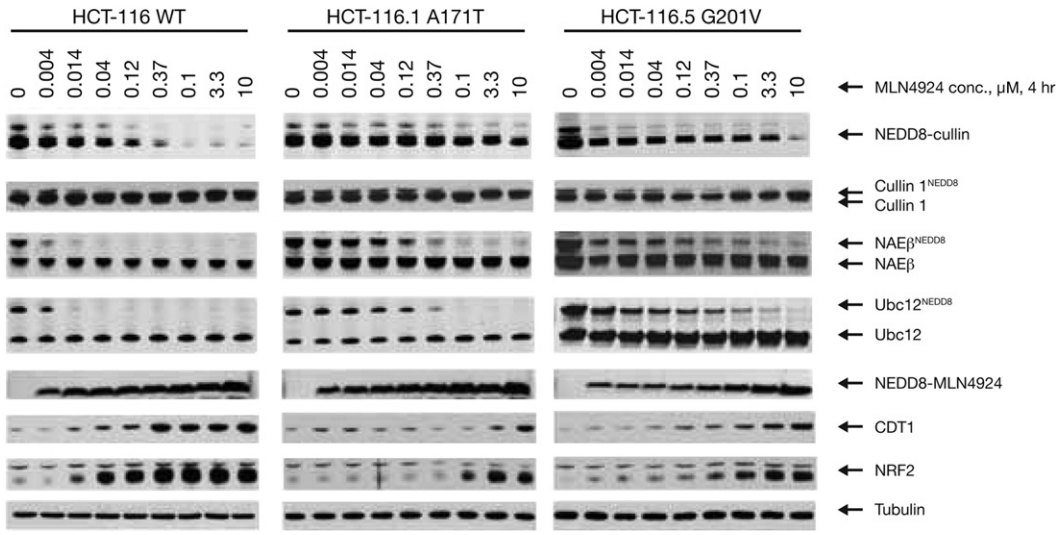

Figure 2. MLN4924-Resistant HCT-116 Clones Show Reduced NEDD8 Pathway Inhibition and Contain a Heterozygous Mutation in NAEβ
HCT-116 WT cells and resistant clones were treated with DMSO or various concentrations of MLN4924 for 4 hr. Western blots were probed for NEDD8-cullin, CUL1, NEDD8-NAEβ, NEDD8-UBC12, NEDD8-MLN4924 adduct, CDT1, NRF2, and tubulin. See also Figure S2.

methods (Table S2). The location of the mutations would be consistent with modification of MLN4924 binding in the nucleotide binding pocket (A171T and A171D) or in affecting the ability of NEDD8 to bind to NAEβ (G201V, E204K, N209K, and C324Y). Of note, a heterozygous mutation in NEDD8 (I44T) was detected in wild-type HCT-116 cells, which was maintained in the resistant clones. However, the activity of this NEDD8 mutant was identical to wild-type NEDD8 in biochemical assays (data not shown).

Pathway analysis by western blotting was performed following a 4 hr incubation of compound to assess the effect of MLN4924 on the NEDD8 pathway in the resistant clones. Two HCT-116 clones were selected for analysis (A171T and G201V), and a reduced effect of inhibition of NEDD8 conjugation to NAEβ, UBC12, and the cullin proteins was demonstrated when compared to wild-type cells (Figure 2). The reduced effect on NAE inhibition was confirmed by a reduced accumulation of two CRL substrates, NRF2 and CDT1 (Figure 2). As expected, NEDD8-MLN4924 adduct could still be detected in the resistant cell lines, since there is still one wild-type copy of NAEβ. In addition, the steady-state neddylation levels of the cullins, and specifically cullin-1 (CUL1), are similar in the three cell lines, and the inhibition of CUL1 neddylation reflects that of the total cullins (Figure 2). MLN4924 induces DNA re-replication in HCT-116 cells (Milhollen et al., 2011), yet the cell-cycle distribution of HCT-116-resistant A171T and G201V clones treated with MLN4924 is not significantly altered, consistent with their insensitivity to MLN4924 (Figure S3). Similar effects of reduced potency of MLN4924 on the neddylation pathway and CRL substrate accumulation were observed in NCI-H460 A171D clone (Figure S3). Reduced pathway inhibition was also observed in the Calu-6 N209K clone, but this was not as marked as in other resistant clones (Figure S3). These data demonstrate that in vitro-derived MLN4924-resistant cell lines contain heterozygous mutations in *NAEβ* and are, as a result, less sensitive to NAE inhibition.

HCT-116 Xenografts Become Resistant to Antitumor Effects of MLN4924, Demonstrate Reduced Pharmacodynamic Effects, and Contain Mutations in NAEβ

HCT-116 cells were grown as subcutaneous xenografts in immunocompromised rats and then subcutaneously treated with the maximum tolerated dose of MLN4924 (150 mg/kg) on a dosing schedule of days 1, 4, 8, and 11 of a 21-day therapy cycle. Importantly, this regimen was chosen as it is currently being utilized in phase I clinical studies of MLN4924 in solid and hematologic malignancies. After the first cycle of MLN4924, tumor regressions were observed that were maintained through most of the second cycle of treatment (Figure 3A). However, during cycle 3, ten of eleven tumors began to regrow, even in the presence of MLN4924 (Figure 3A). Tumors were harvested at the end of treatment and the nucleic acid sequence of *NAEβ* was analyzed. Eight of ten tumors were found to contain a heterozygous mutation at A171T of NAEβ (Figure 3A and Table S2). Interestingly, in two tumors, more than one mutation was detected (A171T/E204K and A171T/A171D/Y228H, respectively), indicating that multiple clones may emerge within a tumor population. No mutations were detected in *NAE1*, *COPS5*, or *UBC12*, and the I44T mutation within *NEDD8* was detected, consistent with cells grown in vitro.

To confirm that the tumors were now stably resistant to MLN4924, one xenograft with an A171T mutation was retransplanted into nude rats. The antitumor activity of MLN4924 was dramatically reduced compared to wild-type xenografts; one cycle of MLN4924 150 mg/kg (days 1, 4, 8, and 11) inhibited tumor growth by only 38% compared to 94% (including tumor regressions) that were observed in wild-type xenografts (Figure 3B). The A171T NAEβ mutation was still present in this resistant xenograft model as confirmed by both Sanger and Sequenom methodologies. Pharmacodynamic analysis of NEDD8 pathway inhibition by MLN4924 in HCT-116 wild-type and A171T-resistant xenografts was conducted following a single

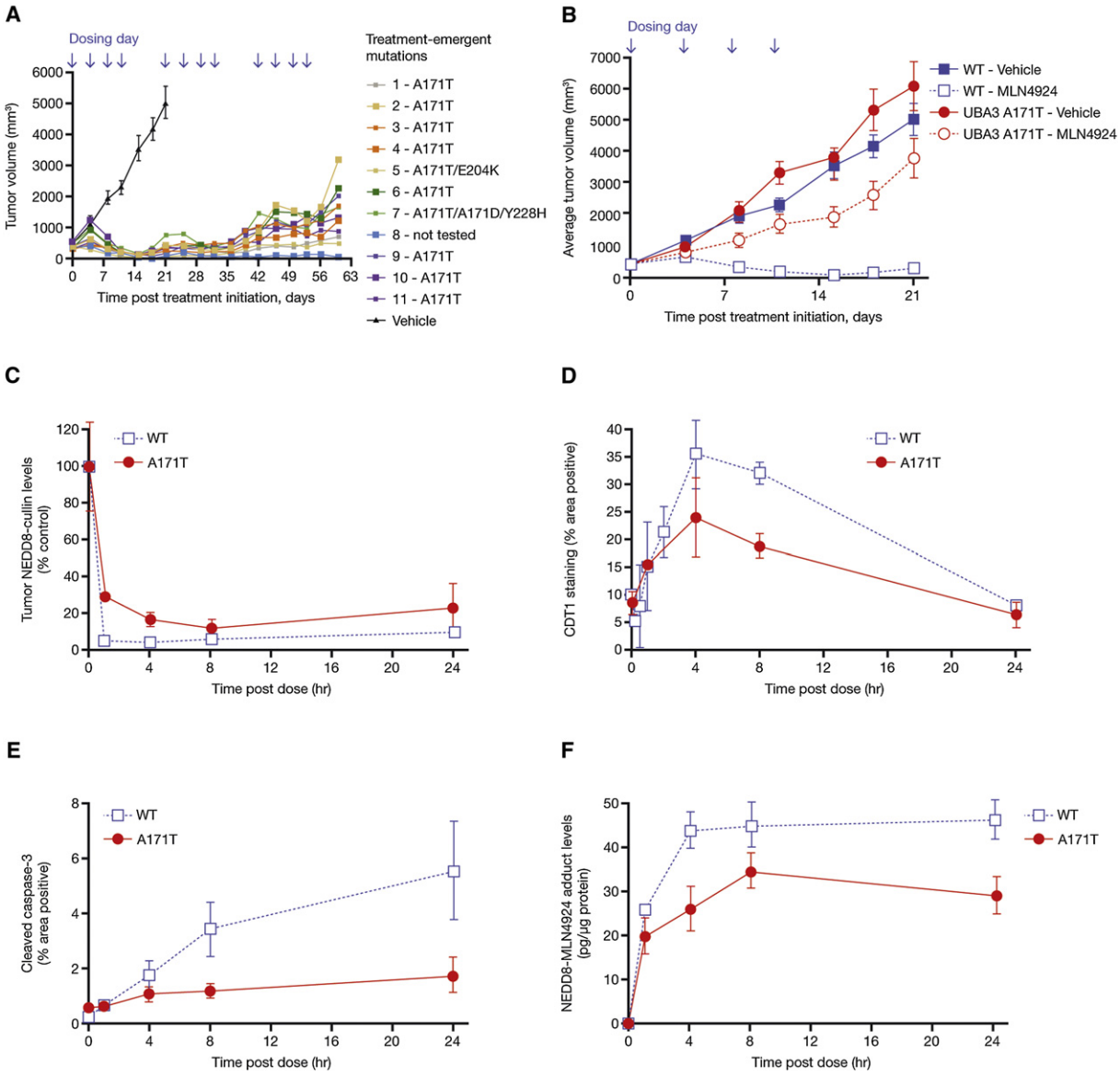

Figure 3. HCT-116 Xenograft-Bearing Nude Rats Become Refractory to MLN4924 Treatment, Contain a Heterozygous Mutation in NAEβ, and Are Resistant to Retreatment

(A) Immunocompromised nude rats bearing HCT-116 xenografts were administered MLN4924 150 mg/kg on days 1, 4, 8, and 11 of a 21-day cycle for three cycles. Tumors were harvested at the end of treatment for analysis, and the mutational status of *NAEβ* was determined. Data shown are mean ± standard error (n = 10) for vehicle group.

(B) A tumor containing an alanine 171 to threonine mutation was re-established in nude rats and treated with MLN4924 150 mg/kg on days 1, 4, 8, and 11 of a 21-day cycle. The response of WT (parental) tumors is included on the graph for comparison. Data shown are mean ± standard error (n = 10).

(C–F) Nude rats bearing HCT-116 parental or A171T xenografts were administered a single dose of 150 mg/kg MLN4924 and tumors were excised at the indicated times and measured for (C) NEDD8-cullin conjugate levels by western blotting; (D) CDT1 levels by immunohistochemistry; (E) cleaved caspase-3 levels by immunohistochemistry; and (F) NEDD8-MLN4924 adduct levels by mass spectrometry. Data shown are mean ± standard deviation (n = 3 replicates). See also Table S2 and Figure S4.

dose of MLN4924 (150 mg/kg). Maximal inhibition of NEDD8-cullin levels occurred as early as 1 hr postdose in HCT-116 wild-type xenografts compared to 8 hr postdose in the A171T-resistant model (Figures 3C and S4A). In agreement with reduced effects on NEDD8-cullin levels in HCT-116 A171T cells was a reduction in CDT1 levels (Figures 3D and S4B), apoptosis as measured by cleaved caspase-3 (Figure 3E and S4C), and NEDD8-MLN4924 adduct (Figure 3F) compared to HCT-116 wild-type xenografts. These data demonstrate that tumor xenografts treated with a clinically relevant dosing schedule can acquire resistance to MLN4924 that is associated with mutations in *NAEβ*.

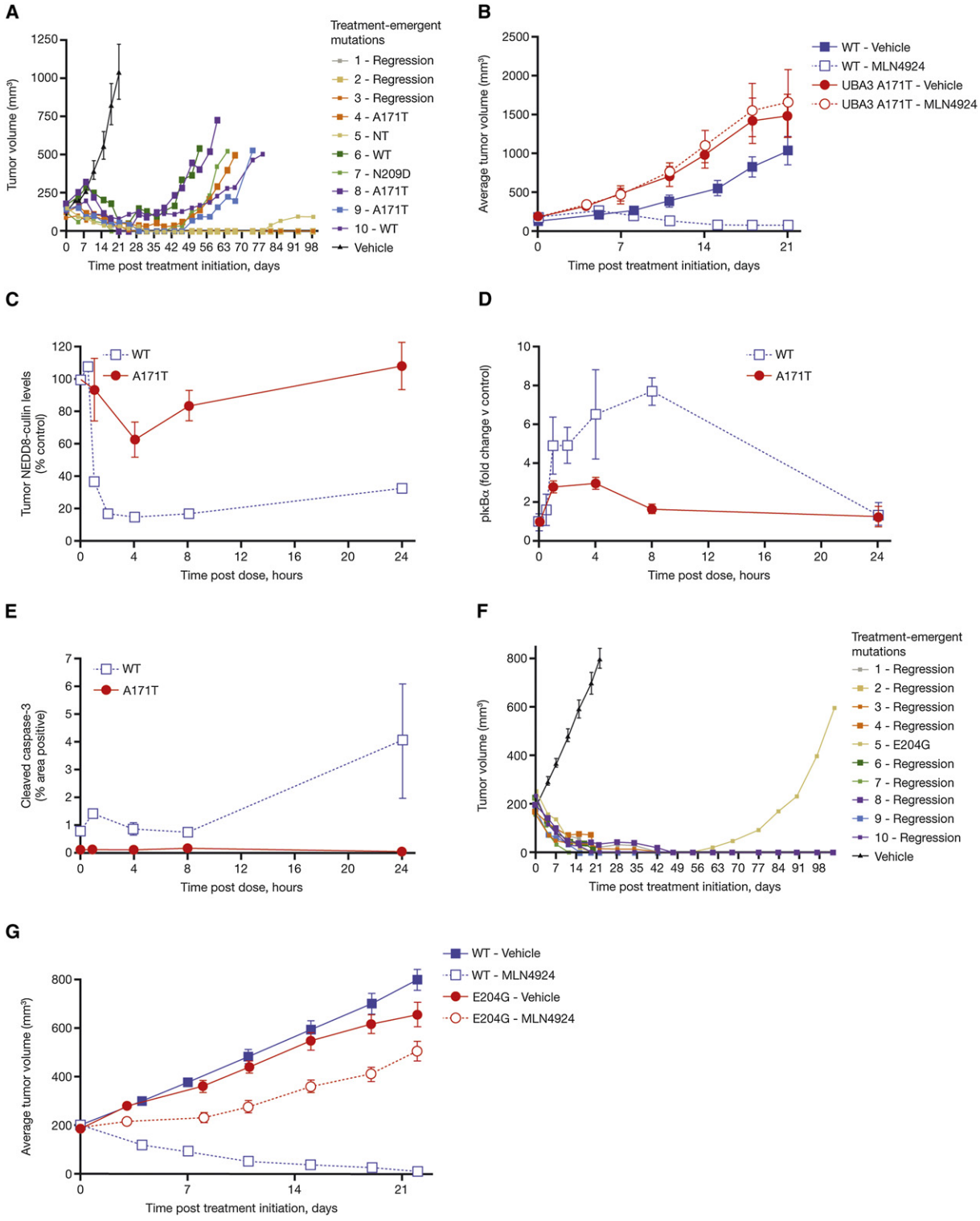

Figure 4. Acute Myelogenous Leukemia and Diffuse Large B Cell Lymphoma Xenograft-Bearing Nude Mice Become Refractory to MLN4924 Treatment, Contain a Heterozygous Mutation in NAEβ, and Are Resistant to Retreatment

(A) CB.17 SCID mice bearing THP-1 AML xenografts were administered MLN4924 90 mg/kg BID on days 1, 4, 8, 11, 15, and 18 of a 21-day cycle for up to five cycles. Tumors were harvested at the end of treatment for analysis, and the mutational status of *NAEβ* was determined. Data shown are mean ± standard error (n = 10) for vehicle group.

(B) A tumor containing an alanine 171 to threonine mutation was re-established in CB.17 SCID mice and treated with MLN4924 90 mg/kg BID on days 1, 4, 8, 11, 15, and 18 of a 21-day cycle. The response of WT (parental) tumors is included on the graph for comparison. Data shown are mean ± standard error (n = 10).

Treatment-Emergent Mutations in *NAEβ* Are Observed in AML and DLBCL Xenografts

MLN4924 has shown clinical activity in patients with AML (Wang et al., 2011). Therefore, we utilized THP-1 cells, a relevant subcutaneous AML preclinical model, to determine whether resistance to MLN4924 could be driven by *NAEβ* mutations. The subcutaneous model was utilized to facilitate harvesting tumors for subsequent analysis. On a clinically relevant schedule, MLN4924 was administered to SCID mice bearing THP-1 xenografts (90 mg/kg BID, twice-weekly), and uniform tumor regressions were observed (Figure 4A). Six of ten THP-1 xenografts regrew during the MLN4924 treatment period and were harvested for analysis. Three of these THP-1 xenografts contained a heterozygous mutation in *NAEβ* at A171T, one contained a heterozygous mutation at N209D, and the remaining two were wild-type for NAEβ so may be refractory through an alternate mechanism (Figure 4A and Table S2). Again, no mutations were observed in *NAE1*, *COPS5*, *UBC12*, or *NEDD8*. One A171T THP-1 xenograft was successfully re-established in SCID mice and shown to be resistant to MLN4924 when dosed at 90 mg/kg BID twice-weekly (Figure 4B). Pharmacodynamic evaluation in THP-1 A171T xenografts showed that MLN4924 produced minimal inhibition of NEDD8-cullin levels (Figures 4C and S5A), resulting in a reduced elevation of the CRL substrate pIκBα (Figures 4D and S5B) and a failure to activate apoptosis (Figures 4E and S5C) in comparison to THP-1 wild-type xenografts.

We have previously shown that activated B cell-like (ABC-) DLBCL may be particularly sensitive to MLN4924 through inhibition of constitutively active NF-κB signaling (Milhollen et al., 2010). To determine whether resistance to MLN4924 through *NAEβ* mutations occurs in models in which re-replication does not drive the terminal outcome, we followed OCI-Ly10 xenograft-bearing mice and administered MLN4924 (90 mg/kg BID, twice-weekly) for more than 100 days. Consistent with our previous findings, MLN4924 induced tumor regressions in the OCI-Ly10 model (Figure 4F). Only one of ten tumors regrew during therapy, and subsequent analysis revealed a heterozygous mutation in *NAEβ* at E204G. The tumor was re-implanted and was, as with the other re-introduced resistant tumors, resistant to MLN4924 treatment at 90 mg/kg BID (Figure 4G). These data demonstrate that, regardless of the MLN4924-dependent terminal outcome or genetic background, certain *NAEβ* mutations can drive resistance to MLN4924.

Mutations in the Nucleotide Binding Pocket and NEDD8 Binding Cleft of NAEβ Affect MLN4924 Adduct Formation and Dissociation from NAEβ

The *NAEβ* mutations that have been detected in MLN4924-resistant cells derived in tissue culture or in vivo occur in two areas of the gene, the nucleotide binding pocket at Alanine 171 and at various residues that are within or close to the NEDD8 binding cleft (Figures 5A and 5B). Mutations at Alanine 171 appear to be a "hotspot," since approximately two-thirds of the mutations detected lie at this residue (Figure 5A). Structural renderings of the A171T and A171D mutants suggest that decreased potency of MLN4924 could occur through a clash with the indane group of MLN4924 and the bulkier threonine or aspartic acid residue in mutant NAEβ (Figure 5B). In contrast, mutations found in the NEDD8 binding region of NAEβ are hypothesized to affect the affinity of NEDD8 and in turn the NEDD8-MLN4924 adduct (Figure 5B). To understand the biochemical consequences of mutations in these regions, recombinant enzymes expressing A171T, A171D, N209K, E204K, or G201V were constructed as representative of the two classes of mutations (Table 2). Structural modeling of A171T or A171D did not predict an effect on ATP binding, yet these mutations did result in weaker affinity for ATP. However, the titration profile and affinity for NEDD8 was largely unaffected by mutations to A171 (Table 2 and Figure S6). In contrast, mutations in the NEDD8 binding cleft (G201V and E204K) resulted in a shift in the NEDD8 titration profile, which attributes to a concomitant increase in the K_M for NEDD8 (Table 2 and Figure S6). Neither of these NEDD8 binding cleft mutations had much effect on the K_M for ATP. Interestingly, a mutation at G201V resulted in an increase in both the K_M for ATP and NEDD8, whereas the K_M for PPi was unaffected by any of these mutations (Table 2). In addition, other than the A171D mutant, the catalytic rate (k_{cat}) of the NAE reaction is not severely affected by any of these mutations; in fact, it appears that the G201V mutant is more catalytically active than is the wild-type enzyme (Table 2).

We have previously demonstrated that MLN4924 inhibits the NEDD8-NAEβ thioester form of NAE by occupying the nucleotide binding site and forming a covalent adduct between NEDD8 and MLN4924 (Brownell et al., 2010). To determine the effect of inhibitory potency of MLN4924 against wild-type and mutant enzymes, the PPi-ATP assay was performed using a concentration of 1 mM ATP. Interestingly, the A171T mutant was still capable of being inhibited by MLN4924 with only a modest 2-fold decrease in potency compared to wild-type enzyme (Table 2). MLN4924 did not inhibit A171D up to a concentration of 100 μM, suggesting that the bulkier aspartic acid residue impedes MLN4924 binding in the nucleotide binding pocket. MLN4924 was approximately 10-fold less active against the NEDD8 binding cleft mutants compared to wild-type enzyme. Compound 1, a structurally similar N6-substituted adenosine sulfamate, was used for comparison with MLN4924 (Brownell et al., 2010). The potency of Compound 1 decreased 7-fold versus the A171T mutant and 17,000-fold versus the A171D mutant (Table 2). A noticeable decrease in potency was

(C–E) CB.17 SCID mice bearing THP-1 parental or A171T xenografts were administered a single dose of MLN4924 90 mg/kg and tumors were excised at the indicated times and measured for (C) NEDD8-cullin conjugate levels by western blotting; (D) pIκBα levels by western blotting; and (E) cleaved caspase-3 levels by immunohistochemistry. Data shown are mean ± standard deviation (n = 3 replicates). (F) CB.17 SCID mice bearing OCI-Ly10 DLBCL xenografts were administered MLN4924 90 mg/kg BID on days 1, 4, 8, 11, 15, and 18 of a 21-day cycle for up to five cycles. Tumors were harvested at the end of treatment for analysis, and the mutational status of *NAEβ* was determined. Data shown are mean ± standard error (n = 10) for vehicle group.
(G) A tumor containing a glutamic acid 204 to glycine mutation was re-established in CB.17 SCID mice and treated with MLN4924 90 mg/kg BID on days 1, 4, 8, 11, 15, and 18 of a 21-day cycle. The response of WT (parental) tumors is included on the graph for comparison. Data shown are mean ± standard error (n = 10). See also Table S2 and Figure S5.

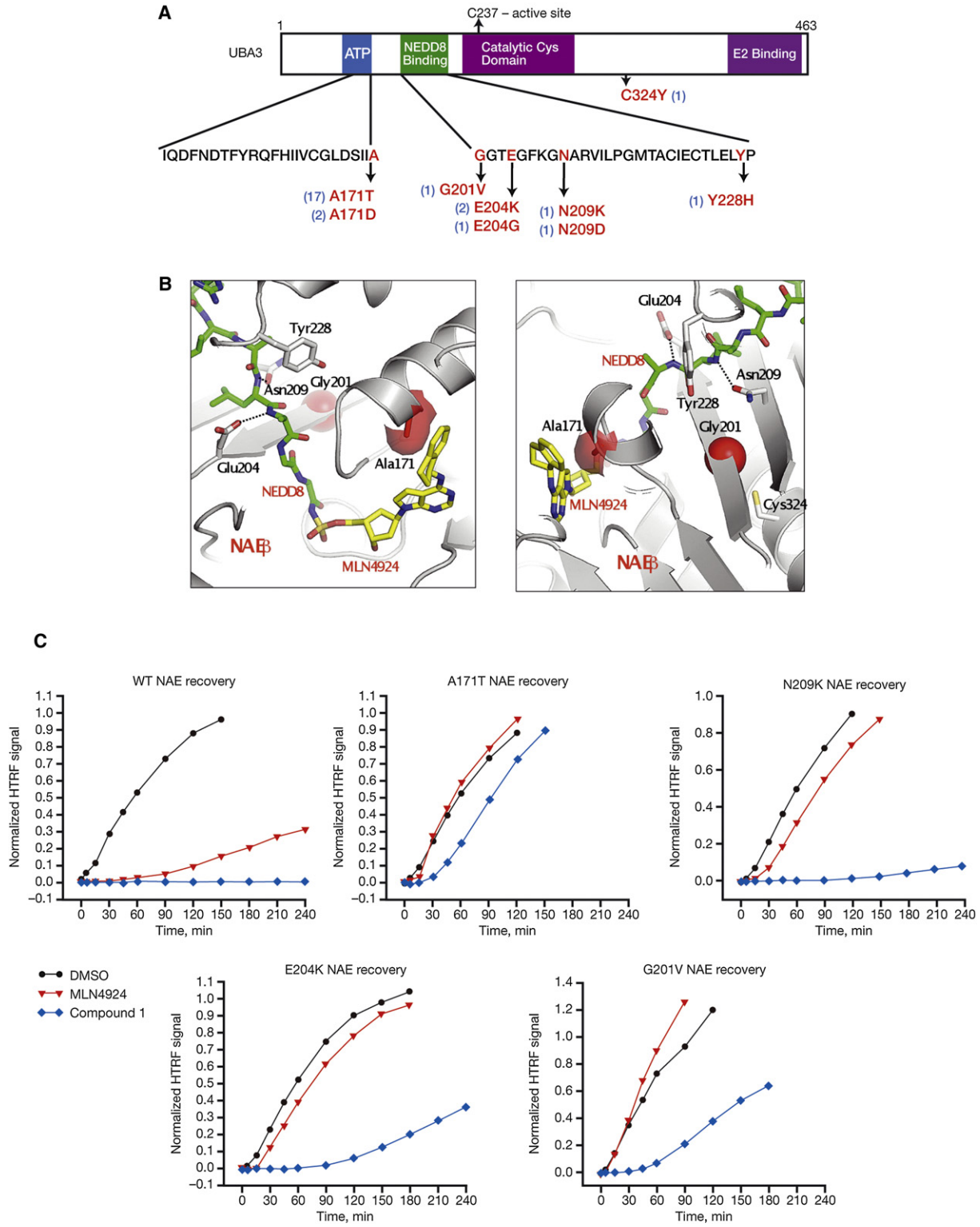

Figure 5. NAEβ Mutants Located in ATP Binding Pocket and NEDD8-Binding Cleft Lead to Faster Recovery from Enzyme Inhibition

(A) Schematic representation of location and frequency of NAEβ mutations detected in cells and xenografts.

(B) Crystal structure of NAE with NEDD8-MLN4924 adduct bound (PDB entry 3GZN; Brownell et al., 2010), highlighting NAEβ mutations.

(C) NAEβ mutants were inhibited with MLN4294 or compound 1 and purified, and complexes were added to transthiolation reaction containing 1 mM ATP to measure recovery of enzyme activity. Data shown are the mean of four replicates. See also Table S3.

Table 2. Biochemical Characterization of NAEβ Mutants.

NAEβ Enzyme	K_M ATP (μM)	K_M NEDD8 (μM)	K_M PPi (μM)	k_{cat} (s^{-1})	MLN4924 IC_{50} (μM)	Compound 1 IC_{50} (μM)
WT	88 ± 3	0.044 ± 0.024	22 ± 2	1.2 ± 0.2	0.049 ± 0.011	0.0041 ± 0.0002
A171T	600 ± 30	0.080 ± 0.018	22 ± 2	1.5 ± 0.4	0.10 ± 0.026	0.030 ± 0.002
A171D	1,900 ± 20	0.016 ± 0.0037	10 ± 2	0.33 ± 0.08	>100	70 ± 20
N209K	31 ± 1	0.43 ± 0.081	24 ± 2	2.0 ± 0.1	0.78 ± 0.16	0.076 ± 0.005
E204K	21 ± 1	0.48 ± 0.053	18 ± 1	1.3 ± 0.5	1.6 ± 0.20	0.17 ± 0.005
G201V	820 ± 36	3.5 ± 0.22	10 ± 1	3.7 ± 0.5	0.51 ± 0.057	0.0057 ± 0.0006

Several NAEβ mutants were characterized in the pyrophosphate exchange assay and analyzed for parameters of K_M for ATP, NEDD8, PPi, and catalytic activity. The K_M for each substrate was determined by titrating each substrate into the PPi-ATP assay and fitting the average of three replicates to the standard Michaelis-Menten equation, $y = V_{max}^{*}[S] / K_M + [S]$, where y is PPi-ATP activity. The standard error was extrapolated from the fit. The k_{cat} for each enzyme using three replicates was determined under optimal conditions (saturating ATP, PPi, and peak [NEDD8]) and using an [α-32P]-ATP standard curve. Each k_{cat} value represents the average and standard deviations of duplicates experiments. NAEβ mutants were tested in the pyrophosphate exchange using 1 mM ATP and measured for potency with MLN4924 and Compound 1. IC_{50} curves using the average of three replicates were fit using a sigmoidal logistics 3-parameter equation, $y = a / (1+([I]/IC_{50})^{b}$, where y is % inhibition, a is amplitude, and b is hill slope. Each IC_{50} value represents the average and standard deviations of duplicate experiments. See also Figure S6.

also observed with Compound 1 in the NEDD8 binding pocket mutants.

Since in vitro IC_{50}s of enzyme inhibition did not fully explain the resistance to MLN4924 observed, further compound characterization was performed to evaluate the rates of enzyme inactivation and the reversibility of compound inhibition. A171D NAEβ mutant was not used in these studies, because it was completely insensitive to MLN4924 inhibition. Enzyme-inhibitor complexes, NEDD8-MLN4924 or NEDD8-Compound 1, were pre-formed on the enzyme, purified, and added to a UBC12 transthiolation reaction to measure the recovery of enzyme activity (Figure 5C). As previously reported, NEDD8-MLN4924 was a tight-binding inhibitor of wild-type NAEβ with enzyme activity, recovering to approximately 30% of dimethylsulfoxide (DMSO) control levels by 240 min. In contrast, the recovery of enzymatic activity following MLN4924 inhibition was similar to that of the DMSO control for A171T, N209K, E204K, and G201V mutants. These data indicate that although the NEDD8-MLN4924 adduct is formed by the mutant enzymes, it is no longer a tight-binding inhibitor. The NEDD8-Compound 1 adduct binds more tightly to wild-type NAEβ than the NEDD8-MLN4924 adduct, with no discernible recovery of enzymatic activity at 240 min (Figure 5C). In addition, the NEDD8-Compound 1 adduct appears to be a tighter binder of all mutant NAE enzymes, suggesting that Compound 1 may be a more potent inhibitor of mutant enzyme in cells compared to MLN4924.

The rate of enzyme inactivation by MLN4924 for both A171T and N209K mutants was also dramatically slower compared to wild-type as opposed to Compound 1, for which the rate of wild-type and mutant enzyme inactivation was more rapid than MLN4924 (Table S3). These data provide a rationale for explaining the resistance that is conferred by mutations in *NAEβ*, namely, the slower rate of inactivation and faster off-rate of the NEDD8-MLN4294 adduct.

Cells Containing Mutations in NAEβ Form Lower Levels of NEDD8-MLN4924 Adduct and Show Increased Recovery of Pathway Activity

HCT-116 mutant cells lines (A171T and G201V) were evaluated during and after MLN4924 treatment to determine the effect of these mutations on pathway activity recovery. Cells were treated with MLN4924 10 μM for 1 hr, after which compound was removed and replaced with drug-free media; cells were harvested at 0 min, 15 min, 2 hr, or 5 hr postdrug washout (Figure 6A). In agreement with previous observations (Brownell et al., 2010), western blot analysis of wild-type cells indicated incomplete recovery of NEDD8-cullin and NEDD8-UBC12 and a persistence of NEDD8-MLN4924 adduct levels at both 1 μM and 10 μM for at least 5 hr postwashout. The prolonged pathway inhibition in the washout setting was corroborated by continued elevation of two CRL substrates, NRF2 and CDT1. In contrast, both A171T and G201V mutant cell lines showed almost-complete recovery of pathway activity as early as 15 min postwashout (Figure 6A). Interestingly, it appeared that the two mutant cell lines contained a reduced amount of NEDD8-MLN4924 adduct compared to wild-type cells, even though the levels of total NAEβ appeared similar. This would support the biochemical findings of a slower rate of adduct formation and weaker binding of adduct in the mutant enzymes.

To determine whether lower amounts of NEDD8-MLN4924 adduct were bound to NAEβ, cells were treated under the same washout conditions but subjected to immunoprecipitation assays with NAEβ (Figure 6B). Similar levels of NAEβ and NAE1 were detected in immunoprecipitates, indicating that the NAE heterodimer had been efficiently extracted from cell lysates. Immunoprecipitates were next probed with the NEDD8-MLN4924 antibody, which detected lower levels bound to A171T and G201V mutants compared to the wild-type enzyme. Lower levels of bound NEDD8-MLN4924 adduct in A171T and G201V mutants compared to wild-type enzyme were confirmed by running the 1 hr incubation samples on the same gel (Figure S7). It is likely that the amount of NEDD8-MLN4294 adduct bound to NAEβ is comprised mostly of an adduct bound to the wild-type but not the mutant enzyme, as the mutant enzyme can form an adduct but not bind the adduct tightly. To determine if higher levels of unbound adduct were present in mutant versus wild-type cells, the flow-through from the immunoprecipitates was probed with the NEDD8-MLN4924 adduct antibody (Figure 6B). However, there did not appear to be a difference in

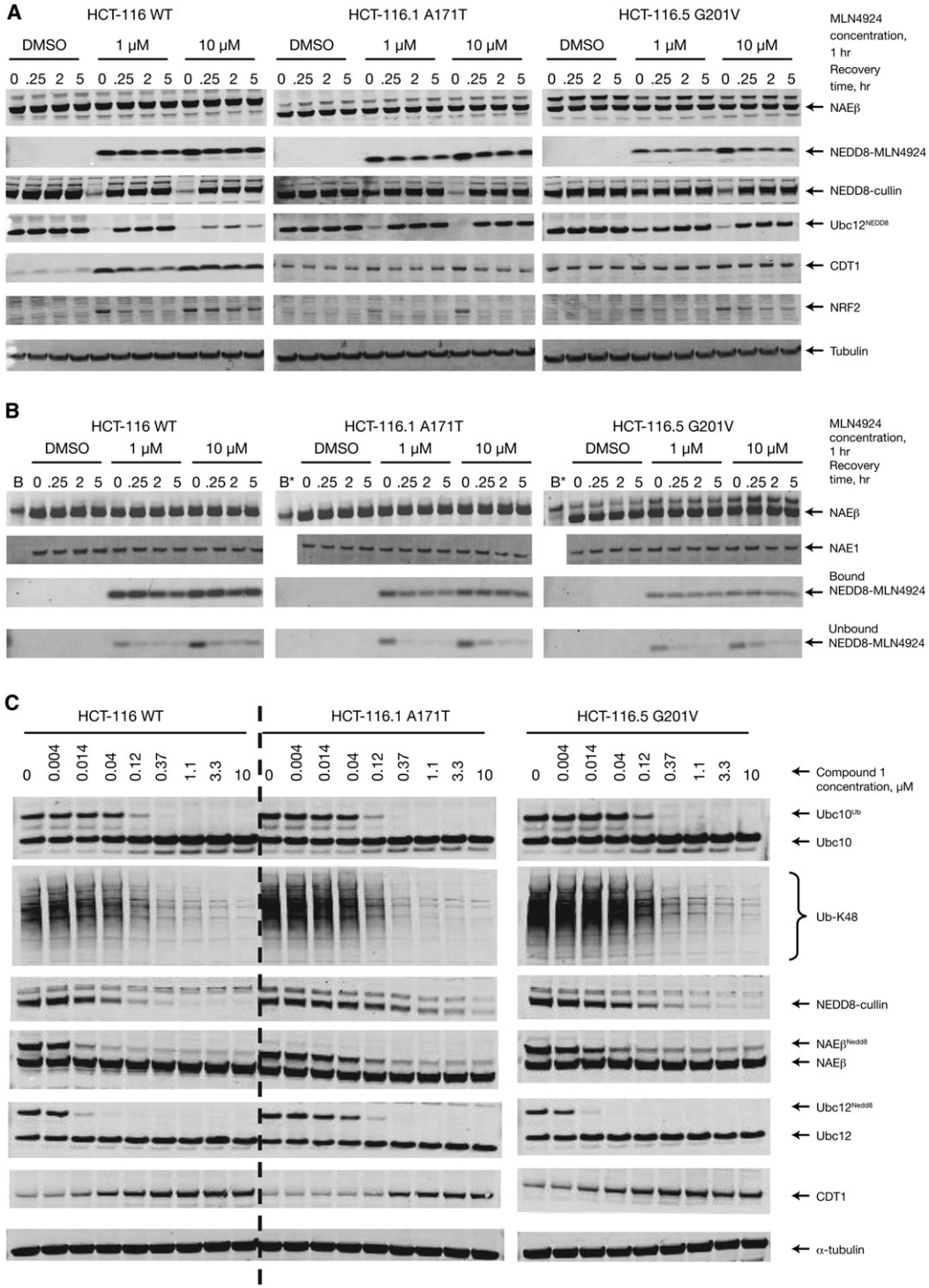

Figure 6. MLN4924-Resistant Cells with a Heterozygous *NAEβ* Mutation Show Reduced Levels of NEDD8-MLN4924 Adduct Formation, Faster Recovery of Pathway Inhibition, and Are More Sensitive to a Tighter-Binding NAE Inhibitor

(A) HCT-116 WT, A171T, or G201V cells were treated with MLN4924 1 μM or 10 μM for 1 hr, the compound was washed out, and the cells were incubated in drug-free media and harvested at the indicated times. Protein lysates were probed by western blotting for NEDD8-cullin, NEDD8-NAEβ, NEDD8-UBC12, NEDD8-MLN4924 adduct, CDT1, NRF2, and tubulin.

(B) Immunoprecipitation assays were performed with a NAEβ antibody and resultant isolates probed with NAEβ, NAE1, and NEDD8-MLN4924 adduct antibody. Flow through from the immunoprecipitation assays was probed with NEDD8-MLN4924 adduct antibody. See also Figure S7.

(C) HCT-116 WT, A171T, or G201V cells were treated with various concentrations of compound 1 for 4 hr, and protein lysates were probed by western blotting for UBC10, ubiquitin K48 chains, NEDD8-cullin, NEDD8-NAEβ, NEDD8-UBC12, CDT1, and α-tubulin.

the amount of free adduct in mutant versus wild-type cells, which may be due to proteolysis of adduct when it is released from NAEβ in cells. These data show that, following inhibition of mutant NAEβ in cells, pathway activity recovers quickly and correlates with lower amounts of NEDD8-MLN4924 adduct bound to the enzyme.

The data in biochemical and cell-based assays would suggest that a NEDD8-inhibitor adduct, which was able to bind more tightly to the enzyme, may overcome resistance to MLN4924 treatment-emergent NAE mutations. To test this hypothesis we used Compound 1, which in biochemical assays had faster rates of enzyme inhibition and slower rates of recovery compared to MLN4924. HCT-116 wild-type, and A171T and G201V mutant cells were exposed to increasing concentrations of Compound 1 for 4 hr and assessed for pathway activity by western blotting (Figure 6C). Since Compound 1 also inhibits UBA1, we could show comparable inhibition of ubiquitination of Ubc10 (an E2 for ubiquitin) and polyubiquitination in all cells (Figure 6C). In contrast to MLN4924 (see Figure 2), Compound 1 was able to produce comparable inhibition of NAEβ-NEDD8, NEDD8-cullin, and NEDD8-UBC12 in G201V mutant versus wild-type cells, and there was only a modest decrease in A171T mutant cells compared to wild-type cells. This likely reflects the quicker recovery of enzyme activity seen with Compound 1 in A171T biochemical assays. These data suggest that NEDD8-inhibitor compounds with improved binding affinities may overcome the resistance observed in the NAEβ mutations we have identified. In addition, to provide complete inhibition of the A171T mutation, alternative strategies may need to be employed, which could include the generation of covalent inhibitors of the enzyme.

Sequencing of DNA from AML, Colon Cancer, and Melanoma Tumor Samples Does Not Detect Preexisting Mutations in *NAEβ*

To determine whether mutations in *NAEβ* could be detected in cancer patients and therefore may exist prior to MLN4924 therapy, DNA from 50 colon cancer and melanoma tumor samples and 41 AML samples were subjected to Sanger and mass spectrometry-based (Sequenom platform) sequencing (Table S4). No *NAEβ* mutations were detected by either method, with the Sequenom platform having a sensitivity limit of approximately 10%. To increase the sensitivity of detection we subjected 21 of the AML samples to next-generation sequencing of *NAEβ* using the illumina platform but did not detect any mutations in *NAEβ*. Similarly, "preexisiting" mutations in *NAEβ* were not detected in wild-type HCT-116, Calu-6, and NCI-H460 cells by next-generation sequencing. Interestingly, one heterozygous *NAEβ* mutation (C249Y resulting from an amino acid change G > A) has been reported in an ovarian cancer patient in the Catalogue of Somatic Mutations in Cancer (Cosmic) database (total 218 tumor samples tested; http://www.sanger.ac.uk/perl/genetics/CGP/cosmic?action = bygene&ln = UBA3&start = 1&end = 1392&coords = AA%3Abp). This mutation is in a region of NAEβ that binds NAE1 (Walden et al., 2003) and so may interfere with heterodimer formation and enzyme activity. Thus, we were not able to detect a preexisting mutation in *NAEβ* in DNA isolated from patient tumors, leukemic blasts, or cancer cell lines.

DISCUSSION

MLN4924, a small-molecule inhibitor of an E1-activating enzyme (NAE) that is being tested as a cancer therapy in humans, has shown clinical activity with reports of complete responses in patients with AML (Wang et al., 2011). In this report we sought to characterize potential mechanisms of resistance to MLN4924 in preclinical models of cancer. We demonstrated that human tumor cell lines and xenografts grown in immunocompromised rodents can acquire resistance to MLN4924 through coding sequence mutations in *NAEβ*. These studies reveal a potential strategy for designing second-generation inhibitors that could overcome resistance mediated by mutations in *NAEβ*.

The occurrence of amino acid substitutions has been described as a common form of resistance for cancer drugs, such as tyrosine kinase inhibitors, including imatinib, gefitinib, and erlotinib (Shah et al., 2002; Kobayashi et al., 2005; Pao et al., 2005). More recent examples include amino acid substitutions in the anaplastic lymphoma kinase (ALK) following crizotinib therapy that occurred in lung cancer patients harboring an *EML4-ALK* translocation (Choi et al., 2010). Mutations in *ALK* that reduced sensitivity to crizotinib were originally described in preclinical studies using models of *NPM-ALK* translocations, which led to the studies' predictions that the mutations may occur in *EML4-ALK* cancers (Lu et al., 2009). These data demonstrate two important points: confirmation that the enzyme targets of these drugs "drive" the cancer, and that the activity of the inhibitors is through inhibition of the target. Furthermore, these observations have led to treatment paradigms that include retreating relapsed patients with a second-generation inhibitor that can target enzymes with amino acid substitutions (Cortes et al., 2011). This approach may be useful for NAEβ amino acid substitutions that are mechanisms of resistance to MLN4924 in clinical studies.

Treatment-emergent mutations in *NAEβ* were detected in the ATP binding pocket and NEDD8 binding cleft with approximately two-thirds at Alanine 171, representing a potential hotspot. Though mutations in both areas generally led to changes in affinities for ATP or NEDD8, this did not lead to a dramatic change in catalytic rate of NAE (except in the case of A171D and G201V). However, mutations in both areas of NAEβ led to a slower rate of enzyme inhibition and a NEDD8-MLN4924 adduct that was no longer tightly bound. We have previously demonstrated that NEDD8-MLN4924 adduct formation is necessary for potent NAE inhibition by MLN4924 and the tight binding nature of the adduct is required for in vitro and cellular potency (Brownell et al., 2010). In keeping with this notion, we demonstrated reduced pathway inhibition in cells and a more rapid recovery from compound inhibition in cell washout experiments. We used a nonselective E1 inhibitor (Compound 1) to probe the effects of more potent enzyme inhibition in vitro and in cells. Compound 1 forms an adduct with NEDD8 in vitro and shows a slower rate of recovery from enzyme inhibition compared to MLN4924 in the wild-type and mutant enzymes tested. These data indicate that the NEDD8-Compound 1 adduct is a tighter binder of wild-type and mutant NAEβ enzymes compared to MLN4924. Indeed, in A171T and G201V mutant HCT-116 cells Compound 1 was able to more potently inhibit

NEDD8-cullin and NEDD8-UBC12 thioester levels than did MLN4924. However, pathway inhibition in the A171T mutant HCT-116 cells was less pronounced than in the G201V mutant HCT-116 cells, which may indicate the need for a tighter binding inhibitor or a molecule capable of covalent inactivation of the A171T mutant. Nevertheless, these data support our notion that a NAE-selective, NEDD8-compound adduct with high affinity for mutant and wild-type enzymes should overcome resistance in cells and tumor xenografts. Unfortunately, it was not possible to test this in cell viability or xenograft experiments, as Compound 1 is nonselective for other E1 enzymes whose inhibition can result in viability effects (Brownell et al., 2010). It will be of interest to complete a thorough characterization of all *NAEβ* mutants and the mechanism by which they are conferring resistance to MLN4924. For example, the Y228H mutation corresponds with a residue previously shown to be important for "clamping" the C-terminus of NEDD8 into the adenylation domain, and the mutation of Y228 has been previously shown to diminish NEDD8 adenylation (Walden et al., 2003). This would suggest that this mutant enzyme is inefficient for NEDD8-activation. In addition, the mutation detected at C324Y is in a region of NAEβ that may also impact NEDD8 binding through structural perturbation of the NEDD8 binding cleft (see Figure 5B). Interestingly, Alanine at position 171 is conserved in most E1-activating enzymes, including UBA1, UBA6, and Sumo-activating enzyme, suggesting that selective inhibitors of these enzymes that are potential drug targets may also be susceptible to the same resistance mechanism.

The resistant cell lines were selected following a short exposure (four days) to high concentrations of MLN4924. All cell lines were isolated as clonal populations, shown to be resistant to MLN4924 and still sensitive to other chemotherapies, including proteasome inhibition (bortezomib), an anthracycline (doxorubicin), and a topoisomerase I inhibitor (SN-38). Reverse transcription-polymerase chain reaction analysis of the clones indicated an elevation of drug efflux mechanisms with increased detection of mRNA for Pgp and BCRP in some cell lines. However, it appears that the elevation of drug efflux does not significantly contribute to the resistance, as cotreating cells with a number of Pgp, BCRP, and MRP2 inhibitors did not sensitize cells to MLN4924 (dipyridamole, Shalinsky et al., 1993; MK519, Gekeler et al., 1995; GF120918, Hyafil et al., 1993; K0143, Allen et al., 2002; LY5979, Dantzig et al., 1996). These data, in addition to the presence of mutations in NAEβ, indicate that the resistance is driven by mutations in the target enzyme.

MLN4924 induces DNA damage in cells via re-replication (Milhollen et al., 2011), and this mechanism of inducing hyperreplication of DNA may aid in the development of resistance through increased random mutagenesis. HCT-116, H460, and Calu-6 cells all undergo DNA re-replication, whereas OCI-Ly10 cells do not (Milhollen et al., 2010). We were able to detect an *NAEβ* mutation in the OCI-Ly10 model, suggesting that resistant mutants can emerge irrespective of the mechanism of action of MLN4924. Interestingly, HCT-116 cells have a deficiency in the DNA mismatch repair protein MLH1 (Taverna et al., 2000), and this may make them more susceptible to resistance mutations by virtue of increased genomic instability. This assertion may be supported by the increased number of mutations detected in HCT-116 cell lines and xenografts compared to others used in these studies that do not possess the same defect in DNA repair. It will be of interest to understand whether the mechanism of DNA re-replication and/or defects in DNA repair make cells more likely to develop resistance to MLN4924 through mutations in *NAEβ*.

In these studies we have detected heterozygous mutations in *NAEβ*, where cells maintain one wild-type copy of *NAEβ*. An important model system to conclusively prove that mutations in *NAEβ* drive resistance would be an engineered cell line that only expresses the mutant, not the wild-type, enzyme. Thus far, we have not been successful in developing such a model system. It is possible that a wild-type enzyme is required to support growth and that the role of the mutant enzyme is to enable NEDD8 conjugation when the wild-type enzyme is under transient inhibition by MLN4924 in cells and xenografts. Since the mutation frequency of *NAEβ* in cell and xenograft populations is ~50%, we developed mass spectrometry and next-generation sequencing methodologies that allowed us to detect *NAEβ* mutations to a frequency of ~0.5%. We were not able to detect mutations in *NAEβ* that were preexisting in the cell line, xenograft, or patient tumor DNA samples, suggesting that the mutations are acquired during the selection process. A search of single-nucleotide polymorphism databases did not reveal the existence of the mutations reported in human populations, but we cannot rule out the possibility that mutations do exist at a lower frequency than 0.5% in tumors. Indeed, a mutation in *NAEβ* has been reported in the Cosmic database in an ovarian cancer sample at C249Y. This residue is in a region of NAEβ that is involved in binding NAE1 (Walden et al., 2003), and so it is possible that this would interfere with heterodimer formation and enzyme activity. It will be important to continue efforts to establish whether mutations are preexisiting, as this may predict patients who are more likely to relapse following MLN4924 administration.

These studies demonstrate that treatment-emergent mutations in *NAEβ* can confer resistance to MLN4924 in preclinical models. Since *NAEβ* mutations appear to be the most common cause of resistance in our studies, irrespective of the cellular outcome following NAE inhibition, this confirms the selectivity of MLN4924 for its target. We did observe the regrowth of THP-1 AML xenografts that did not contain a mutation in *NAEβ*, suggesting that other mechanisms of resistance to MLN4924 are also likely to occur. Mechanisms of MLN4924 resistance will be explored further so that continued clinical strategies can be employed in responding patients. These may take the form of combination partners based on complimentary biology in the context of NAE inhibition or next-generation NAE inhibitors targeted to mutant NAEβ that may emerge in MLN4924-relapsed patients.

EXPERIMENTAL PROCEDURES

Materials

[32P]-PPi (Cat. No. NEX019), [α-32P]-ATP (Cat. No. BLU003H250UC), and [α-32P]-ATP (Cat. No.BLU002250UC) were obtained from Perkin Elmer (Boston, MA, USA). Other chemicals were purchased from Sigma-Aldrich (St. Louis, MO, USA). N-terminal FLAG-tagged NEDD8 with the sequence of N-MDYKDDDDK-NEDD8 was expressed and purified as described (Soucy

et al., 2009a). Untagged NEDD8 and N15- and C13-labeled, untagged NEDD8 (NEDD8*) was expressed and purified similarly. N-terminal GST-tagged Ubc12 was expressed and purified as described (Soucy et al., 2009a). His-tagged NAE proteins (*NAE1* and His-tagged *NAEβ* wild-type and mutants) were cloned into Rosetta (DE3) cells and complexes were generated by co-expression into *Escherichia coli*. Expressed proteins were purified by affinity (Ni-NTA agarose; Qiagen, Valencia, CA, USA) or conventional chromatography. GST-tagged NAE proteins (NAE1 and GST-tagged NAEβ wild-type and mutants) were generated by co-infection of Sf9 cells (Soucy et al., 2009a). GST-NAE proteins were purified by affinity chromatography (Glutathione Sepharose 4B; GE Healthcare, Piscataway, NJ, USA) followed by Hi-Trap Q HP (GE Healthcare).

Cell Culture, Cell Viability, and Western Blot Analysis

Cell line cultures were maintained using the appropriate cell culture media as recommended by ATCC and as previously reported (Soucy et al., 2009a; Milhollen et al., 2010). To derive resistant cell lines HCT-116, Calu-6, and NCI-H460 cells were incubated with high concentrations of MLN4924 ($\geq EC_{90}$ concentrations) for four days, after which the remaining cells were removed, plated as single-cell clones, and cultured in drug-free media. Cell viability assays were completed using a 96 hr ATPlite assay (Perkin Elmer) as previously reported (Soucy et al., 2009a). Whole-cell extracts were prepared and immunoblotting assays performed as previously described (Soucy et al., 2009a) with primary antibodies as follows: CDT1, NRF2, NEDD8, NAEβ, UBC12, and MLN4924-NEDD8-ADS (MIL22; Millennium, Cambridge, MA, USA); UBC10 (Boston Biochem, Cambridge, MA, USA); K48 (Millipore, Billerica, MA, USA); NAE1 (Sigma-Aldrich); and tubulin (Santa Cruz, Santa Cruz, CA, USA). Secondary Alexa-680-labeled antibodies to rabbit/mouse IgG (Molecular Probes, Grand Island, NY, USA) were used as was appropriate, and blots were imaged using the Li-Cor Odyssey Infared Imaging system.

Cell Culture Washout and Immunoprecipitation Analysis

HCT-116 wild-type, A171, and G201V cells were treated with either MLN4924 1 μM or 10 μM or DMSO for 1 hr. Cells were washed with media to remove the drug, replaced with fresh media, and harvested at 0 hr, 0.25 hr, 2 hr, or 5 hr postwashout. Lysates were prepared as previously reported (Soucy et al., 2009a). Washout lysate (100 μg) was incubated with 5 μg NAEβ antibody on ice for 1 hr. Slurry Protein G agarose (Upstate, Billerica, MA, USA; 50 μl of 50%) was added and tumbled for 1 hr at 4°C. Samples were spun down and supernatant removed to fresh tube (unbound fraction), and beads were washed three times with buffer. Sample buffer (50 μl 2X) was added to beads (bound fraction), and samples were fractionated on sodium dodecyl sulfate polyacrylamide gel electrophoresis gels and immunobloted as indicated. For the unbound fraction, the above procedure was repeated using 2 μg MLN4924-NEDD8-ADS (MIL22) antibody and 50 μl of 50% slurry Protein A agarose (Pierce, Rockford, IL, USA).

Immunocompromised Rat and Mouse Antitumor Studies

Female NCr nude rats (Taconic Farms, Germantown, NY, USA), aged 6–8 weeks, were inoculated with 10×10^6. HCT-116 cells were subcutaneously injected in the right flank. Tumor growth was measured using digital vernier calipers. When mean tumor growth reached ~500 mm^3, rats were assigned randomly to treatment groups and dosed subcutaneou sly with vehicle (20% hydroxypropyl-beta-cyclodextrin) or MLN4924. Rats received one dose per day twice-weekly for two weeks (days 1, 4, 8, and 11) of a 21-day therapy cycle. After three cycles of treatment, refractory tumors were collected. Female CB-17 SCID mice (Charles River Laboratories, Wilmington, MA, USA), aged 6–8 weeks, were inoculated with 2×10^6 THP-1 or OCI-Ly10 cells with Matrigel support (1:1, v/v). When mean tumor growth reached 200 mm^3, mice were assigned randomly to treatment groups and dosed subcutaneously with vehicle (20% hydroxypropyl-beta-cyclodextrin) or MLN4924. Mice received two doses per day twice-weekly (days 1, 4, 8, 11, 15, 18, 22, and so on) until tumors reached ~500–800 mm^3. Tumors were then collected and one 40 mg–50 mg piece of tumor was subcutaneously implanted using a 13-gauge trocar needle into 6–8 naive animals for further study. In addition, tumor DNA was extracted for mutational analysis as described in the Supplemental Experimental Procedures. All studies were done in accordance with the standards of ethical treatment approved by the Institutional Animal Care and Use Committee (IACUC) and Association for the Assessment and Accreditation of Laboratory Animal Care (AAALAC). All animal experiments were approved by the Institutional Animal Care and Use Committee of Millennium Pharmaceuticals Inc.

Pharmacodynamic Marker Analysis

Mice and rats bearing HCT-116, THP-1, or OCI-Ly10 tumors were administered a single MLN4924 dose, and at the indicated times, tumors were excised and extracts prepared. The relative levels of NEDD8-cullin and plκBα were estimated by quantitative immunoblot analysis (Li-Cor Odyssey system) using Alexa680-labeled anti-IgG (Molecular Probes) as the secondary antibody. For the analysis of CDT1 and cleaved caspase-3 levels in tumor sections, formalin-fixed, paraffin-embedded tumor sections were stained with the relevant antibodies, amplified with HRP-labeled secondary antibodies, and detected with the ChromoMap DAB Kit (Ventana Medical Systems, Tuscon, AZ, USA). Slides were counterstained with hematoxylin. Images were captured using an Eclipse E800 microscope (Nikon Instruments, Melville, NY, USA) and Retiga EXi color digital camera (QImaging, Surrey, BC, Canada) and processed using Metamorph software (Molecular Devices, Sunnyvale, CA, USA). CDT1 and cleaved caspase-3 are expressed as a function of the DAB signal area.

Measurement of NEDD8-MLN4924 Adduct Levels in Tumor Xenografts

To quantify the absolute level of NEDD8-MLN4924 adduct in tumor xenografts, 30 μg total protein of each lysate sample was mixed with 0.1 pmol (0.9 ng) NEDD8*-MLN4924 followed by NuPAGE Bis-Tris 4%–12% SDS gel separation (Invitrogen); NEDD8 gel fractions were excised and in-gel tryptic digestion was performed as described previously (Brownell et al., 2010). The digests were analyzed on an LC/MS/MS system (Brownell et al., 2010). The NEDD8-MLN4924 adduct amount in each sample was calculated from the ratio of the peak areas of Gly-Gly-MLN4924 to Gly*-Gly*-MLN4924 in the chromatogram.

Biochemical Characterization of NAEβ and Mutant Enzymes

Biochemical characterization and IC_{50} determinations were performed using an improved pyrophosphate exchange assay developed by Bruzzese et al. (2009). ATP-PPi exchange reactions were performed in buffer containing 50 mM HEPES (pH 7.5), 25 mM NaCl, 10 mM $MgCl_2$, 0.05% BSA, 0.01% Tween-20, and 1 mM DTT. NEDD8 titrations were performed by serial dilution of NEDD8 into a 96-well assay plate containing 10 nM NAE, 1 mM ATP, and 0.2 mM PPi (50 cpm/pmol [32P] PPi). Assays were incubated for 30 min at 37°C in a final volume of 50 μl and were stopped with the addition of 500 μl of 5% (w/v) trichloroacetic acid containing 10 mM PPi. The quenched reactions were transferred to a dot-blot apparatus fitted with activated charcoal filter paper as described previously (Bruzzese et al., 2009). CPM was converted to pM/min using an [α-P32] ATP standard curve. Since NEDD8 was inhibitory at higher concentrations for wild-type and A171T/D NAEβ, inhibited top points for these particular mutants were excluded before fitting for an estimated K_M. All K_Ms were fit using the standard Michaelis-Menten equation for enzyme kinetics. ATP K_Ms were determined by serial diluting ATP into a 96-well assay plate under similar assay conditions. Reactions were initiated with addition of NEDD8 (0.16 μM for wild-type, A171T/D and 2.5 μM for N209K, E204K, and G201V). Assays were incubated for 30 min at 37°C. PPi titrations were performed under similar conditions, except with serial dilution of PPi instead and using 1 mM ATP.

IC_{50}s were determines by serial dilution of each compound into a 96-well assay plate containing 5 nM NAE, 1 mM ATP, and 0.2 mM PPi (50 cpm/pmol [32P] PPi). Reactions were initiated with addition of NEDD8 (0.16 μM for wild-type, A171T/D, and 2.5 μM for N209K, E204K, and G201V). Assays were incubated for 60 min at 37°C in a final volume of 50 μl and were stopped as previously described.

The enzyme reversibility assay was run in the FLAG-NEDD8-GST-UBC12 HTRF transthiolation assay described previously (Soucy et al., 2009a; Brownell et al., 2010). Final concentrations of each enzyme after dilution were 10 pM wild-type NAEβ, 12.5 pM A171T NAEβ, 30 pM N209K NAEβ, and 33 pM E204K/G201V NAEβ.

Clinical Human Tumor Testing

All human tumor samples were obtained from commercial vendors (Supplemental Experimental Procedures) and were de-identified prior to purchase and analysis.

AML

Forty one unique malignant AML patient tumors (21 bone marrow aspirates and 20 bone marrow mononuclear cells) were genotyped for mutations found in preclinical models using the sequenom NAEβ assays (Supplemental Experimental Procedures), and the full gene was sequenced by an Illumina Next-Generation sequencing assay. All samples were found to be wild-type for NAEβ. The AML tumors represented newly diagnosed and relapsed patients with M1-M5 diagnosis classification. The blast tumor count ranged from 2% to 94%. Matched peripheral blood mononuclear cells were also sequenced and found to be wild-type.

Colon Cancer

A collection of 50 unique mucinous and sigmoidal colon adenocarcinomas with representative histologies of poor, moderate, and well-differentiated and 10% to 100% tumor per tissue were genotyped for mutations found in preclinical models using the Sequenom NAEβ assays, and the full gene was sequenced by Sanger sequencing. All samples were found to be wild-type for NAEβ.

Melanoma

A collection of 25 unique epithelioid and spindle cell-type melanoma adenocarcinomas, ranging from 25% to 100% tumor per tissue, were genotyped for mutations found in preclinical models using the Sequenom NAEβ assays, and the full gene was sequenced by Sanger sequencing. All samples were found to be wild-type for NAEβ.

SUPPLEMENTAL INFORMATION

Supplemental Information includes seven figures, four tables, and Supplemental Experimental Procedures and can be found with this article online at doi:10.1016/j.ccr.2012.02.009.

ACKNOWLEDGMENTS

All authors were employees of Millennium Pharmaceuticals, Inc., at the time of this work. Millennium Pharmaceuticals, Inc., is developing MLN4924.

Received: October 5, 2011
Revised: December 12, 2011
Accepted: February 6, 2012
Published: March 19, 2012

REFERENCES

Allen, J.D., van Loevezijn, A., Lakhai, J.M., van der Valk, M., van Tellingen, O., Reid, G., Schellens, J.H., Koomen, G.J., and Schinkel, A.H. (2002). Potent and specific inhibition of the breast cancer resistance protein multidrug transporter in vitro and in mouse intestine by a novel analogue of fumitremorgin C. Mol. Cancer Ther. *1*, 417–425.

Brownell, J.E., Sintchak, M.D., Gavin, J.M., Liao, H., Bruzzese, F.J., Bump, N.J., Soucy, T.A., Milhollen, M.A., Yang, X., Burkhardt, A.L., et al. (2010). Substrate-assisted inhibition of ubiquitin-like protein-activating enzymes: the NEDD8 E1 inhibitor MLN4924 forms a NEDD8-AMP mimetic in situ. Mol. Cell *37*, 102–111.

Bruzzese, F.J., Tsu, C.A., Ma, J., Loke, H.K., Wu, D., Li, Z., Tayber, O., and Dick, L.R. (2009). Development of a charcoal paper adenosine triphosphate: pyrophosphate exchange assay: kinetic characterization of NEDD8 activating enzyme. Anal. Biochem. *394*, 24–29.

Choi, Y.L., Soda, M., Yamashita, Y., Ueno, T., Takashima, J., Nakajima, T., Yatabe, Y., Takeuchi, K., Hamada, T., Haruta, H., et al; ALK Lung Cancer Study Group. (2010). EML4-ALK mutations in lung cancer that confer resistance to ALK inhibitors. N. Engl. J. Med. *363*, 1734–1739.

Cortes, J., Hochhaus, A., Hughes, T., and Kantarjian, H. (2011). Front-line and salvage therapies with tyrosine kinase inhibitors and other treatments in chronic myeloid leukemia. J. Clin. Oncol. *29*, 524–531.

Dantzig, A.H., Shepard, R.L., Cao, J., Law, K.L., Ehlhardt, W.J., Baughman, T.M., Bumol, T.F., and Starling, J.J. (1996). Reversal of P-glycoprotein-mediated multidrug resistance by a potent cyclopropyldibenzosuberane modulator, LY335979. Cancer Res. *56*, 4171–4179.

Gekeler, V., Ise, W., Sanders, K.H., Ulrich, W.R., and Beck, J. (1995). The leukotriene LTD4 receptor antagonist MK571 specifically modulates MRP associated multidrug resistance. Biochem. Biophys. Res. Commun. *208*, 345–352.

Hyafil, F., Vergely, C., Du Vignaud, P., and Grand-Perret, T. (1993). In vitro and in vivo reversal of multidrug resistance by GF120918, an acridonecarboxamide derivative. Cancer Res. *53*, 4595–4602.

Kobayashi, S., Boggon, T.J., Dayaram, T., Jänne, P.A., Kocher, O., Meyerson, M., Johnson, B.E., Eck, M.J., Tenen, D.G., and Halmos, B. (2005). EGFR mutation and resistance of non-small-cell lung cancer to gefitinib. N. Engl. J. Med. *352*, 786–792.

Lin, H.K., Chen, Z., Wang, G., Nardella, C., Lee, S.W., Chan, C.H., Yang, W.L., Wang, J., Egia, A., Nakayama, K.I., et al. (2010a). Skp2 targeting suppresses tumorigenesis by Arf-p53-independent cellular senescence. Nature *464*, 374–379.

Lin, J.J., Milhollen, M.A., Smith, P.G., Narayanan, U., and Dutta, A. (2010b). NEDD8-targeting drug MLN4924 elicits DNA rereplication by stabilizing Cdt1 in S phase, triggering checkpoint activation, apoptosis, and senescence in cancer cells. Cancer Res. *70*, 10310–10320.

Lu, L., Ghose, A.K., Quail, M.R., Albom, M.S., Durkin, J.T., Holskin, B.P., Angeles, T.S., Meyer, S.L., Ruggeri, B.A., and Cheng, M. (2009). ALK mutants in the kinase domain exhibit altered kinase activity and differential sensitivity to small molecule ALK inhibitors. Biochemistry *48*, 3600–3609.

Milhollen, M.A., Traore, T., Adams-Duffy, J., Thomas, M.P., Berger, A.J., Dang, L., Dick, L.R., Garnsey, J.J., Koenig, E., Langston, S.P., et al. (2010). MLN4924, a NEDD8-activating enzyme inhibitor, is active in diffuse large B-cell lymphoma models: rationale for treatment of NF-kappaB-dependent lymphoma. Blood *116*, 1515–1523.

Milhollen, M.A., Narayanan, U., Soucy, T.A., Veiby, P.O., Smith, P.G., and Amidon, B. (2011). Inhibition of NEDD8-activating enzyme induces rereplication and apoptosis in human tumor cells consistent with deregulating CDT1 turnover. Cancer Res. *71*, 3042–3051.

Nalepa, G., Rolfe, M., and Harper, J.W. (2006). Drug discovery in the ubiquitin-proteasome system. Nat. Rev. Drug Discov. *5*, 596–613.

Pao, W., Miller, V.A., Politi, K.A., Riely, G.J., Somwar, R., Zakowski, M.F., Kris, M.G., and Varmus, H. (2005). Acquired resistance of lung adenocarcinomas to gefitinib or erlotinib is associated with a second mutation in the EGFR kinase domain. PLoS Med. *2*, e73.

Sellers, W.R. (2011). A blueprint for advancing genetics-based cancer therapy. Cell *147*, 26–31.

Schulman, B.A., and Harper, J.W. (2009). Ubiquitin-like protein activation by E1 enzymes: the apex for downstream signalling pathways. Nat. Rev. Mol. Cell Biol. *10*, 319–331.

Shah, N.P., Nicoll, J.M., Nagar, B., Gorre, M.E., Paquette, R.L., Kuriyan, J., and Sawyers, C.L. (2002). Multiple BCR-ABL kinase domain mutations confer polyclonal resistance to the tyrosine kinase inhibitor imatinib (STI571) in chronic phase and blast crisis chronic myeloid leukemia. Cancer Cell *2*, 117–125.

Shalinsky, D.R., Jekunen, A.P., Alcaraz, J.E., Christen, R.D., Kim, S., Khatibi, S., and Howell, S.B. (1993). Regulation of initial vinblastine influx by P-glycoprotein. Br. J. Cancer *67*, 30–36.

Soucy, T.A., Smith, P.G., Milhollen, M.A., Berger, A.J., Gavin, J.M., Adhikari, S., Brownell, J.E., Burke, K.E., Cardin, D.P., Critchley, S., et al. (2009a). An inhibitor of NEDD8-activating enzyme as a new approach to treat cancer. Nature *458*, 732–736.

Soucy, T.A., Smith, P.G., and Rolfe, M. (2009b). Targeting NEDD8-activated cullin-RING ligases for the treatment of cancer. Clin. Cancer Res. *15*, 3912–3916.

Swords, R.T., Kelly, K.R., Smith, P.G., Garnsey, J.J., Mahalingam, D., Medina, E., Oberheu, K., Padmanabhan, S., O'Dwyer, M., Nawrocki, S.T., et al. (2010). Inhibition of NEDD8-activating enzyme: a novel approach for the treatment of acute myeloid leukemia. Blood *115*, 3796–3800.

Taverna, P., Liu, L., Hanson, A.J., Monks, A., and Gerson, S.L. (2000). Characterization of MLH1 and MSH2 DNA mismatch repair proteins in cell lines of the NCI anticancer drug screen. Cancer Chemother. Pharmacol. *46*, 507–516.

Walden, H., Podgorski, M.S., and Schulman, B.A. (2003). Insights into the ubiquitin transfer cascade from the structure of the activating enzyme for NEDD8. Nature *422*, 330–334.

Wang, M., Medeiros, B.C., Erba, H.P., DeAngelo, D.J., Giles, F.J., and Swords, R.T. (2011). Targeting protein neddylation: a novel therapeutic strategy for the treatment of cancer. Expert Opin. Ther. Targets *15*, 253–264.

Watson, I.R., Irwin, M.S., and Ohh, M. (2011). NEDD8 pathways in cancer, sine quibus non. Cancer Cell *19*, 168–176.

Cancer Cell
Article

Marginating Dendritic Cells of the Tumor Microenvironment Cross-Present Tumor Antigens and Stably Engage Tumor-Specific T Cells

John J. Engelhardt,[1] Bijan Boldajipour,[1] Peter Beemiller,[1] Priya Pandurangi,[1] Caitlin Sorensen,[1] Zena Werb,[2] Mikala Egeblad,[2,3] and Matthew F. Krummel[1,*]
[1]Department of Pathology
[2]Department of Anatomy
University of California San Francisco, San Francisco, CA 94143, USA
[3]Cold Spring Harbor Laboratory, 1 Bungtown Road, Cold Spring Harbor, NY 11724, USA
*Correspondence: matthew.krummel@ucsf.edu
DOI 10.1016/j.ccr.2012.01.008

SUMMARY

The nature and site of tumor-antigen presentation to immune T cells by bone-marrow-derived cells within the tumor microenvironment remains unresolved. We generated a fluorescent mouse model of spontaneous immunoevasive breast cancer and identified a subset of myeloid cells with significant similarity to dendritic cells and macrophages that constitutively ingest tumor-derived proteins and present processed tumor antigens to reactive T cells. Using intravital live imaging, we determined that infiltrating tumor-specific T cells engage in long-lived interactions with these cells, proximal to the tumor. In vitro, these cells capture cytotoxic T cells in signaling-competent conjugates but do not support full activation or sustain cytolysis. The spatiotemporal dynamics revealed here implicate nonproductive interactions between T cells and antigen-presenting cells on the tumor margin.

INTRODUCTION

Despite the recruitment of tumor-specific $CD8^+$ tumor-infiltrating lymphocytes (TILs) to the tumor microenvironment, the immune response is limited in its ability to clear tumors (Drake et al., 2006). Numerous lines of evidence suggest that tolerance to tumors relies on presentation of peptide antigens on major histocompatibility complex (MHC) molecules on the surface of bone-marrow-derived antigen-presenting cells (APCs), as is the case for other peripheral tissues (Adler et al., 1998; Heath and Carbone, 2001; Kusmartsev et al., 2005; Sotomayor et al., 2001). In recent years, broad classes of cell types derived from the mononuclear phagocyte system (MPS), such as myeloid-derived suppressor cells (MDSCs) and tumor-associated macrophages (TAMs), have been implicated in promoting tumor growth and metastasis while inhibiting a productive immune response by T cells (Gabrilovich and Nagaraj, 2009; Pollard, 2009). TAMs increase metastasis in the PyMT breast cancer model (Lin et al., 2006), partly as a result of T cell skewing toward a Th2 phenotype (DeNardo et al., 2009). Isolated MDSCs bearing the marker Gr-1, in contrast, inhibit T cell activation and suppress the activation of T cells by secondary APCs or other stimuli (Gabrilovich and Nagaraj, 2009; Terabe et al., 2003). There has, however, been no direct identification of the cell type that physically mediates antigen uptake and presentation in the tumor microenvironment.

Dendritic cells (DCs), another cell type derived from the MPS that is very similar to macrophages, are the preeminent APCs for T cells in lymphoid organs and in tissues. DCs in this setting are clearly integral in activating T cells but may also serve to tolerize them (Hawiger et al., 2001). The role of DCs in tumors (TuDC) is less well understood, but their presence is extensively documented. While the elicitation of a potent T cell expansion by DCs is clearly an integral part of a successful immunotherapy and can be augmented by transferring antigen-pulsed DCs to hosts (Mayordomo et al., 1995), DCs in the

Significance

The cells involved in presenting antigens to T cells at the tumor site are not defined. To better study the T cell response to tumors, we developed a fluorescent- and antigen-linked spontaneous model of breast cancer. The primary cells responsible for ingesting tumor antigens and presenting them to T cells are low-motility myeloid cells localized along tumor margins. These cells fail to stimulate T cells and may serve as a barrier to an effective T cell response. This model demonstrates the behavior of tolerized T cells within tumors and provides a target for immunotherapies. Marker analysis demonstrates that the cells presenting antigens to T cells are a large subset of cells implicated in tumor remodeling.

tumor microenvironment may also be an important aspect of immune dysregulation. For example, the presence of specific subsets of DCs, especially CD123$^+$ plasmacytoid DCs (pDCs), are associated with negative prognosis in human patients (Ambe et al., 1989; Treilleux et al., 2004).

Delineating cell types of the MPS purely on surface phenotype has proven difficult because TAMs, MDSCs, and DCs share many common lineage markers. While direct staining of these cells from sections provides information about the populations in aggregate, it is likely that the MPS contributes a variety of cell types to the microenvironment, all of which might be the primary APCs for T cells. Real-time intravital imaging has shed light on key processes during priming in the lymph node, including the priming of T cells on DCs (Miller et al., 2002; Mempel et al., 2004), and holds promise for delineating subsets of APCs that are responsible for interacting with T cells. It has the benefit of complementing phenotypic surface marker data with morphological and behavioral phenotypes. Imaging of ectopic thymomas (EL4s) using labeled T cell receptor (TCR) transgenic cells has revealed long-lived antigen-dependent contacts as well as effective killing between T cells and the tumor cells during tumor rejection (Mrass et al., 2006). However, in those models, there was no possibility to visualize or define the APCs of the microenvironment or to study T cell interaction with such bone-marrow-derived APCs. Furthermore, introduction of tumor-specific T cells in these models leads to tumor regression, unlike the case in typical refractory tumors. Thus, the interactions of T cells and APCs that accompany tumor tolerance have, as yet, remained largely unresolved.

To gain insights into the nature of tumor antigen presentation and the nature of interactions between T cells and APCs in refractory tumors, we have generated a spontaneous tumor model of human breast cancer based on the well-described MMTV-PyMT model (Guy et al., 1992) that incorporates tags for both imaging and for T-cell characterization. This model allows us to track uptake of a coexpressed protein-fluorophore from tumor into the APC compartment. This study effectively exposes a key cell type and its antigen uptake, presentation, and activation capacities, as well as placing these activities spatially within the tumor microenvironment.

RESULTS

Recruitment and Inactivity of Tumor-Specific T Cells in a Spontaneous Model of Breast Cancer

To provide a method for tracking the flow of antigens from tumor to T cell, we generated a spontaneous mouse model for breast cancer in which the initiating oncogene and a neotumor antigen are coexpressed with the stable fluorescent protein mCherry, under a common breast epithelium-specific promoter. For this, we adapted the extensively characterized mouse mammary tumor virus-polyoma middle T (MMTV-PyMT) transgenic cassette (Guy et al., 1992), whose expression gives rise to disease in mice that closely models many aspects of spontaneous luminal breast cancer, including characteristic stages from hyperplasia to adenoma to carcinoma and ultimately to metastatic disease (Lin et al., 2003). We introduced two self-cleaving P2A sequences (de Felipe et al., 2003) downstream of the PyMT cDNA to produce the mCherry and ovalbumin proteins (OVA) (Figure 1A). We included mCherry expression to aid in visualization of transformed cells and to track antigen uptake in the microenvironment. We included OVA to generate germline-encoded self-antigens that were specific to cells expressing the oncogene (“tumor self”) and could be recognized by well-characterized CD8 T cells expressing the OT-I TCR. By coexpressing these genes in a common MMTV-driven transcript, we ensured the coproduction of each protein, in concert with onset of transformation, and yet allowed both mCherry and OVA to be processed independently, thus preventing premature degradation. The expression of these proteins as distinct polypeptides was demonstrated by western blotting (Figure 1B), where each individual protein is detected as a single band at the expected molecular weight. The onset of tumors in this “PyMT ChOVA” line was approximately 20 weeks of age on the C57BL/6 background (Figure S1 available online). The >95% penetrance of tumors and onset at times similar to those of the parental PyMT strain on C57/BL6 background (data not shown) suggested that the inclusion of the mCherry and OVA proteins provided little benefit to the immune system’s ability to recognize or control the tumor.

A sizeable fraction of the tumor antigens that have been isolated from human tumors to date are nonmutated, germline-encoded, tissue-specific proteins that are more dominantly expressed by transformed cells (Finn et al., 1995; Kawakami et al., 1994; van der Bruggen et al., 1991). In these cases, their presumed expression in the thymus apparently leads to negative selection of T cells bearing high-affinity TCRs, and data show a prevalence of cytotoxic T cells (CTLs) with low avidity to these tumor antigens (Gervois et al., 1996), with some notable exceptions identified using tetramers (Lee et al., 1999; Yee et al., 1999). The MMTV promoter used in the PyMT ChOVA model also drove expression in the thymus, as indicated by the negative selection of developing anti-OVA/antitumor OT-I TCR transgenic T cells (Figure 1C). Thus, OVA in this mouse replicates partial central tolerance to tumor antigens.

We next investigated the ability of high-affinity anti-OVA OT-I T cells, introduced into mice already bearing tumors, to respond in situ. Tumor-antigen presentation in PyMT ChOVA lymph nodes was quite robust, as evidenced by proliferation-dependent dilution of the vital dye CFSE specifically in naive tumor-specific T cells (OT-I) in PyMT ChOVA mice, but not in the PyMT mouse strain (Figure 1D). Similarly, introduced GFP-labeled tumor-specific OT-I T cells were present in the tumor and specifically proliferated and accumulated in the lymph node, whereas nonspecific T cells did not expand or significantly populate the tumor (Figure 1E). That the tumor antigen-specific T cells expanded to over 10% of the CD45$^+$ cells and then persisted at high percentages at lymph nodes and tumor for over 30 days (Figure 1F) indicates that the primed cells were not subject to strong deletional tolerance.

Tumor-Specific T Cells Are Incapable of Eliminating PyMT ChOVA Tumors

Tumor-reactive naive T cells are efficiently activated in the secondary lymphoid organs of PyMT ChOVA mice. However, naive high-avidity T cells had only a slight effect in slowing tumor growth and were unable to eliminate tumors when transferred to tumor-bearing hosts (Figures 2A and 2B). These results are

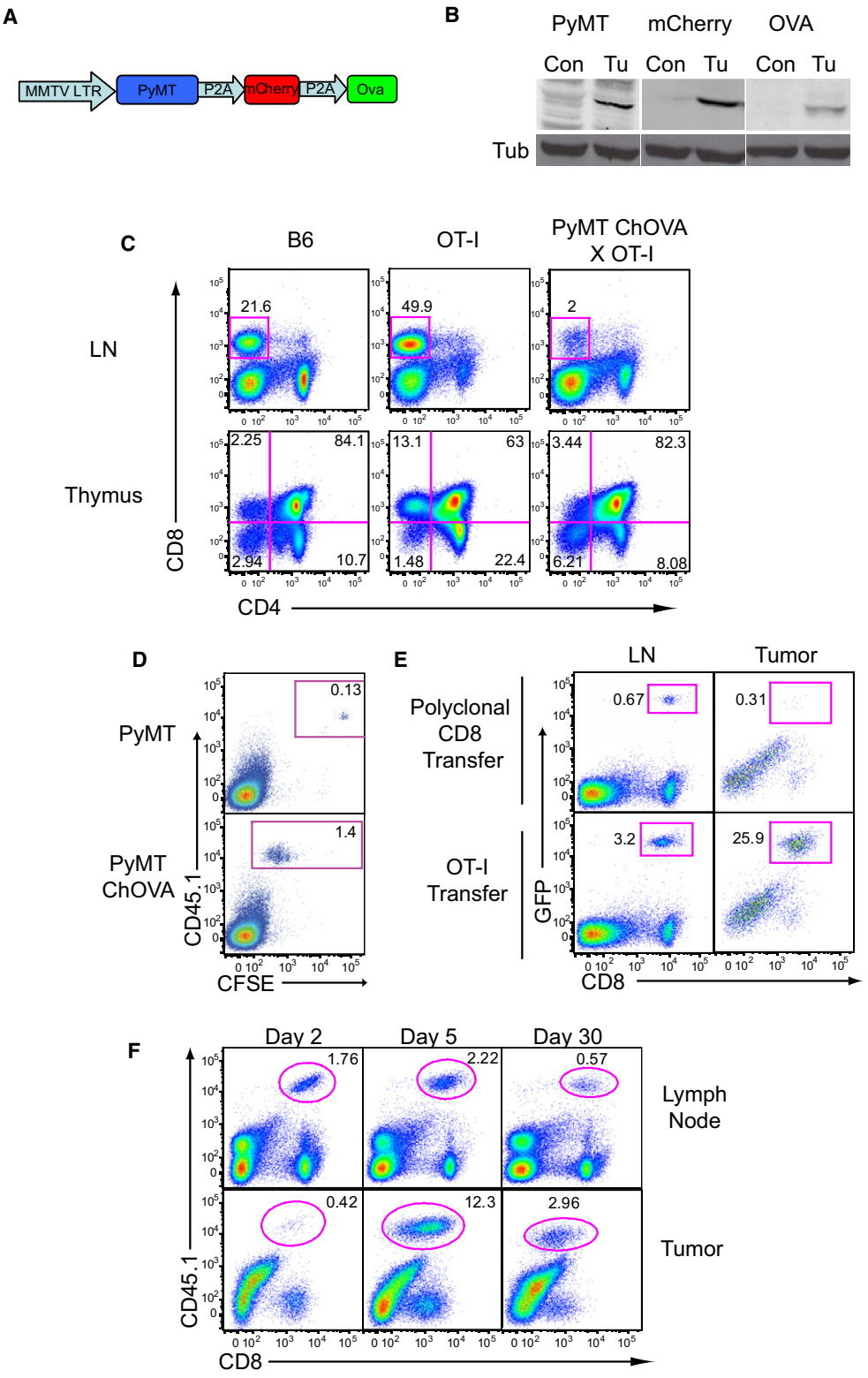

Figure 1. Recruitment and Ineffectiveness of Tumor-Specific T Cells in a Spontaneous Model of Breast Cancer

(A) Schematic of PyMT ChOVA transgenic construct.

(B) Western blots displaying the expression of PyMT, mCherry, and Ova from tumor cells and control T cells in PyMT ChOVA mice.

(C) Thymic negative selection of high-affinity TCRs in the PyMTChOVA spontaneous breast cancer model. Lymph nodes and thymii from wild-type B6, OT-I, or PyMT ChOVA x OT-I mice were analyzed by flow cytometry for CD4 and CD8 expression.

consistent with adoptive transfer of tumor-specific T cells in another spontaneous mouse model, TRAMP, in which lymph node CTL activation fails to be sufficient to induce rejection (Anderson et al., 2007). Notably, in our model, whereas tumor-specific T cells primed for 5 days in the lymph node of tumor-bearing mice demonstrated excellent cytolytic function against antigen-bearing targets, CTL found in the tumor at that time were effectively nonlytic (Figure 2C). That the latter were derived from the former is suggested by the earlier kinetics of accumulation and CFSE dilution in the lymph node relative to the tumor (Figure 1F; data not shown). Overall, this result is similar to human cancers such as melanoma in which tumor-antigen-specific Melan-A/MART-1 tetramer staining demonstrates expanded levels of tumor-specific cells in TILs relative to peripheral sites, coupled with the same profound failure to reject the tumor (Lee et al., 1999; Romero et al., 1998).

We thus sought to determine the in vivo behavior of T cells in our model. To this end, we turned to intravital imaging (Egeblad et al., 2008), adoptively transferring naive GFP-labeled OT-I T cells, allowing them to activate and traffic to tumors and subsequently imaging their interactions in the tumor. We observed significant accumulations of T cells, often in multicellular clusters and at distinct foci along the tumor borders (Figure 2D; Movie S1). As motility appeared much slower near the tumor, we defined a cutoff at 5 μm and considered cells within this radius "proximal," whereas those further away are considered "distal." In tumor-distal regions, T cells were largely motile, moving at 6 μm/min (Figure 2E), a speed only slightly slower than those reported for unrestricted movements in lymph nodes (Miller et al., 2002). However, in the proximal regions, where clusters formed on the tumor margins, speeds were largely reduced to an average of 3 μm/min, with many cells much slower. Radial tracking plots of randomly selected cells supported the theory that most of these cells were in fact swarming or jittering in the proximal clustered regions (Figure 2F), whereas distally located cells quickly diverged from the origin. We did not observe any evidence for destruction of tumor cells by OVA-specific (OT-I) T cells in these tumors, such as single-step loss of mCherry fluorescence in cell-sized voxel regions, consistent with tumor measurements that had previously shown that T cells had little effect on tumor growth.

Phenotypic Characterization of Tumor Antigen Cross-Presenting Dendritic Cells

In engineering the PyMT ChOVA model to coexpress mCherry, we exploited this protein's apparent resistance to degradation to allow us to track antigens that are taken up from tumor cells for presentation by neighboring cells. By flow cytometry, we detected a population of mCherry$^+$/CD45$^+$ cells of hematopoietic origin in single-cell suspensions of PyMT ChOVA but not original PyMT tumors (Figure 3A). A majority of CD45$^+$ cells positive for mCherry above background also expressed high levels of CD11c, an integrin enriched in the dendritic cell lineage. To demonstrate that the mCherry in these cells derived from ingestion of the protein, as opposed to production, we generated bone marrow chimeras in which nontransgenic CD45.1$^+$ bone marrow introduced into PyMT ChOVA mice resulted in mCherry fluorescence in CD11c$^+$ cells of the adopted (transgene-negative) lineage (Figure 3B). We observed mCherry fluorescence as puncta in isolated cells consistent with phagosomes (data not shown) but were unable to detect significant levels of mCherry transcripts in these cells (data not shown), consistent with uptake.

Analysis of CD11c versus Gr-1 staining in the CD45$^+$ mCherry^{hi} cells demonstrated that approximately 3/4 of the mCherry^{hi} cells expressed CD11c and less than 5% of them expressed Gr-1, a marker closely associated with MDSC (Figure 3C). We performed a similar analysis of CD11c and Gr-1 from the entire CD45$^+$ gate (Figure 3D) to characterize the infiltrate in aggregate and thereby defined four populations: CD11c$^+$Gr-1$^-$ (CD11c$^+$), CD11c$^-$ Gr-1$^+$ (Gr-1$^+$), double-positive (CD11c$^+$, Gr-1$^+$), and double-negative (DN). Staining for additional surface proteins showed that none of these subsets expressed CD123, a marker for pDCs; CD135, a marker for bone marrow progenitors; or CD115, the CSF-1R. CD11c$^+$ subsets coexpressed moderate CD11b, whereas Gr-1$^+$ cells expressed distinctly high levels (Figure 3E). The CD11c$^+$ populations also expressed high levels of F4/80 and MHC II. The F4/80 expression together with the CD11b positivity would also qualify this subset as a TAM (Ojalvo et al., 2009). The CD11c$^+$ population also had taken up significantly more of the tumor-derived mCherry than the Gr-1$^+$ or DN populations, although we note that this is bimodal, suggesting the population is not homogeneous in this respect (Figure 3E). The higher levels of both MHC II and mCherry suggests that the CD11c$^+$ cells are most likely to be effective antigen-presenting cells for incoming effector T cells. We also note that they are considerably more abundant within the tumor relative to the other three populations. On an absolute scale, the DP populations were most homogeneously mCherry positive but represented less than 1% of the total isolate. Less than 1% of CD11c$^+$ cells expressed the pDC markers CD123 (Figure 3E) and B220 (data not shown). The best correlation with mCherry positivity was the marker F4/80 (data not shown).

As we were interested in these cells as putative APCs, we next compared the entire lineage of CD11c-positive cells from tumors to splenic DCs and to in-vitro-matured, bone-marrow-derived DCs (BMDCs). CD11c levels were just slightly lower on tumor APCs as compared to BMDCs or splenic DCs (Figure 3F, left panel). When CD11c$^+$ TuDC cells were analyzed, we observed roughly similar levels of MHCs and costimulatory molecule expression in the tumor-associated cells and splenic DCs,

(D) Flow cytometry of tumor-draining lymph nodes 48 hr after 1 × 10^6 CFSE-labeled CD45.1 OT-I T cells were transferred to either a PyMT tumor-bearing mouse or a PyMT ChOVA tumor-bearing mouse.
(E) A total of 5 × 10^6 OT-I-UbGFP T cells or polyclonal Ub-GFP CD8 T cells were transferred to PyMT ChOVA tumor-bearing mice. Five days posttransfer, tumor-draining lymph nodes and tumors were removed and analyzed by flow cytometry. Plots from tumor were previously gated for CD45$^+$ leukocytes.
(F) Tumor-bearing PyMT ChOVA mice received 1 × 10^6 CD45.1 OT-I cells intravenously and were sacrificed at the specified day posttransfer. Tumor-draining lymph nodes and tumor were removed and analyzed by flow cytometry. Plots from tumor were previously gated for CD45$^+$ leukocytes.
See also Figure S1.

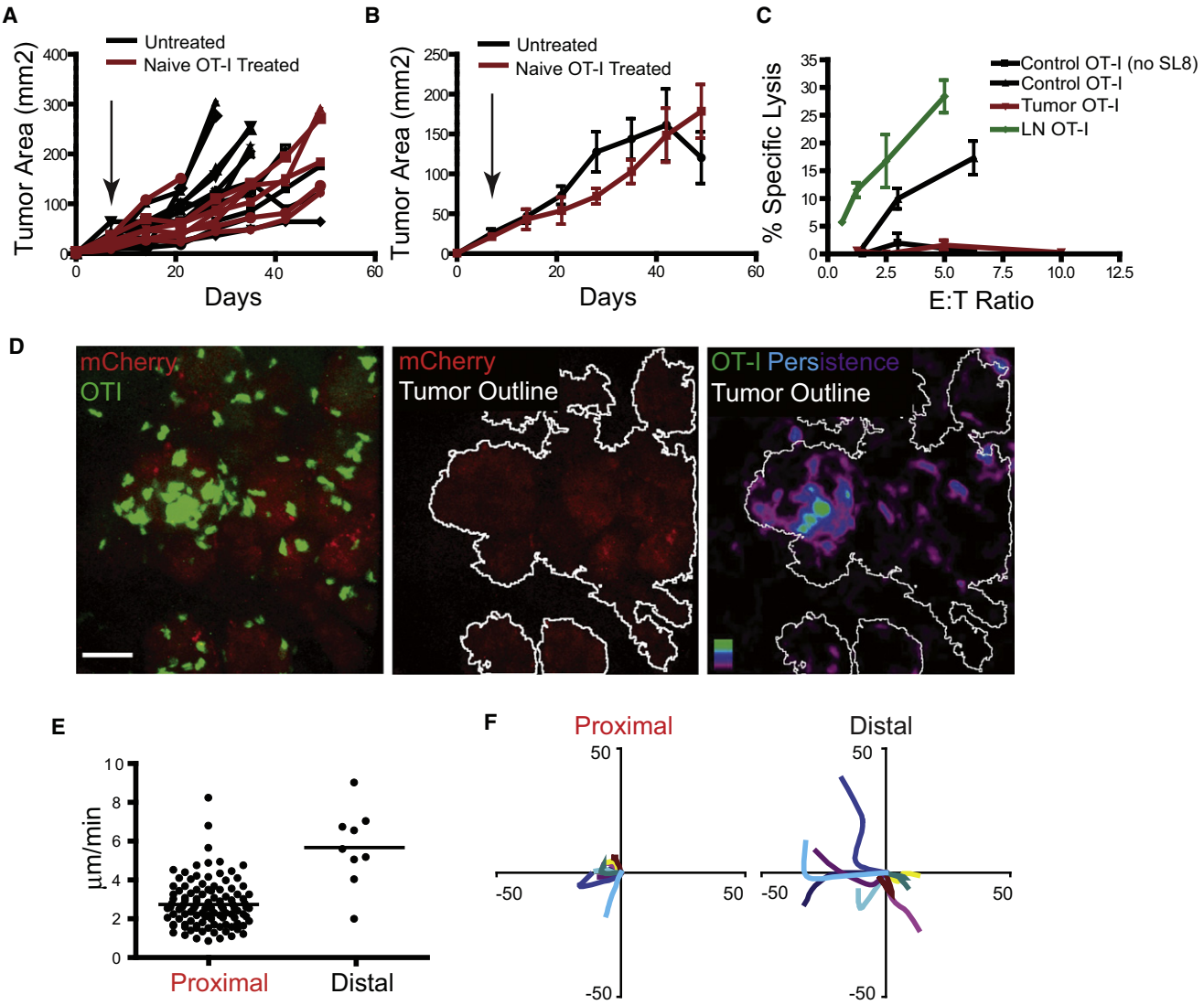

Figure 2. Tumor-Specific T Cells Are Defective in Their Ability to Eliminate PyMT ChOVA Tumors

(A) Tumor burden in individual PyMT ChOVA mice after adoptive transfer of 5 × 10^6 naive OT-I cells (red lines, n = 7) or untreated controls (black lines, n = 12). Arrow indicates date of adoptive transfer.

(B) Average combined tumor burden in PyMT ChOVA mice after adoptive transfer of 5 × 10^6 naive OT-I cells (red line: mean (M) ± SEM, N = 7) or untreated controls (black line: M ± SEM, N = 12).

(C) Cytotoxic activity of OT-I T cells isolated from the lymph nodes (LNs; green) or tumor (red) of PyMTChOva mice 5 days after adoptive transfer, compared to in-vitro-activated control OT-I T cells (black line with triangles) or control OT-I lysis of unpulsed EL4s (black line with squares). A total of 10^4 EL-4 cells (±100 ng/ml SL8 peptide pulse) were used as targets. All lines: M ± SEM, N = 3.

(D) Spinning disc confocal live imaging of OT-I GFP T cells 5 days after adoptive transfer into PyMT ChOVA mice. Representative image of T cell localization at the site of a mCherry fluorescent tumor (left), image displaying tumor area outlined using a threshold mask (middle), and time-average image of T cell persistence at the tumor site with tumors outlined (right). Scale bar, 50 µm.

(E) Average velocity of individual T cell tracks of cells located proximal (within 5 µm) or distal to the tumor.

(F) Representative displacement tracks from T cells located either proximal (within 5 µm) or distal to the tumor border.

See also Movie S1.

suggesting that they would be similarly capable of presenting antigen to naive T cells (Figure 3F). Although many $CD11c^+$ cells at the tumor site were $mCherry^+$, there was still significant heterogeneity within the $CD11c^+$ population for the amount of mCherry that had been ingested. This could reflect that not all cells are in a position to effectively take up the antigen or that the cells degrade the protein over time.

Live Imaging of Tumor Dendritic Cell Behavior

Given the presence of the CD11c protein on the majority of the $mCherry^{hi}$ cells of interest, we interbred PyMT ChOVA mice with mice that express yellow fluorescent protein (YFP) under the control of the CD11c promoter (Lindquist et al., 2004), permitting us to visualize the location and behavior of these APCs directly through real-time intravital live imaging of exposed

tumor masses. Using the same 5 μm proximity cutoffs as in Figure 2, we characterized tumor-proximal CD11c$^+$ cells that were closely juxtaposed with the tumor and had very low motility compared to distal cells (Figures 4A–4C and 4H; Movies S2 and S3). The proximal CD11c-YFP$^+$ cells of the tumors also had the highest level of mCherry fluorescence (Figures 4D, 4E, and 4G; Movie S3). The observation of the behavior of these cells in vivo supported our previous observation that CD11c$^+$ cells ingested tumor antigens and eliminated the possibility that the mCherry fluorescence that we observe by flow cytometry is simply an artifact of in vitro digestion of the tumor. Flow cytometry of tumor from PyMT ChOVA x CD11c YFP mice also demonstrated that CD11c-YFP$^+$ cells from the tumor had taken up mCherry to an extent similar to that in cells stained with antibodies against CD11c supporting the finding that the transgene is generally faithful to the native protein (Figure 4F). Proximal CD11c-YFP$^+$ cells contained significant amounts of mCherry signal in their cytoplasm, often in puncta suggestive of endocytic vesicles, while distal CD11c-YFP$^+$ cells did not contain these structures(Figure 4G). Despite not moving their cell bodies along the tumor margin, these proximal cells dynamically extended and retracted dendrites, which is suggestive of ongoing sampling of the environment (Figure 4H; Movie S3). Morphological data complement phenotypic markers in supporting an assignment of CD11c$^+$ cells from the tumor as DCs, although it is important to remember that the lineages are highly plastic as previously discussed, and these cells may equally be called TAMs on the basis of flow cytometry.

Changes in Myeloid Cell Populations during Tumor Development

Having identified CD11c$^+$ cells as important in ingesting tumor antigens, we sought to characterize whether they were a consistent feature of the tumor across multiple stages. An advantage of the PyMT model is that tumors of distinct developmental stages exist in the same mouse. We identified mice with large carcinomas (area > 100 mm^2) and adenomas (barely palpable tumors < 9 mm^2) at different mammary glands (Figure 5A) and dissociated these tumors for analysis by flow cytometry. After gating on the CD45$^+$ leukocytic infiltrate, we again analyzed the levels of the common myeloid markers, Gr-1, CD11c, CD11b, and F4/80 (Figure 5B). We found that the numbers of cells positive for Gr-1 were significantly higher in carcinomas than adenomas, while CD11c and F4/80 were only modestly increased (Figure 5C). Together, these data suggest that the CD11c$^+$ population is a consistent component of tumors across multiple stages and not restricted to early or late tumors.

Tumor DCs Interact with Tumor-Specific T Cells In Vitro and In Vivo

Armed with the knowledge that this population of CD11c$^+$ cells ingest tumor antigens specifically along the tumor margin, we noted that this location would also ideally place them in a position to interact with the swarming/arrested antigen-specific T cells that we had visualized earlier. To test whether this was the case, we modified our cell-labeling approach to allow direct assessment of interactions between T cells and CD11c$^+$. For this, we transferred OT-I cells derived from mice interbred with the CD2RFP strain, which expresses the RFP protein at a very high level in T cells. We thereby could coimage reactive T cells and the proximal CD11c$^+$ DC in a PyMT ChOVA x CD11c-YFP mouse. In this setting, the mCherry expression of the tumor was considerably less than the RFP-expressing T cells, allowing the latter to be viewed distinctly. We observed both clusters and individual T cells interacting for prolonged periods with tumor-marginal DCs (Figure 6A; Movie S4). We also observed interactions of multiple T cells and DCs that were stable (white arrows) and conjugates of a single T cell with a single DC that formed (blue arrow) or dissipated (yellow arrow) over time.

Analysis of larger fields, using color coding that differentiates lone T cells and DCs from those that are interacting, visually demonstrated that interactions between T cells and DCs were less frequent and more transient in the distal region of the tumor as compared to the proximal region (Figure 6B; Movie S5). Quantification of T cell behaviors over multiple sites demonstrated that the majority of those in clusters, as observed in Figure 6A, were attached to a tumor-proximal DC. Additionally, when individual contacts between T cells and DCs were scored, a large fraction persisted in contact with one another for more than 5 min, with some persisting beyond the 30 min of our standard imaging session. Many of the T cells in the dense clusters persisted there for at least the 30 min periods of our observation. Additionally, when we analyzed whether individual T cells had interacted with a DC during the course of our 30 min imaging session, we found that, by 30 min, 96% (147/153) of T cells had interacted with DCs (defined as contacting DCs), while at the start of acquisition, 56% (85/153) were in contact with DCs. This evidence supports the theory that tumor-proximal T cells are preferentially localized together with the mCherry^{hi} CD11c$^+$ cells in this local environment and that they are effectively engaged in both prolonged and ongoing interactions.

We thus sought to test specifically whether these APCs were more likely to form stable interactions with tumor-specific T cells compared to the OVA$^+$ tumor cells themselves. As it was not possible to distinguish all cell types simultaneously during intravital imaging, we turned to an in vitro system to study T cell coupling frequencies with specific cells of the tumor microenvironment. We prepared single-cell suspensions of all cells from a PyMT ChOVA tumor and allowed the collections of tumor and stromal cells to form couples with a significant excess of in-vitro-activated OT-I T cells and then stained for surface markers to delineate the tumor-derived populations that had interacted. Using CD45$^+$ and MHC II$^+$ as a strategy to highlight all potential APCs with tumor, we demonstrated that T cells preferentially coupled with bone-marrow-derived APCs by this definition compared to tumor cells, even though the latter vastly outnumber them (Figures 6C and 6D). Strikingly, T-cell-engaged APCs had higher levels of mCherry fluorescence than those that failed to couple, suggesting that the T cells differentially couple to the mCherry^{hi} cells (Figure 6E), corresponding to the high frequency of T cell arrest on those proximal mCherry^{hi} cells in vivo (Figure 6B). We applied the same technique to determine if CD11c$^+$ or GR-1$^+$ cells were more likely to interact with OT-I T cells and found that CD11c$^+$ cells were significantly better at forming couples with T cells (Figures 6F and 6G). These results corroborate the observations made during intravital imaging and confirm that T cells preferentially interact with CD11c$^+$ cells when given the opportunity to choose their partner.

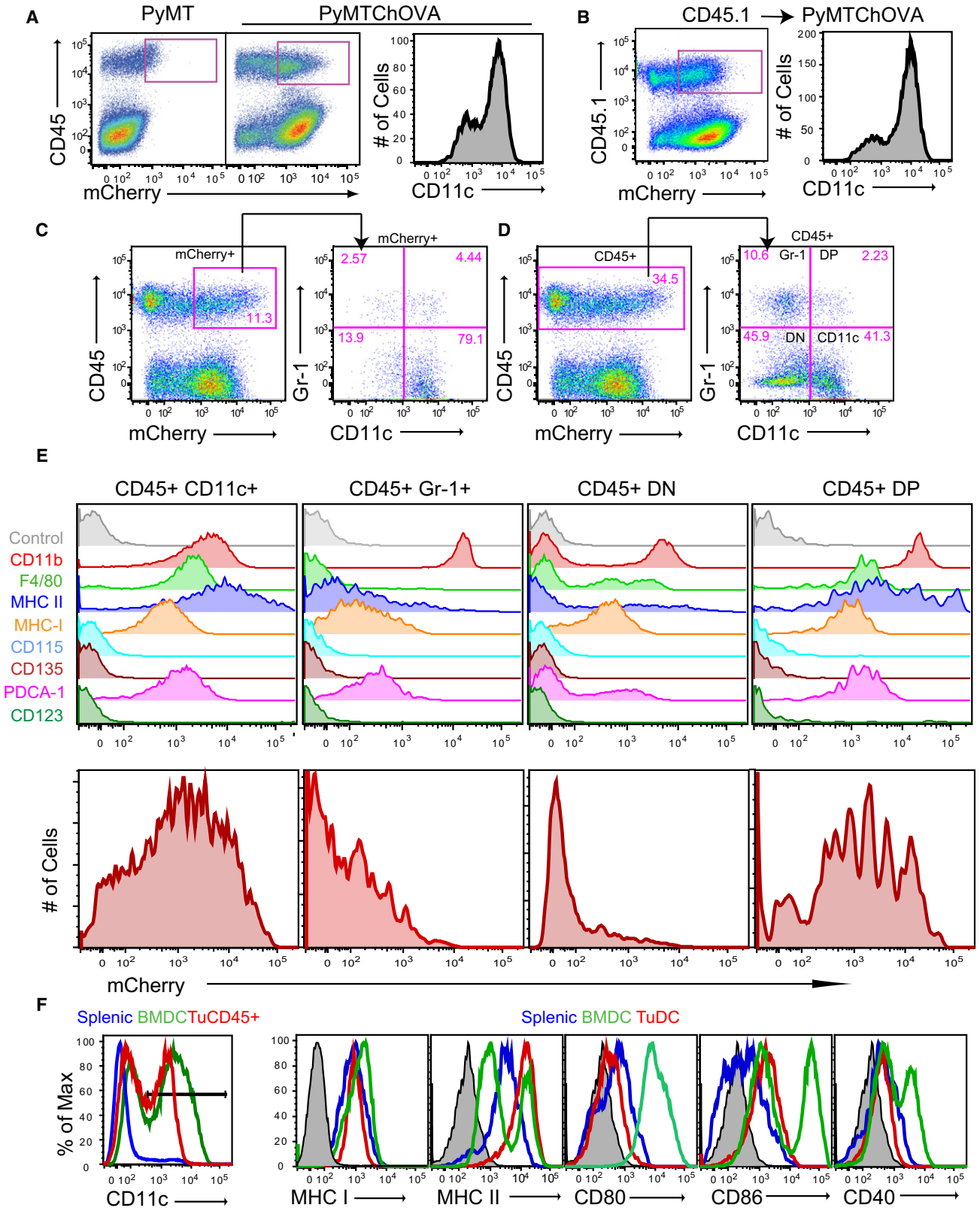

Figure 3. Phenotypic Characterization of Tumor-Antigen Cross-Presenting DCs

(A) Flow cytometry of CD45 expression versus mCherry levels from digested tumor from PyMT (left) or PyMT ChOVA (middle) mice. CD11c levels of gated CD45$^+$ mCherry$^+$ cells (right) from a previous dot plot.

Finally, we investigated the status of TCR levels and the ability to bind pMHC since overall downregulation of the complex is associated with recent signaling (Valitutti et al., 1995) but absence of pMHC binding with presence of the α/β complex has been previously associated with tumor tolerance (Nagaraj et al., 2007). We thus tested the ability of both lymph-node- and tumor-infiltrating T cells to bind to OVA-labeled Kb pentamers 5 days after adoptive transfer into tumor-bearing hosts. We found that both lymph node and tumor OT-I cells both showed decreased levels of pentamer binding in comparison to OT-I cells that were stimulated and then rested for 6 days in vitro, with tumor OT-I showing the lowest level of staining (Figure S2). We similarly determined by staining for the Vβ5 of the OTI TCR that this was decreased in a similar hierarchy in these cells compared to blasted/rested OT-I (Figure S2). We interpret these data as being consistent with ongoing TCR engagement at both lymph node and tumor, leading to downregulation of the entire TCR complex, but not a specific alteration of TCR binding capabilities (e.g., Nagaraj et al., 2007).

Tumor DCs Activate Naive but Not Previously Activated OT-I T Cells

Since activated T cells preferentially interact with the $CD11c^+$ cell populations both in vitro and in vivo, we sought to define the ability of these $CD11c^+$ cells to interact with and stimulate T cells in vitro. Given their cell surface similarity to splenic DC and their mCherry positive phenotype, we were not surprised to find that a total $CD11c^+$/MHC II^+ population, freshly isolated from tumors and without added antigen (TuDCs), stimulated the proliferation of naive OVA-specific (OT-I) T cells in vitro (Figure 7A) at lower but still significantly above background levels compared to BMDCs that had been pulsed with exogenous peptides. This finding established that the TuDCs process and display antigens in peptide-MHC complexes and are capable of stimulating naive T cells, a feature sometimes associated with mature myeloid populations such as mature DCs. However, when assayed for the ability to support proliferation of established CTLs, the tumor-derived antigen-bearing DCs proved unexpectedly incapable of driving cell division. This deficit was true across a wide range of concentrations of DCs and even when exogenous peptides were added to the TuDCs (Figure 7B), suggesting that the block was profound.

However, live imaging of CTLs, labeled with the calcium dye FURA-2 and interacting with TuDCs, demonstrated that proximal activation occurred in CTL and that peptide-MHC triggering of TCRs at the site of these interactions was not defective (Figure 7C; Movies S6 and S7). Both the percentage of cells that generated calcium transients during interaction (Figure 7D) and the magnitude of calcium curves generated by a panel of cells (Figure 7E) were similar between TuDCs and the stimulatory BMDC population pulsed with exogenous peptides. These results are consistent with peptide-MHC expression on these cells but suggest that TuDCs apparently might bear inhibitory ligands that function distal to synapse formation and TCR signaling and inhibit productive responses. We also tested the ability of TuDCs to induce upregulation of CD69 on previously activated T cells and found that CD69 is upregulated by T cells stimulated by both BMDCs pulsed with peptide and TuDCs (Figure S3). These data support the conclusion that TuDCs are indeed antigen positive and are also able to initiate early events of TCR signaling. We screened a large number of candidate molecules and pathways and eliminated the canonical T cell inhibitory pathways that are suggested to function in MDSCs, M2 macrophages, and other APCs, including both surface receptors and soluble factors (Figure S3). That none of these restored proliferation suggests an unknown mechanism of T cell inhibition.

Given the ability of these TuDCs to support antigen-dependent coupling with CTLs in vitro and in vivo, we sought to determine the downstream effects of these signaling interactions. We therefore tested the ability of CTLs encountering the TuDCs to maintain CTL function, a key deficit in T cells that had homed to the tumor (Figure 2). Comparisons of cytolysis by T cells cultured with TuDCs showed that this interaction does not sustain cytolytic function, similar to T cells cultured alone or T cells stimulated with BMDCs without peptide. In contrast, T cells cultured with BMDC pulsed with peptides or T cells cultured alone or with TuDCs in the presence of interleukin-2 (IL-2) did maintain cytolytic acitivity (Figure 7F).

As we were unable to restore proliferation effectively by blocking established inhibitory pathways in these assays, we also sought to reverse the phenotype by modulating the DC. Maturing the TuDCs by adding either imiquimod or CpG to the stimulation reaction strikingly relicensed them to stimulate CTLs to further divide (Figure 7G). These two agents are agonists for APC-expressed toll-like receptors (TLRs) 7 and 9, respectively, and neither agent had significant effects on the T cells (data not shown). As a control, cells were treated without effect by applying lipopolysaccharide (LPS), an agonist to TLR4, which is poorly expressed by TuDCs (data not shown). Supplementing the stimulation reaction with exogenous cytokines, whether IL-2, IL-12, or IL-15, also was able to rescue the proliferative defect (Figure 7H). Together, our data suggest a specific stimulatory defect of TuDCs in their interactions with CTL, separate from antigen processing and presentation.

Given the ability of these TuDCs to support antigen-dependent interactions with CTLs, we finally sought to determine whether TuDCs suppress CTLs from responding to other antigen-presenting cells. While, in some experiments, inhibition was profound, it was inconsistent over 13 experiments with an

(B) Flow cytometry of CD45.1 expression versus mCherry levels from bone marrow chimera made by adoption of CD45.1 bone marrow cells into an irradiated PyMT ChOVA mouse.
(C) CD45 expression versus mCherry levels from digested tumor from PyMT ChOVA mouse, gated $CD45^+$ $mCherry^{hi}$ cells were propagated to subsequent dot plot and analyzed for their expression of CD11c and Gr-1.
(D) CD45 expression versus mCherry levels from digested tumor from PyMT ChOVA mouse, gated $CD45^+$ cells were propagated to subsequent dot plot and analyzed for their expression of CD11c and Gr-1.
(E) Gated and labeled populations from (3D) were analyzed for their expression of the listed cell surface markers or for their mCherry fluorescence level.
(F) $CD11c^+$ cells from the spleens of B6 mice, BMDC cultures, or the tumor of PyMT ChOVA mice. Gate in left histogram propagated to subsequent histograms.

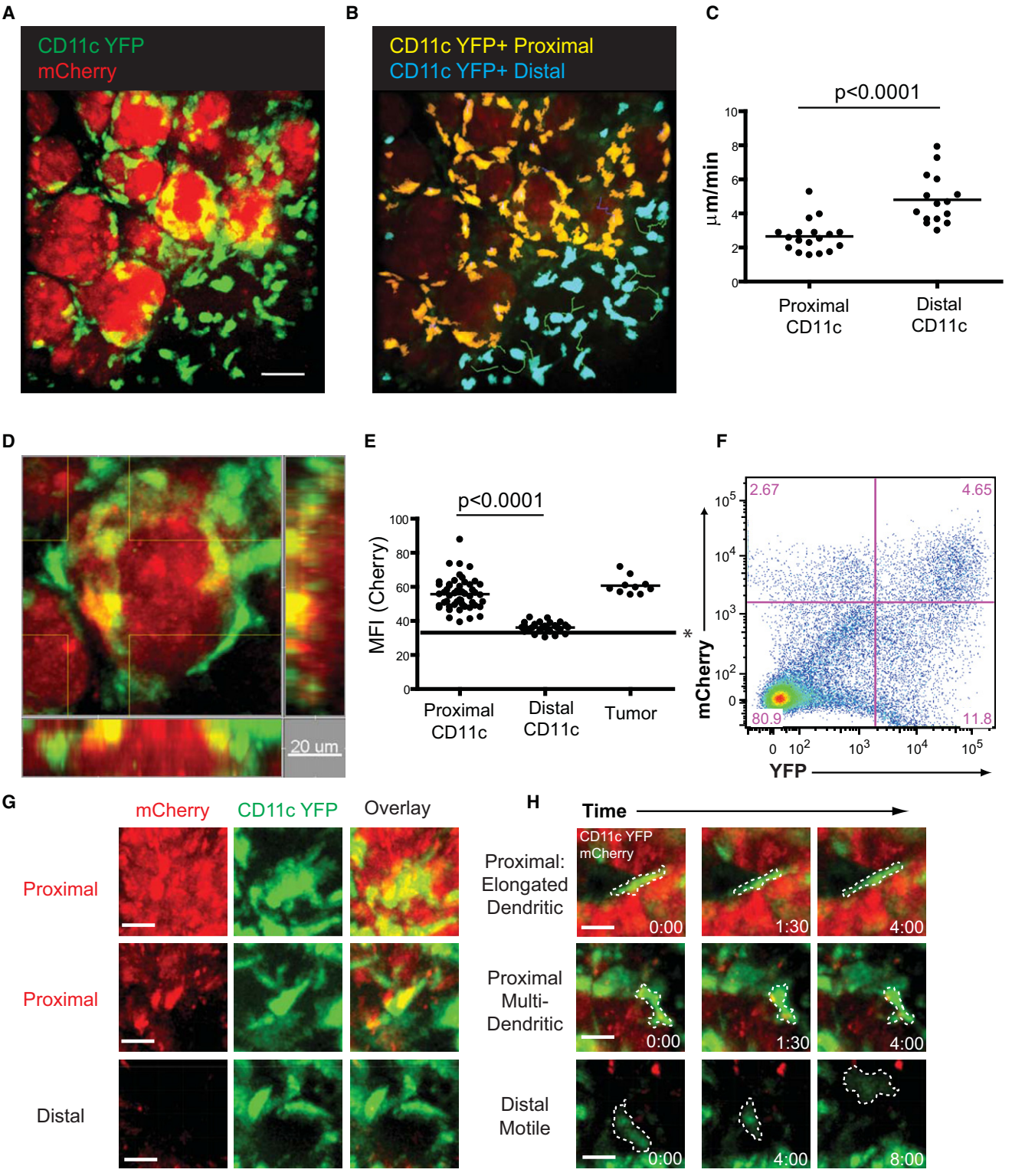

Figure 4. Live Imaging of Tumor-DC Behavior

(A) Representative still image acquired by intravital spinning disc confocal microscopy of mCherry$^+$ CD11c YFP$^+$ DCs in PyMT ChOVA x CD11c YFP mice. Scale bar, 10 μm.

(B) DCs are color coded based on their proximity to the tumor border. Proximal DCs (within 5 μm) are coded yellow, and distal DCs (>5 μm from tumor border) are coded blue. Color-coded DCs with representative tracks of their movement during imaging.

(C) Average velocity of individual CD11c YFP$^+$ cells located proximal or distal to the tumor border.

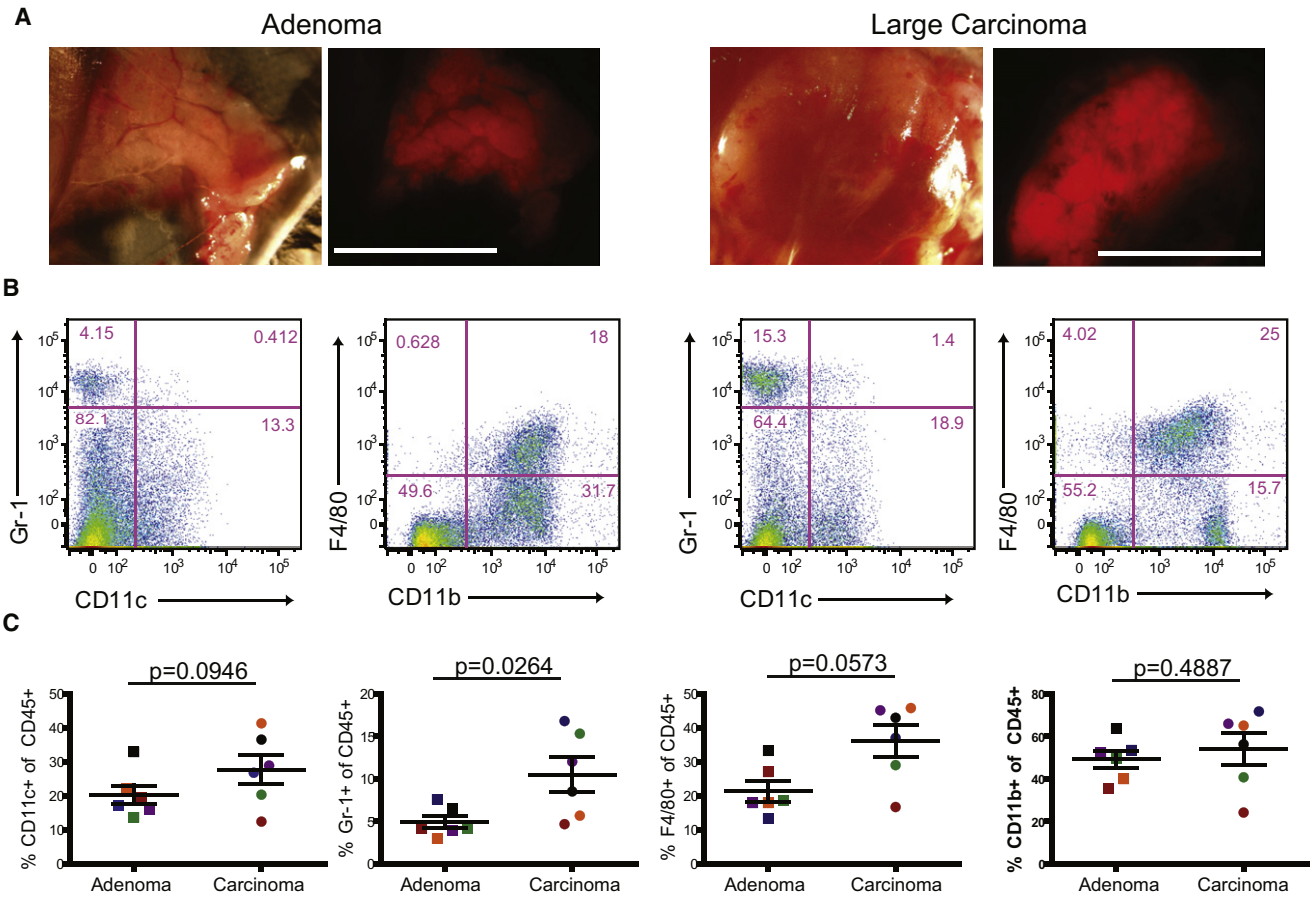

Figure 5. Alteration of Leukocytic Infiltrate with Tumor Development

(A) Transmitted and mCherry-fluorescent images of tumors from PyMT ChOVA mouse taken on a dissecting scope. Scale bar, 1 cm.

(B) Cells from either an adenoma or a late carcinoma tumor were dissociated and analyzed by flow cytometry. $CD45^+$ cells were analyzed for the cell surface markers CD11c, Gr-1, CD11b, and F4/80.

(C) Plots depict percent positive for specified cell surface markers out total $CD45^+$ cells from tumors at different stages. Each data point represents one tumor, and matched colors indicate tumors were from the same mouse.

average of just 30% inhibition (Figure S3). Since we do not yet understand the mechanisms utilized, any dominant suppression, if present, may also be sensitive to culture conditions or may be reversible (e.g., see Figure 7G). Alternatively, given the paucity of other effective APCs in the tumor microenvironment, tolerance may result purely from ineffective or defective repriming.

DISCUSSION

Delineating APCs in Tumors

Using a spontaneous mouse model of breast cancer, we have identified a population of myeloid cells that is optimized for ingesting and presenting tumor antigens to CD8 T cells and, thus, is a clear and relevant APC of the tumor microenvironment. This formal identification is an important finding since many cells are likely capable of antigen presentation in vitro when pulsed appropriately with peptides, yet no previous study has been able to unequivocally define the cells that interact with tumor-specific T cells within tumors. The direct demonstration of their presence at the site of T cell arrest along the margin suggest that they fill this roll in vivo as well as in vitro.

Ojalvo et al. recently described TAMs as c-fmsGFP$^+$ F4/80$^+$ and dextran$^+$ (Ojalvo et al., 2009); by this definition, the mCherry$^+$ cells that we describe here could also be classified as TAMs, as they are CD11b$^+$ and F4/80$^+$ and their mCherry positivity largely substitutes for dextran$^+$ as a marker of phagocytic ability (J.J.E.

(D) Representative still image acquired by intravital spinning disc confocal microscopy of mCherry$^+$ CD11c YFP$^+$ DCs in PyMT ChOVA x CD11c YFP mice.

(E) Mean fluorescent intensity of CD11c YFP$^+$ cells located proximal or distal to the tumor border, and tumor masses. Line indicated with an asterisk represents background fluorescence of image.

(F) Flow cytometry analysis of CD11c-YFP x PyMT ChOVA mouse displaying CD11c YFP$^+$ mCherry$^+$ DCs.

(G) Representative YFP, mCherry, and overlay still images of DCs either proximal or distal to the tumor. Scale bar, 10 μm.

(H) Representative still images of YFP$^+$ cells displaying either dendritic-like or motile cell behaviors. Cell outlines are marked in dashed lines. Scale bar, 10 μm. See also Movies S2 and S3.

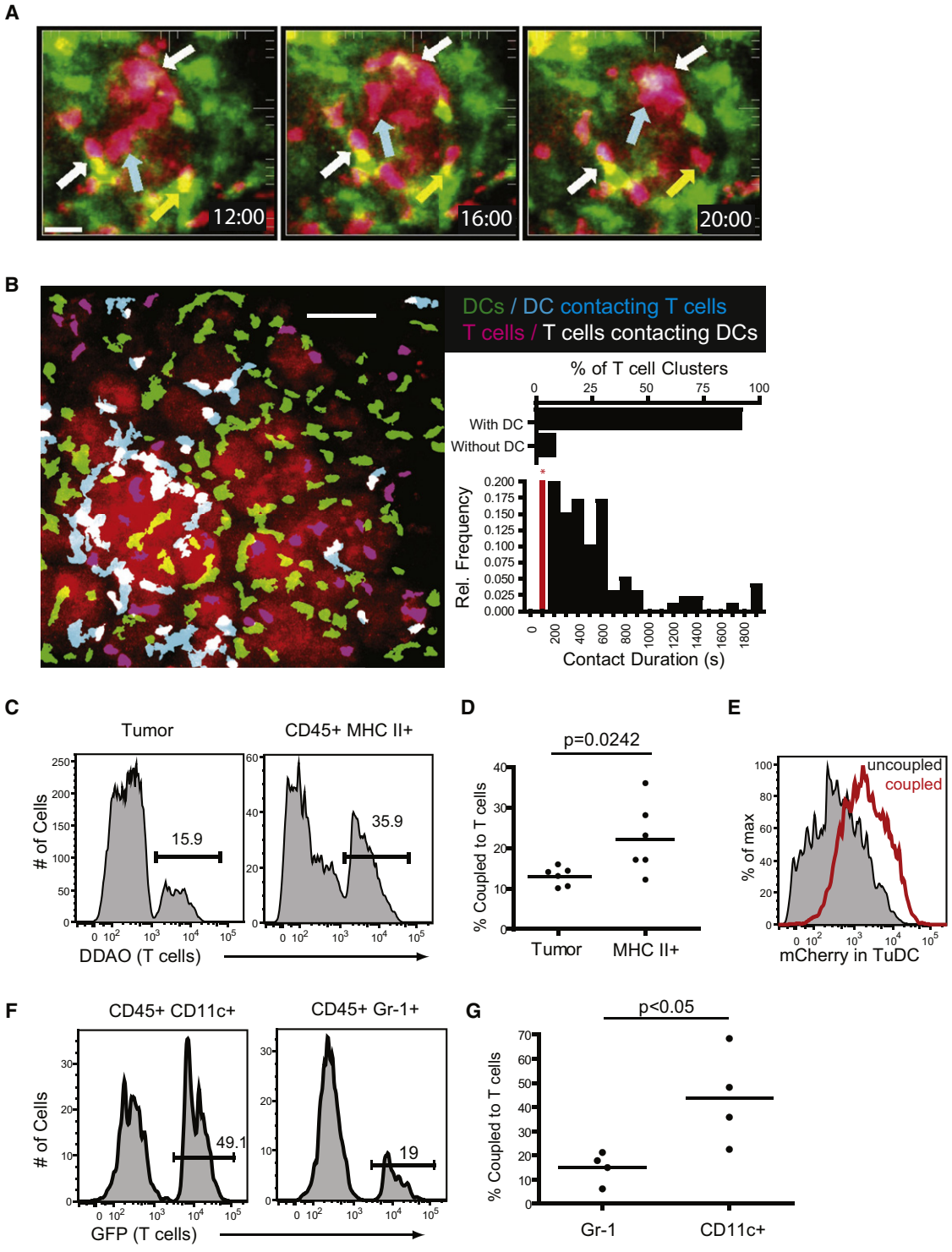

Figure 6. Tumor DCs Interact with Tumor-Specific T Cells In Vitro and In Vivo

(A) Spinning disc confocal imaging of CD2RFP OT-I T cells 5 days after adoptive transfer to PyMT ChOVA x CD11c-YFP mice. A representative image sequence of CD2RFP T cells (red) interacting with CD11c-YFP (green) DCs at the tumor site; white arrows indicate T cells interacting with DCs throughout the time lapse, yellow arrows indicate a T cell leaving an interaction with a DC, and blue arrows indicate a T cell moving to a DC. Scale bar, 30 μm.

(B) Representative image displaying T cells (red) and DCs (green) at the tumor site. Blue cells indicate DCs contacting T cells (defined by overlapping red and green fluorescence), and white cells indicate T cells contacting DCs. Scale bar, 50 μm. Inset/top: Graph of the number of T cell clusters (defined as stable groups of greater than 2 T cells) that occur with DCs present or without DCs present. Inset/bottom: Relative frequency of contact duration between OT-I T cells and TuDCs. Pairs with contact durations lower than 200 s were not considered.

and M.F.K., unpublished data). Although we do not find significant expression of CD115, the protein product of the c-fms GFP reporter, the TuDC population we describe otherwise can be considered a substantial subset of TAMs as well, and the nomenclature discrepancy in the literature may ultimately resolve these on the basis of data such as ours. The plasticity and overlap of cell surface markers makes the study and classification of these cells difficult, but we suggest classifying these cells as dendritic cells for immunological purposes, based on their cell surface marker expression and in vivo morphology and behavior. This apparent equivalency in the literature is then intriguing, as some of the same cells that are implicated in tolerizing T cells are also those implicated in remodeling and angiogenesis (Schoppmann et al., 2002; Qian and Pollard, 2010).

We have excluded tumor APCs from the MDSC population because of their lack of expression of the defining marker for this population, Gr-1, and furthermore because the CD11c$^+$ cells do not function in analogous manner; namely, defective proliferation is not restored with iNOS and/or Arginase inhibition (Figure S2) (Gabrilovich and Nagaraj, 2009). Although we identify CD11c$^+$ cells to be a distinct subset of cells from the entire lineage of the MPS, we acknowledge that some of these cells have previously been described by others as TAMs (DeNardo et al., 2009) or MDSCs or that some of our cells may share phenotypic or functional characteristics of these populations. However, the method that we have used clearly highlights this population of cells on the basis of location, morphology, phagocytosis, and their unique interactions with infiltrating T cells. It is also important to note that transient TCR-triggering interactions might occur with other APCs at sites besides the proximal region, and we cannot rule out interactions between T cells and the few CD11c$^-$ mCherry$^+$ APCs. We have demonstrated in the lymph nodes that even transient interactions can trigger TCR clustering and/or internalization (Friedman et al., 2010). Although, with our in vitro coupling experiments and in vivo behavioral studies, we established that CD11c$^+$ TuDC are the predominant partners for T cells, this by no means excludes other members of the MPS from ever acting on T cells via antigen receptors.

Despite the robust mCherry signal in tumor CD45+ cells, we were unable to detect mCherry$^+$ DCs in the tumor-draining lymph nodes (data not shown). It thus remains unknown how and by which cells antigen is being presented to lymph node T cells. DCs from the tumor site may be trafficking to lymph nodes but degrading the mCherry protein, or soluble tumor antigens may travel through the lymph directly.

The Behavior of Tumor-Specific T Cells in Refractory Tumors

In addition to identifying the tumor antigen cross-presenting DCs at the tumor site, we were also able to study the behavior of tumor antigen-specific T cells in a spontaneous and progressive model that is refractory to large numbers of infiltrating tumor-specific T cells. While activation and proliferation of naive tumor-specific T cells was robust in the lymph node, these T cells were shown to be defective at lysis of targets after exposure to the tumor microenvironment. This lack of cytolytic ability correlated with a lack of therapeutic benefit to adoptive transfer of T cells. This inactivity is similar to what is seen in human vaccination trials where large numbers of tumor-specific T cells can be elicited without eliminating tumors (Gattinoni et al., 2006; Rosenberg et al., 2005), suggesting a later defect, as we are observing in this model. The ability of exogenous γc cytokines to restore proliferation of T cells is also consistent with higher levels of efficacy of adoptive cell therapy when combined with IL-2 or IL-15 administration (Gattinoni et al., 2005; Overwijk et al., 2003; Epardaud et al., 2008).

Intravital imaging in our model revealed strong long-lasting interactions between tumor-specific T cells and DCs at the tumor site. The importance of interactions between T cells and DCs at the effector site of an immune response is an emerging field of study; in the case of viral infections, the stimulation of memory or effector cells by DCs at peripheral sites is thought to be important for effective viral immunity (Wakim et al., 2008). The behavior of these ineffective tumor-specific T cells is different from the behavior of tumor-rejecting T cells described in previous studies of ectopic tumor models (Mrass et al., 2006). While that study highlighted the activity of a strongly productive T cell response to a tumor, our study represents the activity occurring in a tumor setting that is more representative of naturally occurring human disease, where TILs are not effective in controlling tumor growth. It remains to be determined why T cells preferentially interact with TuDCs as compared to other cells of the tumor, and it is intriguing to conjecture that a specific chemokine-driven interaction may also contribute both to cell positioning within the tumor and, perhaps, to the limited stimulation capacity.

Tolerance Induction through T-APC Interactions within the Tumor

The concept that a BMDC serves to tolerize T cells that interact with them as cognate APCs is not unprecedented. Tolerance in the lymph node occurs when antigens are directed to DEC205$^+$ DCs in the lymph nodes in the absence of additional stimuli (Hawiger et al., 2001). Adler et al. broadly described the requirement for MHC-matched BMDCs in the tolerance to a tissue-restricted antigen (Adler et al., 1998), and induction of tolerance to an A20 lymphoma required matched bone marrow cells and not the tumors themselves (Sotomayor et al., 2001).

Based on our in vitro studies, we propose that the interaction between T cells and DCs may in fact inhibit the ongoing T cell response or, alternatively, may simply fail to effectively restimulate T cells to control the tumor while diverting them into such "sterile" interactions. After isolation of tumor DCs, we found that they were capable of activating naive T cells to proliferate but not in-vitro-generated activated T cells. A recent report

(C) Histogram displaying the percentage of tumor cells (left) or MHC II$^+$ cells (right) from PyMT ChOVA tumors that form couples with DDAO-labeled T cells.
(D) Results from six separate coupling assays plotted as percentage of tumor or MHC II$^+$ cells coupled to T cells. Bar represents mean.
(E) mCherry fluorescence of CD45$^+$ MHC class II$^+$ cells that were not coupled to T cells (shaded histogram) or were coupled to T cells (red histogram).
(F) Histogram displaying the percentage of mCherry$^+$ CD11c$^+$ or CD45$^+$ Gr-1$^+$ cells that form couples with OT-I GFP T cells.
(G) Results from four separate coupling assays plotted as percentage of CD11c or GR-1$^+$ cells coupled to T cells. Bar represents mean.
See also Figure S2 and Movies S4 and S5.

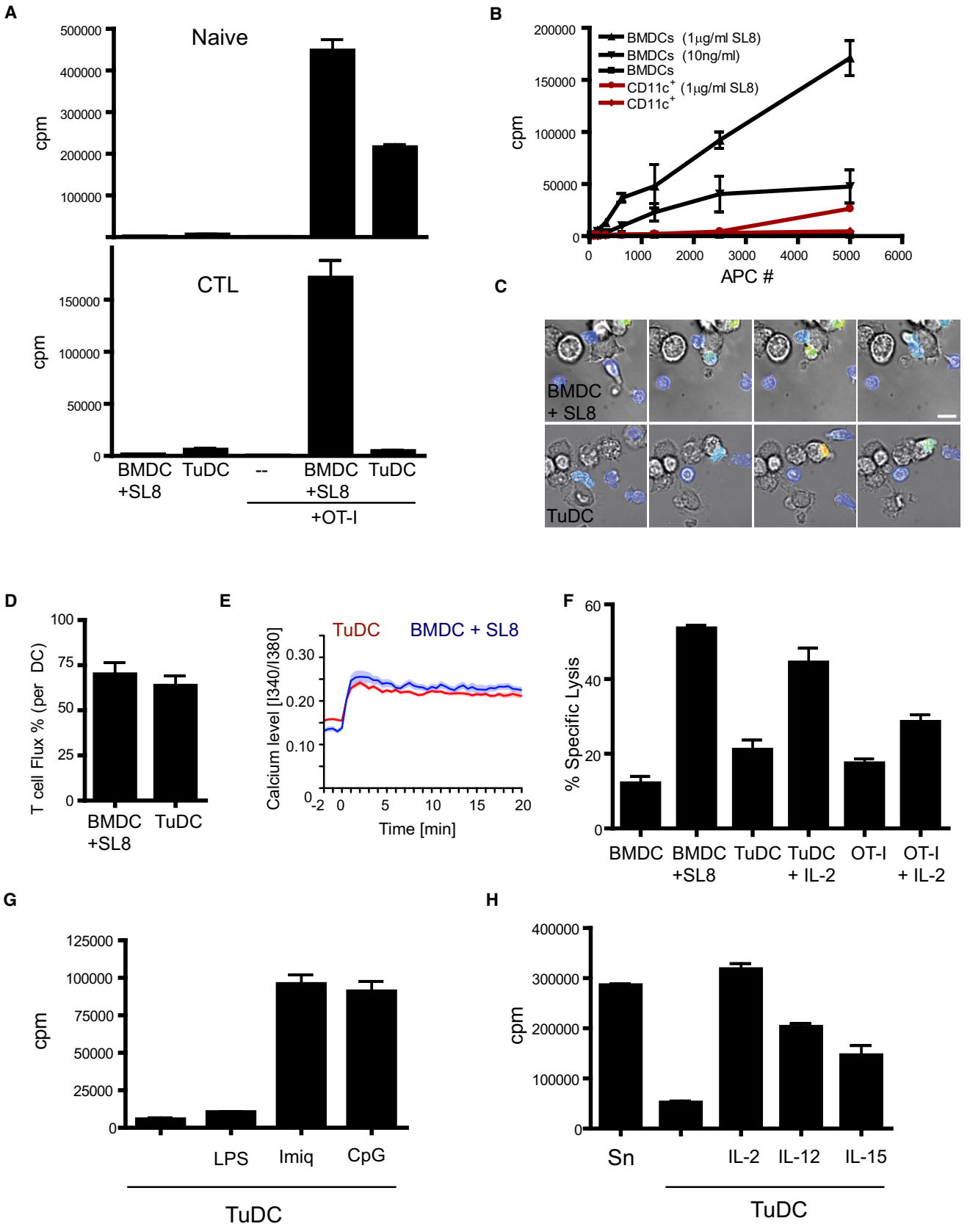
A
Naive
CTL
cpm
BMDC +SL8
TuDC
--
BMDC +SL8
TuDC
+OT-I
B
BMDCs (1μg/ml SL8)
BMDCs (10ng/ml)
BMDCs
CD11c+ (1μg/ml SL8)
CD11c+
APC #
C
BMDC + SL8
TuDC
D
T cell Flux % (per DC)
E
TuDC
BMDC + SL8
Calcium level [I340/I380]
Time [min]
F
% Specific Lysis
BMDC
BMDC +SL8
TuDC
TuDC + IL-2
OT-I
OT-I + IL-2
G
LPS
Imiq
CpG
TuDC
H
Sn
IL-2
IL-12
IL-15
TuDC

describing TuDCs isolated from the NeuT model of mammary carcinoma demonstrated an inhibitory phenotype for these cells when exogenously pulsed with peptides and used to stimulate naive CD8 T cells (Norian et al., 2009). While similar to our findings, the differences—that our cells are able to stimulate naive CD8s while theirs are not and that their inhibition was mediated by arginine metabolism—suggest that the mechanism of inhibition is distinct.

The defect in T cell restimulation exhibited by TuDCs could be rescued by treatment of the cultures with the TLR agonists CpG DNA and imiquimod. These data suggest that TuDCs are either specifically lacking a stimulatory signal or are actively giving an inhibitory signal that is distinct from other stimulatory DCs. These data are consistent with a previous study in another spontaneous tumor model, RIP-Tag, where adoptive cell therapy was only effective in conjunction with CpG administration (Garbi et al., 2004) Similarly, topical administration of imiquimod was effective against some established tumors in an ectopic model (Lu et al., 2010), and it is tempting to speculate that this TuDC/CTL axis is being modulated in that case. Topical application of imiquimod to breast tissue was not effective in our hands (data not shown). TuDCs from imiquimod-treated mice or after treatment in vitro had similar levels of MHC II, CD80, and CD86 when compared to untreated TuDCs. Our highest doses of imiquimod sometimes led to tumor hemorrhaging, and so we suspect that a more direct approach toward modifying TuDC function will be necessary.

Additional in vitro data correlate the functionally inactive T cells at the tumor site to DC interactions. T cells cultured with tumor DCs, but not stimulatory BMDCs, are unable to maintain lytic activity against targets, again suggesting that this interaction is deficient in its ability to promote a strong tumor response. Both the intravital imaging detailing interactions between T cells and DCs at the tumor site and in vitro coupling assays indicate that T cells are preferentially drawn to DCs as they enter the tumor microenvironment. Since this interaction fails to promote T cell effector function, it may be a significant impediment to the ongoing tumor response.

Does this represent a new mechanism of T cell tolerance? We have examined a large variety of surface receptor and soluble mediators and find that these do not revert inhibition and allow proliferation. It is interesting that we can demonstrate that proximal signaling, both as assessed by calcium signaling and, indirectly, through the formation of stable T cell and TuDC couples, is intact. Otten and Germain had previously described a state of "split anergy" in CTL clones; T cells retained cytotoxicity but lost proliferation and IL-2 secretion, when these lines engaged partially fixed APCs (Otten and Germain, 1991). The situation in response to TuDCs has interesting parallels, although inverted; the key defect for tumor rejection may in fact be the loss of CTL function.

Implications for Immunotherapy

Current immunotherapies focus on promoting a strong antitumor T cell response by altering the T cells themselves, either by increasing tumor-specific T cell frequency by adoptive cell transfer (Dudley et al., 2002), increasing the reactivity of responding T cells by engineering of high-avidity TCRs specific for tumors (Park et al., 2011), or by eliciting more potent T cells by blockade of inhibitory costimulatory molecules such as CTLA-4 or PD-1. While CTLA-4 blockade, in particular, has shown promise in treating human melanoma, many patients still show no clinical response after treatment (Hodi et al., 2010). The reasons behind this are unknown, but our data suggest that tumor-based APCs may function by a unique mechanism and that combination therapy to boost T cell responses via CTLA-4 blockade in conjunction with treatments that alter TuDC stimulatory capacity may be particularly effective. Our model in many ways represents a best-case scenario for immunotherapy in that we have available a large number of high-avidity, tumor-specific T cells for adoptive therapy. That treatment with this therapy still fails highlights the need to search for other ways to enhance the T cell response within tumors.

EXPERIMENTAL PROCEDURES

Mice and Genotyping

PyMT ChOVA transgenic C57BL/6 founder mice were generated as described in the associated Supplemental Information. All other mice are as described in the Supplemental Information. All mice were maintained in microisolator cages and treated in accordance with National Institutes of Health (NIH) and American Association of Laboratory Animal Care standards, consistent with the animal care and use regulations of the Institutional Animal Care and Use Committee of the University of California, San Francisco (UCSF).

Cell Tracking and Imaging Analysis

We visualized and analyzed data using Imaris 5.7.2 and 7.0 Software (Bitplane). Individual cells were identified and tracked by Imaris, and cell speed

Figure 7. Tumor DCs Activate Naive but Not Previously Activated OT-I T Cells

(A) Proliferation of either naive (upper) or previously activated (lower) OT-I T cells activated with either sorted TuDCs (50,000) or BMDCs (5,000) pulsed with 100 ng/ml SL8 peptide. N = 3 M ± SEM.

(B) Proliferation of previously activated OT-I T cells cultured with varying numbers of TuDCs or BMDCs pulsed with the specified amount of SL8 peptide. N = 3 M ± SEM.

(C) Live imaging of previously activated and Fura-2 labeled OT-I T cells interacting with BMDCs pulsed with 100 ng/ml SL8 peptide or with TuDCs. Brightfield images are overlaid with a pseudocolor image of the ratiometric Fura-2 fluorescence values, with low intracellular calcium levels represented in blue and high intracellular calcium represented in red. Scale bar, 10 μm.

(D) Frequency of cell contacts with SL8 peptide-pulsed BMDCs or TuDCs that lead to calcium transients in previously activated OT-I T cells. N = 3 M ± SEM.

(E) Intracellular calcium levels of previously activated OT-I T cells contacting BMDCs pulsed with 100 ng/ml SL8 peptide or TuDC. Mean values with standard errors are shown.

(F). Cytolytic activity of in-vitro-activated T cells after overnight culture with BMDCs, TuDCs, or BMDCs pulsed with 100 ng/ml SL8 peptide. N = 3 M ± SEM.

(G) Proliferation of OT-I T cells cultured with TuDCs alone or TuDCs with the TLR ligands, LPS (1 μg/ml), imiquimod (2.5 μg/ml), or CpG (10 μg/ml). N = 3 M ± SEM.

(H) Proliferation of OT-I T cells cultured with either control splenocytes pulsed with 100 ng/ml SL8 peptide or TuDCs alone or in the presence of IL-2 (3 U/ml), IL-12 (10 ng/ml), or IL-15(10 ng/ml). N = 3 M ± SEM.

See also Figure S3 and Movies S6 and S7.

and displacement were calculated from tracks. Mean fluorescence intensity of mCherry in CD11c YFP DCs was calculated using iso-surfaces of masked DCs from MATLAB segmentation. Contact duration was determined by calculated track duration of masked T cell and DC couples that were tracked using Imaris. T cell clusters for analysis of presence of DCs in couples were defined as clusters of T cells containing more than two T cells. The presence of DCs contacting these clusters was determined by visual inspection. Statistical analysis of speeds, stopping times, mean fluorescence intensity, and interaction times was conducted with Prism 4.0 (GraphPad Software), using an unpaired t test and a two-tailed 95% confidence interval.

Statistical Analysis

Statistical analyses were performed with GraphPad Prism. Unless specifically noted, all data are representative of >3 separate experiments. Error bars represent SEM, were calculated using Prism, and are derived from triplicate experimental conditions. Specific statistical tests used were paired and unpaired t tests, and all p values < 0.05 were considered statistically significant.

SUPPLEMENTAL INFORMATION

Supplemental Information includes three figures, Supplemental Experimental Procedures, and seven movies and can be found with this article online at doi:10.1016/j.ccr.2012.01.008.

ACKNOWLEDGMENTS

We thank A. Ma, L. Lanier, and N. Matsumoto for advice and the generous sharing of materials. We also thank Nigel Killeen and the UCSF Transgenic Core for assistance in the production of transgenic mice and Cliff MacArthur and Shu-Wei Jiang for assistance with cell sorting. This work was supported by NIH Grants R01CA134622, R01CA129523, U01CA141451, and by the Cancer Research Institute. B.B. was supported by an EMBO fellowship, and J.J.E. was supported by NIH Training Grant CA108462. We thank Mark Anderson, Alexis Madrid, and Emily Thornton for critical reading of the manuscript. We thank Lisa Coussens, David Denardo, Brian Ruffell, and Vicki Plaks for helpful discussions.

Received: July 29, 2011
Revised: November 18, 2011
Accepted: January 13, 2012
Published: March 19, 2012

REFERENCES

Adler, A.J., Marsh, D.W., Yochum, G.S., Guzzo, J.L., Nigam, A., Nelson, W.G., and Pardoll, D.M. (1998). CD4+ T cell tolerance to parenchymal self-antigens requires presentation by bone marrow-derived antigen-presenting cells. J. Exp. Med. *187*, 1555–1564.

Ambe, K., Mori, M., and Enjoji, M. (1989). S-100 protein-positive dendritic cells in colorectal adenocarcinomas. Distribution and relation to the clinical prognosis. Cancer *63*, 496–503.

Anderson, M.J., Shafer-Weaver, K., Greenberg, N.M., and Hurwitz, A.A. (2007). Tolerization of tumor-specific T cells despite efficient initial priming in a primary murine model of prostate cancer. J. Immunol. *178*, 1268–1276.

de Felipe, P., Hughes, L.E., Ryan, M.D., and Brown, J.D. (2003). Co-translational, intraribosomal cleavage of polypeptides by the foot-and-mouth disease virus 2A peptide. J. Biol. Chem. *278*, 11441–11448.

DeNardo, D.G., Barreto, J.B., Andreu, P., Vasquez, L., Tawfik, D., Kolhatkar, N., and Coussens, L.M. (2009). CD4(+) T cells regulate pulmonary metastasis of mammary carcinomas by enhancing protumor properties of macrophages. Cancer Cell *16*, 91–102.

Drake, C.G., Jaffee, E., and Pardoll, D.M. (2006). Mechanisms of immune evasion by tumors. Adv. Immunol. *90*, 51–81.

Dudley, M.E., Wunderlich, J.R., Robbins, P.F., Yang, J.C., Hwu, P., Schwartzentruber, D.J., Topalian, S.L., Sherry, R., Restifo, N.P., Hubicki, A.M., et al. (2002). Cancer regression and autoimmunity in patients after clonal repopulation with antitumor lymphocytes. Science *298*, 850–854.

Egeblad, M., Ewald, A.J., Askautrud, H.A., Truitt, M.L., Welm, B.E., Bainbridge, E., Peeters, G., Krummel, M.F., and Werb, Z. (2008). Visualizing stromal cell dynamics in different tumor microenvironments by spinning disk confocal microscopy. Dis. Model Mech. *1*, 155–167.

Epardaud, M., Elpek, K.G., Rubinstein, M.P., Yonekura, A.R., Bellemare-Pelletier, A., Bronson, R., Hamerman, J.A., Goldrath, A.W., and Turley, S.J. (2008). Interleukin-15/interleukin-15R alpha complexes promote destruction of established tumors by reviving tumor-resident CD8+ T cells. Cancer Res. *68*, 2972–2983.

Finn, O.J., Jerome, K.R., Henderson, R.A., Pecher, G., Domenech, N., Magarian-Blander, J., and Barratt-Boyes, S.M. (1995). MUC-1 epithelial tumor mucin-based immunity and cancer vaccines. Immunol. Rev. *145*, 61–89.

Friedman, R.S., Beemiller, P., Sorensen, C.M., Jacobelli, J., and Krummel, M.F. (2010). Real-time analysis of T cell receptors in naive cells in vitro and in vivo reveals flexibility in synapse and signaling dynamics. J. Exp. Med. *207*, 2733–2749.

Gabrilovich, D.I., and Nagaraj, S. (2009). Myeloid-derived suppressor cells as regulators of the immune system. Nat. Rev. Immunol. *9*, 162–174.

Garbi, N., Arnold, B., Gordon, S., Hämmerling, G.J., and Ganss, R. (2004). CpG motifs as proinflammatory factors render autochthonous tumors permissive for infiltration and destruction. J. Immunol. *172*, 5861–5869.

Gattinoni, L., Klebanoff, C.A., Palmer, D.C., Wrzesinski, C., Kerstann, K., Yu, Z., Finkelstein, S.E., Theoret, M.R., Rosenberg, S.A., and Restifo, N.P. (2005). Acquisition of full effector function in vitro paradoxically impairs the in vivo antitumor efficacy of adoptively transferred CD8+ T cells. J. Clin. Invest. *115*, 1616–1626.

Gattinoni, L., Powell, D.J., Jr., Rosenberg, S.A., and Restifo, N.P. (2006). Adoptive immunotherapy for cancer: building on success. Nat. Rev. Immunol. *6*, 383–393.

Gervois, N., Guilloux, Y., Diez, E., and Jotereau, F. (1996). Suboptimal activation of melanoma infiltrating lymphocytes (TIL) due to low avidity of TCR/MHC-tumor peptide interactions. J. Exp. Med. *183*, 2403–2407.

Guy, C.T., Cardiff, R.D., and Muller, W.J. (1992). Induction of mammary tumors by expression of polyomavirus middle T oncogene: a transgenic mouse model for metastatic disease. Mol. Cell. Biol. *12*, 954–961.

Hawiger, D., Inaba, K., Dorsett, Y., Guo, M., Mahnke, K., Rivera, M., Ravetch, J.V., Steinman, R.M., and Nussenzweig, M.C. (2001). Dendritic cells induce peripheral T cell unresponsiveness under steady state conditions in vivo. J. Exp. Med. *194*, 769–779.

Heath, W.R., and Carbone, F.R. (2001). Cross-presentation, dendritic cells, tolerance and immunity. Annu. Rev. Immunol. *19*, 47–64.

Hodi, F.S., O'Day, S.J., McDermott, D.F., Weber, R.W., Sosman, J.A., Haanen, J.B., Gonzalez, R., Robert, C., Schadendorf, D., Hassel, J.C., et al. (2010). Improved survival with ipilimumab in patients with metastatic melanoma. N. Engl. J. Med. *363*, 711–723.

Kawakami, Y., Eliyahu, S., Delgado, C.H., Robbins, P.F., Rivoltini, L., Topalian, S.L., Miki, T., and Rosenberg, S.A. (1994). Cloning of the gene coding for a shared human melanoma antigen recognized by autologous T cells infiltrating into tumor. Proc. Natl. Acad. Sci. USA *91*, 3515–3519.

Kusmartsev, S., Nagaraj, S., and Gabrilovich, D.I. (2005). Tumor-associated CD8+ T cell tolerance induced by bone marrow-derived immature myeloid cells. J. Immunol. *175*, 4583–4592.

Lee, P.P., Yee, C., Savage, P.A., Fong, L., Brockstedt, D., Weber, J.S., Johnson, D., Swetter, S., Thompson, J., Greenberg, P.D., et al. (1999). Characterization of circulating T cells specific for tumor-associated antigens in melanoma patients. Nat. Med. *5*, 677–685.

Lin, E.Y., Jones, J.G., Li, P., Zhu, L., Whitney, K.D., Muller, W.J., and Pollard, J.W. (2003). Progression to malignancy in the polyoma middle T oncoprotein mouse breast cancer model provides a reliable model for human diseases. Am. J. Pathol. *163*, 2113–2126.

Lin, E.Y., Li, J.-F., Gnatovskiy, L., Deng, Y., Zhu, L., Grzesik, D.A., Qian, H., Xue, X.N., and Pollard, J.W. (2006). Macrophages regulate the angiogenic switch in a mouse model of breast cancer. Cancer Res. *66*, 11238–11246.

Lindquist, R.L., Shakhar, G., Dudziak, D., Wardemann, H., Eisenreich, T., Dustin, M.L., and Nussenzweig, M.C. (2004). Visualizing dendritic cell networks in vivo. Nat. Immunol. *5*, 1243–1250.

Lu, H., Wagner, W.M., Gad, E., Yang, Y., Duan, H., Amon, L.M., Van Denend, N., Larson, E.R., Chang, A., Tufvesson, H., and Disis, M.L. (2010). Treatment failure of a TLR-7 agonist occurs due to self-regulation of acute inflammation and can be overcome by IL-10 blockade. J. Immunol. *184*, 5360–5367.

Mayordomo, J.I., Zorina, T., Storkus, W.J., Zitvogel, L., Celluzzi, C., Falo, L.D., Melief, C.J., Ildstad, S.T., Kast, W.M., Deleo, A.B., et al. (1995). Bone marrow-derived dendritic cells pulsed with synthetic tumour peptides elicit protective and therapeutic antitumour immunity. Nat. Med. *1*, 1297–1302.

Mempel, T.R., Henrickson, S.E., and Von Andrian, U.H. (2004). T-cell priming by dendritic cells in lymph nodes occurs in three distinct phases. Nature *427*, 154–159.

Miller, M.J., Wei, S.H., Parker, I., and Cahalan, M.D. (2002). Two-photon imaging of lymphocyte motility and antigen response in intact lymph node. Science *296*, 1869–1873.

Mrass, P., Takano, H., Ng, L.G., Daxini, S., Lasaro, M.O., Iparraguirre, A., Cavanagh, L.L., von Andrian, U.H., Ertl, H.C., Haydon, P.G., and Weninger, W. (2006). Random migration precedes stable target cell interactions of tumor-infiltrating T cells. J. Exp. Med. *203*, 2749–2761.

Nagaraj, S., Gupta, K., Pisarev, V., Kinarsky, L., Sherman, S., Kang, L., Herber, D.L., Schneck, J., and Gabrilovich, D.I. (2007). Altered recognition of antigen is a mechanism of CD8+ T cell tolerance in cancer. Nat. Med. *13*, 828–835.

Norian, L.A., Rodriguez, P.C., O'Mara, L.A., Zabaleta, J., Ochoa, A.C., Cella, M., and Allen, P.M. (2009). Tumor-infiltrating regulatory dendritic cells inhibit CD8+ T cell function via L-arginine metabolism. Cancer Res. *69*, 3086–3094.

Ojalvo, L.S., King, W., Cox, D., and Pollard, J.W. (2009). High-density gene expression analysis of tumor-associated macrophages from mouse mammary tumors. Am. J. Pathol. *174*, 1048–1064.

Otten, G.R., and Germain, R.N. (1991). Split anergy in a CD8+ T cell: receptor-dependent cytolysis in the absence of interleukin-2 production. Science *251*, 1228–1231.

Overwijk, W.W., Theoret, M.R., Finkelstein, S.E., Surman, D.R., de Jong, L.A., Vyth-Dreese, F.A., Dellemijn, T.A., Antony, P.A., Spiess, P.J., Palmer, D.C., et al. (2003). Tumor regression and autoimmunity after reversal of a functionally tolerant state of self-reactive CD8+ T cells. J. Exp. Med. *198*, 569–580.

Park, T.S., Rosenberg, S.A., and Morgan, R.A. (2011). Treating cancer with genetically engineered T cells. Trends Biotechnol. *29*, 1–8.

Pollard, J.W. (2009). Trophic macrophages in development and disease. Nat. Rev. Immunol. *9*, 259–270.

Qian, B.-Z., and Pollard, J.W. (2010). Macrophage diversity enhances tumor progression and metastasis. Cell *141*, 39–51.

Romero, P., Dunbar, P.R., Valmori, D., Pittet, M., Ogg, G.S., Rimoldi, D., Chen, J.L., Liénard, D., Cerottini, J.C., and Cerundolo, V. (1998). Ex vivo staining of metastatic lymph nodes by class I major histocompatibility complex tetramers reveals high numbers of antigen-experienced tumor-specific cytolytic T lymphocytes. J. Exp. Med. *188*, 1641–1650.

Rosenberg, S.A., Sherry, R.M., Morton, K.E., Scharfman, W.J., Yang, J.C., Topalian, S.L., Royal, R.E., Kammula, U., Restifo, N.P., Hughes, M.S., et al. (2005). Tumor progression can occur despite the induction of very high levels of self/tumor antigen-specific CD8+ T cells in patients with melanoma. J. Immunol. *175*, 6169–6176.

Schoppmann, S.F., Birner, P., Stöckl, J., Kalt, R., Ullrich, R., Caucig, C., Kriehuber, E., Nagy, K., Alitalo, K., and Kerjaschki, D. (2002). Tumor-associated macrophages express lymphatic endothelial growth factors and are related to peritumoral lymphangiogenesis. Am. J. Pathol. *161*, 947–956.

Sotomayor, E.M., Borrello, I., Rattis, F.M., Cuenca, A.G., Abrams, J., Staveley-O'Carroll, K., and Levitsky, H.I. (2001). Cross-presentation of tumor antigens by bone marrow-derived antigen-presenting cells is the dominant mechanism in the induction of T-cell tolerance during B-cell lymphoma progression. Blood *98*, 1070–1077.

Terabe, M., Matsui, S., Park, J.M., Mamura, M., Noben-Trauth, N., Donaldson, D.D., Chen, W., Wahl, S.M., Ledbetter, S., Pratt, B., et al. (2003). Transforming growth factor-beta production and myeloid cells are an effector mechanism through which CD1d-restricted T cells block cytotoxic T lymphocyte-mediated tumor immunosurveillance: abrogation prevents tumor recurrence. J. Exp. Med. *198*, 1741–1752.

Treilleux, I., Blay, J.Y., Bendriss-Vermare, N., Ray-Coquard, I., Bachelot, T., Guastalla, J.P., Bremond, A., Goddard, S., Pin, J.J., Barthelemy-Dubois, C., and Lebecque, S. (2004). Dendritic cell infiltration and prognosis of early stage breast cancer. Clin. Cancer Res. *10*, 7466–7474.

Valitutti, S., Müller, S., Cella, M., Padovan, E., and Lanzavecchia, A. (1995). Serial triggering of many T-cell receptors by a few peptide-MHC complexes. Nature *375*, 148–151.

van der Bruggen, P., Traversari, C., Chomez, P., Lurquin, C., De Plaen, E., Van den Eynde, B., Knuth, A., and Boon, T. (1991). A gene encoding an antigen recognized by cytolytic T lymphocytes on a human melanoma. Science *254*, 1643–1647.

Wakim, L.M., Waithman, J., van Rooijen, N., Heath, W.R., and Carbone, F.R. (2008). Dendritic cell-induced memory T cell activation in nonlymphoid tissues. Science *319*, 198–202.

Yee, C., Savage, P.A., Lee, P.P., Davis, M.M., and Greenberg, P.D. (1999). Isolation of high avidity melanoma-reactive CTL from heterogeneous populations using peptide-MHC tetramers. J. Immunol. *162*, 2227–2234.

Cancer Cell
Article

Enzymatic Targeting of the Stroma Ablates Physical Barriers to Treatment of Pancreatic Ductal Adenocarcinoma

Paolo P. Provenzano,[1] Carlos Cuevas,[4] Amy E. Chang,[1] Vikas K. Goel,[1] Daniel D. Von Hoff,[5] and Sunil R. Hingorani[1,2,3,*]
[1]Clinical Research Division
[2]Public Health Sciences Division
Fred Hutchinson Cancer Research Center, Seattle, WA 98109, USA
[3]Division of Medical Oncology, University of Washington School of Medicine, Seattle, WA 98195, USA
[4]Department of Radiology, University of Washington, Seattle, WA 98195, USA
[5]Clinical Translational Research Division, Translational Genomics Research Institute, Scottsdale, AZ 85259, USA
*Correspondence: srh@fhcrc.org
DOI 10.1016/j.ccr.2012.01.007

SUMMARY

Pancreatic ductal adenocarcinomas (PDAs) are characterized by a robust fibroinflammatory response. We show here that this desmoplastic reaction generates inordinately high interstitial fluid pressures (IFPs), exceeding those previously measured or theorized for solid tumors, and induces vascular collapse, while presenting substantial barriers to perfusion, diffusion, and convection of small molecule therapeutics. We identify hyaluronan, or hyaluronic acid (HA), as the primary matrix determinant of these barriers and show that systemic administration of an enzymatic agent can ablate stromal HA from autochthonous murine PDA, normalize IFP, and re-expand the microvasculature. In combination with the standard chemotherapeutic, gemcitabine, the treatment permanently remodels the tumor microenvironment and consistently achieves objective tumor responses, resulting in a near doubling of overall survival.

INTRODUCTION

Pancreatic ductal adenocarcinoma (PDA) is the fourth leading cause of cancer-related deaths in the United States (Jemal et al., 2010). The inherent biology of the disease makes it not only uniformly but also rapidly lethal: overall 5-year survival for PDA is less than 5%, with a median survival of 4–6 months (Hidalgo, 2010). Gemcitabine, a deoxycytosine analog, represents the current standard of care for advanced disease and improves quality of life in a minority of patients while prolonging survival by several weeks (Burris et al., 1997). A recent advance involving targeted inhibition of epidermal growth factor receptor (EGFR) with erlotinib extends median survival by an additional 14 days (Moore et al., 2007). Moreover, despite notable advances in surgical technique and postoperative care, and the use of adjuvant chemical and radiotherapies, virtually all early-stage patients who undergo resection also eventually succumb to recurrent and/or metastatic disease (Allison et al., 1998; Farnell et al., 2005; Oettle et al., 2007). Understanding the unusual resistance of pancreas cancer and finding ways to treat it at all stages of disease are clear and imperative needs.

Most preclinical drug evaluations to date have relied on in vitro assays and in vivo cell transplantation models. However, tumor cells arising in situ in the native organ are categorically distinct from the same cells grown in culture or engrafted into an immunocompromised mouse (Bissell and Radisky, 2001). Indeed, transplanted pancreas carcinoma cells respond readily to conventional chemotherapeutic agents (Hertel et al., 1990), in marked contrast to autochthonous tumors in mice (Olive et al., 2009) and humans (Tempero et al., 2003). This problem cuts both ways: in failing to fully appreciate the unique challenges imposed by the complex cancer "organ," opportunities to target

Significance

More than 90% of cancer drugs brought to the clinic fail. The gap between preclinical promise and clinical reality arises, in part, from the inability of traditional model systems to sufficiently represent the cellular and structural complexity of the solid tumor "organ." In failing to fully account for the tremendous obstacles to efficacy in autochthonous tumors, potential opportunities to identify and target the most clinically meaningful barriers are also lost. We have found that an unusually abundant matrix glycosaminoglycan fortifies the epithelium and creates a drug-free sanctuary in PDA. Ablating this constituent renders the cancer profoundly vulnerable to standard cytotoxics and holds promise as a distinct therapeutic strategy, while compelling reassessment of conventional chemotherapies previously thought to be ineffective.

and exploit the most clinically relevant mechanisms may also be missed. Thus, there are noncell autonomous factors, including unique cell-cell and cell-matrix interactions and evolving intratumoral physical dynamics, that contribute to the in vivo resistance of cancers.

Prior work in a number of experimental systems has suggested that altered intratumoral fluid dynamics can limit the effectiveness of systemic therapies (reviewed in Bouzin and Feron, 2007; Heldin et al., 2004; Jain, 1987; Trédan et al., 2007). Mammalian organs and tissues typically possess interstitial fluid pressures (IFPs) at or below the intravascular pressures (IVPs) in the terminal arterioles and capillaries that supply them. As first proposed by Starling in 1896, an IFP less than IVP permits ready perfusion and favors diffusive and convective forces necessary for solute and fluid flow into the interstitium (Starling, 1896; see Supplemental Information available online). The solutes are consumed by cells, while the venous vasculature and functional lymphatic channels return excess fluid to the systemic circulation (reviewed in Michel, 1984). Although these processes governing the delivery and diffusion of cancer drugs have been studied extensively in xenograft models, very few experiments have been performed in autochthonous carcinomas, and no rigorous analyses before and after perturbation of the tumor microenvironment have been described.

PDAs are characterized by an unusually intense desmoplastic reaction composed of fibroblasts, immune cells, and endothelial cells embedded within a dense and complex extracellular matrix (ECM). The ECM component hyaluronic acid (HA), or hyaluronan, is inordinately abundant, inviting speculation on its role in disease biology and resistance. HA is a large linear glycosaminoglycan (GAG), composed of repeating N-acetyl glucosamine and glucuronic acid units, and figures prominently in the architecture, integrity, and malleability of tissues, particularly in dynamic processes such as embryogenesis and oncogenesis (Toole, 2004). Its viscoelastic properties underlie its unique role in tissue homeostasis and its appeal in cosmetic and clinical applications (Balazs and Denlinger, 1989). HA also communicates directly with cells in health and disease through interactions with several distinct types of surface receptors. However, the abundance of HA varies widely across tumors, and it has been shown to both promote and suppress tumor growth (Toole, 2004). Even its potential contribution to IFP is controversial. Local injection of hyaluronidase into osteosarcoma xenografts has been shown to decrease IFP (Brekken et al., 2000; Eikenes et al., 2005), although enforced overexpression of HA in thyroid and colon carcinoma xenografts did not increase it (Jacobson et al., 2003). Thus, although HA has been implicated in a variety of cell autonomous and noncell autonomous processes, its precise role(s) in therapeutic resistance of cancers has remained elusive and is likely context specific (reviewed in Toole and Slomiany, 2008; Trédan et al., 2007).

As an alternative to transplanted cells and tumors, we have developed genetically engineered mouse (GEM) models of PDA that faithfully recapitulate the clinical syndrome, histopathology, and molecular progression of human pancreas cancer from inception to invasion. *Kras*$^{LSL\text{-}G12D/+}$*;Cre* (*KC*) (Hingorani et al., 2003) and *Kras*$^{LSL\text{-}G12D/+}$*;Trp53*$^{LSL\text{-}R172H/+}$*;Cre* (*KPC*) (Hingorani et al., 2005) mice conditionally express endogenous, physiologic levels of the respective oncogene and tumor suppressor gene mutations in pancreatic progenitor cells, resulting in the stochastic development and spontaneous progression of preinvasive ductal lesions to invasive and metastatic carcinomas. In collaborative studies using the *KPC* model, we have recently suggested that the unusually hypovascular microenvironment of PDA compromises the delivery of even small molecule therapeutics such as gemcitabine. These studies showed further that targeting stromal fibroblasts by disrupting paracrine Hedgehog signaling between the epithelial and mesenchymal tumor compartments transiently increased the apparent microvascular density through neoangiogenesis and improved drug delivery, resulting in a modest survival benefit (Olive et al., 2009). Interestingly, disease resistance rapidly re-emerged along with a return of the profound hypovascularity. Moreover, the mechanisms giving rise to and sustaining this paucity of vessels remained unclear. In the present study, we pursue a mechanistic understanding of the biophysical barriers to perfusion, diffusion, and convection imposed by the desmoplastic reaction in autochthonous PDA and investigate strategies to surmount them.

RESULTS

Cellular and Molecular Evolution of Desmoplasia in PDA

As part of a systematic effort to characterize the evolving stromal dynamics and potential therapeutic vulnerabilities during disease progression, we performed specific histochemical and immunohistochemical assays to identify components of the ECM and infiltrating cells in preinvasive, invasive, and metastatic PDA in mice and humans (Figure 1 and Figures S1A–S1D). A robust and definable stromal reaction develops in association with early precursor lesions and includes a dense collagen content organized in a fibrillary structure in both primary tumors and metastases, as revealed by intravital second harmonic generation (SHG) imaging (Figures S1E–S1J). The tight association of this fibrillar collagen with epithelial carcinoma cells became evident in *Kras*$^{LSL\text{-}G12D/+}$*;Trp53*$^{LSL\text{-}R172H/+}$*;R26*$^{LSL\text{-}GFP/+}$*;Cre* (*KPGC*) mice. Interestingly, the relative concentrations of collagen and glycosaminoglycans (GAGs) appear to alter during disease progression, shifting toward higher GAG content at more advanced and metastatic stages of disease (Figures 1A–1J). One particular GAG, HA, was especially abundant (Figures 1K–1O), which was confirmed by treating tissue sections with hyaluronidase (Figures S1K–S1N). We note that significant HA deposition begins with early precursor lesions (Figures 1G and 1L). In addition, activated stromal pancreatic stellate cells (PSCs), or myofibroblasts, also infiltrate early and are prevalent throughout disease progression (Figures 1P–1T). Conversely, a decrease in vessel number is seen with progression (Figures S1O–S1Q), as described previously (Olive et al., 2009), and is accompanied by a decrease in cross-sectional (luminal) area (Figure S1R).

This same overall molecular and cellular stromal composition is observed in human PDA (Figures 1E, 1J, 1O, and 1T). We note, in particular, the expression of moderate-to-high levels of HA in all human PDAs tested (n = 30; Figures 1J and 1O and data not shown), suggesting that this substrate may be an essential component of disease architecture, biology, and resistance.

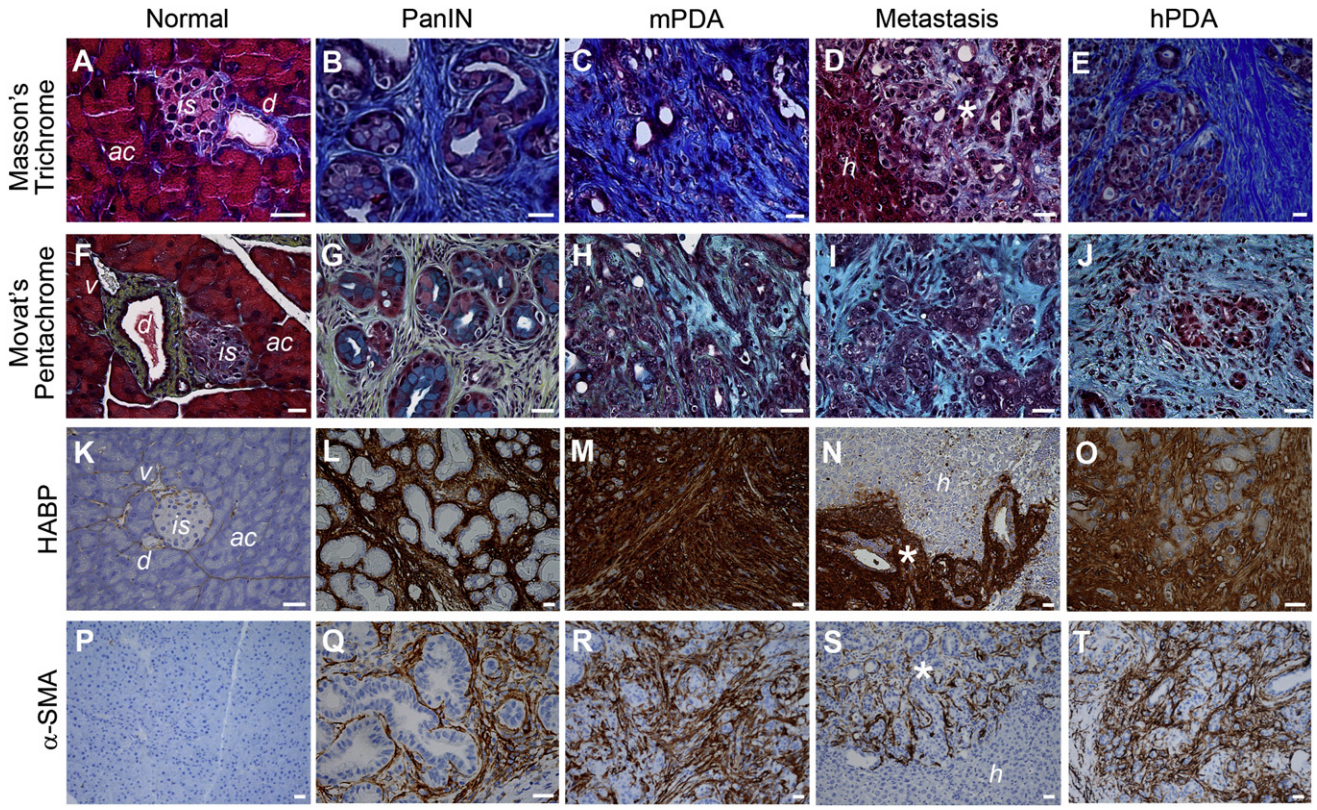

Figure 1. Evolution of the Desmoplastic Reaction in Murine and Human PDA

(A–E) Masson's trichrome histochemistry shows robust collagen deposition (blue) at all stages of disease.

(F–J) Movat's pentachrome histochemistry reveals collagen (yellow), GAGs and mucins (blue), and their colocalization (turquoise/green).

(K–O) Histochemistry with HA-binding protein (HABP) reveals intense HA content beginning with preinvasive disease (PanIN).

(P–T) Activated PSC express α-smooth muscle actin (α-SMA) and are abundant in preinvasive (Q), invasive (R) and metastatic mPDA (S) and hPDA (T), but not in normal pancreata (P). *ac,* acini; *is,* islet; *d,* duct; *v*, venule; *h*, hepatic parenchyma; *, metastatic lesions. Scale bars, 25 μm. See also Figure S1.

Dramatically Elevated IFP in PDA

To directly measure IFP in normal pancreata and in autochthonous PDAs in live animals, we used a system coupling a miniature piezoelectric pressure transducer to a pressure control unit and data acquisition module (Figure 2A). Anesthetized animals underwent laparotomy followed by needle-guided placement of the pressure transducer probe enabling real-time in vivo IFP measurements (Figures 2B and 2C). As expected, the normal pancreas possesses an IFP ranging between 8 and 13 mm Hg (mean = 10.4 mm Hg; n = 8) (Figure 2D). In contrast, we observed dramatically elevated IFPs in autochthonous PDA that far exceeded the normal range for the pancreas (Figure 2D). Tumor IFPs ranged from 75 to 130 mm Hg (mean = 99 mm Hg, n = 7, in *KPC* PDA; mean = 87 mm Hg, n = 4, in *KC* tumors), which vastly exceeded typical arteriolar and capillary pressures of 40–80 mm Hg and 15–40 mm Hg, respectively (Sherwood, 1997) and rivaled mean arterial pressure (Janssen et al., 2000; Mattson, 1998). Pressures of this magnitude suggest not only major impediments to delivery and convection of small molecules, but also imply a profound reorganization and remodeling of the tumor architecture and the forces operant within it (see also Supplemental Information).

Enzymatic Targeting of Stromal HA Restores Tumor IFP and Functional Perfusion

We began our studies on the ability of HA to elevate IFP using reconstituted three-dimensional matrices. Purified primary murine PDA cells were embedded in matrices with differing HA concentrations, the tumor plugs were implanted in immunodeficient mice, and IFPs were recorded (Figures S2A–S2C). HA concentrations of 3 mg/ml more than doubled the baseline IFP of carcinoma cells engrafted in collagen alone, suggesting that the presence of HA in the tumor can contribute directly to elevated IFP.

The abundance of HA in PDA and its demonstrated capacity to significantly elevate IFP prompted us to investigate whether a systemically delivered agent could ablate HA in the stroma of an autochthonous PDA and decrease pressures. We first tested the ability of intravenously administered PEGPH20 to deplete HA from normal tissues in wild-type (*WT*) mice and assessed for any untoward effects (Figures S2D–S2F). Several organs in the body including heart, lung, bowel, and liver contain modest levels of detectable HA (Figure S2E), whereas joints possess very high levels (Figure S2F). HA was efficiently ablated from all of these sites except cartilage and the surrounding joint space. Cartilage

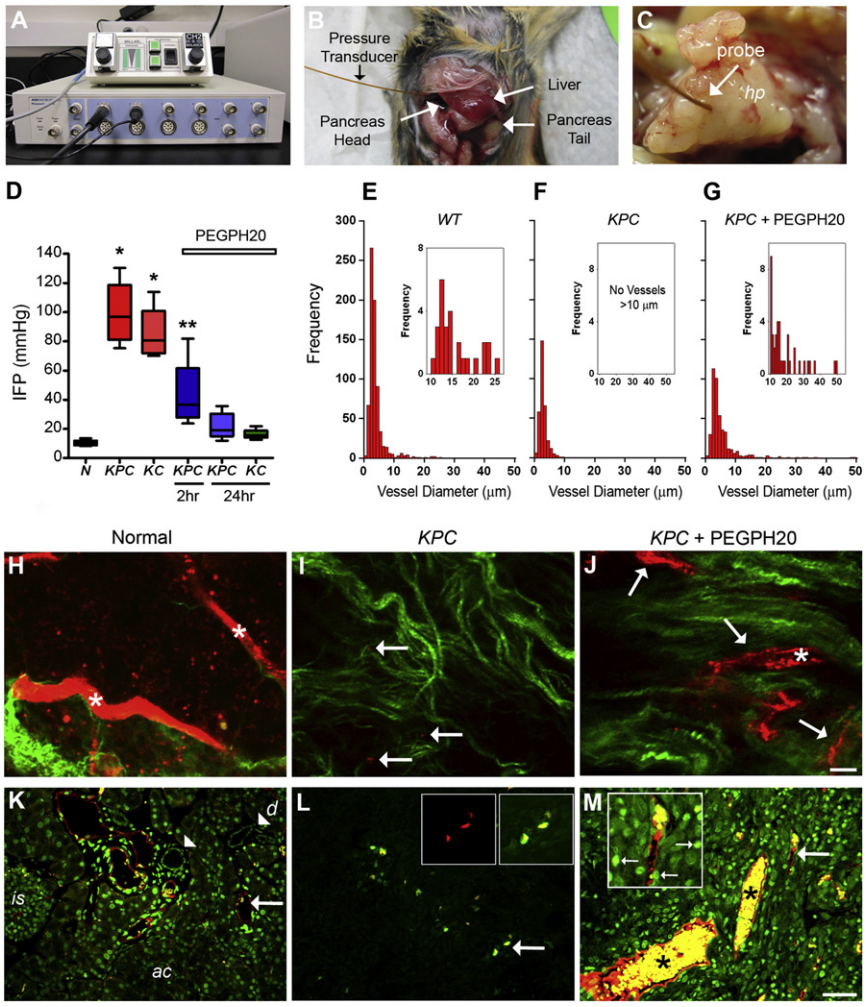

Figure 2. Elevated IFP Compromises Vascular Function in PDA

(A) Experimental apparatus to measure IFP.

(B and C) IFP probe positioned in PDA at the head of the pancreas (*hp*). In (B), the probe ends in a tumor obscured by the overlying liver.

(D) IFP measurements in normal pancreata (*N*), untreated *KPC* and *KC* tumors and tumors 2 and 24 hr after PEGPH20 treatment. *p < 0.01 for comparison between normal pancreata and PEGPH20 treatment groups; **p < 0.05 for difference from all other groups with 1-way ANOVA and Newman-Keuls posthoc multiple comparison test. Note that IFP levels in normal pancreata and PEGPH20-treated *KC* (mean = 16 mm Hg, n = 4) and *KPC* (mean = 22 mm Hg, n = 5) tumors 24 hr after treatment were not statistically different. Box and whisker plots: boxes display the lower (25^{th}) and upper (75^{th}) quartiles with a line at the median; whiskers extend from the minimum to the maximum observation.

(E–G) Distribution of $CD31^+$ vessel diameter in normal pancreata (E), untreated *KPC* tumors (F), and *KPC* tumors 24 hr after PEGPH20 treatment (G). Insets show data for vessels of diameter > 10 μm. Data represent evaluations from four independent sections from each of four separate animals for each condition and are significantly different ($p < 0.0001$) in the pairwise comparisons with *KPC*.

(H–J) Multiphoton excitation of fluorescently conjugated lectin (red) and second harmonic generation imaging of collagen (green) within intact normal pancreas (H), untreated *KPC* tumors (I), and *KPC* tumors 24 hr after PEGPH20 treatment (J). Asterisks in (H) and (J) highlight examples of large functional vessels. Arrows in (I) and (J) indicate perfused (functional) vessels. Note that when a rare functional vessel in untreated *KPC* tumors is identified, it is extremely small relative to those in normal pancreata and PEGPH20 treated tumors. Scale bar, 10 μm for (H–J).

(K–M) Direct fluorescence analysis of Alexa-647-conjugated lectin (red) and doxorubicin (green) in intact normal pancreas (K), untreated *KPC* tumors (L), and *KPC* tumors 24 hr after PEGPH20 treatment (M). Arrow in (K) shows an example of a widely patent, thin-walled vessel, and arrowheads indicate ductal epithelium. Large arrows in (L) and (M) highlight regions magnified in respective inset boxes. The left inset box in (L) shows signal in the far-red Alexa-647 channel (lectin) alone, and the right inset box shows merged green (doxorubicin) and red (lectin) channels. Small arrows in inset box of panel (M) identify examples of specific nuclear staining from DNA-bound doxorubicin, as well as the presence of free doxorubicin in the tumor. Asterisks in (M) highlight examples of large, functional lectin-positive vessels loaded with doxorubicin. *ac,* acini; *is,* islet; *d,* duct. Scale bar, 50 μm for (K–M). See also Figure S2.

represents an essentially avascular compartment completely excluding delivery of PEGPH20. Interestingly, depletion of HA from these sites had no discernible effects on organ function or animal health; animals remained active without apparent changes in energy level or mobility and also maintained their body weight (Figure S2D). We next demonstrated that intravenous administration of PEGPH20 to *KC* and *KPC* mice could deplete HA in autochthonous PDAs (Figure S2G). Moreover, after a single intravenous dose of PEGPH20, IFP was significantly decreased within 2 hr and approached the range for normal pancreata 24 hr after treatment (Figure 2D). The restoration of near normal tumor IFP after degradation of stromal HA suggested that treatment with PEGPH20 should also significantly and rapidly improve blood flow if indeed mechanical compression of the vasculature was the primary mechanism limiting perfusion. To assess the effects on the tumor microvasculature of IFP normalization, we performed a systematic survey of vessel number and lumen diameter in WT pancreata as well as untreated and treated murine PDA (Figures 2E–2G). We found a significant shift in the distribution of $CD31^+$ vessel diameters in murine and human PDA compared with the normal pancreas and, in particular, an almost complete absence of large diameter (>10 μm) vessels (Figures 2E–2G and Figures S2H and S2I). The normal pancreas contains a range of small-to-moderate sized vessels, more than 80% of which possess a readily discernible and patent lumen; conversely, the majority (~75%) of vessels in PDA lacked an apparent lumen, consistent with vascular collapse from elevated extrinsic fluid pressures. Following treatment with PEGPH20, vessel diameter was significantly increased and lumens clearly discernible in ~71% of $CD31^+$ vessels (Figure 2G and Figure S2H).

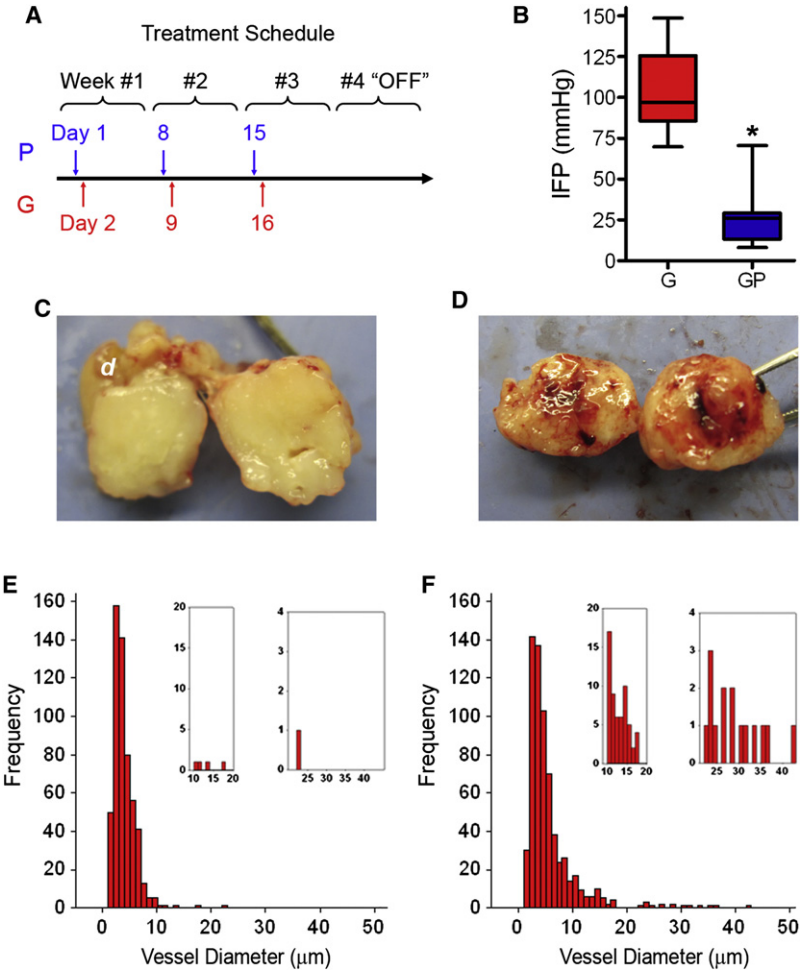

Figure 3. Gemcitabine+PEGPH20 Combination Therapy Fundamentally Changes the Tumor Vasculature

(A) Treatment schedule for administration of PEGPH20 (P) or placebo and gemcitabine (G). Mice undergoing gemcitabine monotherapy also received placebo (vehicle) injections. Each 4-week course represents one cycle of therapy.

(B) Tumor IFP at survival endpoint after treatment with gemcitabine (G; n = 9) or Gem+PEGPH20 (GP; n = 9), *p < 0.0001. Box and whisker plots: boxes display the lower (25th) and upper (75th) quartiles with a line at the median; whiskers extend from the minimum to the maximum observation.

(C) Gross pathology of transected PDA at endpoint after gemcitabine monotherapy. *d*, duodenum.

(D) Gross pathology of transected PDA at endpoint after combination therapy.

(E and F) Distribution of significantly different ($p < 0.0001$) CD31$^+$ vessel diameter in Gem (E) and Gem+PEGPH20 (F) treated *KPC* tumors at survival endpoint. Inset graphs show significantly different ($p < 0.0001$) distribution also for subsets of vessels with diameters between 10–20 μm and > 20 μm. Data are from four independent sections from five separate animals for each treatment arm. See also Figure S3.

We next performed functional analyses of the vasculature with intravital multiphoton laser scanning microscopy (MPLSM). Normal pancreata revealed a rich, widely patent vasculature (Figure 2H) with excellent delivery of the small molecule therapeutic doxorubicin throughout the parenchyma (Figure 2K). In contrast, vessels in PDA were difficult to detect and appeared collapsed (Figure 2I), and penetration of doxorubicin into the tumor bed was extremely limited (Figure 2L). Even when rare perfusion was observed (Figure 2L), the distribution of drug into the tumor was low, suggesting limited diffusion and convection into the interstitium. A single intravenous dose of PEGPH20 resulted in the immediate appearance of significant numbers of patent vessels (Figures 2J and 2M), reflecting their increased diameters (Figure 2G). These changes were accompanied by a >6.5-fold increase in doxorubicin fluorescence intensity over baseline ($p = 0.013$, $n = 4$ each for treated and untreated *KPC* cohorts; and $p = 0.04$, $n = 3$ per group for *KC* PDAs). We note that overall vessel number did not significantly change (data not shown), which, together with the rapidity of the effect and lack of significant endothelial cell proliferation (see below), suggest that neoangiogenesis did not contribute substantively. Rather, it appears that the inordinately high IFP produces vascular collapse in PDA and reversal of these elevated pressures restores functional perfusion and unimpeded delivery of drug into the carcinoma.

Combined Enzymatic and Cytotoxic Chemotherapy Alters Tumor Biology and Increases Disease Response and Overall Survival in PDA

We next sought to assess the effects of combination chemotherapy on the gross morphological, physicomechanical, cellular, and molecular properties of autochthonous PDA. In previous studies of gemcitabine in *KPC* mice (Olive et al., 2009), we used a dose, route, and schedule modeled on the original preclinical investigations of gemcitabine in subcutaneously engrafted tumors (Hertel et al., 1990; Schultz et al., 1993). For the present studies, we treated *KPC* cohorts according to the route and schedule used in the clinic. Specifically, we performed a randomized, placebo-controlled study of the combination regimen involving intravenous drug administration in cycles consisting of the 3-weeks "on" and 1-week "off" schedule used in patients (Figure 3A). Animals were first assessed with serial high-resolution ultrasound measurements until they achieved a requisite enrollment tumor diameter of 2–5 mm. Studies were performed on separate cohorts of animals to measure early and intermediate effects, and also to establish overall survival.

As expected, IFP normalized in Gem+PEGPH20-treated tumors, confirming that the addition of gemcitabine did not impede the ability of PEGPH20 to influence this physicomechanical property (Figure 3B). Interestingly, no change in baseline tumor IFP occurred in Gem+Placebo-treated animals, reflecting the inability of gemcitabine to effectively penetrate tumors and induce responses. The gross findings at necropsy underscored these differences, as tumors recovered from Gem+Placebo-treated animals (Figure 3C and Figure S3A) revealed the hard,

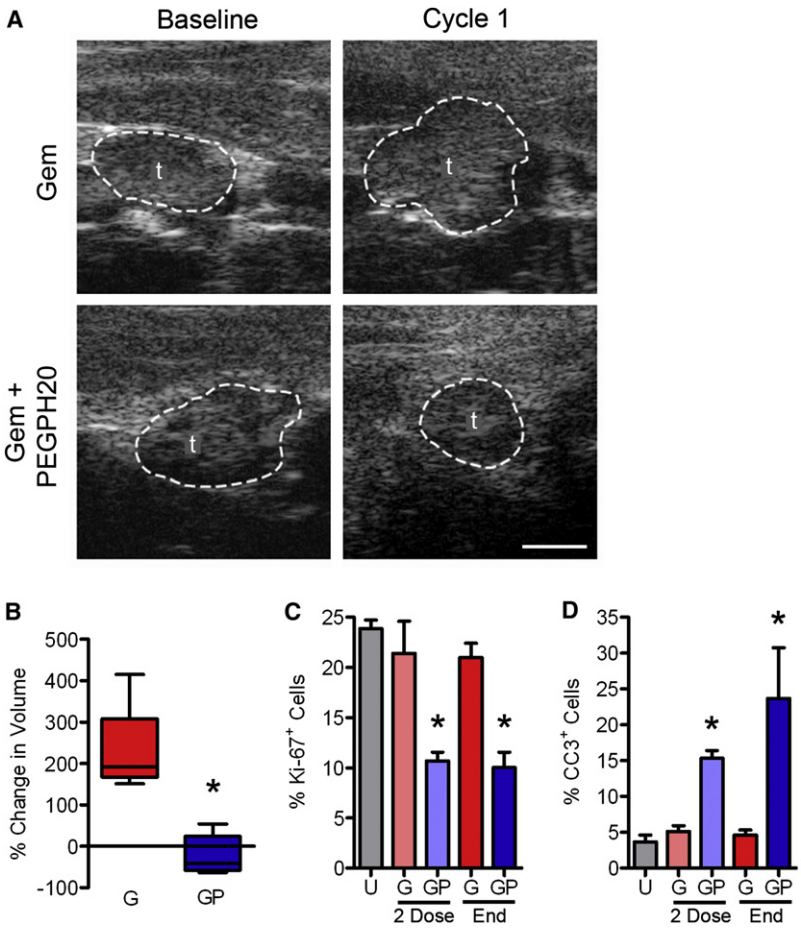

Figure 4. Gemcitabine+PEGPH20 Induces Objective Responses through Reduced Proliferation and Increased Apoptosis

(A) High-resolution ultrasound images of PDA before and after the indicated treatment. Scale bar, 1 mm. t, tumor.

(B) Quantitative analysis of tumor volume in Gem (G; n = 5) and Gem+PEGPH20 (GP; n = 6) treated mice after one cycle of therapy (*p = 0.009). Box and whisker plots: boxes display the lower (25th) and upper (75th) quartiles with a line at the median; whiskers extend from the minimum to the maximum observation.

(C) Quantitative analysis of proliferation assessed as percentage of Ki-67^{+} cells per image field in untreated (U) and Gem (G) or Gem+PEGPH20 (GP) treated tumors after either two weekly doses of therapy (2 Dose; *p < 0.035) or at endpoint (End; *p = 0.0009).

(D) Quantitative analysis of apoptosis assessed as percentage of cleaved caspase-3 (CC3)$^{+}$ cells per image field in untreated (U) and Gem (G) or Gem+PEGPH20 (GP) treated tumors after two doses of therapy (*p = 0.035) or at endpoint (*p = 0.01). Data in (C and D) are plotted as mean ± SEM. See also Figure S4.

white, fibrous, and overtly hypovascular composition typical of the untreated disease (Figure S3B). In contrast, tumors from animals receiving Gem+PEGPH20 were notably soft, highly vascularized, and even hemorrhagic when transected (Figures 3D and Figures S3C–S3F). A blood-rich microenvironment in combination treated tumors was readily apparent even by routine histology (Figures S3G–S3L). Quantitative analysis confirmed significant differences in vessel diameter between Gem+Placebo- and Gem+PEGPH20-treated PDA (Figures 3E and 3F) without significant differences in vessel number (data not shown). Importantly, these findings were observed in all mice immediately after initiating therapy (Figures S3G–S3L), during active treatment (Figures S3M and S3N), and persisted even after treatment cessation (Figures S3O–S3T). Even nearly 3 months after completing combination therapy, functional vessels were retained suggesting an irreversible change in tumor physiology (Figures S3S and S3T).

Objective measures of clinical response were frequently apparent after only one cycle of combination therapy. Notably, of the subset of Gem+Placebo-treated animals that underwent quantitative volumetric imaging both before and after treatment, none experienced an objective tumor response affirming the collective clinical (Burris et al., 1997; Casper et al., 1994) and preclinical experience with this agent in autochthonous PDA (Olive et al., 2009) (Figures 4A and 4B). In contrast, 83% of Gem+PEGPH20-treated tumors decreased in size after one cycle of treatment (Figures 4A and 4B) with all tumors responding after three cycles (see example in Figure S4A). Consistent with its known mechanisms of inhibiting DNA and RNA synthesis (Hertel et al., 1990; Ueno et al., 2007), combination therapy both decreased proliferation and increased apoptosis of primary tumor cells compared with Gem+Placebo, contributing to the observed differences in objective responses (Figures 4C and 4D and Figures S4B–S4E). Thus, when able to penetrate the tumor bed, gemcitabine can indeed be an effective agent against this disease.

The numbers of total stromal PSCs (Figure S5A) and activated PSCs (Figures 5A–5C and Figure S5B) were also significantly decreased, and the tumor stroma was extensively remodeled (Figures 5D–5G). Although unaffected by PEGPH20 alone, collagen content and distribution were both significantly decreased by the combined regimen, likely as a secondary consequence of depleting collagen-secreting activated PSCs. Finally, no discernible effects on endothelial cell proliferation (Figure S5C) or apoptosis (Figure S5D) were observed, consistent with the expected restricted activity of a conventional cytotoxic agent to actively dividing cells. Thus, the depleted HA and diminished IFP seen with the combined enzymatic and cytotoxic regimen restores and preserves a functional vasculature while inducing tumor epithelial and stromal cells to die.

Similar restrictions and responses were observed in metastases. Metastatic lesions to the liver (Figures 1D, 1I, 1N, and 1S) and lung (Figure 6A) possessed a robust and complex desmoplasia, with notable HA content and a paucity of vessels (Figures S6A–S6G). Perhaps surprisingly, given their typically smaller size compared with primary tumors, the metastatic deposits were also poorly perfused by small molecules (Figures S6H–S6K). As with primary tumors, PEGPH20 efficiently ablated HA from metastases (Figure 6B) and restored functional perfusion (Figure S6K).

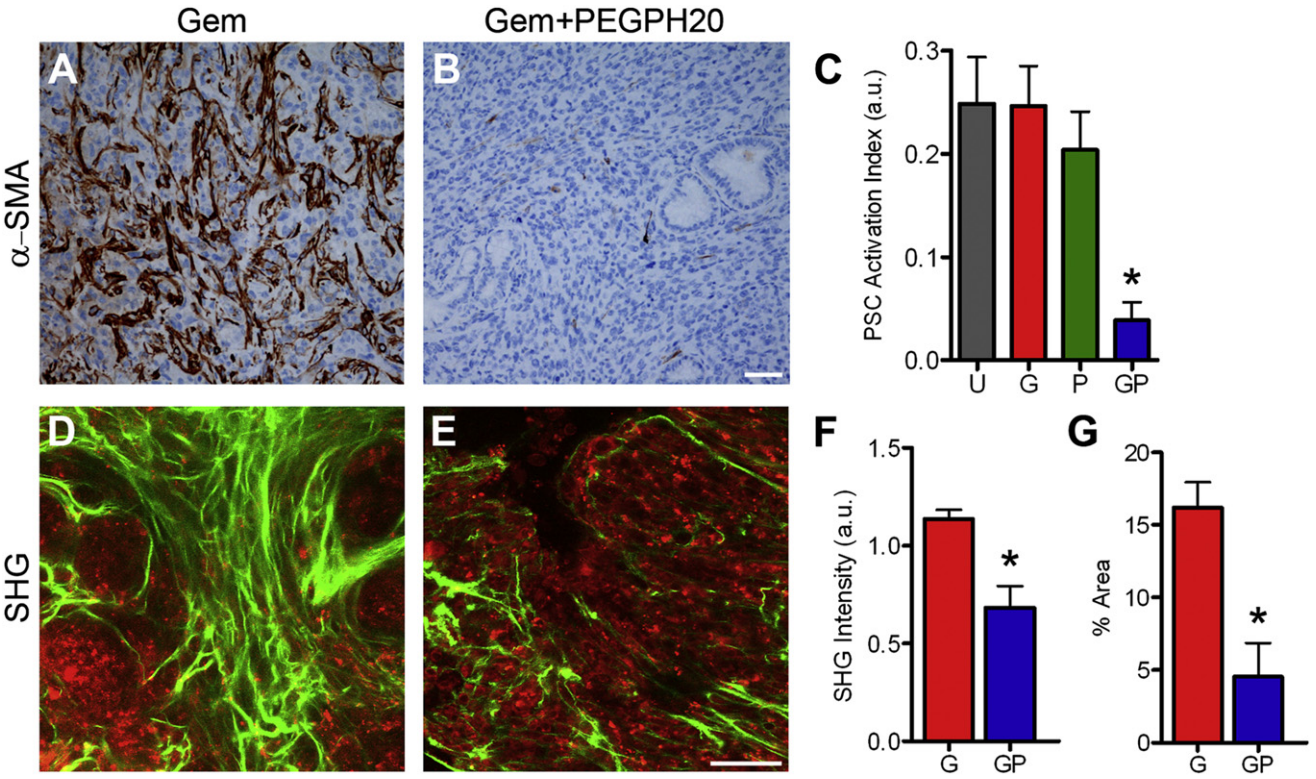

Figure 5. Combination Therapy with Gemcitabine+ PEGPH20 Remodels the Tumor Stroma

(A and B) IHC for the PSC activation marker α-SMA in PDA at survival endpoint after the indicated treatment. Scale bar, 50 μm.

(C) Quantitative analysis of PSC activation in untreated tumors (U) or tumors treated with Gem (G), PEGPH20 (P), or Gem+PEGPH20 (GP) at survival endpoint (*p = 0.005).

(D and E) Representative micrographs from intravital SHG imaging of collagen (green) combined with multiphoton excitation of endogenous fluorescence from NADH (red) in PDA at survival endpoint just prior to euthanasia. Scale bar, 50 μm.

(F) Mean SHG intensity in PDAs at endpoint as a measure of fibrillar collagen concentration (*p = 0.028).

(G) Percent area occupied by fibrillar collagen in tumors at endpoint (*p = 0.028). Data in (C), (F), and (G) are plotted as mean ± SEM. See also Figure S5.

When given together with gemcitabine, the combination regimen decreased proliferation (Figure 6C) and increased apoptosis (Figure 6D) in metastases to both distant sites.

The aforementioned encouraging results notwithstanding, the most clinically relevant measure of efficacy is survival. We therefore performed a prospective, randomized, placebo-controlled trial in *KPC* mice with overall survival as the primary endpoint. Secondary endpoints included changes in intratumoral IFP and objective response rates, as well as metastatic disease burden.

Median overall survival increased from 55.5 days for Gem+Placebo to 91.5 days for Gem+PEGPH20, an 83% increase (Figure 6E). These results likely do not reflect the maximal achievable benefit from combination therapy as the treatment course was limited to 3 months because of sclerosing of the vein after repeated intravenous injections. In fact, only 29% of Gem+PEGPH20-treated animals died during the course of therapy and approximately 30% of animals lived an additional 4–11 weeks after completing three full months of treatment. In contrast, more than 80% of animals receiving Gem+Placebo died during treatment; of the remaining four animals, three died in the very next week after cessation of therapy (Figure 6E and Table S1).

The metastatic tumor burden was also significantly diminished with combination therapy (Figure 6F, Table 1, and Table S1). The frequency of malignant ascites as well as metastases to the liver, lungs, diaphragm, and mesenteric lymph nodes were all decreased in the Gem+PEGPH20 cohort. Thus, the combination regimen effectively treated both the primary and metastatic disease burdens.

DISCUSSION

The defining features of PDA are a penchant for metastatic spread and a notorious resistance to chemical and radiotherapies. These features, in turn, establish the major hurdles to meaningful treatment of the disease. A perhaps prosaic, albeit unexpected and critically important, barrier to systemic therapy is a profoundly diminished functional vasculature in PDA. We show here that the primary mechanism limiting perfusion in PDA is significant collapse of resident vessels by inordinately high fluid pressures. Small molecules that are delivered to the tumor bed are subsequently impeded from penetrating the interstitium by constraints on diffusion and convection, completing a trifecta of stromal barriers to chemotherapy. Enzymatic

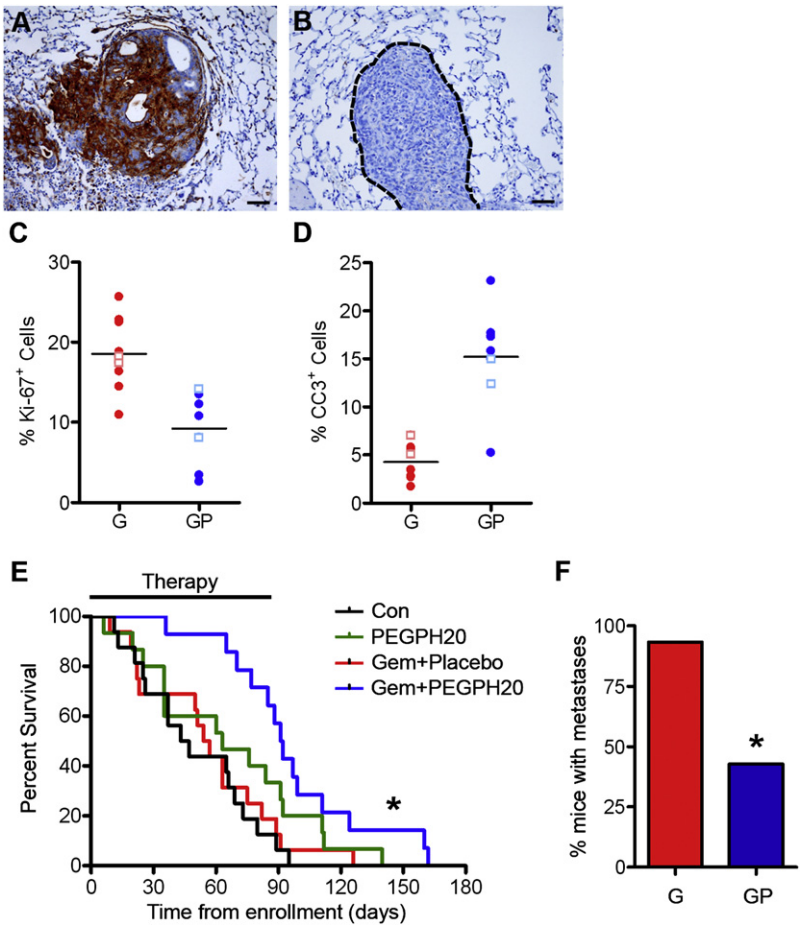

Figure 6. Gemcitabine+PEGPH20 Combination Therapy Decreases Metastatic Tumor Burden and Improves Survival

(A and B) HA expression in lung metastases from untreated (A) and PEGPH20-treated (B) animals.

(C) Quantitative analyses of proliferation assessed as percentage of Ki-67$^+$ cells in metastases to liver (filled circles) and lung (open squares) after gemcitabine monotherapy (G) or Gem+PEGPH20 (GP) combination therapy ($p = 0.0012$). Horizontal bars represent means.

(D) Quantitative analysis of apoptosis assessed as percentage of CC3$^+$ cells in liver (filled circles) and lung (open squares) metastases ($p = 0.0001$). Horizontal bars represent means.

(E) Kaplan-Meier survival curves from time of enrollment in control (Con; n = 16), Gem (n = 16), PEGPH20 (n = 15), and Gem+PEGPH20-treated *KPC* animals (n = 14). (Black bar indicates maximum duration of therapy.) Median overall survival of Gem (55.5 days) and Gem+PEGPH20 (91.5 days) treated mice are significantly different (*$p = 0.004$). Treatment with PEGPH20 alone showed a trend toward increased survival (median = 63 days) that did not reach statistical significance ($p = 0.1$).

(F) Metastatic burden in Gem+PEGPH20 (GP) treated mice is significantly decreased compared with Gem treatment alone (G) (*$p = 0.014$). See also Figure S6 and Table S1.

degradation of hyaluronan results in a rapid reduction of IFP accompanied by the appearance of widely patent functioning vessels. Removing these barriers permits high concentrations of chemotherapy to reach the tumor, resulting in improved survival and revealing an unappreciated sensitivity of the disease to conventional cytotoxic agents.

The theory governing the movement of fluid and solute across a semipermeable membrane dividing two compartments (e.g., vascular and extravascular) is readily derived from fundamental thermodynamic principles (Kedem and Katchalsky, 1958; Kedem and Katchalsky, 1961; Staverman, 1952) (reviewed in Ogston and Michel, 1978) and incorporates hydrostatic and osmotic pressure gradients as the primary determinants of fluid flow, and concentration gradients as the driving force for solute flux. The resultant equations, in turn, explain the inability to achieve effective chemotherapy concentrations in PDA given the extremely high IFPs observed (see Supplemental Information for a detailed treatment of these equations). They do not, however, adequately address how such dramatically elevated IFPs arise in the first place. The prevailing hypotheses envision the intravascular and interstitial compartments to be in contiguity or communication, suggesting that changes in IFP chronicle and directly reflect intratumoral vascular pressures largely as a consequence of "leaky" or damaged vessels (Boucher and Jain, 1992; Netti et al., 1999). However, the essentially complete collapse of the microvasculature in invasive PDA implies that this relationship no longer holds and that forces other than intravascular pressure must be maintaining the dramatically elevated IFP. Indeed, we have observed a sustained elevation of tumor IFP even after the cessation of cardiac function (unpublished observations), underscoring the disconnect between intravascular pressure and IFP in this setting. Some models also postulate an elevated interstitial permeability in tumors (Jain, 1990), which appears not to be the case in PDA and, in any event, would favor not hinder delivery of (macro)molecules. Thus, despite an extensive history of studies in experimental systems and limited work in human cancers in situ (Boucher et al., 1991; Curti et al., 1993; Less et al., 1992), the magnitude of interstitial hypertension in solid tumors has clearly been underestimated, particularly with respect to PDA, and the mechanisms driving its genesis have remained elusive.

Plausible mechanisms to further elevate interstitial pressure include an ECM production sufficiently prolific to increase tumor density more rapidly than volume, and/or robust cell contractility that actively compacts the tumor (Reed et al., 1992). In this regard, the ability of a systemically delivered enzyme to dissipate the high IFPs in PDA not only holds great therapeutic promise but also provides insight into the underlying physicomechanical processes operant within this complex cancer environment (Figure 7). Intact HA functions as a hydrated gel generating an immobile fluid phase that secondarily also diminishes compressibility (tethered collagen fibers under tension provide the primary framework for rigid structure). We propose that PEGPH20 first liberates water bound to HA through cleavage of the extended polymer into substituent units. The release of trapped water

Table 1. Summary of Metastatic Disease Burden in *KPC* Mice

Treatment	Mice with Metastatic Disease (%)	No. of Macroscopic Metastases/ Mouse (mean ± SEM)	No. of Metastases/ Mouse (mean ± SEM)	Mice with Liver Metastases (%)	Mice with Lung Metastases (%)	Mice with Diaphragm Metastases (%)	Mice with Lymph Node Involvement (%)	Mice with Malignant Ascites (%)
Gem+Placebo	93	1.7 ± 0.35	2.4 ± 0.35	73	40	40	73	47
Gem+PEGPH20	43	0.86 ± 0.4	1.1 ± 0.4	43	21	21	36	21

rapidly decreases IFP to a range of 20–30 mm Hg, enabling collapsed arterioles and capillaries to open. Without additional treatment, HA is replenished, in part by α-SMA(+) myofibroblasts, and intratumoral physical dynamics are restored. Together with a concomitant cytotoxic agent, however, the resultant death of activated PSC leads to the additional loss of collagen I content through decreased synthesis, while also unraveling its architecture, which itself has been implicated in promoting carcinoma invasion and metastasis (Provenzano et al., 2006; Wang et al., 2002), impeding drug delivery (Eikenes et al., 2004; Netti et al., 2000; Ramanujan et al., 2002), and conferring gemcitabine resistance (Dangi-Garimella et al., 2011). Thus, enzymatic degradation of HA removes the central barrier, allowing drugs to breach the previously impenetrable sanctuary of PDA. A subsequent feed-forward mechanism results in depletion of stromal fibroblasts and carcinoma cells, dissolution of the collagen network, and irrevocable remodeling of the tumor microenvironment. Uniform objective responses ensue, at least until cells can evolve secondary mechanisms of resistance. This gap in time represents an unprecedented opportunity for therapeutic advantage. The persistence of patent vessels enables switching sequentially from one chemotherapeutic regimen to another in hopes of prolonging this window of vulnerability. In this context, revisiting the extensive list of previously presumed "ineffective" agents against PDA (Nieto et al., 2008) represents an obvious starting point, even as additional targets within the tumor stroma are identified and explored (Izeradjene and Hingorani, 2007).

In the context of our current findings, two very recent reports of combination regimens to treat advanced PDA are particularly notable for their shared pharmacokinetic features and their improved success over the current standard. One regimen combined gemcitabine with nab-paclitaxel, an albumin-coated formulation of taxol with an extended half-life of >10 hr in the circulation (Von Hoff et al., 2011). A second regimen, FOLFIRINOX, added bolus dosing of two conventional cytotoxic agents onto a base of prolonged (46 hr) continuous infusion of fluorouracil with each treatment cycle (Conroy et al., 2011). In each case, the sustained exposure to cytotoxic therapy may have helped surmount the relative barriers to perfusion imposed by the ECM of PDA.

Finally, the prospect that augmenting blood flow to a lethal carcinoma may increase its ability to seed metastatic deposits gives pause; however, the dramatically decreased metastatic tumor burden in animals treated with combination therapy is reassuring and no doubt contributes to the observed benefit in overall survival. Indeed, that Gemcitabine+PEGPH20 improves survival in animals with advanced and metastatic disease underscores its potential utility for the majority of patients who present with PDA. These findings also reflect the similar physicochemical principles operant in metastases as in the primary tumor; in fact, our molecular characterization of the ECM suggests that the metastatic microenvironment is further enriched in GAGs (including HA) relative to collagen as compared with primary tumors. Understanding the precise mechanism of achieving a decreased metastatic tumor burden has important implications for specific clinical uses of PEGPH20. The decreased metastatic burden may have been achieved by regression of established metastases (which we have observed) and/or decreased seeding of metastases either by killing primary tumor cells or altering their ability to spread. HA has been directly implicated in increasing the metastatic potential of cancer cells (Zhang et al., 1995). However, HA depletion may also inhibit the ability of already seeded cells to establish clinically relevant metastases. In other words, HA may represent a necessary component of the microenvironmental niche in order for a circulating tumor cell or nest of cells to blossom fully into a life-limiting lesion. Thus, there may be additional potential uses for and benefits from a stromal targeting therapy including, for example, as part of an adjuvant regimen. Given that more than two thirds of patients with resected PDA eventually succumb to metastatic disease (Hidalgo, 2010), incorporating an enzymatic agent that degrades HA in the adjuvant setting may extend survival by preventing, or at least delaying, the establishment of a critical metastatic disease burden.

EXPERIMENTAL PROCEDURES

Mouse Strains

All animal studies were approved by the Institutional Animal Care and Use Committee of the Fred Hutchinson Cancer Research Center. *Kras*$^{LSL\text{-}G12D/+}$; *Trp53*$^{LSL\text{-}R172H/+}$;*Cre* (*KPC*) mice have been previously described in detail (Hingorani et al., 2005). *KPC* mice conditionally express endogenous physiologic levels of activated *Kras* and point mutant *Trp53* targeted to progenitor cells of the developing pancreas. The animals spontaneously develop the full spectrum of precursor ductal lesions (pancreatic intraepithelial neoplasias, PanINs) which progress to invasive and metastatic PDA, faithfully mimicking the clinical syndrome, histopathology, and molecular progression of the human disease from inception to invasion and metastasis. A subset of experiments were also performed on *Kras*$^{LSL\text{-}G12D/+}$;*Cre* (*KC*) mice, which similarly develop invasive and metastatic disease along the PanIN-to-PDA progression scheme, albeit with a slower time course than *KPC* mice (Hingorani et al., 2003). *ROSA26*$^{LSL\text{-}EGFP}$ mice (obtained from Jackson Laboratory) contain enhanced green fluorescent protein (EGFP) cDNA sequence flanked by *LoxP* sites knocked-in to the *ROSA26* locus.

Measuring Interstitial Fluid Pressure

Interstitial fluid pressure (IFP) measurements were performed using a Millar Mikro-Tip pressure catheter transducer (SPR-1000, 0.33 mm diameter) with a dynamic pressure range from −50 to 300 mm Hg, possessing a shielded side-mounted sensor. The catheter was connected to PCU-2000 Pressure

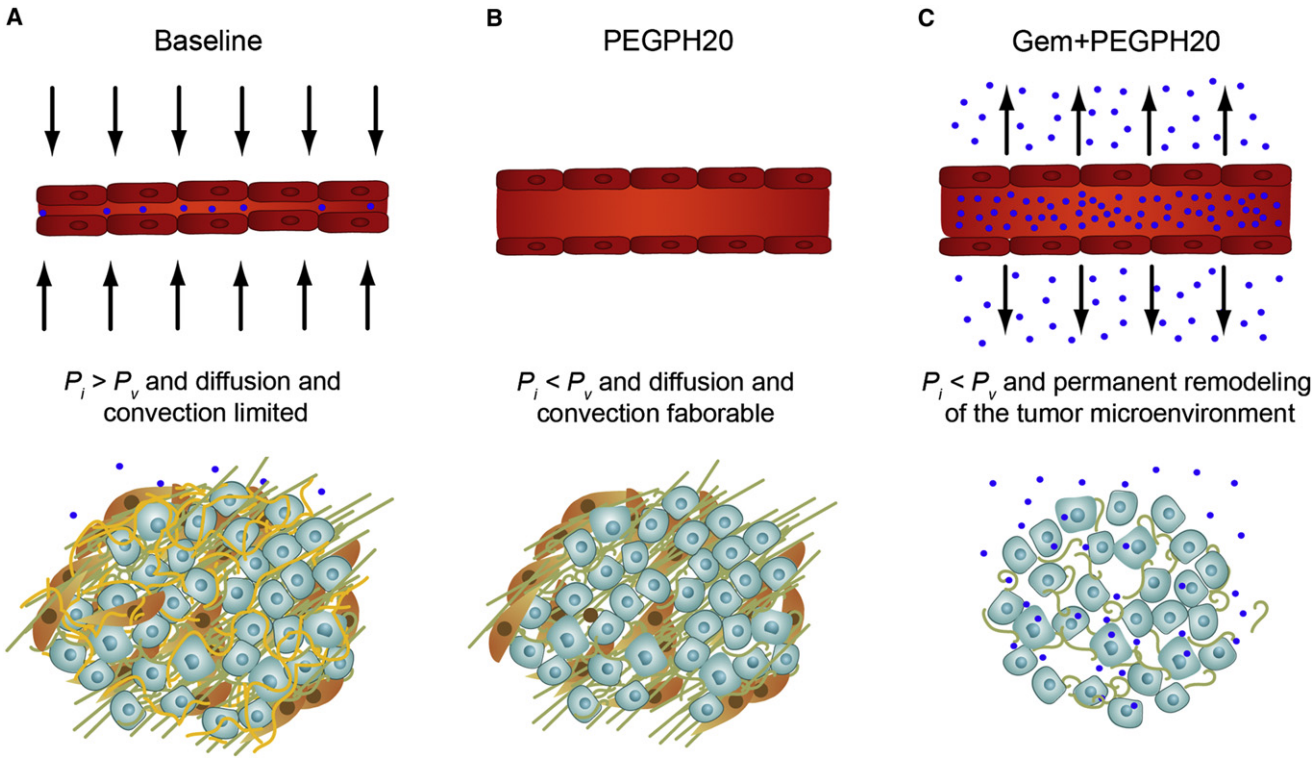

Figure 7. Altering Physicomechanics and Remodeling the Stroma in PDA to Therapeutic Advantage

(A) Intratumoral mechanics in PDA impede diffusion and convection of small molecules.

(B) Enzymatic degradation of stromal HA decreases IFP and relieves physical constraints on small molecule perfusion, which can reconstitute in the absence of additional therapy.

(C) Combined enzymatic and cytotoxic therapy permanently remodels the tumor microenvironment to favor the delivery and distribution of small molecules.

Blue spheres represent chemotherapy molecules, vessels are shown in red, carcinoma cells in light blue, activated PSC in brown, collagen in green, and HA in yellow. P_i, interstitial fluid pressure; P_v, intravascular fluid pressure. See text for details.

Control Unit and an ADInstruments PowerLab data acquisition system (Millar Instruments, Inc.) (Ozerdem and Hargens, 2005; Thompson et al., 2010). Data were recorded and analyzed using LabChart software (Millar Instruments, Inc.). The system was calibrated to 0, 25, and 100 mm Hg prior to each measurement following the manufacturer's recommendations; calibration was reconfirmed after each study. To place the microtip pressure catheter, a 25-gauge needle (~2× the diameter of the probe) was first introduced into the tissue or tumor of interest, and the probe was inserted into the space after needle withdrawal.

Assessment of Vascular Function and Molecular Diffusion

To assess vascular function, 425 μl of biotin-conjugated *Lycopersicon esculentum* lectin (B1175-1mg, Vector Laboratories) was mixed with 75 μl of Streptavidin-AlexaFluor-488 (S32354, Molecular Probes) for whole-tissue MPLSM imaging or with Streptavidin-AlexaFluor-647 (S21375) for analyses of tissue sections following coadministration of doxorubicin (Sigma). Mice were anesthetized by inhalation of isofluorane gas. Five minutes prior to euthanasia, 100 μl of the conjugated lectin was administered into the left ventricle. For coadministration experiments, 20 mg/kg doxorubicin solution was injected immediately after fluorescently conjugated lectin. While under terminal anesthesia, mice were perfused with 4% paraformaldehyde. For histologic analyses, harvested tissues were additionally fixed overnight in 4% paraformaldehyde.

Treatment Schedule and Survival Study

Enrollment of *KPC* mice was based on primary tumor burden and informed by age. Specifically, animals 12–14 weeks old and with a palpable pancreas mass were enrolled. Ultrasound imaging was performed in the initial 11 mice enrolled to confirm the physical examination findings of estimated tumor burden. *KPC* mice were genotyped and then randomized by one investigator (A.E.C.) to receive Gemcitabine+Placebo or Gemcitabine+PEGPH20, which were administered by another investigator (P.P.P.). Objective response was assessed by high-resolution ultrasound performed by a third investigator (C.C.) who was blinded to the treatments administered. The treatment schedule was modeled on the standard clinical management of patients with pancreas cancer (Figure 3A). Gemcitabine was administered intravenously (i.v.) once weekly at 50 mg/kg in a three weeks on/one week off schedule; PEGPH20 (or vehicle) was administered i.v. 24 hr prior to gemcitabine.

Statistical Analyses

Data were tested to determine whether they met the assumption of normality using the Kolmogorov-Smirnov test. Normally distributed two-group data were analyzed using a t test. Multigroup data were analyzed using ANOVA followed with the Newman-Kuels multiple comparison post test. In the instance that two-group data did not conform to normality, the nonparametric Mann-Whitney sum rank test was performed. Kaplan-Meier survival data were analyzed using a log rank test. Metastatic disease burden was analyzed using Fisher's exact test.

SUPPLEMENTAL INFORMATION

Supplemental Information includes six figures, one table, and Supplemental Experimental Procedures and can be found with this article online at doi:10.1016/j.ccr.2012.01.007.

ACKNOWLEDGMENTS

We thank Randi Simmons, Markus Carlson, and Simon Bennett for assistance with animal husbandry and care; Julie Randolph-Habecker and members of FHCRC Experimental Histopathology for assistance with histology and immunohistochemistry; and members of the Hingorani and Olson laboratories for helpful discussions. We thank Shelley Thorsen for expert assistance with figure and manuscript preparation, John Potter for helpful discussions and comments on the manuscript, and Gregory Frost and Michael Shepard for providing PEGPH20 and for helpful discussions. TMA sections were kindly provided by Galen Hostetter and Clifford Whatcott. D.D.V.H. has a consulting agreement with Halozyme Therapeutics. This work was supported by the National Cancer Institute (grants CA161112 and CA114028 to S.R.H., CA152249 to P.P.P. and S.R.H., and CA109552 to D.D.V.H.), the Giles W. and Elise G. Mead Foundation (support to S.R.H.), donated funds from David Jones and Maryanne Tagney-Jones (support to S.R.H.), donated funds from Safeway (support to S.R.H.), and a Jaconette L. Tietze Young Scientist Award (to P.P.P.).

Received: September 30, 2011
Revised: November 26, 2011
Accepted: January 11, 2012
Published: March 19, 2012

REFERENCES

Allison, D.C., Piantadosi, S., Hruban, R.H., Dooley, W.C., Fishman, E.K., Yeo, C.J., Lillemoe, K.D., Pitt, H.A., Lin, P., and Cameron, J.L. (1998). DNA content and other factors associated with ten-year survival after resection of pancreatic carcinoma. J. Surg. Oncol. *67*, 151–159.

Balazs, E.A., and Denlinger, J.L. (1989). Clinical uses of hyaluronan. Ciba Found. Symp. *143*, 265–275, discussion 275–280, 281–265.

Bissell, M.J., and Radisky, D. (2001). Putting tumours in context. Nat. Rev. Cancer *1*, 46–54.

Boucher, Y., and Jain, R.K. (1992). Microvascular pressure is the principal driving force for interstitial hypertension in solid tumors: implications for vascular collapse. Cancer Res. *52*, 5110–5114.

Boucher, Y., Kirkwood, J.M., Opacic, D., Desantis, M., and Jain, R.K. (1991). Interstitial hypertension in superficial metastatic melanomas in humans. Cancer Res. *51*, 6691–6694.

Bouzin, C., and Feron, O. (2007). Targeting tumor stroma and exploiting mature tumor vasculature to improve anti-cancer drug delivery. Drug Resist. Updat. *10*, 109–120.

Brekken, C., Hjelstuen, M.H., Bruland, O.S., and de Lange Davies, C. (2000). Hyaluronidase-induced periodic modulation of the interstitial fluid pressure increases selective antibody uptake in human osteosarcoma xenografts. Anticancer Res. *20* (5B), 3513–3519.

Burris, H.A., 3rd, Moore, M.J., Andersen, J., Green, M.R., Rothenberg, M.L., Modiano, M.R., Cripps, M.C., Portenoy, R.K., Storniolo, A.M., Tarassoff, P., et al. (1997). Improvements in survival and clinical benefit with gemcitabine as first-line therapy for patients with advanced pancreas cancer: a randomized trial. J. Clin. Oncol. *15*, 2403–2413.

Casper, E.S., Green, M.R., Kelsen, D.P., Heelan, R.T., Brown, T.D., Flombaum, C.D., Trochanowski, B., and Tarassoff, P.G. (1994). Phase II trial of gemcitabine (2,2′-difluorodeoxycytidine) in patients with adenocarcinoma of the pancreas. Invest. New Drugs *12*, 29–34.

Conroy, T., Desseigne, F., Ychou, M., Bouché, O., Guimbaud, R., Bécouarn, Y., Adenis, A., Raoul, J.L., Gourgou-Bourgade, S., de la Fouchardière, C., et al; Groupe Tumeurs Digestives of Unicancer; PRODIGE Intergroup. (2011). FOLFIRINOX versus gemcitabine for metastatic pancreatic cancer. N. Engl. J. Med. *364*, 1817–1825.

Curti, B.D., Urba, W.J., Alvord, W.G., Janik, J.E., Smith, J.W., 2nd, Madara, K., and Longo, D.L. (1993). Interstitial pressure of subcutaneous nodules in melanoma and lymphoma patients: changes during treatment. Cancer Res. *53* (10, Suppl), 2204–2207.

Dangi-Garimella, S., Krantz, S.B., Barron, M.R., Shields, M.A., Heiferman, M.J., Grippo, P.J., Bentrem, D.J., and Munshi, H.G. (2011). Three-dimensional collagen I promotes gemcitabine resistance in pancreatic cancer through MT1-MMP-mediated expression of HMGA2. Cancer Res. *71*, 1019–1028.

Eikenes, L., Bruland, O.S., Brekken, C., and Davies, Cde.L. (2004). Collagenase increases the transcapillary pressure gradient and improves the uptake and distribution of monoclonal antibodies in human osteosarcoma xenografts. Cancer Res. *64*, 4768–4773.

Eikenes, L., Tari, M., Tufto, I., Bruland, O.S., and de Lange Davies, C. (2005). Hyaluronidase induces a transcapillary pressure gradient and improves the distribution and uptake of liposomal doxorubicin (Caelyx) in human osteosarcoma xenografts. Br. J. Cancer *93*, 81–88.

Farnell, M.B., Pearson, R.K., Sarr, M.G., DiMagno, E.P., Burgart, L.J., Dahl, T.R., Foster, N., and Sargent, D.J.; Pancreas Cancer Working Group. (2005). A prospective randomized trial comparing standard pancreatoduodenectomy with pancreatoduodenectomy with extended lymphadenectomy in resectable pancreatic head adenocarcinoma. Surgery *138*, 618–628, discussion 628–630.

Heldin, C.H., Rubin, K., Pietras, K., and Ostman, A. (2004). High interstitial fluid pressure: an obstacle in cancer therapy. Nat. Rev. Cancer *4*, 806–813.

Hertel, L.W., Boder, G.B., Kroin, J.S., Rinzel, S.M., Poore, G.A., Todd, G.C., and Grindey, G.B. (1990). Evaluation of the antitumor activity of gemcitabine (2′,2′-difluoro-2′-deoxycytidine). Cancer Res. *50*, 4417–4422.

Hidalgo, M. (2010). Pancreatic cancer. N. Engl. J. Med. *362*, 1605–1617.

Hingorani, S.R., Petricoin, E.F., Maitra, A., Rajapakse, V., King, C., Jacobetz, M.A., Ross, S., Conrads, T.P., Veenstra, T.D., Hitt, B.A., et al. (2003). Preinvasive and invasive ductal pancreatic cancer and its early detection in the mouse. Cancer Cell *4*, 437–450.

Hingorani, S.R., Wang, L., Multani, A.S., Combs, C., Deramaudt, T.B., Hruban, R.H., Rustgi, A.K., Chang, S., and Tuveson, D.A. (2005). Trp53R172H and KrasG12D cooperate to promote chromosomal instability and widely metastatic pancreatic ductal adenocarcinoma in mice. Cancer Cell *7*, 469–483.

Izeradjene, K., and Hingorani, S.R. (2007). Targets, trials, and travails in pancreas cancer. J. Natl. Compr. Canc. Netw. *5*, 1042–1053.

Jacobson, A., Salnikov, A., Lammerts, E., Roswall, P., Sundberg, C., Heldin, P., Rubin, K., and Heldin, N.E. (2003). Hyaluronan content in experimental carcinoma is not correlated to interstitial fluid pressure. Biochem. Biophys. Res. Commun. *305*, 1017–1023.

Jain, R.K. (1987). Transport of molecules across tumor vasculature. Cancer Metastasis Rev. *6*, 559–593.

Jain, R.K. (1990). Vascular and interstitial barriers to delivery of therapeutic agents in tumors. Cancer Metastasis Rev. *9*, 253–266.

Janssen, B.J., Leenders, P.J., and Smits, J.F. (2000). Short-term and long-term blood pressure and heart rate variability in the mouse. Am. J. Physiol. Regul. Integr. Comp. Physiol. *278*, R215–R225.

Jemal, A., Siegel, R., Xu, J., and Ward, E. (2010). Cancer statistics, 2010. CA Cancer J. Clin. *60*, 277–300.

Kedem, O., and Katchalsky, A. (1958). Thermodynamic analysis of the permeability of biological membranes to non-electrolytes. Biochim. Biophys. Acta *27*, 229–246.

Kedem, O., and Katchalsky, A. (1961). A physical interpretation of the phenomenological coefficients of membrane permeability. J. Gen. Physiol. *45*, 143–179.

Less, J.R., Posner, M.C., Boucher, Y., Borochovitz, D., Wolmark, N., and Jain, R.K. (1992). Interstitial hypertension in human breast and colorectal tumors. Cancer Res. *52*, 6371–6374.

Mattson, D.L. (1998). Long-term measurement of arterial blood pressure in conscious mice. Am. J. Physiol. *274*, R564–R570.

Michel, C.C. (1984). Fluid movements through capillary walls. In Handbook of Physiology, Section 2, Vol. IV, Microcirculation, E.M. Renkin and C.C. Michel, eds. (Washington, D.C: American Physiological Society), pp. 375–409.

Moore, M.J., Goldstein, D., Hamm, J., Figer, A., Hecht, J.R., Gallinger, S., Au, H.J., Murawa, P., Walde, D., Wolff, R.A., et al; National Cancer Institute of Canada Clinical Trials Group. (2007). Erlotinib plus gemcitabine compared with gemcitabine alone in patients with advanced pancreatic cancer: a phase

III trial of the National Cancer Institute of Canada Clinical Trials Group. J. Clin. Oncol. *25*, 1960–1966.

Netti, P.A., Hamberg, L.M., Babich, J.W., Kierstead, D., Graham, W., Hunter, G.J., Wolf, G.L., Fischman, A., Boucher, Y., and Jain, R.K. (1999). Enhancement of fluid filtration across tumor vessels: implication for delivery of macromolecules. Proc. Natl. Acad. Sci. USA *96*, 3137–3142.

Netti, P.A., Berk, D.A., Swartz, M.A., Grodzinsky, A.J., and Jain, R.K. (2000). Role of extracellular matrix assembly in interstitial transport in solid tumors. Cancer Res. *60*, 2497–2503.

Nieto, J., Grossbard, M.L., and Kozuch, P. (2008). Metastatic pancreatic cancer 2008: is the glass less empty? Oncologist *13*, 562–576.

Oettle, H., Post, S., Neuhaus, P., Gellert, K., Langrehr, J., Ridwelski, K., Schramm, H., Fahlke, J., Zuelke, C., Burkart, C., et al. (2007). Adjuvant chemotherapy with gemcitabine vs observation in patients undergoing curative-intent resection of pancreatic cancer: a randomized controlled trial. JAMA *297*, 267–277.

Ogston, A.G., and Michel, C.C. (1978). General descriptions of passive transport of neutral solute and solvent through membranes. Prog. Biophys. Mol. Biol. *34*, 197–217.

Olive, K.P., Jacobetz, M.A., Davidson, C.J., Gopinathan, A., McIntyre, D., Honess, D., Madhu, B., Goldgraben, M.A., Caldwell, M.E., Allard, D., et al. (2009). Inhibition of Hedgehog signaling enhances delivery of chemotherapy in a mouse model of pancreatic cancer. Science *324*, 1457–1461.

Ozerdem, U., and Hargens, A.R. (2005). A simple method for measuring interstitial fluid pressure in cancer tissues. Microvasc. Res. *70*, 116–120.

Provenzano, P.P., Eliceiri, K.W., Campbell, J.M., Inman, D.R., White, J.G., and Keely, P.J. (2006). Collagen reorganization at the tumor-stromal interface facilitates local invasion. BMC Med. *4*, 38.

Ramanujan, S., Pluen, A., McKee, T.D., Brown, E.B., Boucher, Y., and Jain, R.K. (2002). Diffusion and convection in collagen gels: implications for transport in the tumor interstitium. Biophys. J. *83*, 1650–1660.

Reed, R.K., Rubin, K., Wiig, H., and Rodt, S.A. (1992). Blockade of beta 1-integrins in skin causes edema through lowering of interstitial fluid pressure. Circ. Res. *71*, 978–983.

Schultz, R.M., Merriman, R.L., Toth, J.E., Zimmermann, J.E., Hertel, L.W., Andis, S.L., Dudley, D.E., Rutherford, P.G., Tanzer, L.R., and Grindey, G.B. (1993). Evaluation of new anticancer agents against the MIA PaCa-2 and PANC-1 human pancreatic carcinoma xenografts. Oncol. Res. *5*, 223–228.

Sherwood, L. (1997). Human Physiology from Cells to Systems, Third Edition (Florence, KY: Wadsworth Publishing Company).

Starling, E.H. (1896). On the absorption of fluids from the connective tissue spaces. J. Physiol. *19*, 312–326.

Staverman, A.J. (1952). Non-equilibrium thermodynamics of membrane processes. Trans. Faraday Soc. *48*, 176–185. 10.1039/TF9524800176.

Tempero, M., Plunkett, W., Ruiz Van Haperen, V., Hainsworth, J., Hochster, H., Lenzi, R., and Abbruzzese, J. (2003). Randomized phase II comparison of dose-intense gemcitabine: thirty-minute infusion and fixed dose rate infusion in patients with pancreatic adenocarcinoma. J. Clin. Oncol. *21*, 3402–3408.

Thompson, C.B., Shepard, H.M., O'Connor, P.M., Kadhim, S., Jiang, P., Osgood, R.J., Bookbinder, L.H., Li, X., Sugarman, B.J., Connor, R.J., et al. (2010). Enzymatic depletion of tumor hyaluronan induces antitumor responses in preclinical animal models. Mol. Cancer Ther. *9*, 3052–3064.

Toole, B.P. (2004). Hyaluronan: from extracellular glue to pericellular cue. Nat. Rev. Cancer *4*, 528–539.

Toole, B.P., and Slomiany, M.G. (2008). Hyaluronan: a constitutive regulator of chemoresistance and malignancy in cancer cells. Semin. Cancer Biol. *18*, 244–250.

Trédan, O., Galmarini, C.M., Patel, K., and Tannock, I.F. (2007). Drug resistance and the solid tumor microenvironment. J. Natl. Cancer Inst. *99*, 1441–1454.

Ueno, H., Kiyosawa, K., and Kaniwa, N. (2007). Pharmacogenomics of gemcitabine: can genetic studies lead to tailor-made therapy? Br. J. Cancer *97*, 145–151.

Von Hoff, D.D., Ramanathan, R.K., Borad, M.J., Laheru, D.A., Smith, L.S., Wood, T.E., Korn, R.L., Desai, N., Trieu, V., Iglesias, J.L., et al. (2011). Gemcitabine plus nab-paclitaxel is an active regimen in patients with advanced pancreatic cancer: a phase I/II trial. J. Clin. Oncol. *29*, 4548–4554.

Wang, W., Wyckoff, J.B., Frohlich, V.C., Oleynikov, Y., Hüttelmaier, S., Zavadil, J., Cermak, L., Bottinger, E.P., Singer, R.H., White, J.G., et al. (2002). Single cell behavior in metastatic primary mammary tumors correlated with gene expression patterns revealed by molecular profiling. Cancer Res. *62*, 6278–6288.

Zhang, L., Underhill, C.B., and Chen, L. (1995). Hyaluronan on the surface of tumor cells is correlated with metastatic behavior. Cancer Res. *55*, 428–433.

Cancer Cell
Article

Transient Low Doses of DNA-Demethylating Agents Exert Durable Antitumor Effects on Hematological and Epithelial Tumor Cells

Hsing-Chen Tsai,[1,2,10] Huili Li,[2,10] Leander Van Neste,[3,10] Yi Cai,[2] Carine Robert,[4] Feyruz V. Rassool,[4] James J. Shin,[2,5] Kirsten M. Harbom,[2] Robert Beaty,[2] Emmanouil Pappou,[2,5] James Harris,[2,5] Ray-Whay Chiu Yen,[2] Nita Ahuja,[2,5] Malcolm V. Brock,[2,5] Vered Stearns,[2,6] David Feller-Kopman,[7] Lonny B. Yarmus,[7] Yi-Chun Lin,[8] Alana L. Welm,[8] Jean-Pierre Issa,[9] Il Minn,[2] William Matsui,[1,2] Yoon-Young Jang,[2] Saul J. Sharkis,[1,2] Stephen B. Baylin,[1,2,*] and Cynthia A. Zahnow[2,6,*]

[1]The Graduate Program in Cellular and Molecular Medicine, Johns Hopkins University School of Medicine, Baltimore, MD 21231, USA
[2]The Sidney Kimmel Comprehensive Cancer Center at Johns Hopkins, Baltimore, MD 21231, USA
[3]MDxHealth PharmacoDx BVBA, Technologiepark 4, 9052 Ghent, Belgium
[4]Department of Radiation Oncology, Greenebaum Cancer Center, University of Maryland School of Medicine, Baltimore, MD 21201, USA
[5]Department of Surgery, School of Medicine, Johns Hopkins University, Baltimore, MD 21231, USA
[6]Breast Cancer Program, The Sidney Kimmel Comprehensive Cancer Center at Johns Hopkins, Baltimore, MD 21231, USA
[7]Bronchoscopy and Interventional Pulmonology, Johns Hopkins Hospital, Baltimore, MD 21205, USA
[8]Department of Oncological Sciences, Huntsman Cancer Institute, University of Utah, Salt Lake City, UT 84112, USA
[9]Department of Leukemia, The University of Texas M.D. Anderson Cancer Center, Houston, TX, 77030 USA
[10]These authors contributed equally to this work
*Correspondence: sbaylin@jhmi.edu (S.B.B.), zahnoci@jhmi.edu (C.A.Z.)
DOI 10.1016/j.ccr.2011.12.029

SUMMARY

Reversal of promoter DNA hypermethylation and associated gene silencing is an attractive cancer therapy approach. The DNA methylation inhibitors decitabine and azacitidine are efficacious for hematological neoplasms at lower, less toxic, doses. Experimentally, high doses induce rapid DNA damage and cytotoxicity, which do not explain the prolonged time to response observed in patients. We show that transient exposure of cultured and primary leukemic and epithelial tumor cells to clinically relevant nanomolar doses, without causing immediate cytotoxicity, produce an antitumor "memory" response, including inhibition of subpopulations of cancer stem-like cells. These effects are accompanied by sustained decreases in genomewide promoter DNA methylation, gene reexpression, and antitumor changes in key cellular regulatory pathways. Low-dose decitabine and azacitidine may have broad applicability for cancer management.

INTRODUCTION

Decitabine (DAC) and its analog azacitidine (AZA), two major DNA demethylating agents (Jones and Taylor, 1980), have recently emerged as potent therapies for the preleukemic hematological disease myelodysplastic syndrome (MDS), and for established leukemias (Blum et al., 2007; Cashen et al., 2010; Issa et al., 2004), leading to approval from the Food and Drug Administration for patients with MDS (Kantarjian et al., 2006; Silverman et al., 2002). Remarkably, the improved clinical efficacy and safety profile have emerged only as doses of the drugs, given either alone (Issa et al., 2004; Kantarjian et al., 2006, 2007) or in combination with histone deacetylase (HDAC) inhibitors (Gore et al., 2006), were significantly reduced. Despite the clinical efficacy observed in hematological neoplasms, these lower dosing regimens have not been thoroughly tested in

Significance

The mechanisms underlying clinical efficacies of the DNA methylation inhibitors decitabine and azacitidine are unclear. Understanding how these drugs work would be a pivotal step in furthering epigenetic therapy. Clinical clues suggest that these drugs work in myelodysplastic syndrome because low doses provide antitumor effects over time rather than acutely exerting cytotoxic effects. We show that nanomolar doses of both drugs have, without acute cytotoxic effects, antitumor effects on both cultured and primary human leukemic and epithelial tumor cells, including the most tumorigenic, self-renewing, and drug-resistant cell populations. These effects are accompanied by sustained, genomewide changes in promoter DNA methylation and gene expression which affect multiple key regulatory pathways that are high-priority targets for pharmacologic anticancer strategies.

patients with common solid tumors. Past trials with high doses have been plagued by extreme toxicities that have probably confounded the ability to document true clinical responses (Abele et al., 1987; Momparler et al., 1997). Even for the successes in hematologic neoplasms, it is still under debate whether epigenetic effects of the drugs account for all, or even some, of the therapeutic response (Issa and Kantarjian, 2009). In a recently completed clinical trial for advanced lung cancer using a low-dose regimen that has efficacy in MDS, we have seen some very durable, complete, partial, and stable responses in a subset of patients who have failed multiple previous chemotherapy regimens (Juergens et al., 2011). These results emphasize the importance of deciphering the mechanisms involved with therapeutic efficacy of DAC and AZA and understanding how low, nanomolar doses of DAC and AZA are effective at inducing sustained antitumor responses.

RESULTS

Transient, Low-Dose DAC Decreases Tumorigenicity of Cultured Leukemia Cells with Minimal Acute DNA Damage, Cell Cycle Alterations, or Apoptosis

DAC and AZA were originally designed as nucleoside analogs that, at high doses, clearly produce DNA damage and cytotoxicity (Karpf et al., 2001; Palii et al., 2008). However, these effects may not be the primary mechanisms responsible for the clinical efficacy in patients with MDS or leukemia. We, thus, first sought to separate low-dose, from high-dose effects of DAC on cultured leukemia cells. We used the very low doses, indicated by pharmacokinetic studies to be in the nanomolar range for DAC (20 to 300 nM) (Cashen et al., 2008; Schrump et al., 2006), to which tumor cells in responding patients with MDS/AML are most likely exposed in settings of clinical efficacy. Kasumi-1 cells, an acute myelogenous leukemia (AML) line with a stem-cell-like phenotype characterized by a high fraction of $CD34^+$ early progenitor cells (Asou et al., 1991) (Figure S1A available online), are known to be sensitive to cytotoxic effects of high-dose DAC (Berg et al., 2007). Indeed, daily doses of 500 nM DAC for 3 days produced 50% apoptosis, which reached over 90% by 4 days after drug withdrawal (Figure S1B), while 10 nM produces little or no cell death at 3 days in Kasumi-1, KG-1, and KG-1a AML cells and in histiocytic lymphoma U-937 cells (Figures 1A and S1C). It is important to note that this lack of early cytotoxicity at 10 nM is subsequently followed, after drug withdrawal, by sustained rates of apoptosis, leveling off at ~40% for Kasumi-1 and ~25% for KG-1 leukemia cells (Figure S1D). Consistent with these observations, the 3-day 10 nM DAC exposures produce little cell cycle changes between mock and treated Kasumi-1 cells at Day 3 (Figure 1B) and 4 and 11 days after drug withdrawal (Figure S1E) or significant increases in double-strand DNA breaks in $CD34^+$ and $CD34^-$ Kasumi-1 cells at Day 3 (Figure 1C). In contrast, 100 nM of cytarabine (Ara-C), a compound structurally similar to DAC and a standard cytotoxic chemotherapeutic agent used for AML therapy, causes distinct prolongation of S-phase (Figure 1B).

Despite the aforementioned lack of acute cytotoxic effects, the 3-day, 10 nM dose of DAC can fully (for Kasumi-1, KG-1, and KG-1a cells and partially for U-937 cells) inhibit subsequent colony formation in methylcellulose assays performed over 20 days in drugfree media (Figures 1A and S1C). Similarly, 100 nM DAC produces no initial apoptosis in chronic myelogenous leukemia, K-562 cells, but sharply reduces subsequent colony formation (Figure S1C). Acute promyelocytic leukemia NB4 cells are sensitive to both early apoptosis and diminishing of proliferation at 10 nM DAC (Figure S1C).

It is important to note that these anticloning effects for sensitive cells such as Kasumi-1 are sustained and wane only slowly after drug removal. First, the 10 nM dose of DAC blunts clonogenic potential of the cells in repeated methylcellulose colony-forming assays performed without subsequent drug exposure over 28 days (Figure S1F). Second, the transient 3-day exposure of 10 nM also inhibits, in serial methylcellulose replating assays, colony formation for Kasumi-1 (Figure 1D) and KG-1 (Figure S1G) cells and markedly decreases this ability for U-937 and K-562 cells (Figure S1G). In contrast, 10 or 100 nM doses of Ara-C produce much less inhibition of colony growth (Figure 1A). Finally, 10 nM DAC for 3 days also markedly blunts cloning of Kasumi-1 and KG-1 cells in a 5-week, drugfree, feeder layer assay that supports long-term culture-initiating cells (LTC-IC) (Figure 1E). Ara-C, again, fails to reduce LTC-IC (Figure 1E), which is consistent with the known poor capability of this drug to target such leukemic cell populations (Guzman et al., 2001).

The ultimate test of tumor initiation for leukemia and solid tumor cells (Lapidot et al., 1994; Al-Hajj et al., 2003; Li et al., 2007; O'Brien et al., 2007; Ricci-Vitiani et al., 2007; Schatton et al., 2008; Singh et al., 2004) is engraftment capability and tumor growth of the most tumorigenic or more "stem-like" cells in mice (Jordan et al., 2006). Kasumi-1 has a high percentage of stem-like $CD34^+$ cells. Only purified $CD34^+$, and not $CD34^-$, Kasumi cells are tumorigenic in mice (Figure 1F). Of note, our transient, low-dose treatment with DAC inhibits colony formation of both $CD34^+$ and $CD34^-$ Kasumi-1 cells (Figure 1G). Most strikingly, a 3-day treatment of Kasumi-1 cells to 10 nM DAC markedly delays, without any drug treatment of recipient animals, detectable engraftment of Kasumi-1 cells in the peripheral blood and the bone marrow of NOD/Shi-*scid*/IL-2Rγ^{null} mice (Figures 1H and 1I) and decreases the percentage of $CD34^+$ leukemic stem/progenitor cells that do appear in bone marrow (Figure 1J). Thus, a 10 nM transient DAC exposure markedly inhibits subsequent leukemia-initiating $CD34^+$ in vivo.

Low-Dose DAC, without Acute Cytoxicity, Blunts Clonogenicity of Primary Leukemia Cells but Not Primary Normal Bone Marrow Cells

Low-dose DAC can produce many of the same effects observed earlier on primary AML cells without the toxic effects on primary bone marrow cells. Thus, a 3-day transient 10 nM dose of DAC markedly blunts the ability of five of six primary samples from patients with newly diagnosed AML to subsequently clone in methylcellulose (Figure 2A) without causing early cell apoptosis or change in cell cycle (Figures 2B and 2C). This same 10 nM dose of DAC fails to blunt the ability of a normal bone marrow sample to generate progenitor colonies for multiple marrow lineages and did not cause significant apoptosis (Figures 2D and 2E). All of the aforementioned results are consistent with clinical results for MDS/AML, wherein delayed, robust antitumor responses can be produced while the normal bone marrow parameters are restored.

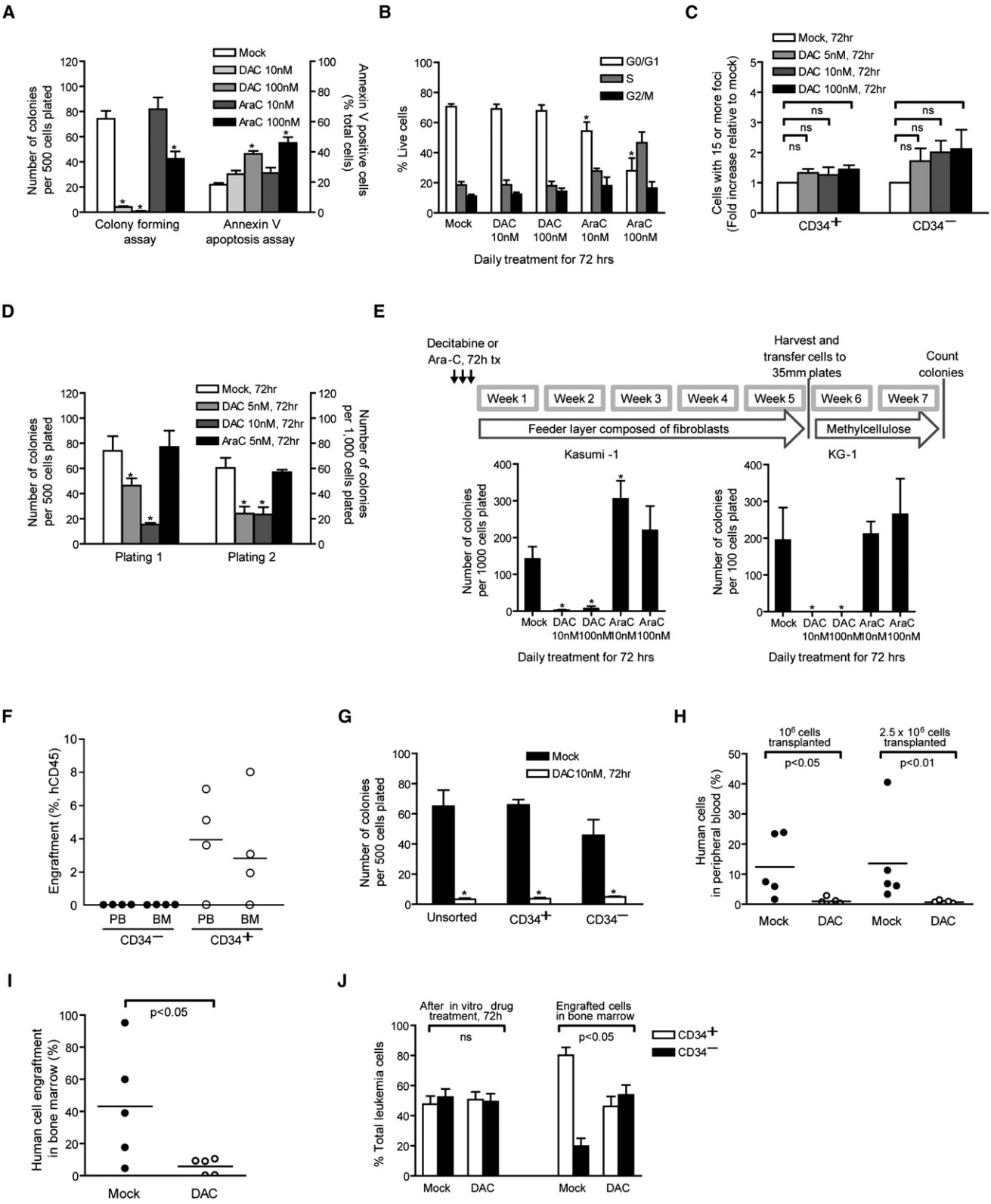

Figure 1. Low-Dose DAC Treatment Diminishes Self-Renewing and Leukemia-Initiating Capacities in Cultured Leukemia Cells

(A) Apoptosis and methylcellulose colony-forming assays of Kasumi-1 cells after 72 hr daily treatment with DAC or cytarabine (Ara-C). *p < 0.05 compared to mock by analysis of variance (ANOVA) and Dunnett's multiple comparison test.

(B) Cell cycle analysis of Kasumi-1 after DAC or Ara-C daily treatment for 72 hr. *p < 0.05 by ANOVA and Bonferroni posttests.

Transient Low Doses of DAC and AZA Inhibit Cultured Solid Tumor Stem-like Cells and Diminish Tumorigenicity

We next determined doses of DAC/AZA that were acutely nontoxic to cultured breast cancer cells but that might affect their tumorigenic properties. We found that transient 3-day exposure of MCF7 cells to 100 nM DAC at Day 3 of drug treatment or 4 days after drug withdrawal (day 7), or an equivalent dose of 500 nM AZA at 7 days after drug withdrawal (day 10), produced little apoptosis (Figure S2A). Similarly, 3 days of exposure to 100 nM DAC or 500 nM AZA led to minimal cell cycle changes over time (Figure S2B). Significant decreases were observed for MCF7 cells in anchorage-independent growth in soft agar, a classic in vitro transformation assay, for both 100 nM DAC and 500 nM AZA (Figure S2C). Similarly, 3-day treatments with 10 nM DAC (Figure S2D), 100 nM DAC (Figure 3B), and 500 nM AZA (Figure 3C), followed by subcutaneous injection into untreated nonobese diabetic (NOD)/SCID mice (Figure 3A), significantly reduced the size of MCF7 xenografts. This diminished tumorigenicity persisted in serially transplanted secondary xenografts (Figures 3A and 3B). An even stronger decrease was produced in tumor growth for T-47D breast cancer cells. Growth was also suppressed for HCT116 colon and H2170 lung cancer lines (Figure 3C). Moreover, for clinical relevance, we tested several short cycles and therapeutic doses of AZA in mice bearing established xenografts of MDA-MB-231, MCF7, and T-47D breast cancer cells. In MDA-MB-231 and T-47D xenografts, the lowest dose of drug led to the largest reduction in tumor size, whereas in MCF7 xenografts, all doses were comparable (Figure 3D). There were, again, no changes in proliferative capacity of cells in the treated MCF7 tumors (Figure S2E).

Transient Low Doses of AZA Inhibit Primary Breast Cancer Stem-like and Self-Renewing Cells

We further investigated the effects of transient, low-dose AZA treatment on the self-renewal potential of primary cancer cells isolated from the pleural effusions of four patients with metastatic breast cancer of the luminal type. These cells were treated for 3 days with 500 nM AZA, followed by drug withdrawal and culture in suspension as tumor spheres and serial passaged to test for self-renewal capacity and stem-like cell activity (Figure 4A) (McDermott and Wicha, 2010; Korkaya et al., 2009; Charafe-Jauffret et al., 2009; Dontu et al., 2003; Ginestier et al., 2007; Liu et al., 2006). There was dramatic inhibition of primary sphere formation and an inhibitory effect that persisted through two subsequent serial passages (Figure 4B), while spheres from mock-treated cells showed a trend toward enrichment from passage two to passage three (see patients #103, #PE1, and #105; Figure 4B). Thus, 3 days of exposure to low-dose AZA reduces the self-renewal capacity of primary breast cancer cells consistent with our observation that AZA treatment decreases a self-renewing population in breast cancer cell lines. Aldehyde dehydrogenase (ALDH1) and $CD44^+/CD24^{lo}$ have emerged as markers for cancer stem-like cells in breast and are predictive for metastasis and poor prognosis (Al-Hajj et al., 2003; Ginestier et al., 2007). We find, in agreement with others, that the MCF7 breast cancer line has ~0.5% $ALDH1^+$ cells (Charafe-Jauffret et al., 2009) and T47Ds contain ~5% $CD44^+/CD24^{lo}$ (data not shown). A 3-day treatment with 500 nM AZA and 10 nM DAC significantly reduced $CD44^+/ALDH1^+$ cells for up to 17 days after drug withdrawal (Figure 4C), with no changes observed in the larger $CD44^+/ALDH1^-$ cell population (data not shown). Similar results were observed for 100 nM DAC (data not shown). For T-47D cells, a similar 3-day treatment with 500 nM AZA reduced the $CD44^+/CD24^{lo}$ population for up to 11 days after drug withdrawal (Figure 4C). Likewise, 3 days of 500 nM AZA decreased the $CD44^+/CD24^{lo}$ population in mammospheres from patient #105 (Figure 4C).

Last, we tested the effects of low-dose AZA on primary tumor tissue from breast cancer patients. Therapeutic administration of AZA (0.5 mg/kg) significantly inhibited the growth of three preestablished, patient-derived tumors, engrafted orthotopically into immunodeficient mice (Figure 4D) (DeRose et al., 2011)

Low-Dose DAC Inhibits Gene Promoter DNA Methylation and Causes Re-Expression of Hypermethylated Genes

The ability of transient low doses of DAC to sustain long-term antitumor effects is associated, at least temporally, with the retained ability of this drug to target DNA methylation processes and alter gene expression, in each of the cell types under study. DAC and AZA, after their incorporation into DNA, are known to bind to and block the catalytic site of DNA methyltransferases (DNMTs). This covalent binding effectively traps DNMTs as adducts to DNA (Ferguson et al., 1997; Gabbara and Bhagwat, 1995; Santi et al., 1984). Additionally, DAC and AZA can trigger proteosomal degradation of the maintenance DNMT, DNMT1

(C) γH2AX foci formation in $CD34^+$ and $CD34^-$ Kasumi-1 cells after 72 hr DAC treatment. For each treatment, cells containing more than 15 foci are counted and calculated as fold change relative to that of mock treatment. ns, not statistically significant by ANOVA and Bonferroni posttests.
(D) Serial methylcellulose replating assays of Kasumi-1 after 72 hr daily treatment of DAC or Ara-C. Equal numbers of viable cells were plated for each plating. *$p < 0.01$ compared to mock by ANOVA and Bonferroni posttests.
(E) Long-term culture-initiating cell assay of Kasumi-1 and KG-1 AML cells after 72 hr daily treatment of DAC or Ara-C. *$p < 0.05$ compared to mock by Mann-Whitney test.
(F) Engraftment assay in NOD/Shi-scid/IL-2Rγ^{null} mice of $CD34^+$ versus $CD34^-$ Kasumi-1 cells. Human $CD45^+$ cells were analyzed in the peripheral blood (PB) and bone marrow (BM) of transplant mice 4 to 5 months posttransplantation. No engraftment was observed in any mice receiving $CD34^-$ cells.
(G) Methylcellulose colony-forming assay of $CD34^+$ and $CD34^-$ Kasumi-1 cells after 72 hr daily treatment with 10 nM DAC. *$p < 0.001$, compared to mock, by ANOVA with Bonferroni posttests.
(H and I) Engraftment assay in NOD/Shi-scid/IL-2Rγ^{null} mice of Kasumi-1 cells pretreated daily with 10 nM DAC for 72 hr. Percentage of human leukemia cells in peripheral blood (H) and in bone marrow (I) is shown. p values were calculated by Mann-Whitney test.
(J) Percentage of $CD34^+$ and $CD34^-$ Kasumi-1 AML cells after daily treatment of 10 nM DAC for 72 hr in vitro and after engraftment in mouse bone marrow. *$p < 0.05$ by Mann-Whitney test. All error bars represent standard errors.
See also Figure S1.

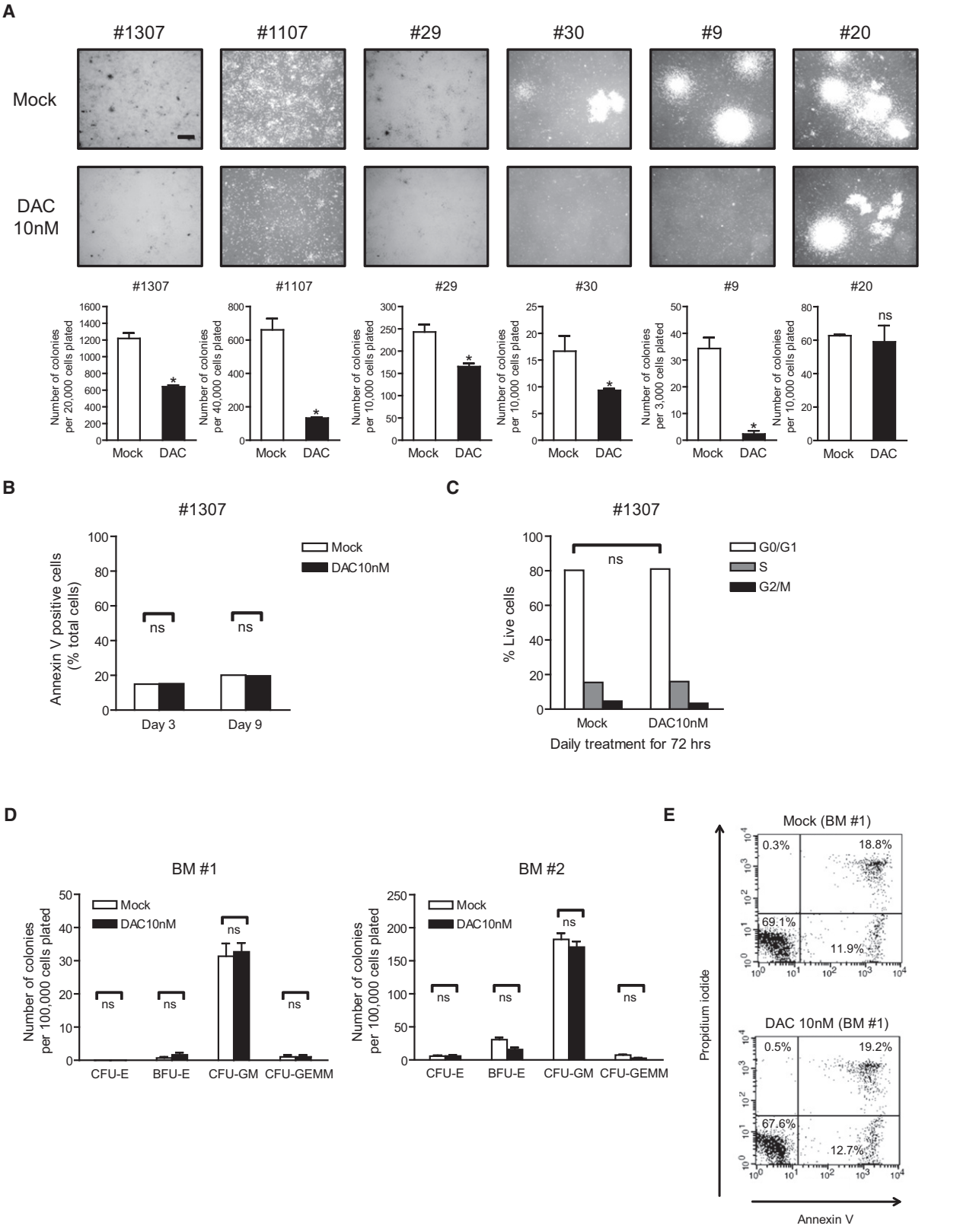

Figure 2. DAC at Non-Acutely Cytotoxic Doses Blunts Clonogenicity of Primary Human Leukemia Cells but Not Normal Bone Marrow Cells

(A) Methylcellulose colony-forming assay of bone marrow mononuclear cells from six patients with newly diagnosed AML after 72 hr daily DAC treatment and 4-day recovery period in vitro. Images and quantifications of colonies are shown in upper and lower panels, respectively. *$p < 0.05$ compared to mock by ANOVA

(Ghoshal et al., 2005). Three days of 10 nM DAC leads to early depletion of DNMT1 protein in Kasumi-1, KG-1, and KG-1a leukemia cells, and 100 nM gives a similar effect in three different breast cancer lines (Figure 5A). Despite these similar effects on early depletion of DNMT1 in all tested cell lines, the duration of the effect does not correlate with the later phenotypic consequences of drug treatment described earlier. Thus, while DNMT1 protein levels quickly recover in most of the lines, DNMT1 depletion lasts for at least 25 days after drug withdrawal in Kasumi-1 cells, although the phenotypic responses of these cells are similar to those of KG-1 cells (Figure 5A). Thus, transient or sustained inhibition of DNMT1 protein expression by 3 days of DAC treatment accompanies prolonged, subsequent, antitumor effects.

In keeping with the early depletion of DNMT1 protein levels, low-dose DAC causes demethylation and reexpression of DNA hypermethylated and epigenetically silenced genes. A 3-day exposure to 10 nM DAC produces, in both $CD34^+$ and $CD34^-$ Kasumi-1 cells, significant demethylation of the completely methylated and silenced tumor suppressors *CDKN2B* and *CDH1* (Figures 5B and 5C). One particularly important finding with respect to the cellular phenotypes observed involves the expression of some initially silenced genes. In the treatment schema used wherein cells are not acutely killed, we see in both Kasumi-1 and KG-1a cells increased transcription long after drug withdrawal. This is exemplified by *CDKN2B*, for which the peak expression is reached at Day 14, or 11 days after cessation of drug administration (Figure 5D).

It is important to note that these methylation effects are seen across the genome in analyses of DNA methylation by using the Methylation 27 BeadChip for cultured cells and the more probe-dense HumanMethylation450 BeadChip 450K for the treated 1107 and 1307 primary leukemia cells (Figure 2A). DAC (10 nM) for 72 hr causes a distinct decrease in methylation for essentially all probes and genes with high initial levels of DNA methylation in Kasumi-1 cells (Figures 6A and 6B), many of which are also heavily methylated in DNA from primary AML samples (Figure S3A). The decreases can be seen in promoter regions of both CpG island- and non-CpG island-containing genes (Figure 6C). This dose similarly reduces global methylation of highly methylated genes in KG-1 and KG-1a cells, as does 100 nM in breast cancer MCF7 cells (Figure S3B). Treatment of a primary leukemia sample (PL6347) with 10 nM DAC, after proliferation stimulation with cytokines, similarly causes decreases in gene promoter region DNA methylation (Figures 6B and S3B). Virtually identical results have been seen for primary, treated leukemia samples 1107 and 1307 using the 450K platform (data not shown).

The aforementioned genomic promoter demethylation induced by low-dose DAC is accompanied by widespread increases in gene expression (scatter plot for Kasumi-1 cells; Figures S3C and S3D). In fact, up to 50% of genes whose expression increase after transient low dose exposure remain increased for up to 14 days (Figure S3E). Among such genes are those having decreases in their cancer-specific promoter hypermethylation after drug treatment, such as *CDKN2B* in Kasumi-1 (Figure 5C) and KG-1a AML cells (Figure S5), *CDKN2A* in KG-1a cells, and six hypermethylated genes (Figure 6D) studied by Lubbert and colleagues (Flotho et al., 2009), or our lab, in Kasumi-1 cells, *DAPK1*, *CDKN1C* (also known as *p57KIP2*), *HOXA9*, *HGF*, *DLK1*, and *RAB13*. All these eight genes have increased expression by Day 3 of low-dose decitabine treatment, and seven have sustained increases at least 11 days after treatment cessation (Figure 6D).

Transient Low Doses of DAC and AZA Induce Sustained Alterations in Major Cancer Cell Signaling Pathways

Cancer is driven by alterations of gene function in key cellular pathways (Hanahan and Weinberg, 2011). We find, using Metacore analyses of gene expression, changes in many key antitumor pathways (Figures 7A, 7B, S4A, and S4B; Tables S1 and S2).

Changes in gene expression, which would block cell proliferation and decrease tumor self-renewing populations, were often correlated with increases in expression of more than one cyclin-dependent kinase inhibitors (*CDKN2B*, *CDKN2A*, *CDKN1A*) and were associated with CpG island DNA demethylation for *CDKN2B* in leukemia cells (Figures 7A and 7B). The upregulation of *p14ARF*, *CDKN2A*, *CDKN1A*, and other key hypermethylated pathway genes, such as *SLIT2* and *ROBO3*, were validated in cultured leukemia cells (Figure 8A). The FOXM1-polo-kinase (PLK)-Aurora kinase pathway would be predicted to be downregulated secondary to the aforementioned gene increases (Koo et al., 2012). We observed this in both cultured (KG-1a AML) and primary leukemia cells (#1107 in Figure 2A) and in primary breast cancer mammosphere samples (#103 and #104 in Figure 4A; Figure 7B). In each case, *CDKN1A* expression was increased and could be linked to DNA demethylation in a DNA methylated region (Figure 7C) just upstream from a nonhypermethylated CpG island. This pathway, required for cells to enter and perform cell division and to maintain DNA damage-triggered cell cycle check points, is increased in tumors with poor prognosis

and Dunnett's multiple comparison test. Scale bar, 500 μm. #1307 and #29, AML with FLT3-ITD mutation; #1107, AML FAB M2; #30, AML with mutated NPM1; #9, secondary AML; #20, AML FAB M5.

(B) Annexin V apoptosis assay of one representative AML patient sample (#1307) after 72 hr daily DAC treatment in vitro. Bone marrow mononuclear cells were harvested for analysis at the end of 72 hr drug treatment (Day 3) and 6 days after drug removal (Day 9). ns, not statistically significant by ANOVA with Bonferroni posttests.

(C) Cell cycle analysis on one representative AML patient sample (#1307) was performed 4 days after drug removal (Day 7) with DNA content measured using propidium iodide staining. ns, not statistically significant by ANOVA with Bonferroni posttests.

(D) Methylcellulose colony-forming assays of human normal bone marrow mononuclear cells (BM #1 and #2) after 72 hr daily DAC treatment in vitro. CFU-E, colony-forming unit erythroid; BFU-E, burst-forming unit erythroid; CFU-GM, colony-forming unit granulocyte, macrophage; CFU-GEMM, colony-forming unit granulocyte, erythrocyte, macrophage, megakaryocyte. ns, not statistically significant by ANOVA with Bonferroni posttests.

(E) Annexin V apoptosis assay in one representative bone marrow sample (BM #1) after DAC treatment in vitro. Cells were double-stained with Annexin-V and propidium iodide, and percentage of cells relative to total cells is shown in each quadrant. All error bars represent standard errors.

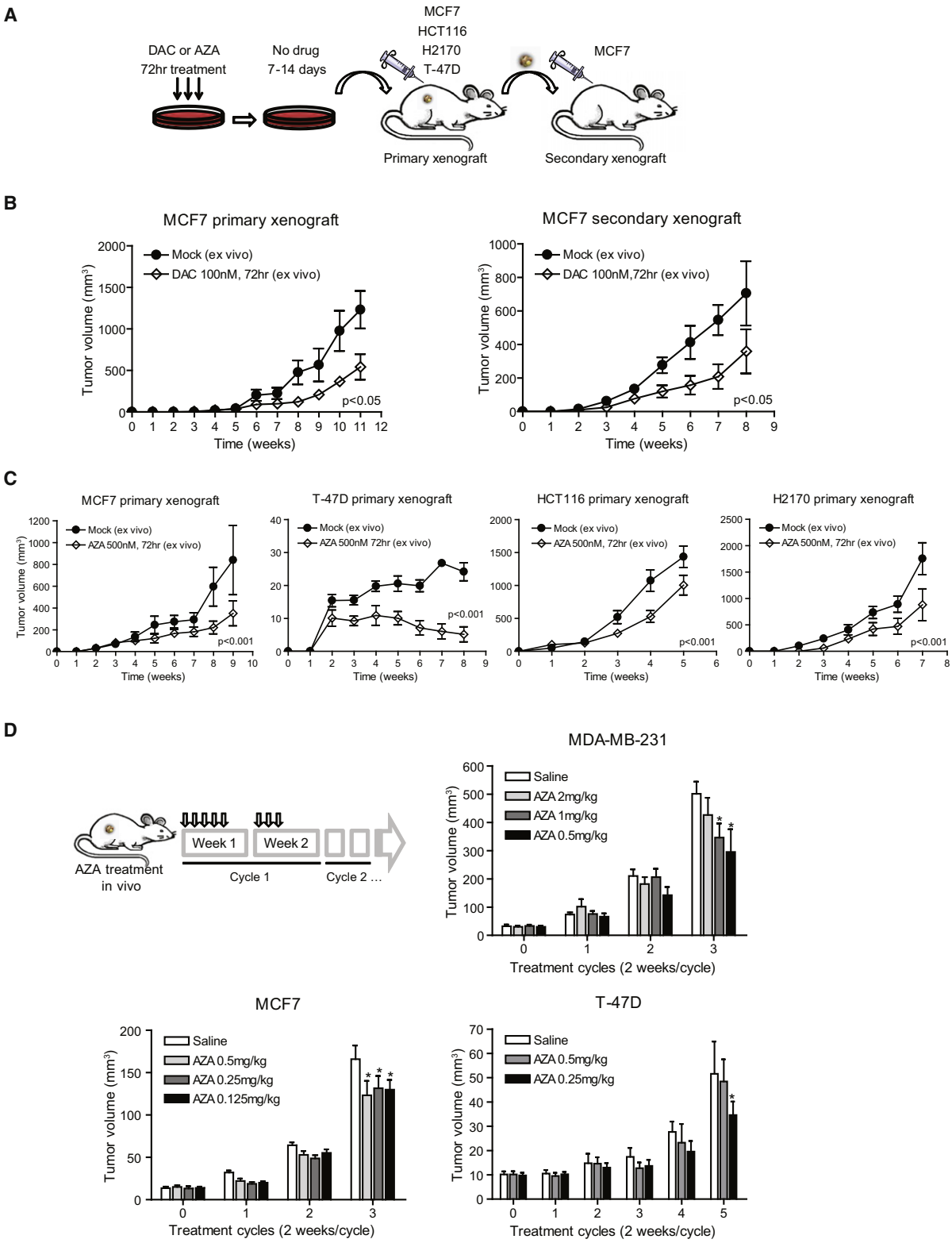

Figure 3. DAC and AZA at Noncytotoxic Doses Decrease Tumorigenicity in Mouse Tumor Xenografts

(A) Schematic outline of xenograft tumorigenicity assay in NOD/SCID mice for MCF7 (breast), T-47D (breast), HCT116 (colon), and H2170 (lung) cancer cells after 7- to 14-day recovery period after 100 nM DAC or 500 nM AZA daily treatment for 72 hr.

(B) Primary and secondary xenograft assays of MCF7 cells pretreated with 100 nM DAC. Equal numbers of viable cells were injected in each transplantation. p value is calculated by ANOVA. n = 6 for each treatment group.

and has been linked to progenitor cell renewal and increased cellular invasion, motility, and metastatic potential (Koo et al., 2012; Raychaudhuri and Park, 2011). Loss of G2M cell cycle checkpoint control and the downregulation of *FOXM1*, aurora kinases, polo kinases, *CHK1*, *CHK2*, and *MYT1* represent proteins currently targeted by the pharmaceutical industry to induce cancer cell apoptosis and/or sensitization to cytotoxic drugs (Carrassa and Damia, 2011; Merry et al., 2010). In bone marrow samples from two leukemia patients who responded to DAC treatment in a clinical trial, sustained DNA demethylation and increased expression of *CDKN2B* is detected at early time points before reduction of the leukemic tumor clone and coincident with decreases in *FOXM1* RNA (Figures 8B and 8C).

We also saw decreased *AKT* mRNA, and downregulation of key regulatory genes, *TWIST*, *SLUG*, and *SNAIL* (Hanahan and Weinberg, 2011), which activate epithelial to mesenchymal transition (EMT) (Figure 7A). EMT has been closely linked to stem-like populations in breast cancer and we observe down regulation of EMT genes in treated, self-renewing primary mammosphere cells from patients 103 and 104 (Figure 4A; Table S2). Correlative studies in the laboratory reveal decreased phosphorylation of AKT in cultured MCF7 breast cancer cells (Figure 8D).

In the self-renewing, primary mammosphere cultures, we saw changes predictive of diminished cell motility, invasiveness, induction of angiogenesis, and metastatic potential including decreased mRNA expression for genes encoding the integrins, metalloproteinases, and the key cytoskeletal remodeling protein ezrin (Figure S4A; Table S2). These genes can be overexpressed in breast cancer, and their downregulation is matched by upregulation of mRNA for genes that suppress these cell processes, such as the often hypermethylated tissue inhibitors of metalloproteinases (*TIMP*s), thrombospondin, and the complement receptor, *C5AR* (Table S2). It is important to note that breast cancer sample PE1, after 3-day treatment with 500 nM AZA, appears less invasive and forms a more compact sphere in matrigel (Figure 8E).

Finally, both cultured and primary cells harbored gene expression changes that predict cell maturation events. Kasumi-1 AML and primary AML sample 1107 had decreased expression of the *G-CSF* receptor and of the *c-myc* gene and increased expression, with decreased DNA methylation of the transcription region, for the transcription factor *RARA* (Figures 8A and S5). Coordinately, myeloid commitment at the progenitor cell level was indicated by DNA demethylation and increased expression of the normally methylated early myeloid lineage genes, *LYZ* and *ELANE* (Figures S4B and S5; and Table S1); increases in *CD13* (Figure S4B), a marker of cells with bipotential maturation to erythroid and granulocyte cells (Chen et al., 2007); and mature granulocyte formation (Levy et al., 1990) by increased *p47-phox*, *p67-phox*, and *Gp91-phox* (Figure S4B; Table S1). All of these changes were observed both in DAC-treated total AML cells and tumorigenic $CD34^+$ cells from Kasumi-1 AML (Figure S4B). Also, increased TGF-beta signaling was observed, and this is known to promote maturation and inhibition of leukemic progenitor cell renewal (Figure 7A) (Lewis et al., 2001; Watabe and Miyazono, 2009). Concomitantly, there is decreased canonical WNT pathway signaling associated with reduced methylation; increased expression of *WIF1* (Figures 7A and S5), a Wnt antagonist gene; and downstream decrease in expression of *c-myc* (Figure 7A), a canonical target for Wnt pathway activation (He et al., 1998). Of note, we validated myelocyte differentiation by flow cytometric analysis of a surface marker for mature granulocyte, CD11b, in a treated primary AML sample 29 (Figure 8F). Sustained increase of cytokeratin 18 (CK18) in DAC- or AZA-treated MCF7 cells, as well as in tumor xenografts from mice treated for 6 weeks with AZA (Figure 8G), was also observed. CK18 expression reflects maturation of breast luminal cells, and loss of CK18 is associated with poor prognosis in breast cancer patients (Woelfle et al., 2004).

DISCUSSION

Our present studies indicate that treatment of cancer cells with clinically relevant low doses of DAC and AZA can exert sustained changes in gene expression and critical signaling pathways involved in tumorigenesis without inducing immediate cytotoxic effects such as DNA damage, apoptosis, and cell cycle arrest. Our preclinical use of transient 3-day exposure to such doses ex vivo produces a ''memory'' type of antitumor response in mice bearing transplanted tumor xenografts, which may resemble the prolonged time to response seen in patients with hematologic neoplasms (Kantarjian et al., 2006; Oki et al., 2008; Silverman et al., 2002). In patient tumors and mammospheres, the antitumor response occurred more quickly and appeared to be more sensitive to AZA than that observed for cancer-cell-line-generated tumors. This may be explained by the fact that the human tumors were exposed to a longer, more sustained treatment and that primary tissues may be initially more sensitive to AZA. All of these aforementioned dynamics after transient drug exposure are accompanied by genomewide, prolonged gene promoter DNA demethylation and sustained increases in gene expression, some of which occur for key tumor suppressor genes in leukemia and breast cancer cells.

There are several reasons to suggest that at least one key mechanism underlying the antitumor responses we demonstrate may involve a resetting of abnormal epigenetic states in treated cancer cells. First, we have achieved a sustained change in the pattern of gene expression without changing primary DNA sequence. Second, as defined for an epigenetic change, these sustained changes persist for significant periods of time after a transient, subsequently withdrawn, signal (i.e., in this case, drug treatment). Third, altered expression patterns are accompanied by antitumor effects. It is important to note that we probably have brought out these aspects of DAC and

(C) Primary xenograft assays of MCF7, T-47D, HCT116, and H2170 cells pretreated with 500 nM AZA. p value is calculated by ANOVA. n = 10 for each treatment group.
(D) AZA treatment of mice with pre-established MDA-MD-231, MCF7, or T-47D breast tumors. Tumor volumes are measured at the end of each cycle. *Statistical significance determined by two-way ANOVA ($p < 0.05$). All error bars represent standard errors.
See also Figure S2.

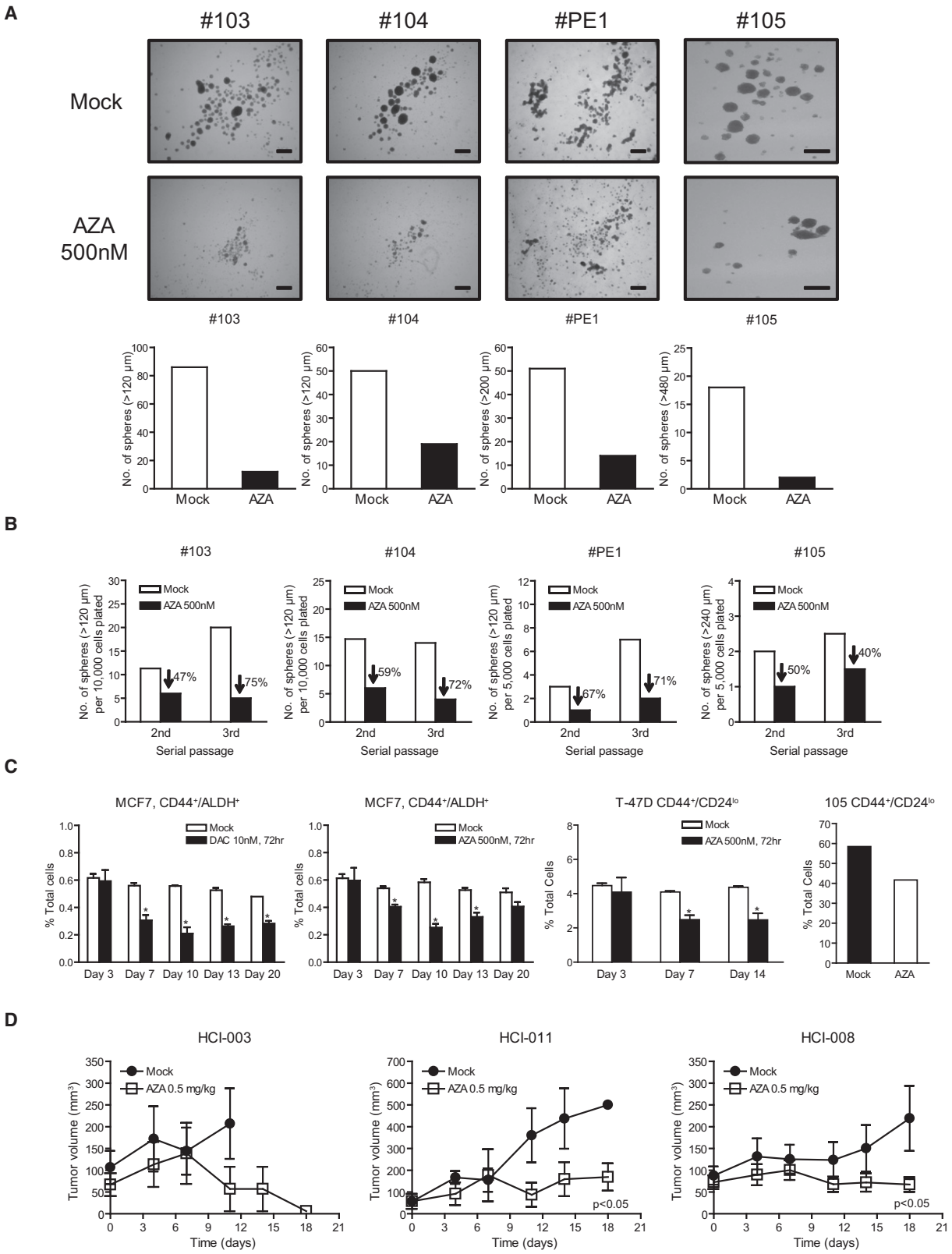

Figure 4. Low-Dose DAC and AZA Decrease Self-Renewal and Tumorigenesis in Primary Breast Cancer Tissue from Patients

(A) Tumor sphere assays of primary breast cancer cells from pleural effusions after 500 nM AZA daily treatment for 3 days in vitro. Images and quantifications of tumor spheres are shown in upper and lower panels, respectively. Scale bars, 500 μm.

AZA treatment by using doses that do not acutely kill cells and, thus, allow the sustained alterations in both gene expression patterns and appearance of, to our knowledge, a new phenotype to emerge. Of note, these changes include antitumor events in multiple key pathways, such as apoptosis, increased lineage commitment, downregulation of cell cycling, and others, which continue well after drug removal. Reprogramming might, then, be considered a very desirable type of targeted therapy that can blunt multiple tumor signaling pathways simultaneously.

Perhaps one of the most striking effects observed in our study concerns the fact that nanomolar doses of both DAC and AZA appear to target, in both cell lines and primary samples of leukemia and breast cancers, self-renewing and/or tumorigenic cell subpopulations. This involves stem-like $CD34^+$ cells in leukemia and $CD44^+/ALDH1^+$, $CD44^+/CD24^{LO}$, and mammosphere-forming cells in breast cancer. These findings should be considered in the context that one of the most important problems in cancer therapy is the failure of most therapies to target the subpopulations that are most responsible for sustained tumor cell renewal (Jordan et al., 2006). Our findings suggest that the often prolonged time course to response in patients with myelodysplasia or frank AML might involve a progressive exhaustion of cell populations. This hypothesis is supported by recent reports that depleting DNMT1, by nonpharmacologic means, in normal mouse hematopoietic and human epithelial cells blocks self-renewal and proper cell maturation, leading to cellular depletion of progenitor cells (Bröske et al., 2009; Sen et al., 2010; Trowbridge et al., 2009). DAC and AZA do deplete DNMT1 in leukemia and breast cancer cells for variable time periods after transient exposure (Figure 4A). However, the mechanisms underlying our pharmacologically induced responses are certainly more complex since both DAC and AZA inhibit the catalytic sites of DNMT3a and DNMT3b as well. Also, all the DNMTs assuredly participate in complex protein interactions where they may exert scaffolding functions with effects on other chromatin regulatory features (Robertson et al., 2000; Rountree et al., 2000). They also, experimentally, have effects for repressing gene expression that may not require their directly catalyzing DNA methylation (Bachman et al., 2001). This complexity may actually give DAC and AZA an important advantage in treating cancer cells where they may target all of these functions and their role in governing the epigenetic aberrancies present in cancer. If so, the activities we find for low nanomolar doses may be very important in rendering these drugs as gold standards for the development of agents to target DNA methylation and other epigenetic abnormalities as an anticancer strategy to inhibit the most tumorigenic subpopulations of cells.

In summary, our findings have much relevance for strategies to use DAC and AZA more widely for the management of cancer. These drugs are already making an impact for patients with hematological malignancies. Our findings now suggest ways and biomarkers that might be used to predict and/or monitor clinical efficacy. The similar "memory" type of responses we find for primary and cultured breast cancer cells, and the key pathway changes seen, indicate that the treatment of many cancers may be considered and with doses that will be not only efficacious but also minimally toxic to patients. Such possibilities are emerging in our recently completed trial, sponsored by Lung Cancer SPORE and Stand Up to Cancer (SU2C), for patients with advanced non-small-cell lung carcinoma (Juergens et al., 2011). SU2C trials in breast cancer have now begun that might be well informed by the preclinical studies we now report. Moreover, it is especially appealing to consider that DAC and AZA might sensitize tumor cells to other drugs, as is suggested by Juergens et al. (2011), that target the oncogenic pathways we have shown to be altered and allow use of reduced, less toxic, doses for these other agents.

EXPERIMENTAL PROCEDURES

Methylcellulose Colony-Forming Assay and Serial Replating Assay

After a 3-day drug treatment, equal numbers of viable cells were plated in triplicate on to MethoCult H4434 Classic or MethoCult H4435 Enriched (StemCell Technologies, Vancouver, British Columbia, Canada). Colonies containing more than 40 cells were quantified at 10-16 days under an inverted microscope. For serial replating assays, equal numbers of viable cells from the first plating were plated in triplicate in the second plating. Colonies were again scored after 16-21 days.

Long-Term Culture-Initiating Cell Assay

After a 3-day drug treatment, equal numbers of viable leukemia cells (trypan blue negative) were plated on to a feeder layer of irradiated M2-10B4 mouse fibroblasts (StemCell Technologies) and maintained via biweekly one-half medium changes in MyeloCult H5100 according to the manufacturer's instructions (StemCell Technologies). After 5 weeks, cells were harvested and plated on to MethoCult H4435 Enriched (StemCell Technologies), and colonies were counted after 14-18 days.

Immunophenotypic Staining and Fluorescence-Activated Cell Sorting

Human anti-CD34-FITC, anti-CD34-APC, anti-CD38-PE, anti-CD33-APC, anti-CD15-FITC, anti-CD14-PE, anti-CD11b-APC, anti-CD45-perCP, anti-CD45-APC, anti-CD44-APC, anti-CD24-PE, and corresponding isotype controls were obtained from BD Biosciences, San Jose, CA, USA. The ALDEFLUOR Assay kit (StemCell Technologies) was used to identify cells expressing high levels of aldehyde dehydrogenase (ALDH). Cells were stained according to the manufacturer's instructions and analyzed on a FACSCalibur Flow Cytometer (BD Biosciences) using BD CellQuest Pro v.5.2 (BD Biosciences). For sorting, CD34 cells with upper or lower 10% fluorescent intensity were collected (FACSVantage Cell sorter or BD FACSAria II cell sorter; BD Biosciences).

Leukemia Engraftment Assay

Cells were tail vein injected into sublethally irradiated (3.0 cG) female NOD/Shi-*scid*/IL-2Rγ^{null} mice 6-8 weeks of age. Peripheral blood was sampled every

(B) Serial passages of tumor spheres formed by primary breast cancer cells after the initial 3-day AZA treatment. Equal numbers of viable cells were plated in each passage. The data show a sustained decrease in self-renewal capacity of tumor spheres.
(C) Flow cytometric analyses of $CD44^+/ALDH^+$ in MCF7 cells, $CD44^+/CD24^{lo}$ cells in T-47D, and primary breast cancer sample #105 after AZA or DAC daily treatment for 3 days and subsequent drug removal. Statistical significance was determined via two-way ANOVA.
(D) In vivo AZA treatment of immunodeficient mice bearing orthotopically transplanted primary breast cancer cells from patients. AZA (0.5 mg/kg) was administered intraperitoneally 5 days/week. All error bars represent standard errors.

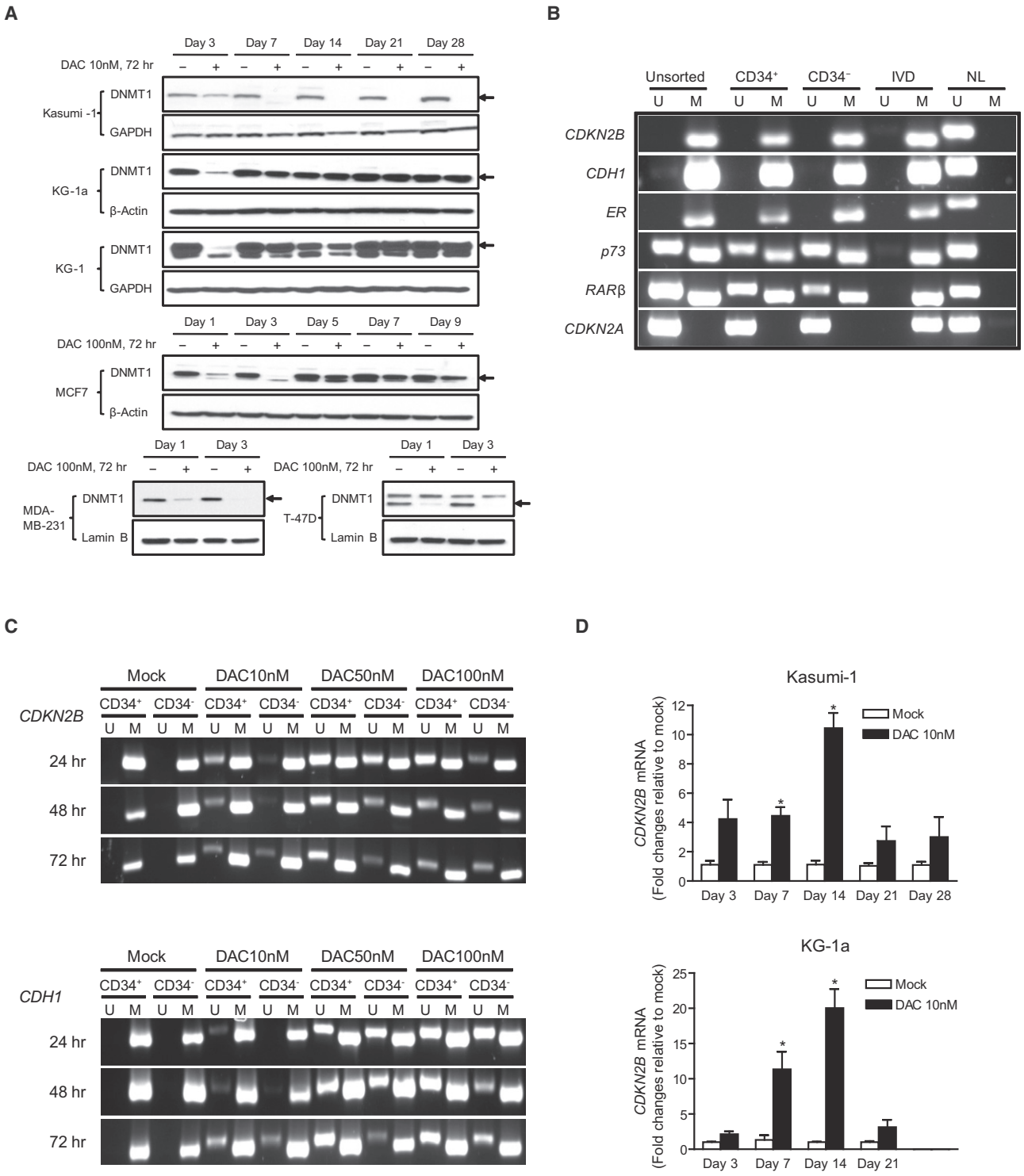

Figure 5. Low-Dose DAC Inhibits Gene Promoter DNA Methylation and Causes Sustained Re-expression of Hypermethylated Genes

(A) Western blot of DNMT1 expression levels in human leukemia cells (Kasumi-1, KG-1a, and KG-1) and breast cancer cells (MCF7, MDA-MB-231, and T-47D) after 72 hr daily treatment of 10 nM (leukemia) or 100 nM (breast cancer) DAC.

(B) Methylation-specific PCR (MSP) analyses of gene promoter DNA methylation in unsorted, $CD34^+$, and $CD34^-$ Kasumi-1 cells before DAC treatment. U, unmethylated sequence amplifications; M, methylated sequence amplifications; IVD, in vitro methylated DNA; NL, normal lymphocyte DNA.

(C) MSP analyses of *CDKN2B* and *CDH1* promoters in $CD34^+$ and $CD34^-$ Kasumi-1 cells at 24, 48, and 72 hr of DAC treatment.

(D) Quantitative real-time PCR analyses of *CDKN2B* gene expression over time in Kasumi-1 and KG-1a cells after 72 hr daily treatment of 10 nM DAC. Expression levels are adjusted to *GAPDH* for each sample and graphed as fold changes relative to mock. All error bars represent standard errors.

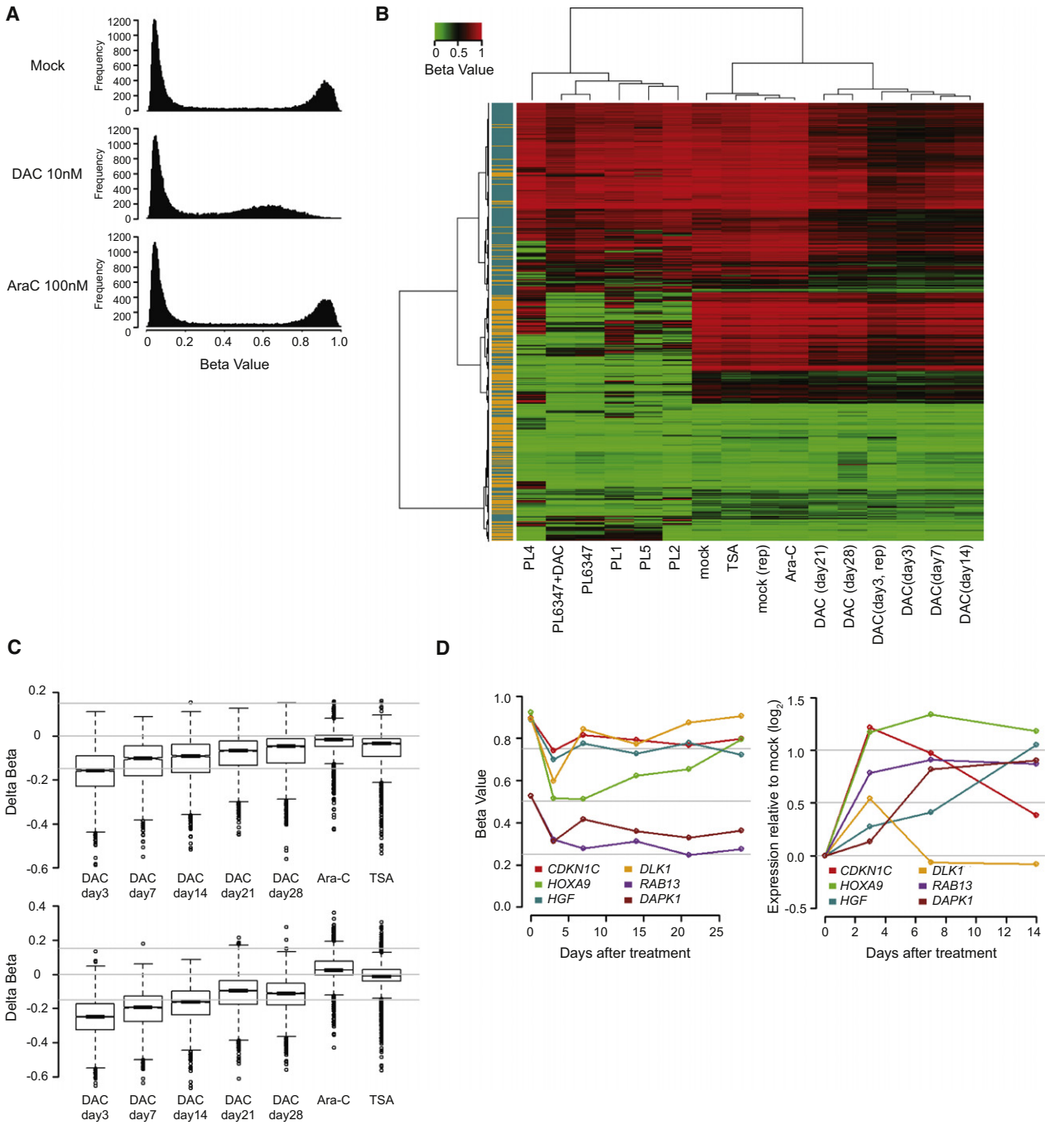

Figure 6. Genome-wide Methylation and Expression Analyses after Short-Term Exposure to Low-Dose DAC

(A) Histogram of Infinium results for Kasumi-1 methylation profiles after daily DAC or ARA-C treatment for 72 hr. y axis, frequency of probes; x axis, CpG probe beta scores (lowest to highest = increasing DNA methylation).

(B) Heat map composed of minimal variation beta probes located at −1,000 to +200 bp surrounding transcription start site (~5,500 genes). Blue and orange colors on the left denote non-CpG and CpG island promoters, respectively. PL6347, PL1, PL2, PL4, PL5 are the primary leukemia samples. PL6347+DAC: primary leukemia after 72 hr 10 nM DAC treatment. mock and mock (rep), untreated Kasumi-1 cells and its replicate. Ara-C, Kasumi-1 cells treated with 100 nM Ara-C daily for 72 hr. TSA, Kasumi-1 cells treated with 300 nM trichostatin A for 9 hr. DAC (day 3, day 3 rep, day 7, day 14, day 21, day 28), Kasumi-1 cells harvested at various time points after 72 hr daily treatment of 10 nM DAC.

(C) Box plots showing beta value changes over time in CpG island (upper panel) and non-CpG island gene promoters (lower panel) in Kasumi-1 cells after 72 hr daily treatment of 10 nM DAC. Ara-C, 100 nM AraC treatment for 72 hr. TSA, 300 nM TSA treatment for 9 hr.

(D) Left panel shows beta value changes after 72 hr, 10 nM DAC treatment for six genes in Kasumi-1 with basal beta values ≥ 0.5. Right panel shows corresponding Agilent expression changes normalized to Day 0. Gray horizontal lines: bottom to top, no change ($\log_2$ scale = 0), 1.4-fold (0.5), and 2.0-fold (1.0). See also Figure S3.

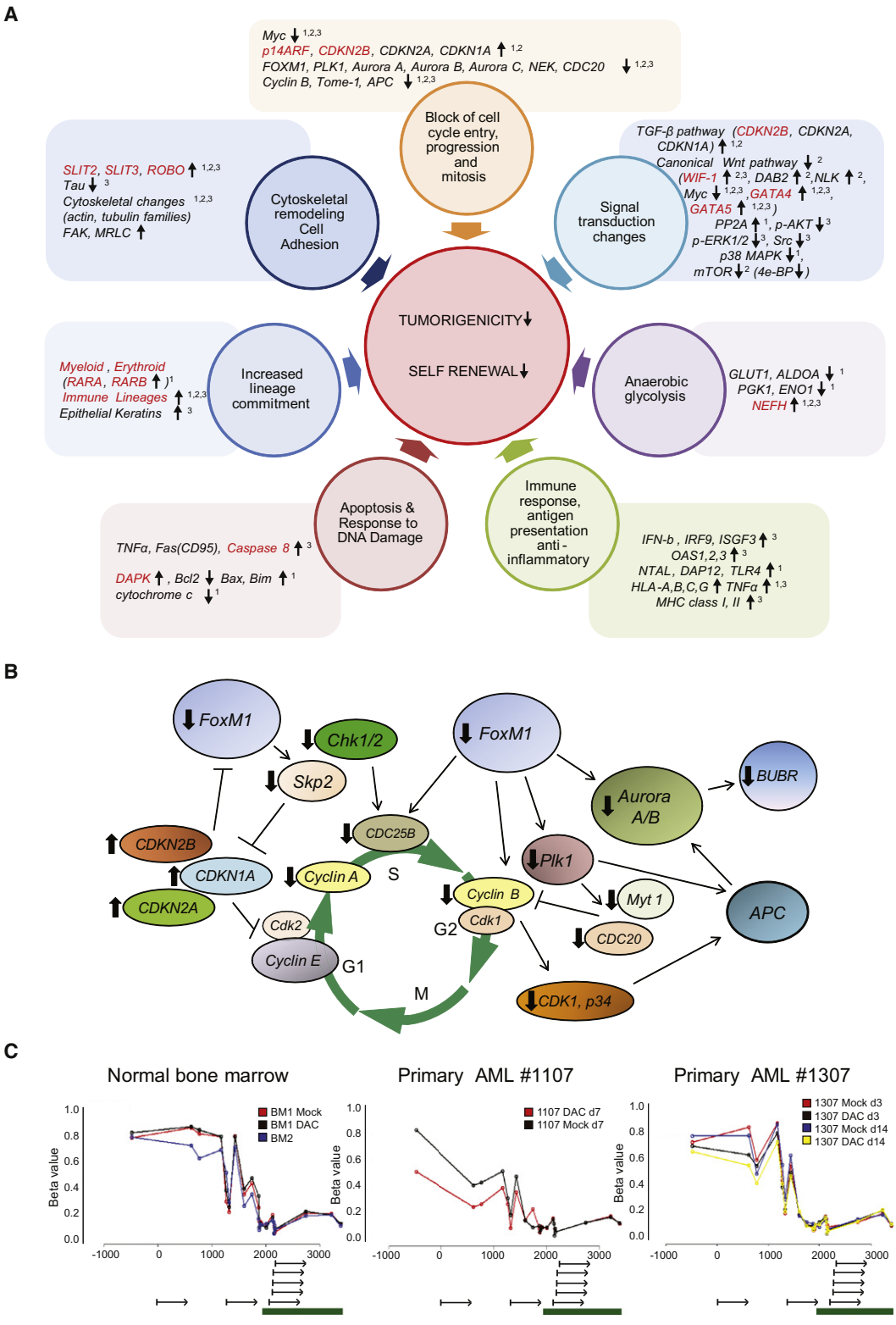

Figure 7. Metacore Pathway Analyses of Agilent Expression Changes after DAC or AZA Treatment

(A) Key pathways and/or master genes, shown here for studies in cultured cells. Genes in black type indicate genes with expression changes not directly linked to promoter DNA methylation. Genes in red type indicate genes with basal promoter hypermethylation, drug-induced demethylation, and corresponding increases in expression. Superscript 1, 2, and 3 by genes or pathways indicate, respectively, Kasumi-1 AML cells, KG-1a AML cells, and MCF7 breast cancer cells with expression changes concordant in the indicated cell line.

4 weeks, and bone marrow was harvested from each mouse at 13-15 weeks. Engraftment was determined by immunophenotypic staining using human anti-CD45-perCP and anti-CD34-APC (BD Biosciences).

Solid Tumor Xenograft Tumorigenicity Assay

MCF7, T-47D, HCT116, and H2170 cells were pretreated with 100 nM decitabine, 500 nM azacytidine, or PBS (Mock) for 72 hr, followed by another 4-7 days in culture without drug. Harvested cells were injected (1×10^6) subcutaneously into both flanks of 4- to 6-week-old NOD/SCID mice. Female mice receiving MCF7 cells were implanted with estrogen pellets (0.72 mg/60 days; Innovative Research of America, Sarasota, FL, USA). Secondary xenografts were generated by collagenase dissociation of primary MCF7 tumors at 8 weeks, followed by reinjection of 1×10^6 viable cells into mice.

Therapeutic Administration of AZA to NOD-SCID Mice with Pre-established Tumors

Mice with preestablished MDA-MB-231, MCF7, or T-47D xenotumors (0.3–0.5 cm) received subcutaneous daily saline (mock) or azacitidine injections (2, 1, 0.5, 0.25, or 0.125 mg/kg) for 8 days over a 14-day period per cycle, as outlined in Figure 2D. Five mice (10 tumors) were used per treatment group.

For xenograft experiments using cell lines, tumors were measured weekly and volume was calculated as $0.5 \times (L \times W^2)$(mm3). Protocols for all animal experiments conducted at Johns Hopkins were approved by the John Hopkins University Animal Care and Use Committee and guidelines were strictly enforced. Experiments using human tumor xenografts and conducted at the Huntsman Cancer Institute were reviewed and approved by the University of Utah Institutional Animal Care and Use Committee.

In Vitro Culture of Primary Human Leukemia and Normal Bone Marrow Cells

Frozen bone marrow mononuclear cells from patients with freshly diagnosed acute myelgenous leukemia (#1107 and #1307) or healthy controls (BM #1 and #2) were thawed and cultured in Poietics HPGM (Lonza, Inc., Walkersville, MD, USA) supplemented with multiple cytokines described in the Supplemental Experimental Procedures. Provision of all primary bone marrow and leukemia samples was through protocols approved by the institutional review boards (IRBs) at the University of Maryland School of Medicine, The Johns Hopkins Medical Institutions, and The University of Texas M.D. Anderson Cancer Center.

Tumor Sphere Assays of Primary Breast Cancer Cells

Malignant plueral effusions were collected under an IRB-approved protocol at the Johns Hopkins Medical Institutions from women with metastatic breast cancer undergoing thoracentesis as part of clinical care and who provided a written consent for use of leftover fluid. The fluid was enriched for malignant epithelial cells via centrifugation and lysing of red blood cells. Tumorspheres were maintained on ultralow adherent plates (Corning Inc., Lowell, MA, USA) in MammoCult (StemCell Technologies) or MCF10A media. (See the Supplemental Experimental Procedures for details.) Tumorspheres were treated daily for 3 days with 500 nM AZA and were cultured 4 more days after drug withdrawal. Primary spheres were counted and digested with 0.05% trypsin (Invitrogen, Carlsbad, CA, USA) into single cells. Equal numbers of live cells were plated in ultralow attachment plates to generate the second spheres. Again, spheres were counted on Day 7 and digested to generate the third spheres.

Global Gene Expression and Methylation Analysis

Gene expression profiles were analyzed, for queried cells, with Agilent Human 4× 44K expression arrays (Agilent Technologies, Santa Clara, CA, USA. Global methylation analysis was performed with the Illumina Infinium Human Methylation27 BeadChip or HumanMethylation450 BeadChip (Illumina, Inc., San Diego, CA, USA). Data were processed using R and BioConductor.

Metacore Pathway Analysis

All probes from the Agilent Human 4× 44K expression arrays with a change of at least .5 ($\log_2$ scale) up or down at any of the investigated time points were selected for further analysis and used as input for the Metacore (GeneGo, Inc.) pathway analysis. Details are described in the Supplemental Experimental Procedures.

ACCESSION NUMBERS

All microarray data are deposited in the GEO database under accession number GSE20945.

SUPPLEMENTAL INFORMATION

Supplemental Information includes five figures, two tables, and Supplemental Experimental Procedures and can be found with this article online at doi:10.1016/j.ccr.2011.12.029.

ACKNOWLEDGMENTS

We thank Drs. Peter A. Jones and Charles M. Rudin and multiple other members of our SU2C team, charged with bringing epigenetic therapy to the clinical management of all types of cancer, for critically reviewing the paper and for making helpful suggestions throughout. We thank Dr. Ying Ye for providing part of the primary leukemia samples used in this study. We thank Ada J. Tam from the flow cytometry core facility and Wayne Yu from the microarray core facility at Sidney Kimmel Comprehensive Cancer Center for their technical assistance. We also thank Stacie Jeter and Shannon Slater for regulatory support and recruitment of patients to the clinical study.

This work was, in part, supported by Grant CA 116160 from the National Institutes of Health, the Lung Spore in Cancer NCI Grant CA058184, and by funds from the Entertainment Industry Foundation and Lee Jeans, SU2C, the Samuel Waxman Cancer Research Foundation, the Irving A. Hansen Memorial Foundation (C.A.Z.), the Safeway Foundation (C.A.Z.), the Department of Defense Breast Cancer Research Program (BC075015 to A.L.W.), and The Huntsman Cancer Foundation (A.L.W.). H.-C.T. is a David Workman Student Scholar of the Samuel Waxman Cancer Research Foundation, and C.A.Z. is an Evelyn Grollman Glick Scholar. The clinical study was supported by the Cindy Rosencrans Fund for Triple Negative Breast Cancer Research.

H-C.T., C.A.Z., and S.B.B. designed the study, analyzed data, and wrote the article. L.V.N. performed bioinformatic analyses. C.A.Z. designed and conducted animal studies for solid tumors. Y.-Y.J. and S.J.S. helped design animal studies for leukemia. H.-C.T., H.L., J.J.S., K.H., E.P., J.H., and I.M. conducted solid tumor xenograft mouse experiments. H.-C.T., R.-W.C.Y. and H.L. performed all in vitro assays for leukemia and breast cancer cells. Y.C. and H.L. performed western assays. C.R. and F.V.R. conducted DNA damage assays and provided primary leukemia samples. H-C.T. and R-W.C.Y performed methylation and gene expression studies. W.M. provided primary leukemia samples and helped with study design. V.S. was responsible for all

(B) An example of pathway diagram summarizes gene changes for cultured and primary AML and breast cancer samples after transient in vitro treatment of DAC or AZA. Events depicted illustrate key expression increases in cyclin-dependent kinase inhibitors (*CDKN2B*, *CDKN2A*, *CDKN1A*), which are known to trigger decreased activity of the *FOXM1* pathway and all of the decreases shown earlier for *FOXM1* itself and the other key participants for cycle entry and progression and including the oncogene *Skp2*.

(C) Analyses of DNA methylation by HumanMethylation450 BeadChip for multiple CpG sites in the *CDKN1A* proximal promoter region. Note that a normally heavily methylated (two normal bone marrow samples) region 5′ to the unmethylated CpG island (large green bar), surrounding an alternate gene start site (small arrow), is distinctly demethylated after 10 nM DAC treatment in #1107 primary AML cells, which show all of the pathway changes but not to the same degree as in #1307 AML cells, where *CDKN1A* expression is not increased and the pathway changes seen are not present.

See also Figure S4 and Tables S1 and S2

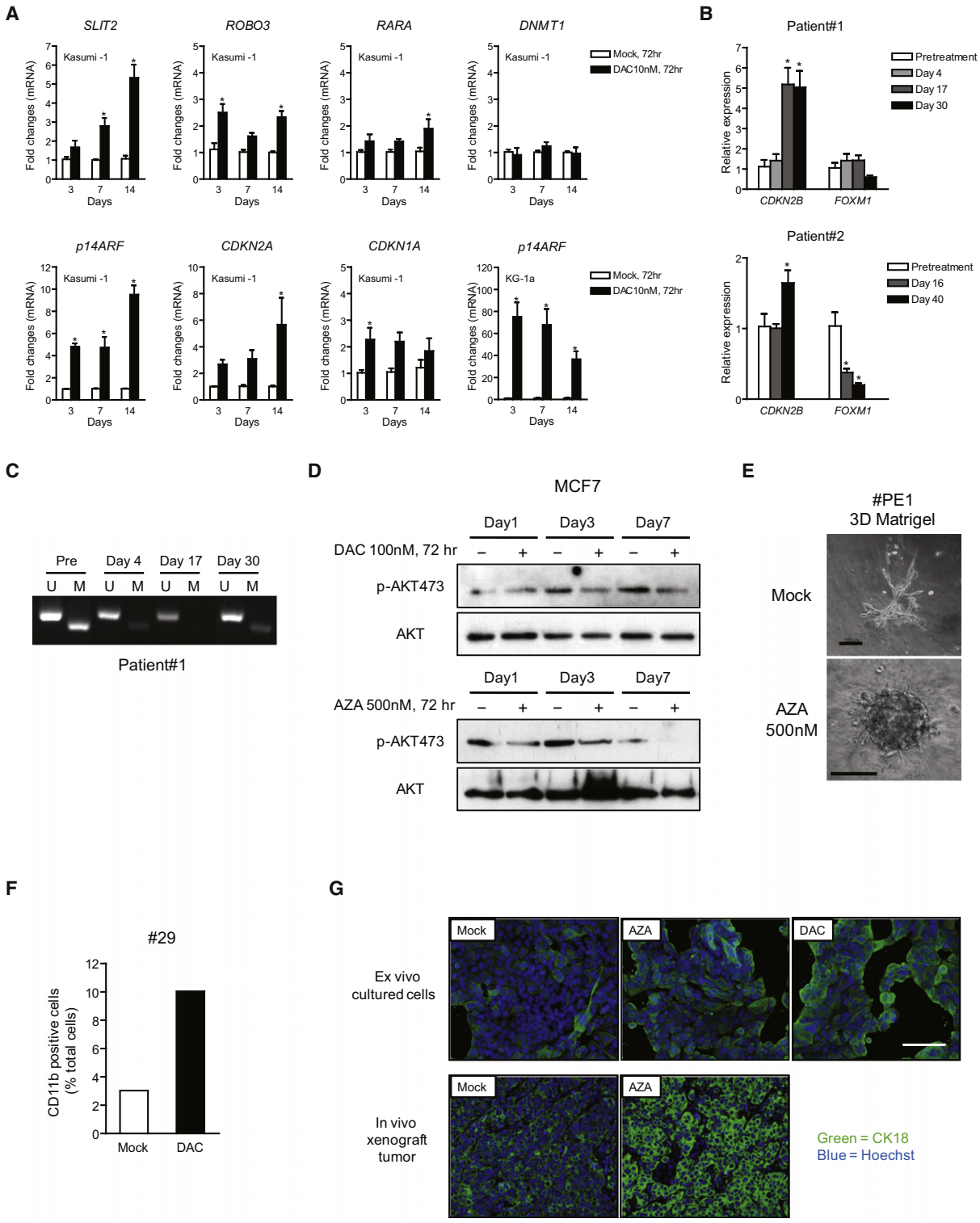

Figure 8. Validation of Changes in Multiple Signaling Pathways after DAC or AZA Treatment

(A) Quantitative real-time PCR verification for selected genes with expression changes indicated by the Metacore analyses. *$p < 0.05$ determined by ANOVA and Bonferroni posttests.

(B) Quantitative real-time PCR analyses of gene expression changes in bone marrow samples taken from patients #1 (partial responder with AML) and #2 (complete responder with CMML) at pretreatment and various time points during or after administration of DAC (20 mg/m^2 IV over 1 hr daily × 5 days every 4 weeks). mRNA levels of two genes, *CDKN2B* and *FOXM1*, at each time point were plotted relative to the baseline level after adjusted by a control housekeeping gene, *GAPDH*.

regulatory aspects of patient recruitment to the clinical study that provided primary effusion samples, and D.F.-K. and L.B.Y. assisted with patient recruitment and conducted thoracentesis. A.L.W. and Y.-C.L. provided and treated primary human xenografts with AZA. J.-P.I. provided DNA and RNA samples from DAC-treated leukemia patients. S.B.B., C.A.Z., L.V.N., and H.-C.T. contributed to pathway analyses.

Received: November 3, 2010
Revised: June 20, 2011
Accepted: December 30, 2011
Published: March 19, 2012

REFERENCES

Abele, R., Clavel, M., Dodion, P., Bruntsch, U., Gundersen, S., Smyth, J., Renard, J., van Glabbeke, M., and Pinedo, H.M. (1987). The EORTC Early Clinical Trials Cooperative Group experience with 5-aza-2′-deoxycytidine (NSC 127716) in patients with colo-rectal, head and neck, renal carcinomas and malignant melanomas. Eur. J. Cancer Clin. Oncol. *23*, 1921–1924.

Al-Hajj, M., Wicha, M.S., Benito-Hernandez, A., Morrison, S.J., and Clarke, M.F. (2003). Prospective identification of tumorigenic breast cancer cells. Proc. Natl. Acad. Sci. USA *100*, 3983–3988.

Asou, H., Tashiro, S., Hamamoto, K., Otsuji, A., Kita, K., and Kamada, N. (1991). Establishment of a human acute myeloid leukemia cell line (Kasumi-1) with 8;21 chromosome translocation. Blood *77*, 2031–2036.

Bachman, K.E., Rountree, M.R., and Baylin, S.B. (2001). Dnmt3a and Dnmt3b are transcriptional repressors that exhibit unique localization properties to heterochromatin. J. Biol. Chem. *276*, 32282–32287.

Berg, T., Guo, Y., Abdelkarim, M., Fliegauf, M., and Lübbert, M. (2007). Reversal of p15/INK4b hypermethylation in AML1/ETO-positive and -negative myeloid leukemia cell lines. Leuk. Res. *31*, 497–506.

Blum, W., Klisovic, R.B., Hackanson, B., Liu, Z., Liu, S., Devine, H., Vukosavljevic, T., Huynh, L., Lozanski, G., Kefauver, C., et al. (2007). Phase I study of decitabine alone or in combination with valproic acid in acute myeloid leukemia. J. Clin. Oncol. *25*, 3884–3891.

Bröske, A.M., Vockentanz, L., Kharazi, S., Huska, M.R., Mancini, E., Scheller, M., Kuhl, C., Enns, A., Prinz, M., Jaenisch, R., et al. (2009). DNA methylation protects hematopoietic stem cell multipotency from myeloerythroid restriction. Nat. Genet. *41*, 1207–1215.

Carrassa, L., and Damia, G. (2011). Unleashing Chk1 in cancer therapy. Cell Cycle *10*, 2121–2128.

Cashen, A.F., Shah, A.K., Todt, L., Fisher, N., and DiPersio, J. (2008). Pharmacokinetics of decitabine administered as a 3-h infusion to patients with acute myeloid leukemia (AML) or myelodysplastic syndrome (MDS). Cancer Chemother. Pharmacol. *61*, 759–766.

Cashen, A.F., Schiller, G.J., O'Donnell, M.R., and Dipersio, J.F. (2010). Multicenter, phase II study of decitabine for the first-line treatment of older patients with acute myeloid leukemia. J Clin Oncol. *28*, 556–561.

Charafe-Jauffret, E., Ginestier, C., Iovino, F., Wicinski, J., Cervera, N., Finetti, P., Hur, M.H., Diebel, M.E., Monville, F., Dutcher, J., et al. (2009). Breast cancer cell lines contain functional cancer stem cells with metastatic capacity and a distinct molecular signature. Cancer Res. *69*, 1302–1313.

Chen, L., Gao, Z., Zhu, J., and Rodgers, G.P. (2007). Identification of CD13+CD36+ cells as a common progenitor for erythroid and myeloid lineages in human bone marrow. Exp. Hematol. *35*, 1047–1055.

DeRose, Y.S., Wang, G., Lin, Y.-C., Bernard, P.S., Buys, S.S., Ebbert, M.T.W., Factor, R., Matsen, C., Milash, B.A., Nelson, E., et al. (2011). Tumor grafts derived from women with breast cancer authentically reflect tumor pathology, growth, metastasis and disease outcomes. Nat. Med. *17*, 1514–1520.

Dontu, G., Abdallah, W.M., Foley, J.M., Jackson, K.W., Clarke, M.F., Kawamura, M.J., and Wicha, M.S. (2003). In vitro propagation and transcriptional profiling of human mammary stem/progenitor cells. Genes Dev. *17*, 1253–1270.

Ferguson, A.T., Vertino, P.M., Spitzner, J.R., Baylin, S.B., Muller, M.T., and Davidson, N.E. (1997). Role of estrogen receptor gene demethylation and DNA methyltransferase. DNA adduct formation in 5-aza-2′deoxycytidine-induced cytotoxicity in human breast cancer cells. J. Biol. Chem. *272*, 32260–32266.

Flotho, C., Claus, R., Batz, C., Schneider, M., Sandrock, I., Ihde, S., Plass, C., Niemeyer, C.M., and Lübbert, M. (2009). The DNA methyltransferase inhibitors azacitidine, decitabine and zebularine exert differential effects on cancer gene expression in acute myeloid leukemia cells. Leukemia *23*, 1019–1028.

Gabbara, S., and Bhagwat, A.S. (1995). The mechanism of inhibition of DNA (cytosine-5-)-methyltransferases by 5-azacytosine is likely to involve methyl transfer to the inhibitor. Biochem. J. *307*, 87–92.

Ghoshal, K., Datta, J., Majumder, S., Bai, S., Kutay, H., Motiwala, T., and Jacob, S.T. (2005). 5-Aza-deoxycytidine induces selective degradation of DNA methyltransferase 1 by a proteasomal pathway that requires the KEN box, bromo-adjacent homology domain, and nuclear localization signal. Mol. Cell. Biol. *25*, 4727–4741.

Ginestier, C., Hur, M.H., Charafe-Jauffret, E., Monville, F., Dutcher, J., Brown, M., Jacquemier, J., Viens, P., Kleer, C.G., Liu, S., et al. (2007). ALDH1 is a marker of normal and malignant human mammary stem cells and a predictor of poor clinical outcome. Cell Stem Cell *1*, 555–567.

Gore, S.D., Baylin, S., Sugar, E., Carraway, H., Miller, C.B., Carducci, M., Grever, M., Galm, O., Dauses, T., Karp, J.E., et al. (2006). Combined DNA methyltransferase and histone deacetylase inhibition in the treatment of myeloid neoplasms. Cancer Res. *66*, 6361–6369.

Guzman, M.L., Neering, S.J., Upchurch, D., Grimes, B., Howard, D.S., Rizzieri, D.A., Luger, S.M., and Jordan, C.T. (2001). Nuclear factor-kappaB is constitutively activated in primitive human acute myelogenous leukemia cells. Blood *98*, 2301–2307.

Hanahan, D., and Weinberg, R.A. (2011). Hallmarks of cancer: the next generation. Cell *144*, 646–674.

He, T.C., Sparks, A.B., Rago, C., Hermeking, H., Zawel, L., da Costa, L.T., Morin, P.J., Vogelstein, B., and Kinzler, K.W. (1998). Identification of c-MYC as a target of the APC pathway. Science *281*, 1509–1512.

Issa, J.P., and Kantarjian, H.M. (2009). Targeting DNA methylation. Clin. Cancer Res. *15*, 3938–3946.

Issa, J.P., Garcia-Manero, G., Giles, F.J., Mannari, R., Thomas, D., Faderl, S., Bayar, E., Lyons, J., Rosenfeld, C.S., Cortes, J., and Kantarjian, H.M. (2004). Phase 1 study of low-dose prolonged exposure schedules of the hypomethylating agent 5-aza-2′-deoxycytidine (decitabine) in hematopoietic malignancies. Blood *103*, 1635–1640.

Jones, P.A., and Taylor, S.M. (1980). Cellular differentiation, cytidine analogs and DNA methylation. Cell *20*, 85–93.

Jordan, C.T., Guzman, M.L., and Noble, M. (2006). Cancer stem cells. N. Engl. J. Med. *355*, 1253–1261.

(C) Methylation-specific PCR analysis of *CDKN2B* promoter on the bone marrow sample of patient #1 at pretreatment, Day 4, Day 17, and Day 30 during the treatment cycle. U, unmethylated sequence amplifications; M, methylated sequence amplifications.
(D) Western blot analysis of total and phosphorylated AKT in MCF7 breast cancer cells after 100 nM DAC (upper panel) and 500 nM AZA (lower panel) treatment.
(E) Three-dimensional assay in Matrigel of a primary breast cancer sample PE1 after 3-day treatment with 500 nM AZA and subsequent drug removal. Scale bars, 100 μm.
(F) Flow cytometric analysis of surface CD11b expression in primary AML sample #29 at 14 days after 72 hr 10 nM DAC treatment.
(G) Immunofluoresence staining of cytokeratin 18 in cultured MCF7 cells 4 days after 72 hr 100 nM DAC or 500 nM AZA daily treatment (upper panel) and in MCF7 xenograft tumors removed from mock- and AZA-treated mice (lower panel) at 6 weeks. Scale bars, 100 μm. All error bars represent standard errors.
See also Figure S5.

Juergens, R.A., Wrangle, J., Vendetti, F.P., Murphy, S.C., Zhao, M., Coleman, B., Sebree, R., Rodgers, K., Hooker, C.M., Franco, N., et al. (2011). Combination epigenetic therapy has efficacy in patients with refractory advanced non-small cell lung cancer. Cancer Discovery *1*, 598–607.

Kantarjian, H., Issa, J.P., Rosenfeld, C.S., Bennett, J.M., Albitar, M., DiPersio, J., Klimek, V., Slack, J., de Castro, C., Ravandi, F., et al. (2006). Decitabine improves patient outcomes in myelodysplastic syndromes: results of a phase III randomized study. Cancer *106*, 1794–1803.

Kantarjian, H., Oki, Y., Garcia-Manero, G., Huang, X., O'Brien, S., Cortes, J., Faderl, S., Bueso-Ramos, C., Ravandi, F., Estrov, Z., et al. (2007). Results of a randomized study of 3 schedules of low-dose decitabine in higher-risk myelodysplastic syndrome and chronic myelomonocytic leukemia. Blood *109*, 52–57.

Karpf, A.R., Moore, B.C., Ririe, T.O., and Jones, D.A. (2001). Activation of the p53 DNA damage response pathway after inhibition of DNA methyltransferase by 5-aza-2′-deoxycytidine. Mol. Pharmacol. *59*, 751–757.

Koo, C.Y., Muir, K.W., and Lam, E.W. (2012). FOXM1: From cancer initiation to progression and treatment. Biochim Biophys Acta *1819*, 28–37.

Korkaya, H., Paulson, A., Charafe-Jauffret, E., Ginestier, C., Brown, M., Dutcher, J., Clouthier, S.G., and Wicha, M.S. (2009). Regulation of mammary stem/progenitor cells by PTEN/Akt/beta-catenin signaling. PLoS Biol. *7*, e1000121.

Lapidot, T., Sirard, C., Vormoor, J., Murdoch, B., Hoang, T., Caceres-Cortes, J., Minden, M., Paterson, B., Caligiuri, M.A., and Dick, J.E. (1994). A cell initiating human acute myeloid leukaemia after transplantation into SCID mice. Nature *367*, 645–648.

Levy, R., Rotrosen, D., Nagauker, O., Leto, T.L., and Malech, H.L. (1990). Induction of the respiratory burst in HL-60 cells. Correlation of function and protein expression. J. Immunol. *145*, 2595–2601.

Lewis, J.L., Chinswangwatanakul, W., Zheng, B., Marley, S.B., Nguyen, D.X., Cross, N.C., Banerji, L., Glassford, J., Thomas, N.S., Goldman, J.M., et al. (2001). The influence of INK4 proteins on growth and self-renewal kinetics of hematopoietic progenitor cells. Blood *97*, 2604–2610.

Li, C., Heidt, D.G., Dalerba, P., Burant, C.F., Zhang, L., Adsay, V., Wicha, M., Clarke, M.F., and Simeone, D.M. (2007). Identification of pancreatic cancer stem cells. Cancer Res. *67*, 1030–1037.

Liu, S., Dontu, G., Mantle, I.D., Patel, S., Ahn, N.S., Jackson, K.W., Suri, P., and Wicha, M.S. (2006). Hedgehog signaling and Bmi-1 regulate self-renewal of normal and malignant human mammary stem cells. Cancer Res. *66*, 6063–6071.

McDermott, S.P., and Wicha, M.S. (2010). Targeting breast cancer stem cells. Mol. Oncol. *4*, 404–419.

Merry, C., Fu, K., Wang, J., Yeh, I.J., and Zhang, Y. (2010). Targeting the checkpoint kinase Chk1 in cancer therapy. Cell Cycle *9*, 279–283.

Momparler, R.L., Bouffard, D.Y., Momparler, L.F., Dionne, J., Belanger, K., and Ayoub, J. (1997). Pilot phase I-II study on 5-aza-2′-deoxycytidine (Decitabine) in patients with metastatic lung cancer. Anticancer Drugs *8*, 358–368.

O'Brien, C.A., Pollett, A., Gallinger, S., and Dick, J.E. (2007). A human colon cancer cell capable of initiating tumour growth in immunodeficient mice. Nature *445*, 106–110.

Oki, Y., Jelinek, J., Shen, L., Kantarjian, H.M., and Issa, J.P. (2008). Induction of hypomethylation and molecular response after decitabine therapy in patients with chronic myelomonocytic leukemia. Blood *111*, 2382–2384.

Palii, S.S., Van Emburgh, B.O., Sankpal, U.T., Brown, K.D., and Robertson, K.D. (2008). DNA methylation inhibitor 5-Aza-2′-deoxycytidine induces reversible genome-wide DNA damage that is distinctly influenced by DNA methyltransferases 1 and 3B. Mol. Cell. Biol. *28*, 752–771.

Raychaudhuri, P., and Park, H.J. (2011). FoxM1: a master regulator of tumor metastasis. Cancer Res. *71*, 4329–4333.

Ricci-Vitiani, L., Lombardi, D.G., Pilozzi, E., Biffoni, M., Todaro, M., Peschle, C., and De Maria, R. (2007). Identification and expansion of human colon-cancer-initiating cells. Nature *445*, 111–115.

Robertson, K.D., Ait-Si-Ali, S., Yokochi, T., Wade, P.A., Jones, P.L., and Wolffe, A.P. (2000). DNMT1 forms a complex with Rb, E2F1 and HDAC1 and represses transcription from E2F-responsive promoters. Nat. Genet. *25*, 338–342.

Rountree, M.R., Bachman, K.E., and Baylin, S.B. (2000). DNMT1 binds HDAC2 and a new co-repressor, DMAP1, to form a complex at replication foci. Nat. Genet. *25*, 269–277.

Santi, D.V., Norment, A., and Garrett, C.E. (1984). Covalent bond formation between a DNA-cytosine methyltransferase and DNA containing 5-azacytosine. Proc. Natl. Acad. Sci. USA *81*, 6993–6997.

Schatton, T., Murphy, G.F., Frank, N.Y., Yamaura, K., Waaga-Gasser, A.M., Gasser, M., Zhan, Q., Jordan, S., Duncan, L.M., Weishaupt, C., et al. (2008). Identification of cells initiating human melanomas. Nature *451*, 345–349.

Schrump, D.S., Fischette, M.R., Nguyen, D.M., Zhao, M., Li, X., Kunst, T.F., Hancox, A., Hong, J.A., Chen, G.A., Pishchik, V., et al. (2006). Phase I study of decitabine-mediated gene expression in patients with cancers involving the lungs, esophagus, or pleura. Clin. Cancer Res. *12*, 5777–5785.

Sen, G.L., Reuter, J.A., Webster, D.E., Zhu, L., and Khavari, P.A. (2010). DNMT1 maintains progenitor function in self-renewing somatic tissue. Nature *463*, 563–567.

Silverman, L.R., Demakos, E.P., Peterson, B.L., Kornblith, A.B., Holland, J.C., Odchimar-Reissig, R., Stone, R.M., Nelson, D., Powell, B.L., DeCastro, C.M., et al. (2002). Randomized controlled trial of azacitidine in patients with the myelodysplastic syndrome: a study of the cancer and leukemia group B. J. Clin. Oncol. *20*, 2429–2440.

Singh, S.K., Hawkins, C., Clarke, I.D., Squire, J.A., Bayani, J., Hide, T., Henkelman, R.M., Cusimano, M.D., and Dirks, P.B. (2004). Identification of human brain tumour initiating cells. Nature *432*, 396–401.

Trowbridge, J.J., Snow, J.W., Kim, J., and Orkin, S.H. (2009). DNA methyltransferase 1 is essential for and uniquely regulates hematopoietic stem and progenitor cells. Cell Stem Cell *5*, 442–449.

Watabe, T., and Miyazono, K. (2009). Roles of TGF-beta family signaling in stem cell renewal and differentiation. Cell Res. *19*, 103–115.

Woelfle, U., Sauter, G., Santjer, S., Brakenhoff, R., and Pantel, K. (2004). Down-regulated expression of cytokeratin 18 promotes progression of human breast cancer. Clin. Cancer Res. *10*, 2670–2674.

SnapShot: Non-Small Cell Lung Cancer

Cancer Cell

Rebecca S. Heist and Jeffrey A. Engelman
Massachusetts General Hospital, Boston, MA, 02114, USA

Stage	Est. %[a]	General treatment recommendations	5-year overall survival[b]	
			clinical stage	path. stage
IA	14%	Surgical resection	50%	73%
IB	10%	Surgical resection, can consider adjuvant chemotherapy in selected cases (e.g. tumor size > 4cm)	43%	58%
IIA	6%	Surgical resection followed by adjuvant chemotherapy	36%	46%
IIB	5%	Surgical resection followed by adjuvant chemotherapy	25%	36%
IIIA	16%	Multimodality treatment: chemotherapy, radiation, +/- surgery	19%	24%
IIIB	8%	Multimodality treatment: chemotherapy and radiation	7%	9%
IV	41%	Chemotherapy, consider targeted therapies according to driver mutations	2%	N/A

[a]Estimated from SEER validation set of proposed 7th edition IASLC staging.
[b]Overall survival is higher by pathologic stage because clinical stage, which is estimated by clinical characteristics based on CT scan, PET, etc., can underestimate the true stage.

Mutation spectrum in Adenocarcinoma

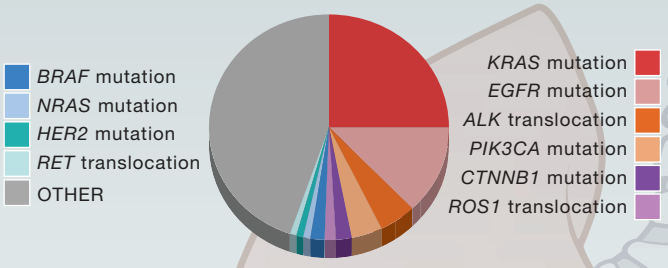

Mutations in *TP53* and *STK11/LKB1* are common occurrences, not included in pie chart due to high overlap with other mutations

Mutation spectrum in Squamous Cell Carcinoma

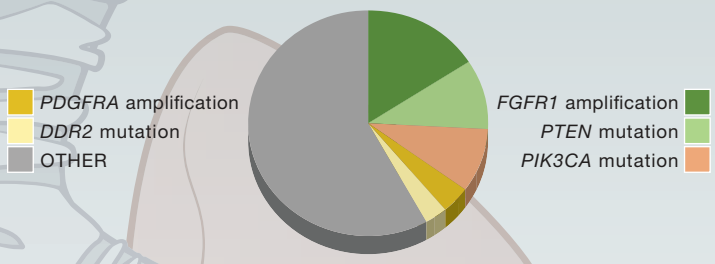

Mutations in *TP53* are a common occurrence, not included in pie chart due to high overlap with other mutations

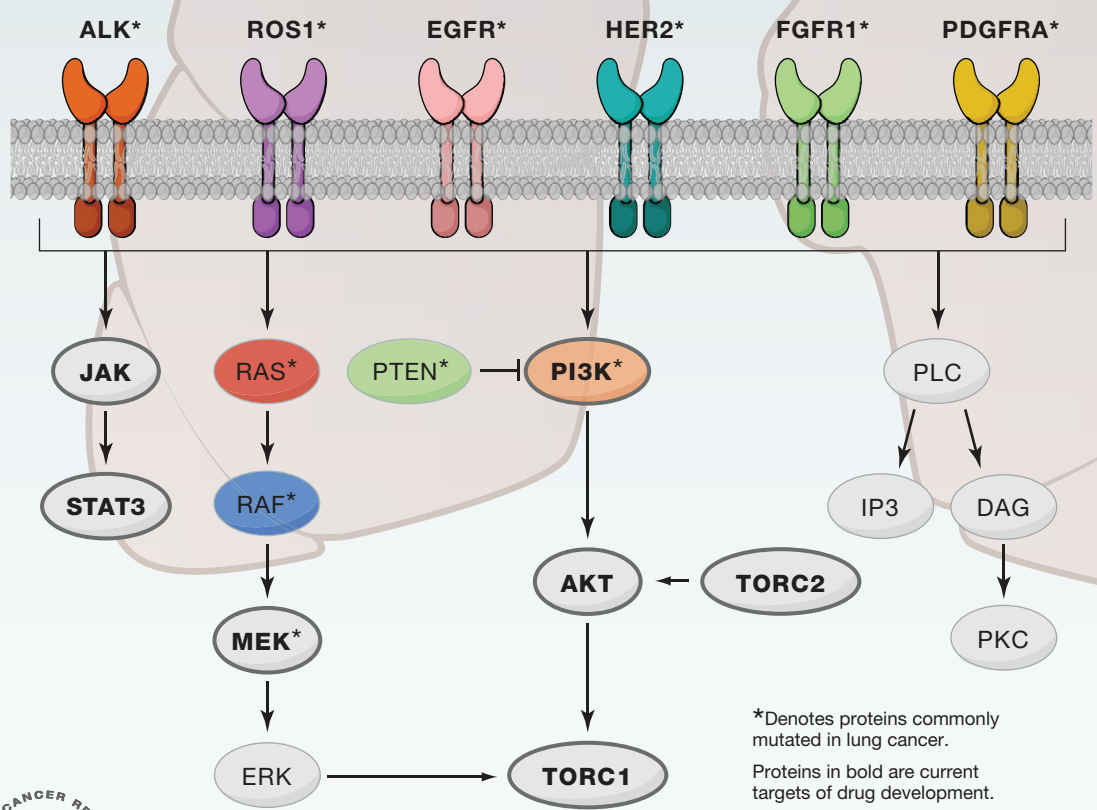

*Denotes proteins commonly mutated in lung cancer.

Proteins in bold are current targets of drug development.

Target	Drug
EGFR	Erlotinib (approved)
	Gefitinib (approved)
	PF299804
	Afatinib (BIBW2992)
ALK	Crizotinib (approved)
	LDK378
	AP26113
	AF802
ROS1	Crizotinib
HER2	PF299804
	Afatinib (BIBW2992)
FGFR	BGJ398
	FP1039 (HGS1036)
	Ponatinib (AP24534)
FGFR/ PDGFRA/ VEGFR	BIBF1120
	Pazopanib
	Lenvatinib (E7080)
	Brivanib (BMS-582,664)
	Dovitinib (TKI258)
PDGFRA	MEDI575
	IMC-3G3
PI3K	BKM120
	PX-866
	GDC-0941
	SAR245408
PI3K/ MTOR	GDC-0980
	BEZ235
	SAR245409
MEK	MEK162
	GDC-0973
	GSK1120212
	MSC1936369B
STAT3	OPB51602
AKT	MK2206

See online version for legend and references.

SnapShot: Non-Small Cell Lung Cancer

Rebecca S. Heist and Jeffrey A. Engelman
Massachusetts General Hospital, Boston, MA, 02114, USA

Cancer Cell

The treatment and diagnosis of non-small cell lung cancer (NSCLC) has been revolutionized by the development of targeted agents for cancers harboring specific genetic mutations. The top table in the adjacent figure summarizes the current clinical landscape of NSCLC. Several somatic "driver" mutations have been described in lung cancer, with the spectra and frequencies of mutations differing between adenocarcinoma and squamous cell carcinoma. The pie charts display the current understanding of the mutation frequencies in these subsets of NSCLC.

Routine genetic testing for somatic mutations from lung cancer biopsies is becoming the standard for providing optimal patient care. Identification of specific mutations such as in *EGFR* and *ALK* directs use of FDA-approved targeted therapies that are likely to provide clinical benefit. The identification of other genetic mutations can direct patients and physicians toward appropriate clinical trials with new targeted agents. Many of the therapies currently under development target activated receptor tyrosine kinases (RTKs) or associated downstream signaling pathways, particularly the RAS-RAF-MAPK and PI3K-AKT pathways. The accompanying pathway diagram highlights the proteins that are currently being targeted in NSCLC, and the accompanying table lists the targeted therapies that are FDA approved or currently under active development for treating NSCLC. There are numerous clinical trials currently underway assessing how to best target specific pathways (alone or in combination) in cancers harboring specific mutations.

EGFR

Activating EGFR mutations are located in the tyrosine kinase domain and result in constitutive EGFR signaling. Mutant EGFR activates the PI3K-AKT and RAS-MEK-ERK pathways that are central to the growth, survival, and migration of cancer cells. The most common activating mutations are in-frame deletions in exon 19 and a missense mutation at codon 858 that leads to an arginine to leucine substitution (L858R). Lung cancers with *EGFR* mutations are highly sensitive to EGFR tyrosine kinase inhibitors (TKIs). Currently, genotype screening for mutations in *EGFR* is often used to select patients with stage IV NSCLC who will receive EGFR TKIs in the first-line setting. Current research is focused on improving the duration of response and finding effective ways to target the resistance mechanisms that develop at the time of progression. The most common resistance mechanism is the *EGFR* T790M mutation found in ~50% of resistant tumors, but several others, such as *MET* amplification, *PIK3CA* mutations, and transformation to SCLC, have also been described.

ALK

An inversion in chromosome 2 results in a fusion gene combining *EML4* and *ALK*, which encodes a fusion protein with constitutive activation of ALK resulting from ligand-independent dimerization. ALK signaling leads to cellular proliferation and growth through activation of RAS-MEK-ERK, JAK3-STAT3, and PI3K-AKT pathways. *ALK* translocations in NSCLC are associated with adenocarcinoma histology and signet ring cell morphology and with younger patient age and nonsmoking history. A large phase I study of crizotinib, which inhibits ALK and several other kinases, demonstrated an overall response rate of 57% and disease control rate of 90% in patients whose cancers harbor *ALK* translocations, leading to FDA approval in this indication. More potent ALK inhibitors and strategies targeting acquired resistance are currently being investigated.

ROS1

Chromosomal rearrangements involving the *ROS1* gene are identified in ~1.5% of lung adenocarcinomas. Similar to ALK-positive cancers, patients with ROS1-positive cancers tend to be younger, never-smokers, and with adenocarcinoma. Responses to crizotinib in patients whose cancers harbor *ROS1* translocations have been identified.

KRAS

KRAS is one of the most frequently mutated genes in lung cancer, occurring in ~25% of adenocarcinomas. *KRAS* mutations in lung cancer localize primarily to codons 12 and 13. *KRAS* mutations in lung cancer appear to be mutually exclusive with *EGFR* mutations and with *ALK* translocations and are more often associated with patients with a smoking history. *KRAS* mutations are associated with resistance to EGFR TKI therapy. Although no drugs are currently in development that directly target mutant KRAS, strategies using newer targeted therapies in combination with chemotherapy or other targeted therapies, for example, combined PI3K and MEK inhibition, are under clinical development.

PI3K

Mutations in *PIK3CA* are clustered in two hotspot regions, exons 9 and 20, encoding the helical and kinase domains of the protein, respectively. These mutations result in heightened lipid kinase activity and constitutive PI3K-AKT signaling. There are multiple PI3K inhibitors in development, with specificity ranging from dual PI3K/MTOR inhibition to pan-PI3K to isoform-selective PI3K inhibitors. Preclinical data suggest that cancers harboring activating mutations in *PIK3CA* are among the most sensitive to single-agent PI3K pathway inhibitors, and clinical trials are underway in lung cancer examining this hypothesis.

PTEN

The tumor suppressor gene *PTEN* encodes a lipid phosphatase that negatively regulates the PI3K-AKT pathway, and loss of *PTEN* leads to constitutive PI3K-AKT signaling. *PTEN* is inactivated in many cancers through various mechanisms. PTEN loss is more common in squamous cell cancers than adenocarcinomas. Clinical trials are assessing the efficacy of PI3K inhibitors in cancers with *PTEN* loss.

FGFR1

FGFR1 is a potential target in squamous cell lung cancer. FGFR1 is a member of the FGFR family of RTKs. FGFR1 activation leads to downstream signaling via PI3K-AKT and RAS-MEK-MAPK. *FGFR1* amplification is observed in ~20% of squamous cell cancer. In laboratory studies, inhibition of FGFR1 both in cancer cell lines and in mouse models harboring *FGFR1* amplification leads to growth inhibition and apoptosis. Multiple FGFR inhibitors are in clinical development, many of which inhibit multiple tyrosine kinases in addition to FGFR1.

PDGFRA

PDGFRA amplification is observed in lung squamous cell cancers. Inhibition of PDGFRA via shRNA knockdown or small molecule inhibition impairs cell survival and anchorage-independent growth, suggesting that *PDGFRA* may be a driver oncogene in a subset of cancers with *PDGFRA* amplification. Multiple PDGFR inhibitors are in clinical development. Similar to the FGFR1 inhibitors, many of these agents inhibit multiple kinases.

DDR2

DDR2 is a RTK that binds collagen and promotes cell migration, proliferation, and survival. *DDR2* mutations were identified in squamous cell lung cancers and cell lines. In cell lines with *DDR2* mutations, suppression of DDR2 activity led to inhibition of proliferation. Ectopic expression of mutant DDR2 led to cellular transformation, although different mutations had varying levels of transformative capability. These results suggest that *DDR2* mutations may be oncogenic and that cancers with these mutations may be sensitive to DDR2 kinase inhibitors.

BRAF

BRAF mutations are found in 1%–3% of NSCLC. While V600E is the most common mutation, multiple other types of *BRAF* mutations have been reported in lung cancer, including G469A and D594G. While specific drugs such as vemurafenib are highly active in melanomas harboring *BRAF* V600E mutations, the activity of these drugs in *BRAF* mutant lung cancer remains to be assessed. Multiple trials assessing the activity of BRAF and MEK inhibitors are underway for cancers harboring *BRAF* mutations.

Targeted therapies are being developed in the metastatic, or stage IV, lung cancer setting. In metastatic lung cancer, surgery and radiation therapy are usually not indicated, and treatment centers on systemic therapy. Because these novel drugs show promise in the metastatic setting when used in cancers with specific genetic mutations, future directions may include implementing these treatment strategies in the adjuvant setting to improve cure rates.

  DOI 10.1016/j.ccr.2012.03.007

SnapShot: Non-Small Cell Lung Cancer

Rebecca S. Heist and Jeffrey A. Engelman
Massachusetts General Hospital, Boston, MA, 02114, USA

Cancer Cell

REFERENCES

Bergethon, K., Shaw, A.T., Ignatious Ou, S.H., Katayama, R., Lovly, C.M., McDonald, N.T., Massion, P.P., Siwak-Tapp, C., Gonzalez, A., Fang, R., et al. (2012). ROS1 rearrangements define a unique molecular class of lung cancers. J. Clin. Oncol. *30*, 863-870.

Engelman, J.A. (2009). Targeting PI3K signaling in cancer: opportunities, challenges and limitations. Nat. Rev. Cancer *9*, 550–562.

Hammerman, P.S., Sos, M.L., Ramos, A.H., Xu, C., Dutt, A., Zhou, W., Brace, L.E., Woods, B.A., Lin, W., Zhang, J., et al. (2011). Mutations in the DDR2 kinase gene identify a novel therapeutic target in squamous cell lung cancer. Cancer Discov. *1*, 78–89.

Hollander, M.C., Blumenthal, G.M., and Dennis, P.A. (2011). PTEN loss in the continuum of common cancers, rare syndromes and mouse models. Nat. Rev. Cancer *11*, 289–301.

Kwak, E.L., Bang, Y.J., Camidge, D.R., Shaw, A.T., Solomon, B., Maki, R.G., Ou, S.H., Dezube, B.J., Jänne, P.A., Costa, D.B., et al. (2010). Anaplastic lymphoma kinase inhibition in non-small-cell lung cancer. N. Engl. J. Med. *363*, 1693–1703.

Linardou, H., Dahabreh, I.J., Kanaloupiti, D., Siannis, F., Bafaloukos, D., Kosmidis, P., Papadimitriou, C.A., and Murray, S. (2008). Assessment of somatic k-RAS mutations as a mechanism associated with resistance to EGFR-targeted agents: a systematic review and meta-analysis of studies in advanced non-small-cell lung cancer and metastatic colorectal cancer. Lancet Oncol. *9*, 962–972.

Mok, T.S., Wu, Y.L., Thongprasert, S., Yang, C.H., Chu, D.T., Saijo, N., Sunpaweravong, P., Han, B., Margono, B., Ichinose, Y., et al. (2009). Gefitinib or carboplatin-paclitaxel in pulmonary adenocarcinoma. N. Engl. J. Med. *361*, 947–957.

Sequist, L.V., Waltman B.A., Dias-Santagata, D., Diqumarthy, S., Turke, A.B., Fidias, P., Bergethon, K., Shaw, AT., Gettinger, S., Cosper, A.K., et al. (2011). Genotypic and histological evolution of lung cancers acquiring resistance to EGFR inhibitors. Sci. Transl. Med. *3*, 75ra26.

Shaw, A.T., Yeap, B.Y., Mino-Kenudson, M., Digumarthy, S.R., Costa, D.B., Heist, R.S., Solomon, B., Stubbs, H., Admane, S., McDermott, U., et al. (2009). Clinical features and outcome of patients with non-small-cell lung cancer who harbor EML4-ALK. J. Clin. Oncol. *27*, 4247–4253.

Weiss, J., Sos, M.L., Seidel, D., Peifer, M., Zander, T., Heuckmann, J.M., Ullrich, R.T., Menon, R., Maier, S., Soltermann, A., et al. (2010). Frequent and focal FGFR1 amplification associates with therapeutically tractable FGFR1 dependency in squamous cell lung cancer. Sci. Transl. Med. *2*, 62ra93.

  DOI 10.1016/j.ccr.2012.03.007